DISSERTATION

AQUEOUS ATMOSPHERIC ORGANIC PROCESSING: EFFECTS OF FOG AND CLOUD COMPOSITION

Submitted by

Alexandra Jeanne Boris

Department of Atmospheric Science

In partial fulfillment of the requirements

For the Degree of Doctor of Philosophy

Colorado State University

Fort Collins, Colorado

Summer 2016

Doctoral Committee:

Advisor: Jeffrey L. Collett, Jr.

Delphine K. Farmer
Sonia M. Kreidenweis
Jeffrey R. Pierce

ABSTRACT

AQUEOUS ATMOSPHERIC ORGANIC PROCESSING: EFFECTS OF FOG AND CLOUD COMPOSITION

Cloud and fog droplets are well-suited venues for organic reactions leading to the formation of suspended particulate matter in the atmosphere. Suspended particulate matter formed through aqueous reactions is called "aqueous secondary organic aerosol" or aqSOA, and can interact with solar radiation and adversely impact human and ecosystem health. Although atmospheric observations and lab simulations have verified the formation of aqSOA, little is known about where and when it occurs in the atmosphere. The organic (carbonaceous) reactions leading to aqSOA formation also degrade chemicals in the atmosphere, impacting the potential health effects of fog water deposited to ecosystems and crops. In the present work, studies are described that approach these aqueous oxidation reactions from field and lab perspectives, capturing both complex and simple experiments. Some results will be presented that capture the dynamics of aqSOA formation from studies of *in-situ* fog chemistry, but the lack of control over environmental variables in these observations will be highlighted. Lab-based reactions of fog and cloud water will also be presented, which oppositely underscore the missing variables in such simplified lab experiments. Despite the need for more advanced experimental design to quantify aqSOA formation and identify its sensitivities to real atmospheric variables, these field and lab approaches have garnered new insight into some key aspects of aqueous oxidation.

Fog at Baengnyeong Island (BYI) in the Yellow Sea of Korea was collected in July 2014. Fog chemistry was exemplary of aged atmospheric components: sulfur was almost entirely oxidized (98.9 to 99.8% was present as S(VI) versus S(IV)), and peroxides, which can serve as oxidants, were depleted. Organic acids at times accounted for >50% of the total organic carbon (TOC) by carbon mass, indicating that organic matter was highly oxidized. Although formic and acetic acids were the most abundant, concentrations of ten out of the 18 organic acids quantified were above 1 μM. Some organic sulfur and organic nitrogen species were additionally observed, which may have formed during aqueous reactions in the fog or in humid conditions as air traveled to BYI. Back trajectories demonstrated that the relative humidities of the air masses arriving at BYI were typically >80%, suggesting that oxidation could have taken place in the aqueous phase.

The Southern California coast is frequently foggy during the summer months, but in contrast to BYI, is closer to many atmospheric chemical emissions sources. Fog water was collected at Casitas Pass (CP) near Ventura, California in June 2015. Regional oil drilling and/or refinery emissions influenced the composition of foggy air, as did biogenic and marine emissions. Only 20% of TOC on average was contributed by organic acids, suggesting influence of fresher organic emissions than observed at BYI. After 3-5 hours of foggy conditions, however, organic sulfur and organic nitrogen species were observed, suggesting possible in-fog oxidation. A contrast between the 2015 study and a 1985/6 study demonstrated improved air quality compared to 1985/6, with lower concentrations of anthropogenically derived species (NH_4^+, NO_3^-, SO_4^{2-}, acetate, formate, and formaldehyde), but similar concentrations of naturally derived species (Na^+, Cl^-, Ca^{2+}, and Mg^{2+}).

Lab work involving aqueous oxidation within real cloud water revealed that organic constituents of cloud water caused oxidation reactions to slow due to competition for oxidant. Inorganic species (NH_4^+, SO_4^{2-} and NO_3^-) at concentrations relevant to polluted cloud water did not have a statistically significant effect on oxidation. Mechanisms of oxidation were also surprisingly unaffected by cloud water components: similar low molecular mass organic acids were observed as products of oxidation in pure and cloud water.

Oxidation of real cloud water sample constituents in the lab revealed that organosulfate species were produced when sufficient SO_4^{2-} and organic species concentrations were present. Four fog and cloud water samples were oxidized, demonstrating different oxidation regimes: a BYI fog was clearly more aged such that organosulfate esters were formed; cloud water from Mount Tai, China contained biomass burning and anthropogenic aromatic emissions and produced organic acids similar to those observed from nitrophenol chemical standard oxidations; and fog water from CP containing fresher emissions produced mainly low molecular mass organic acids.

The aqueous oxidation of biomass burning emissions collected using a mist chamber resulted in the formation of a variety of low molecular mass organic acids. No apparent structure-activity relationship was observed: aliphatic and aromatic species were oxidized at similar rates when exposed to $^{\bullet}OH$ radicals. The degradation of potentially toxic organic nitrogen species as well as net production of semi-volatile organic acid products were observed, demonstrating that in-cloud oxidation of biomass burning emissions likely contributes to the chemical evolution and organic aerosol mass within smoke plumes.

Overall, there is still a need for advanced experiment development in the field of aqueous organic atmospheric chemistry. The finding that physical processes obscured effects of aqueous reactions during fog field

studies should, likewise, guide future field work toward the concurrent measurement of microphysical parameters and possible development of higher efficiency techniques for droplet collection and/or real-time chemical analyses. However, the combination of bulk reactions and fog studies employed within this thesis has allowed the effects of real fog and cloud water chemistry on aqSOA formation to be demonstrated. The common oxidation products identified under most aqueous atmospheric regimes, including low molecular mass organic acid species, but specific environmental requirements for other products such as organosulfates, should guide future research in identifying molecular tracers of aqSOA and sensitivity studies of aqSOA formation to environmental factors.

ACKNOWLEDGMENTS

I would like to acknowledge the following important contributions to this thesis. Funding for this work was provided mainly by National Science Foundation (NSF) Grant AGS-1050052; collection of Mt. Tai cloud samples was funded by NSF Grant ATM-0711102; purchase of the ESI-HR-ToF-MS system was supported through an NSFMRI grant (ATM-0521643). Work in Korea was completed with the help of the Korean National Institute for Environmental Research Baengnyeong Island Atmospheric Research Center, and with support from an East Asia and Pacific Summer Institutes (EAPSI) Fellowship (1414725), which was funded in part by the National Research Foundation (NRF) of Korea (NRF2014R1A1A1007947). Mt. Tai cloud samples used in this research were collected by Drs. Taehyoung Lee and Xinhua Shen, Tao Wang, Wenxing Wang, and Xinfeng Wang. HYbrid Single Particle Lagrangian Integrated Trajectory Model (HySPLIT) back trajectories were run in collaboration with Sam Atwood, and the HySPLIT transport and dispersion model (http://www.ready.noaa.gov) was provided by the NOAA Air Resources Laboratory (ARL). My advisor, Dr. Jeff Collett, has provided me with many wonderful opportunities, and has made time for me whenever I needed it. He is an inspiring scientist and I am grateful that I have been able to work with him in the past five years. Dr. Yury Desyaterik has also been invaluable as a mentor to me: his expert advice on experimental design allowed me to start work on this thesis, and his knowledge of chromatography/mass spectrometry analyses was vital in each of my chapters. Dr. Amy Sullivan has also been a mentor to me, particularly in field studies and in the use of ion chromatographs. Her enduring optimism and tenacity in fixing and troubleshooting instruments has motivated me in tough situations. Dr. Taehyoung Lee is one of the most dedicated researchers I have met. He provided space, supplies, and support for me so that I could collect fog samples at Baengnyeong Island, an experience that is a highlight of my graduate work, and will be a highlight of my lifetime. I would also like to thank his students, Jungmin Yeom, Sungwon Cho, and Taehyun Park, whose efforts made that experience possible and added a dose of fun and culture. Dr. Arsineh Hecobian's incredible strength, breadth of knowledge, and willingness to help has been essential as I navigated new challenges and deadlines. Dr. Andrea Clements has also supported me with her wonderful attention to detail, and brilliant organizational and troubleshooting skill on our adventure to Southern California. I would like to thank my fellow graduate students at CSU, especially (but not exclusively) Dr. Misha Schurman, Ashley Evanoski-Cole, Brad Wells, and Dr. Katie Benedict for collaborations and for their camaraderie during these past four years. I would like to thank my

committee members, Drs. Delphine Farmer, Jeff Pierce, and Sonia Kreidenweis, for their support while I learned to think more cohesively as a scientist, and for their love of thinking about and doing atmospheric chemistry and microphysics. Finally, I would like to acknowledge the love and support of my friends and my family, especially my parents Peter Boris, Terri Fessler-Boris, Godmother Ceil Fessler, and Stepmother Teddi Boris throughout my graduate work. I could not have done this without you, and I certainly would not have had such a memorable adventure without you. Thank you.

TABLE OF CONTENTS

Abstract ii
Acknowledgements v
1. Introduction 1
1.1 The Importance of Atmospheric Water 1
1.2 Formation of Aqueous Secondary Organic Aerosol Mass 2
1.3 Microphysical Considerations of Fog and Cloud Chemistry 4
1.4 Fog Chemical Composition Overview 5
1.5 Equilibrium between Gas and Atmospheric Water Droplets 11
1.6 Aqueous Atmospheric Organic Processing 12
1.7 Aqueous Photo-Oxidation Reaction Mechanisms 14
1.8 Methods of Observing Aqueous Photo-Oxidation Reactions: Field Studies 19
1.8.1 Collection of Fog and Cloud Water 20
1.9 Methods of Observing Aqueous Photo-Oxidation Reactions: Bulk Phase Lab Studies 21
1.9.1 Aqueous Photo-Oxidation Oxidant 24
1.9.2 Aqueous Photo-Oxidation Precursors 27
1.9.3 Aqueous Photo-Oxidation Measurement Techniques 28
1.10 Key Findings and Objectives of Thesis 30
References 31
2. Fog Composition at Baengnyeong Island in the Eastern Yellow Sea: Detecting Markers of Aqueous Atmospheric Oxidation Reactions 44
2.1 Introduction 44
2.2 Methods 47
2.2.1 Study Overview 47
2.2.2 Fog Collection and Handlng 47
2.2.3 Fog Water Analysis 50
2.3 Results and Discussion 51
2.3.1 Fog Characteristics and Major Contributing Species 52
2.3.2 Marine Source Contribution 54
2.3.3 Inorganic Sulfur 55
2.3.4 Total Organic Carbon 56
2.3.5 Carboxylic Acids 56
2.3.6 Mass Spectral Analysis 58
2.3.7 Nitrophenols 60
2.3.8 Organic Sulfur Species 61
2.3.9 Atmospheric Aqueous Organic Processing 62
2.3.10 Size and Microphysical Considerations 62
2.4 Conclusions 64
References 65
3. Evolving Anthropogenic Emissions and Aqueous Aging within Fog on the Southern California Coast 71
3.2. Introduction 72
3.3. Materials and Methods 74
3.4. Results and discussion 77
3.4.1. Overview of Fog Composition 77
3.4.2. Contrast of Fog between 2015 and 1985/6 79
3.4.3. Contribution of Low Molecular Mass Organic Acids to Fog Organic Matter 81
3.4.4. Polar Organic Fog Water Constituents (≥C4) 85
3.4.5. Fog Water Non-Polar Constituents 87
3.4.6. Volatile Organic Compounds 88
3.5. Conclusions 91
References 93
4. How Do Components of Real Cloud Water Affect Aqueous Pyruvate Aging? 99
4.2. Introduction 100

4.3. Material and Methods 103
4.2.1. Mt. Tai Cloud Samples 104
4.2.1. Control Experiments 105
4.2.2. Photon Flux, $^{\bullet}$OH Concentrations and Rate Constants 106
4.2.3. Online Mass Spectrometry Analysis 107
4.2.4. Offline analysis 107
4.3. Results and Discussion 109
4.3.1. Pyruvate Oxidation 109
4.3.2. Effects of a Cloud Water Matrix on aqSOA Formation Reactions 113
4.3.3. Oxidation of Pyruvate within Less Polluted Real Cloud Water 113
4.3.4. Oxidation of Pyruvate within More Polluted Real Cloud Water 115
4.3.5. Can Inorganic Cloud Constituents Account for Impeded Pyruvate Oxidation in Cloud Water? 115
4.4. Conclusions 117
References 119
5. Aqueous Atmospheric Oxidation Processes in Real Fog and Cloud Water 123
5.1. Introduction 124
5.2. Material and Methods 126
5.2.1. Material and Methods: Photoreaction 127
5.2.2. Material and Methods: Chemical Analyses 128
5.2.3. Material and Methods: Online Analyses 129
5.2.4. Material and Methods: Offline Analyses 130
5.3. Results and Discussion 131
5.3.1. Initial Chemical Composition of Real Fog and Cloud Samples 131
5.3.2. Evolution of Carboxylic Acids 133
5.3.3. Mechanisms of Oxidation: Standards 138
5.3.4. Precursors of Oxidation: Samples 142
5.3.5. Products of Oxidation: Samples 145
5.3.6. Atmospheric Implications 150
5.4. Conclusions 151
References 154
6. Laboratory Simulated Cloud Processing of Biomass Burning Emissions 161
6.1. Introduction 162
6.2. Material and Methods 164
6.2.1. Methods: Simulated Wildfire Burns at the Powerhouse Building 164
6.2.2. Methods: Emissions Sample Collection 164
6.2.3. Methods: Aqueous Photoreaction 165
6.2.4. Methods: Online Analyses 166
6.2.5. Methods: Offline Analyses 166
6.2.6. Methods: Calculations 167
6.3. Results and Discussion 167
6.3.1. Initial Composition of Biomass Burning Emissions 167
6.3.2. Aqueous Oxidation Results: Organic Carbon 170
6.3.3. Aqueous Oxidation Results: Organic Acids 171
6.3.4. Aqueous Oxidation Results: Mechanisms of Oxidation and Qualitative Chemical Analysis 171
6.3.5. Atmospheric Implications 177
6.4. Conclusions 180
References 181
7. Conclusions and Future Research 186
7.1. Can We Observe Aqueous Aging of Organics in the Real Atmosphere? 186
7.2. Can We Accurately Simulate Aqueous Aging using Bulk Phase Reactions in the Lab? 187
7.3. Priorities for Further Research 188
References 190
Appendix 1: Standard operating procedures for Fog and cloud water analyses 193
Appendix 2: Fog composition at Baengnyeong Island in the eastern Yellow Sea: detecting markers of aqueous atmospheric oxidations 248

Appendix 3: Evolving Anthropogenic Emissions and Aqueous Aging within Fog on the Southern California Coast 259
Appendix 4: How Do Components of Real Cloud Water Affect Aqueous Pyruvate Oxidation? 289
Appendix 5: Aqueous Atmospheric Oxidation Processes in Real Fog and Cloud Water 293
Appendix 6: Laboratory Simulated Cloud Processing of Biomass Burning Emissions 310
Appendix 7: Standard Operating Procedures for Oxidations and Offline IC and LC/MS Analyses 322
Appendix 8: Case Study: Organic Acids at Mount Tai, China 344
Appendix 9: Materials for outreach programs 353

1. INTRODUCTION

1.1 The Importance of Atmospheric Water

The atmosphere contains a vast number of molecules that continually react and shift between phases of matter. Atmospheric chemical reactions occur, then, in multiple phases: in the gas phase, within/at the surface of suspended particles, or within/at the surface of water droplets. Liquid water contributes 30-80% of aerosol mass at typical ambient relative humidity (Graedel and Weschler, 1981; Khlystov et al., 2005) such that atmospheric aqueous phase reactions are relevant under most environmental circumstances. However, additional lab and field work is needed to capture atmospheric aqueous reactions in models (Chen et al., 2015), since chemical analyses are carried out on these phases separately.

Water suspended within the atmosphere as either droplets of fog or cloud, or as wet aerosol particles, is referred to as atmospheric water. These droplets play important roles as processors of atmospheric pollutants by multiple mechanisms: (a) removing chemicals from the atmosphere via physical deposition (wind- or sedimentation-driven "occult" deposition of droplets onto surfaces or wet deposition via precipitation of drops); (b) hosting reactions that degrade chemicals to products with different properties; or (c) hosting reactions that produce lower volatility chemicals, which can form aerosol mass. For example, the transfer of gaseous sulfur dioxide (SO_2) to the particle phase occurs mainly through aqueous oxidation to sulfuric acid (H_2SO_4; Finlayson-Pitts and Pitts, 2000a). Rain is also a form of atmospheric liquid water, but is typically dilute and short-lived; fog and cloud droplets are smaller in diameter (~1-25 μm in fog/cloud versus ~150-1500 μm in rain; Herrmann et al., 2015) and typically contain lesser chemical concentrations due mainly to competitive water vapor deposition onto ice particles (Borys et al., 2000; Collett et al., 1991). The typically greater concentrations of chemical constituents in fog and cloud water make the study of fog and cloud chemistry relevant for pollutant transfer to terrestrial ecosystems, photochemical and dark transformations of chemicals in the atmospheric aqueous phase, and climate implications of atmospheric chemistry occurring within water. However, the distinction between aqueous and gas-phase phenomena in the atmosphere is made difficult by the coexistence of multiple phases of matter. All liquid water is suspended in the air for some period of time, and is influenced heavily by particles and gases in the surrounding air.

Atmospheric chemistry within water droplets is often mechanistically similar to gas phase chemistry, but there are some key differences that lead to typically greater reaction rates and some different products (Altieri et al., 2006; Monod et al., 2005). The most widely applicable chemical influences of water as a medium for reactions include: (a) the solvent cage effect, which increases the time spent in an interaction between two or more chemicals (although this may be counteracted by slow aqueous molecular movement); (b) the chemical changes in conformation of species as they become dissolved: deprotonation, hydration of aldehyde groups, and chelation of metals by polar organic molecules; and (c) interactions with low volatility or non-volatile species such as inorganic anions that aren't found in the gas phase (Finlayson-Pitts and Pitts, 2000a).

The fate of chemicals in the atmosphere is altered by wet/occult deposition of water: wet deposition is faster for most species than dry deposition when cloud/fog or rain is present. For example, ~75% of nitrogen species deposition at Rocky Mountain National Park is caused by wet deposition, (Benedict et al., 2013), while 95-97% of nitrogen species deposition in the San Joaquin Valley is occult (fog) deposition during foggy periods (Lillis et al., 1999). The overall impact of fog and cloud uptake of many atmospheric chemical constituents is a balance between removal from the atmosphere (0.05-0.2 μg m^{-3} SO_4^{2-}, 3-6 μg m^{-3} NO_3^-, and 1-3 μg m^{-3} NH_4^+ removed during California Central Valley radiation fogs) and aqueous formation reactions (Lillis et al., 1999). The microphysical and chemical transformations that govern concentrations and properties of atmospheric chemicals in the presence of liquid water are complex, even for systems in which organic species are not considered (Pandis et al., 1990).

1.2 Formation of Aqueous Secondary Organic Aerosol Mass

The layers of the Earth's atmosphere are composed of chemicals in the gas as well as solid and liquid states. Those chemicals in the condensed phases form particles, which, in combination within their surrounding gases, are called aerosol. Aerosol is important for many aspects of atmospheric science. Clouds cannot be formed without aerosol particles due to the high water super-saturations (more than 400%) theoretically required for activation of a droplet without a preexisting particle (Pruppacher and Klett, 2010). This effect is thus similar for fog formation. Ice crystals also form on aerosol particles, the majority of which have been identified as mineral dust, biological particles, and metallic particles (DeMott et al., 2003; Murray et al., 2012). The change in the radiative balance of the atmosphere due to the reflection and absorption of light by aerosol particles as well as droplets or ice crystals nucleated on aerosol particles has not yet been precisely estimated, as noted in the most recent reports of the Intergovernmental Panel on Climate Change (Alexander et al., 2013; Forster et al., 2007). There are other

interactions between aerosol and atmospheric radiation, including the Twomey effect, which describes the high reflectivity of a cloud containing a large number of small droplets nucleated on abundant aerosol particles (Alexander et al., 2013). More acute effects have been described for aerosol on weather events, such as a decrease in the likelihood of tropical cyclogenesis when aerosol particles are abundant (Reale et al., 2014) and decreased precipitation during monsoonal flow patterns caused by biomass burning aerosol (Lee et al., 2014). Individual particles are too small to see, but en-masse can substantially impact the radiative balance of the atmosphere (Alexander et al., 2013; Booth et al., 2012).

Organic aerosol is complex. There are many thousands of chemicals within its composition (Hamilton et al., 2004), originating from multiple sources and changing depending on both natural and human-activity related processes. Organic species typically account for about half of fine aerosol composition (Jimenez et al., 2009), but are also key in the gas and aqueous phases of the atmosphere (Goldstein and Galbally, 2007b; Herckes et al., 2013). There are a variety of analytical techniques available to speciate these chemicals, but even when used in combination, only about 30% of organic aerosol particle mass can be identified by chemical structure (El Haddad et al., 2009; Graham et al., 2002; Jaoui and Kamens, 2003; Rogge et al., 1993; Yu et al., 1999).

Discrepancies between the measured and modeled concentrations of secondary organic aerosol (SOA; organic-containing particles formed through reactions in the atmosphere) from several studies around the world show that current SOA formation mechanisms underestimate the mass observed (Carlton et al., 2008; Heald et al., 2005; Hodzic et al., 2009; Volkamer et al., 2006). The chemical properties of SOA are also not in agreement between what is modeled and observed: the degree of oxygenation of aerosol particle components, often expressed as the oxygen to carbon (O/C) ratio, is consistently higher in the troposphere than in lab-generated aerosol or in model studies (Aiken et al., 2008; Simon et al., 2011). Despite efforts to simplify and parameterize atmospheric oxidation processes (Kroll et al., 2011; Kuwata et al., 2013; Ng et al., 2010), O/C ratios and products of oxidation reactions of OPM constituents are highly varied (Lambe et al., 2011; Yu et al., 1999). One explanation for the discrepancies between ambient and lab-generated SOA is that most current lab studies and models do not consider, or inadequately consider, aqSOA formation within atmospheric water (Ervens, 2015; McNeill, 2015).

Formation of aqSOA is a new organic aerosol formation mechanism relative to the ideas of particle nucleation and gas-particle partitioning (Blando and Turpin, 2000). Briefly, aqSOA mass is produced by aqueous atmospheric

organic processing (AAOP) reactions occurring within atmospheric water, followed by evaporation of the water and remainder of low volatility products in the particle phase. There is strong evidence suggesting that aqSOA could explain part or all of the discrepancy between observed and expected organic aerosol. This support includes the improvement of SOA models by adding aqueous processes (Carlton et al., 2008), the strong correlation of the organic fraction in the particle phase with relative humidity above 49% (El-Sayed et al., 2015; Hennigan et al., 2008, 2009), and a long list of lab study results demonstrating that low molecular mass (LMM) products such as oxalic acid can be formed through aqueous oxidation of single precursors (Herrmann et al., 2015). Some important aqSOA reactions are known, but a more complete understanding of the chemicals involved and interactions within atmospheric water matrices is needed to properly estimate and attribute the aerosol formed via aqueous reactions.

1.3 Microphysical Considerations of Fog and Cloud Chemistry

Fog formation can be caused by radiation, subsidence, advection, or frontal passage (Ahrens, 2000). A radiation fog forms when heat escapes from the warm land surface during a clear night, creating a cool layer of air in contact with the ground. Once the dewpoint is reached in this layer, water can condense onto available particles and form fog. Radiation fog formation can be enhanced by topography: when air cools on a hilltop, this denser air sinks into the valley below and causes the valley surface air to cool more rapidly (this is referred to as valley fog; Ahrens, 2000). Advection fog occurs when a moist air mass moves over a colder region of air, water and cools to dewpoint. Sea fog is an example of advection fog that forms as the result of air advection from over a warmer to a colder water body, such as in the Yellow Sea (Zhang et al., 2009). In contrast, fog along many coastlines, such as the California coastline, is formed by subsidence of stratocumulus clouds (Johnstone and Dawson, 2010).

During the lifetime of clouds and fogs, the liquid water content (LWC, the mass of liquid water per volume of ambient air) and droplet size distribution change with the maturity of the fog/cloud. Chemical composition changes with microphysical structure of the fog/cloud, since constituent concentration as well as gas-to-droplet partitioning processes are dependent on the volume of liquid water and surface area of each droplet, the number of droplets, and other microphysical variables in complex, interdependent, and often spatially and temporally varying relationships (see Section 1.5). Fog development is classically recognized as having three stages (Pruppacher and Klett, 2010): onset, wherein droplets are activated, causing the number concentration and LWC to increase but the droplet size distribution to remain constant; maturity, which is characterized by somewhat regular cycles in the droplet size distribution and LWC, even in the case of stagnant radiation fogs, while droplets grow, evaporate, and may be

deposited out; and dissipation, during which the droplets are evaporating and the droplet size, LWC, and droplet number all correspondingly decrease. The variation of fog LWC is typically between 30 and 500 mg m^{-3}, and the droplet mean size of 10-20 μm (Pruppacher and Klett, 2010). Clouds, on the other hand, typically have larger droplets, particularly in cumuliform clouds and maritime or low particle concentration environments. Cloud LWCs are most often between 100 and 500 mg m^{-3}, but for turbulent cumuliform clouds such as cumulonimbus, 3-5 g m^{-3} is possible. The same three stages represent the general development of a cloud, but turbulent collision/coalescence processes occurring within clouds cause the size distribution to broaden during maturation, and drops to precipitate (i.e. wet deposit) during the dissipation stage of the cloud (Pruppacher and Klett, 2010). Despite some differences between fog and cloud characteristics in these generalized cases, the distinction between fogs and clouds is sometimes ambiguous, especially when clouds touch the ground as in the case of coastal stratiform clouds as they move inland, or orographic clouds at low elevation.

1.4 Fog Chemical Composition Overview

Particles and gases are both dissolved into water during fog events, such that fog chemistry is representative of the air quality of a region (Herckes et al., 2013). The fog chemistries of many regions of the world have been documented; campaigns examining the organic content of fogs/clouds from the 1980s-2010s have been summarized by Herckes et al. (2013) and Collett et al. (2002). The dissolution of ionic species from aerosol particles acting as condensation nuclei, dissolution of gases, and aqueous-phase oxidation reactions contribute to fog water composition. Three inorganic species are typically dominant: NH_4^+, from the particle phase or gaseous NH_3, NO_3^-, mainly from oxidation of NO_x to gas phase HNO_3, and SO_4^{2-}, which is mainly from oxidation of SO_2 to particle phase H_2SO_4 and SO_4^{2-} (Finlayson-Pitts and Pitts, 2000a). The overall composition of fog water maintains charge balance through variable concentrations of inorganic and organic ions, as well as induced concentrations of H_3O^+/H^+ and ^-OH. The balance of these ions as well as the overall LWC of the fog/cloud water dictates the resulting pH, although other species including sea salt/dust cations and carboxylic acids, can be influential as well (Finlayson-Pitts and Pitts, 2000a). The acidity of atmospheric water has historically been a driver for research of fog, cloud, and rain chemistry (e.g., Jacob, 1985; Pandis et al., 1990), and remains an influential characteristic of atmospheric water on ecosystem and human health. Fog water typically ranges in pH between approximately 2 and 7 (Figure 1-1). Since CO_2 reacts with liquid water in the atmosphere, the theoretical pH of natural waters at equilibrium with atmospheric CO_2 is 5.6 (based on a [CO_2] of 405 ppmv, accurate for Mauna Loa Observatory, HI in spring of 2016, NOAA

ESRL Global Monitoring Division, 2016). Thus, fog water samples above this value are considered alkaline, while values below are acidic. The true neutral pH of approximately 5.6 is approximately one pH unit greater than the median value for cloud and fog water pH values globally (Figure 1-1), suggesting that studied fogs/clouds have been slightly acidic. Even in background atmospheres, uptake of naturally produced acids (e.g., H_2SO_4, HCCOH, or H_3CCOOH) can lower pH to 5.0 or below (Gioda et al., 2011).

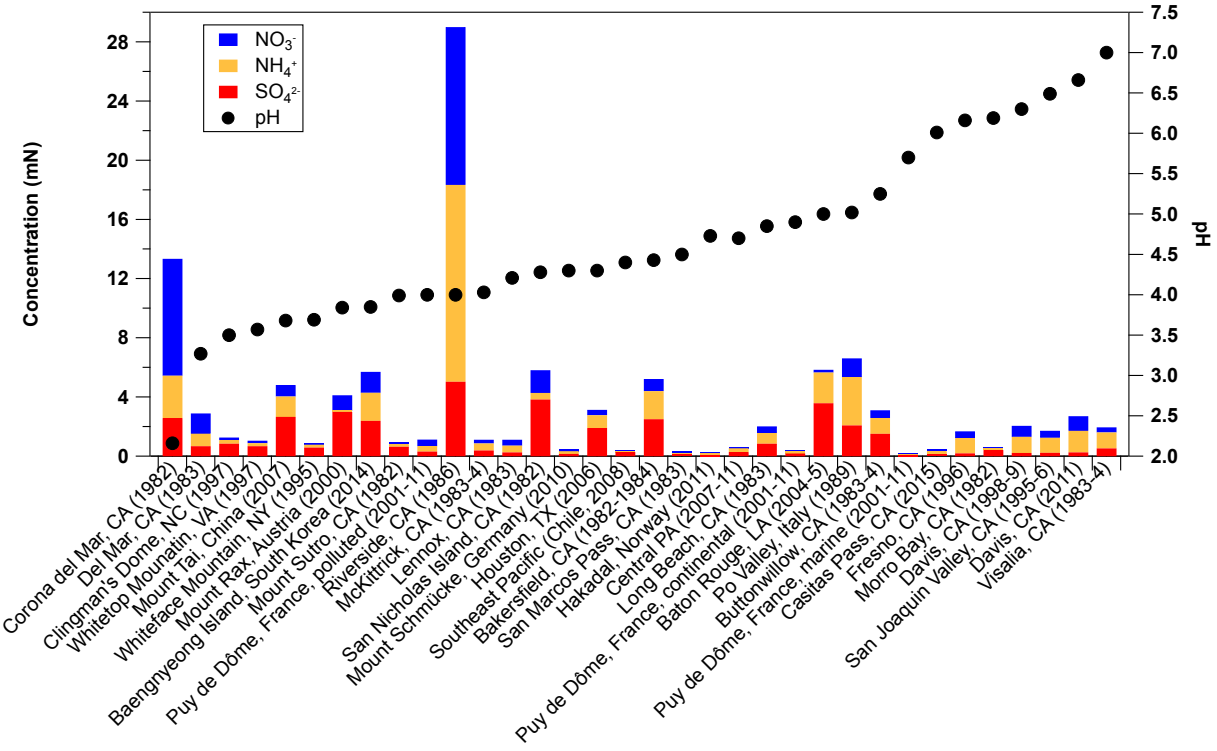

Figure 1-1. Compiled NH_4^+, NO_3^-, and SO_4^{2-} concentrations (mN = millinormal), and pH values in fog and cloud water samples collected within the United States and internationally. Sources: Jacob, 1985 (Corona del Mar, CA (1982), Del Mar, CA (1983), Mount Sutro, CA (1982), Lennox, CA (1983), San Nicholas Island, CA (1982), Bakersfield, CA (1982-1984), San Marcos Pass, CA (1983), Long Beach, CA (1983), Morro Bay, CA (1982)), Anderson et al., 1999 (Clingman's Dome, NC (1997), Whitetop Mountain, VA (1997), Whiteface Mountain, NY (1995)), Wang et al., 2011 (Mount Tai, China (2007)), Löflund et al., 2002 (Mount Rax, Austria (2000)), Boris et al., 2015 (Baengnyeong Island, South Korea (2014)), Deguillaume et al., 2014 (Puy de Dôme, France (2001-11)), Munger et al., 1990 (Riverside, CA (1986)), Jacob et al., 1986 (McKittrick, CA (1983-4), Buttonwillow, CA (1983-4), Visalia, CA (1983-4)), van Pinxteren et al., 2016 (Mt. Schmücke (2010)), Raja et al., 2008 (Houston, TX (2006), Baton Rouge, LA (2004-5)), Benedict et al., 2012 (Chile, 2008), Wang et al., 2014 (Hakadawl, Norway (2011)), Straub et al., 2012 (Central PA (2007-11)), Fuzzi et al., 1992 (Po Valley, Italy (1989)), Chapter 3 (Casitas Pass, CA (2015)), Collett et al., 1999 (Fresno, CA (1996), San Joaquin Valley, CA (1995-5)), Collett et al., 2002 and Moore et al., 2004a (Davis, VA (1998-1999)), Herckes et al., 2015 (Davis, CA (2011)).

In general, fog concentrations of inorganic pollutants depend on the same primary sources and oxidation processes as in aerosol, and regional trends are therefore expected to be similar to those of aerosol species. For example, aerosol SO_4^{2-} concentrations tend to be greater in the Eastern U.S., where coal contains greater

concentrations of sulfur impurities versus in the Western U.S. In contrast, NO_x emissions, and therefore aerosol NO_3^- concentrations, are abundant in the Southern California urban areas and the Ohio River Valley (Heald et al., 2012; Park et al., 2004, 2006). The concentrations of NH_4^+ are mainly controlled by farming practices and fertilizer use, as demonstrated by the distribution primarily in the Midwest and San Joaquin Valley (SJV) of California (Heald et al., 2012). These trends in general are also visible in fog chemical measurements made throughout the U.S. as well as the world. Fog water acidity is contributed, for example, by HNO_3 at California sites while H_2SO_4 is more abundant at North Carolina, Virginia, and New York sites (Figure 1-1, left side of plot). In agreement with the aerosol NH_4^+ sources in regions with substantial agricultural land use, the fog concentrations of NH_4^+ are greatest in the SJV of California (Bakersfield, Davis, and downwind in Riverside) and areas such as the Po Valley in Italy, which is mainly farmland. The concentration of NO_3^- in fog is typically greatest downwind of cities, due to formation of gaseous HNO_3 and particle NO_3^- from urban NO_x sources such as vehicles. Aside from Riverside (downwind of Los Angeles), high fog concentrations of NO_3^- were observed at Corona del Mar and San Nicholas Island (also near Los Angeles), Del Mar (near San Diego), the Po Valley in Italy and Mount Tai in China (within industrial/agricultural valleys), Baengnyeong Island in South Korea (downwind of major cities in China), and Mount Rax in Austria (near Vienna). Oxidation of SO_2 is the primary source of particle SO_4^{2-} in the atmosphere (Finlayson-Pitts and Pitts, 2000a), and thus is also most abundant within fog downwind of industrial and urban areas. Foggy locations with greatest SO_4^{2-} concentrations are therefore similar to those with abundant NO_3^-, with less influence in the west due to the coal/oil impurities in the eastern U.S. The location of a fog measurement site with respect to the prevailing meteorology during fog events and the regional topography are clearly important: measured Riverside, CA fog concentrations of NH_4^+ (as well as other pollutants) are high due to the typical conditions during fog events, which include flow from the nearby L.A. urban area and farms in the Chino area, and stagnation against the San Bernardino Mountains and under a temperature inversion (Munger et al., 1990). Organic matter (OM) is also abundant within fog water, constituting 10-50% of the fog constituent mass, similar to individual inorganic components (Figure 1-2). The OM concentrations (from an OM/organic carbon ratio of 1.8 and a mean molecular mass of 100 g mol^{-1}) overall do not follow any apparent trend with region or proximity to urban areas because a vast number of sources of organic species exist in the atmosphere. Reported values of the total organic carbon (TOC) concentration in fog and cloud water range from 1 mg C L^{-1} (ppm C) to nearly 300 mg C L^{-1}, with most values between 10 and 50 mg C L^{-1} (Herckes et al., 2013). Fog OM can originate from biogenic sources, which emit almost

ten times more volatile organic compounds by mass than anthropogenic sources globally (Goldstein and Galbally, 2007). Forest fires are additionally substantial contributors (Lee et al., 2012; Shen et al., 2012). Concentrations of OM are often greatest when nocturnal boundary layers form, trapping air pollutants near the ground (Herckes et al., 2013); this is a common feature of urban areas in valleys or against mountain ranges, such as the Los Angeles Basin and Po Valley. While some of the fog TOC is insoluble in water and might be located within a surface layer or undissolved organic phase, the soluble fraction, dissolved organic carbon (DOC), is typically largest (54% in Po Valley fog, Facchini et al., 1999, to 95% in Zurich, Switzerland fog, Capel et al., 1990).

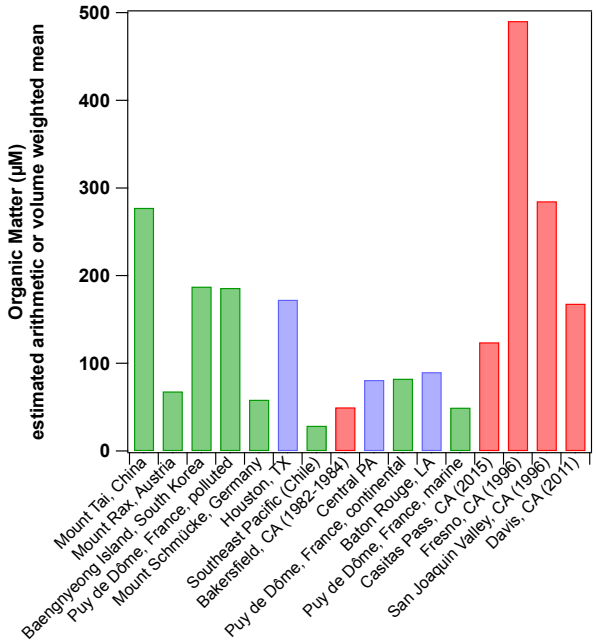

Figure 1-2. Compiled organic matter (OM) concentrations in fog water samples collected within the United States (blue, with California sites in red), and internationally (green). Values were estimated from total or dissolved organic carbon measurements, assuming an organic mass/organic carbon ratio of 1.8 and a mean molecular mass of 100 g mol^{-1}. See Figure 1-1 for references.

Bulk characterization of the TOC or DOC has been carried out using a range of techniques, which are listed elsewhere (Fuzzi et al., 2002; Herckes et al., 2013). Characteristics of OM have been explored using other techniques: proton nuclear magnetic resonance spectroscopy (^{1}H NMR) demonstrated that polyacids, as well as mono- and di-carboxylic acids, account for ~5-35% and ~17-51% of DOC, respectively, with primarily aliphatic character in Po Valley fog (Decesari et al., 2000, 2005). Size exclusion chromatography and electrospray ionization mass spectrometry (ESI-MS) approximated the typical range of Po Valley fog OM between mass-to-charge ratios (m/z^-) 50-500, with a peak at m/z^- 250 (for singly or doubly charged anions). The elemental abundance within the TOC in fog water was also analyzed using high resolution mass spectrometry (Fourier Transform ion cyclotron

resonance mass spectrometry, FT-ICR-MS), demonstrating that structures with not only the elements C, H, and O were present in the fog, 88% of which were identified as "oligomers" (polymers with a small number of monomer subunits), but also N (36% of structures) and S (12% of structures, including N and S-containing species), indicating the presence of organic species containing CHNO, CHOS, and CHNOS atoms (Mazzoleni et al., 2010). Analysis of OM in fog is a somewhat recent focus that has been driven in part by the advancement of analytical techniques but also by an understanding that organic species are a substantial fraction of fog composition and charge balance (Herckes et al., 2013).

The quantification of carboxylic acids is becoming common in fog studies. The most abundant carboxylic acids are typically analyzed: formate, acetate, oxalate, and sometimes propionate, pyruvate, succinate, malonate, maleate, lactate, and methanesulfonate. Limbeck and Puxbaum (1999) documented the species diversity of carboxylic acids in aerosol samples from both rural and urban sites; since the solubilities of carboxylic acids in water are typically high (Saxena and Hildemann, 1996), these relative concentrations are relevant for fog water as well, although some of the carboxylic acids in fog also originate from the gas phase (including formate and acetate). In general, the sources of carboxylic acids are similar to those of hydrocarbons, mainly because they are formed as photo-oxidation products (Kawamura and Ikushima, 1993): combustion of fossil fuel, biogenic emissions, combustion of biomass (Limbeck and Puxbaum, 1999). Primary sources are also regularly cited for carboxylic acids and even dicarboxylic acids (Kawamura et al., 1996), so distinguishing between fresh and photo-oxidized emissions in the atmosphere is challenging. Although there are a large number of atmospheric sources of carboxylic acids, photochemical aging is a substantial source, and, especially in the case of dicarboxylic acids, their abundance is used in determining whether or not a sample has been photochemically aged (e.g., Sorooshian et al., 2010).

Because the pH of fog and cloud water is typically between 3 and 7, and many logarithmic acid dissociation constants pK_a are in the lower part of this range (Table 1-1), carboxylic acids are mainly deprotonated in the aqueous phase (one or both protons removed for dicarboxylic acids). The coulombic attraction between deprotonated carboxylic acids and H_3O^+, NH_4^+, and other cations causes them to be favorably in the aqueous phase. Fog or cloud water carboxylic acids may originate from gas phase, particle phase, or formation in the aqueous phase. There are multiple aqueous phase mechanisms for carboxylic acid formation. The mechanism typically begins with hydration of an aldehyde functionality, which occurs especially at low pH because the process can be acid-catalyzed (e.g., Pocker et al., 1969). The resulting gem-diol structure is easily further reacted to form a carboxylic acid species,

especially as in a dehydration reaction (which will only occur at high organic concentration and in the aqueous phase) or by hydroxyl radical ($^{\bullet}OH$) removal of the geminal hydrogen atom, peroxyradical formation, and subsequent carbonyl formation (which will occur in the gas phase as well; Lim et al., 2010, 2013).

Table 1-1. Empirical acid dissociation constants of organic species with reactive proton sites (expressed as pK_{a1} and pK_{a2}, the negative logarithms of the first and second acid dissociation constants) (source: Haynes et al., 2013). Formulae for acidic species ($pK_a<7$) are listed as singly deprotonated anions ($[M-H]^-$) as typically found in atmospheric water; basic species ($pK_a>7$) are listed as uncharged species. Values were measured at approximately 25°C.

Species Name	Formula	pK_{a1}	pK_{a2}
Oxalate	C_2HO_4	1.25	3.81
Maleate	$C_4H_3O_4$	1.92	6.23
Pyruvate	$C_3H_3O_3$	2.39	
Hydroxymalonate	$C_3H_3O_5$	2.42	4.54
2-Oxo-glutarate	$C_5H_5O_5$	2.47	4.68
Oxaloacetate	$C_4H_3O_5$	2.55	4.37
Malonate	$C_3H_3O_4$	2.85	5.7
Phthalate	$C_8H_5O_4$	2.94	5.43
Fumarate	$C_4H_3O_4$	3.02	4.38
meso-Tartarate	$C_4H_5O_6$	3.17	4.91
Glyoxylate	C_2HO_3	3.18	
Malate	$C_4H_5O_5$	3.4	5.11
Glycerate	$C_3H_5O_4$	3.52	
Formate	CHO_2	3.75	
Glycolate	$C_2H_3O_3$	3.83	
Lactate	$C_3H_5O_3$	3.86	
Salicylate	$C_7H_5O_3$	4.08	9.92
Benzoate	$C_7H_5O_2$	4.2	
Succinate	$C_4H_5O_4$	4.21	5.64
Methylmalonate	$C_4H_5O_4$	3.07	5.76
Acrylate	$C_3H_3O_2$	4.25	
Glutarate	$C_5H_7O_4$	4.32	5.42
3-Butenoate	$C_4H_5O_2$	4.34	
3-Hydroxypropanoate	$C_3H_5O_3$	4.51	
trans-3-Pentenoate	$C_5H_7O_2$	4.51	
Heptanedioate	$C_7H_{11}O_4$	4.71	5.58
4-Hydroxybutanoate	$C_4H_7O_3$	4.72	
Acetate	$C_2H_3O_2$	4.76	
Butanoate	$C_4H_7O_2$	4.83	
Pentanoate	$C_5H_9O_2$	4.83	
3-Hydroxybutanoate	$C_4H_7O_3$	4.84	
Propanoate	$C_3H_5O_2$	4.87	
Heptanoate	$C_7H_{13}O_2$	4.89	
4-Nitrophenol	$C_6H_5NO_3$	7.15	
4-Hydroxybenzenesulfonate	$C_6H_6O_4S$	9.07	
para-Hydroquinone	$C_6H_6O_2$	9.85	11.4
Phenol	C_6H_6O	9.99	
meta-Cresol	C_7H_8O	10.09	
para-Cresol	C_7H_8O	10.26	
ortho-Cresol	C_7H_8O	10.29	
Formaldehyde	CH_2O	13.27	

While photo-oxidation in the gas and aqueous phases is a primary source of carboxylic acids, it can also be a sink. The oxidation of carboxylic acids by $^{\bullet}OH$ has been well documented (e.g., Boris et al., 2014; Lim et al., 2010), and formation and photolysis of transition metal-carboxylate complexes has been suggested to degrade carboxylic acids (Safarzadeh-Amiri et al., 1997; Zuo and Hoigné, 1992, 1994). Sorooshian and colleagues (2013) found that the Fe(III)-oxalate complex formation was non-linearly related to total iron concentration, and may be a result of the predominance of Fe(II) during the day, as well as the formation of complexes with other carboxylic acids. Although

other relevant carboxylic acids are typically less abundant than oxalate, their complexes with transition metals may be more stable (Weller et al., 2013, 2014). These metal-carboxylato complexes may also influence volatile organic carbon (VOC) concentrations, and even new particle formation (Nie et al., 2014). Such a process not only brings a direct relationship between organic and inorganic constituents of atmospheric water, but also underscores the overall complexity of aqueous atmospheric processes.

1.5 Equilibrium between Gas and Atmospheric Water Droplets

Multiple processes are responsible for the transfer of a volatile species between the gas and aqueous phases: (1) gas phase transport (diffusion) to the droplet; (2) mass transfer across the air-water interface of the droplet; (3) protonation/hydration/establishment of aqueous-phase chemical equilibria; and (4) aqueous-phase transport (diffusion; Finlayson-Pitts and Pitts, 2000a). For a dilute, aqueous solution in equilibrium with the surrounding gas phase, Henry's Law can be used to describe the concentrations of a species in the aqueous and gas phases:

$$K_H = \frac{[A]_{aq}}{[A]_g} \qquad \text{Equation 1}$$

where K_H is the Henry's Law constant (given typically in M atm^{-1}), $[A]_{aq}$ is the aqueous concentration of a chemical substance A (in M) and $[A]_g$ is the gas phase partial pressure of A (in atm). The value of K_H is empirically derived for pure water, and often is accompanied by modifiers to account for enhanced solubility. Values of K_H can be compared to show the solubility of gases in the atmospheric aqueous phase, and discuss the likelihood that species will be in the aqueous phase. For example, H_2O_2, K_H=0.7-1.4×10^5 M atm^{-1}, is more soluble in pure water at 20-25 °C than $^{\bullet}$OH, K_H=5-30 M atm^{-1} (Finlayson-Pitts and Pitts, 2000b), and measured ambient aqueous concentrations of $^{\bullet}$OH are lower.

For carboxylic acids, the deprotonation or hydration that occurs once the species enters a droplet can further drive the partitioning of the species to the aqueous phase. This can be thought about using Le Chatelier's principle: as increased quantities of formic acid are deprotonated in a solution in which pH > pK_a for formic acid (~3.75; Haynes et al., 2013), an increased quantity of formic acid is drawn into the aqueous phase from the gas phase according to the following chemical equilibrium: $[HA]_{gas} \Leftrightarrow [HA]_{aq} \Leftrightarrow [A^-]_{aq} + [H^+]_{aq}$. For carboxylic acids, the K_H is therefore inversely dependent upon the $[H^+]_{aq}$ of the solution. Similarly, for aldehydes, the hydration to give gem-diol forms of the species can increase the equilibrium concentration of the species in the aqueous phase. The hydration of ketones is sterically hindered, and therefore typically unfavorable (Solomons and Fryhle, 2004). Other

interactions, including oligomerization and oxidation reactions, can also increase effective Henry's Law constants (Ervens and Volkamer, 2010). Equilibrium, however, may not be reached for volatile species between the gas phase and the aqueous phase of the atmosphere. Ambient measurements of fog chemistry have demonstrated that volatile species may be sub-saturated and super-saturated with respect to complex modeled equilibria. The observed departures from ideality might be caused by: (a) sampling droplets with differing chemical concentrations (Pandis and Seinfeld, 1991; Ricci et al., 1998); (b) sampling droplets with differing droplet sizes (Moore et al., 2004b); or (c) sampling changing water/air within a single bulk sample of atmospheric water (Winiwarter et al., 1992). Ervens et al. (2003b) found that larger droplets and more soluble species (greater K_H) required longer times for equilibration.

Departure from equilibrium is indeed observed in real, collected atmospheric water. Collected fog water has been 1000-fold supersaturated in NH_4^+, up to 3-fold sub-saturated in NO_3^-, and up to 7-fold sub-saturated in formaldehyde relative to effective K_H values (Ricci et al., 1998). For a bulk sample of atmospheric water, Winiwarter et al. (1992) and Pandis and Seinfeld (1991) showed that a bulk fog/cloud water sample is chemically dependent on changes in meteorological, microphysical, and chemical properties of the air mass during the collection time period, and its equilibrium $[A]_{aq}$ cannot be accurately described as by its bulk characteristics. The simplified case in which equilibrium is reached can therefore only be used to approximate the expected distribution of a volatile species between the gas and the aqueous phase. This limitation in using common sampling techniques for atmospheric water is an example of the many challenges in capturing an accurate depiction of aqueous atmospheric processes. In contrast, variables can easily be controlled in models and lab simulations, but may oppositely be too simplified to be accurate. Finding a set of conditions to best represent atmospheric water chemistry between the two boundaries of complex real atmospheric samples and simplified models/lab simulations is a fundamental goal in the present thesis.

1.6 Aqueous Atmospheric Organic Processing

Water in the atmosphere can act as a medium for chemical reactions, including organic oxidation reactions. Oxidation of organic species involves the attack of an oxidant and production of more oxygenated and typically smaller molecules. This process is known by many names; these include, but are not limited to: mineralization, aging, degradation, oxidation, advanced oxidation, and photo-oxidation. Many of these terms are rooted in studies of water pollution and remediation, or terrestrial aqueous phase organic matter (Kavitha and Palanivelu, 2005;

Schwarzenbach et al., 2003). In the context of non-atmospheric processes, oxidative degradation may refer to catalytically assisted oxidant formation mechanisms, such as titanium dioxide (TiO_2) catalysis, which generates $^{\bullet}OH$ but may cause somewhat differing oxidation mechanisms (Barndõk et al., 2015; Grčić and Puma, 2013). In the context of the atmosphere, AAOP will be used in the present work.

Oxidation by $^{\bullet}OH$ is almost exclusively studied within the present literature on AAOP reactions, because of the ubiquity and non-selective reactivity of $^{\bullet}OH$ (Ervens and Volkamer, 2010; Ervens et al., 2014b). The complexity of the organic content of atmospheric water makes this simplification attractive, and the predominance of $^{\bullet}OH$ in the aqueous phase has been shown via models (Ervens et al., 2003a). Other molecules have been shown to participate as oxidants, however, such as H_2O_2, $^{\bullet}NO_3$, or $SO_4^{\bullet-}$, or O_3, but are not as ubiquitous and/or non-selective as $^{\bullet}OH$; for example, O_3 does not react with alkanes, but instead can oxidize alkenes such as methacrolein and methylvinylketone (Chen et al., 2008). Organic molecules acting as AAOP precursors (reactants) are often partitioned from the gas phase due to their high volatility (Figure 1-3). As organic species come to equilibrium in the aqueous phase, a fraction of carboxylic acids will deprotonate (increasingly, if their pKa is less than the pH of the droplet, which typically depends on the inorganic composition of the droplet) and aldehydes will be hydrated to form gem-diols, particularly at low pH, or form complexes with S(IV) species (Epstein et al., 2013; Finlayson-Pitts and Pitts, 2000a; Rao and Collett, 1995). Approximately 50% of a given aldehyde molecule will be hydrated in solution at typical atmospheric water pH (~2-7), with the exception of formaldehyde, which will be almost entirely hydrated (Buschmann et al., 1982; Finlayson-Pitts and Pitts, 2000a).

AAOP reactions occur more rapidly in the atmosphere than do gas-phase oxidation reactions: for example, the lifetime of phenol due to $^{\bullet}OH$ reaction is two-fold shorter when clouds are present; likewise, the lifetime of succinic acid is estimated to be 10^5 times shorter when clouds are present (Monod et al., 2005). Such short lifetimes in the aqueous phase also reflect quick reactions to form organic oxidation products, including succinic acid, possibly resulting in equilibrium concentrations of such species. Despite these differences in reaction rates, many of the reaction mechanisms are similar between gas and aqueous phase organic photo-oxidation reactions.

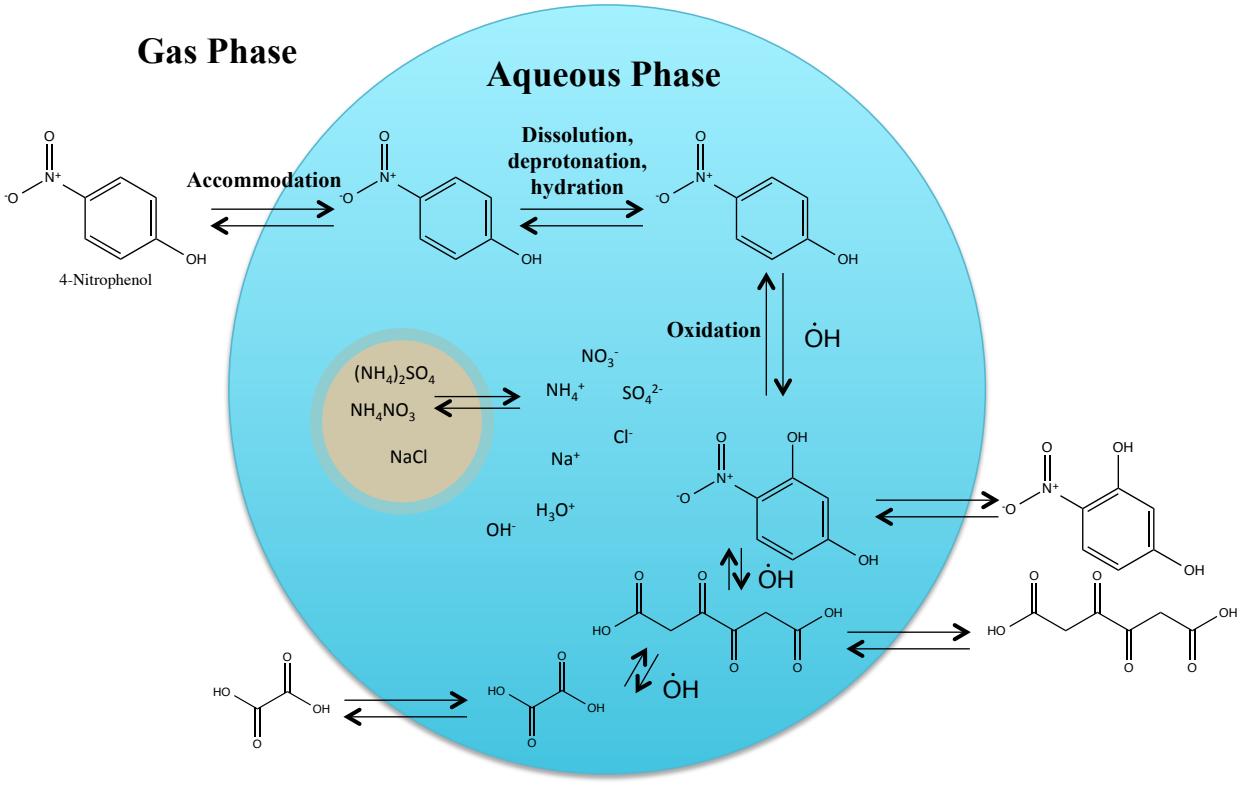

Figure 1-3. Aqueous atmospheric organic processing reaction example of 4-nitrophenol within a droplet. Brown inner circle represents fog/cloud nucleating particle, from which ionic species are dissolved. Oxidation is shown in multiple steps, leading to the formation of sequentially smaller and more fragmented products, all of which may be re-volatilized to the gas phase.

1.7 Aqueous Photo-Oxidation Reaction Mechanisms

Three competing types of products are formed via aqueous organic oxidation reactions: oxygenated precursor molecules resulting from functionalization mechanisms, low molecular mass (LMM) carboxylic or carbonyl-containing species such as formaldehyde, oxalic and pyruvic acids from fragmentation mechanisms, and high molecular mass (HMM) "oligomeric" products formed via radical-radical combinations of either radicalized precursor molecules or radicalized LMM carboxylic acids (Lim et al., 2010). Precursor and oxygen concentrations determine the degree to which HMM radical-radical products are formed; it has even been suggested that at low precursor concentrations such as those observed in fog or cloud water samples in pristine regions, these HMM products may not be formed (Tan et al., 2010). The decay of oligomeric products will occur when the precursor has been entirely reacted, causing an overall cyclic scheme of oxidation wherein primary LMM products combine as radicals to form HMM products, which again are fragmented to form LMM final products (Ervens et al., 2014a; Renard et al., 2014). There are differences between the chemical environments of different types of atmospheric

water, particularly based on the volumes individual droplets and the proximity of anthropogenic or natural atmospheric gas and particle sources. The concentrations of chemicals in atmospheric water are typically considered to be within the cloud, fog, or wet aerosol regime. For a cloud droplet, it is assumed that the solution is nearly pure water (i.e., the activities of solution constituents are ~1; Pankow, 1991): 10-100 μM of a given inorganic species such as NO_3^- and 10 nm-10 μM of an abundant organic species such as glyoxal (Tan et al., 2009) might be present. However, for a wet aerosol particle, which is typically concentrated with respect to inorganics (10-100 mM) and organics (1-10 mM), the behavior of each species will be non-ideal (the chemical activities will likely diverge from one, and charge layers surrounding molecules should be considered; Pankow, 1991). Fogs typically contain inorganic and organic constituents at concentrations intermediate to those present in clouds and wet aerosols. These different concentration regimes may determine which organic chemical reactions are dominant: non-radical reactions such as esterifications and aldol condensations may only occur, for example, within wet aerosol particles (Ervens et al., 2011; Tan et al., 2009). In all atmospheric water, however, chemical structure and behavior of molecules differ from those in the gas-phase due to interactions with water and other dissolved, ionic species.

Organic emissions to the atmosphere are complex, and oxidation reactions result in a large number of products; such complexity requires visualization schemes that can simplify the overall observed changes during AAOPs. A distinction between functionalization and fragmentation regimes has been suggested in the overall oxidation processes observed in lab and field studies, in agreement with the predominance of these two radical mechanisms in AAOP reactions, and can be characterized by plotting mean hydrogen/carbon (H/C) versus oxygen/carbon (O/C) atom ratios of a sample (van Krevelen space; Chen et al., 2015), or O/C ratio versus the carbon number of each molecule (difference Kroll diagrams; Kroll et al., 2009; Aljawhary et al., 2015). More complex visualizations of the oxidation state and aging process of atmospheric organic components have also been suggested, including double bond equivalent and categorization of species based on the presence of heteroatoms (Wei et al., 2012; Fig. 1-4).

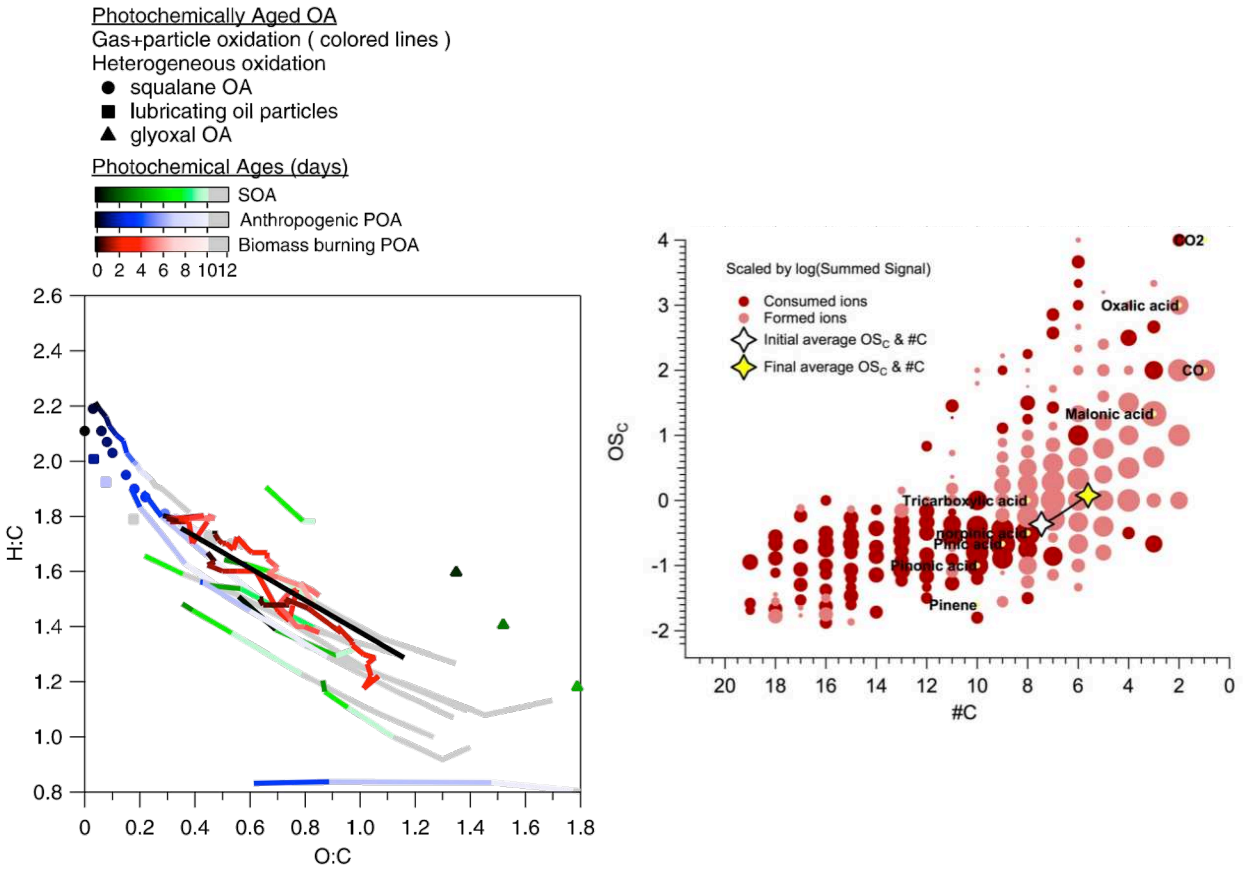

Figure 1-4. Visualizations of organic oxidation reactions. Left: example van Krevelen diagram demonstrating the typical oxidation scheme (dark to greyed colors) in lab simulated aerosol oxidation data from various literature sources (Chen et al., 2015). Right: Kroll diagram demonstrating a typical oxidation from greater carbon number (#C), lower oxidation state (OS_c) compounds to lower #C and greater OS_c compounds (Aljawhary et al., 2013). Data are aqueous oxidation gas phase precursors and products of terpenoid secondary organic aerosol, as measured via iodide chemical ionization mass spectrometry (CIMS). Heterogeneous oxidation refers to surface and aqueous processes. Figures reprinted with permissions from John Wiley & Sons and Copernicus Publications.

Despite the complexity of atmospheric samples and the need for simplifying schematics, the predominant chemical mechanisms within AAOPs are surprisingly simple. The typical reaction is initiated via one of two main mechanisms of electrophilic attack of •OH on an organic chemical: H or functional group abstraction, leaving an alkyl radical, or •OH-addition across a double bond forming an alcohol group and an adjacent alkyl radical. The following steps are formation of functionalized intermediates with alcohol and oxo-groups, and finally fragmentation to produce LMM oxygenated species, and eventually CO_2. For example, Figure 1-5 depicts the oxidation of 4-nitrophenol in which a H atom is abstracted, followed by addition of molecular O_2 to form a peroxy radical. In the case of cyclic structures, the peroxy radical undergoes an intramolecular cyclization, which initiates the fragmentation of the molecule into LMM oxygenated products (Atkinson, 1997; Fig. 1-5).

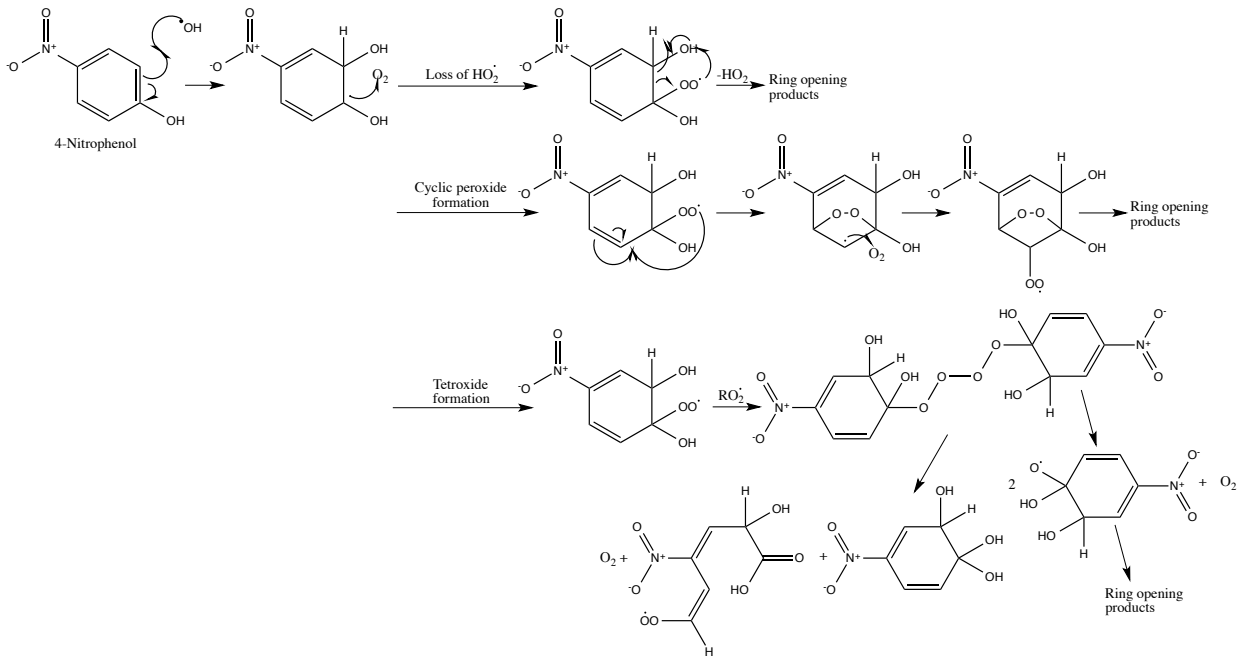

Figure 1-5. Mechanisms for the oxidation of 4-nitrophenol, as an example of the $^{\bullet}$OH oxidation of an organic species in water. The dominant pathway of oxidation with $^{\bullet}$OH for aromatic species is the addition of $^{\bullet}$OH to an aromatic C=C bond, followed by addition of O_2 to form a peroxy radical. The top mechanism demonstrates removal of $HO_2^{\bullet}$ to form a carbonyl, the middle mechanism follows a bicyclic peroxide formation, similar to gaseous reaction (e.g., Ziemann and Atkinson, 2012), and in the bottom mechanism the reaction proceeds via a tetroxide formation, followed by decomposition to either (left) an alcohol and carbonyl, or (right) an alkoxy radical. The steps shown demonstrate functionalization, while smaller product molecules resulting from further ring opening steps demonstrate fragmentation. Mechanisms are based on the 4-nitrophenol oxidation mechanism from Zhang et al. (2003) as well as other mechanisms (Baltaretu et al., 2009; Cooper et al., 2009; Lim et al., 2013).

Peroxy radicals also form in the oxidation of non-aromatic molecules, including, for example, methylglyoxal (Lim and Turpin, 2015); in this case, the peroxy radical can be reduced to form an alkoxy radical and eventually a carbonyl (Figure 1-6), or combine with a second alkoxy radical to form a tetroxide, which dissociates into alcohol and carbonyl-containing molecules (Lim et al., 2013).

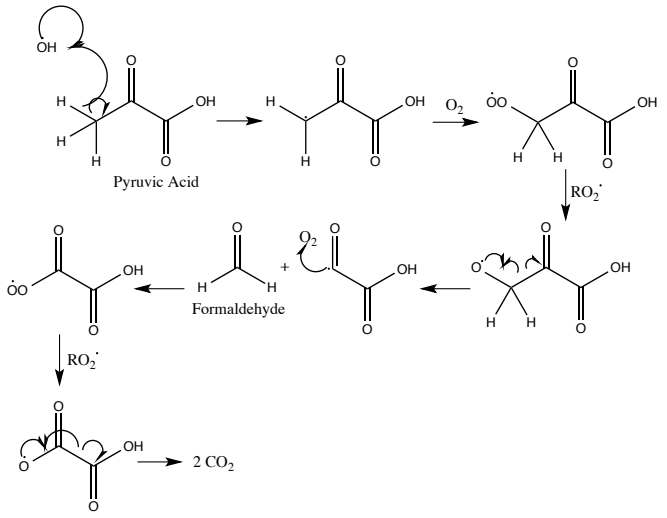

Figure 1-6. Mechanism for the oxidation of pyruvic acid, as an example of the •OH oxidation of a non-aromatic organic species in water. Based on the methylglyoxal oxidation mechanism from Lim et al. (Lim and Turpin, 2015; Lim et al., 2010). $RO_2^{\bullet}$ represents a peroxy radical, which allows tetroxide formation and decomposition to form an alkoxy radical (Figure 1-5).

Alternatively, Lim et al. (2015) proposed that the peroxy radical could abstract a hydrogen from a separate molecule (e.g., $HO_2^{\bullet}$ to form O_2) to produce organic peroxides. Organic radical-radical reaction to form oligomers occurs when sufficient concentrations of organic compounds are present in the oxidation solution. For example, the abstraction of a H atom from two acetic acid molecules, followed by combination of the two radicals causes the formation of succinic acid (Fig. 1-7 Altieri et al., 2008; Wang et al., 2001).

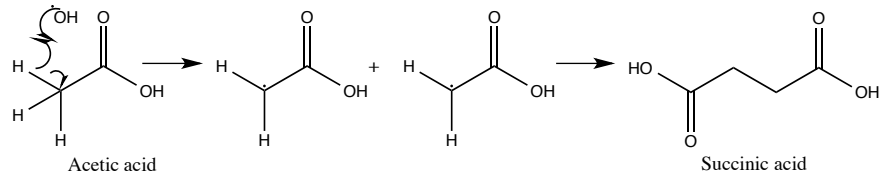

Figure 1-7. Mechanism for the oxidation and radical-radical reaction of acetic acid resulting in the formation of succinic acid (Altieri et al., 2008; Wang et al., 2001).

An oligomerization scheme for the unsaturated species methylvinyl ketone (MVK) was proposed by Ervens et al. (2014), which included a strong dependence of the onset of oligomerization on oxygen content, and the combination of organic radicals on the initial MVK (precursor) concentration. Two competing processes of fragmentation and oligomerization were identified, and were similar to those demonstrated in Figure 1-6 and Figure 1-7, respectively. The reaction of organic radicals with oxygen to form peroxy radicals is more favorable than the alkyl radical combination such that if the concentration of dissolved oxygen is high or that of organic radicals is low,

the formation LMM products will dominate. In the real atmosphere, fog/cloud droplets are likely to be saturated with oxygen due to continuous uptake of available gases to the aqueous phase, unless there is some physical or chemical barrier limiting the oxygen uptake. This might include a hydrophobic layer on the surface of a droplet, such as that observed by Gill et al. (1983), or wet aerosol (Ervens et al., 2014a). Modeled aqSOA formation from methylglyoxal oxidation produced predominantly LMM products when fog/cloud relevant precursor concentrations (1 μM-mM) were used, and predominantly HMM radical-radical oligomers when wet aerosol relevant precursors concentrations (10 M) were used (Lim et al., 2013). It should be noted that oligomers are not formed specifically in the atmospheric aqueous phase: dimerization can also occur from the gas phase, as in ozonolysis of alpha-pinene in a dry environment (Kristensen et al., 2014).

1.8 Methods of Observing Aqueous Photo-Oxidation Reactions: Field Studies

Experiments at ground measurement sites and aboard airplanes have shown evidence of aqSOA formation, many of which are summarized by Ervens et al. (2011) and Blando & Turpin (2000). Approaches have included the measurement of possible tracer molecules, observation of the droplet size mode (suggested to result from the growth of fine particles within droplets, Crahan et al., 2004), and observation of changing chemical or physical bulk aerosol characteristics in the presence of liquid water.

Molecular tracers (also known as chemical markers) are an elegant tool for quantifying the contribution of sources or processes within the atmosphere, when readily available. For example, pinic and pinonic acids, among other species, are used as tracer compounds for α-pinene secondary organic aerosol formation (Kleindienst et al., 2007). However, no unambiguous molecular tracers of aqSOA have been identified. Possible tracers originate from multiple sources, and correlating the concentration of a molecule with aqueous rather than gaseous oxidation is difficult. Frequently discussed candidate aqSOA tracers include summed LMM carboxylic acids, oxalic acid, and "humic-like substances" (HULIS). LMM carboxylic acids are produced during AAOPs, and have been measured at elevated concentrations in aerosol coincident with fogs and clouds (Kaul et al., 2012, 2011; Lu et al., 2008; Sorooshian et al., 2013, 2007). Dicarboxylic and oxo-acid species such as pyruvic, succinic, and oxalic acids are prominent products of AAOP carried out in the lab (Ervens et al., 2011), but have also been identified as gas-phase oxidation products in the atmosphere (as in the ozonolysis of cyclohexene, Hamilton et al., 2006; Kalberer et al., 2000; Kawamura and Bikkina, 2016). Similarly, oxalic acid originates from aqueous phase oxidation reactions, but also gas-phase oxidation reactions of aromatic species (Borrás and Tortajada-Genaro, 2012; Edney et al., 2000;

Kalberer et al., 2000; Kamens et al., 2011; Kleindienst et al., 1999). Finally HULIS, which is a class of HMM species containing many oxygenated functional groups, and having characteristics similar to those of the soil constituent humic acid, has been associated with secondary SO_4^{2-} formation (Kuang et al., 2015) and can form via radical-radical oligomerization of aromatic species originating from biomass burning processes and their oxidation products (Hoffer et al., 2004).

The droplet mode contains particles from the condensation mode (~0.2 μm diameter) that have increased in diameter (~0.7 μm diameter) due to aqueous reactions lowering the volatility of organic material (John et al., 1990; Meng and Seinfeld, 1994). SO_4^{2-}, formed primarily through aqueous oxidation, and oxalic acid are often observed in the droplet size mode of aerosol particles (Yu et al., 2005). Correlations between aerosol oxalate and sulfate were observed in data from several studies of Asian air masses, with a predominance in the droplet size mode and an additional positive relationship with relative humidity (Jiang et al., 2013; Wonaschuetz et al., 2012; Yu et al., 2005).

Concentrations of aerosol mass in changing conditions can also indicate the formation of aqSOA. The irreversible formation of aqSOA was demonstrated through the transition of observed organic carbon species from the gas to the particle phase, with no effect of drying of the particles after collection (El-Sayed et al., 2015). Similarly, aerosol concentration enhancements were observed during foggy versus non-foggy periods in Kanpur, India (Kaul et al., 2011) and adjacent to clouds, as observed from satellite retrievals (Eck et al., 2014) and aircraft measurements (Wonaschuetz et al., 2012).

1.8.1 Collection of Fog and Cloud Water

Fog and cloud water chemical analysis has been an area of research since at least the 1930s, with varying applications including ecosystem chemical flux analysis and cloud microphysics (Daube et al., 1987 and therein). Challenges of developing fog/cloud water collectors include the need for large volumes of water (high throughput and collection efficiency) so that chemical analyses can be performed, but the competing need to resolve the evolution of fog/cloud chemistry with time, the interference of aerosol particles, and the deployment in wet, remote conditions. Passive collectors, while advantageous in their simplicity and lack of requirement for electricity, depend on wind for consistent and efficient collection, which can be challenging, and their open designs render them often prone to contamination by rain/snow (Roman et al., 2013). Active collectors instead use a controlled air intake to sample droplets with characterized efficiency. The most widely used device for fog and cloud water collection is the

Caltech Active Strand Cloudwater Collector (CASCC), which was first described as a "Screen Collector" by Jacob et al. (1985) and later characterized in detail by Demoz et al. (1996). A second common variation of an active collector is the rotating arm collector (RAC; Jacob et al., 1984), which uses inertia of a spinning long-arm propeller mounted on the front of a weather vane to collect fog water into small bottles on the ends of the propeller. The CASCC and RAC were compared in real fog events; the primary difference was the superior collection efficiency of the CASCC, particularly at small droplet sizes (Collett et al., 1990).

The CASCCs now include a series of instruments devised for the purpose of collecting large volumes of cloud and fog water with high efficiency (Daube et al., 1987). The design consists of a 15-30 cm wide polycarbonate or stainless steel rectangular duct through which droplet-laden air is pulled at a constant flow rate. The water droplets are impacted onto angled rows of Teflon strands or rods, then pulled downward into collection troughs via gravity and air moving through the duct. The collector droplets coalesce and drain through tubing to collection bottles. Versions of the CASCCs have been built for various applications. The single-stage CASCC (Daube et al., 1987) employs rows of Teflon strands to generate one bulk sample containing all sizes of droplets, while the size-fractionating CASCC (sf-CASCC) employs two or three rows of Teflon rods/strands to collect size-fractionated droplet fractions (Demoz et al., 1996; Munger, 1989; Raja et al., 2008). The CSU five-stage collector has been employed to distinguish between five separate sizes of fog/cloud water droplets (Herckes et al., 2007; Moore et al., 2004a, 2004b; van Pinxteren et al., 2016; Straub and Collett, 2002). Even for similar fog events, the size distribution can vary broadly depending on a variety of factors, such as aerosol particle size distribution and composition, or age of the air mass (van Pinxteren et al., 2016). Stainless steel versions were developed because organic species may adhere to the Teflon of the standard CASCCs (Herckes et al., 2002). In addition, a small version (CASCC2) was developed for simpler deployment and shipping (Demoz et al., 1996). All CASCCs can be deployed either using mains power, or if unavailable, using battery power and an inverter for shorter periods of time (Chang, 2004).

1.9 Methods of Observing Aqueous Photo-Oxidation Reactions: Bulk Phase Lab Studies

Bulk phase reactions have been the most common approach for studying aqSOA formation and AAOP in a lab (Table 1-2), although other experimental designs have been applied. A bulk reaction is carried out in a 100 to 1000 mL jar-like quartz or glass photoreactor with outlets for sampling and measurement. The photoreactor may have a recirculating water jacket for temperature stabilization e.g., (Figure 1-8). Aqueous sample or a chemical standard is

introduced to the photoreactor, along with a solution of oxidant. In most cases, hydroxyl radical (•OH) produced from UV-C (254 nm) photolysis of hydrogen peroxide (H_2O_2) is used as the oxidant. Solar simulators are also used.

Figure 1-8. Photoreaction vessel used in the study of aqueous atmospheric oxidation processes of organics (e.g., in Boris et al., 2014). Recirculating water jacket inlet is pictured on the left of the vessel; UV-C light source is u-shaped bulb submerged into solution; outlet for online MS analysis is brown tubing placed into reaction solution.

Despite the substantial number of studies that have been performed in the lab using bulk photo-oxidation reactions (Table 1-2), there are fundamental differences between the environments in simulations and droplets in the real atmosphere. Firstly, precursor concentrations in many of the studies are greater than typically observed in fog/cloud droplets (nM-μM for most organic species), and are instead relevant for wet aerosol or as a proxy for total organics. Secondly, no gas/aqueous exchange is allowed, limiting oxidant/precursor uptake and product removal during reaction. Finally, evaporation/condensation are not allowed, which may impact the formation of product molecules (Lim et al., 2010), and unless an atomization step is carried out (Lee et al., 2011b; Ortiz-Montalvo et al., 2012), no aerosol mass formation is measured. Chamber studies have been conducted at high relative humidity (RH) to address problems with bulk reactions, although wall losses are a concern (Daumit et al., 2014; Nguyen et al., 2011). Chamber experiments can indeed capture aspects of AAOP that bulk reactions cannot. A contrast of aqueous oxidation in bulk reactions vs. suspended droplets was made by Daumit et al. (2014) by conducting experiments in a photoreactor and also a chamber (7.5 m^3), respectively. The results demonstrated that the mass of aqSOA produced during a bulk simulation was substantially underestimated due to a lack of exchange between the gas and aqueous phases. Hoppel et al. (1994) used a large chamber (590 m^3; 9.14 m high) to study aqueous SO_4^{2-} formation from SO_2/O_3 reaction in the presence of liquid water droplets over several pressure-induced "cloud cycles". Size distributions were monitored to show the formation of the droplet size mode and "Hoppel minimum" at 0.6-1.0 μm.

Table 1-2. Aqueous bulk photo-oxidation and dark experiments from the literature demonstrating the reaction of •OH with organic species and dark reactions with inorganic species.

Precursor	Organic precursor conc.	H_2O_2 conc. (•OH)	Inorganic solutes	Instrumentation	Products	Source
Glyoxal	30 μM-3 mM	0.15-15 mM	0-840 μM H_2SO_4	ESI-MS, IC, FT-ICR-MS	Carboxylic acids	Tan et al., 2009
	30 μM-3 mM	0.15-15 mM	--	ESI-MS, IC, FT-ICR-MS	Carboxylic acids, oligomers	Lim et al., 2010
	1 mM	5mM	1.68 mM HNO_3, 840 μM $(NH_4)_2SO_4$	ESI-MS, FT-ICR-MS, IC	Carboxylic acids (no OS or ON)	Kirkland et al., 2013
Methylglyoxal	2 mM	10 mM	--	LC-ESI-MS, IC, FT-ICR-MS, ESI-MS/MS	Carboxylic acids, oligomers	Altieri et al. 2008
	30 μM-3 mM	0.15-15 mM	0-840 μM H_2SO_4	ESI-MS, IC	Carboxylic acids, oligomers	Tan et al. 2010
	1 mM	--	0.001-0.1 mM sulfate salts	ESI-MS/MS	Oligomers (no OS or ON)	Yasmeen et al. 2010
	10 mM	20 mM	--	FT-ICR-MS, FT-ICR-MS/MS	Organic peroxides	Lim & Turpin 2015
	0-2 M	--	3.1 M $(NH_4)_2SO_4$, 5.1 M NaCl, 1.18 M Na_2SO_4, 8.7 M NH_4NO_3 (Atomization)	UV, SMPS, Aerosol-CIMS	Carboxylic acids, oligomers, OS and ON	Sareen et al., 2010
Methanol	0.23-0.31 mM	2.3-11 mM	--	GC-FID, LC-UV, LC-fluorescence, IC		
Limonene ozonolysis products	0.3 g L^{-1}	--	2.3 μM-23 mM $(NH_4)_2SO_4$ (Evaporation)	UV, ESI-MS, nano-DESI-MS	Oligomers, ON, OS	Nguyen et al., 2012
Methylglyoxal, glyoxal	1 mM-1 M	--	(Evaporation)	FT-IR	Non-radical oligomers (~reversible)	Loeffler et al., 2006
Methylvinylketone	0.2-20 mM	4-400 mM	--	LC-ESI-MS, LC-UV, IC-ESI-MS, HR-AMS	Oligomers followed by carboxylic acids	Renard et al., 2014
Methylvinylketone, isoprene, α-pinene, methacrolein,	0.1-11 M	(some UV photolysis)	~5 M SO_4^{2-} salts	LC-ESI-MS, LC-ESI-MS/MS	OS	Nozière et al., 2010
Glycolaldehyde	1 mM	5 mM	--	ESI-MS, FT-ICR-MS, IC	Carboxylic acids, oligomers	Perri et al., 2009
	1 mM	5 mM	1 mM H_2SO_4	ESI-MS, FT-ICR-MS	Carboxylic acids, oligomers, OS	Perri et al., 2010
Pyruvic acid	10-20 mM	0.5 mM	--	LC-ESI-MS	Carboxylic acids, oligomers	Altieri et al., 2006
	5-10 mM	20-100 mM	--	LC-UV, ESI-MS	Carboxylic acids	Carlton et al., 2006
Phenol, guaiacol, syringol	0.1 mM	0.1 mM	(H_2SO_4 or $Na_2B_4O_7$ for pH)	HR-AMS, IC	Carboxylic acids, oligomers	Sun et al., 2010
Phenols	10 mM	1 mM	--	UV, ESI-MS, FT-IR, NMR, fluorescence	Oligomers (light absorbing)	Chang and Thompson, 2010
Green leaf volatiles (e.g., methyl jasmonate)	50 μM	0.5-1 mM	--	LC-UV	--	Richards-Henderson et al., 2014

FT-ICR-MS = Fourier Transform Ion Cyclotron Resonance Mass Spectrometer; MS/MS = tandem mass spectrometry; UV = ultraviolet/visible absorption spectrometer HR-AMS = High Resolution Aerosol Mass Spectrometer; CIMS = Chemical Ionization Mass Spectrometer; GC = gas chromatograph, FID = flame ionization detector; nano-DESI-MS = nanospray desorption electrospray ionization mass spectrometer; FT-IR = Fourier Transform Infrared spectrometer; fluorescence = fluorescence spectrometry; NMR = Nuclear Magnetic Resonance spectroscopy. OS = organic sulfur; ON = organic nitrogen.

In a third experiment, contrasted oxidation of isoprene at low and high (90%) RH demonstrated that condensation reactions are limited in the presence of liquid water, but overall the two conditions produced similar quantities of organic aerosol (Nguyen et al., 2011). Additional chamber-based and bulk studies have been reviewed in a publication by Herrmann et al. (2015), with a focus on the aqueous phase reaction mechanisms that have been uncovered recently.

1.9.1 Aqueous Photo-Oxidation Oxidant

The supply of oxidant during bulk reactions may not be atmospherically realistic due to high and/or diminishing concentrations. The largest sources of aqueous $^{\bullet}OH$ is uptake from the gas phase and transition metal-catalyzed H_2O_2 photolysis (photo-Fenton reactions; Arakaki and Faust, 1998; Nguyen et a l., 2013); the direct photolysis of H_2O_2 (up to 99% of $^{\bullet}OH$ production; Bianco et al., 2015) and NO_3^- (Zepp et al., 1989) are also estimated to be important. These sources are complex and it is therefore difficult to directly correlate oxidation of fog components with measured oxidant quantities, such as aqueous H_2O_2 concentration. In bulk aqueous oxidation studies, the photolysis of H_2O_2 is typically used to generate $^{\bullet}OH$. Photolysis of H_2O_2 must be initiated by a high-energy light source such as a UV-C (254 nm) light, but this wasvelength is not relevant for the troposphere because it is removed by the stratospheric ozone layer (Finlayson-Pitts and Pitts, 1999). Solar simulators can also be used to initiate photo-oxidation; while more accurate for tropospheric light, however, H_2O_2 photolysis is not efficient at wavelengths provided by a typical solar simulator (Oriel, 2015).

Actual $^{\bullet}OH$ concentrations in real atmospheric water are typically only estimated. Aqueous phase concentrations of $^{\bullet}OH$ have been modeled, giving typical concentrations in remote cloud droplets of 6×10^{-14} M, in urban wet aerosol particles of 4×10^{-13} M, and greater concentrations over maritime regions of 2×10^{-12} M in cloud and 1×10^{-13} M in wet aerosol (Herrmann et al., 2010). The formation rate of $^{\bullet}OH$ has been estimated within real samples using radical scavenger/probe species, resulting in rates on the order of $0.1\text{-}10\times10^{-6}$ M hr^{-1} (hydroxymethanesulfonate: Zuo, 2003; benzene: Faust & Allen, 1993, Arakaki & Faust, 1998, Anastasio & McGregor, 2001; benzoate: Anastasio & McGregor, 2001, Richards-Henderson et al., 2014; terephthalate: Bianco et al., 2015). Reaction rates of aqueous $^{\bullet}OH$ with organic molecules typically occur so rapidly that aqueous diffusion of the oxidant and precursor molecules is the limiting step ($k=10^8\text{-}10^9$ $M^{-1}s^{-1}$; Monod et al., 2005). In agreement with this, Ervens et al. (2014b) found a strong gradient in the distribution of $^{\bullet}OH$ within a cloud droplet or wet aerosol particle, with greater concentrations and reaction rates at the outer edge of the droplet.

Factors affecting fog oxidant concentrations and reaction rates are manifold. The dependence of reaction rates on pH and other aqueous parameters is known, although not entirely understood. For example, the reduced sulfur ($S(IV) = SO_2 \bullet H_2O + HSO_3^- + SO_3^{2-}$) oxidation mechanism is dependent on pH: at low pH, protonated sulfurous acid (H_2SO_3) molecules are available for reaction with peroxides, while at high pH, the formation of primary ozonide analogs is prevalent, and at mid-range pH, formation of aldehyde complexes is dominant (Figure 1-9).

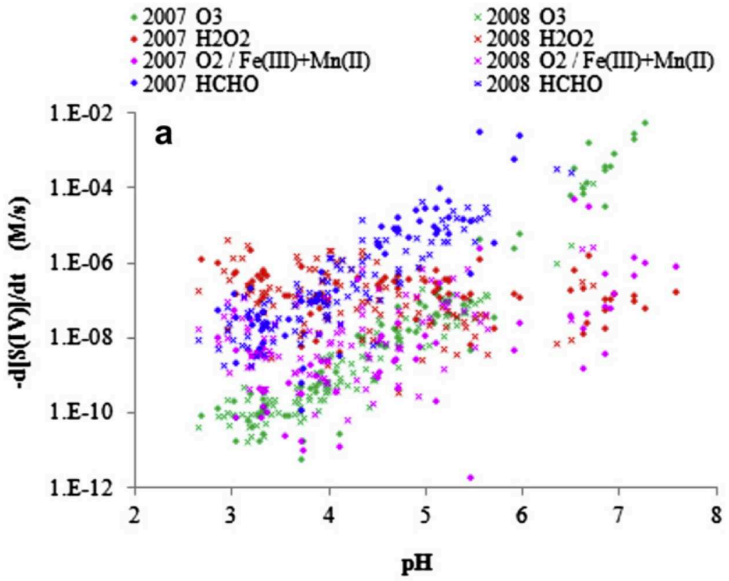

Figure 1-9. Predominance of differing oxidation mechanisms due to effects on oxidant and reactant molecules of pH, as observed within montane cloudwater intercepted at Mount Tai in Southeastern China (image reprinted from Shen et al., 2012 with permission from Elsevier).

Patterns of oxidation mechanisms for organic molecules are unlikely to parallel those of S(IV) because of differences in chemical structures, but deprotonation of carboxylic acids and hydration of carbonyls, which are both pH-dependent, are known to enhance reaction rates with $^{\bullet}OH$, H_2O_2, and O_3 (Schöne and Herrmann, 2014). In addition, non-radical reactions are dependent on pH. The mechanisms for oligomerization proposed by Lim et al. (2010) are acid catalyzed, including aldol reaction and esterification. Thus at lower pH as highly polluted cloud samples (Herckes et al., 2013), these HMM species will be formed more readily.

The availability of oxidant can be highly dependent on location and meteorology: the concentration of $^{\bullet}OH$ will increase with hydrogen peroxide (H_2O_2) concentration, light availability, and metal concentrations, but decrease with TOC (Arakaki and Faust, 1998; Ervens et al., 2003). The influence of urban versus marine/clean air masses, however, does not seem to affect aqueous $^{\bullet}OH$ concentrations in transported air: marine air masses at a mountaintop in France produced on average 0.26 μM hr^{-1} $^{\bullet}OH$, while continental air masses produced 0.52 μM hr^{-1} (Bianco et al.,

2015). At night, when no photolysis occurs, the nitrate radical ($^{\bullet}NO_3$) is likely to be the most active oxidant in fog, cloud, or wet aerosol events. Sufficient NO_x and O_3 concentrations must be available since the main formation process of $^{\bullet}NO_3$ is the gas-phase reaction of $^{\bullet}NO_2$ with O_3 to form $^{\bullet}NO_3$ and O_2. The solubility of $^{\bullet}NO_3$ is lower than that of $^{\bullet}OH$, but $^{\bullet}NO_3$ still might partition into the aqueous phase or react at the surface of water to form HNO_3 ($^{\bullet}NO_3$: K_H = 0.6-1.8 M atm^{-1}; $^{\bullet}OH$: K_H = 30 M atm^{-1}, Finlayson-pitts and Pitts, 1999; Rudich et al., 1996). Night-time "dark" reactions with ammonia and/or amines at wet aerosol relevant concentrations (high relative to atmospheric water droplets), may also be responsible for formation of ON (O'Brien et al., 2014).

The inorganic constituents in fog or wet aerosol water can dictate not only the pH and oxidant species present, but also can act as reactants. The formation of N and S-containing organic species has been observed in lab and field AAOP experiments, typically at wet aerosol or fog relevant concentrations (Table 1-2). Organic S (OS) species have been observed during $^{\bullet}OH$ oxidation of organics in the presence of H_2SO_4 (Perri et al., 2010) and other SO_4^{2-} salts (Galloway et al., 2011; Nozière et al., 2010), but only in some studies (Kirkland et al., 2013). The aqueous phase formation mechanism is proposed to occur via H atom abstraction from both the SO_4^{2-}/H_2SO_4 and organic precursors, followed by radical-radical reaction (Perri et al., 2010), although there are other possible mechanisms (Liggio and Li, 2006; Schindelka et al., 2013). While OS species are observed under photo-oxidizing conditions, organic N (ON) species are observed in dark reactions, often as a result of droplet evaporation. For example, Nozière et al. (2009) found that evaporation of droplets containing methylglyoxal/$(NH_4)_2SO_4$ formed products with C=N bonds (as well as catalyzing the formation of non-nitrogen-containing oligomers) as a result of NH_3 nucleophilic attack on the C atom of carbonyl groups. De Haan and coworkers (2011) likewise found that evaporating droplets containing methylglyoxal/amine resulted in the formation of various imidazoles (five-member aromatic rings with two N heteroatoms). Note that these reactions would not be possible in bulk photo-oxidation experiments. Real fog and cloud water samples contain ON, some of which is likely nitrophenols, and some that must be heteroatom-containing aromatic species such as imines (Boone et al., 2015; Mazzoleni et al., 2010; Zhao et al., 2013).

Oxidants in addition to $^{\bullet}OH$ including ozone (O_3; Chen et al., 2008), the sulfate radical ($SO_4^{-\bullet}$; Nozière et al., 2010), triplet excited state organics, and halide radicals ($^{\bullet}Cl$ and $^{\bullet}Br$) may be players in aqSOA formation. These species can all produce similar products to $^{\bullet}OH$ (Herrmann et al., 2010). In terrestrial waters, $^{\bullet}Cl$ and $^{\bullet}Br$ as well as carbonate radicals are also recognized as abundant radical oxidizers (Glover and Rosario-Ortiz, 2013), but are not

typically discussed in an atmospheric context; excited triplet states of carbonyls, on the other hand, have been found to react more quickly with $^{\bullet}OH$ and give similar products (Anastasio et al., 1997; Smith et al., 2014; Yu et al., 2014).

1.9.2 Aqueous Photo-Oxidation Precursors

AAOP reactions occur via the interaction of an oxidant molecule with a "precursor" molecule in lab and modeling studies; the latter is typically a volatile carbonaceous molecule such as methylglyoxal or methyl vinyl ketone (Renard et al., 2013; Tan et al., 2010) to maximize the potential transfer of mass from the gas to the particle phase. Gas-phase oxidation followed by gas-to-particle partitioning can generate secondary organic aerosol (SOA) from HMM species, while, in contrast, AAOPs allow the transfer of organic matter from the gas to the particle phase for LMM as well as HMM precursors. The transition of organic mass from lighter volatile species to particle mass is specific to the aqueous phase (Ervens et al., 2011). For this reason, the oxidation products of isoprene, such as glyoxal, methylglyoxal, and similar chemicals have been a focus in aqSOA formation studies (Table 1-2). However, the oxidation of aromatic species, as from biomass burning emissions, can form humic-like substances (HULIS). These HMM organics have been suggested to form a substantial fraction of atmospheric organic matter that has been only minimally characterized: HULIS (Hoffer et al., 2004). The photo-oxidation of a variety of species within the aqueous phase is therefore important for the formation of aqSOA.

Bulk reaction studies have focused almost exclusively on the reaction of a single precursor within a given reaction: for example, oxidation of a glyoxal or methylglyoxal chemical standard (Table 1-2; Ervens et al., 2011). However, in the real atmosphere, the number of organic species may be in the thousands or even ten thousands within a single air mass (Hamilton et al., 2004; Mazzoleni et al., 2010), such that the chemistry may differ substantially due to synergistic effects or the summed oxidation of many organic species. The effect of photosensitization has been studied by reaction of phenol in the presence of 1-nitronaphthalene (De Laurentiis et al., 2013) and glyoxal in the presence of imidazole-2-carboxaldehyde (Rossignol et al., 2014). Dissolved organic matter from terrestrial water sources oxidized phenols via photosensitization in one study (Canonica et al., 1995), but decreased the oxidation rates of several phenols and herbicides in a later study (Canonica and Laubscher, 2008). Such complex interactions between organic molecules and their resulting oxidation rates are influential in AAOP reactions, but are not typically included in bulk studies.

A second role of AAOP reactions is the degradation of organic species. Organic substances, including potentially toxic trace substances such as pesticides and nitrophenols (Agency for Toxic Substances and Disease Registry, 1992; Hung et al., 2005; Mason et al., 2011; Tremp, 1992) can be degraded to produce LMM species such as carboxylic acids and aldehydes with lesser toxicity (Santos et al., 2006).

1.9.3 Aqueous Photo-Oxidation Measurement Techniques

There are a variety of organic molecular characterization and quantification techniques that have been used for monitoring AAOP reactions in real-time (online) and from discrete samples (offline). Online techniques include aerosol mass spectrometry (AMS), for aerosolized solutions (e.g., Lee et al., 2011), and electrospray ionization mass spectrometry (ESI-MS) for bulk, aqueous solutions (Carlton et al., 2006). Offline measurements are varied, and include bulk sample characteristics such as TOC and pH, and molecular identification and quantification techniques. Since the media are aqueous, techniques requiring non-polar solvents such as gas chromatography/electron impact mass spectrometry (GC/MS) are not typically used. Liquid chromatography (LC) and ion chromatography (IC) are frequently used instead for larger (typically $\geq C_4$) and smaller ($\leq C_4$) ionizable organic species, respectively. While the following techniques do not provide an exhaustive list of those used for characterizing AAOP reactants and products, the most common techniques are briefly discussed.

ESI-MS is one of the most powerful techniques for monitoring aqueous photo-oxidation reactions in the lab because it allows for the specific identification of many reactants, intermediates, and products of the reactions at real-time resolution. The principle of ESI is the transformation of an aqueous solution flow into ions via the competition within formed droplets between electrostatic repulsion of ions and surface tension (Cech and Enke, 2002). Negative or positive ionization mode can be applied (depending on the direction of the current applied at the ionization source), resulting in either positive ions ($[M+H]^+$ or $[M+N]^+$ where M represents the analyte molecule and N represents a cation such as K^+, Na^+, or NH_4^+), or deprotonated ions ($[M-H]^-$); because carboxylic acids are a substantial fraction of known AAOP products, negative ionization mode is typically used (Ervens et al., 2011). The major drawback of this technique is its qualitative rather than quantitative measurement due to environmentally dependent and highly varying sensitivities of the ionization process to different species (Tang et al., 2004). So-called "matrix effects" of the ESI process are a result of competition between ions present in the sample for charge imparted by the applied current; at high concentration, only the species that are more favorably ionized will gain a charge. This ionization preference can be related to the acid or ion dissociation constant of the analyte since, for

most inorganic and LMM organic species, ionization will occur through ejection of an already charged ion from a droplet (as opposed to the drying and eventual gas-phase ionization; Cech and Enke, 2002). This leads to a wide variation in sensitivity of the instrument to different analytes, and also to a varying response to analytes depending on the solvent matrix (Tang et al., 2004). Therefore, ESI-MS, although powerful for identification of specific analytes in real-time during aqueous oxidation reactions, is not readily applicable for quantitation of the analytes.

A similar technique with greater resolution and sensitivity (limit of detection) to analytes is Fourier Transform Ion Cyclotron Resonance MS (FT-ICR-MS; Marshall et al., 1998). Again, this technique is qualitative, but allows the identification of thousands of compounds within a given sample. For example, fog water organic composition was explored using FT-ICR-MS and resulted in the identification of 715 compounds with C, H, and O atoms, 487 CHNO compounds, and 166 CHOS and CHNOS compounds (Mazzoleni et al., 2010); similarly, cloud water contained 700-850 CHO compounds, 1450-1650 CHNO compounds, 220-280 CHOS compounds, and 360-380 CHNOS compounds (Zhang et al., 2013). One substantial advantage of this technique due to its superior sensitivity is the identification of oligomeric species in real samples: in real atmospheric water samples, the concentrations of such species appears to be quite low and therefore only detectable using powerful instrumentation such as FT-ICR-MS (Mazzoleni et al., 2010). The analysis, however, is computationally and financially expensive using this instrument.

In contrast to real-time monitoring during an oxidation reaction, discrete sample analysis is typically used for quantitation of reactants and products. Samples are drawn at 10-15 minute intervals from the oxidation solution and analyzed via techniques such as LC and IC to quantify organic species. The application of LC and IC allows the quantitation of $\geq C_4$ organics (LC) and smaller ($\leq C_4$) carboxylic acids (IC), respectively. Derivatization (dinitrophenylhydrazine, DNPH) followed by LC has been used for the quantitation of aldehydes as well (e.g., Monod et al., 2000). The typical detector for LC is either MS or ultraviolet/visible absorption spectrometry (UV/vis), while IC is typically paired with conductivity or in some cases MS.

Total organic carbon (TOC) measurements made throughout an AAOP reaction demonstrate that the degradation of an organic compound such as nitrophenol results in inorganic carbon production (CO_2 and equilibrated species; Stefan and Bolton, 1999; Zhang et al., 2003). Under the conditions provided by water treatment processes with high concentrations of oxidant and precursors relative to those found in cloud and fog droplets, TOC can be entirely

removed (Zhang et al., 2003). However, the same measurements in the more dilute environments of real fog and cloud water might demonstrate that TOC does not degrade entirely at atmospherically relevant concentrations. The biggest drawback to TOC analysis is the need for a substantial amount of sample (~1-30 mL per analysis).

The techniques applied in bulk AAOP studies primarily focus on the chemical characterization of organic species within aqueous samples; it is desirable, however, to quantify and speciate the chemicals within resulting aerosol mass that has been formed from the aqueous solution during/after oxidation. Samples can be nebulized/atomized, then analyzed using an aerosol mass spectrometer (AMS), which allows quantification of various fragments of aerosol components (Lee et al., 2011a, 2011b). While specific chemical speciation is difficult for organics using AMS, the quantitation of fragments allows calculation of O/C and H/C ratios for all non-refractory organic aerosol mass, and also quantification of signatures for oxidized and less oxidized species (for example, particular fractions of m/z 44^+ and m/z^+ 43 represent more and less oxygenated organic species; Ng et al., 2011).

1.10 Key Findings and Objectives of Thesis

The field of aqueous secondary organic aerosol formation studies has developed in the previous 10-15 years, and is based around findings from laboratory experimentation using simplified, "simulated cloud and fog water" solutions, as well as a growing number of somewhat conclusive field studies. The work included in this dissertation aims to show whether the reactions carried out in simulated atmospheric water solutions can successfully approximate aqSOA formation reactions occurring in real cloud, fog, and wet aerosol droplets.

While lab studies can be oversimplified, field studies in the real atmospheric aqueous phase can involve a variety of variables that cannot be controlled. There must be some balance of lab and field work to accurately represent and characterize AAOP reactions and their effects. The present thesis will explore lab and field approaches to the study of AAOP and aqSOA formation in search of an ideal experimental design, or the combination of experiments.

REFERENCES

Agency for Toxic Substances and Disease Registry: Toxicological profile for nitrophenols: 2-nitrophenol, 4-nitrophenol, Atlanta, Georgia. [online] Available from: http://www.atsdr.cdc.gov/toxprofiles/tp50.pdf, 1992.

Ahrens, C. D.: Essentials of meteorology: an invitation to the atmosphere, Third., Brooks Cole., 2000.

Alexander, L., Allen, S., Bindoff, N. L., Bréon, F.-M., Church, J., Cubasch, U., Emori, S., Forster, P., Friedlingstein, P., Gillett, N., Gregory, J., Hartmann, D., Jansen, E., Kirtman, B., Knutti, R., Kanikicharla, K. K., Lemke, P., Marotzke, J., Masson-Delmotte, V., Meehl, G., Mokhov, I., Piao, S., Plattner, G.-K., Dahe, Q., Ramaswamy, V., Randall, D., Rhein, M., Rojas, M., Sabine, C., Shindell, D., Stocker, T. F., Talley, L., Vaughan, D. and Xie, S.-P.: Working Group I Contribution to the IPCC Fifth Assessment Report Climate Change 2013: The Physical Science Basis Summary for Policymakers., 2013.

Aljawhary, D., Lee, A. K. Y. and Abbatt, J. P. D.: Application of high resolution Chemical Ionization Mass Spectrometry (CI-ToFMS) to study SOA composition: focus on formation of oxygenated species via aqueous phase processing, Atmos. Meas. Tech., 6(4), 6147–6186, doi:10.5194/amtd-6-6147-2013, 2013.

Altieri, K. E., Carlton, A. G., Lim, H.-J., Turpin, B. J. and Seitzinger, S. P.: Evidence for oligomer formation in clouds: Reactions of isoprene oxidation products, Environ. Sci. Technol., 40(16), 4956–60, 2006.

Altieri, K. E., Seitzinger, S. P., Carlton, A. G., Turpin, B. J., Klein, G. C. and Marshall, A. G.: Oligomers formed through in-cloud methylglyoxal reactions: Chemical composition, properties, and mechanisms investigated by ultra-high resolution FT-ICR mass spectrometry, Atmos. Environ., 42, 1476–1490, doi:10.1016/j.atmosenv.2007.11.015, 2008.

Anastasio, C., Faust, B. C. and Rao, C. J.: Aromatic carbonyl compounds as aqueous-phase photochemical sources of hydrogen peroxide in acidic sulfate aerosols, fogs, and clouds 1. Non-phenolic methoxybenzaldehydes and methoxyacetophenones with reductants (phenols), Environ. Sci. Technol., 31(1), 218–232, doi:10.1021/es960359g, 1997.

Anastasio, C. and McGregor, K. G.: Chemistry of fog waters in California's Central Valley: 1. In situ photoformation of hydroxyl radical and singlet molecular oxygen, Atmos. Environ., 35(6), 1079–1089, doi:10.1016/S1352-2310(00)00281-8, 2001.

Anderson, J. B., Baumgardner, R. E., Mohnen, V. a. and Bowser, J. J.: Cloud chemistry in the eastern United States, as sampled from three high-elevation sites along the Appalachian Mountains, Atmos. Environ., 33(30), 5105–5114, doi:10.1016/S1352-2310(99)00193-4, 1999.

Arakaki, T. and Faust, B. C.: Sources, sinks, and mechanisms of hydroxyl radical (•OH) photoproduction and consumption in authentic acidic continental cloud waters from Whiteface Mountain, New York: The role of the Fe(r) (r = II, III) photochemical cycle, J. Geophys. Res., 103(D3), 3487, doi:10.1029/97JD02795, 1998.

Atkinson, R.: Atmospheric reactions of alkoxy and -hydroxyalkoxy radicals, Int. J. Chem. Kinet., 29(2), 99–111 [online] Available from: http://onlinelibrary.wiley.com/doi/10.1002/(SICI)1097-4601(1997)29:2<99::AID-KIN3>3.0.CO;2-F/abstract, 1997.

Baltaretu, C. O., Lichtman, E. I., Hadler, A. B. and Elrod, M. J.: Primary Atmospheric Oxidation Mechanism for Toluene, J. Phys. Chem. A, 113(December 2008), 221–230, 2009.

Barndõk, H., Merayo, N., Blanco, L., Hermosilla, D. and Blanco, Á.: Application of on-line FTIR methodology to study the mechanisms of heterogeneous advanced oxidation processes, Appl. Catal. B Environ., doi:10.1016/j.apcatb.2015.12.036, 2015.

Benedict, K. B., Carrico, C. M., Kreidenweis, S. M., Schichtel, B., Malm, W. C. and Collett, J. L.: A seasonal nitrogen deposition budget for Rocky Mountain National Park., Ecol. Appl., 23(5), 1156–69 [online] Available from: http://www.ncbi.nlm.nih.gov/pubmed/23967583, 2013.

Benedict, K. B., Lee, T. and Collett, J. L.: Cloud water composition over the southeastern Pacific Ocean during the VOCALS regional experiment, Atmos. Environ., 46, 104–114, doi:10.1016/j.atmosenv.2011.10.029, 2012.

Bianco, A., Passananti, M., Perroux, H., Voyard, G., Mouchel-Vallon, C., Chaumerliac, N., Mailhot, G., Deguillaume, L. and Brigante, M.: A better understanding of hydroxyl radical photochemical sources in cloud waters collected at the puy de Dôme station – experimental versus modelled formation rates, Atmos. Chem. Phys., 15(16), 9191–9202, doi:10.5194/acp-15-9191-2015, 2015.

Blando, J. and Turpin, B.: Secondary organic aerosol formation in cloud and fog droplets: A literature evaluation of plausibility, Atmos. Environ., 34, 1623–1632, 2000.

Boone, E. J., Laskin, A., Laskin, J., Wirth, C., Shepson, P. B., Stirm, B. H. and Pratt, K. a.: Aqueous Processing of Atmospheric Organic Particles in Cloud Water Collected via Aircraft Sampling, Environ. Sci. Technol., 49(8523-8530), 150611113115005, doi:10.1021/acs.est.5b01639, 2015.

Boris, A. J., Desyaterik, Y. and Collett, J. L.: How do components of real cloud water affect aqueous pyruvate oxidation?, Atmos. Res., 143, 95–106, doi:10.1016/j.atmosres.2014.02.004, 2014.

Boris, A. J., Lee, T., Park, T., Choi, J., Seo, S. and Collett, J. L.: Fog composition at Baengnyeong Island in the eastern Yellow Sea: detecting markers of aqueous atmospheric oxidations, Atmos. Chem. Phys. Discuss., 15(17), 24871–24908, doi:10.5194/acpd-15-24871-2015, 2015.

Borrás, E. and Tortajada-Genaro, L. A.: Secondary organic aerosol formation from the photo-oxidation of benzene, Atmos. Environ., 47, 154–163, doi:10.1016/j.atmosenv.2011.11.020, 2012.

Borys, R. D., Lowenthal, D. H. and Mitchell, D. L.: The relationships among cloud microphysics, chemistry, and precipitation rate in cold mountain clouds, Atmos. Environ., 34(16), 2593–2602, doi:10.1016/S1352-2310(99)00492-6, 2000.

Buschmann, H.-J., Dutkiewicz, E. and Knoche, W.: The reversible hydration of carbonyl compounds in aqueous solution part II: The kinetics of the keto/gem-diol transition, Berichte der Bunsengesellschaft für Phys. Chemie, 86(2), 129–134, 1982.

Canonica, S., Jans, U. R. S., Stemmler, K. and Hoigne, J.: Transformation Kinetics of Phenols in Water: Photosensitization by Dissolved Natural Organic Material and Aromatic Ketones, Environ. Sci. Technol., 29(7), 1822–1831, 1995.

Canonica, S. and Laubscher, H.-U.: Inhibitory effect of dissolved organic matter on triplet-induced oxidation of aquatic contaminants, Photochem. Photobiol. Sci., 7(5), 547–551, doi:10.1039/b719982a, 2008.

Capel, P. D., Gunde, R., Ziircher, F. and Gigert, W.: Carbon Speciation and Surface Tension of Fog, Environ. Sci. Technol., 24(5), 722–727, doi:10.1021/es00075a017, 1990.

Carlton, A. G., Turpin, B. J., Lim, H., Altieri, K. E. and Seitzinger, S. P.: Link between isoprene and secondary organic aerosol (SOA): Pyruvic acid oxidation yields low volatility organic acids in clouds, Geophys. Res. Lett., 33(L06822), 1–4, doi:10.1029/2005GL025374, 2006.

Cech, N. B. and Enke, C. G.: Practical implications of some recent studies in electrospray ionization fundamentals., Mass Spectrom. Rev., 20(6), 362–87, doi:10.1002/mas.10008, 2002.

Chang, H.: The Processing of Aerosol Particles and Soluble Trace Gases by Chemically Heterogeneous Radiation Fogs, Colorado State University., 2004.

Chang, J. L. and Thompson, J. E.: Characterization of colored products formed during irradiation of aqueous solutions containing H2O2 and phenolic compounds, Atmos. Environ., 44(4), 541–551, doi:10.1016/j.atmosenv.2009.10.042, 2010.

Chen, Q., Heald, C. L., Jimenez, J. L., Canagaratna, M. R., He, L.-Y., Huang, X.-F., Campuzano-Jost, P., Palm, B. B., Poulain, L., Kuwata, M., Martin, S. T., Abbatt, J. P. D., Lee, A. K. Y. and Liggio, J.: Elemental Composition of Organic Aerosol: The Gap Between Ambient and Laboratory Measurements, Geophys. Res. Lett., 42, 1–8, doi:10.1002/2015GL063693, 2015.

Chen, Z. M., Wang, H. L., Zhu, L. H., Wang, C. X., Jie, C. Y. and Hua, W.: Aqueous-phase ozonolysis of methacrolein and methyl vinyl ketone: a potentially important source of atmospheric aqueous oxidants, Atmos. Chem. Phys., 8(8), 2255–2265, doi:10.5194/acp-8-2255-2008, 2008.

Collett, J. L., Bator, A., Sherman, D. E., Moore, K. F., Hoag, K. J., Demoz, B. B., Rao, X. and Reilly, J. E.: The

chemical composition of fogs and intercepted clouds in the United States, Atmos. Res., 64, 29–40, doi:10.1016/S0169-8095(02)00077-7, 2002.

Collett, J. L., Daube, B. C., Munger, W. J. and Hoffmann, M. R.: A Comparison of two cloudwater/fogwater collectors: The rotating arm collector and the Caltech active strand cloudwater collector, Atmos. Environ., 24A(7), 1685–1692, 1990.

Collett, J. L. J., Hoag, K. J., Sherman, D. E., Bator, A. and Richards, L. W.: Spatial and temporal variations in San Joaquin Valley fog chemistry, Atmos. Environ., 33, 129–140, doi:10.1016/S1352-2310(98)00136-8, 1999.

Collett, J. L. J., Prevot, A. S. H., Staehelin, J. and Waldvogel, A.: Physical Factors Influencing Winter Precipitation Chemistry, Environ. Sci. Technol., 25(4), 782–788, 1991.

Cooper, W. J., Cramer, C. J., Martin, N. H., Mezyk, S. P. and Shea, K. E. O.: Free Radical Mechanisms for the Treatment of Methyl tert -Butyl Ether (MTBE) via Advanced Oxidation/Reductive Processes in Aqueous Solutions, Chem. Rev., 1302–1345, 2009.

Crahan, K. K., Hegg, D., Covert, D. S. and Jonsson, H.: An exploration of aqueous oxalic acid production in the coastal marine atmosphere, Atmos. Environ., 38(23), 3757–3764, doi:10.1016/j.atmosenv.2004.04.009, 2004.

Daube, B. J., Kimball, K. D., Lamar, P. A. and Weathers, K. C.: Two new ground-level cloud water sampler designs which reduce rain contamination, Atmos. Environ., 21(4), 893–900 [online] Available from: http://www.sciencedirect.com/science/article/pii/0004698187900850 (Accessed 18 July 2014), 1987.

Daumit, K. E., Carrasquillo, A. J., Hunter, J. F. and Kroll, J. H.: Laboratory studies of the aqueous-phase oxidation of polyols: submicron particles vs. bulk aqueous solution, Atmos. Chem. Phys., 14(19), 10773–10784, doi:10.5194/acp-14-10773-2014, 2014.

Decesari, S., Facchini, M. C., Fuzzi, S. and Tagliavini, E.: Characterization of water-soluble organic compounds in atmospheric aerosol ' A new approach mixture of aerosol / fog, , 105, 1481–1489, 2000.

Decesari, S., Facchini, M., Fuzzi, S., Mcfiggans, G., Coe, H. and Bower, K.: The water-soluble organic component of size-segregated aerosol, cloud water and wet depositions from Jeju Island during ACE-Asia, Atmos. Environ., 39(2), 211–222, doi:10.1016/j.atmosenv.2004.09.049, 2005.

Deguillaume, L., Charbouillot, T., Joly, M., Vaïtilingom, M., Parazols, M., Marinoni, a., Amato, P., Delort, a.-M., Vinatier, V., Flossmann, a., Chaumerliac, N., Pichon, J. M., Houdier, S., Laj, P., Sellegri, K., Colomb, a., Brigante, M. and Mailhot, G.: Classification of clouds sampled at the puy de Dôme (France) based on 10 yr of monitoring of their physicochemical properties, Atmos. Chem. Phys., 14(3), 1485–1506, doi:10.5194/acp-14-1485-2014, 2014.

DeMott, P. J., Cziczo, D. J., Prenni, a J., Murphy, D. M., Kreidenweis, S. M., Thomson, D. S., Borys, R. and Rogers, D. C.: Measurements of the concentration and composition of nuclei for cirrus formation., Proc. Natl. Acad. Sci., 100(25), 14655–60, doi:10.1073/pnas.2532677100, 2003.

Demoz, B. B., Collett, J. L. and Daube, B. C.: On the Caltech Active Strand Cloudwater Collectors, Atmos. Res., 41(1), 47–62, doi:10.1016/0169-8095(95)00044-5, 1996.

Eck, T. F., Holben, B. N., Reid, J. S., Arola, A., Ferrare, R. A., Hostetler, C. A., Crumeyrolle, S. N., Berkoff, T. A., Welton, E. J., Lolli, S., Lyapustin, A., Wang, Y., Schafer, J. S., Giles, D. M., Anderson, B. E., Thornhill, K. L., Minnis, P., Pickering, K. E., Loughner, C. P., Smirnov, A. and Sinyuk, A.: Observations of rapid aerosol optical depth enhancements in the vicinity of polluted cumulus clouds, Atmos. Chem. Phys., 14(21), 11633–11656, doi:10.5194/acp-14-11633-2014, 2014.

Edney, E. O., Driscoll, D. J., Speer, R. E., Weathers, W. S., Kleindienst, T. E., Li, W. and Smith, D. F.: Impact of aerosol liquid water on secondary organic aerosol yields of irradiated toluene/propylene/NOx/(NH4)2SO4/air mixtures, Atmos. Environ., 34, 3907–3919, 2000.

El-Sayed, M. M. H., Wang, Y. and Hennigan, C. J.: Direct atmospheric evidence for the irreversible formation of aqueous secondary organic aerosol (aqSOA), Geophys. Res. Lett., doi:10.1002/2015GL064556, 2015.

Epstein, S. A., Tapavicza, E., Furche, F. and Nizkorodov, S. A.: Direct photolysis of carbonyl compounds dissolved in cloud and fog droplets, Atmos. Chem. Phys. Discuss., 13(4), 10905–10937, doi:10.5194/acpd-13-10905-2013, 2013.

Ervens, B.: Modeling the Processing of Aerosol and Trace Gases in Clouds and Fogs, Chem. Rev., 115(10), 4157–4198, doi:10.1021/cr5005887, 2015.

Ervens, B., George, C., Williams, J. E., Buxton, G. V., Salmon, G. A., Bydder, M., Wilkinson, F., Dentener, F., Mirabel, P., Wolke, R. and Herrmann, H.: CAPRAM 2.4 (MODAC mechanism): An extended and condensed tropospheric aqueous phase mechanism and its application, J. Geophys. Res., 108(D14), 1–21, doi:10.1029/2002JD002202, 2003a.

Ervens, B., Herckes, P., Feingold, G., Lee, T., Collett, J. L. and Kreidenweis, S. M.: On the drop-size dependence of organic acid and formaldehyde concentrations in fog, J. Atmos. Chem., 46(3), 239–269, doi:10.1023/A:1026393805907, 2003b.

Ervens, B., Renard, P., Ravier, S., Clément, J.-L. and Monod, A.: Aqueous phase oligomerization of methyl vinyl ketone through photooxidation – Part 2: Development of the chemical mechanism and atmospheric implications, Atmos. Chem. Phys. Discuss., 14(15), 21565–21609, doi:10.5194/acpd-14-21565-2014, 2014a.

Ervens, B., Sorooshian, A., Lim, Y. B. and Turpin, B. J.: Key parameters controlling OH-initiated formation of secondary organic aerosol in the aqueous phase (asSOA), J. Geophys. Res. Atmos., 119(119), 3997–4016, doi:10.1002/2013JD021021, 2014b.

Ervens, B., Turpin, B. and Weber, R.: Secondary organic aerosol formation in cloud droplets and aqueous particles (aqSOA): A review of laboratory, field and model studies, Atmos. Chem. Phys., 11, 11069–11102, doi:10.5194/acp-11-11069-2011, 2011.

Ervens, B. and Volkamer, R.: Glyoxal processing by aerosol multiphase chemistry: towards a kinetic modeling framework of secondary organic aerosol formation in aqueous particles, Atmos. Chem. Phys., 10(17), 8219–8244, doi:10.5194/acp-10-8219-2010, 2010.

Facchini, M. C., Fuzzi, S., Zappoli, S., Andracchio, a, Gelencsér, a, Kiss, G., Krivácsy, Z., Mészáros, E., Hansson, H. C., Alsberg, T. and Zebühr, Y.: Partitioning of the organic aerosol component between fog droplets and interstitial air, J. Geophys. Res., 104(D21), 26821–26832, doi:10.1029/1999jd900349, 1999.

Faust, B. C. and Allen, J. M.: Aqueous-phase photochemical formation of hydroxyl radical in authentic cloudwaters and fogwaters, Environ. Sci. Technol., 27(6), 1221–1224 [online] Available from: http://pubs.acs.org/doi/abs/10.1021/es00043a024, 1993.

Finlayson-Pitts, B. J. and Pitts, J. N.: Acid Deposition: Formation and Fates of Inorganic and Organic Acids in the Troposphere, in Chemistry of the Upper and Lower Atmosphere: Theory, Experiments, and Applications, p. 969, Academic Press, San Diego, CA., 2000a.

Finlayson-Pitts, B. J. and Pitts, J. N.: Chemistry of the Upper and Lower Atmosphere: Theory, Experiments, and Applications, First Ed., Academic Press, San Diego, CA. [online] Available from: http://www.sciencedirect.com/science/book/9780122570605, 2000b.

Finlayson-Pitts, B. J. and Pitts, J. N. J.: Homogeneous and Heterogeneous Chemistry in the Stratosphere, in Chemistry of the Upper and Lower Atmosphere: Theory, Experiments, and Applications, pp. 657–726, Academic Press, San Diego, CA., 1999.

Forster, P., Ramaswamy, V., Artaxo, P., Berntsen, T., Betts, R., Fahey, D. W., Haywood, J., Lean, J., Lowe, D. C., Myhre, G., Kganga, J., Prinn, R., Raga, G., Schulz, M. and Van Dorland, R.: Changes in Atmospheric Constituents and in Radiative Forcing., 2007.

Fuzzi, S., Facchini, M. C., Decesari, S., Matta, E. and Mircea, M.: Soluble organic compounds in fog and cloud droplets: What have we learned over the past few years?, Atmos. Res., 64, 89–98, doi:10.1016/S0169-8095(02)00082-0, 2002.

Fuzzi, S., Facchini, M. C., Orsi, G., Lind, J. A., Wobrock, W., Kessell, M., Maser, R., Jaeschke, W., Enderle, K. H., Arends, B. G., Berner, A., Solly, I., Kruisz, C., Reischl, G., Pahl, S., Kaminski, U., Winkler, P., Ogren, J. A., Noone, K. J., Hallberg, A., Fierlinger-Oberlinninger, H., Puxbaum, H., Marzorati, A., Hansson, H.-C., Wiedensohler, A., Svenningsson, I. B., Martinsson, B. G., Schell, D. and Georgii, H. W.: The Po Valley Fog Experiment 1989: An Overview, Tellus B, 44B(5), 448–468, doi:10.1034/j.1600-0889.1992.t01-4-00002.x, 1992.

Galloway, M. M., Loza, C. L., Chhabra, P. S., Chan, A. W. H., Yee, L. D., Seinfeld, J. H. and Keutsch, F. N.:

Analysis of photochemical and dark glyoxal uptake: Implications for SOA formation, Geophys. Res. Lett., 38, L17811, doi:10.1029/2011GL048514, 2011.

Gill, P. S., Graedel, T. E. and Weschler, C. J.: Organic films on atmospheric aerosol particles, fog droplets, cloud droplets, raindrops, and snowflakes, Rev. Geophys., 21(4), 903, doi:10.1029/RG021i004p00903, 1983.

Gioda, A., Reyes-Rodríguez, G. J., Santos-Figueroa, G., Collett, J. L., Decesari, S., Ramos, M. D. C. K. V., Bezerra Netto, H. J. C., de Aquino Neto, F. R. and Mayol-Bracero, O. L.: Speciation of water-soluble inorganic, organic, and total nitrogen in a background marine environment: Cloud water, rainwater, and aerosol particles, J. Geophys. Res., 116(D5), D05203, doi:10.1029/2010JD015010, 2011.

Glover, C. M. and Rosario-Ortiz, F. L.: Impact of halides on the photoproduction of reactive intermediates from organic matter, Environ. Sci. Technol., 47(24), 13949–13956, doi:10.1021/es4026886, 2013.

Goldstein, A. and Galbally, I.: Known and unexplored Organic constituents in the Earth's atmosphere, Environ. Sci. Technol., 41(5), 1514–1521 [online] Available from: http://pubs.acs.org/doi/abs/10.1021/es072476p (Accessed 7 August 2013a), 2007.

Goldstein, A. H. and Galbally, I. E.: Known and unexpected organic constituents in the Earth's atmosphere, Environ. Sci. Technol., 41(5), 1514–1521, doi:10.1021/es072476p, 2007b.

Graedel, T. E. and Weschler, C. J.: Chemistry within aqueous atmospheric aerosols and raindrops., 1981.

Grčić, I. and Puma, G. L.: Photocatalytic degradation of water contaminants in multiple photoreactors and evaluation of reaction kinetic constants independent of photon absorption, irradiance, reactor geometry, and hydrodynamics, Environ. Sci. Technol., 47(23), 13702–13711, doi:10.1021/es403472e, 2013.

De Haan, D. O., Hawkins, L. N., Kononenko, J. A., Turley, J. J., Corrigan, A. L., Tolbert, M. A. and Jimenez, J. L.: Formation of nitrogen-containing oligomers by methylglyoxal and amines in simulated evaporating cloud droplets., Environ. Sci. Technol., 45(3), 984–91, doi:10.1021/es102933x, 2011.

Hamilton, J. F., Lewis, a. C., Reynolds, J. C., Carpenter, L. J. and Lubben, A.: Investigating the composition of organic aerosol resulting from cyclohexene ozonolysis: low molecular weight and heterogeneous reaction products, Atmos. Chem. Phys., 6, 4973–4984, doi:10.5194/acpd-6-6369-2006, 2006.

Hamilton, J., Webb, P., Lewis, a., Hopkins, J., Smith, S. and Davy, P.: Partially oxidised organic components in urban aerosol using GCXGC-TOF/MS, Atmos. Chem. Phys. Discuss., 4(2), 1393–1423, doi:10.5194/acpd-4-1393-2004, 2004.

Haynes, W. M., Bruno, T. J. and Lide, D. R., Eds.: Handbook of Chemistry and Physics, 94th ed., CRC Press, Cleveland, OH. [online] Available from: http://ezproxy2.library.colostate.edu:2767/ (Accessed 21 September 2013), 2013.

Heald, C. L., Collett, J. L., Lee, T., Benedict, K. B., Schwandner, F. M., Li, Y., Clarisse, L., Hurtmans, D. R., Van Damme, M., Clerbaux, C., Coheur, P. F., Philip, S., Martin, R. V. and Pye, H. O. T.: Atmospheric ammonia and particulate inorganic nitrogen over the United States, Atmos. Chem. Phys., 12(21), 10295–10312, doi:10.5194/acp-12-10295-2012, 2012.

Hennigan, C. J., Bergin, M. H., Dibb, J. E. and Weber, R. J.: Enhanced secondary organic aerosol formation due to water uptake by fine particles, Geophys. Res. Lett., 35(18), 1–5, doi:10.1029/2008GL035046, 2008.

Hennigan, C. J., Bergin, M. H., Russell, a G., Nenes, a and Weber, R. J.: Gas/particle partitioning of water-soluble organic aerosol in Atlanta, Atmos. Chem. Phys. Discuss., 9(1), 3613–3628 [online] Available from: http://www.atmos-chem-phys-discuss.net/9/635/2009/, 2009.

Herckes, P., Chang, H., Lee, T. and Collett, J. L.: Air Pollution Processing by Radiation Fogs, Water Air Soil Pollut., 181, 65–75, doi:10.1007/s11270-006-9276-x, 2007.

Herckes, P., Hannigan, M. P., Trenary, L., Lee, T. and Collett, J. L.: Organic compounds in radiation fogs in Davis (California), Atmos. Res., 64(1-4), 99–108, doi:10.1016/S0169-8095(02)00083-2, 2002.

Herckes, P., Marcotte, A. R., Wang, Y. and Collett, J. L.: Fog composition in the Central Valley of California over three decades, Atmos. Res., 151, 20–30, doi:10.1016/j.atmosres.2014.01.025, 2015.

Herckes, P., Valsaraj, K. T. and Collett, J. L.: A review of observations of organic matter in fogs and clouds: Origin, processing and fate, Atmos. Res., 132-133, 434–449, doi:10.1016/j.atmosres.2013.06.005, 2013.

Herrmann, H., Hoffmann, D., Schaefer, T., Bräuer, P. and Tilgner, A.: Tropospheric aqueous-phase free-radical chemistry: radical sources, spectra, reaction kinetics and prediction tools., ChemPhysChem, 11(18), 3796–822, doi:10.1002/cphc.201000533, 2010.

Herrmann, H., Schaefer, T., Tilgner, A., Styler, S. A., Weller, C., Teich, M. and Otto, T.: Tropospheric Aqueous-Phase Chemistry: Kinetics, Mechanisms, and Its Coupling to a Changing Gas Phase, Chem. Rev., 115(10), 4259–4334, doi:10.1021/cr500447k, 2015.

Hoffer, A., Kiss, G., Blazsó, M. and Gelencsér, A.: Chemical characterization of humic-like substances (HULIS) formed from a lignin-type precursor in model cloud water, Geophys. Res. Lett., 31, L06115, doi:10.1029/2003GL018962, 2004.

Hoppel, W. A., Frick, G. M., Fitzgerald, J. W. and Watter, B. J.: A Cloud Chamber Study of the Effect That Nonprecipitating Water Clouds Have on the Aerosol Size Distribution, Aerosol Sci. Technol., 20(1), 1–30, 1994.

Hung, H., Blanchard, P., Halsall, C. J., Bidleman, T. F., Stern, G. A., Fellin, P., Muir, D. C. G., Barrie, L. A., Jantunen, L. M., Helm, P. A., Ma, J. and Konoplev, A.: Temporal and spatial variabilities of atmospheric polychlorinated biphenyls (PCBs), organochlorine (OC) pesticides and polycyclic aromatic hydrocarbons (PAHs) in the Canadian Arctic: Results from a decade of monitoring, Sci. Total Environ., 342(1-3), 119–144, doi:10.1016/j.scitotenv.2004.12.058, 2005.

Jacob, D. J.: The origins of inorganic acidity in fogs, California Intitute of Technology., 1985.

Jacob, D. J., Munger, J. W., Waldman, J. E. D. M. and Hoffmann, M. R.: The H2SO4-HNO3-NH3 System at High Humidities and in Fogs 1. Spatial and Temporal Patterns in the San Joaquin Valley of California, J. Geophys. Res., 91(D1), 1073–1088, 1986.

Jacob, D. J., Waldman, J. M., Haghi, M., Hoffmann, M. R. and Flagan, R. C.: Instrument to collect fogwater for chemical analysis, Rev. Sci. Instrum., 56(6), 1291–1293, doi:10.1063/1.1137995, 1985.

Jacob, D. J., Wang, R.-F. T. and Flagan, R. C.: Fogwater collector design and characterization, Environ. Sci. Technol., 18(11), 827–833, doi:10.1021/es00129a005, 1984.

Jiang, Y., Zhuang, G., Wang, Q., Liu, T., Huang, K., Fu, J. S., Li, J., Lin, Y., Zhang, R. and Deng, C.: Aerosol oxalate and its implication to haze pollution in Shanghai, China, Chinese Sci. Bull., 59(2), 227–238, doi:10.1007/s11434-013-0009-4, 2013.

Jimenez, J. L., Canagaratna, M. R., Donahue, N. M., Prevot, a. S. H., Zhang, Q., Kroll, J. H., DeCarlo, P. F., Allan, J. D., Coe, H., Ng, N. L., Aiken, a. C., Docherty, K. S., Ulbrich, I. M., Grieshop, A. P., Robinson, a. L., Duplissy, J., Smith, J. D., Wilson, K. R., Lanz, V. a., Hueglin, C., Sun, Y. L., Tian, J., Laaksonen, A., Raatikainen, T., Rautiainen, J., Vaattovaara, P., Ehn, M., Kulmala, M., Tomlinson, J. M., Collins, D. R., Cubison, M. J., Dunlea, J., Huffman, J. A., Onasch, T. B., Alfarra, M. R., Williams, P. I., Bower, K., Kondo, Y., Schneider, J., Drewnick, F., Borrmann, S., Weimer, S., Demerjian, K., Salcedo, D., Cottrell, L., Griffin, R., Takami, a., Miyoshi, T., Hatakeyama, S., Shimono, A., Sun, J. Y., Zhang, Y. M., Dzepina, K., Kimmel, J. R., Sueper, D., Jayne, J. T., Herndon, S. C., Trimborn, a. M., Williams, L. R., Wood, E. C., Middlebrook, A. M., Kolb, C. E., Baltensperger, U., Worsnop, D. R., Dunlea, E. J., Huffman, J. A., Onasch, T. B., Alfarra, M. R., Williams, P. I., Bower, K., Kondo, Y., Schneider, J., Drewnick, F., Borrmann, S., Weimer, S., Demerjian, K., Salcedo, D., Cottrell, L., Griffin, R., Takami, a., Miyoshi, T., Hatakeyama, S., Shimono, A., Sun, J. Y., Zhang, Y. M., Dzepina, K., Kimmel, J. R., Sueper, D., Jayne, J. T., Herndon, S. C., Trimborn, a. M., Williams, L. R., Wood, E. C., Middlebrook, A. M., Kolb, C. E., Baltensperger, U., Worsnop, D. R., Dunlea, J., Huffman, J. A., et al.: Evolution of Organic Aerosols in the Atmosphere, Science (80-.)., 326(5959), 1525–1529, doi:10.1126/science.1180353, 2009.

John, W., Wall, S., Ondo, J. and Winklmayr, W.: Modes in the size distributions of atmospheric inorganic aerosol, Atmos. Environ., 24(9), 2349–2359 [online] Available from: http://www.sciencedirect.com/science/article/pii/096016869090327J (Accessed 25 April 2013), 1990.

Johnstone, J. A. and Dawson, T. E.: Climatic context and ecological implications of summer fog decline in the coast redwood region., Proc. Natl. Acad. Sci., 107(10), 4533–8, doi:10.1073/pnas.0915062107, 2010.

Kalberer, M., Yu, J., Cocker, D. R., Flagan, R. C. and Seinfeld, J. H.: Aerosol Formation in the Cyclohexene-

Ozone System, Environ. Sci. Technol., 34(23), 4894–4901, doi:10.1021/es001180f, 2000.

Kalina, M. F., Stopper, S., Zambo, E. and Puxbaum, H.: Altitude-dependent wet, dry and occult nitrogen deposition in an Alpine Region - Achenkirch, Austria, 920m-1758m a.s.l, Environ. Sci. Pollut. Res., 2(2), 16–22 [online] Available from: <Go to ISI>://000202839700004, 2002.

Kamens, R. M., Zhang, H., Chen, E. H., Zhou, Y., Parikh, H. M., Wilson, R. L., Galloway, K. E. and Rosen, E. P.: Secondary organic aerosol formation from toluene in an atmospheric hydrocarbon mixture: Water and particle seed effects, Atmos. Environ., 45, 2324–2334, doi:10.1016/j.atmosenv.2010.11.007, 2011.

Kaul, D. S., Gupta, T., Tripathi, S. N., Tare, V. and Collett, J. L.: Secondary Organic Aerosol: A Comparison between Foggy and Nonfoggy Days, Environ. Sci. Technol., 45(17), 7307–7313 [online] Available from: http://www.ncbi.nlm.nih.gov/pubmed/21790145, 2011.

Kavitha, V. and Palanivelu, K.: Degradation of nitrophenols by Fenton and photo-Fenton processes, J. Photochem. Photobiol. A Chem., 170, 83–95, doi:10.1016/j.jphotochem.2004.08.003, 2005.

Kawamura, K. and Bikkina, S.: A review of dicarboxylic acids and related compounds in atmospheric aerosols: Molecular distributions, sources and transformation, Atmos. Res., 170, 140–160, doi:10.1016/j.atmosres.2015.11.018, 2016.

Kawamura, K. and Ikushima, K.: Seasonal changes in the distribution of dicarboxylic acids in the urban atmosphere, Environ. Sci. Technol., 27(10), 2227–2235, doi:10.1021/es00047a033, 1993.

Kawamura, K., Kasukabe, H. and Barrie, L. A.: Source and reaction pathways of dicarboxylic acids, ketoacids and dicarbonyls in arctic aerosols: One year of observations, Atmos. Environ., 30(10/11), 1709–1722, doi:10.1016/1352-2310(95)00395-9, 1996.

Khlystov, A., Stanier, C. O., Takahama, S. and Pandis, S. N.: Water content of ambient aerosol during the Pittsburgh air quality study, J. Geophys. Res. Atmos., 110(7), 1–10, doi:10.1029/2004JD004651, 2005.

Kirkland, J., Lim, Y., Tan, Y., Altieri, K. and Turpin, B.: Glyoxal secondary organic aerosol chemistry: effects of dilute nitrate and ammonium and support for organic radical-radical oligomer formation, Environ. Chem., 10, 158–166, doi:dx.doi.org/10.1071.EN13074, 2013.

Kleindienst, T. E., Jaoui, M., Lewandowski, M., Offenberg, J. H., Lewis, C. W., Bhave, P. V. and Edney, E. O.: Estimates of the contributions of biogenic and anthropogenic hydrocarbons to secondary organic aerosol at a southeastern US location, Atmos. Environ., 41(37), 8288–8300, doi:10.1016/j.atmosenv.2007.06.045, 2007.

Kleindienst, T. E., Smith, D. F., Li, W., Edney, E. O., Driscoll, D. J., Speer, R. E. and Weathers, W. S.: Secondary organic aerosol formation from the oxidation of aromatic hydrocarbons in the presence of dry submicron ammonium sulfate aerosol, Atmos. Environ., 33, 3669–3681, doi:10.1016/S1352-2310(99)00121-1, 1999.

Kristensen, K., Cui, T., Zhang, H., Gold, a., Glasius, M. and Surratt, J. D.: Dimers in α-pinene secondary organic aerosol: effect of hydroxyl radical, ozone, relative humidity and aerosol acidity, Atmos. Chem. Phys., 14(8), 4201–4218, doi:10.5194/acp-14-4201-2014, 2014.

Kroll, J. H., Smith, J. D., Dung, L. C., Kessler, S. H., Worsnop, D. R. and Wilson, K. R.: Measurement of fragmentation and functionalization pathways in the heterogeneous oxidation of oxidized organic aerosol, Phys. Chem. Chem. Phys., 11, 8005–8014, doi:10.1039/b916865f, 2009.

Kuang, B. Y., Lin, P., Huang, X. H. H. and Yu, J. Z.: Sources of humic-like substances in the Pearl River Delta, China: Positive matrix factorization analysis of PM2.5 major components and source markers, Atmos. Chem. Phys., 15(4), 1995–2008, doi:10.5194/acp-15-1995-2015, 2015.

De Laurentiis, E., Sur, B., Pazzi, M., Maurino, V., Minero, C., Mailhot, G., Brigante, M. and Vione, D.: Phenol transformation and dimerisation, photosensitised by the triplet state of 1-nitronaphthalene: A possible pathway to humic-like substances (HULIS) in atmospheric waters, Atmos. Environ., 70, 318–327, doi:10.1016/j.atmosenv.2013.01.014, 2013.

Lee, A. K. Y., Hayden, K. L., Herckes, P., Leaitch, W. R., Liggio, J., Macdonald, A. M. and Abbatt, J. P. D.: Characterization of aerosol and cloud water at a mountain site during WACS 2010: secondary organic aerosol formation through oxidative cloud processing, Atmos. Chem. Phys., 12(15), 6019–6047, doi:10.5194/acpd-12-6019-2012, 2012.

Lee, A. K. Y., Herckes, P., Leaitch, R. W., Macdonald, A. M. and Abbatt, J. P. D.: Aqueous OH oxidation of ambient organic aerosol and cloud water organics: Formation of highly oxidized products, Geophys. Res. Lett., 38(L11805), 1–5, doi:10.1029/2011GL047439, 2011a.

Lee, A. K. Y., Zhao, R., Gao, S. S. and Abbatt, J. P. D.: Aqueous-phase OH oxidation of glyoxal: application of a novel analytical approach employing aerosol mass spectrometry and complementary off-line techniques, J. Phys. Chem. A, 115, 10517–10526 [online] Available from: http://pubs.acs.org/doi/abs/10.1021/jp204099g (Accessed 23 September 2013b), 2011.

Lee, D., Sud, Y. C., Oreopoulos, L., Kim, K.-M., Lau, W. K. and Kang, I.-S.: Modeling the influences of aerosols on pre-monsoon circulation and rainfall over Southeast Asia, Atmos. Chem. Phys., 14(13), 6853–6866, doi:10.5194/acp-14-6853-2014, 2014.

Liggio, J. and Li, S. M.: Organosulfate formation during the uptake of pinonaldehyde on acidic sulfate aerosols, Geophys. Res. Lett., 33(May), 2–5, doi:10.1029/2006GL026079, 2006.

Lillis, D., Cruz, C. N., Collett, J., Willard Richards, L. and Pandis, S. N.: Production and removal of aerosol in a polluted fog layer: Model evaluation and fog effect on PM, Atmos. Environ., 33(29), 4797–4816, doi:10.1016/S1352-2310(99)00264-2, 1999.

Lim, Y. B., Tan, Y., Perri, M. J., Seitzinger, S. P. and Turpin, B. J.: Aqueous chemistry and its role in secondary organic aerosol (SOA) formation, Atmos. Chem. Phys., 10, 10521–10539, doi:10.5194/acp-10-10521-2010, 2010.

Lim, Y. B., Tan, Y. and Turpin, B. J.: Chemical insights, explicit chemistry, and yields of secondary organic aerosol from OH radical oxidation of methylglyoxal and glyoxal in the aqueous phase, Atmos. Chem. Phys., 13(17), 8651–8667, doi:10.5194/acp-13-8651-2013, 2013.

Lim, Y. B. and Turpin, B. J.: Organic peroxide and OH formation in aerosol and cloud water: laboratory evidence for this aqueous chemistry, Atmos. Chem. Phys. Discuss., 15(12), 17367–17396, doi:10.5194/acpd-15-17367-2015, 2015.

Limbeck, A. and Puxbaum, H.: Organic acids in continental background aerosols, , 33(June 1998), 1847–1852, 1999.

Loeffler, K. W., Koehler, C. A., Paul, N. M. and De Haan, D. O.: Oligomer formation in evaporating aqueous glyoxal and methylglyoxal solutions, Environ. Sci. Technol., 40(20), 6318–6323, doi:10.1021/es060810w, 2006.

Löflund, M., Kasper-Giebl, A., Schuster, B., Giebl, H., Hitzenberger, R. and Puxbaum, H.: Formic, acetic, oxalic, malonic and succinic acid concentrations and their contribution to organic carbon in cloud water, Atmos. Environ., 36(9), 1553–1558, doi:Pii S1352-2310(01)00573-8\rDoi 10.1016/S1352-2310(01)00573-8, 2002.

Marshall, A. G., Hendrickson, C. L. and Jackson, G. S.: Fourier transform ion cyclotron resonance mass spectrometry: A primer, Mass Spectrom. Rev., 17, 1–35, 1998.

Mason, J. B., Fujita, E. M., Campbell, D. E. and Zielinska, B.: Evaluation of passive samplers for assessment of community exposure to toxic air contaminants and related pollutants., Environ. Sci. Technol., 45(6), 2243–9, doi:10.1021/es102500v, 2011.

Mazzoleni, L. R., Ehrmann, B. M., Shen, X., Marshall, A. G. and Collett, J. L.: Water-soluble atmospheric organic matter in fog: Exact masses and chemical formula identification by ultrahigh-resolution fourier transform ion cyclotron resonance mass spectrometry., Environ. Sci. Technol., 44(10), 3690–3697, doi:10.1021/es903409k, 2010.

McNeill, V. F.: Aqueous organic chemistry in the atmosphere: Sources and chemical processing of organic aerosols, Environ. Sci. Technol., 49(3), 1237–1244, doi:10.1021/es5043707, 2015.

Meng, Z. and Seinfeld, J. H.: On the Source of the Submicrometer Droplet Mode of Urban and Regional Aerosols, Aerosol Sci. Technol., 20(3), 253–265, doi:10.1080/02786829408959681, 1994.

Monod, A., Chebbi, A., Durand-Jolibois, R. and Carlier, P.: Oxidation of methanol by hydroxyl radicals in aqueous solution under simulated cloud droplet conditions, Atmos. Environ., 34(29-30), 5283–5294, doi:10.1016/S1352-2310(00)00191-6, 2000.

Monod, A., Poulain, L., Grubert, S., Voisin, D. and Wortham, H.: Kinetics of OH-initiated oxidation of

oxygenated organic compounds in the aqueous phase: new rate constants, structure–activity relationships and atmospheric implications, Atmos. Environ., 39(40), 7667–7688, doi:10.1016/j.atmosenv.2005.03.019, 2005.

Moore, K. F., Sherman, D. E., Reilly, J. E. and Collett, J. L.: Drop size-dependent chemical composition in clouds and fogs. Part I. Observations, Atmos. Environ., 38(10), 1389–1402, doi:10.1016/j.atmosenv.2003.12.013, 2004a.

Moore, K. F., Sherman, D. E., Reilly, J. E., Hannigan, M. P., Lee, T. and Collett, J. L.: Drop size-dependent chemical composition of clouds and fogs. Part II: Relevance to interpreting the aerosol/trace gas/fog system, Atmos. Environ., 38(10), 1403–1415, doi:10.1016/j.atmosenv.2003.12.014, 2004b.

Munger, J. W.: The chemical composition of fogs and clouds in Southern California, California Institute of Technology., 1989.

Munger, J. W., Collett, J., Daube, B. and Hoffmann, M. R.: Fogwater chemistry at Riverside, California, Atmos. Environ., 24B(2), 185–205, 1990.

Murray, B. J., O'Sullivan, D., Atkinson, J. D. and Webb, M. E.: Ice nucleation by particles immersed in supercooled cloud droplets., Chem. Soc. Rev., 41(19), 6519–54, doi:10.1039/c2cs35200a, 2012.

Ng, N. L., Canagaratna, M. R., Jimenez, J. L., Chhabra, P. S., Seinfeld, J. H. and Worsnop, D. R.: Changes in organic aerosol composition with aging inferred from aerosol mass spectra, Atmos. Chem. Phys., 11(13), 6465–6474, doi:10.5194/acp-11-6465-2011, 2011.

Nguyen, T. B., Coggon, M. M., Flagan, R. C. and Seinfeld, J. H.: Reactive uptake and photo-fenton oxidation of glycolaldehyde in aerosol liquid water, Environ. Sci. Technol., 47(9), 4307–16, doi:10.1021/es400538j, 2013.

Nguyen, T. B., Lee, P. B., Updyke, K. M., Bones, D. L., Laskin, J., Laskin, A. and Nizkorodov, S. A.: Formation of nitrogen- and sulfur-containing light-absorbing compounds accelerated by evaporation of water from secondary organic aerosols, J. Geophys. Res. Atmos., 117(1), D01207, doi:10.1029/2011JD016944, 2012.

Nguyen, T. B., Roach, P. J., Laskin, J., Laskin, a. and Nizkorodov, S. a.: Effect of humidity on the composition of isoprene photooxidation secondary organic aerosol, Atmos. Chem. Phys., 11(14), 6931–6944, doi:10.5194/acp-11-6931-2011, 2011.

Nie, W., Ding, A., Wang, T., Kerminen, V.-M., George, C., Xue, L., Wang, W., Zhang, Q., Petäjä, T., Qi, X., Gao, X., Wang, X., Yang, X., Fu, C. and Kulmala, M.: Polluted dust promotes new particle formation and growth, Sci. Rep., 4, 6634, doi:10.1038/srep06634, 2014.

NOAA ESRL Global Monitoring Division: Trends in Atmospheric Carbon Dioxide, Recent Mon. Aver. Mauna Loa CO2 [online] Available from: http://www.esrl.noaa.gov/gmd/ccgg/trends/#mlo, 2016.

Nozière, B., Dziedzic, P. and Córdova, A.: Products and kinetics of the liquid-phase reaction of glyoxal catalyzed by ammonium ions (NH4+), J. Phys. Chem. A, 113(1), 231–237, doi:10.1021/jp8078293, 2009.

Nozière, B., Ekström, S., Alsberg, T. and Holmström, S.: Radical-initiated formation of organosulfates and surfactants in atmospheric aerosols, Geophys. Res. Lett., 37(5), doi:10.1029/2009GL041683, 2010.

O'Brien, R. E., Laskin, A., Laskin, J., Rubitschun, C. L., Surratt, J. D. and Goldstein, A. H.: Molecular characterization of S- and N-containing organic constituents in ambient aerosols by negative ion mode high-resolution nanospray desorption electrospray ionization mass spectrometry: CalNex 2010 field study, J. Geophys. Res. Atmos., 119, 12706–12720, doi:10.1002/2014JD021955.Received, 2014.

Oriel: Solar Simulator, Stratford, CT. [online] Available from: https://assets.newport.com/webDocuments-EN/images/12298.pdf, 2015.

Ortiz-Montalvo, D. L., Lim, Y. B., Perri, M. J., Seitzinger, S. P. and Turpin, B. J.: Volatility and Yield of Glycolaldehyde SOA Formed through Aqueous Photochemistry and Droplet Evaporation, Aerosol Sci. Technol., 46(9), 1002–1014, doi:10.1080/02786826.2012.686676, 2012.

Pandis, S. N. and Seinfeld, J. H.: Should bulk cloudwater or fogwater samples obey henrys law, J. Geophys. Res.-Atmos., 96(91), 10791–10798, doi:10.1029/91JD01031, 1991.

Pandis, S. N., Seinfeld, J. H. and Pilinis, C.: The smog-fog-smog cycle and acid deposition, J. Geophys. Res.,

95(D11), 18489–18500, doi:10.1029/JD095iD11p18489, 1990.

Pankow, J. F.: Aquatic Chemistry Concepts, First., Lewis Publishers, Chelsea, MI., 1991.

Park, R. J., Jacob, D. J., Field, B. D. and Yantosca, R. M.: Natural and transboundary pollution influences on sulfate-nitrate-ammonium aerosols in the United States: Implications for policy, J. Geophys. Res., 109(D15), D15204, doi:10.1029/2003JD004473, 2004.

Park, R. J., Jacob, D. J., Kumar, N. and Yantosca, R. M.: Regional visibility statistics in the United States: Natural and transboundary pollution influences, and implications for the Regional Haze Rule, Atmos. Environ., 40(28), 5405–5423, doi:10.1016/j.atmosenv.2006.04.059, 2006.

Perri, M. J., Lim, Y. B., Seitzinger, S. P. and Turpin, B. J.: Organosulfates from glycolaldehyde in aqueous aerosols and clouds: Laboratory studies, Atmos. Environ., 44(21-22), 2658–2664, doi:10.1016/j.atmosenv.2010.03.031, 2010.

Perri, M. J., Seitzinger, S. and Turpin, B. J.: Secondary organic aerosol production from aqueous photooxidation of glycolaldehyde: Laboratory experiments, Atmos. Environ., 43(8), 1487–1497, doi:10.1016/j.atmosenv.2008.11.037, 2009.

van Pinxteren, D., Fomba, K. W., Mertes, S., Müller, K., Spindler, G., Schneider, J., Lee, T., Collett, J. and Herrmann, H.: Cloud water composition during HCCT-2010: Scavenging efficiencies, solute concentrations, and droplet size dependence of inorganic ions and dissolved organic carbon, Atmos. Chem. Phys., 16, 3185–3205, doi:10.5194/acpd-15-24311-2015, 2016.

Pocker, Y., Meany, J. E., Nist, B. J. and Zadorojny, C.: The Reversible Hydration of Pyruvic Acid I. Equilibrium Studies, J. Phys. Chem., 73(9), 2879–2882, 1969.

Pruppacher, H. R. and Klett, J. D.: Microphysics of Clouds and Precipitation, Springer Netherlands, Dordrecht., 2010.

Raja, S., Raghunathan, R., Yu, X.-Y., Lee, T., Chen, J., Kommalapati, R. R., Murugesan, K., Shen, X., Qingzhong, Y., Valsaraj, K. T. and Collett, J. L.: Fog chemistry in the Texas–Louisiana Gulf Coast corridor, Atmos. Environ., 42(9), 2048–2061, doi:10.1016/j.atmosenv.2007.12.004, 2008.

Rao, X. and Collett, J. L.: Behavior of S(IV) and formaldehyde in a chemically heterogeneous cloud, Environ. Sci. Technol., 29(4), 1023–1031, doi:10.1021/es00004a024, 1995.

Reale, O., Lau, K. M., da Silva, a. and Matsui, T.: Impact of assimilated and interactive aerosol on Tropical Cyclogenesis., Geophys. Res. Lett., n/a–n/a, doi:10.1002/2014GL059918, 2014.

Renard, P., Siekmann, F., Gandolfo, A., Socorro, J., Salque, G., Ravier, S., Quivet, E., Clément, J.-L., Traikia, M., Delort, A. M., Voisin, D., Vuitton, V., Thissen, R. and Monod, A.: Radical mechanisms of methyl vinyl ketone oligomerization through aqueous phase OH-oxidation: on the paradoxical role of dissolved molecular oxygen, Atmos. Chem. Phys., 13(13), 6473–6491, doi:10.5194/acp-13-6473-2013, 2013.

Renard, P., Siekmann, F., Salque, G., Smaani, A., Demelas, C., Coulomb, B., Vassalo, L., Ravier, S., Temime-Roussel, B., Voisin, D. and Monod, A.: Aqueous phase oligomerization of methyl vinyl ketone through photooxidation – Part 1: Aging processes of oligomers, Atmos. Chem. Phys. Discuss., 14(10), 15283–15322, doi:10.5194/acpd-14-15283-2014, 2014.

Ricci, L., Fuzzi, S., Laj, P., Lazzari, A., Orsi, G., Berner, A., Gunther, A., Jaeschke, W., Wendisch, M. and Arends, B. G.: Gas-liquid equilibria in polluted fog, Contrib. to Atmos. Phys., 71(1), 159–170, 1998.

Richards-Henderson, N. K., Hansel, A. K., Valsaraj, K. T. and Anastasio, C.: Aqueous oxidation of green leaf volatiles by hydroxyl radical as a source of SOA: Kinetics and SOA yields, Atmos. Environ., 95, 105–112, doi:10.1016/j.atmosenv.2014.06.026, 2014.

Roman, P., Polkowska, Ż. and Namieśnik, J.: Sampling Procedures in Studies of Cloud Water Composition: A Review, Crit. Rev. Environ. Sci. Technol., 43(14), 1517–1555, doi:10.1080/10643389.2011.647794, 2013.

Rossignol, S., Aregahegn, K. Z., Tinel, L., Fine, L., Nozière, B. and George, C.: Glyoxal induced atmospheric photosensitized chemistry leading to organic aerosol growth., Environ. Sci. Technol., 48(6), 3218–27, doi:10.1021/es405581g, 2014.

Rudich, Y., Talukdar, R. K., Ravishankara, A. R. and Fox, R. W.: Reactive uptake of NO3 on pure water and ionic solutions, J. Geophys. Res. Atmos., 101(D15), 21023–21031, doi:10.1029/96JD01844, 1996.

Safarzadeh-Amiri, A., Bolton, J. R. and Cater, S. R.: Ferrioxalate-mediated photodegradation of organic pollutants in contaminated water, Water Res., 31(4), 787–798 [online] Available from: http://www.sciencedirect.com/science/article/pii/S0043135496003739 (Accessed 30 December 2013), 1997.

Santos, A., Yustos, P., Rodriguez, S. and Garcia-Ochoa, F.: Wet oxidation of phenol, cresols and nitrophenols catalyzed by activated carbon in acid and basic media, Appl. Catal. B Environ., 65(3-4), 269–281, doi:10.1159/000093525, 2006.

Sareen, N., Schwier, A. N., Shapiro, E. L., Mitroo, D. and McNeill, V. F.: Secondary organic material formed by methylglyoxal in aqueous aerosol mimics, Atmos. Chem. Phys., 10(3), 997–1016, doi:10.5194/acp-10-997-2010, 2010.

Saxena, P. and Hildemann, L. M.: Water-Soluble Organics in Atmospheric Particles : A Critical Review of the Literature and Application of Thermodynamics to Identify Candidate Compounds, , 57–109, 1996.

Schindelka, J., Iinuma, Y., Hoffmann, D. and Herrmann, H.: Sulfate radical-initiated formation of isoprene-derived organosulfates in atmospheric aerosols, Faraday Discuss., 165, 237–259, doi:10.1039/c3fd00042g, 2013.

Schöne, L. and Herrmann, H.: Kinetic measurements of the reactivity of hydrogen peroxide and ozone towards small atmospherically relevant aldehydes, ketones and organic acids in aqueous solutions, Atmos. Chem. Phys., 14(9), 4503–4514, doi:10.5194/acp-14-4503-2014, 2014.

Schwarzenbach, R. P., Gschwend, P. M. and Imboden, D. M.: Indirect Photolysis in Surface Waters: Reactions with Photooxidants in Natural Waters and in the Atmosphere, in Environmental Organic Chemistry, p. 1313, John Wiley & Sons, Inc., Hoboken, New Jersey., 2003.

Shen, X., Lee, T., Guo, J., Wang, X., Li, P., Xu, P., Wang, Y., Ren, Y., Wang, W., Wang, T., Li, Y., Carn, S. A. and Collett, J. L.: Aqueous phase sulfate production in clouds in eastern China, Atmos. Environ., 62, 502–511, doi:10.1016/j.atmosenv.2012.07.079, 2012.

Smith, J. D., Sio, V., Yu, L., Zhang, Q. and Anastasio, C.: Secondary organic aerosol production from aqueous reactions of atmospheric phenols with an organic triplet excited state., Environ. Sci. Technol., 48(2), 1049–57, doi:10.1021/es4045715, 2014.

Solomons, T. W. G. and Fryhle, C. B.: Organic Chemistry, 8th ed., John Wiley & Soons, Hoboken, New Jersey., 2004.

Sorooshian, A., Murphy, S. M., Hersey, S., Bahreini, R., Jonsson, H., Flagan, R. C. and Seinfeld, J. H.: Constraining the contribution of organic acids and AMS m/z 44 to the organic aerosol budget: On the importance of meteorology, aerosol hygroscopicity, and region, Geophys. Res. Lett., 37(21), n/a–n/a, doi:10.1029/2010GL044951, 2010.

Sorooshian, A., Wang, Z., Coggon, M. M., Jonsson, H. H. and Ervens, B.: Observations of Sharp Oxalate Reductions in Stratocumulus Clouds at Variable Altitudes: Organic Acid and Metal Measurements During the 2011 E-PEACE Campaign, Environ. Sci. Technol., 47, 7747–7756, 2013.

Stefan, M. I. and Bolton, J. R.: Reinvestigation of the Acetone Degradation Mechanism in Dilute Aqueous Solution by the UV/H2O2 Process, Environ. Sci. Technol., 33(6), 870–873 [online] Available from: http://pubs.acs.org/doi/abs/10.1021/es9808548 (Accessed 21 September 2013), 1999.

Straub, D. J. and Collett, J. L. J.: Development of a multi-stage cloud water collector Part 2: Numerical and experimental calibration, Atmos. Environ., 36, 45–56, 2002.

Straub, D. J., Hutchings, J. W. and Herckes, P.: Measurements of fog composition at a rural site, Atmos. Environ., 47, 195–205, doi:10.1016/j.atmosenv.2011.11.014, 2012.

Sun, Y. L., Zhang, Q., Anastasio, C. and Sun, J.: Insights into secondary organic aerosol formed via aqueous-phase reactions of phenolic compounds based on high resolution mass spectrometry, Atmos. Chem. Phys., 10, 4809–4822, doi:10.5194/acp-10-4809-2010, 2010.

Tan, Y., Carlton, A. G., Seitzinger, S. P. and Turpin, B. J.: SOA from methylglyoxal in clouds and wet aerosols:

Measurement and prediction of key products, Atmos. Environ., 44(39), 5218–5226, doi:10.1016/j.atmosenv.2010.08.045, 2010.

Tan, Y., Perri, M. J., Seitzinger, S. P. and Turpin, B. J.: Effects of Precursor Concentration and Acidic Sulfate in Aqueous Glyoxal-OH Radical Oxidation and Implications for Secondary Organic Aerosol, Environ. Sci. Technol., 43(21), 8105–8112, 2009.

Tang, K., Page, J. S. and Smith, R. D.: Charge competition and the linear dynamic range of detection in electrospray ionization mass spectrometry., J. Am. Soc. Mass Spectrom., 15(10), 1416–23, doi:10.1016/j.jasms.2004.04.034, 2004.

Tremp, J.: Sources and Fate of Nitrate Phenols in the Atmospheric Environment, Swiss Federal Institute of Technology Zürich., 1992.

Wang, W. F., Schuchmann, M. N., Schuchmann, H. P. and Von Sonntag, C.: The importance of mesomerism in the termination of α-carboxymethyl radicals from aqueous malonic and acetic acids, Chem. - A Eur. J., 7(4), 791–795, doi:10.1002/1521-3765(20010216)7:4<791::AID-CHEM791>3.0.CO;2-2, 2001.

Wang, Y., Guo, J., Wang, T., Ding, A., Gao, J., Zhou, Y., Collett, J. L. and Wang, W.: Influence of regional pollution and sandstorms on the chemical composition of cloud/fog at the summit of Mt. Taishan in northern China, Atmos. Res., 99(3-4), 434–442, doi:10.1016/j.atmosres.2010.11.010, 2011.

Wang, Y., Zhang, J., Marcotte, A. R., Karl, M., Dye, C. and Herckes, P.: Fog chemistry at three sites in Norway, Atmos. Res., doi:10.1016/j.atmosres.2014.04.016, 2014.

Wei, Y., Cao, T. and Thompson, J. E.: The chemical evolution & physical properties of organic aerosol: A molecular structure based approach, Atmos. Environ., 62, 199–207, doi:10.1016/j.atmosenv.2012.08.029, 2012.

Weller, C., Horn, S. and Herrmann, H.: Photolysis of Fe (III) carboxylato complexes: Fe (II) quantum yields and reaction mechanisms, J. Photochem. Photobiol. A Chem., 268, 24–36, doi:10.1016/j.jphotochem.2013.06.022, 2013.

Weller, C., Tilgner, A., Bräuer, P. and Herrmann, H.: Modelling the impact of iron-carboxylate photochemistry on radical budget and carboxylate degradation in cloud droplets and particles, Environ. Sci. Technol., 140328152101005, doi:10.1021/es4056643, 2014.

Winiwarter, W., Brantner, B. and Puxbaum, H.: Comment on "Should Bulk Cloudwater or Fogwater Samples Obey Henry's Law?" by S.N. Pandis and J.H. Seinfeld, J. Geophys. Res. Atmos., 97, 6075–6078, 1992.

Wonaschuetz, A., Sorooshian, A., Ervens, B., Chuang, P. Y., Feingold, G., Murphy, S. M., de Gouw, J., Warneke, C. and Jonsson, H. H.: Aerosol and gas re-distribution by shallow cumulus clouds: An investigation using airborne measurements, J. Geophys. Res., 117(D17), D17202, doi:10.1029/2012JD018089, 2012.

Yu, J. Z., Huang, X.-F., Xu, J. and Hu, M.: When aerosol sulfate goes up, so does oxalate: implication for the formation mechanisms of oxalate., Environ. Sci. Technol., 39(1), 128–133, doi:10.1021/es049559f, 2005.

Yu, L., Smith, J., Laskin, a., Anastasio, C., Laskin, J. and Zhang, Q.: Chemical characterization of SOA formed from aqueous-phase reactions of phenols with the triplet excited state of carbonyl and hydroxyl radical, Atmos. Chem. Phys., 14(24), 13801–13816, doi:10.5194/acp-14-13801-2014, 2014.

Zepp, R. G., Hoigné, J. and Bader, H.: Nitrate-Induced Photooxidation of Trace Organic Chemicals in Water, J. Chem. Inf. Model., 53(5), 160, doi:10.1017/CBO9781107415324.004, 1989.

Zhang, R., Cao, X., Liu, Y. and Chang, X.: Development of a simple cataluminescence sensor system for detecting and discriminating volatile organic compounds at different concentrations., Anal. Chem., 85(8), 3802–6, doi:10.1021/ac400208k, 2013.

Zhang, S.-P., Xie, S.-P., Liu, Q.-Y., Yang, Y.-Q., Wang, X.-G. and Ren, Z.-P.: Seasonal Variations of Yellow Sea Fog: Observations and Mechanisms, J. Clim., 22(24), 6758–6772, doi:10.1175/2009JCLI2806.1, 2009.

Zhang, W., Xiao, X., An, T. and Song, Z.: Kinetics, degradation pathway and reaction mechanism of advanced oxidation of 4-nitrophenol in water by a UV/H2O2 process, J. Chem. Technol. Biotechnol., 794(April), 788–794, doi:10.1002/jctb.864, 2003.

Zhao, Y., Hallar, a. G. and Mazzoleni, L. R.: Atmospheric organic matter in clouds: exact masses and molecular

formula identification using ultrahigh-resolution FT-ICR mass spectrometry, Atmos. Chem. Phys., 13(24), 12343–12362, doi:10.5194/acp-13-12343-2013, 2013.

Ziemann, P. J. and Atkinson, R.: Kinetics, products, and mechanisms of secondary organic aerosol formation, Chem. Soc. Rev., 41(19), 6582, doi:10.1039/c2cs35122f, 2012.

Zuo, Y.: Light-induced formation of hydroxyl radicals in fog waters determined by an authentic fog constituent, hydroxymethanesulfonate, Chemosphere, 51(3), 175–179, doi:10.1016/S0045-6535(02)00803-2, 2003.

Zuo, Y. and Hoigné, J.: Formation of hydrogen peroxide and depletion of oxalic acid in atmospheric water by photolysis of iron (III)-oxalato complexes, Environ. Sci. Technol., 26(5), 1014–1022 [online] Available from: http://pubs.acs.org/doi/abs/10.1021/es00029a022 (Accessed 15 August 2013), 1992.

Zuo, Y. and Hoigné, J.: Photochemical decomposition of oxalic, glyoxalic and pyruvic acid catalysed by iron in atmospheric waters, Atmos. Environ., 2(7), 1231–1239, doi:10.1016/1352-2310(94)90270-4, 1994.

2. FOG COMPOSITION AT BAENGNYEONG ISLAND IN THE EASTERN YELLOW SEA: DETECTING MARKERS OF AQUEOUS ATMOSPHERIC OXIDATION REACTIONS*

Samples of fog water were collected at Baengnyeong Island (BYI) in the Yellow Sea during the summer of 2014. The most abundant chemical species in the fog water were NH_4^+ (mean of 2220 μM), NO_3^- (1260 μM), SO_4^{2-} (730 μM), and Na^+ (551 μM), with substantial contributions from other species consistent with marine and biomass burning influence on some dates. The pH of the samples ranged between 3.48 and 5.00, with a mean of 3.94, intermediate within pH values of fog/cloud water reported previously in Southeast Asia. Back trajectories (72 hr) showed that high relative humidity (>80%) was encountered upwind of the sampling site by all but one of the sampled air masses, and that the fog composition at BYI can be impacted by several different source regions, including the Sea of Japan, southeastern China, northeastern China, and the East China Sea. Sulfur in the collected fog was highly oxidized: low S(IV) concentrations were measured (mean of 2.36 μM) in contrast to SO_4^{2-} and in contrast to fog/cloud S(IV) concentrations from pollutant source regions; organic sulfur species were also observed and were most likely formed through aging of mainly biogenic volatile organic compounds. LMM carboxylic acids were major contributors to total organic carbon (TOC; 36–69%), comprising a fraction of TOC at the upper end of that seen in fogs and clouds in other polluted environments. Large contributions were observed from not only acetic and formic acids but also oxalic, succinic, maleic, and other carboxylic acids that can be produced in aqueous atmospheric organic processing (AAOP) reactions. These samples of East Asian fog water containing highly oxidized components represent fog downwind of pollutant sources and can provide new insight into the fate of regional emissions. In particular, these samples demonstrate the result of extensive photochemical aging during multiday transport, including oxidation within wet aerosols and fogs.

2.1 Introduction

The chemistry of the atmosphere occurs within multiple phases, one of which is the aqueous phase. Atmospheric water includes fog droplets, cloud droplets, and wet aerosol particles, all of which can act as miniature aqueous

* Reprinted from original publication: Boris, A.J., Lee, T., Park, T., Choi, J., Seo, S.J., Collett, J.L., 2016. Fog composition at Baengnyeong Island in the eastern Yellow Sea: detecting markers of aqueous atmospheric oxidations. Atmos. Chem. Phys. 16, 437–453.

reaction vessels. Distinct chemical phenomena occur within the atmospheric aqueous phase: formation of organic hydrates and protonation/deprotonation occur frequently, time spent by reactants in proximity to one another increases, and interactions involving metals such as the Fenton reactions and iron oxalate complexes are possible (Lelieveld and Crutzen, 1991; Zuo and Hoigné, 1994). The study of carbonaceous species is particularly pertinent to understanding particle-, gas-, and aqueous-phase atmospheric processes because the composition and formation of organics are complex. Particle-phase organics in particular cannot yet be modeled well by laboratory or computer experiments (Aiken et al., 2008; Chen et al., 2015; Heald et al., 2010, 2005) and can account for a large fraction of aerosol mass (Fu et al., 2008; Lin et al., 2014; Liu et al., 2012). Uptake of organic components into atmospheric water represents a pathway for their removal from the atmosphere, via deposition and/or chemical degradation (Collett et al., 2008). Aqueous atmospheric organic processing (AAOP) can yield low molecular mass (LMM) products with typically increased volatilities, effectively reducing pollutant concentrations in an air mass via chemical water treatment (Brinkmann et al., 2003; Zhang et al., 2003). Some reactions of organic material within atmospheric water form aqueous secondary organic aerosol (aqSOA) by oxidation of dissolved organic precursors to form lower-volatility products that remain in the particle phase as fog drops evaporate (Ervens et al., 2011).

The most common approach to studying AAOP reactions in the lab is to introduce $^{\bullet}OH$ oxidant into a bulk solution of a standard carbonaceous "precursor" molecule such as glyoxal and monitor the reaction as it proceeds (Lim et al., 2010). Some assumptions of this common type of simulation can also be studied within a lab: for example, real cloud water constituents have been shown to cause an effective kinetic slowing, via oxidant competition, of a given organic chemical reaction (Boris et al., 2014). However, while these commonly applied lab simulations are useful for studying specific AAOP reactions, more accurate representations of fogs and clouds are needed to validate simulation results and elucidate more complex phenomena. Daumit et al., (2014) demonstrated that microphysical dynamics of in-droplet diffusion and bidirectional air–water mass transfer are inaccurate in simple "bulk reactions": carrying out a reaction within a photoreactor does not allow species, including oxidants, to continuously partition into and out of solution, as in the real atmosphere (Ervens et al., 2003). Bulk photoreactions also do not correctly simulate differences in chemical constituents between droplets within a cloud (Bator and Collett, 1997; Collett et al., 1994), gradients inside individual droplets (Ervens et al., 2014), or physical processes of fogs and clouds such as evaporation and deposition (Collett et al., 2008; Herckes et al., 2002a; Pandis et al., 1990).

Unequivocal evidence of AAOP reactions within the real atmosphere is challenging to show because no specific molecular or physical tracers for AAOP have been identified. Known products of aqueous oxidation reactions including oxalic acid and SO_4^{3-} are frequently used as non-specific molecular tracers. Successful approaches toward identifying the location and timing of AAOP reactions have included the use of coincident non-specific molecular tracers such as carboxylic acids (Sorooshian and Varutbangkul, 2006; Sorooshian et al., 2013), the predominance of oxalic acid and SO_4^{2-} in a size mode generated from aqueous processes (the droplet size mode, Crahan et al., 2004), and high carbon oxidation states (Chen et al., 2015). Additional observations of AAOP evidence have been summarized by Blando and Turpin (2000) and Ervens et al. (2011). Although oxalic acid in particular has been used as a molecular tracer for AAOP reactions (Sorooshian and Varutbangkul, 2006; Wonaschuetz et al., 2012; Yu et al., 2005), other sources for oxalic acid in the atmosphere have been proposed: gas-phase oxidation of aromatic and anthropogenic molecules (Borrás and Tortajada-Genaro, 2012; Edney et al., 2000; Kalberer et al., 2000; Kamens et al., 2011; Kleindienst et al., 1999), diesel exhaust emissions (Kawamura and Kaplan, 1987), and forest fire emissions (Narukawa and Kawamura, 1999; Yamasoe et al., 2000).

High aerosol concentrations near major cities in China have been attributed in large part to secondary aerosol formation processes from various sources of carbonaceous emissions (Bian et al., 2014; Zhang et al., 2005). Cloud water collected on Mount Tai in Shandong Province (west of the Yellow Sea) contained some of the highest total organic carbon (TOC) concentrations measured in the world (Herckes et al., 2013; Shen et al., 2012; Wang et al., 2011), consistent with strong regional organic pollutant sources, including agricultural burning (Desyaterik et al., 2013). AAOP reactions could produce measurable quantities of aqSOA and LMM carboxylic acids during atmospheric transport of chemicals, especially at high concentrations and within humid environments as observed in Southeast Asia. Anthropogenic emissions from mainland China and Korea frequently impact remote sites around the Yellow Sea (Kim et al., 2011). Oxygenated organic species observed within atmospheric water and aerosol samples at coastal sites in South Korea (Decesari et al., 2005; Lee et al., 2015) are evidence for AAOP reactions occurring in this part of the world.

Fog water was collected at BYI to characterize the composition of fog formed in aged air masses intercepted in the eastern Yellow Sea. Frequent sea fog events are observed at BYI, particularly during the late spring and early summer (Cho et al., 2000; Zhang et al., 2009). In addition to gathering new information about the composition of fogs in this little-studied region, chemical measurements discussed herein helped to determine whether AAOP

reactions occurred at BYI, either within the fog or upwind of the sampling site within cloud droplets/wet aerosol particles. Specifically, it was hypothesized that highly oxidized sulfur and oxidized organics (*e.g.,* LMM carboxylic acids such as oxalic acid) would be measured within the fog water, indicating that AAOP reactions had occurred.

2.2 Methods

2.2.1 Study Overview

Fog water was collected from 29 June through 21 July 2014 on BYI at an established atmospheric research center (ARC) run by the Korean National Institute for Environmental Research (NIER; 37°58'0" N, 124°37'4" E). The collection site was approximately 100 m above sea level (Yoo et al., 2010; Zhang et al., 2009) and was collocated with a meteorological station and an international Interagency Monitoring of Protected Visual Environments (IMPROVE) network site. Meteorological data were accessed online (http://rp5.ru/Weather_archive_on_Baengnyeong_Island). The ARC is on the northwest corner of the island; to the east and south are local agricultural sources of emissions and small towns that are home to approximately 4000 total permanent residents. Regular transport of air masses from eastern China and mainland South Korea were expected to provide a high loading of pollutants to the island (Kim et al., 2006), and frequent haze events were indeed encountered during the study. Three-day (72 hr) back trajectories generated using the NOAA HySPLIT model (online version: http://ready.arl. noaa.gov/HYSPLIT.php; 0.5° global GDAS archived meteorological data) were used to determine the upwind histories of air masses sampled during fog events. The model was initiated using the coordinates of the research station, a height of 100 m, and the approximate beginning time of each fog event. Latitude, longitude, and air mass relative humidity (RH) as estimated by the model were outputted at each 1 hr interval. Periods during which large-scale fires may have impacted fog samples were detected using MODIS archived graphics retrieved from the Naval Research Lab 7 SEAS Data Repository (http://www.nrlmry.navy.mil/aerosol-bin/ 7seas/view_7seas_by_date_t.cgi) and NASA FIRMS (produced by the University of Maryland and provided by NASA FIRMS operated by NASA/GSFC/ESDIS; https://earthdata. nasa.gov/active-fire-data-tab-content-6).

2.2.2 Fog Collection and Handling

A size-fractionating Caltech Active Strand Cloudwater Collector (sf-CASCC; Demoz et al., 1996) was used to collect small and large fog droplets (diameters predominantly 4–16 and <16 μm, respectively). The sf-CASCC is a

polycarbonate structure outfitted with a fan at the rear to pull droplet-laden air into the body of the collector (at 19 m^3 min^{-1}). Droplets were impacted onto rows of forward-tilted Teflon rods and strands and pulled by gravity and aerodynamic drag into Teflon sampling troughs at the bottom of the collector. Fog water was collected for durations of 1 to 3 hr; four events (1, 2, 5, and 18 July) were long enough for collection of multiple fog samples. A Gerber Particulate Volume Monitor (PVM-100; Gerber, 1991) was used to determine the liquid water content (LWC) of the atmosphere during the study; an approximate threshold of 30 mg m^{-3} was used to initiate fog sampling. When fog was not present, the sf-CASCC inlet and outlet were covered to prevent collection of contaminants onto the inner surfaces of the collector. The sf-CASCC was cleaned after each fog event: a high-power sprayer was used to rinse deionized water (approx. 2-3 L) through the collector body. Field blanks were collected after each cleaning, and were stored and analyzed in the same manner as samples. Limits of detection (LODs) were calculated using these blanks and are tabulated in Table 2-1.

Table 2-1. Mean, minimum, and maximum concentrations of species quantified in fog samples collected at BYI.

			Aqueous Concentration				Uncertainty	Air Equivalent Concentration	
Chemical	Unit	Samples	Mean	Min	Max	LOD	(95% CI)	Mean	Unit
pH	--	11	3.94	3.48	5	--	--	11.8	nmol m^{-3}
NH_4^+	µM	13	2220	253	6090	7.41	4	97.8	nmol m^{-3}
NO_3^-	µM	13	1260	185	4900	0.34	10	49	nmol m^{-3}
SO_4^{2-}	µM	13	730	72	2270	7.16	0.4	26.6	nmol m^{-3}
Na^+	µM	13	551	24	2920	2.06	2	7.55	nmol m^{-3}
Cl^-	µM	13	253	22	900	0.76	3	9.29	nmol m^{-3}
K^+	µM	13	83	16	172	0.7	2	3.17	nmol m^{-3}
Ca^{2+}	µM	13	77	12	217	0.22	1	3.23	nmol m^{-3}
Mg^{2+}	µM	13	73	13	276	0.54	1	2.53	nmol m^{-3}
Peroxides	µM	11	7.8	0.4	58.9	0.17	0.2	0.45	nmol m^{-3}
S(IV)	µM	11	2.36	0.25	6.27	0.18	0.001	0.12	nmol m^{-3}
NO_2^-	µM	13	2.1	0.3	5.6	0.05	0.9	0.18	nmol m^{-3}
TOC	mg C L^{-1}	8	17	4.66	24.8	0.26	0.03	413	ng C m^{-3}
Acetate	µM	11	138	19.3	640	2.36	0.007	4.77	nmol m^{-3}
Formate	µM	11	120	1.77	532	1.47	0.05	8.47	nmol m^{-3}
Oxalate	µM	11	41.5	5.86	110	1.47	0.03	1.99	nmol m^{-3}
Succinate	µM	11	22.9	3.31	52.6	0.74	0.002	1.29	nmol m^{-3}
Maleate	µM	11	21.1	3.04	58.8	0.29	0.02	0.72	nmol m^{-3}
Malonate	µM	11	10.7	1.48	24.8	0.45	0.002	0.46	nmol m^{-3}
Pyruvate	µM	11	9.19	0.79	38.8	0.23	0.02	0.48	nmol m^{-3}
MSA	µM	11	7.75	1.77	18.6	0.18	0.009	0.3	nmol m^{-3}
HCHO	µM	10	7	3	21	4.81	2	0.65	nmol m^{-3}
Glutarate	µM	11	6.5	0.92	18.3	0.66	0.02	0.3	nmol m^{-3}
Valerate	µM	11	1.03	0.21	3.78	0.06	0.004	0.11	nmol m^{-3}
Propionate	µM	11	0.88	0.35	1.36	0.06	0.004	0.11	nmol m^{-3}
Adipate	µM	11	0.09	*<LOD*	0.24	0.006	0.04	0.01	nmol m^{-3}
Salicylate	µM	11	0.06	0.001	0.15	0.0003	0.04	0.006	nmol m^{-3}
Benzoate	µM	11	0.06	*<LOD*	0.15	0.002	0.02	0.005	nmol m^{-3}
Pinate	µM	11	0.009	*<LOD*	0.03	0.001	0.01	0.0005	nmol m^{-3}
Azelate	µM	11	0.02	*<LOD*	0.09	0.001	0.03	0.0009	nmol m^{-3}
All Carboxylic acids	µM	11	379	138	1000	--	--	19	nmol m^{-3}

Deep cleanings were also performed periodically by removing the Teflon strands, rods, and troughs from the body of the sf-CASCC and scrubbing all surfaces with Triton X-100 detergent, then thoroughly rinsing all surfaces with deionized water. Collected fog water was refrigerated for a short period of time (<3 hr) prior to separation into aliquots for specific chemical analyses.

Contamination from Triton X-100 detergent in the fog water samples between 14 and 19 July and (seven samples) was discovered by positive ionization HR-ToF-MS analysis. TOC concentrations are not reported for the affected samples; however, duplicate analyses of standards of inorganic ions and carboxylic acids containing Triton X-100 were not different from uncontaminated standards. Peroxides, formaldehyde, and S(IV) were also assumed to be unaffected by the contamination.

Deionized water used in analyses and sample collection at BYI was obtained from a distillation and ion exchange–UV light purification system at the ARC. The calculated charge balance and sample volume were used to determine whether measurements made from a given fog sample were accurate and should be included in results (most samples not containing balanced ionic charges consisted of small liquid volumes). If charge balance, which

included all organic and inorganic ionic species, was not within 1.0±0.3 (positive/negative charge), that sample was not included (4 of 17 samples were excluded). Directly after sample collection, liquid water from samples with only small collected volumes was dispensed to aliquots according to volume needed and importance of analysis to the study purpose; therefore, in some cases, only some analyses could be carried out for a given sample. For those samples with insufficient volumes (<2 mL) of the small droplet fraction due to a predominance of large droplets in the sampled fog, the large droplet fraction was assumed to be representative of the entire fog water sample in data analyses. Chemical and physical interactions differ between droplet sizes, and the collection of different sizes of droplets helps preserve real differences in drop composition as compared to bulk fog sampling (Hoag et al., 1999; Moore et al., 2004; Reilly et al., 2001). Mean fog constituent concentrations were calculated from the two droplet fractions (e.g., [(small drop sample volume × small sample concentration) + (large drop volume × large drop concentration)]/total sample volume); mean, median, maximum, and minimum values calculated over the size fraction weighted values of all samples were used in further discussion of the fog chemical composition. Air equivalent concentrations (also referred to as loadings) were calculated from molar concentrations in water to establish trends in fog water constituents independent (or less dependent) of the amount of liquid water present during a given fog event. Equation 2-1 was used, where *i* represents a given chemical constituent of interest.

$$\frac{\text{nmol } i}{\text{m}^3 \text{ air}} \times \frac{\mu\text{mol } i}{\text{L sample}} \times \frac{\text{L}}{1000 \text{ mL}} \times \frac{\text{mL}}{1.00 \text{ g}} \times \text{mass sampled (g)} \times \frac{\text{hr}}{\text{m}^3 \text{ air}} \times \frac{1}{\text{time sampled (hr)}} \times \frac{1000 \text{ nmol } i}{\mu\text{mol } i} \qquad \text{Equation 2-1}$$

The collection rate of the sf-CASCC was assumed to be 19.0 m^3 air min^{-1} (Demoz et al., 1996) and the density of water was assumed to be 1.00 g mL^{-1}.

2.2.3 Fog Water Analysis

Samples were each weighed and divided into aliquots for analyses, and remaining fog water was stored frozen in Nalgene wide-mouth HDPE plastic bottles (also used for collection). Measurement of fog water pH was carried out at the BYI ARC using a Cole-Parmer microelectrode and pH meter, calibrated with pH 4 and 7 buffers. The mean of three replicate measurements was recorded for each sample. Preservation of other aliquots for chemical analyses (as performed previously; *e.g.,* Benedict et al., 2012) was as follows: peroxides were preserved with parahydroxyphenylacetic acid (POPHA) and ethylenediaminetetraacetic acid (EDTA), S(IV) was stabilized using formaldehyde and trans-1,2-cyclohexylenedinitrilotetraacetic acid (CDTA) and bovine catalase enzyme was added to eliminate hydrogen peroxide, formaldehyde was preserved with Na_2SO_3 and CDTA, samples for analysis of

major ionic species (Cl^-, NO_2^- , NO_3^-, SO_4^{2-}, Na^+, NH_4^+, K^+, Mg^{2+}, Ca^{2+}) were aliquoted without added reagents, and microbial activity was eliminated for the storage of carboxylic acids and other organic components by addition of chloroform. Aliquots for TOC and carbohydrates (including levoglucosan) analysis were taken from thawed samples after arrival at Colorado State University (CSU). Additional organic molecules were identified and/or quantified via high-performance liquid chromatography (HPLC) followed by negative electrospray ionization high-resolution time-of-flight mass spectrometry ((-)-ESI- HR-ToF-MS) from the aliquot preserved for carboxylic acids analysis. Levoglucosan and other carbohydrates were measured using high-performance anion exchange chromatography with pulsed amperometric detection (HPAEC-PAD) as described previously (Sullivan et al., 2008) from frozen remaining fog water samples; only some samples were analyzed for carbohydrates.

2.3 Results and Discussion

Fog water was collected during nine fog events (17 total samples) at the BYI ARC during July 2014; seven events and 13 samples were included in mean chemical concentrations calculated over the duration of the sampling campaign and will be discussed here (Figure 2-1).

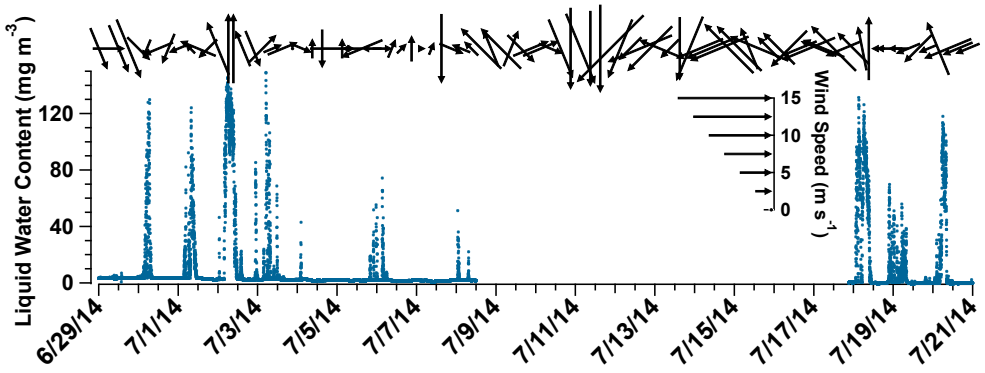

Figure 2-1. Wind speed and direction during fog sampling period, shown as vector arrows (top): speed is displayed as the length of each arrow and direction is displayed as tilt, pointing away from wind origin. LWC measured during the entire study period is shown in blue along the bottom of the plot. Fog was not collected in mid- July during the monsoonal period.

Events on 2 and 18 July persisted for several hours, allowing collection of up to five samples per event. Air masses sampled during the seven fog events traveled either from the south over the Yellow Sea as documented in Zhang et al., (2009), from the west over eastern China, from the east over the Sea of Japan, or from the north over northeastern China (Figure 2-2).

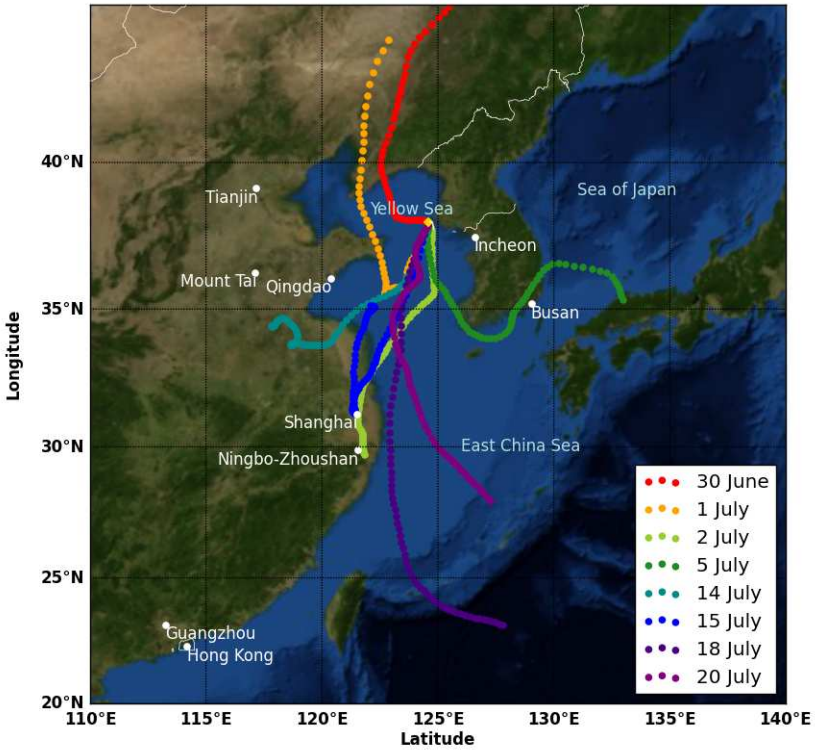

Figure 2-2. Back trajectories of air masses intercepted during fog events (72 hr at 1 h time resolution; HySPLIT). Locations labeled on plot include Mount Tai, where previous atmospheric water chemical measurements were made, and the highest throughput shipping ports in the region pictured. The BYI ARC is shown as a gold diamond. Sectors were defined to determine whether particular source regions existed for chemical constituents of the fog: northerly (30 June and 1 July), westerly (2, 14, and 15 July), southerly (18 and 20 July), and easterly (5 July). Each trajectory was initiated at the approximate beginning of a fog event. Imagery from NASA Blue Marble; plot generated using Python Matplotlib Toolkit BaseMap.

2.3.1 Fog Characteristics and Major Contributing Species

A moderately acidic pH was observed (study mean 3.94, ranging between 3.48 and 5.00). This value is intermediate between values measured in fog and cloud samples from Southeast Asia (Mount Tai: pH 3.68, Wang et al., 2011; Jeju Island, Korea: pH 5.2, Kim et al., 2006; Daekwanreung, Korea: pH 4.7, Kim et al., 2006; and Shanghai, China: pH 5.97, Li et al., 2011). Major inorganic species contributing to the measured acidity of the fog water at BYI (Table 2-1; Figure 2-3) were NH_4^+ (mean concentration of 2220 µM), followed by NO_3^- (1260 µM) and SO_4^{2-} (730 µM); these concentrations were elevated compared to fog and cloud samples collected globally (e.g., Collett et al., 2002; Raja et al., 2008; Wang et al., 2011).

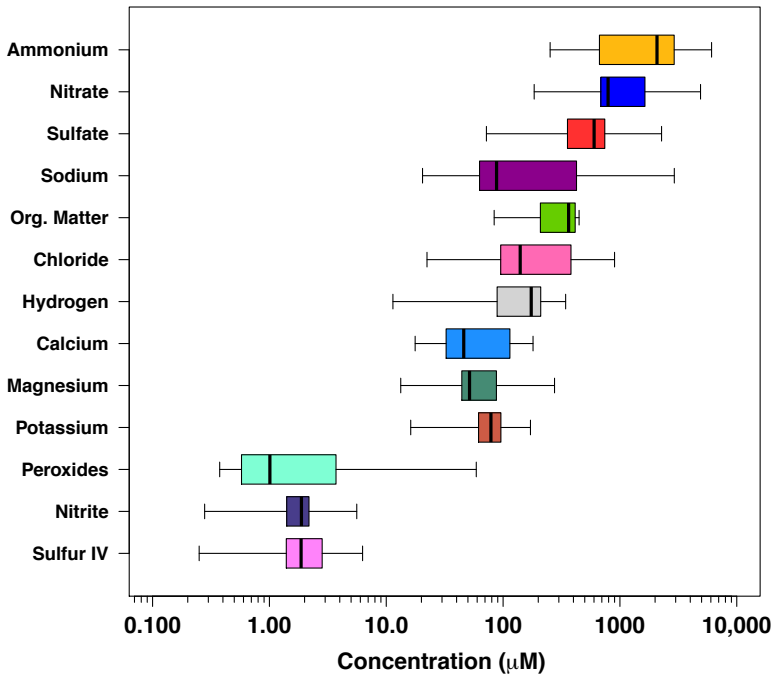

Figure 2-3. Concentrations of major components quantified in BYI fog samples. Boxes show 25th and 75th percentiles with the median bar in the center, and whiskers show outliers. Total organic matter was calculated from measured TOC using a ratio of 1.8 g/1.0 g OM/OC (Zhang et al., 2005) and an estimated mean molecular mass of 100 g mol^{-1}. Note that for most ions, *n*=13; for pH, S(IV), and peroxides, *n*=11; for formaldehyde, *n*=10; and for total organic matter, *n*=7.

Sea salt was also an abundant constituent of the fog water (mean concentrations of 551 μM Na^+ and 253 μM Cl^-), as was organic matter (mean 276 μM, estimated using a molecular mass of 100 g mol^{-1} and OM/OC=1.8, Zhang et al., 2005). The mean NH_4^+ concentration measured at BYI was within the upper range of measured NH_4^+ in fog and cloud samples (similar to, for example, the Po Valley, Italy, Fuzzi et al., 1992, and Baton Rouge, Louisiana; Raja et al., 2008). Although agriculture was a main land use on BYI, no correlation between wind direction and fog NH_4^+ concentrations was observed (Figure A2-1), suggesting long-range transport of fine particle NH_4^+ as an important source. The concentrations of Ca^{2+} (mean 77 μM) were within the range of previous studies in other, remote parts of the world (Benedict et al., 2012; Munger et al., 1989), indicating that inputs to fog water chemistry by mineral dust were likely unimportant during the study period (Arimoto et al., 2004; Kawamura et al., 2004; Mattigod et al., 1990).

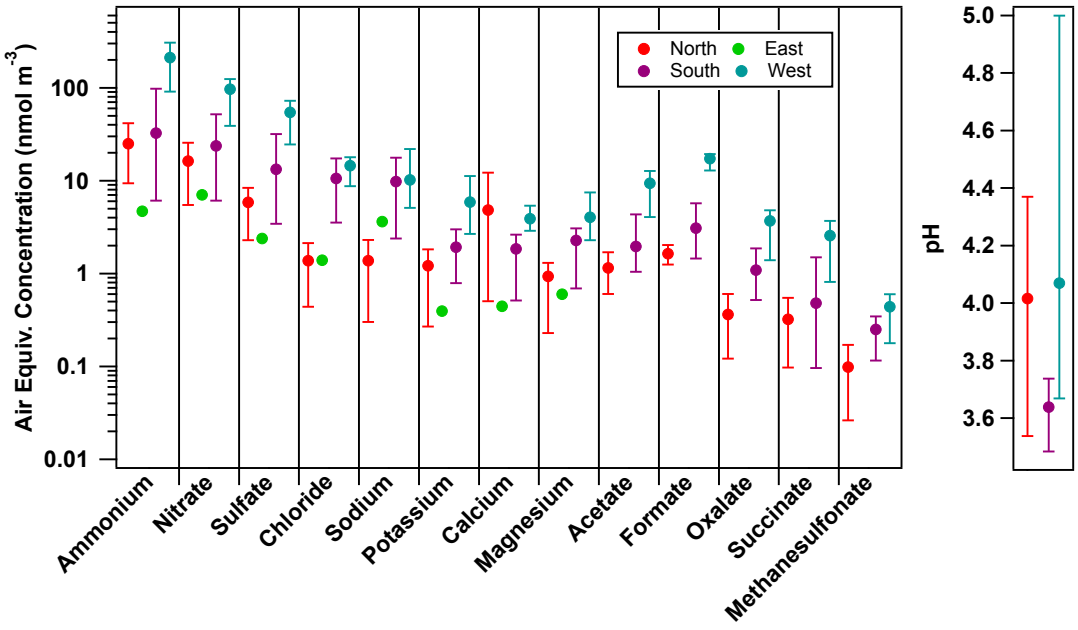

Figure 2-4. Sector analysis of most abundant inorganic fog water components, as well as selected carboxylic acids. Highest concentrations of most species originated from the west. For Na^+ and Cl^-, high concentrations were also observed from the south. Ca^{2+} concentrations were also heightened within samples with northerly trajectories, which may suggest a continental dust source. In agreement with high measured NH_4^+ concentrations, pH was highest from the west. Note that samples were low in volume in some cases so that pH analyses were not performed. For inorganic species except pH, n=1 easterly, n=3 northerly, n=4 southerly, and n=5 for westerly trajectories. For organic species and pH, n=0 easterly, n=2 northerly, n=3 southerly, and n=4 westerly.

Concentrations of nearly all species were highest in samples with westerly back trajectories (Figure 2-4). Anthropogenic influence was likely greatest from this sector because of the large number of urban areas and major industry in Shandong Province and surrounding regions (Cao et al., 2006). The lowest concentrations of most species originated from the east (note that only one sample included in the analyses originated from the east). The only exceptions were Na^+, from the north, and H^+, which was least abundant from the west due to the contribution of NH_4^+ to fog acidity.

2.3.2 Marine Source Contribution

Evidence of a marine contribution to fog composition was clear. Upwind trajectories of all air masses sampled included some duration over the Yellow Sea, and in some cases the Sea of Japan (Figure 2-2). Measured Ca^{2+} was contributed in part by sea salt particle scavenging: 21% was attributed to sea salt (Figure A2-2) using an observed ratio in seawater of 0.022 mol Ca^{2+}/mol Na^+ (Lee, 2007; Radojevic and Bashkin, 2006). Depletion of particle-phase Cl^- appears to have occurred in some scavenged sea salt particles, likely due to displacement of HCl to the gas phase by NO_3^- and SO_4^{2-} (Mouri and Okada, 1993) or carboxylic acids (Wang et al., 2015). Measured Cl^-/Na^+ molar ratios

ranged as low as 0.08, with a mean value of 1.20; this mean value is within measurement error (Table 2-1) of the typical sea salt ratio of 1.16 (Radojevic and Bashkin, 2006). In some samples, the Cl^- concentration was in excess of the sea salt ratio, indicating possible contributions from other sources such as incineration or coal combustion (McCulloch et al., 1999). Small contributions of K^+ (study mean 83 µM) and SO_4^{2-} were estimated to derive from scavenged sea salt particles: only 12% of the measured K^+ and 6% of the SO_4^{2-} were attributed to a marine source on average. This estimate of nss-SO_4^{2-} does not account for SO_4^{2-} formed via oxidation of biogenic, marine dimethyl sulfide, which could be as much as 12% (Yang et al., 2009). Elevated concentrations of cations including K^+ in aerosol have also been associated with the influence of biomass burning activities (Andreae, 1983; Lee et al., 2010), mineral dust from arid regions (Zhang et al., 1993), and/or construction in urban areas (Li et al., 2011).

2.3.3 Inorganic Sulfur

Aqueous sulfur oxidation in the pH range measured in this study (3.48-5.00) is expected to be dominated by reaction with H_2O_2 (Rao and Collett, 1995). The mean concentrations of total peroxides and S(IV) (7.8 and 2.36 µM, respectively; Table 2-1) were low compared to the mean S(IV) and peroxides concentrations measured during summer 2007 and 2008 field campaigns at Mount Tai, China (Shen et al., 2012), consistent with a low potential for additional S(IV) oxidation within the BYI fog samples (Figure 2-5).

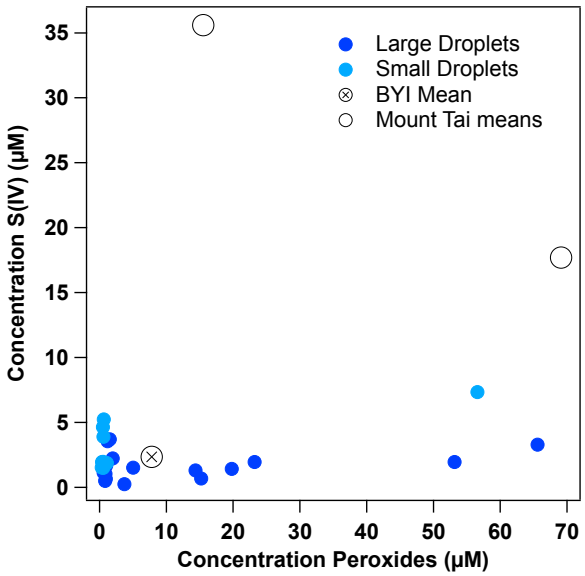

Figure 2-5. Droplet size-segregated concentrations of S(IV) and peroxides quantified in BYI fog samples. S(IV) concentrations were low in BYI fog as compared to those measured at Mount Tai (summer 2007 and 2008; Shen et al., 2012). For both, *n*=11.

Since Mount Tai is located west across the Yellow Sea from BYI and is influenced by the abundant SO_2 sources in Shandong Province, including large numbers of coal-fired power plants, these observations are consistent with extensive aging of S(IV) during transport to the BYI fog collection site. In contrast to BYI measurements, cloud samples from remote areas contain high concentrations of peroxides and low concentrations of S(IV) (1.9–610 μM peroxides, <0.91–3.7 μM S(IV); Benedict et al., 2012; Straub et al., 2007). Measured SO_4^{2-} was abundant within BYI samples, demonstrating that sources of atmospheric sulfur existed upwind, and that oxidation of sulfur occurred prior to arrival at BYI. Between 98.9 and 99.8% of sulfur measured (as the sum of SO_4^{2-} and S(IV)) was in the form of SO_4^{2-}. International shipping lanes could also contribute to the measured SO_4^{2-} concentrations in BYI fog: some of the world's largest shipping ports are located in the Yellow Sea (Streets et al., 2000). The contribution of fine particle (<1μm diameter) SO_4^{2-} has been estimated at ≤15% from ship oil combustion in this region (Lauer et al., 2007), and shipping routes in the Yellow Sea have been identified as major SO_2 source regions (Kang et al., 2006). Shipping emissions have also been associated with elevated concentrations of other atmospheric constituents, including NO_3^- (Prabhakar et al., 2014). Methanesulfonic acid (MSA) was also observed within all fog samples collected at BYI, indicating that oxidation of marine emissions via either $^{\bullet}OH$ or $^{\bullet}NO_3$ reaction occurred upwind of fog collection at BYI (Kukui et al., 2003; Scaduto, 1995; Seinfeld and Pandis, 2006).

2.3.4 Total Organic Carbon

Concentrations of fog water TOC measured at BYI were 4.66-24.8 mg C L^{-1}, with a mean of 17.0 mg C L^{-1}, comparable to concentrations measured in polluted environments globally (Herckes et al., 2013). Although the mean BYI TOC was also similar to that measured in cloud water from Mount Tai during the summer of 2008 (15.8 mg C L^{-1}), several samples impacted by agricultural burning were collected during the latter campaign ranging between 100 and 200 mg C L^{-1} (Shen, 2011).

2.3.5 Carboxylic Acids

The products of AAOP reactions commonly include C_2-C_4 (two to four carbon) oxo- and di-carboxylic acid molecules (Lim et al., 2010). The percent BYI fog TOC accounted for by carboxylic acids was 36–69% (mean 52% by mole; *n*=6), which is at the upper end of values typical for fog samples (e.g., 16% at Davis, CA, Herckes et al., 2002b; 18% at Angiola, CA, Ervens et al., 2003; 43% at Fresno, CA, Collett et al., 2008; and 44% at Baton Rouge, LA, and 51% at Houston, TX, Raja et al., 2008). Among the carboxylic acids quantified, major contributions to

TOC came not only from acetate and formate but also succinate, maleate and oxalate, with lesser but substantial contributions from other acids (Figure 2-6).

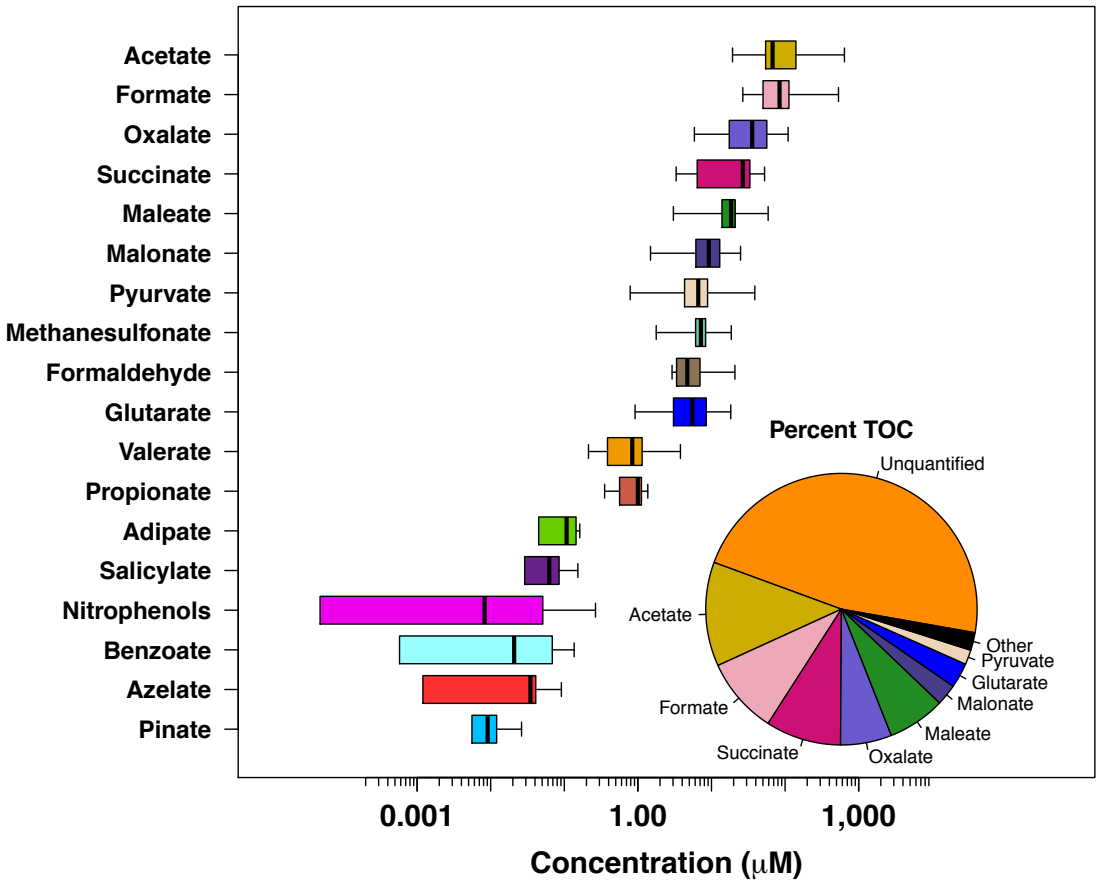

Figure 2-6. Concentrations of major carbonaceous components quantified in BYI fog samples. Box-and-whisker plot shows 25th and 75th percentiles with the median bar in the center, and whiskers at the min and max. Note that for C_1-C_5 carboxylic acids, n=11; for formaldehyde, n=10; and for components with C_6 or greater, n=11. Pie chart (inset) shows carbonaceous composition as a percentage of TOC (only those samples with results from all organic analyses included, n=6).

Concentrations of LMM carboxylic acids were strongly correlated with one another (air equivalent concentrations): r^2=0.83 on average, with probability $p \leq 0.01$ of random correlation, ranging from 0.47 to 0.99 ($p \leq 0.001$ to 0.2) for C_1–C_6 mono- and di-carboxylic acids. The predominance of succinate suggests a major anthropogenic source of carboxylic acids at BYI (Kawamura and Ikushima, 1993). While substantial contributions of oxalate to TOC suggest that AAOP reactions took place, they are not unequivocal evidence of it, since other atmospheric sources for oxalate have been documented (e.g., Kawamura and Kaplan, 1987; Yamasoe et al., 2000). The presence of MSA in the observed samples and its correlation with other measured carboxylic acids ($r^2 \leq 0.7$ and

$p \leq 0.02$ with all LMM carboxylic acids, $r^2=0.88$ and $p \leq 0.001$ with oxalate) additionally supports the occurrence of AAOP upwind of fog water collection.

2.3.6 Mass Spectral Analysis

Polar organic components of the fog water with $\geq C_4$ were tentatively identified using HPLC-(-)-ESI-HR-ToF-MS. These compounds were biogenic and anthropogenic in origin, including pinic acid and monoterpene-derived organic sulfur (CHOS) species, and phthalic acid (Table 2-2).

Table 2-2. Chemical formulae and possible structures of organic components identified via HPLC-(-)-ESI-HR-ToF-MS within BYI fog water samples. Formulae with multiple isomers (different retention times) are marked with an asterisk (*). Only species with mass spectral abundances ≥500 abundance units were included.

m/z⁻	Molecular Formula	t_R (min)	O/C	H/C	Possible Identification and References
85.0311	C_4H_6O2	3.182	0.5	0.67	Methacrylic acid
105.034		9.32			
113.027	$C_5H_6O_3$	3.67	0.6	1.2	Oxo-pentenoic acid
117.057	$C_5H_{10}O_3$	4.54	0.6	2	Hydroxy-pentanoic acid*
117.057	$C_5H_{10}O_3$	3.43	0.6	2	Hydroxy-pentanoic acid*
121.031	$C_7H_6O_2$	9.82	0.29	0.86	Hydroxy-benzaldehyde
127.042	$C_6H_8O_3$	5.79	0.5	1.3	Oxo-hexeneoic acid
129.022	$C_5H_6O_4$	3.67	0.8	1.2	Pentenedioic acid*
129.021	$C_5H_6O_4$	3.18	0.8	1.2	Pentenedioic acid*
129.057	$C_6H_{10}O_3$	5.96	0.5	1.7	Methyl-oxo-pentanoic acid*
129.057	$C_6H_{10}O_3$	7	0.5	1.7	Methyl-oxo-pentanoic acid*
131.036	$C_5H_8O_4$	3.18	0.8	1.6	Methyl-succinic acid
131.036	$C_5H_8O_4$	4.34	0.8	1.6	Glutaric acid
131.073	$C_6H_{12}O_3$	9.82	0.5	2	Hydroxy-Hexanoic acid*
131.073	$C_6H_{12}O_3$	7.95	0.5	2	Hydroxy-Hexanoic acid*
137.026	$C_7H_6O_3$	16.17	0.43	0.86	Salicylic acid
138.021	$C_6H_5NO_3$	13.18	0.5	0.83	4-Nitrophenol
143.036	$C_6H_8O_4$	3.18	0.67	1.7	Hexenedioic acid*
143.037	$C_6H_8O_4$	6.86	0.67	1.7	Hexenedioic acid*
143.073	$C_7H_{12}O_3$	11.43	0.43	1.7	Methyl-pentenedioic acid
145.051	$C_6H_{10}O_4$	8.93	0.67	1.7	Methyl-glutaric acid*
145.052	$C_6H_{10}O_4$	7.1	0.67	1.7	Adipic acid
145.052	$C_6H_{10}O_4$	9.52	0.67	1.7	Methyl-glutaric acid*
149.026	$C_8H_6O_3$	9.32	0.38	0.75	Formyl-benzoic acid
152.036	$C_7H_7NO_3$	17.85	0.43	1	Methyl-nitrophenol
152.037	$C_7H_7NO_3$	19.33	0.43	1	2-Methyl-4-nitrophenol
154.016	$C_6H_5NO_4$	10.46	0.67	0.83	Nitroguaiacol
157.052	$C_7H_{10}O_4$	6.32	0.57	1.4	Heptenedioic acid*
157.053	$C_7H_{10}O_4$	5.22	0.57	1.4	Heptenedioic acid*
159.068	$C_7H_{12}O_4$	10.79	0.57	1.7	Pimelic acid
163.042	$C_9H_8O_3$	12.63	0.33	0.89	Previously identified (Desyaterik et al., 2013)
165.021	$C_8H_6O_4$	10.13	0.5	0.75	Phthalic acid
165.021	$C_8H_6O_4$	12.06	0.5	0.75	Benzenedicarboxylic acid
166.053	$C_8H_9NO_3$	23.61	0.38	1.1	Dimethyl-nitrophenol
171.067	$C_8H_{12}O_4$	8.33	0.5	1.5	Octenedioic acid*
171.068	$C_8H_{12}O_4$	6.95	0.5	1.5	Octenedioic acid*
171.983		19.712			
173.047	$C_7H_{10}O_5$	4.22	0.71	1.4	Isoprene photooxidation product (Nguyen et al., 2011)
179.037	$C_9H_8O_4$	15.23	0.44	0.89	Phthalic acid, methyl ester
181.016	$C_8H_6O_5$	5.65	0.63	0.75	Hydroxy-benzene-dicarboxylic acid*
181.016	$C_8H_6O_5$	8.81	0.63	0.75	Hydroxy-benzene-dicarboxylic acid*
181.019	$C_5H_{10}O_5S$	2.82	1	2	Previously identified (Nguyen et al., 2014a)

Dicarboxylic and hydroxy dicarboxylic acids are prominent within the polar organic matter of the BYI fog samples. A van Krevelen diagram (Chen et al., 2015; Heald et al., 2010; Mazzoleni et al., 2010; Noziere et al., 2015)

was used to illustrate the distribution of organic species identified within all fog water samples (CHO, CHNO, CHOS, CHNOS; Figure 2-7), with the objectives of showing groupings of like species within the fog samples, and comparing the fog composition to previously analyzed atmospheric samples.

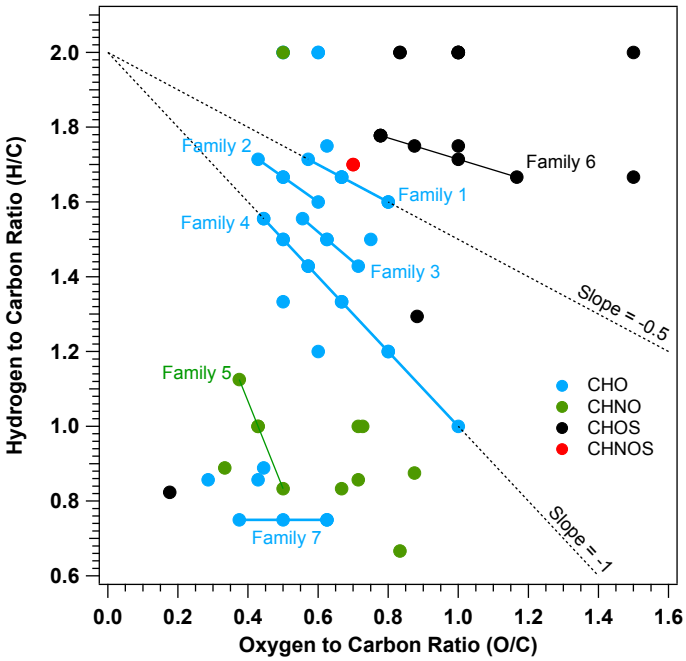

Figure 2-7. Polar organic compounds identified within fog samples using HPLC-(-)-ESI-HR-ToF-MS detection illustrated via a van Krevelen diagram. Colors of points distinguish compound elemental composition; solid lines show families differing by methylene groups of di-carboxylic acids (blue, families 1-4), nitrophenols (green, family 5), and organic S species (black, family 6); aromatic oxygenated species differing by an O atom are also shown (blue, family 7). Dashed lines show slopes typical of samples in previous studies (Chen et al., 2015) of -0.5 for remote/rural (top) and -1 for urban (bottom); carboxylic acid families fit within the space of these previously analyzed atmospheric samples.

Molecules differing by specific, oxygen-containing elemental combinations can be identified in van Krevelen space by slope: *i.e.,* addition of carbonyl (-2H, +1O; slope=-2); carboxylic acid (-2H, +2O; slope = -1); alcohol (or oxidation of an aldehyde to a carboxylic acid group; slope = 0); or water (slope =+2). In BYI fog samples, families of species differing by methylene (CH_2) are visible: (1) saturated di-carboxylic acids (C_5-C_7; slope =-0.5), (2) hydroxy di-carboxylic acids (C_5-C_7; slope=-0.7), (3) hydroxy monounsaturated di-carboxylic acids (C_7-C_9; slope =-0.8), (4) monounsaturated di-carboxylic acids (C_4–C_9; slope =-1), (5) nitrophenols (dimethyl nitrophenol, methyl nitrophenol, and nitrophenol; slope =-2.3), and (6) organic S species ($C_9H_{16}O_7S$ through $C_6H_{10}O_7S$; slope =-0.3). The slopes between points in these families vary because the O content remains constant while the C and H contents differ. A family of phthalate derivatives (7) with differing oxygen contents ($C_8H_6O_3$ through $C_8H_6O_5$; slope = 0) is also visible. Several CHO species were additionally identified as both biogenic and anthropogenic secondary

organic species; for example, 3- methyl-1,2,3-butanetricarboxylic acid (MBTCA) was tentatively identified (m/z^- 203.058 and formula $C_8H_{12}O_6$), as was diaterpenylic acid (m/z^- 189.078; $C_8H_{14}O_5$), which are gas-phase oxidation products of α-pinene (Szmigielski et al., 2007; Yasmeen et al., 2010). Based on a qualitative analysis of mass spectral peak areas, westerly air masses brought the greatest quantities of anthropogenic species to BYI fog water, while the greatest biogenic species quantities were contributed by air masses from the west and east (depending on the constituent; note that only one sample with an easterly back trajectory was available; see Figure A2-5). Mean O/C and H/C of ambient aerosol samples (mass-normalized, from aerosol mass spectrometry; Chen et al., 2015; Heald et al., 2010; Ng et al., 2011) typically fall on a line within van Krevelen space at a slope of -1 and *y*-intercept of 2 for samples with fresh emissions and a slope of -0.5 for rural/remote samples. Within the molecular level analysis employed here, the slopes between -1 and -0.5 appear to correspond to families of carboxylic acids differing by a CH_2 group, with differing levels of unsaturation and/or number of hydroxyl groups. The space within the van Krevelen diagram occupied by these identified families indicates they are chemically similar to aged aerosol from previous studies (Chen et al., 2015) and may be analogous to ring-opened and oxygenated species present within the fragmentation scheme of the atmospheric aging process (Kroll et al., 2009).

2.3.7 Nitrophenols

Four identified nitrophenols were quantified via HPLC-(-)-ESI-HR-ToF-MS (Table A2-4): 4-nitrophenol (20.9±1.8 nM; max 1440 nM), 2-methyl-4-nitrophenol (3.6±0.5 nM; max 40 nM), 2,4-dinitrophenol (20.2±0.1 nM; max 70 nM). Concentrations detected in most previous fog and cloud water field studies were 1–300 nM (Harrison et al., 2005), in the same range as identified in this study. However, the concentrations of 4-nitrophenol measured within cloud water from Mount Tai were as high as 15 μM (Desyaterik et al., 2013). The lower concentrations measured at BYI versus at Mount Tai likely reflect the strong influence of aged biomass burning emissions in the Mount Tai region, and may also be a result of aqueous aging in the samples collected at BYI, since species such as 4-nitrophenol are oxidized by $^{\bullet}OH$ in the aqueous phase (Zhang et al., 2003). Other N-containing species (tentatively identified; Table 2-2) included a second methyl nitrophenol isomer (m/z^- 152.04, $C_7H_7NO_3$), a hydroxy nitrophenol (also called a nitrocatechol; m/z^- 154.02, $C_6H_5NO_4$), a dimethyl nitrophenol (m/z^- 166.05, $C_8H_9NO_3$), and three other oxygenated nitrophenols (m/z^- 228.02, $C_8H_7NO_7$; m/z^- 284.05, $C_{11}H_{11}NO_8$; and m/z^- 361.16, $C_{15}H_{26}N_2O_8$). These N-containing organic species may have originated from biomass burning and/or wildfires in Southeast Asia and eastern Russia during the fog study period. For the three events with quantified fog nitrophenol concentrations above

detection limits, large-scale fires were detected in upwind source regions (MODIS data). Levoglucosan (a biomass burning marker) concentrations measured within fog samples from BYI were below background concentrations measured in aerosol samples (Weber et al., 2007); however, those concentrations measured within the fog from 2 July were high relative to other fog samples (Figure A2-7), and thus may have been impacted by biomass burning emissions. Aqueous solubility of levoglucosan as well as oxidation processes may have affected the concentrations measured in BYI fog samples. Concentrations of the biomass burning marker K^+ were additionally above the study mean on dates when regional fires were detected (Figure A2-6) and a correlation of r^2=0.93 (n=11, $p \leq 0.001$) was observed between nss-K^+ and total quantified nitrophenols as air equivalent concentrations (nmol m^{-3}).

2.3.8 Organic Sulfur Species

CHOS species were identified within BYI fog samples (Table 2-2), some of which have also been found within rainwater (samples collected in urban and rural New Jersey; Altieri et al., 2009). Most organic S species identified were likely from oxidation and sulfation of biogenic emissions, including *m/z*$^-$ 225.01, 253.04, and 267.06 corresponding to $C_6H_{10}O_7S$, $C_8H_{14}O_7S$, and $C_9H_{16}O_7S$, respectively; however, no isoprene-derived organosulfates were detected in the BYI samples (Surratt et al., 2008). Nguyen et al., (2014) observed a compound with the formula $C_8H_{14}O_7S$ in aerosol samples, and Surratt et al., (2008) showed that the source may have been esterification of a *d*-limonene oxidation product with SO_4^{2-} An observed compound at *m/z*$^-$ 239.02 with a formula of $C_7H_{12}O_7S$ was previously identified by Praplan et al., (2014) as an oxidation product of the anthropogenic species 1,3,5-trimethylbenzene. Several pairs of organic S species appear to have originated from loss of a hydroxyl group: for example, *m/z*$^-$ 195.03 and 211.03, corresponding to $C_6H_{12}O_5S$ and $C_6H_{12}O_6S$; the latter species was noted to possibly be formed from the sulfation of a fatty acid (Surratt et al., 2008). CHONS species were also found in the fog samples from BYI, two of which were identified previously as monoterpene oxidation products (Iinuma et al., 2007; Surratt et al., 2008): *m/z*$^-$ 294.07 with formula $C_{10}H_{17}NO_7S$ and *m/z*$^-$ 310.06 with formula $C_{10}H_{17}NO_8S$. A compound with the formula $C_{10}H_{17}NO_7S$ was also identified within Fresno fog samples (Mazzoleni et al., 2010). These species were likely formed via NO addition to monoterpene-derived peroxy radicals (Surratt et al., 2008) or reaction of monoterpenes with $^{\bullet}NO_3$ (Iinuma et al., 2007) in the presence of acidic sulfate.

2.3.9 Atmospheric Aqueous Organic Processing

Many features of the fog water at BYI, including the organic composition and the humid conditions encountered prior to arrival at the collection site, suggest that components in the fog were oxidized in the atmospheric aqueous phase. The oxidation may have occurred in the fogs themselves or during upwind transport of wet aerosol later scavenged by the fog. The RH upwind of fog-producing air masses as they traveled to BYI was high, with only a few time periods at <50%, and mean 65–91% (Figure A2-7). Only the air mass intercepted during the fog event on 30 June did not encounter RH>80% within 72 hr of fog formation at BYI. Mixtures of organic and inorganic components can easily take up water (growth factors ≤1.71 at 85% RH for several carboxylic acids, Wise et al., 2003; and ≤1.16 at 85% RH for chamber-generated secondary organic aerosol (Varutbangkul et al., 2006). It is therefore likely that the aerosol LWC was sufficient to allow radical or even non-radical aqueous reactions to occur upwind of the BYI fog collection site (Lim et al., 2013, 2010). The high abundance and large diversity of carboxylic acids, oxidized S, lack of peroxides, and organic S species identified within fog samples also support the hypothesis that AAOP reactions took place within wetted aerosol particles, in-cloud/fog during transit of the intercepted air masses to BYI, or within the fog at BYI (Lim et al., 2005; McNeill, 2015).

2.3.10 Size and Microphysical Considerations

Changes in LWC, species concentrations, and enrichments of species within large or small droplets can be indicative of many simultaneous microphysical processes: coalescence or condensational growth, evaporation, deposition, and collisions between droplets and interstitial particles (Degefie et al., 2015; Fahey et al., 2005; Seinfeld and Pandis, 2006). Figure 2-8 shows differences in large and small droplet concentrations of abundant chemical constituents in the BYI fog samples collected on the two stages of the sf-CASCC.

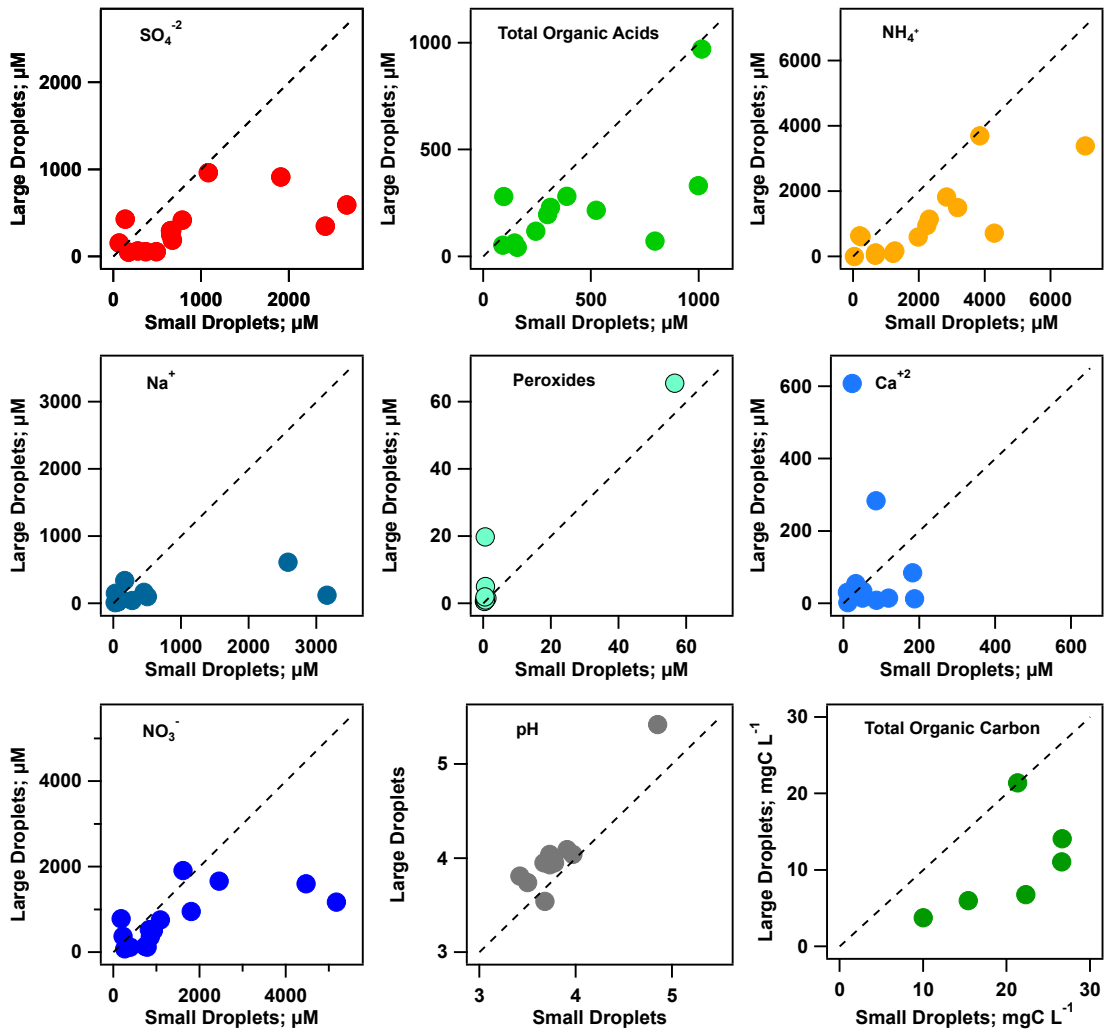

Figure 2-8. Scatter plots showing size distribution of major species in BYI fog water samples. All species shown, with the exception of peroxides, were enriched in small droplets.

Much higher volumes of liquid water were typically collected into the large droplet fraction (>16 µm) than the small droplet fraction (4-16 µm) at BYI; on average, the small fraction comprised only 10% of the total liquid water volume, indicating relatively large fog droplets made up most of the LWC. All species shown are enriched in the small droplet (4-16 µm) size fraction, with the exception of peroxides; similar observations have previously been reported in many clouds and fogs, especially for species typically associated with submicron aerosol, including SO_4^{2-}, NO_3^-, NH_4^+, and TOC (Bator and Collett, 1997; Herckes et al., 2007; Munger et al., 1989). As in most of these prior observations, the pH in large BYI fog droplets was also typically higher than in small droplets. Differences in pH among cloud drops can give rise to differences in the rates of pH-dependent chemical reaction rates, including the aqueous oxidation of S(IV) to SO_4^{2-} by ozone or by oxygen in the presence of trace metal

catalysts (Collett et al., 1994; Hegg and Larson, 1990; Rao and Collett, 1998). Enrichment of solutes in large or small fog drops can also affect rates of removal by fog drop deposition (e.g., Fahey et al., 2005; Herckes et al., 2007; Hoag et al., 1999).

2.4 Conclusions

The fogs at BYI were on average slightly acidic, and the chemical composition was dominated by NH_4NO_3 from long-range transport, with contributions from anthropogenic nss-SO_4^{2-}, marine NaCl, and a variety of organic compounds. Biomass burning activities throughout eastern Russia and Southeast Asia appear to have contributed K^+ and organic species, including nitrophenols, in some periods. Organic S species deriving from oxidation products of monoterpenes (e.g., Nguyen et al., 2014; Surratt et al., 2008) were tentatively observed, several of which have been identified in aqueous atmospheric samples in the past (Altieri et al., 2009; Mazzoleni et al., 2010). Low concentrations of S(IV), high concentrations of SO_4^{2-}, and generally low concentrations of peroxides suggest that chemical components of the fog water were highly oxidized during upwind transport and/or within the local fog. LMM carboxylic acids accounted for 36-69% of TOC, a higher fraction than observed in fogs from other environments, with acetate, formate, succinate, oxalate, and maleate each contributing >5% of TOC on average. Further analysis of the fog organic matter via HPLC-(-)-ESI-HR-ToF-MS revealed homologous families of dicarboxylic acids and nitrophenols. The position within van Krevelen space occupied by identified organics matches well with the fragmentation aging regime (at high oxidation state) shown by Kroll et al. (2009).

Future studies of fog or cloud water composition in the region should include the characterization of carbonyl species, which have been cited as important AAOP reactants (Ervens, 2015) and are direct oxidation precursors of carboxylic acids. Additional studies to analyze the evolution of gaseous, particulate, and aqueous-phase organics during fog events as well as the advancement of laboratory-simulated reactions will be essential in more fully characterizing AAOP reactions and aqSOA formation.

REFERENCES

Aiken, A.C., Decarlo, P.F., Kroll, J.H., Worsnop, D.R., Huffman, J.A., Docherty, K.S., Ulbrich, I.M., Mohr, C., Kimmel, J.R., Super, D., Sun, Y., Zhang, Q., Trimborn, A., Northway, M., Zieman, P.J., Canagaratna, M.R., Onasch, T.B., Alfarra, M.R., Prevot, A.S.H., Dommen, J., Duplissy, J., Metzger, A., Baltensperger, U., Jimenez, J.L., 2008. O/C and OM/OC Ratios of Primary, Secondary, and Ambient Organic Aerosols with High-Resolution Time-of-Flight Aerosol Mass Spectrometry. Environ. Sci. Technol. 42, 4478–4485.

Altieri, K.E., Turpin, B.J., Seitzinger, S.P., 2009. Oligomers, organosulfates, and nitrooxy organosulfates in rainwater identified by ultra-high resolution electrospray ionization FT-ICR mass spectrometry. Atmos. Chem. Phys. 9, 2533–2542.

Andreae, M.O., 1983. Soot carbon and excess fine potassium: Long-range transport of combustion-derived aerosols. Science 220, 1148–1151.

Arimoto, R., Zhang, X.Y., Huebert, B.J., Kang, C.H., Savoie, D.L., Prospero, J.M., Sage, S.K., Schloesslin, C.A., Khaing, H.M., Oh, S.N., 2004. Chemical composition of atmospheric aerosols from Zhenbeitai, China, and Gosan, South Korea, during ACE-Asia. J. Geophys. Res. 109, D19S04.

Bator, A., Collett, J.L., 1997. Cloud chemistry varies with drop size. J. Geophys. Res. 102, 28071–28078.

Benedict, K.B., Lee, T., Collett, J.L., 2012. Cloud water composition over the southeastern Pacific Ocean during the VOCALS regional experiment. Atmos. Environ. 46, 104–114.

Bian, Q., Huang, X.H.H., Yu, J.Z., 2014. One-year observations of size distribution characteristics of major aerosol constituents at a coastal receptor site in Hong Kong – Part 1: Inorganic ions and oxalate. Atmos. Chem. Phys. 14, 9013–9027.

Blando, J., Turpin, B., 2000. Secondary organic aerosol formation in cloud and fog droplets: A literature evaluation of plausibility. Atmos. Environ. 34, 1623–1632.

Boris, A.J., Desyaterik, Y., Collett, J.L., 2014. How do components of real cloud water affect aqueous pyruvate oxidation? Atmos. Res. 143, 95–106.

Borrás, E., Tortajada-Genaro, L.A., 2012. Secondary organic aerosol formation from the photo-oxidation of benzene. Atmos. Environ. 47, 154–163.

Brinkmann, T., Hörsch, P., Sartorius, D., Frimmel, F.H., 2003. Photoformation of low-molecular-weight organic acids from brown water dissolved organic matter. Environ. Sci. Technol. 37, 4190–8.

Cao, G., Zhang, X., Zheng, F., 2006. Inventory of black carbon and organic carbon emissions from China. Atmos. Environ. 40, 6516–6527.

Chen, Q., Heald, C.L., Jimenez, J.L., Canagaratna, M.R., He, L.-Y., Huang, X.-F., Campuzano-Jost, P., Palm, B.B., Poulain, L., Kuwata, M., Martin, S.T., Abbatt, J.P.D., Lee, A.K.Y., Liggio, J., 2015. Elemental Composition of Organic Aerosol: The Gap Between Ambient and Laboratory Measurements. Geophys. Res. Lett. 42, 1–8.

Cho, Y., Kim, M., Kim, B., 2000. Sea fog around the Korean Peninsula. J. Appl. Meteorol. 39, 2473–2479.

Collett, J.L., Bator, A., Rao, X., Demoz, B.B., 1994. Acidity variations across the cloud drop size spectrum and their influence on rates of atmospheric sulfate production. Geophys. Res. Lett. 21, 2393–2396.

Collett, J.L., Bator, A., Sherman, D.E., Moore, K.F., Hoag, K.J., Demoz, B.B., Rao, X., Reilly, J.E., 2002. The chemical composition of fogs and intercepted clouds in the United States. Atmos. Res. 64, 29–40.

Collett, J.L., Herckes, P., Youngster, S., Lee, T., 2008. Processing of atmospheric organic matter by California radiation fogs. Atmos. Res. 87, 232–241.

Crahan, K.K., Hegg, D., Covert, D.S., Jonsson, H., 2004. An exploration of aqueous oxalic acid production in the coastal marine atmosphere. Atmos. Environ. 38, 3757–3764.

Daumit, K.E., Carrasquillo, A.J., Hunter, J.F., Kroll, J.H., 2014. Laboratory studies of the aqueous-phase oxidation of polyols: submicron particles vs. bulk aqueous solution. Atmos. Chem. Phys. 14, 10773–10784.

Decesari, S., Facchini, M., Fuzzi, S., Mcfiggans, G., Coe, H., Bower, K., 2005. The water-soluble organic component of size-segregated aerosol, cloud water and wet depositions from Jeju Island during ACE-Asia. Atmos. Environ. 39, 211–222.

Degefie, D.T., El-Madany, T.-S., Hejkal, J., Held, M., Dupont, J.-C., Haeffelin, M., Klemm, O., 2015. Microphysics and energy and water fluxes of various fog types at SIRTA, France. Atmos. Res. 151, 162–175.

Demoz, B.B., Collett, J.L., Daube, B.C., 1996. On the Caltech Active Strand Cloudwater Collectors. Atmos. Res. 41, 47–62.

Desyaterik, Y., Sun, Y., Shen, X., Lee, T., Wang, X., Wang, T., Collett, J.L., 2013. Speciation of "brown" carbon in cloud water impacted by agricultural biomass burning in eastern China. J. Geophys. Res. Atmos. 118, 7389–7399.

Edney, E.O., Driscoll, D.J., Speer, R.E., Weathers, W.S., Kleindienst, T.E., Li, W., Smith, D.F., 2000. Impact of aerosol liquid water on secondary organic aerosol yields of irradiated toluene/propylene/NOx/(NH4)2SO4/air mixtures. Atmos. Environ. 34, 3907–3919.

Ervens, B., 2015. Modeling the Processing of Aerosol and Trace Gases in Clouds and Fogs. Chem. Rev. 115, 4157–4198.

Ervens, B., Herckes, P., Feingold, G., Lee, T., Collett, J.L., Kreidenweis, S.M., 2003. On the drop-size dependence of organic acid and formaldehyde concentrations in fog. J. Atmos. Chem. 46, 239–269.

Ervens, B., Sorooshian, A., Lim, Y.B., Turpin, B.J., 2014. Key parameters controlling OH-initiated formation of secondary organic aerosol in the aqueous phase (asSOA). J. Geophys. Res. Atmos. 119, 3997–4016.

Ervens, B., Turpin, B., Weber, R., 2011. Secondary organic aerosol formation in cloud droplets and aqueous particles (aqSOA): A review of laboratory, field and model studies. Atmos. Chem. Phys. 11, 11069–11102.

Fahey, K.M., Pandis, S.N., Collett, J.L., Herckes, P., 2005. The influence of size-dependent droplet composition on pollutant processing by fogs. Atmos. Environ. 39, 4561–4574.

Fu, T.-M., Jacob, D.J., Wittrock, F., Burrows, J.P., Vrekoussis, M., Henze, D.K., 2008. Global budgets of atmospheric glyoxal and methylglyoxal, and implications for formation of secondary organic aerosols. J. Geophys. Res. 113, D15303.

Fuzzi, S., Facchini, M.C., Orsi, G., Lind, J.A., Wobrock, W., Kessell, M., Maser, R., Jaeschke, W., Enderle, K.H., Arends, B.G., Berner, A., Solly, I., Kruisz, C., Reischl, G., Pahl, S., Kaminski, U., Winkler, P., Ogren, J.A., Noone, K.J., Hallberg, A., Fierlinger-Oberlinninger, H., Puxbaum, H., Marzorati, A., Hansson, H.-C., Wiedensohler, A., Svenningsson, I.B., Martinsson, B.G., Schell, D., Georgii, H.W., 1992. The Po Valley Fog Experiment 1989: An Overview. Tellus B 44B, 448–468.

Gerber, H., 1991. Direct measurement of suspended particulate volume concentration and far-infrared extinction coefficient with a laser-diffraction instrument. Appl. Opt. 30, 4824–31.

Harrison, M., Barra, S., Borghesi, D., Vione, D., Arsene, C., Iulianolariu, R., 2005. Nitrated phenols in the atmosphere: a review. Atmos. Environ. 39, 231–248.

Heald, C.L., Jacob, D.J., Park, R.J., Russell, L.M., Huebert, B.J., Seinfeld, J.H., Liao, H., Weber, R.J., 2005. A large organic aerosol source in the free troposphere missing from current models. Geophys. Res. Lett. 32, 2–5.

Heald, C.L., Kroll, J.H., Jimenez, J.L., Docherty, K.S., DeCarlo, P.F., Aiken, A.C., Chen, Q., Martin, S.T., Farmer, D.K., 2010. A simplified description of the evolution of organic aerosol composition in the atmosphere. Geophys. Res. Lett. 37.

Hegg, D.A., Larson, T. V., 1990. The effects of microphysical parameterization on model predictions of sulfate production in clouds. Tellus 42B, 272–284.

Herckes, P., Chang, H., Lee, T., Collett, J.L., 2007. Air Pollution Processing by Radiation Fogs. Water Air Soil Pollut. 181, 65–75.

Herckes, P., Hannigan, M.P., Trenary, L., Lee, T., Collett, J.L., 2002a. Organic compounds in radiation fogs in Davis (California). Atmos. Res. 64, 99–108.

Herckes, P., Lee, T., Trenary, L., Kang, G., 2002b. Organic Matter in Central California Radiation Fogs. Environ. Sci. Technol. 36, 4777–4782.

Herckes, P., Valsaraj, K.T., Collett, J.L., 2013. A review of observations of organic matter in fogs and clouds: Origin, processing and fate. Atmos. Res. 132-133, 434–449.

Hoag, K.J., Collett, J.L., Pandis, S.N., 1999. The influence of drop size-dependent fog chemistry on aerosol processing by San Joaquin Valley fogs. Atmos. Environ. 33, 4817–4832.

Iinuma, Y., Muller, C., Berndt, T., Boge, O., Claeys, M., Herrmann, H., 2007. Evidence for the Existence of Organosulfates from β-Pinene Ozonolysis in Ambient Secondary Organic Aerosol. Environ. Sci. Technol. 41, 6678–6683.

Kalberer, M., Yu, J., Cocker, D.R., Flagan, R.C., Seinfeld, J.H., 2000. Aerosol Formation in the Cyclohexene-Ozone System. Environ. Sci. Technol. 34, 4894–4901.

Kamens, R.M., Zhang, H., Chen, E.H., Zhou, Y., Parikh, H.M., Wilson, R.L., Galloway, K.E., Rosen, E.P., 2011. Secondary organic aerosol formation from toluene in an atmospheric hydrocarbon mixture: Water and particle seed effects. Atmos. Environ. 45, 2324–2334.

Kang, C.-M., Kang, B.-W., Lee, H.S., 2006. Source identification and trends in concentrations of gaseous and fine particulate principal species in Seoul, South Korea. J. Air Waste Manag. Assoc. 56, 911–921.

Kawamura, K., Ikushima, K., 1993. Seasonal changes in the distribution of dicarboxylic acids in the urban atmosphere. Environ. Sci. Technol. 27, 2227–2235.

Kawamura, K., Kaplan, I., 1987. Motor exhaust emissions as a primary source for dicarboxylic acids in Los Angeles ambient air. Environ. Sci. Technol. 21, 105–110.

Kawamura, K., Kobayashi, M., Tsubonuma, N., Mochida, M., Watanabe, T., Lee, M., 2004. Organic and inorganic compositions of marine aerosols from East Asia: Seasonal variations of water-soluble dicarboxylic acids, major ions, total carbon and nitrogen, and stable C and N isotopic composition, in: Geochemical Investigations in Earth and Space Science: A Tribute to Isaac R. Kaplan. The Geochemical Society, Amsterdam, The Netherlands, pp. 243–265.

Kim, J.H., Yum, S.S., Shim, S., Yoon, S.-C., Hudson, J.G., Park, J., Lee, S.-J., 2011. On aerosol hygroscopicity, cloud condensation nuclei (CCN) spectra and critical supersaturation measured at two remote islands of Korea between 2006 and 2009. Atmos. Chem. Phys. 11, 12627–12645.

Kim, M.-G., Lee, B.-K., Kim, H.-J., 2006. Cloud/Fog Water Chemistry at a High Elevation Site in South Korea. J. Atmos. Chem. 55, 13–29.

Kleindienst, T.E., Smith, D.F., Li, W., Edney, E.O., Driscoll, D.J., Speer, R.E., Weathers, W.S., 1999. Secondary organic aerosol formation from the oxidation of aromatic hydrocarbons in the presence of dry submicron ammonium sulfate aerosol. Atmos. Environ. 33, 3669–3681.

Kukui, A., Borissenko, D., Laverdet, G., Le Bras, G., 2003. Gas-phase reactions of OH radicals with dimethyl sulfoxide and methane sulfinic acid using turbulent flow reactor and chemical ionization mass spectrometry. J. Phys. Chem. A 107, 5732–5742.

Lauer, A., Eyring, V., Hendricks, J., Jöckel, P., Lohmann, U., 2007. Global model simulations of the impact of ocean-going ships on aerosols, clouds, and the radiation budget. Atmos. Chem. Phys. Discuss. 7, 9419–9464.

Lee, T., 2007. Characterizing ionic components of aerosol in rural environments: temporal variability, size distributions, and the form of particle nitrate. Colorado State University.

Lee, T., Sullivan, A.P., Mack, L., Jimenez, J.L., Kreidenweis, S.M., Onasch, T.B., Worsnop, D.R., Malm, W., Wold, C.E., Hao, W.M., Collett, J.L., 2010. Chemical Smoke Marker Emissions During Flaming and Smoldering Phases of Laboratory Open Burning of Wildland Fuels. Aerosol Sci. Technol. 44.

Lee, T.T., Choi, J.J., Lee, G., Ahn, J.J.Y., Park, J.S., Atwood, S.A., Schurman, M., Choi, Y., Chung, Y., Collett, J.L., Choi, J.J., Ahn, J.J.Y., Park, J.S., Atwood, S.A., Schurman, M., Chung, Y., Collett, J.L., 2015. Characterization of Aerosol Composition, Concentrations, and Sources at Baengnyeong Island, Korea using an Aerosol Mass Spectrometer. Atmos. Environ. 120, 297–306.

Lelieveld, J., Crutzen, P., 1991. The role of clouds in tropospheric photochemistry. J. Atmos. Chem. 12, 229–267.

Li, P., Li, X., Yang, C., Wang, X., Chen, J., Collett, J.L., 2011. Fog water chemistry in Shanghai. Atmos. Environ. 45, 4034–4041.

Lim, H., Carlton, A.G., Turpin, B.J., 2005. Isoprene Forms Secondary Organic Aerosol through Cloud Processing: Model Simulations. Environ. Sci. Technol. 39, 4441–4446.

Lim, Y.B., Tan, Y., Perri, M.J., Seitzinger, S.P., Turpin, B.J., 2010. Aqueous chemistry and its role in secondary organic aerosol (SOA) formation. Atmos. Chem. Phys. 10, 10521–10539.

Lim, Y.B., Tan, Y., Turpin, B.J., 2013. Chemical insights, explicit chemistry, and yields of secondary organic aerosol from OH radical oxidation of methylglyoxal and glyoxal in the aqueous phase. Atmos. Chem. Phys. 13, 8651–8667.

Lin, G., Sillman, S., Penner, J.E., Ito, A., 2014. Global modeling of SOA: the use of different mechanisms for aqueous-phase formation. Atmos. Chem. Phys. 14, 5451–5475.

Liu, Y., Monod, A., Tritscher, T., Praplan, A.P., DeCarlo, P.F., Temime-Roussel, B., Quivet, E., Marchand, N., Dommen, J., Baltensperger, U., 2012. Aqueous phase processing of secondary organic aerosol from isoprene photooxidation. Atmos. Chem. Phys. 12, 5879–5895.

Mattigod, S.., Rai, D., Eary, L.., Ainsworth, C.., 1990. Geochemical factors controlling the mobilisation of inorganic constituents from fossil fuel combustion residues: I. Review of the major elements. J. Environ. Qual. 19, 188–201.

Mazzoleni, L.R., Ehrmann, B.M., Shen, X., Marshall, A.G., Collett, J.L., 2010. Water-soluble atmospheric organic matter in fog: Exact masses and chemical formula identification by ultrahigh-resolution fourier transform ion cyclotron resonance mass spectrometry. Environ. Sci. Technol. 44, 3690–3697.

McCulloch, A., Aucott, M.L., Benkovitz, C.M., Graedel, T.E., Kleiman, G., Midgley, P.M., Li, Y.-F., 1999. Global emissions of hydrogen chloride and chloromethane from coal combustion, incineration and industrial activities: Reactive Chlorine Emissions Inventory. J. Geophys. Res. 104, 8391–8403.

McNeill, V.F., 2015. Aqueous organic chemistry in the atmosphere: Sources and chemical processing of organic aerosols. Environ. Sci. Technol. 49, 1237–1244.

Moore, K.F., Sherman, D.E., Reilly, J.E., Hannigan, M.P., Lee, T., Collett, J.L., 2004. Drop size-dependent chemical composition of clouds and fogs. Part II: Relevance to interpreting the aerosol/trace gas/fog system. Atmos. Environ. 38, 1403–1415.

Mouri, H., Okada, K., 1993. Shattering and modification of sea-salt particles in the marine atmosphere. Geophys. Res. Lett. 20, 49–52.

Munger, J.W., Collett, J., Daube, B., Hoffmann, M.R., 1989. Chemical composition of coastal stratus clouds: Dependence on droplet size and distance from the coast. Atmos. Environ. 23, 2305–2320.

Narukawa, M., Kawamura, K., 1999. Distribution of dicarboxylic acids and carbon isotopic compositions in aerosols from 1997 Indonesian forest fires. Geophys. Res. Lett. 26, 3101–3104.

Ng, N.L., Canagaratna, M.R., Jimenez, J.L., Chhabra, P.S., Seinfeld, J.H., Worsnop, D.R., 2011. Changes in organic aerosol composition with aging inferred from aerosol mass spectra. Atmos. Chem. Phys. 11, 6465–6474.

Nguyen, Q.T., Christensen, M.K., Cozzi, F., Zare, A., Hansen, A.M.K., Kristensen, K., Tullinius, T.E., Madsen, H.H., Christensen, J.H., Brandt, J., Massling, A., Nojgaard, J.K., Glasius, M., 2014. Understanding the anthropogenic influence on formation of biogenic secondary organic aerosols in Denmark via analysis of organosulfates and related oxidation products. Atmos. Chem. Phys. 14, 8961–8981.

Noziere, B., Kalberer, M., Claeys, M., Allan, J., Anna, B.D., Decesari, S., Finessi, E., Glasius, M., Grgic, I., Hamilton, J.F., Ho, T., Iinuma, Y., Jaoui, M., Kahnt, A., Kampf, C.J., Kourtchev, I., Maenhaut, W., Marsden, N., Saarikoski, S., Schnelle-kreis, J., Surratt, J.D., Szidat, S., Szmigielski, R., Wisthaler, A., 2015. The molecular identification of organic compounds in the atmosphere: State of the art and challenges. Chem. Rev. 115, 3919–3983.

Pandis, S.N., Seinfeld, J.H., Pilinis, C., 1990. The smog-fog-smog cycle and acid deposition. J. Geophys. Res. 95, 18489–18500.

Prabhakar, G., Ervens, B., Wang, Z., Maudlin, L.C., Coggon, M.M., Jonsson, H.H., Seinfeld, J.H., Sorooshian, A., 2014. Sources of nitrate in stratocumulus cloud water: Airborne measurements during the 2011 E-PEACE and 2013 NiCE studies. Atmos. Environ. 97, 166–173.

Praplan, A., Hegyi-Gaeggeler, K., Barmet, P., Pfaffenberger, L., Dommen, J., Baltensperger, U., 2014. Online measurements of water-soluble organic acids in the gas and aerosol phase from the photooxidation of 1, 3, 5-trimethylbenzene. Atmos. Chem. Phys. 14, 8665–8677.

Radojevic, M., Bashkin, V.N., 2006. Practical Environmental Analysis. The Royal Society of Chemistry, Cambridge, UK.

Raja, S., Raghunathan, R., Yu, X.-Y., Lee, T., Chen, J., Kommalapati, R.R., Murugesan, K., Shen, X., Qingzhong, Y., Valsaraj, K.T., Collett, J.L., 2008. Fog chemistry in the Texas–Louisiana Gulf Coast corridor. Atmos. Environ. 42, 2048–2061.

Rao, X., Collett, J.L., 1995. Behavior of S(IV) and formaldehyde in a chemically heterogeneous cloud. Environ. Sci. Technol. 29, 1023–1031.

Rao, X., Collett, J.L., 1998. The drop size-dependence of iron and manganese concentrations in clouds and fogs: Implications for sulfate production. J. Atmos. Chem. 30, 273–289.

Reilly, J.E., Rattigan, O. V, Moore, K.F., Judd, C., Eli Sherman, D., Dutkiewicz, V. a, Kreidenweis, S.M., Husain, L., Collett, J.L., 2001. Drop size-dependent S(IV) oxidation in chemically heterogeneous radiation fogs. Atmos. Environ. 35, 5717–5728.

Scaduto, R.C.J., 1995. Oxidation of DMSO and methanesulfinic acid by the hydroxyl radical. Free Radic. Biol. Med. 18, 271–277.

Seinfeld, J.H., Pandis, S.N., 2006. Atmospheric Chemistry and Physics: From Air Pollution to Climate Change. John Wiley & Sons, Inc., Hoboken, New Jersey.

Shen, X., 2011. Aqueous Phase Sulfate Production in Clouds at Mt. Tai in Eastern China. Colorado State University.

Shen, X., Lee, T., Guo, J., Wang, X., Li, P., Xu, P., Wang, Y., Ren, Y., Wang, W., Wang, T., Li, Y., Carn, S.A., Collett, J.L., 2012. Aqueous phase sulfate production in clouds in eastern China. Atmos. Environ. 62, 502–511.

Sorooshian, A., Varutbangkul, V., 2006. Oxalic acid in clear and cloudy atmospheres: Analysis of data from International Consortium for Atmospheric Research on Transport and Transformation 2004. J. Geophys. Res. 111, 1–10.

Sorooshian, A., Wang, Z., Coggon, M.M., Jonsson, H.H., Ervens, B., 2013. Observations of Sharp Oxalate Reductions in Stratocumulus Clouds at Variable Altitudes: Organic Acid and Metal Measurements During the 2011 E-PEACE Campaign. Environ. Sci. Technol. 47, 7747–7756.

Straub, D.J., Lee, T., Collett, J.L., 2007. Chemical composition of marine stratocumulus clouds over the eastern Pacific Ocean. J. Geophys. Res. 112, D04307.

Streets, D.G., Guttikunda, S.K., Carmichael, G.R., 2000. The growing contribution of sulfur emissions from ships in Asian waters, 1988–1995. Atmos. Environ. 34, 4425–4439.

Sullivan, A.P., Holden, A.S., Patterson, L.A., McMeeking, G.R., Kreidenweis, S.M., Malm, W.C., Hao, W.M., Wold, C.E., Collett, J.L., 2008. A method for smoke marker measurements and its potential application for determining the contribution of biomass burning from wildfires and prescribed fires to ambient PM 2.5 organic carbon. J. Geophys. Res. 113, D22302.

Surratt, J.D., Gómez-González, Y., Chan, A.W.H., Vermeylen, R., Shahgholi, M., Kleindienst, T.E., Edney, E.O., Offenberg, J.H., Lewandowski, M., Jaoui, M., Maenhaut, W., Claeys, M., Flagan, R.C., Seinfeld, J.H., 2008. Organosulfate formation in biogenic secondary organic aerosol. J. Phys. Chem. A 112, 8345–78.

Szmigielski, R., Surratt, J.D., Gómez-González, Y., van der Veken, P., Kourtchev, I., Vermeylen, R., Blockhuys, F., Jaoui, M., Kleindienst, T.E., Lewandowski, M., Offenberg, J.H., Edney, E.O., Seinfeld, J.H., Maenhaut, W., Claeys, M., 2007. 3-methyl-1,2,3-butanetricarboxylic acid: An atmospheric tracer for terpene secondary organic aerosol. Geophys. Res. Lett. 34, 2–7.

Varutbangkul, V., Brechtel, F.J., Bahreini, R., Ng, N.L., Keywood, M.D., Kroll, J.H., Flagan, R.C., Seinfeld, J.H., Lee, A., Goldstein, a. H., 2006. Hygroscopicity of secondary organic aerosols formed by oxidation of cycloalkenes, monoterpenes, sesquiterpenes, and related compounds. Atmos. Chem. Phys. 6, 2367–2388.

Wang, B., O'Brien, R.E., Kelly, S.T., Shilling, J.E., Moffet, R.C., Gilles, M.K., Laskin, A., 2015. Reactivity of Liquid and Semisolid Secondary Organic Carbon with Chloride and Nitrate in Atmospheric Aerosols. J. Phys. Chem. A 119, 4498–4508.

Wang, Y., Guo, J., Wang, T., Ding, A., Gao, J., Zhou, Y., Collett, J.L., Wang, W., 2011. Influence of regional pollution and sandstorms on the chemical composition of cloud/fog at the summit of Mt. Taishan in northern China. Atmos. Res. 99, 434–442.

Weber, R.J., Sullivan, A.P., Peltier, R.E., Russell, A., Yan, B., Zheng, M., de Gouw, J., Warneke, C., Brock, C., Holloway, J.S., Atlas, E.L., Edgerton, E., 2007. A study of secondary organic aerosol formation in the anthropogenic-influenced southeastern United States. J. Geophys. Res. Atmos. 112.

Wise, M.E., Surratt, J.D., Curtis, D.B., Shilling, J.E., Tolbert, M.A., 2003. Hygroscopic growth of ammonium sulfate/dicarboxylic acids. J. Geophys. Res. 108, 4368–4376.

Wonaschuetz, A., Sorooshian, A., Ervens, B., Chuang, P.Y., Feingold, G., Murphy, S.M., de Gouw, J., Warneke, C., Jonsson, H.H., 2012. Aerosol and gas re-distribution by shallow cumulus clouds: An investigation using airborne measurements. J. Geophys. Res. 117, D17202.

Yamasoe, M., Artaxo, P., Miguel, A., Allen, A., 2000. Chemical composition of aerosol particles from direct emissions of vegetation fires in the Amazon Basin: water-soluble species and trace elements. Atmos. Environ. 34, 1641–1653.

Yang, G.-P., Zhang, H.-H., Su, L.-P., Zhou, L.-M., 2009. Biogenic emission of dimethylsulfide (DMS) from the North Yellow Sea, China and its contribution to sulfate in aerosol during summer. Atmos. Environ. 43, 2196–2203.

Yasmeen, F., Vermeylen, R., Szmigielski, R., Iinuma, Y., Böge, O., Herrmann, H., Maenhaut, W., Claeys, M., 2010. Terpenylic acid and related compounds: precursors for dimers in secondary organic aerosol from the ozonolysis of α- and β-pinene. Atmos. Chem. Phys. 10, 9383–9392.

Yoo, J.-M., Jeong, M.-J., Hur, Y.M., Shin, D.-B., 2010. Improved fog detection from satellite in the presence of clouds. Asia-Pacific J. Atmos. Sci. 46, 29–40.

Yu, J.Z., Huang, X.-F., Xu, J., Hu, M., 2005. When aerosol sulfate goes up, so does oxalate: implication for the formation mechanisms of oxalate. Environ. Sci. Technol. 39, 128–133.

Zhang, Q., Worsnop, D.R., Canagaratna, M.R., Jimenez, J.-L., 2005. Hydrocarbon-like and oxygenated organic aerosols in Pittsburgh: insights into sources and processes of organic aerosols. Atmos. Chem. Phys. 5, 3289–3311.

Zhang, S.-P., Xie, S.-P., Liu, Q.-Y., Yang, Y.-Q., Wang, X.-G., Ren, Z.-P., 2009. Seasonal Variations of Yellow Sea Fog: Observations and Mechanisms. J. Clim. 22, 6758–6772.

Zhang, W., Xiao, X., An, T., Song, Z., 2003. Kinetics, degradation pathway and reaction mechanism of advanced oxidation of 4-nitrophenol in water by a UV/H2O2 process. J. Chem. Technol. Biotechnol. 794, 788–794.

Zhang, X., Arimoto, R., An, Z., Chen, T., Zhang, G., Zhu, G., Wang, X., 1993. Atmospheric trace elements over source regions for Chinese dust: concentrations, sources and atmospheric deposition on the Loess plateau. Atmos. Environ. Part A. Gen. Top. 27, 2051–2067.

Zuo, Y., Hoigné, J., 1994. Photochemical decomposition of oxalic, glyoxalic and pyruvic acid catalysed by iron in atmospheric waters. Atmos. Environ. 2, 1231–1239.

3 EVOLVING ANTHROPOGENIC EMISSIONS AND AQUEOUS AGING IN FOG ON THE SOUTHERN CALIFORNIA COAST

Fog acts as a reservoir and mode of transport for chemicals in the atmosphere, altering their distribution between the gas and particle phases, and allowing deposition of nutrients and pollutants alike into ecosystems and onto crops. Southern California coastal fog water and gaseous grab samples were collected from Casitas Pass (CP) in June 2015 to identify emissions sources and aqueous processes impacting the fog. Air was often advected over the coastline near oil extraction/refining operations, urban areas, and agricultural areas. Fog water composition was dominated by NH_4^+ (volume weighted mean, VWM, concentration 250 μM) with lesser contributions from NO_3^- (VWM 153 μM) and SO_4^{2-} (only 30.9 μM), causing the VWM pH to be 6.03. Organic carbon contributed substantially to the fog composition (8.27 mg C L^{-1}). Carboxylic acids were abundant (20% on average by C mass), with >1% contributions from not only acetate and formate, but also oxalate, malonate, succinate, and lactate, which can be produced through aqueous oxidation reactions. S-containing organic species (CHOS), N-containing organic species (CHNO) and N- and S-containing organic species (CHNOS) were also detected in the fog, often after fog had persisted for 3-5 hours, suggesting possible aqueous formation. Regional oil and natural gas processing and mobile sources were the most influential organic emissions sources at CP. The fog chemical composition at CP in 2015 was contrasted with that from a previous fog sampling campaign in July-September 1985/6. The concentrations of major fog constituents appear to have decreased in response to successful air quality regulations. While natural species concentrations in fog were similar (2015 mean: 120 μM Na^+; 1985/6: 129 μM Na^+), anthropogenic species concentrations were indeed lower in 2015. Acidity of the fog was two orders of magnitude greater in 1985/6 (VWM pH of 3.92), due mainly to the lower concentrations of NO_3^- (483 μM) and SO_4^{2-} (222 μM), since the NH_4^+ concentration was also greater in the 1985/6 fog water campaign (VWM of 584 μM). The concentrations of formaldehyde, formate, and acetate were also lower in 2015 than in 1985/6. These results overall highlight the changes in air quality issues in Southern California, including improvement of some anthropogenic emissions, but the current influence of organic emissions from industrial and mobile sources. This study demonstrates how fog chemistry can be used to survey regional air quality. Further work is needed to better characterize the in-fog organic aging processes such as CHNO and CHOS formation illustrated here.

3.1 Introduction

Interaction of atmospheric trace compounds with fogs, clouds, and wet aerosols can substantially alter chemical fates and effects. Chemical transformations within the aqueous phase, for example, can decrease atmospheric lifetimes of organic species from those in the gas phase (e.g., ~2 times shorter lifetime for phenol; ~3.5 times shorter for acetic acid; Monod et al., 2005). Unfortunately, many atmospheric aqueous processes are not well understood, despite their potential to strongly impact air quality; for example, aqueous-phase oxidation reactions can alter partitioning of volatile organic compounds (VOCs) and semi-VOCs into fog droplets (Ehrenhauser et al., 2012; Herckes et al., 2002a, 2002b). Volatile species such as formate, acetate, and formaldehyde have been found both at sub- and super-saturation concentrations in fog with respect to the gas phase (Facchini et al., 1992). Pandis and Seinfeld found that the fog water mean pH, which depends mainly on inorganic ion concentrations, was a predictor in fog concentrations of weak acids and bases, based on sub- or super-saturation within the droplets with respect to Henry's Law constants, along with aqueous-phase reactions, acid dissociation constants, and the variation in pH over the droplet size spectrum (Pandis and Seinfeld, 1991). A variety of environmental variables and processes bring about the observed concentrations of constituents and additional research is needed to demonstrate the relationships and importance of these factors; in particular, aqueous organic oxidation processes (AAOPs) affecting organic species concentrations in the gas, aqueous and particle phases of the atmosphere must be studied.

Fog is a driver of climate and ecosystem health in many regions of the world, including along the west coast of the United States, where approximately 30% of water collected in redwood forests originates from fog (Dawson, 1998). The chemical composition of fog is therefore important for residential, agricultural, and ecosystem water resources: fog deposition of major ionic species can exceed annual dry deposition (Collett et al., 1989). Fog composition varies with regional emissions sources, oxidant concentrations, temperature, liquid water content (LWC), and meteorology (Jacob et al., 1984). Even within the well-studied areas of the Southern California Coastline, where frequent fog events are observed due to lowering/advection of North Pacific High stratus layers (Johnstone and Dawson, 2010), mean seasonal concentrations of carboxylic acids and inorganic ions in fog demonstrate widely varying values (Collett et al., 1999; Herckes et al., 2007, 2002b; Jacob, 1985; J. Munger et al., 1989; J. W. Munger et al., 1989; Munger, 1989; Munger et al., 1990).

Land use and climatological changes can give rise to spatial and temporal changes in fog water chemistry. Industrial processes such as oil and natural gas (O&NG) extraction and production, agriculture, and urban combustion processes are the main anthropogenic contributors to non-methane VOCs (Middleton et al., 1990), and can also emit sulfur oxides and nitrogen oxides (Finlayson-Pitts and Pitts, 2000). The state of California has increased in population dramatically between the 1980s and 2015: from 26 million in 1985 to more than 39 million in 2015 (U.S. Census Bureau, 2015). Agricultural land use has also increased: the value of crops in Ventura County were 613 million in 1986, and had increased to 2.09 billion by 2013 (Ventura County Office of the Agricultural Commissioner, 2014). Despite these increases in population and agriculture, mean annual measured $[NO_2]_{gas}$, $[O_3]_{gas}$, and $[PM_{2.5}]_{gas}$ steadily decreased between 1990 and 2014 in Ventura, located on the Channel, in response to regulation of emissions. Similar trends were observed just northwest in Santa Barbara, although in both locations, $[SO_2]_{gas}$ remained fairly constant between 1990 and 2014 (U.S. Environmental Protection Agency, 2015). The Ventura Oil Field in the Ojai River Valley has been a thriving oil extraction location since the mid 1920s (Adamson, 2008), but production has decreased in recent years: in 1986, 7.4 million barrels were extracted; in 2014, 5.0 million barrels of oil were extracted from the Ventura Oil Field (California Department of Conservation, 2015, 1987). Deposits of O&NG also exist offshore along the Santa Barbara Channel, which seep naturally from the ocean floor (Hornafius et al., 1999); the O&NG is also extracted via wells drilled from offshore platforms. The emission rates of non-methane VOCs from natural offshore O&NG deposits were estimated to be double that from on-road vehicle traffic affecting nearby Santa Barbara County in 1999 (Hornafius et al., 1999), although O&NG extraction processes reduced some offshore VOC seepage between 1973 and 1999 (Hornafius et al., 1999).

Fog water and gaseous grab samples were collected at Casitas Pass (CP), north of Ventura, California, and inland of the Santa Barbara Channel in June 2015. The objectives of the field campaign were two-fold: (1) to build upon current understanding of AAOPs and other factors determining chemical composition in the presence of fog; and (2) to study the changes in fog chemical composition along the Southern California Coast over time by contrasting results between the June 2015 campaign and a study in 1985/6 (Jacob et al., 1985; J. W. Munger et al., 1989). It was hypothesized that substantial changes between current and previous fog chemistry in the Santa Barbara Channel coastal region would be observed, due to increases in population density and changes in land use. Organic markers of urban activities, O&NG extraction, and agricultural activities were expected to be present in the fog water, as well as possible aged, particle- and gas-phase emissions.

3.2 Materials and Methods

Fog water was collected between 8 and 14 June 2015; four fog events will be discussed that contained sufficient liquid water for chemical analyses (~50 mL; events ending on the mornings of 11-14 June, and referred to as events 1-4, respectively). The fog events 1 and 3 were captured from the summit of CP (34,3863, -119.3809, 350 m A.S.L.), event 2 from a location below the CP summit along Highway 150 near an avocado grove (34.3896, -119.4158, 290 m A.S.L.), and event 4 was captured from a second location along Highway 150 near an orange grove (34.3904, -119.4197, approx. 250 m A.S.L.), as in Figure 3-1. All three 2015 sampling sites were on gravel pull-offs adjacent to Highway 150, 2-10 m from the roadway. Motor vehicle traffic was infrequent between 10:00 pm and 4:00 am (during most sampling periods), and increased somewhat through the final morning hours of each fog sampling period. A 1985/6 study was carried out at a site along Highway 150, 50-150 m from the roadway, and only 200 m from the event 2 sampling site (34.3865, -119.4171). Based on the similarities between fog composition at the sites used in the present study, it is unlikely that the micrometeorology or location of the sites used in 1985/6 and 2015 were substantial contributors to differences in fog composition between the two studies.

Two Caltech Active Strand Cloudwater Collectors (CASCCs) were deployed at CP to collect fog water. Droplets are impacted onto rows of forward-tilted strands and pulled by gravity and aerodynamic drag imparted by an electric fan into a sampling trough at the bottom of each collector. A stainless steel CASCC (ss-CASCC; Herckes et al., 2002a), with stainless steel strands and sampling trough, was used to collect fog droplets for analysis of organic fog constituents. A smaller collector (CASCC2) was used to collect fog droplets for analysis of ionic fog constituents onto Teflon collection surfaces (Demoz et al., 1996). Fog water was collected for durations of one to three hours, depending on the time required to collect sufficient volume (~50 mL) for fog chemical analyses. Samples of fog water were immediately massed and pH was measured on-site using a Cole-Parmer microelectrode and pH meter, calibrated with pH 4 and 7 buffers.

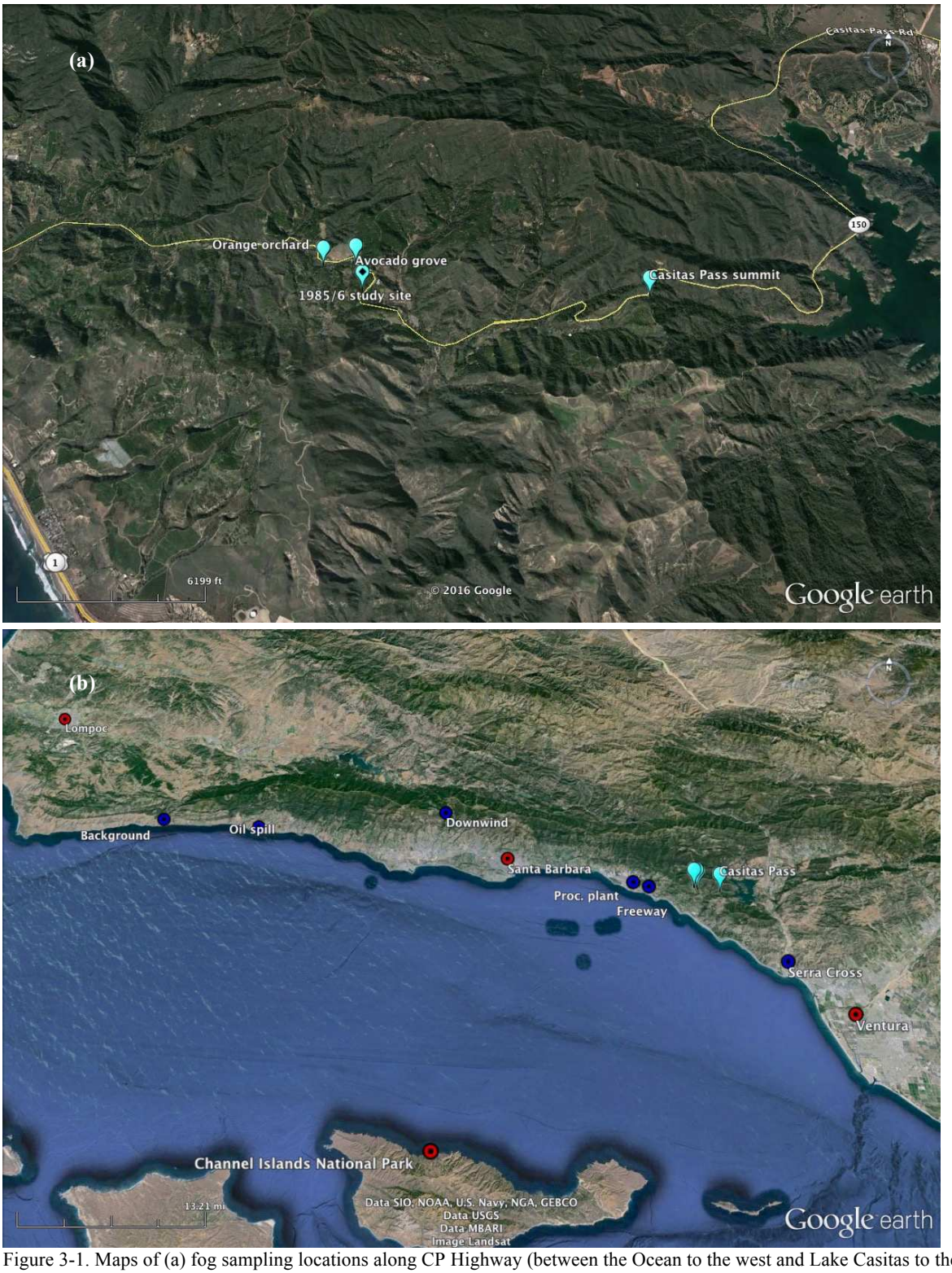

Figure 3-1. Maps of (a) fog sampling locations along CP Highway (between the Ocean to the west and Lake Casitas to the east), and (b) all fog water, VOC, and aerosol sampling sites. Red points denote cities/landmarks, dark blue points denote whole air grab sampling sites, and light blue markers represent fog sampling sites. Labels are as follows: "Background" = upwind of main VOC sources at Gaviota State Park, "Oil spill" = along I-5 at oil spill, "Downwind" = road above Goleta downwind of oil spill, "Freeway" = site along I-5 near CP Highway, "Proc. Plant" = O&NG processing site, and "Serra Cross" = Serra Cross Park above Ventura where aerosol samples were collected.

Preservation methods of aliquots for formaldehyde and carboxylic acids analyses have been described previously (Boris et al., 2016). Samples for inorganic ions and total organic carbon (TOC) were aliquotted without added reagents.

Chemical analyses were carried out using procedures applied previously (Benedict et al., 2012; Boris et al., 2016; Collett et al., 1999), but will be described here in brief. Formaldehyde was quantified using chemical derivatization and fluorescence spectrometry (Dong and Dasgupta, 1987), TOC was measured using a Sievers Model 800 Turbo TOC Analyzer in Turbo mode, and major inorganic ions as well as carboxylic acids were quantified using ion chromatography (IC; Dionex). Additional organic molecules were identified and/or quantified via high performance liquid chromatography followed by negative electrospray ionization high-resolution time-of-flight mass spectrometry (HPLC-(-)-ESI-HR-ToF-MS; Agilent 1100 series LC with Agilent LC/MSD-ToF). Carbohydrates were analyzed using high performance anion exchange chromatography with pulsed amperometric detection (HPAE-PAD) as described previously (Sullivan et al., 2008). Fog samples remaining after analyses were composited (Table A3-1) for analysis of volatile trace organic compounds via gas chromatography/mass spectrometry (GC/MS; HP Model 6890 with 5973 MS and 30 m×250 μm×0.25 μm i.d.HP-5 capillary column). Additional information about fog water analyses as well as meteorological and satellite data can be found in Appendix 3.

Discrete whole-air grab samples were collected using evacuated electropolished stainless steel canisters (2 L) with inert inner coating during fog events at each sampling site and near areas of possible hydrocarbon emissions. A background measurement was made upwind of the Refugio State Beach site at Gaviota State Park and canisters were additionally collected near possible VOC sources (see below and Appendix 3). Two canister batch blanks were generated by transporting cleaned, evacuated canisters to the sampling site without collection. Individual VOCs (48) were quantified using a three GC analytical system with three flame ionization detectors (FIDs), one electron capture detector (ECD) and one mass spectrometer (MS) as described previously (Russo et al., 2010; Sive, 1998; Zhou et al., 2010) and in Appendix 3.

Back trajectories (12 hrs) were generated using the NOAA HySPLIT model (online version; Draxler and Rolph) and used to determine the upwind histories of air masses sampled during fog events. The model was initiated using the coordinates of the CP summit site, and a height of 1150 m, beginning at each two-hour period between 6 pm and

6 am on evenings when fog was collected. Model vertical velocity was used to track vertical motion, and NARR (32 km) archived meteorological data were used to capture the greatest spatial resolution possible.

Air equivalent concentrations (also called the cloud water loading, CWL, and denoted by $[X]_{air\ eq.}$) were calculated for fog water constituents assuming 100% collection efficiency of fog liquid water, using the calculated flow rate through the cloudwater collector, duration of each sample, and mass of each sample collected (see Supporting Information). Volume weighted mean (VWM) for each chemical species quantified was calculated by multiplying the mass of each sample by the corresponding chemical concentration, summing all values, and dividing by the total summed mass of the samples.

3.3 Results and discussion

3.3.1 Overview of Fog Composition

Measured quantities of fog water constituents at CP in June 2015 are summarized in Figure 3-1 and Table 3-1. The most abundant constituent was NH_4^+ (volume weighted mean, VWM $[NH_4^+]_{aq}$=232 μM), causing the fog to be among the more basic pH values (VWM pH 6.01) of those measured globally (mean pH 3.68 in Mount Tai, China, 2011, Wang et al., 2011; median pH 4.01 in stratus cloud water off the California coast, Straub et al., 2007; mean 4.29 at Mt. Schmücke, Germany, 2010, van Pinxteren et al., 2015; 4.3 at Puy de Dôme, France, 2001-2011, Deguillaume et al., 2014; 5.1 at Sequoia National Park in 1985/6, Collett et al., 1989; 5.97 at Shanghai, China in 2009/2010, Li et al., 2011; median pH 6.73 in the San Joaquin Valley, California, 2000/2001, Herckes et al., 2007; mean pH 7.24 in Kanpur, India in 2010, Kaul et al., 2011). Anion concentrations were dominated by NO_3^- (VWM $[NO_3^-]_{aq}$=126 μM), which likely originated from regional urban and industrial combustion sources of NO_x. The abundant $[Cl^-]_{aq}$ (VWM 85.0 μM) as well as $[Na^+]_{aq}$ (VWM 101 μM) demonstrate a marine influence on fog composition, in agreement with back trajectory analyses and regional wind direction during sampling periods. The total organic carbon concentration ($[TOC]_{aq}$; mean 8.27 mg C L^{-1}) was within the range of $[TOC]_{aq}$ values measured in fogs and ground-based clouds near populated areas in the United States (Herckes et al., 2013: e.g., median values of 6.0 mg C L^{-1} in Baton Rouge, LA, 2004/2005, Raja et al., 2008; 8.1 at Shenandoah National Park, VA, 1990/1991, Anastasio et al., 1994; 10.1 in Angiola, CA, 2000/2001, Herckes et al., 2002b).

Table 3-1. Volume weighted mean (VWM), minimum, and maximum concentrations of organic and inorganic species quantified in fog samples collected at CP in 2015. Values below the LOD are shown in italics. Significant digits were determined based on uncertainties (95% CIs) and digits in raw data.

			Aqueous Concentration				Uncertainty	Air Equiv. Concentration	
Chemical	Unit	Samples	VWM	Min	Max	LOD	(95% CI)	Mean	Unit
pH	--	20	6.01	5.34	6.67	--	--	0.026	nmol m^{-3}
TOC	mg C L^{-1}	20	8.27	4.7	16.8	0.26	0.03	0.17	ng C m^{-3}
NH_4^+	µM	20	232	85	640	0.9	0.7	13.5	nmol m^{-3}
NO_3^-	µM	20	126	30.4	778	0.6	0.4	7	nmol m^{-3}
Na^+	µM	20	101	*<LOD*	320	30	0.4	2	nmol m^{-3}
Cl^-	µM	20	85	30	283	4	1.5	1.9	nmol m^{-3}
SO_4^{2-}	µM	20	28.3	12.1	90	0.5	0.8	0.54	nmol m^{-3}
Ca^{2+}	µM	20	21.2	5	72.8	0.4	0.4	0.41	nmol m^{-3}
Mg^{2+}	µM	20	14.1	*<LOD*	43.9	0.4	0.3	0.29	nmol m^{-3}
K^+	µM	20	10.2	2.74	22.3	0.05	0.5	0.2	nmol m^{-3}
NO_2^-	µM	20	5.6	2.7	15.8	0.2	0.4	0.11	nmol m^{-3}
Formate	µM	20	23	10	38	22	2	0.47	nmol m^{-3}
Acetate	µM	20	12	4	29	22	3	0.11	nmol m^{-3}
Oxalate	µM	20	11.2	5	32.6	0.5	0.5	0.45	nmol m^{-3}
Malonate	µM	20	4.16	0.2	12.5	0.16	0.18	0.09	nmol m^{-3}
MSA	µM	20	3.01	1.5	7.3	0.02	0.02	0.064	nmol m^{-3}
HCHO	µM	20	3.4	1.3	6.6	0.4	0.7	0.067	nmol m^{-3}
Succinate	µM	20	3.03	0.56	6.27	0.12	0.13	0.062	nmol m^{-3}
Lactate	µM	20	3.2	*<LOD*	8.6	11	1.1	0.05	nmol m^{-3}
Pyruvate	µM	20	1.9	0.7	4.7	0.011	0.013	0.04	nmol m^{-3}
Glutarate	µM	20	1.81	0.5	5.5	0.05	0.05	0.038	nmol m^{-3}
Propionate	µM	20	1.4	0.5	2.5	0.2	0.3	0.029	nmol m^{-3}
Maleate	µM	20	0.52	0.2	1.5	0.1	0.11	0.011	nmol m^{-3}
Adipate	µM	20	0.078	0.031	0.206	0.012	0.013	0.003	nmol m^{-3}
All Nitrophenols	µM	20	0.022	0.0053	0.0696	0.0035	0.005	0.0009	nmol m^{-3}
Pinate	µM	20	0.0066	*<LOD*	0.0356	0.0011	0.0012	0.0003	nmol m^{-3}
Pinonate	µM	20	0.042	0.02	0.09	0.0009	0.001	0.002	nmol m^{-3}
Azelate	µM	20	0.09	*<LOD*	0.22	0.02	0.03	0.004	nmol m^{-3}
All Org. Acids	µM	20	66	33	136	2≤2	4	4.1	nmol m^{-3}
Levoglucosan	µM	14	0.0473	*<LOD*	0.112	0.0148	0.0001	1.1	nmol m^{-3}
Galactosan	µM	14	0.0179	*<LOD*	0.06	0.0148	0.0001	0.44	nmol m^{-3}
Galactose	µM	14	0.0143	*<LOD*	0.0208	0.0133	0.0001	0.35	nmol m^{-3}
Glucose	µM	14	0.0153	*<LOD*	0.0364	0.0133	0.0001	0.39	nmol m^{-3}
Mannose	µM	14	0.0153	*<LOD*	0.289	0.0133	0.0001	0.38	nmol m^{-3}
Mannitol	µM	14	0.015	*<LOD*	0.0288	0.0137	0.0001	0.35	nmol m^{-3}
Arabinose	µM	14	0.016	*<LOD*	0.0413	0.016	0.0001	0.4	nmol m^{-3}

Fog water constituent concentrations have a negative trend with atmospheric LWC (Elbert et al., 2000), although not a linear or strong correlation in some environments (Straub et al., 2012). The role of LWC in the differences in chemical concentrations between the two campaigns cannot be entirely ruled out, but the mechanism of dilution cannot explain the observed trends.

Four fog events were sampled with sufficient volume for full chemical analyses (20 samples, five samples per event) in 2015. Sea salt (ss) contributions to fog water constituents were estimated using ratios of ionic concentrations in seawater (Cheng et al., 2000). The measured molar ratio of Cl^-/Na^+ ranged between 0.65 and 3.0, with a mean value of 1.1, while the expected ratio in seawater is 1.16 mole Cl^-/mole Na^+ (Cheng et al., 2000;

Eriksson, 1960; Mouri and Okada, 1993). Samples with higher ratios may have been affected by HCl scavenged to the nucleating particles or fog (Zhang and Iwasaka, 2001). Sea salt contributions of other ions, using Na^+ as a conserved tracer, were as follows: 21% of K^+, 58% of Mg^{2+}, 11% of Ca^{2+}, and 22% of SO_4^{2-}. MSA is also a chemical marker of marine emissions, formed in the atmosphere exclusively as an oxidation product of dimethylsulfide via either $^{\bullet}OH$ or $^{\bullet}NO_3$ reaction (Seinfeld and Pandis, 2006). The air equivalent concentration of MSA $[MSA]_{aireq}$) was strongly ($r^2 \geq 0.80$) correlated with the concentration of sea salt sulfate, $[ss\text{-}SO_4^{2-}]_{aireq}$, during events one, two and four. Oxalate has been suggested as a product of aqueous oxidation from marine carbon emissions (Rinaldi et al., 2011; Warneck, 2003), and $[oxalate]_{aireq}$ was most strongly correlated with $[ss\text{-}SO_4^{2-}]_{aireq}$ in the same events ($r^2 \geq 0.90$), suggesting in-cloud aqueous oxidation of marine emissions as a possible source (see Appendices).

3.3.2 Contrast of Fog between 2015 and 1985/6

Fog water concentrations of the major inorganic species NH_4^+, NO_3^-, and SO_4^{2-} were lower in the more recently collected fog water (VWM $[NH_4^+]_{aq}$ in 2015: 232 μM, and in 1985/6: 536 μM; $NO_3^-]_{aq}$ in 2015: 126 μM, and in 1985/6: 364 μM; $[SO_4^{2-}]_{aq}$ in 2015: 29 μM, and in 1985/6: 147 μM; Figure 3-2). Fog water collected at CP was substantially less acidic in 2015 than 1985/6 (pH 2015: 5.34-6.68, VWM=6.01, n=20; pH 1985/6: 3.28-4.93, VWM=3.96, n=42), despite lower $[NH_4^+]_{aq}$ in 2015. Free acid concentrations introduced as HNO_3 and H_2SO_4 can instead explain this change with time, supported by the excess incarboxylic acidity noted in the 1985/6 study by Munger et al. The NO_3^- acidity, calculated as the ratio of $[NO_3^-]_{aq}$ to $[NH_4^+]_{aq}$ in excess of $[(NH_4)_2SO_4]_{aq}$, was on average 0.7 in 2015, and 1.1 in 1985/6. The change in fog water constituent concentrations between 1985/6 and 2015 was likely due in part to successful mitigation of NO_x and SO_2 emissions in the region. Measured decreases in daily one-hour maximum $[NO_2]_{gas}$ and $[SO_2]_{gas}$ in Ventura County were -0.6 ppb yr^{-1} and -0.2 ppb yr^{-1}, respectively (calculated from slopes of EPA Ventura County monitoring site data: 10 sites with NO_2 data from 1980-2005; four sites with SO_2 data from 1980-2004; U.S. Environmental Protection Agency, 2015). Decreases in solute concentrations have also been observed in the SJV, consistent with emissions reductions (Collett et al., 1999; Herckes et al., 2015).

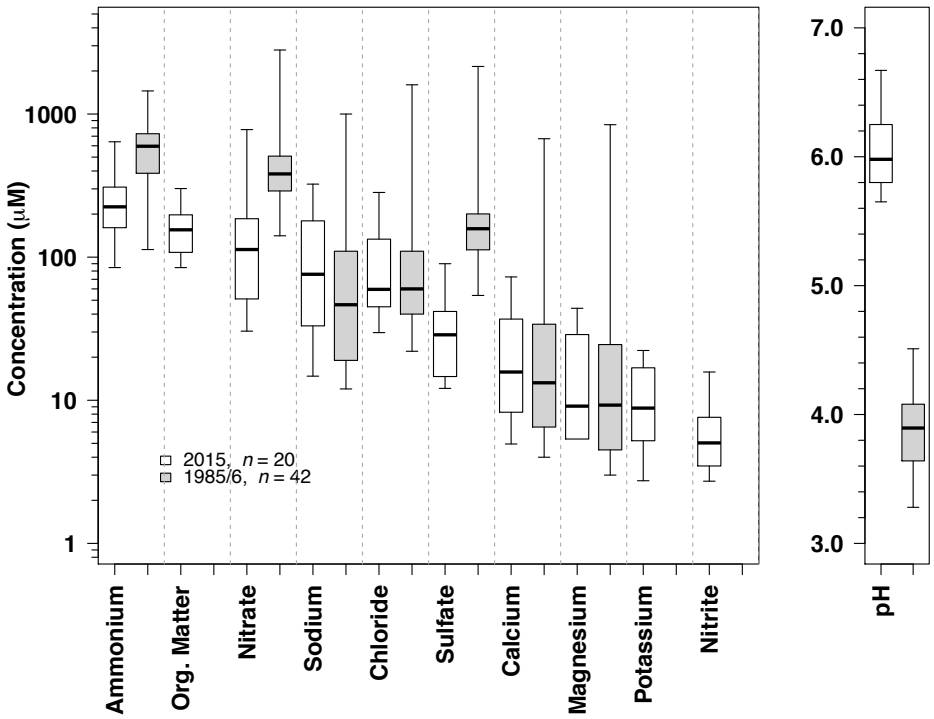

Figure 3-2. Overall composition of CP fog water in 2015, contrasted with the CP fog water composition in 1985/6 (Munger et al., 1989). Chemical species are ordered by mean value. Grey boxes represent 2015 concentrations, while white boxes represent 1985/6 concentrations. Organic matter concentrations was calculated assuming an organic matter/organic carbon mass ratio of 1.8 (Zhang et al., 2005). Centroids of boxes represent median values for each species, box borders extend to interquartile range, and whiskers extend to outliers. Hydrogen concentrations are plotted separately because the concentration range extends to lower values than those of other species plotted. For all 1985/6 analyses, *n*=42; for all 2015 analyses, *n*=20.

Shipping emissions are estimated to contribute substantially to O_3 and aerosol NO_3^- and SO_4^{2-} mass along the Southern California coast (Coggon et al., 2012; Vutukuru and Dabdub, 2008), and regional shipping ports have increased in capacity between the 1980s and 2010s (Andrew et al., 2011; US Department of Transportation Maritime Administration, 2015, 1985). Back trajectories demonstrated onshore flow during the sampled fog events (Fig. A3-14), but trends in fog constituent concentrations decreased, and were therefore minimally affected by increasing shipping emissions. Similarly, atmospheric transport across the Pacific has also been identified as a substantial source of pollutants to the west coast of the U.S. (Heald et al., 2006; Park et al., 2004), but would not explain the observed decreasing trend of pollutants, and especially SO_4^{2-}.

Measured LWC was lower in the 2015 than the 1985/6 study (approximately 150 mg m^{-3} on average in 1985/6, but only 60 mg m^{-3} in 2015). The 1985/6 study took place later in the summer, when fog frequency and density is typically higher (Johnstone and Dawson, 2010). Coastal fog along the California Coast may be declining over time as a function of the changing boundary layer height and coastal temperatures (Johnstone and Dawson, 2010), heat

island effect (Williams et al., 2015), or as a result of climatic cycles (Herckes et al., 2015). Additionally, Munger and others have noted that fog frequency in 1985/6 along the California Coast was anomalously high (Johnstone and Dawson, 2010; Munger, 1989). Since concentrations of fog water constituents were lower in 2015, however, and concentrations would be expected to increase with decreasing LWC (perhaps non-linearly, Straub et al., 2012; van Pinxteren et al., 2015), the expected relationship is not observed.

Hydrocarbon emissions also appear to have decreased between 1985/6 and 2015, based on fog water concentrations of volatile, low molecular mass (LMM) oxidation products of hydrocarbons; specifically, formaldehyde, acetate, and formate. Formaldehyde is mainly produced in the atmosphere via oxidation of hydrocarbons: in the remote and marine atmosphere, methane oxidation is the main production pathway, while non-methane hydrocarbon oxidation contributes a larger fraction of formaldehyde in areas close to urban emissions (Fortems-Cheiney et al., 2012). Isoprene is also a prominent precursor of formaldehyde (Munger and Jacob, 1995). Concentrations of formaldehyde are typically highest near urban areas (Collett et al., 1999). The VWM $[\text{formaldehyde}]_{aq}$ measured in 2015 (3.4 μM) was approximately half that measured in 1986 (7 μM), but within the range of values for remote regions (van Pinxteren et al., 2005). Lower $[\text{acetate}]_{aq}$ and $[\text{formate}]_{aq}$ were measured in 2015 than 1985/6, despite higher fog pH, which should increase uptake to the aqueous phase (2015: VWM $[\text{acetate}]_{aq}$=12 μM, VWM $[\text{formate}]_{aq}$=23 μM; 1985/6: VWM $[\text{acetate}]_{aq}$ = 9 μM, VWM $[\text{formate}]_{aq}$ 24 μM). The ratio between acetate and formate in aerosol has been suggested as a tracer for the dominance of biogenic vs. anthropogenic influence: direct emissions from combustion sources such as vehicles and biomass burning were associated with acetate/formate ratios <1, while growing season acetate/formate values were 1.3 on average in a residential area in eastern Virginia (Talbot et al., 1988). The VWM ratio in 2015 CP fog of 0.56 suggests influence of anthropogenic hydrocarbon oxidation (mass accommodation coefficients of acetate and formate are similar, Jayne et al., 1991). The apparent anthropogenic influence on the concentrations of acetic and formic acids was consistent between 1985/6 and 2015: the VWM value for fog samples collected throughout Southern California in 1985/6 was 0.42, similar to the 2015 study.

3.3.3 Contribution of Low Molecular Mass Carboxylic Acids to Fog Organic Matter

Gaseous and aqueous photo-oxidation reactions are a dominant source of carboxylic acids in the atmosphere, producing a range of carboxylic acid species (Figure 3-3; Chebbi and Carlier, 1996; Kleindienst et al., 1999; Lim et

al., 2010). Correlations were observed between $[oxalate]_{aq}$ and the concentrations of several other carboxylic acids: pyruvate (r^2=0.80), methanesulfonate (r^2=0.87), glutarate (r^2=0.88), and malonate (r^2=0.86). $[Acetate]_{aq}$ and $[propionate]_{aq}$ were also correlated with one another (r^2=0.80). These relationships suggest a similar oxidation process (gas- or aqueous-phase oxidation) leading to the formation of the correlated acids. The percentage of TOC accounted for by C_1-C_9 quantified carboxylic acids from IC and HPLC-(-)-ESI-HR-ToF-MS analyses (abbreviated as percOA) was 20.1% on average, ranging between 9.6% and 30.0% (Table 3-1 and Figure 3-1.). This value is low amongst the other previous measurements of percOA (52% in fog water from the Yellow Sea, Boris et al., 2016; 16% at Davis, California, Herckes et al., 2002b; and 43% at Fresno, California, Collett et al., 2008; Figure 3-4). Formate, acetate, and oxalate typically accounted for most of the carboxylic acid mass, contributing ~3% individually in the CP fog samples: acetate 3.74%, 14 μM; formate 3.40%, 24 μM; and oxalate 3.54%, 13.5 μM (Table 3-1 and Figure 3-3); a similar predominance of these three species has be found in other fog chemistry studies globally (Boris et al., 2016; Löflund et al., 2002; Raja et al., 2008).

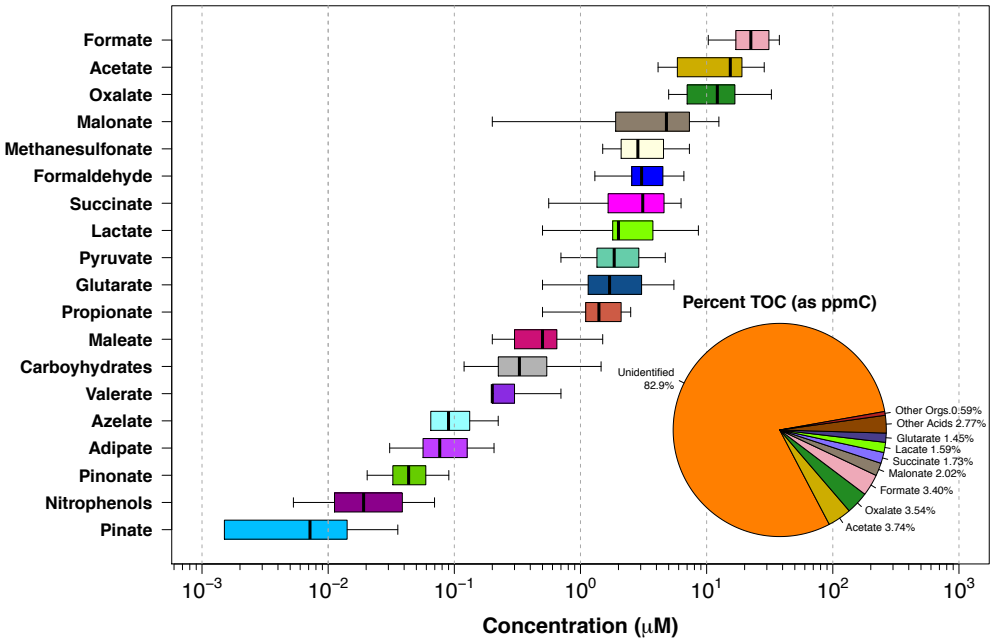

Figure 3-3. Organic constituent concentrations of 2015 CP fog water. Box plot shows summarized organic species (μM) with box outer bounds at 25th and 75th percentiles, center line is median value, and whiskers extend to outliers. Inset pie chart shows percentage of measured organic carbon contributed by specific fog water constituents (colors are the same in box and pie plots unless labeled). On average, carboxylic acids account for 20.1% of TOC. Percentages were calculated using carbon mass concentrations for all organic fog water constituents (in ppmC = mg C L^{-1}). For all species, n=20. The category "other orgs." includes carbohydrates, formaldeyde, and nitrophenols; "other acids" includes methanesulfonate, pyruvate, propionate, maleate, valerate, azelate, adipate, pinonate, and pinate; "carbohydrates" includes galactosan, glucose, mannose, mannitol, arabinose, xylose, levoglucosan, and mannosan; "nitrophenols" includes 4-nitrophenol, 2-methyl-4-nitrophenol, and 2,4-dinitrophenol.

Since LMM carboxylic acids are products of atmospheric oxidation, the large number of carboxylic acids contributing to the percOA in the CP fog water suggests the fog samples contained oxidized organic matter (malonate, succinate, glutarate, and lactate each contributed an additional >1% of TOC).

The uptake of carboxylic acids to aqueous fog droplets is enhanced at basic pH, due to salt formation such as NH_4-oxalate (carboxylic acid pKa values typically between 2 and 5; Ervens et al., 2003; Ortiz-Montalvo et al., 2014, 2012). At CP, fog $[\text{carboxylic acids}]_{aq}$ was correlated with $[NH_4^+]_{aq}$ (r^2=0.79) and $[\text{cations}]_{aq}$ (r^2=0.78; Na^+: r^2=0.40; but not with pH, r^2=0.03). Unexpectedly, the measured percOA was greater at more acidic pH considering published fog/cloud chemistry studies (Figure 3-4).

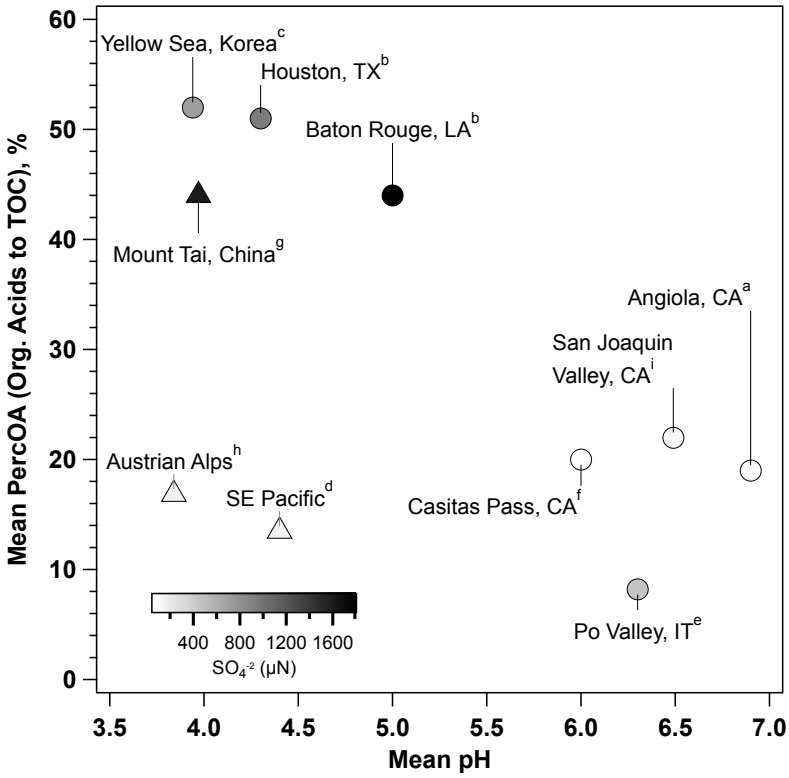

Figure 3-4. Dependence of the mean carboxylic acid percent contribution to TOC concentrations in various studies of fog and cloud water globally. Trend does not reflect expected dependence of volatile carboxylic acid abundance on pH and ionic balance within a solution of atmospheric water. Data points are shaded by $[SO_4^{2-}]_{aq}$ (greater concentrations are darker; ranging from 56 to 1790 µN). Three samples represent cloud water (triangles): the "SE Pacific" and "Austrian Alps" samples demonstrate limited carboxylic acid concentrations in remote environments. No apparent trend with season, number/species of carboxylic acids, or TOC was apparent. References: [a]fog from agricultural land use region in Angiola, CA, December 2000-February 2001 (Herckes et al., 2007); [b]fog from urban Baton Rouge, LA (November 2005-March 2006) and fog from urban Houston, TX (February 2006, Raja et al., 2008); [c]fog from rural but anthropogenically impacted and aged air masses at Baengnyeong Island, Republic of Korea (July 2014, Boris et al., 2016); [d]rural/marine cloud from Southeast Pacific Ocean off the coast of Chile during the VOCALS campaign (marine stratus; October-November 2008, Benedict et al., 2012); [e]fog from agricultural land use region in Po Valley, Italy (November-March 1989-2011, Giulianelli et al., 2014); [f]Casitas Pass, CA (current study; June 2015); [g]orographic cloud from agricultural, biomass burning, and coal combustion impacted region in Mount Tai, China (carboxylic acids concentrations from unpublished data; June-July 2008, Shen et al., 2012); [h]orographic cloud from Mt. Rax, Austria (March/April of 1999/2000, Löflund et al., 2002); [i]radiation fog from Bakersfield, Fresno, and the Kern Wildlife Refuge in the South and Central San Joaquin Valley of California (December 1995-January 1996, Collett et al., 1999).

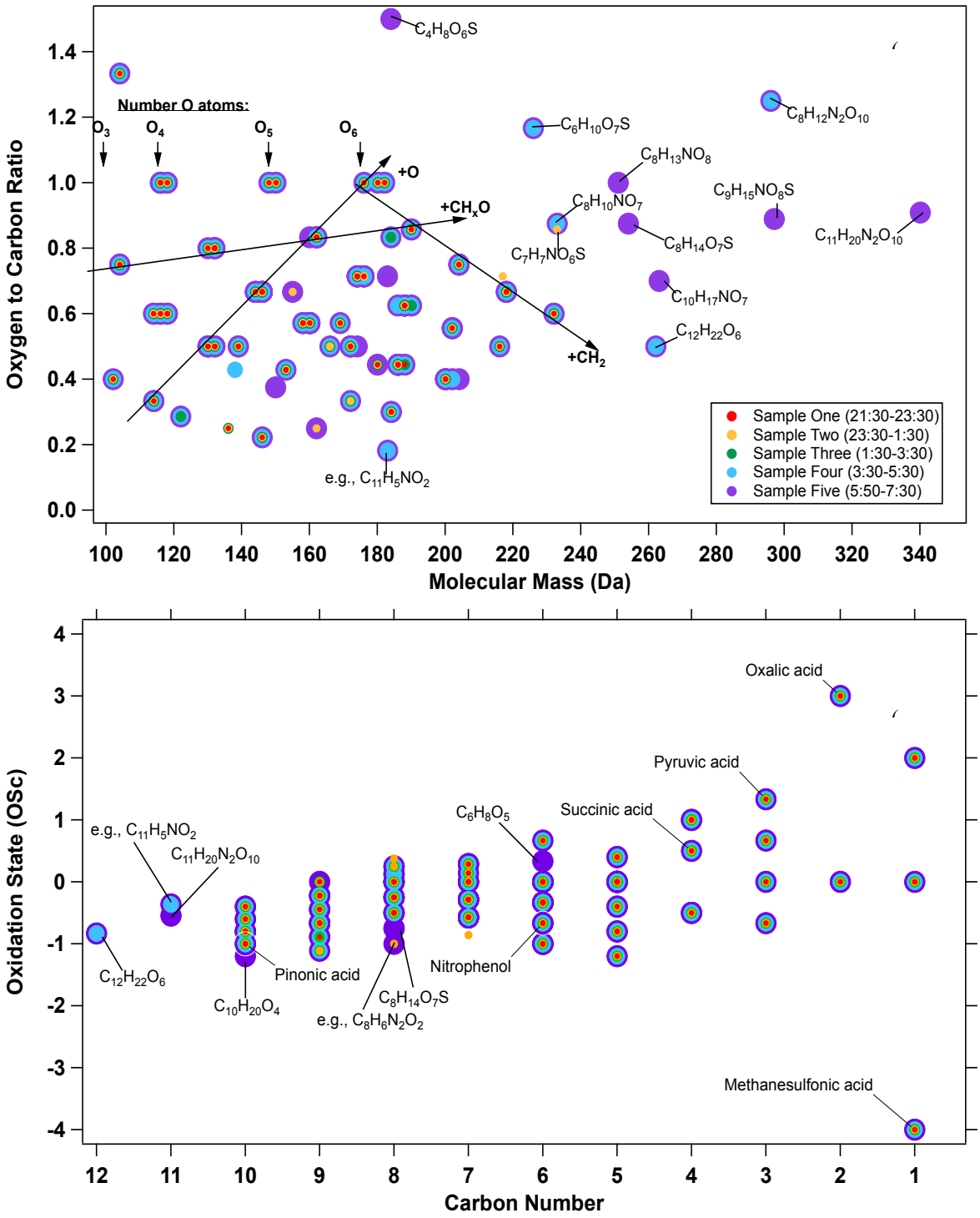

Figure 3-5. Polar, organic compounds identified via LC-(-)-ESI-HR-ToF-MS and IC in event 3 (other events were similar). Molecular composition within the fog is illustrated via (a) a plot of the oxygen/carbon atom ratio versus molecular mass (Da) and (b) oxidation state versus carbon number ("Kroll diagram"). Small, red points represent the first sample in the fog event while large, purple points represent the final sample collected. Series of compounds in (a) appearing diagonally with decreasing O/C ratios at increasing molecular mass differ mostly by CH_2, with the same number of O atoms through each series. The space occupied by fog constituents in (b) corresponds to semi-volatile and low-volatility oxygenated organics (Kroll et al., 2011).

No relationship between sampling season, number of quantified carboxylic acids, TOC, or $[NH_4^+]_{aq}$ with percOA was apparent, but the trend in measured $[SO_4^{2-}]_{aq}$ did somewhat match that of percOA. The percOA must also be dependent on other factors, such as the degree of aging, organic emissions, or LWC (Ervens et al., 2003; Pandis and Seinfeld, 1991; Ricci et al., 1998; Winiwarter et al., 1992).

3.3.4 Polar Organic Fog Water Constituents (≥C_4)

Aged biogenic and aged anthropogenic organic species were identified in the 2015 CP fog water, including nitrophenols, long-chain (C_4-C_{10}) saturated and unsaturated carboxylic acids, and α-pinene and isoprene oxidation products (Table A3-1; tentative identifications made based on formulae). Patterns in identified molecular formulae are shown for fog water collected during event 3, which contained the greatest concentrations of organic species of the fog samples collected (Figure 3-5a and b). Families of similar species, especially carboxylic acids, were present in the samples, differing by CH_2, O, and CH_xO, indicating that there were multiple contributing oxidation pathways of precursor VOCs leading to the complex mixture of aged organics within these fog samples. The molecular difference of CH_2O has been reported previously in high humidity oxidation of biogenic secondary organic aerosol (Nguyen et al., 2011), and observed within products of aqueous oxidation (Chapters 5 and 6). It is currently unclear whether this difference results from a loss or a gain of CH_xO; *i.e.*, whether these products are overall a result of the process of fragmentation, functionalization, or oligomerization. The progression of oxidation can also be visualized by plotting the carbon oxidation state versus carbon number (oxidation state of carbon, OS_c=-$\sum_i OS_i \frac{n_i}{n_c}$ where OSi is the oxidation state of each element i, n_i is the number of atoms of i, and n_c is the number of atoms of carbon, Kroll et al., 2011). This space displays the same three processes, with overall oxidation toward the top right in the diagram and oligomerization to the left; species observed in the final two samples of event three appear to be such oligomerization (and functionalization, with N and S atom) products. During the later hours (after 2:00 am, or after the typical maximum LWC) of each fog event, in fact, differing high molecular mass, oxygenated species were apparently formed, including CHOS and CHNO. The CHO species $C_{12}H_{22}O_6$, $C_{10}H_{20}O_4$, and $C_6H_8O_5$ were also found in only mature fog water. These species may have formed through aqueous oxidation, as suggested in previous studies (CHOS via radical-catalyzed esterification of -OH groups, Surratt et al., 2008, and CHNO via dark reaction with HONO and H_2O_2 or via $^{\bullet}NO_2$ reaction, Vione et al., 2005). These observeations could alternatively reflect the lower (and varying) vapor pressure of organic compounds at the lower temperatures observed during the

later hours of the night, or evaporation of water to leave greater organic species concentrations in the fog. Only minimal wind during fog events was observed, making advection of new air masses containing differing organic species an unlikely explanation.

S-containing organics remain a fraction of organic aerosol that, while ubiquitous, are implicated in many formation mechanisms and research to demonstrate which mechanism is dominant is ongoing (McNeill, 2015). Fog samples at CP contained multiple CHOS and CHNOS species derived from biogenic and anthropogenic molecules, some of which have been observed in fog and aerosol samples previously (Boris et al., 2016). These species (tentatively) included hydroxybutanoic acid, sulfate ester ($C_4H_8O_6S$), a methylglyoxal oxidation product ($C_6H_{10}O_7S$; Sareen et al., 2010), $C_7H_7NO_5S$, methylnitrophenol sulfate ester ($C_7H_7NO_6S$), a limonene oxidation product ($C_8H_{14}O_7S$; Mazzoleni et al., 2010; Surratt et al., 2008), $C_9H_{14}O_7S$, and $C_{21}H_{15}NO_8S$.

Organic nitrogen compounds such as nitrophenols have been recently cited as an important category of chemical species for absorption of sunlight (often cited within the class of "brown carbon" compounds), formed most likely via aqueous reactions in the atmosphere (Desyaterik et al., 2013; Mohr et al., 2013; Zarzana et al., 2012). These species are additionally of atmospheric importance because of their toxicity to animals (Agency for Toxic Substances and Disease Registry, 2011, 1992) as well as plants (Natangelo et al., 1999). CHNO species within CP fog samples included $C_8H_{12}N_2O_{10}$, $C_{11}H_{20}N_2O_{10}$, $C_{11}H_5NO_2$, and $C_{21}H_{15}NO_2$. In addition, a series of nitrophenols were quantified within the CP fog samples (Table A3-1): 4-nitrophenol (mean 6.92 nM), 2,4-dinitrophenol (mean 11.3 nM), and 2-methyl-4-nitrophenol (4-nitro-*o*-cresol; mean 7.93 nM); three additional nitrophenols were quantified above LOD in only two fog samples. These concentrations are lower than those measured within atmospheric water at Baengnyeong Island in the Yellow Sea (mean $[\text{4-nitrophenol}]_{aq}$=36.4 nM, mean $[\text{2,4-dinitrophenol}]_{aq}$=20.7 nM, and mean $[\text{2-methyl-4-nitrophenol}]_{aq}$=3.8 nM; Boris et al., 2016), at Mount Tai on the North China Plain (mean $[\text{4-nitrophenol}]_{aq}$=3.18 μM; Desyaterik et al., 2013), and in Northeastern Bavaria (mean $[\text{4-nitrophenol}]_{aq}$=140 nM, mean $[\text{2,4-dinitrophenol}]_{aq}$=56 nM; Richartz et al., 1990), but are consistently present above the LOD in the fog samples from CP. Primary and secondary biomass burning emissions are a source of nitrophenols (Harrison et al., 2005). However, a signature of biomass burning was unlikely at CP in June 2015: $[\text{levoglucosan}]_{aq}$ was low (Sullivan et al., 2008; Weber et al., 2007), the correlation between $[\text{total nitrophenol}]_{aireq}$ and $[\text{nss-K}^+]_{aireq}$ was weak ($r^2 \leq 0.01$), and $[K^+]_{aq}$ was similar to that observed in Southern California fog previously (Jacob et al., 1985). Nitrophenols can be transported to remote areas and/or formed in the atmosphere downwind of

pollutant source regions; nitrophenols measured at CP were therefore plausibly from secondary reactions with aromatic VOCs such as benzene and toluene (Harrison et al., 2005; Lüttke et al., 1997).

3.3.5 Fog Water Non-Polar Constituents

The concentrations of non-polar (or slightly polar) organic constituents were determined within fog samples that had been composited to represent one measurement per event. Polycyclic aromatic hydrocarbons (PAHs), alkanes, and other species such as hopanes were below detectable limits, as were biogenic VOCs previously detected in Southern California (Arey et al., 1995). This is surprising given the location of the sampling sites within densely vegetated hills, and near urban areas. A series of *n*-alkanoic acids and the pesticide DEET were the only non-polar VOCs identified in the fog water samples. DEET was identified by mass spectral library match and confirmed using a chemical standard. The only reported applications of DEET in Santa Barbara and Ventura Counties between 2009 and 2013 (the most recent data available at the time of query) according to the California Department of Pesticide Regulation Pesticide Information Portal (http://calpip.cdpr.ca.gov/) are small applications (<20 lbs. chemical applied to under 20 acres each) for landscaping, outdoor cut flowers or greens, or greenhouse-contained plants. It has been suggested that only a small fraction (5%) of DEET applied as personal care product would be introduced to the atmosphere, and that the majority of the chemical found in the environment (87.5%) would enter waterways, mainly via washing into wastewater (Weeks et al., 2012). DEET has been reported in wastewater and U.S. waterways, but at concentrations below those measured in fog water here (Sandstrom et al., 2005). The origin of the DEET measured in the CP fog water therefore remains unknown.

The ratio within a given class of compounds of odd/even carbon number molecules is referred to as the carbon preference index (CPI). The CPI was calculated for the homologous series of *n*-alkanoic acids identified within the fog water samples (as methyl esters; Table A3-2). An even carbon number predominance (CPI>1) in *n*-alkanoic acids has been previously associated with a predominant biogenic input to organic carbon, since petroleum contains approximately equivalent concentrations of even and odd carbon number alkanes (which oxidize to *n*-alkanoic acids), while biosynthetic pathways typically produce *n*-alkanoic acids with even carbon numbers (Abas and Simoneit, 1996; Ho et al., 2011). It has also been noted that marine aerosol can contain high fractions of $<C_{20}$ *n*-alkanoic acids, which likely comes from plankton and marine bacteria (Alves et al., 2007). The CPI calculated from

each fog event at CP in Southern California was ≥4.0, indicating that biogenic (including marine biogenic) processes contributed a substantial source of organic matter to the fog water.

3.3.6 Volatile Organic Compounds

Whole air grab samples were collected near VOC sources potentially impacting CP, and at the sampling locations during fog events (Figure 3-1). Concentrations of most VOCs were greatest near the site of the Refugio oil spill along Interstate 5 (Figure 3-6). A distinct odor of oil was present at the spill site, despite the oil spill having been contained and partially cleaned up by the beginning of the fog sampling period (National Oceanographic and Atmospheric Administration, 2015). A study of the Deepwater Horizon Oil Spill impact on atmospheric chemistry (De Gouw et al., 2011) estimated that, emissions of $\leq C_{18}$ oil constituents such as those measured in the present study are theoretically volatilized to the atmosphere within the first day after surfacing of spilled oil. Thus, although gaseous hydrocarbons measured at the oil spill cleanup site included high concentrations of chemical markers for raw O&NG, it is likely that emissions had already subsided, and the oil spill had little impact on regional air quality during the fog sampling campaign. Measured [VOC]s from grab samples were overall similar between fog samples and events. The enhancement ratio of $[iso\text{-pentane}]_{gas}$ to $[n\text{-pentane}]_{gas}$ (iC_5/nC_5 ratio) is used to distinguish raw O&NG extraction emissions from those of vehicles/O&NG processing (Gilman et al., 2013). The iC_5/nC_5 ratio at CP during fog sampling periods was between the ratios indicative of raw O&NG/extraction and vehicles/O&NG processing (Figure 3-6).

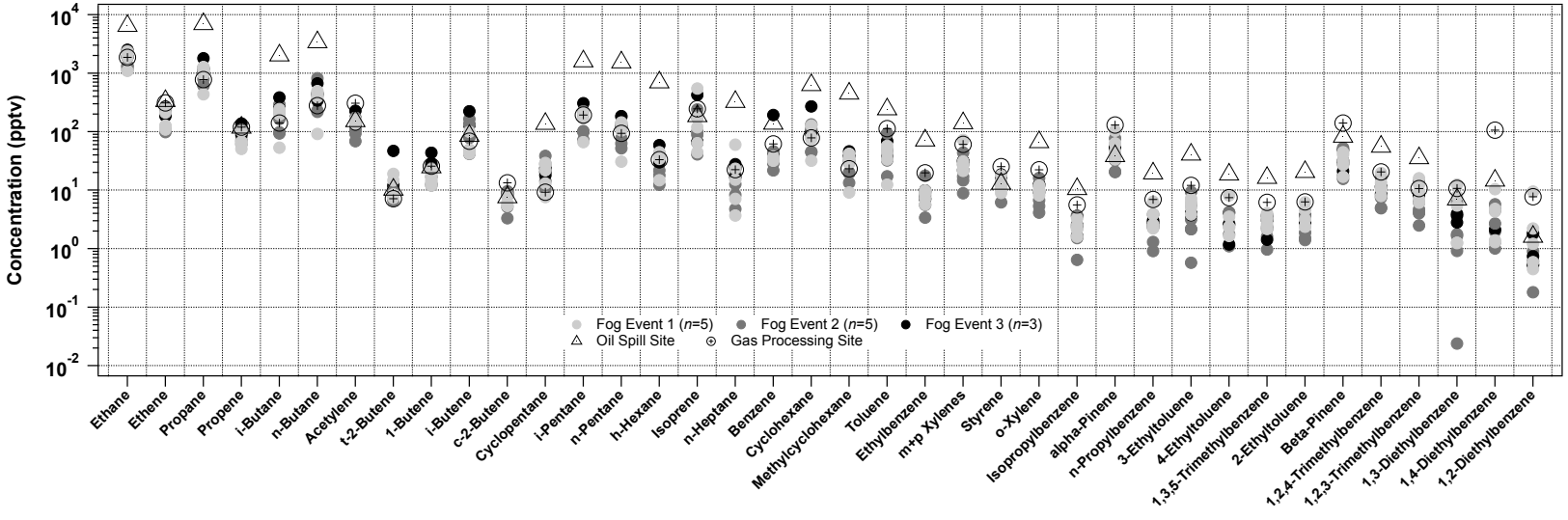

Figure 3-6. VOCs measured from grab samples during fog sampling periods (shades of blue) and near two VOC sources potentially impacting CP: the oil spill cleanup site on I-5, and an O&NG processing site.

No correlation was observed, however, between the O&NG extraction tracer (Gilman et al., 2013) propane and the iC_5/nC_5 ratio (r^2=0.13), causing uncertainty in any O&NG impact on intercepted fog events. A regional VOC signal of O&NG processing (rather than raw O&NG/extraction) was identified during fog sampling periods based on similarities between ratios of measured [VOC]s to those measured near an O&NG processing site (Figure 3-7).

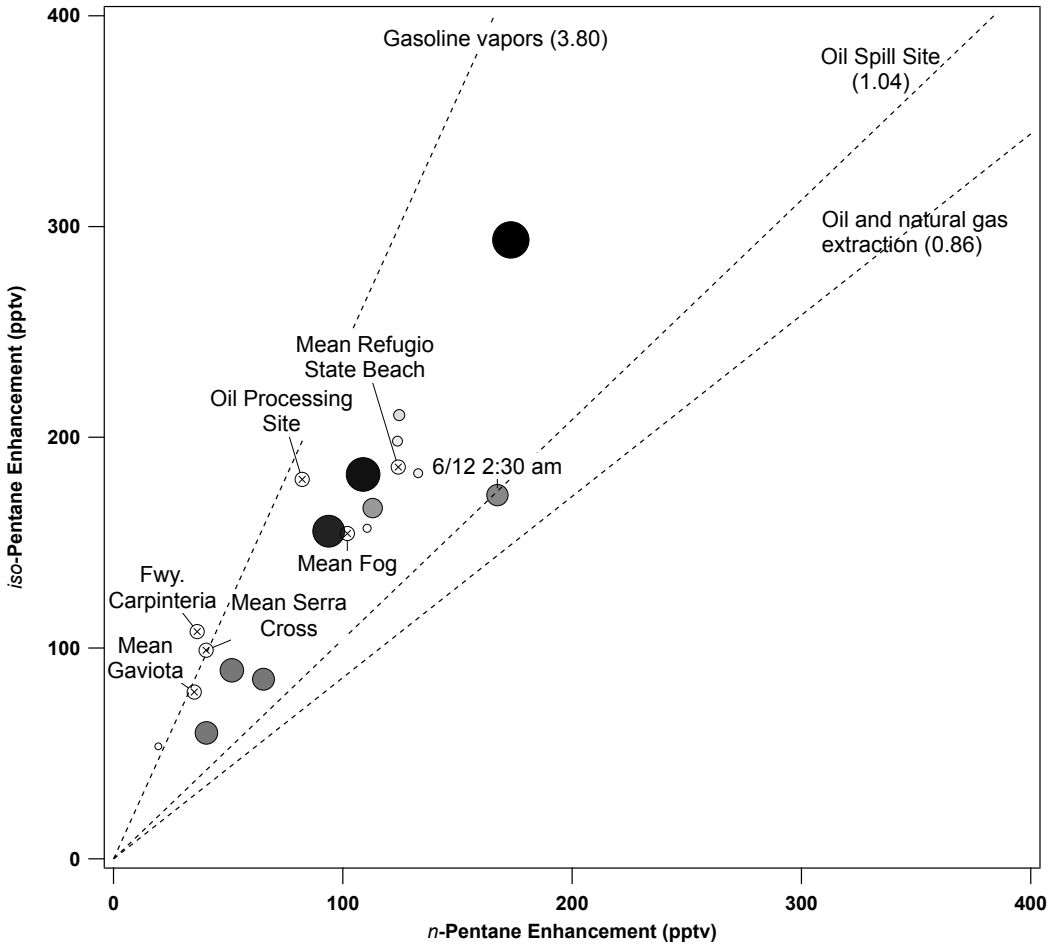

Figure 3-7. Enhancement ratio of the iC_5/nC_5 ratio in grab samples, which demonstrates distinction between VOCs from raw O&NG/extraction versus vehicles/O&NG processing. A sample collected during fog event 2 on 06/12 at 2:30 am (labeled) is likely to have been impacted by VOCs from the oil spill because of the similar iC_5/nC_5 ratio to that measured at the oil spill site (central dashed line). Reference ratios from raw O\&NG extraction (Colorado) measured by Gilman et al. (2013); ratio from vehicle gasoline vapors (California) measured by McGaughey et al. (2004). Fog samples denoted by circles (darker color and larger marker size indicates increasing sampling date and time), while grab samples collected from possible VOC emissions sources are indicated by circled "×" symbols.

A vehicular signal, characterized by $[acetylene]_{gas}$ and $[benzene]_{gas}$ elevated above concentrations in other samples was also observed (See Appendix 3). The concentration of acetylene, which originates mostly from gasoline vehicles, was greatest in the sample from the O&NG processing site and at the Serra Cross (located adjacent to a parking lot, and above the city of Ventura), and near I-5 in Carpinteria. VOCs from wells along and near the Ojai

Valley or offshore platforms cannot be definitively differentiated from those at the oil spill cleanup site because many VOCs are emitted from multiple petroleum and industry processes (U.S. Environmental Protection Agency, 1994). Empirical orthogonal function analysis (similar to principle components analysis) confirmed that O&NG extraction emissions and motor vehicle traffic were the most influential VOC emissions sources at CP (see Supporting Information).

The ratios of alkyl nitrates to parent alkanes can be used to determine air mass age since alkyl nitrates are mainly formed from aging of alkanes in the presence of NO_x (Bertman et al., 1995). Ratios of ethyl, 2-propyl *n*-butyl, and 2-pentyl nitrate to parent alkane concentrations were quantified from the whole air grab samples. No apparent trend was observed in the [ethyl nitrate]/[ethane] ratio, but enhancements were observed before midnight in [2-propyl nitrate]/[2-propane], [*n*-butyl nitrate]/[butane] and [2-pentyl nitrate]/[2-pentane], which is suggested here to indicate advection of emissions containing fresh alkanes overnight as winds shifted from westerly to onshore (also see Fig. A3-12 for wind measurements). Concentrations of carboxylic acids were also expected to be formed from photochemical aging processes in the atmosphere; however, there was no apparent relationship between concentrations of alkyl nitrates and carboxylic acids (e.g., for $[\text{2-propyl nitrate}]_{gas}$ versus $[\text{carboxylic acids}]_{aireq}$, r^2=0.32). This result is probably due to the difference in the lesser extent of oxidation required to form alkyl nitrates versus carboxylic acids (beginning from the emission of a hydrocarbon precursor to the atmosphere), or aqueous oxidation with apt conditions to form carboxylic acids, but not alkyl nitrates (Vione et al., 2005).

3.4 Conclusions

Fog chemical composition on the Southern California Coast was determined from fog water samples collected at a high elevation inland site using a variety of analytical techniques. NH_4^+, NO_3^-, and marine NaCl dominated fog water chemical composition. Fog samples also contained aged organic species of biogenic and anthropogenic origin, including nitrophenols, several families of carboxylic acids with up to six O atoms, and oxidation products of α-pinene and isoprene. Several CHOS species were identified, including some that were only detected after 3-5 hours of persistent foggy conditions, suggesting aqueous phase oxidation of organics. A strong correlation observed in three of four fog events between the aqueous concentrations of oxalate, MSA, and ss-SO_4^{2-} supported an in-cloud oxidation formation of some fog water constituents. The percOA was only 20% on average, typical of alkaline, polluted fog samples (Collett et al., 1999; Giulianelli et al., 2014; Herckes, 2007). The quantified total [carboxylic

acids]$_{aq}$ was correlated with [NH_4^+]$_{aq}$ and [cations]$_{aq}$, suggesting that concentrations of volatile carboxylic acids in the fog water were enhanced by reactive uptake. A mean measured ratio of 0.65 between [acetate]$_{aq}$ and [formate]$_{aq}$ indicated that anthropogenic influence on oxidized hydrocarbons was likely. Regional O&NG processing was determined as a primary contributor to [VOC]s during fog events. Mobile source and biogenic VOCs were also measured in air samples collected during fog events.

The results of this study highlight the successes in control technologies for anthropogenic air emissions. In contrast to fog water collected at the same location in 1985/6, the concentrations of anthropogenic species in the 2015 samples were lower, including NH_4^+, NO_3^-, and SO_4^{2-}, by approximately an order of magnitude. The fog was also less acidic in 2015 by two orders of magnitude [H^+]. These differences in major chemical constituent concentrations between the 2015 and 1985/6 fog sampling campaigns can be explained by reduced gaseous and particle phase anthropogenic pollutant emissions due to effective air quality regulations. This work also demonstrates the need for additional research to determine the extent of in-fog formation of CHOS and CHNO species. The formation of these species can result in increased organic aerosol mass formation (McNeill et al., 2012) and absorption of UV and visible light by aerosol (Lin et al., 2015), both of which are important for climate and air quality. The regional O&NG processing VOC emissions measured in this study are likely to be precursors for the observed N- and S-containing organic species, and impacts of these emissions on air quality in the Southern California urban areas as well as natural areas, including the Channel Island National Park, should be considered.

REFERENCES

Abas, M.R. Bin, Simoneit, B.R.T., 1996. Composition of extractable organic matter of air particles from Malaysia: Initial study. Atmos. Environ. 30, 2779–2793.

Adamson, M.R., 2008. Oil Booms and Boosterism: Local Elites, Outside Companies, and the Growth of Ventura, California. J. Urban Hist. 35, 150–177.

Agency for Toxic Substances and Disease Registry, 1992. Toxicological profile for nitrophenols: 2-nitrophenol, 4-nitrophenol. Atlanta, Georgia.

Agency for Toxic Substances and Disease Registry, 2011. Addendum To the Toxicological Profile for Dinitrophenols. Atlanta, Georgia.

Alves, C., Oliveira, T., Pio, C., Silvestre, A.J.D., Fialho, P., Barata, F., Legrand, M., 2007. Characterisation of carbonaceous aerosols from the Azorean Island of Terceira. Atmos. Environ. 41, 1359–1373.

Anastasio, C., Faust, B.C., Allen, J.M., 1994. Aqueous phase photochemical formation of hydrogen peroxide in authentic cloud waters. J. Geophys. Res. 99, 8231.

Andrew, R.K., Howe, B.M., Mercer, J.A., 2011. Long-time trends in ship traffic noise for four sites off the North American West Coast. J. Acoust. Soc. Am. 129, 642–651.

Arey, J., Crowley, D.E., Crowley, M., Resketo, M., Lester, J., 1995. Hydrocarbon emissions from natural vegetation in California South-Coast-Air-Basin. Atmos. Environ. 29, 2977–2988.

Benedict, K.B., Lee, T., Collett, J.L., 2012. Cloud water composition over the southeastern Pacific Ocean during the VOCALS regional experiment. Atmos. Environ. 46, 104–114.

Bertman, S.B., Roberts, J.M., Parrish, D.D., Buhr, M.P., Goldan, P.D., Kuster, W.C., Fehsenfeld, F.C., Montzka, S. a., Westberg, H., 1995. Evolution of alkyl nitrates with air mass age. J. Geophys. Res. 100, 22805.

Boris, A.J., Lee, T., Park, T., Choi, J., Seo, S.J., Collett, J.L., 2016. Fog composition at Baengnyeong Island in the eastern Yellow Sea: detecting markers of aqueous atmospheric oxidations. Atmos. Chem. Phys. 16, 437–453.

California Department of Conservation, 1987. 72nd Annual Report of the State Oil & Gas Superviesor. Sacramento, CA.

California Department of Conservation, 2015. 2014 Preliminary Report of California Oil and Gas Production Statistics. Sacramento, CA.

Chebbi, A., Carlier, P., 1996. Carboxylic acids in the troposphere, occurrence, sources, and sinks: A review. Atmos. Environ. 30, 4233–4249.

Cheng, Z.L., Lam, K.S., Chan, L.Y., Wang, T., Cheng, K.K., 2000. Chemical characteristics of aerosols at coastal station in Hong Kong. I. Seasonal variation of major ions, halogens and mineral dusts between 1995 and 1996. Atmos. Environ. 34, 2771–2783.

Coggon, M.M., Sorooshian, A., Wang, Z., Metcalf, A.R., Frossard, A.A., Lin, J.J., Craven, J.S., Nenes, A., Jonsson, H.H., Russell, L.M., Flagan, R.C., Seinfeld, J.H., 2012. Ship impacts on the marine atmosphere: insights into the contribution of shipping emissions to the properties of marine aerosol and clouds. Atmos. Chem. Phys. 12, 8439–8458.

Collett, J.L., Daube, B., Munger, J.W., Hoffmann, M.R., 1989. Cloudwater Chemistry in Sequoia National Park. Atmos. Environ. 23, 999–1007.

Collett, J.L., Herckes, P., Youngster, S., Lee, T., 2008. Processing of atmospheric organic matter by California radiation fogs. Atmos. Res. 87, 232–241.

Collett, J.L.J., Hoag, K.J., Sherman, D.E., Bator, A., Richards, L.W., 1999. Spatial and temporal variations in San Joaquin Valley fog chemistry. Atmos. Environ. 33, 129–140.

Dawson, T.E., 1998. Fog in the California redwood forest: ecosystem inputs and use by plants. Oecologia 117, 476–485.

De Gouw, J.A., Middlebrook, A.M., Warneke, C., Ahmadov, R., Atlas, E.L., Bahreini, R., 2011. Organic Aerosol Formation Downwind from the Deepwater Horizon Oil Spill. Science (80-.). 331, 1295–1299.

Deguillaume, L., Charbouillot, T., Joly, M., Vaïtilingom, M., Parazols, M., Marinoni, a., Amato, P., Delort, a.-M., Vinatier, V., Flossmann, a., Chaumerliac, N., Pichon, J.M., Houdier, S., Laj, P., Sellegri, K., Colomb, a., Brigante, M., Mailhot, G., 2014. Classification of clouds sampled at the puy de Dôme (France) based on 10 yr of monitoring of their physicochemical properties. Atmos. Chem. Phys. 14, 1485–1506.

Demoz, B.B., Collett, J.L., Daube, B.C., 1996. On the Caltech Active Strand Cloudwater Collectors. Atmos. Res. 41, 47–62.

Desyaterik, Y., Sun, Y., Shen, X., Lee, T., Wang, X., Wang, T., Collett, J.L., 2013. Speciation of "brown" carbon in cloud water impacted by agricultural biomass burning in eastern China. J. Geophys. Res. Atmos. 118, 7389–7399.

Dong, S., Dasgupta, P., 1987. Fast fluorometric flow injection analysis of formaldehyde in atmospheric water. Environ. Sci. Technol. 2, 581–588.

Draxler, R.R., Rolph, G.D., n.d. HYSPLIT (HYbrid Single-Particle Lagrangian Integrated Trajectory) [WWW Document]. NOAA ARL READY Website. URL http://www.arl.noaa.gov/HYSPLIT.php

Ehrenhauser, F.S., Khadapkar, K., Wang, Y., Hutchings, J.W., Delhomme, O., Kommalapati, R.R., Herckes, P., Wornat, M.J., Valsaraj, K.T., 2012. Processing of atmospheric polycyclic aromatic hydrocarbons by fog in an urban environment. J. Environ. Monit. 14, 2566.

Elbert, W., Hoffmann, M.R., Krämer, M., Schmitt, G., Andreae, M.O., 2000. Control of solute concentrations in cloud and fog water by liquid water content. Atmos. Environ. 34, 1109–1122.

Eriksson, E., 1960. The yearly circulation of chloride and sulfur in nature; meteorological, geochemical and pedological implications. Part I. Tellus A 11, 375–403.

Ervens, B., Herckes, P., Feingold, G., Lee, T., Collett, J.L., Kreidenweis, S.M., 2003. On the drop-size dependence of organic acid and formaldehyde concentrations in fog. J. Atmos. Chem. 46, 239–269.

Facchini, M.C., Fuzzi, S., Lind, J.A., Fierlinger-Oberlinninger, H., Kalina, M., Puxbaum, H., Winiwarter, W., Arends, B.G., Wobrock, W., Jaeschke, W., Berner, A., Kruisz, C., 1992. Phase-partitioning and chemical reactions of low molecular weight organic compounds in fog. Tellus B 44, 533–544.

Finlayson-Pitts, B.J., Pitts, J.N., 2000. Acid Deposition: Formation and Fates of Inorganic and Organic Acids in the Troposphere, in: Chemistry of the Upper and Lower Atmosphere: Theory, Experiments, and Applications. Academic Press, San Diego, CA, p. 969.

Fortems-Cheiney, A., Chevallier, F., Pison, I., Bousquet, P., Saunois, M., Szopa, S., Cressot, C., Kurosu, T.P., Chance, K., Fried, A., 2012. The formaldehyde budget as seen by a global-scale multi-constraint and multi-species inversion system. Atmos. Chem. Phys. 12, 6699–6721.

Gilman, J.B., Lerner, B.M., Kuster, W.C., de Gouw, J. a, 2013. Source signature of volatile organic compounds from oil and natural gas operations in northeastern colorado. Environ. Sci. Technol. 47, 10094.

Giulianelli, L., Gilardoni, S., Tarozzi, L., Rinaldi, M., Decesari, S., Carbone, C., Facchini, M.C., Fuzzi, S., 2014. Fog occurrence and chemical composition in the Po valley over the last twenty years. Atmos. Environ. 98, 394–401.

Harrison, M., Barra, S., Borghesi, D., Vione, D., Arsene, C., Iulianolariu, R., 2005. Nitrated phenols in the atmosphere: a review. Atmos. Environ. 39, 231–248.

Heald, C.L., Jacob, D.J., Park, R.J., Alexander, B., Fairlie, T.D., Yantosca, R.M., Chu, D.A., 2006. Transpacific transport of Asian anthropogenic aerosols and its impact on surface air quality in the United States. J. Geophys. Res. Atmos. 111, 1–13.

Herckes, P., 2007. Comprehensive Characterization of Atmospheric Organic Matter in Fresno, California Fog Water 41, 393–399.

Herckes, P., Chang, H., Lee, T., Collett, J.L., 2007. Air Pollution Processing by Radiation Fogs. Water Air Soil Pollut. 181, 65–75.

Herckes, P., Hannigan, M.P., Trenary, L., Lee, T., Collett, J.L., 2002a. Organic compounds in radiation fogs in Davis (California). Atmos. Res. 64, 99–108.

Herckes, P., Lee, T., Trenary, L., Kang, G., 2002b. Organic Matter in Central California Radiation Fogs. Environ. Sci. Technol. 36, 4777–4782.

Herckes, P., Marcotte, A.R., Wang, Y., Collett, J.L., 2015. Fog composition in the Central Valley of California over three decades. Atmos. Res. 151, 20–30.

Herckes, P., Valsaraj, K.T., Collett, J.L., 2013. A review of observations of organic matter in fogs and clouds: Origin, processing and fate. Atmos. Res. 132-133, 434–449.

Ho, K.F., Ho, S.S.H., Lee, S.C., Kawamura, K., Zou, S.C., Cao, J.J., Xu, H.M., 2011. Summer and winter variations of dicarboxylic acids, fatty acids and benzoic acid in PM2.5 in Pearl Delta River Region, China. Atmos. Chem. Phys. 11, 2197–2208.

Hornafius, J.S., Quigley, D., Luyendyk, B.P., 1999. The world's most spectacular marine hydrocarbon seeps (Coal Oil Point, Santa Barbara Channel, California): Quantification of emissions. J. Geophys. Res. 104, 20703–20711.

Jacob, D.J., 1985. The origins of inorganic acidity in fogs. California Intitute of Technology.

Jacob, D.J., Waldman, J.M., Munger, J.W., Hoffmann, M.R., 1985. Chemical Composition of Fogwater Collected along the California Coast. Environ. Sci. Technol. 19, 730–736.

Jacob, D.J., Wang, R.-F.T., Flagan, R.C., 1984. Fogwater collector design and characterization. Environ. Sci. Technol. 18, 827–833.

Jayne, J.T., Duan, S.X., Davidovits, P., Worsnop, D.R., Zahniser, M.S., Kolb, C.E., 1991. Uptake of Gas-Phase Alcohol and Organic-Acid Molecules by Water Surfaces. J. Phys. Chem. 95, 6329–6336.

Johnstone, J.A., Dawson, T.E., 2010. Climatic context and ecological implications of summer fog decline in the coast redwood region. Proc. Natl. Acad. Sci. 107, 4533–8.

Kaul, D.S., Gupta, T., Tripathi, S.N., Tare, V., Collett, J.L., 2011. Secondary Organic Aerosol: A Comparison between Foggy and Nonfoggy Days. Environ. Sci. Technol. 45, 7307–7313.

Kleindienst, T.E., Smith, D.F., Li, W., Edney, E.O., Driscoll, D.J., Speer, R.E., Weathers, W.S., 1999. Secondary organic aerosol formation from the oxidation of aromatic hydrocarbons in the presence of dry submicron ammonium sulfate aerosol. Atmos. Environ. 33, 3669–3681.

Kroll, J.H., Donahue, N.M., Jimenez, J.L., Kessler, S.H., Canagaratna, M.R., Wilson, K.R., Altieri, K.E., Mazzoleni, L.R., Wozniak, A.S., Bluhm, H., Mysak, E.R., Smith, J.D., Kolb, C.E., Worsnop, D.R., 2011. Carbon oxidation state as a metric for describing the chemistry of atmospheric organic aerosol. Nat. Chem. 3, 133–9.

Li, P., Li, X., Yang, C., Wang, X., Chen, J., Collett, J.L., 2011. Fog water chemistry in Shanghai. Atmos. Environ. 45, 4034–4041.

Lim, Y.B., Tan, Y., Perri, M.J., Seitzinger, S.P., Turpin, B.J., 2010. Aqueous chemistry and its role in secondary organic aerosol (SOA) formation. Atmos. Chem. Phys. 10, 10521–10539.

Lin, P., Liu, J., Shilling, J.E., Kathmann, S.M., Laskin, J., Laskin, A., 2015. Molecular characterization of brown carbon (BrC) chromophores in secondary organic aerosol generated from photo-oxidation of toluene. Phys. Chem. Chem. Phys. 17, 23312–23325.

Löflund, M., Kasper-Giebl, A., Schuster, B., Giebl, H., Hitzenberger, R., Puxbaum, H., 2002. Formic, acetic, oxalic, malonic and succinic acid concentrations and their contribution to organic carbon in cloud water. Atmos. Environ. 36, 1553–1558.

Lüttke, J., Scheer, V., Levsen, K., Wünsch, G., Cape, J.N., Hargreaves, K.J., Storeton-West, R.L., Acker, K., Wieprecht, W., Jones, B., 1997. Occurrence and formation of nitrated phenols in and out of cloud. Atmos. Environ. 31, 2637–2648.

Mazzoleni, L.R., Ehrmann, B.M., Shen, X., Marshall, A.G., Collett, J.L., 2010. Water-soluble atmospheric organic matter in fog: Exact masses and chemical formula identification by ultrahigh-resolution fourier transform ion cyclotron resonance mass spectrometry. Environ. Sci. Technol. 44, 3690–3697.

McGaughey, G.R., Desai, N.R., Allen, D.T., Seila, R.L., Lonneman, W.A., Fraser, M.P., Harley, R.A., Pollack, A.K., Ivy, J.M., Price, J.H., 2004. Analysis of motor vehicle emissions in a Houston tunnel during the Texas Air Quality Study 2000. Atmos. Environ. 38, 3363–3372.

McNeill, V.F., 2015. Aqueous organic chemistry in the atmosphere: Sources and chemical processing of organic aerosols. Environ. Sci. Technol. 49, 1237–1244.

McNeill, V.F., Woo, J.L., Kim, D.D., Schwier, A.N., Wannell, N.J., Sumner, A.J., Barakat, J.M., 2012. Aqueous-phase secondary organic aerosol and organosulfate formation in atmospheric aerosols: A modeling study. Environ. Sci. Technol. 46, 8075–8081.

Middleton, P., Stockwell, W.R., Carter, W.P.L., 1990. Aggregation and analysis of volatile organic compound emissions for regional modeling. Atmos. Environ. Part A. Gen. Top. 24, 1107–1133.

Mohr, C., Lopez-Hilfiker, F.D., Zotter, P., Prévôt, A.S.H., Xu, L., Ng, N.L., Herndon, S.C., Williams, L.R., Franklin, J.P., Zahniser, M.S., Worsnop, D.R., Knighton, W.B., Aiken, A.C., Gorkowski, K.J., Dubey, M.K., Allan, J.D., Thornton, J. a, 2013. Contribution of nitrated phenols to wood burning brown carbon light absorption in Detling, United Kingdom during winter time. Environ. Sci. Technol. 47, 6316–24.

Monod, A., Poulain, L., Grubert, S., Voisin, D., Wortham, H., 2005. Kinetics of OH-initiated oxidation of oxygenated organic compounds in the aqueous phase: new rate constants, structure–activity relationships and atmospheric implications. Atmos. Environ. 39, 7667–7688.

Mouri, H., Okada, K., 1993. Shattering and modification of sea-salt particles in the marine atmosphere. Geophys. Res. Lett. 20, 49–52.

Munger, J., Collett, J., Daube, B., Hoffmann, M., 1989. Carboxylic acids and carbonyl compounds in southern California clouds and fogs. Tellus B 41B, 230–242.

Munger, J., Jacob, D., 1995. Formaldehyde, glyoxal, and methylglyoxal in air and cloudwater at a rural mountain site in Virginia. J. Geophys. Res. 100, 9325–9333.

Munger, J.W., 1989. The chemical composition of fogs and clouds in Southern California. California Institute of Technology.

Munger, J.W., Collett, J., Daube, B., Hoffmann, M.R., 1989. Chemical composition of coastal stratus clouds: Dependence on droplet size and distance from the coast. Atmos. Environ. 23, 2305–2320.

Munger, J.W., Collett, J., Daube, B., Hoffmann, M.R., 1990. Fogwater chemistry at Riverside, California. Atmos. Environ. 24B, 185–205.

Natangelo, M., Mangiapan, S., Bagnati, R., Benfenati, E., Fanelli, R., 1999. Increased concentrations of nitrophenols in leaves from a damaged forestal site. Chemosphere 38, 1495–1503.

National Oceanographic and Atmospheric Administration, 2015. What Type of Oil Spilled at Refugio State Beach?

Nguyen, T.B., Roach, P.J., Laskin, J., Laskin, a., Nizkorodov, S. a., 2011. Effect of humidity on the composition of isoprene photooxidation secondary organic aerosol. Atmos. Chem. Phys. 11, 6931–6944.

Ortiz-Montalvo, D.L., Häkkinen, S. a K., Schwier, A.N., Lim, Y.B., McNeill, V.F., Turpin, B.J., 2014. Ammonium addition (and aerosol pH) has a dramatic impact on the volatility and yield of glyoxal secondary organic aerosol. Environ. Sci. Technol. 48, 255–62.

Ortiz-Montalvo, D.L., Lim, Y.B., Perri, M.J., Seitzinger, S.P., Turpin, B.J., 2012. Volatility and Yield of Glycolaldehyde SOA Formed through Aqueous Photochemistry and Droplet Evaporation. Aerosol Sci. Technol. 46, 1002–1014.

Pandis, S.N., Seinfeld, J.H., 1991. Should bulk cloudwater or fogwater samples obey henrys law. J. Geophys. Res.-Atmos. 96, 10791–10798.

Park, R.J., Jacob, D.J., Field, B.D., Yantosca, R.M., 2004. Natural and transboundary pollution influences on sulfate-nitrate-ammonium aerosols in the United States: Implications for policy. J. Geophys. Res. 109, D15204.

Raja, S., Raghunathan, R., Yu, X.-Y., Lee, T., Chen, J., Kommalapati, R.R., Murugesan, K., Shen, X., Qingzhong, Y., Valsaraj, K.T., Collett, J.L., 2008. Fog chemistry in the Texas–Louisiana Gulf Coast corridor. Atmos. Environ. 42, 2048–2061.

Ricci, L., Fuzzi, S., Laj, P., Lazzari, A., Orsi, G., Berner, A., Gunther, A., Jaeschke, W., Wendisch, M., Arends, B.G., 1998. Gas-liquid equilibria in polluted fog. Contrib. to Atmos. Phys. 71, 159–170.

Richartz, H., Reischl, A., Trautner, F., 1990. Nitrated phenols in fog. Atmos Env. 24, 3067–3071.

Rinaldi, M., Decesari, S., Carbone, C., Finessi, E., Fuzzi, S., Ceburnis, D., O'Dowd, C.D., Sciare, J., Burrows, J.P., Vrekoussis, M., Ervens, B., Tsigaridis, K., Facchini, M.C., 2011. Evidence of a natural marine source of oxalic acid and a possible link to glyoxal. J. Geophys. Res. 116, D16204.

Russo, R.S., Zhou, Y., White, M.L., Mao, H., Talbot, R., Sive, B.C., 2010. Multi-year (2004–2008) record of nonmethane hydrocarbons and halocarbons in New England: seasonal variations and regional sources. Atmos. Chem. Phys. 10, 4909–4929.

Sandstrom, M.W., Kolpin, D.W., Thurman, E.M., Zaugg, S.D., 2005. Widespread detection of N,N-diethyl-m-toluamide in U.S. streams: comparison with concentrations of pesticides, personal care products, and other organic wastewater compounds. Environ. Toxicol. Chem. 24, 1029–1034.

Sareen, N., Schwier, A.N., Shapiro, E.L., Mitroo, D., McNeill, V.F., 2010. Secondary organic material formed by methylglyoxal in aqueous aerosol mimics. Atmos. Chem. Phys. 10, 997–1016.

Seinfeld, J.H., Pandis, S.N., 2006. Atmospheric Chemistry and Physics: From Air Pollution to Climate Change. John Wiley & Sons, Inc., Hoboken, New Jersey.

Shen, X., Lee, T., Guo, J., Wang, X., Li, P., Xu, P., Wang, Y., Ren, Y., Wang, W., Wang, T., Li, Y., Carn, S.A., Collett, J.L., 2012. Aqueous phase sulfate production in clouds in eastern China. Atmos. Environ. 62, 502–511.

Sive, B.C., 1998. Atmospheric nonmethane hydrocarbons: analytical methods and estimated hydroxyl radical concentrations. University of California Irvine.

Straub, D.J., Hutchings, J.W., Herckes, P., 2012. Measurements of fog composition at a rural site. Atmos. Environ. 47, 195–205.

Straub, D.J., Lee, T., Collett, J.L., 2007. Chemical composition of marine stratocumulus clouds over the eastern Pacific Ocean. J. Geophys. Res. 112, D04307.

Sullivan, A.P., Holden, A.S., Patterson, L.A., McMeeking, G.R., Kreidenweis, S.M., Malm, W.C., Hao, W.M., Wold, C.E., Collett, J.L., 2008. A method for smoke marker measurements and its potential application for determining the contribution of biomass burning from wildfires and prescribed fires to ambient PM 2.5 organic carbon. J. Geophys. Res. 113, D22302.

Surratt, J.D., Gómez-González, Y., Chan, A.W.H., Vermeylen, R., Shahgholi, M., Kleindienst, T.E., Edney, E.O., Offenberg, J.H., Lewandowski, M., Jaoui, M., Maenhaut, W., Claeys, M., Flagan, R.C., Seinfeld, J.H., 2008. Organosulfate formation in biogenic secondary organic aerosol. J. Phys. Chem. A 112, 8345–78.

Talbot, R.W., Beecher, K.M., Harriss, R.C., Cofer, W.R.I., 1988. Atmospheric geochemistry of formic and acetic acids at a mid-latitude temperate site. J. Geophys. Res. 93, 1638–1652.

U.S. Census Bureau, 2015. Population Estimates [WWW Document]. URL http://www.census.gov/popest/data/historical/index.html (accessed 2.2.16).

U.S. Environmental Protection Agency, 1994. Locating and Estimating Air Emissions from Sources of Xylene. Research Triangle Park, NC.

U.S. Environmental Protection Agency, 2015. Air Trends [WWW Document]. URL http://www3.epa.gov/airtrends/ (accessed 2.2.16).

US Department of Transportation Maritime Administration, 1985. Containerized Cargo Statistics: Calendar Year 1984.

US Department of Transportation Maritime Administration, 2015. 2002 - 2012 Total Vessel Calls in U.S. Ports, Terminals and Lightering Areas Report.

van Pinxteren, D., Fomba, K.W., Mertes, S., Müller, K., Spindler, G., Schneider, J., Lee, T., Collett, J., Herrmann, H., 2015. Cloud water composition during HCCT-2010: Scavenging efficiencies, solute concentrations, and droplet size dependence of inorganic ions and dissolved organic carbon. Atmos. Chem. Phys. Discuss. 15, 24311–24368.

van Pinxteren, D., Plewka, A., Hofmann, D., Muller, K., Kramberger, H., Svrcina, B., Bachmann, K., Jaeschke, W., Mertes, S., Collett, J.L.J., Herrmann, H., 2005. Schmucke hill cap cloud and valley stations aerosol characterisation during FEBUKO (II): Organic compounds. Atmos. Environ. 39, 4305–4320.

Ventura County Office of the Agricultural Commissioner, 2014. Ventura County's Crop & Livestock Report 2013. Ventura, California.

Vione, D., Maurino, V., Minero, C., Pelizzetti, E., 2005. Aqueous atmospheric chemistry: Formation of 2,4-dinitrophenol upon nitration of 2-nitrophenol and 4-nitrophenol in solution. Environ. Sci. Technol. 39, 7921–7931.

Vutukuru, S., Dabdub, D., 2008. Modeling the effects of ship emissions on coastal air quality: A case study of southern California. Atmos. Environ. 42, 3751–3764.

Wang, Y., Guo, J., Wang, T., Ding, A., Gao, J., Zhou, Y., Collett, J.L., Wang, W., 2011. Influence of regional pollution and sandstorms on the chemical composition of cloud/fog at the summit of Mt. Taishan in northern China. Atmos. Res. 99, 434–442.

Warneck, P., 2003. In-cloud chemistry opens pathway to the formation of oxalic acid in the marine atmosphere. Atmos. Environ. 37, 2423–2427.

Weber, R.J., Sullivan, A.P., Peltier, R.E., Russell, A., Yan, B., Zheng, M., de Gouw, J., Warneke, C., Brock, C., Holloway, J.S., Atlas, E.L., Edgerton, E., 2007. A study of secondary organic aerosol formation in the anthropogenic-influenced southeastern United States. J. Geophys. Res. Atmos. 112.

Weeks, J. a, Guiney, P.D., Nikiforov, a I., 2012. Assessment of the environmental fate and ecotoxicity of N,N-diethyl-m-toluamide (DEET). Integr. Environ. Assess. Manag. 8, 120–34.

Williams, A.P., Schwartz, R.E., Iacobellis, S., Seager, R., Cook, B.I., Still, C.J., Husak, G., Michaelsen, J., 2015. Urbanization causes increased cloud base height and decreased fog in coastal Southern California. Geophys. Res. Lett. 42, 1527–1536.

Winiwarter, W., Brantner, B., Puxbaum, H., 1992. Comment on "Should Bulk Cloudwater or Fogwater Samples Obey Henry's Law?" by S.N. Pandis and J.H. Seinfeld. J. Geophys. Res. Atmos. 97, 6075–6078.

Zarzana, K.J., De Haan, D.O., Freedman, M. a., Hasenkopf, C. a., Tolbert, M. a., 2012. Optical properties of the products of -α-dicarbonyl and amine reactions in simulated cloud droplets. Environ. Sci. Technol. 46, 4845–4851.

Zhang, D., Iwasaka, Y., 2001. Chlorine deposition on dust particles in marine atmosphere. Geophys. Res. Lett. 28, 3613–3616.

Zhang, Q., Worsnop, D.R., Canagaratna, M.R., Jimenez, J.-L., 2005. Hydrocarbon-like and oxygenated organic aerosols in Pittsburgh: insights into sources and processes of organic aerosols. Atmos. Chem. Phys. 5, 3289–3311.

Zhou, Y., Shively, D., Mao, H., Russo, R.S., Pape, B., Mower, R.N., Talbot, R., Sive, B.C., 2010. Air toxic emissions from snowmobiles in Yellowstone National Park. Environ. Sci. Technol. 44, 222–8.

4 HOW DO COMPONENTS OF REAL CLOUD WATER AFFECT AQUEOUS PYRUVATE AGING?*

Chemical oxidation of dissolved volatile or semi-volatile organic compounds within fog and cloud droplets in the atmosphere could be a major pathway for secondary organic aerosol (SOA) formation. This proposed pathway consists of: (1) dissolution of organic chemicals from the gas phase into a droplet; (2) reaction with an aqueous phase oxidant to yield low volatility products; and (3) formation of particle phase organic matter as the droplet evaporates. The common approach to simulating aqueous SOA (aqSOA) reactions is photo-oxidation of laboratory standards in pure water. Reactions leading to aqSOA formation should be studied within real cloud and fog water to determine whether additional competing processes might alter apparent rates of reaction as indicated by rates of reactant loss or product formation. To evaluate and identify the origin of any cloud water matrix effects on one example of observed aqSOA production, pyruvate oxidation experiments simulating aqSOA formation were monitored within pure water, real cloud water samples, and an aqueous solution of inorganic salts. Two analysis methods were used: online electrospray ionization high-resolution time-of-flight mass spectrometry (ESI-HR-ToF-MS), and offline anion exchange chromatography (IC) with quantitative conductivity and qualitative ESI-HR-ToF-MS detection. The apparent rate of oxidation of pyruvate was slowed in cloud water matrices: overall measured degradation rates of pyruvate were lower than in pure water. This can be at least partially accounted for by the observed formation of pyruvate from reactions of other cloud water components. Organic constituents of cloud water also compete for oxidants and/or UV light, contributing to the observed slowed degradation rates of pyruvate. The oxidation of pyruvate was not significantly affected by the presence of inorganic anions (nitrate and sulfate) at cloud-relevant concentrations. Future bulk studies of aqSOA formation reactions using simplified simulated cloud solutions and model estimates of generated aqSOA mass should take into account possible generation of, or competition for, oxidant molecules by organic components found in the complex matrices typically associated with real atmospheric water droplets. Additionally, it is likely that some components of real atmospheric waters have not yet been identified as aqSOA precursors, but could be distinguished through further simplified bulk oxidation reactions of known atmospheric water components.

---

* Reprinted from Atmospheric Research, 143, Boris, A.J., Desyaterik, Y., Collett, J.L., "How do components of real cloud water affect aqueous pyruvate oxidation?" 95–106, Copyright (2014), with permission from Elsevier.

4.1 Introduction

Reactions of organic chemicals occurring within liquid water in the atmosphere, such as cloud or fog droplets, can form low volatility products that add particle-phase mass to the atmosphere after the droplets evaporate. This additional particle mass (called aqueous secondary organic aerosol, or aqSOA) is postulated to be formed primarily through the oxidation of dissolved "precursor" molecules by hydroxyl radical ($^{\bullet}$OH) in cloud and fog droplets, and through non-radical mechanisms in wet aerosol particles (which contain aqSOA higher precursor concentrations) and during droplet evaporation (Ervens et al., 2013, 2011; Loeffler et al., 2006). Formation of aqSOA has been supported by thermodynamic calculations of high molecular mass (HMM) compound production from aqueous reactions (Barsanti and Pankow, 2006), laboratory studies of simulated cloud droplet bulk-phase reactions (Carlton et al., 2006; Lee and Donahue, 2011), and comparison of products of lab bulk-phase reactions with components of real cloud water (Altieri et al., 2008). Particle mass formed through atmospheric aqueous reactions is particularly important because the added mass can shift the geometric mean diameter of particles released from evaporating droplets to larger sizes, making them more effective visible light scatterers (Hegg et al., 2004) and better cloud condensation nuclei (Feingold and Kreidenweis, 2000). The droplet particle size mode, formed through atmospheric aqueous reactions, often contains chemical species that are known or likely products of aqueous reactions, including sulfate, oxalate, glyoxylate, and other low molecular mass (LMM) carboxylic acids (Crahan et al., 2004; John et al., 1990). Such compounds are commonly observed in ambient fogs and clouds (Herckes et al., 2013 and references therein).

The most commonly employed method for experimentally studying aqSOA formation reactions is to simulate oxidation reactions occurring within the bulk phase of atmospheric water droplets. Simplified bulk aqueous oxidation experiments are generally carried out using a glass or quartz photoreactor containing the simulated cloud or fog solution and oxidant, and monitoring composition using offline and online analytical techniques such as chromatographic separation and/or mass spectral detection. A simulated atmospheric water solution generally contains only a few chemical constituents: for example, methylglyoxal or glyoxal with sulfate, nitrate, ammonium, or amines added (De Haan et al., 2011; Kirkland et al., 2013; Tan et al., 2009). Research has also been carried out to show oxidation within real cloud water solutions (Lee et al., 2012), within solutions of atmospherically relevant aromatic compounds in the presence of inorganic radicals or ions (Anastasio et al., 1997; Herrmann et al., 1995; Sun et al., 2010), and on inorganic particles at high relative humidity using various organic aqSOA precursors

(Chan et al., 2013; Galloway et al., 2009; Zhang et al., 2011). It is understood that bulk reactions do not capture the dynamics or heterogeneous chemical interactions that occur at the surface of a droplet (Donaldson and Valsaraj, 2010), but instead are intended to reproduce bulk aqueous chemical reactions. The assumption is also made that the conditions of the reaction provided by the oxidant and simulated atmospheric water solution are chemically relevant for various suspended atmospheric water droplet systems such as cloud, fog, or wet aerosol water. It is possible that additional reactions occur within real atmospheric waters that differ from those proposed for simplified oxidation reactions, and that would alter the kinetics and contributions of particle mass by aqSOA formation processes under real cloud water conditions.

Many interactions of aqSOA precursor and oxidant molecules with trace atmospheric water components are possible, leading to multiple potential effects on observed product formation. Acidity and ionic strength are known to affect the extent of protonation and thus reactivities and photochemical properties of organic molecules and the partitioning of VOCs to atmospheric water (Ervens and Volkamer, 2010). Recently it has been found that very high concentrations of inorganic species are most likely needed for organic–inorganic interactions: sulfuric acid at cloud and fog droplet relevant concentrations (0.2-0.8 mM) does not impact glyoxal or methylglyoxal (0.03-3 mM) aqueous oxidation (Tan et al., 2010, 2009), and only a small decrease in product formation is observed when glyoxal is oxidized in the presence of nitric acid (1 mM glyoxal; Kirkland et al., 2013). At concentrations found in wet aerosol particles, however, aqueous inorganic salts (1-24 M) can react with methylglyoxal (1.6 M) and glyoxal (0.01-2.2 M) to form sulfur and nitrogen-containing organic products with light absorbing properties (Kampf et al., 2012; Sareen et al., 2010; Shapiro et al., 2009). Organic species with nitrogen and sulfur-containing moieties have been observed in fog water samples collected in Fresno, California (Mazzoleni et al., 2010), showing that complex interactions do occur within polluted atmospheric water droplets. Components of real cloud water could inhibit or speed aqueous oxidation reactions (and thus aqSOA formation) by effectively competing for light and/or oxidant molecules (Zhang et al., 2003), or by generating oxidant molecules (Arakaki and Faust, 1998). Such components include inorganic species and a wide range of organic molecules commonly found in cloud droplets (as listed in Herckes et al., 2013). Strong light absorption in the visible range by “brown carbon” species was recently reported, for example, from various organic nitrogen compounds identified in cloud water collected in Eastern China (Desyaterik et al., 2013). An apparent inhibition of organic species aqueous oxidation was observed due to chemical reduction with humic-like substances (HULIS; Canonica and Laubscher, 2008), suggesting that oxidation

reactions within atmospheric waters may be slowed in solutions where high molecular mass (HMM) organic components are present. Formation of reactive oxygen species from reactions of photosensitizers or formation of excited state phenols or HULIS could alternatively increase aqSOA formation reaction rates (Anastasio et al., 1997; Lin and Yu, 2011; Page et al., 2011). Metal–organic charge transfer reactions can also enhance organic radical formation (Zuo and Hoigné, 1994). It is proposed here that oxidants or other radical species (organic or inorganic) found or generated by UV photolysis within atmospheric water samples could enhance oxidation of aqSOA precursor species, or alternatively, that atmospheric water components could compete for oxidant molecules and/or UV light in sufficient amounts to effectively slow the rate of aqSOA product formation. The interactions of different reactants and oxidants within cloud water as compared to chemical standard solutions could also result in different chemical products. For example, if organic radicals are formed through photolysis or $^{\bullet}OH$ oxidation of cloud components, radical–radical reactions forming unique HMM products may occur. As Lim et al. (2013) have suggested, such formation of HMM products could compete with production of LMM carboxylic acids such as oxalate.

Pyruvic acid is the most abundant aqueous reaction product of methylglyoxal (a gas-phase product of the oxidation of isoprene and many anthropogenic volatile organic compounds), and is a chemical intermediate in aqSOA formation pathways (Figure 4-1; Lim et al., 2013).

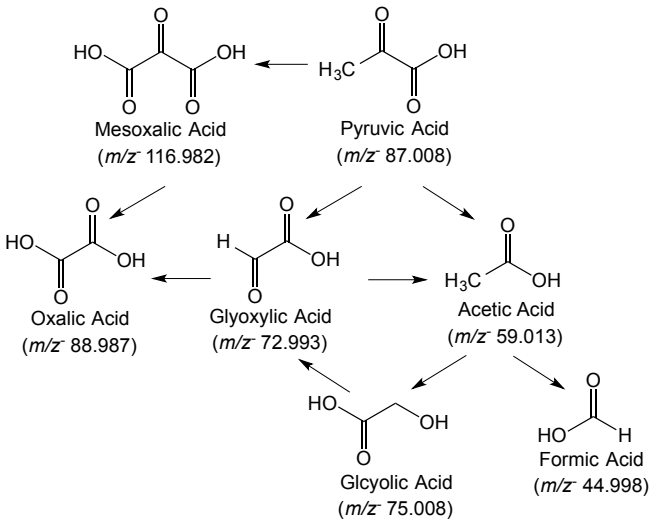

Figure 4-1. Simplified oxidation pathway for pyruvic acid compiled by Lim et al. (2013) showing intermediate and secondary carboxylic acid products. Oxalic and formic acids are the final products in this mechanism.

The mechanism of aqueous phase oxidation of pyruvic acid was proposed by Stefan et al., (1996) and later revised by Lim et al., (2013); it has been verified using simple photoreactions at high pyruvic acid concentration (1 mM), showing the production of glyoxylic acid followed by oxalic acid (Carlton et al., 2006; Tan et al., 2010). Here we report on experiments to examine real cloud water component interactions with the aqSOA precursor pyruvate during in-lab photo-oxidation reactions. The 30 μM pyruvate concentration utilized is cloud-relevant (Brantner et al., 1994; Collett et al., 1989; Herckes et al., 2013; Khwaja et al., 1995) while also sufficient for detection of oxidation products within cloud samples. Four types of oxidation reactions were carried out: pyruvate in pure water, pyruvate within less polluted cloud water, pyruvate within diluted and un-diluted, more polluted cloud water, and pyruvate within an aqueous solution of inorganic constituents. Cloud water samples collected at Mt. Tai in the North China Plain (Shen et al., 2012) were used to show the impacts of pollutant species found in real clouds on aqueous pyruvate oxidation reactions.

4.2 Material and Methods

Photo-oxidation experiments were carried out in a custom-built clear glass photoreactor (150 mL inner volume) equipped with a water jacket to regulate reaction temperature. The reactor was modeled after the work of Lee et al. (2011a, 2011b). Small reaction volumes (50–100 mL) were used to accommodate the small volumes of collected cloud samples. Solutions were continuously stirred (Teflon® magnetic stir bar, ~1 cm in length) throughout the reactions and fed by a peristaltic pump though PEEK™ and Tygon® tubing to an electrospray ionization high-resolution time-of-flight mass spectrometer (ESI-HR-ToF-MS; Agilent LC/MSD-TOF, G1969A) at 0.09 mL min^{-1}. A u-shaped ultraviolet lamp (AA Aquarium, 9 W, peak wavelength 254 nm) was submerged directly into the reaction liquid and turned on after the mass spectrometer (MS) signal from the reaction liquid had equilibrated. Samples were also drawn from the reaction liquid for offline quantitative analyses (see Section 4.2.5 for a more detailed discussion of offline analyses). Chemical standards of LMM carboxylic acids and inorganic salts were obtained as follows: acetic acid from Fluka; glycolic, glyoxylic, maleic, succinic, and pyruvic acids from Aldrich; salicylic and malonic acids from Sigma; potassium iodide and potassium iodate from VWR International; oxalic acid ($C_2H_2O_4 \cdot H_2O$), ammonium nitrate, and ammonium sulfate from Fisher. A small amount of mesoxalate standard was synthesized from diethyl-ketomalonate (Acros) via base-catalyzed hydrolysis and characterized using IC-ESI-HR-ToF-MS. Oxidation reactions of 30 μM pyruvate with $^{\bullet}OH$ generated via photolysis (at 254 nm) of 150 μM H_2O_2 in pure lab water (>18 MΩ-cm) were carried out (Table 4-1).

Table 4-1. Observed species concentrations and rates (measured using IC-conductivity), observed pH values, and TOC concentrations for PyrOx, PyrOxA10, PyrOxA02, PyrIn, and A02 only. Error values shown are CIs at 90% based on replicate experiments. All samples were irradiated using the UV light. Positive pyruvate reaction rates and constants indicate formation of pyruvate. Average $^{\bullet}OH$ concentrations were measured using salicylate oxidation (not pyruvate) within matrices and UV/visible absorbance spectrometry at 202±4 nm after LC separation.

	Pyruvate oxidation in pure water (n=3)	Pyruvate oxidation in A10 (less polluted; n=3)	Pyruvate oxidation in A02 (more polluted; n=1) [a]	Pyruvate oxidation in inorganic salt solution (n=1) [a]	Cloud sample A02 component oxidation (no H_2O_2; n=1) [a]
Solution pH, 0 min	4.9 ± 0.4	6.2 ± 0.4 [a]	6.6 ± 0.4 [b]	---	---
Solution pH, 90 min	3.5 ± 1.2	5.2 ± 1.2 [a]	5.9 ± 1.2 [b]	---	---
H_2O_2 conc., 0 min (μM)	150	150	150	150	---
Pyruvate conc., 0 min (μM)	37 ± 3	34 ± 8	30 ± 3	46 ± 3	1.3
Pyruvate conc., 90 min (μM)	3 ± 1	16 ± 8	30 ± 1	0 *(<LOD)*	0 *(<LOD)*
Oxalate conc., 0 min (μM)	0.2 ± 0.3 *(<LOD)*	3 ± 6	0.9 ± 0.3	0 *(<LOD)*	---
Oxalate conc., 90 min (μM)	10 ± 7	9 ± 18	5 ± 7	20 ± 7	---
Pyruvate TOC, 90 min (%)	19 ± 16	21 ± 13	10 ± 16 [b]	0 ± 16	---
Oxalate TOC, 90 min (%)	33 ± 19	8 ± 17	3 ± 19 [b]	45 ± 19	---
Mesoxalate TOC, 90 min (%)	12 ± 20	0.3 ± 0.5	0.4 ± 20 [b]	7 ± 20	---
Conc. $^{\bullet}OH$, 0 to 15 min (M)	$5.4 \pm 0.5 \times 10^{-14}$	---	1.9×10^{-14} [b]	---	3.8×10^{-15} [b]
Pyruvate reaction rate, 0 to 30 min (μM min^{-1})	-0.9 ± 0.2	-0.5 ± 0.5	-0.1 ± 0.2	-1.2 ± 0.2	+0.2 ± 0.2 [c]
Pyruvate reaction rate constant, 0 to 30 min (μM^{-1} min^{-1})	$-3.6 \pm 0.7 \times 10^{5}$	$-2.1 \pm 2 \times 10^{5}$	$-0.7 \pm 0.7 \times 10^{5}$	$-4.1 \pm 0.7 \times 10^{5}$	---

[a] *Uncertainty applied is that associated with replicate pyruvate in pure water oxidation reactions (90% CL)*
[b] *Calculated using oxidation of pyruvate in cloud water sample A01, collected just prior to A02 (similar composition)*
[c] *Calculated between 0 to 45 minutes oxidation*

The concentration of the pyruvate standard was independently confirmed by measuring the total organic carbon (TOC) concentration in the standard. A concentration of 150 μM H_2O_2 was chosen to give a 5:1 excess of H_2O_2 relative to pyruvate and an atmospherically relevant concentration of $^{\bullet}OH$ (see Section 4.2.3; Anastasio and McGregor, 2001). This H_2O_2 concentration is not unusual for cloud water droplets (Sakugawa et al., 1990) and within the range of concentrations measured in Mt. Tai cloud water (Shen et al., 2012). The light source used was intended to generate $^{\bullet}OH$ from H_2O_2 and not to simulate atmospheric light. An inorganic salt solution with 50 μM ammonium nitrate and 100 μM ammonium sulfate was used to assess effects of common, cloud-relevant inorganic ions on pyruvate oxidation (pH and ionic strength were defined by these solutions, and not otherwise controlled). These concentrations were chosen to be similar to the concentrations of inorganic salts measured in the less polluted Mt. Tai cloud sample used. All oxidation reactions were allowed to proceed for 90 min.

4.2.1 Mt. Tai Cloud Samples

Cloud samples were collected near the summit of Mt. Tai (36.251°N, 117.101°E, 1534 m a.s.l.) in the North China Plain June 14th to July 16th, 2008. High concentrations of inorganic and organic pollutants were encountered in some of the collected cloud samples, originating from a variety of anthropogenic emissions in this heavily developed region of China. Additional information about the samples and sampling techniques can be

found elsewhere (Desyaterik et al., 2013; Guo et al., 2012; Shen et al., 2012). Briefly, cloud water samples were collected using a Caltech Active Strand Cloudwater Collector (CASCC; Demoz et al., 1996). The CASCC collected droplets larger than approximately 3.5 μm in diameter by impaction on Teflon strands. Collected droplets coalesced and drained through a Teflon collection trough and Teflon tube to a polyethylene bottle. Aliquots of samples were prepared on-site for measurement of a suite of chemical species including major inorganic and metal ions, H^+, TOC, H_2O_2, and carboxylic acids (Shen et al., 2012). Remaining sample portions were frozen and stored in the dark; these frozen portions were used for the experiments described here.

Two cloud water samples were selected for use in this study such that the samples differed in TOC concentrations and inorganic composition. This selection aimed to test whether the concentrations of specific cloud water components were related to any observed effects of the cloud water matrices. The more polluted cloud sample (A02) was collected during a period of biomass burning influence between 9:00 and 11:00 pm on June 19th, 2008. The less polluted cloud sample (A10) was collected during a rain event between 12:00 and 1:00 pm on July 4th, 2008. Sample A02 concentrations of inorganic and organic constituents were generally greater: 1110 μM nitrate, 1520 μM sulfate, 2110 μM ammonium, 12.7 μM Fe, 1460 μM TOC, 1.3 μM H_2O_2, pH 3.92; A10 constituent concentrations were: 22.8 μM nitrate, 108.8 μM sulfate, 115 μM ammonium, 22.2 μM Fe, 152 μM TOC, 56.6 μM H_2O_2, pH 6.49.

4.2.2 Control Experiments

To verify that observed products in the oxidation experiments were actually generated from reactions of pyruvate with $^{\bullet}OH$, control experiments were carried out without UV light, and without H_2O_2 (Table A4-1). Pyruvic acid absorbs light in the 315–330 nm range, and can be de-carboxylated in the presence of light at these wavelengths (Griffith et al., 2013; Stefan and Bolton, 1999); the control experiment in this study in which no H_2O_2 was added showed that the photolysis of pyruvate was ~100× slower than oxidation by $^{\bullet}OH$. While in some cases the UV photolysis of pyruvate produces oligomeric products, Guzman et al. (2006) cited 10 mM as the minimum concentration at which oligomer-forming bimolecular reactions become important. Reaction of H_2O_2 with pyruvic acid also occurs (Stefan and Bolton, 1999), but was shown through online ESI-HR-ToF-MS monitoring in our control experiments to be, again, much slower than reaction with $^{\bullet}OH$.

4.2.3 Photon Flux, •OH Concentrations and Rate Constants

The photon flux of the UV lamp used was determined to be 1×10^{-7} Einsteins s^{-1}; this measurement was carried out in a similar manner as reported in Carlton et al. (2007) using an Agilent 1100 series diode array detector (UV/visible absorption spectrophotometer) and an iodide/iodate chemical actinometer (Rahn et al., 2003). The lamp peak wavelength was 253.4 nm (0.4 W m^{-2}) with a spectral bandwidth (full width at half maximum) of 45 nm, as provided by the manufacturer (AA Aquarium Equipment).

The concentrations of •OH in pyruvate oxidation reactions were estimated to ensure they approximated modeled and measured concentrations for ambient atmospheric water samples (~10^{-16} to 10^{-12} M; Anastasio and McGregor, 2001; Ervens et al., 2011; Tan et al., 2010). The •OH degradation of salicylate over 15 min was measured by UV/visible absorption spectrometry after liquid chromatography separation (Agilent 1100 series LC with Phenomenex Kinetex 100×3.00 mm C18 analytical column with 2.6 μm particles and 0.1% formic acid/methanol gradient elution) to quantify the •OH concentration generated in experimental matrices (this was separate from the pyruvate oxidation reactions reported in this work; see Table 4-1 and A4-1). The resulting •OH concentration for pure water matrices was $5.4\pm0.5\times10^{-14}$ M (n=3, accounting for direct photolysis of salicylic acid, and incorporating the second order rate constant of 1.6×10^{10} M^{-1} s^{-1} from Buxton et al., 1988). Second order rate constants k were calculated for each oxidation reaction: $k = d[\text{pyr}] / dt \times (1 / [\text{•OH}][\text{pyr}])$ where t represents reaction time (30 min used in this calculation), and average concentrations of •OH (0 to 15 min measurement) and pyruvate ([pyr]; 0 to 30 min measurement) are in μM. Resulting values of k were used to compare the speed at which pyruvate oxidation occurred in each medium; pyruvate reaction rates were also compared because average [•OH] values measured in cloud water and pure water oxidation reactions differed (Table 4-1), affecting the calculations of k. In contrast to an open reaction system, the bulk reaction approach used in this study does not introduce reactants after the beginning of the reaction (Lim et al., 2013). Although the concentration of •OH is assumed to be approximately at steady state throughout the 90 min reactions based on pyruvate degradation data fits and the concentrations of •OH measured (Figure 4-3), the actual fluctuation in •OH concentration throughout the reactions was not monitored. In the real atmosphere, a constant equilibrium with gaseous •OH would likely be established, and •OH availability would not be limiting.

4.2.4 Online Mass Spectrometry Analysis

The ESI-HR-ToF-MS was mass calibrated before each oxidation reaction using a standard ESI Tuning Mix (Agilent G1969-85000); differences from expected tuning solution m/z^- values were <1.0 ppm during calibration, and differences were <2.0 ppm for most identified species during analysis (Tables A4-2 and 3). Suppression of ionic signal in the ESI source was observed when high concentrations of inorganic constituents such as nitrate and sulfate present in the cloud samples were introduced to the MS. The suppression effects encountered at the inorganic constituent concentrations in the cloud samples used here (Figure A4-1) demonstrate the need for alternative techniques to online ESI-HR-TOF-MS for quantitation of organic compounds within cloud samples. Both online analysis using direct injection to the ESI-HR-ToF-MS and offline analysis with IC separation allowed mass resolution (FWHM, 40-600 Da) of ~5000-15,000, and therefore determination of chemical formulae in most cases. Agilent MassHunter Qualitative Analysis Software (Version B.3.01) was used for analyses of the mass spectra, chromatograms, and species identification. Collected mass spectra were extracted using a minimum peak abundance of 100 a.u., and one-min averaged mass spectra were used for plots and online mass spectral peak formula generation. Background mass spectra from pure water were subtracted from each averaged spectrum prior to formula generation. Abundances of ions shown in individual mass spectra were normalized to the signal of the most abundant ion within each spectrum. Time profiles from online MS monitoring (Figure 4-2) were adjusted to account for the measured sensitivity of the ESI-HR-ToF-MS to each LMM acid, relative to the response of pyruvate (calculated by dividing the slope of the online MS calibration curve for each respective LMM acid by the slope of the online MS calibration curve for pyruvate). Relative sensitivities measured for carboxylic acid chemical standards were as follows: 0.0212 acetate, 0.384 glycolate, 0.994 glyoxylate, 11.9 maleate, 1.31 oxalate, 1.58 succinate, and 3.81 mesoxalate.

4.2.5 Offline Analysis

Discrete samples were drawn from oxidation solutions at 10–15 min intervals. Samples were drawn through PEEK tubing to avoid interrupting the UV light source using Norm-Ject® polypropylene/polyethylene syringes. Bovine catalase (75.6 ng mL^{-1}; Sigma) was added to samples to stop the reactions of H_2O_2 (29.0–32.0% aqueous solution; Sigma). Samples were stored in amber glass vials (for IC analysis), clear HDPE vials (for pH analysis), or amber HDPE bottles (for TOC analysis) at ~7 °C for less than 48 h, until analyzed. The TOC and pH were also measured in each discrete sample using a Sievers 800 Turbo TOC Analyzer and Cole-Parmer EW-5990-45

electrode, respectively. Each sample was diluted (1.5 mL sample to 8.5 mL pure water) prior to TOC analysis to use only a small sample volume and still provide a sufficient TOC concentration to remain within the dynamic range of the instrument in Turbo mode. Precision of the TOC analysis measured as three replicate 30 μM pyruvic acid standard solutions was within 4% relative standard deviation. Pyruvic acid can hydrate at low pH (Pocker et al., 1969) and its pKa is 2.39 (Haynes et al., 2013), changing its reactivity toward $^{\bullet}$OH. The pH of the replicate oxidation reactions of pyruvate at 0 min was reproducible (4.9±0.5, 95% CI); at this pH, deprotonated pyruvate was dominant, which has been noted to be more reactive than pyruvic acid toward $^{\bullet}$OH (Ervens et al., 2003). The pH meter was calibrated prior to and during the analysis of discrete samples (for example, 10, 20, 30 min, and so on of the first pyruvate oxidation) using 4.0, 7.0, and 10.0 buffer solutions (Fisher). The mean of three replicate pH measurements was calculated for each analyzed discrete sample.

Ion chromatography (IC) with conductivity detection was used to quantify carboxylic acids within the discrete oxidation samples; the separated sample was split to the ESI-HR-ToF-MS to aid in identification of components. A Dionex AG11 guard column and AS11-HC weak anion exchange analytical column with a trace anion concentrator (TAC-LP1) column were used to separate carboxylic acids offline using a NaOH gradient elution. A Dionex AS50 autosampler, GP50 gradient pump, LC50 chromatography oven, and ED40 conductivity detector with external conductivity cell were used in this setup. PeakNet (Version 5.21) software was used for collection and analysis of conductivity data. Concentrations were determined based on peak areas using a calibration curve including replicate analyses at all points. Oxalate was used as a surrogate standard to quantify mesoxalate ($C_3H_2O_5$). The assumption of similar sensitivity of the conductivity detector for these two compounds was made based on the similarity in chemical structures and thus in predicted conductivity (di-carboxylic acids), and in measured conductivity sensitivities between the similar species maleate and oxalate. Limits of detection (LODs) using IC-conductivity were 0.35 μM oxalate, 0.23 μM mesoxalate, and 1.9 μM pyruvate. A second calibration was made for the more lengthy IC separation used to quantify components of the more polluted cloud sample (A02); LODs were 0.42 μM oxalate, 0.14 μM mesoxalate, and 1.3 μM pyruvate. All calibration curves were linear (r^2>0.99). The reproducibility of IC-conductivity measurements in cloud water was 9, 26, and 11% relative standard deviation for oxalate, mesoxalate, and pyruvate, respectively (n=3). This degree of variation can be explained by baseline noise in the IC separation, chemical noise of the cloud sample matrices, and uncertainty associated with pre-concentration of a complex sample. Time between oxidation and offline analysis could also affect the LMM

product concentrations, although a correlation was not observed in this work between pre-analysis time and measured oxalate concentration. Variability of the oxidation method was tested by carrying out three similar oxidation reactions of pyruvate in pure water and three similar oxidation reactions of pyruvate added to a cloud sample. Uncertainty associated with replicate pyruvate oxidation reactions in pure water was applied to those experiments carried out without replication (all uncertainties listed throughout the text and within Table 4-1 and A4-1 are 90% CI).

4.3 Results and Discussion

4.3.1 Pyruvate Oxidation

Pyruvate was oxidized in pure water in the presence of $^{\bullet}OH$ (n = 3; experiments abbreviated as "PyrOx") to produce LMM carboxylic acids, in agreement with previous studies (Altieri et al., 2006; Carlton et al., 2006; Tan et al., 2010). In online MS and offline IC-conductivity results (Figure 4-2 and Figure 4-3), this was shown as a decrease in abundance of pyruvate (m/z^- 87.009, $C_3H_4O_3$) and an increase in abundance of products such as oxalate (m/z^- 88.991, $C_2H_2O_4$) and mesoxalate (m/z^-116.983; $C_3H_2O_5$) with elapsed reaction time. The trend in pyruvate ion abundance with time (asymptotic toward approximately 20,000 a.u.; Figure 4-2) was approximated as a pseudo first order reaction rate with respect to pyruvate using the exponential equation $y = y_0 + Ae^{-kx}$, where the initial pyruvate concentration A was set to 37.4 μM, the pseudo first order rate constant k was set to 0.0743 s^{-1} (calculated as the product of the rate constant and $^{\bullet}OH$ concentration measured offline), and the empirical constant y_0 = 3.0155 ± 0.92. This approximation validates the pseudo first order assumption applied to pyruvate degradation (and thus the steady state approximation for $^{\bullet}OH$), and the similarity of the fit to the online MS time profile validates the use of trends in online MS results to show relative reaction rates. The resulting overall change in pH was not significant between 0 and 90 min (Table 4-1); however, changes in pyruvate and oxalate concentrations with reaction time (0 to 90 min) were statistically significant at the 90% CI.

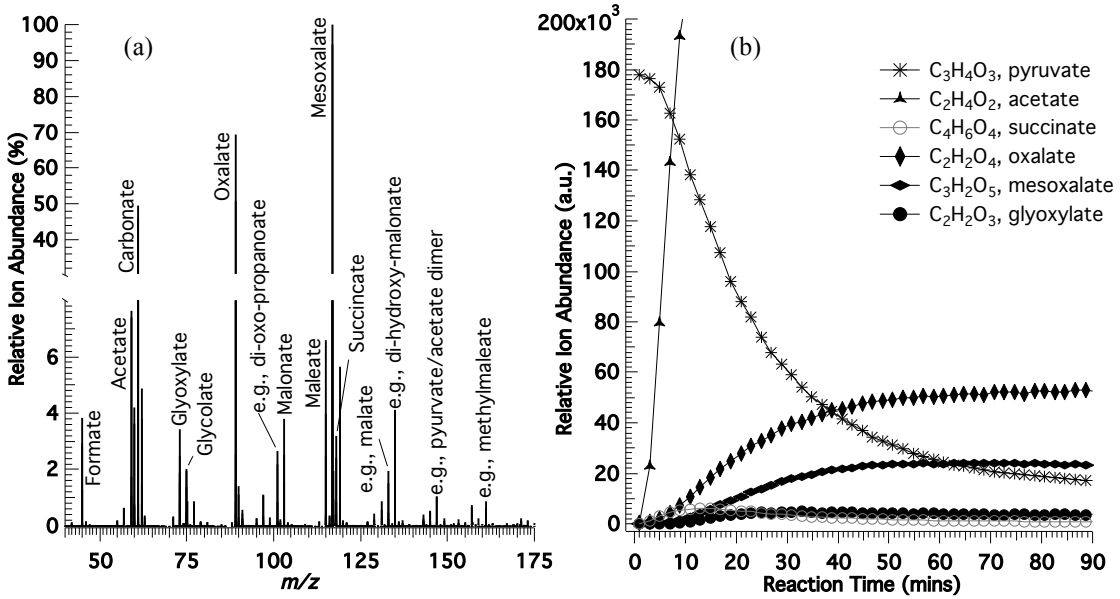

Figure 4-2. Results of pyruvate oxidation from online monitoring using ESI-HR-ToF-MS (example from third pyruvate replicate oxidation). The mass spectrum (a) of pyruvate oxidation products after 60 min shows LMM and HMM (larger than C_3) species. Products were assumed to be adducts and were not labeled if they were not separated using IC. Abundances of reactants at approximately 0 min were subtracted from the 60 min product spectrum to show only products and are relative to mesoxalate (98,012 a.u.; note that y-axis is split). The mechanism proposed by Lim et al. (2013) (Figure 4-1) includes many of the highly abundant products observed, possibly including 3-oxopropanoate ($C_3H_2O_4$). Acetate, followed by oxalate and mesoxalate, appears to be the most abundant ion detected using online MS, as shown in the time profiles (b) of the highest abundance oxidation products of pyruvate (adjusted to account for MS sensitivities; Section 4.2.4). Time profiles were smoothed by averaging every 168 data points (140 s).

This demonstrated that, although there was some variation in observed concentrations between oxidation experiments, the degradation of pyruvate and the quantitation of pyruvate and oxalate were reproducible in this experimental setup.

Oxalate production was important during PyrOx, as suggested by Stefan and Bolton (1999) and later confirmed experimentally by Carlton et al., (2006): the concentration of oxalate accounted for 33±19% (90% CI) of the mean TOC measured after 90 min. Other major products of PyrOx tentatively and positively identified using online MS responses are presented in Table 4-2, including the proposed intermediate 3-oxo-propanoate (Lim et al., 2013).

Table 4-2. High abundance products of pyruvate oxidation as measured in the current study. Formulae were generated using analysis software from observed m/z^- values at 90 min reaction time. Possible identifications were made based on formulae and products identified in previous aqSOA formation reactions or within atmospheric aerosol samples. Formula accuracy was calculated between measured and generated formula m/z^- values.

Neutral Formula	m/z^- (90 min)	Formula Accuracy (mDa)	Identification
CH_2O_2	44.999	-1.23	Formate*
$C_2H_4O_2$	59.015	-1.18	Acetate*
CH_2O_3	60.994	-1.05	Carbonate
$C_2H_2O_3$	72.994	-1.31	Glyoxylate*
$C_3H_6O_2$	73.031	-1.31	e.g., propionate
$C_2H_4O_3$	75.010	-1.09	Glycolate*
$C_3H_8O_2$	75.046	-0.75	---
$C_2H_2O_4$	88.991	-0.83	Oxalate*
$C_3H_2O_4$	100.989	-0.8	e.g., di-oxo-propanoate
$C_3H_4O_4$	103.005	-0.98	Malonate*
$C_4H_4O_4$	115.004	-0.7	Maleate*
$C_3H_2O_5$	116.983	-0.46	Mesoxalate*
$C_4H_6O_4$	117.018	-0.62	Succinate*
$C_4H_6O_5$	133.015	-0.78	e.g., malate
$C_3H_4O_6$	134.994	-0.85	e.g., di-hydroxy-malonate
$C_5H_8O_5$	147.030	-0.28	e.g., pyruvate/acetate dimer
$C_5H_6O_6$	161.009	-0.16	e.g., methylmaleate

**Positive ID using real standard retention time*

The intermediate acetate, formate, and, glyoxylate were present in approximately constant, low mass spectral abundance (3000–10,000 a.u.) after 20 min reaction time, indicating that an equilibrium had likely been reached between formation and further oxidation of these intermediates (these species were not quantified, however, due to low resolution in the IC-conductivity chromatograms). Other oxygenated organic products including succinate exhibited more dynamic online MS time profiles in which a peak in abundance appeared between 10 and 20 min, followed by a decrease toward 90 min (Figure 4-2).

The chemical mechanism for aqSOA formation reactions has been proposed to change from LMM to HMM production when high (≥1 mM) concentrations of precursor are used (Guzman et al., 2006; Lim et al., 2010); however, products with relatively HMM (greater carbon number than pyruvate) were observed in online MS time profiles with only 30 μM initial pyruvate concentrations. The concentration of pyruvic acid used during the experiments conducted by Altieri et al., (2006) and Carlton et al., (2006) in which HMM oxidation products reported were 5–10 mM. Tan et al., (2010) showed that oxidation of 30 μM methylglyoxal allowed formation of mesoxalate, but not formation of products with four or greater carbon atoms at low precursor concentration. HMM products observed herein with initial concentrations of 30 μM pyruvate included m/z^- 115.004 ($C_4H_4O_4$; maleate), m/z^- 117.019 ($C_4H_6O_4$; succinate; Tan et al., 2010), m/z^- 133.014 ($C_4H_6O_5$; *e.g.*, malate), m/z^- 147.030 ($C_4H_4O_6$, *e.g.*, pyruvate/acetate dimer; Altieri et al., 2006), m/z^- 161.009 (e.g., $C_5H_6O_6$ methylmaleate), at 1000 a.u. or greater after 90 min oxidation. Other HMM products were observed in PyrOx samples using online MS response, but were not separated using IC; these were assumed to be adducts generated in the electrospray process. The formation of

products from the oxidation of 30 μM pyruvate with carbon numbers greater than that of the precursor molecule suggests the possibility of HMM compound production from pyruvate aqSOA formation pathways at cloud-relevant concentrations.

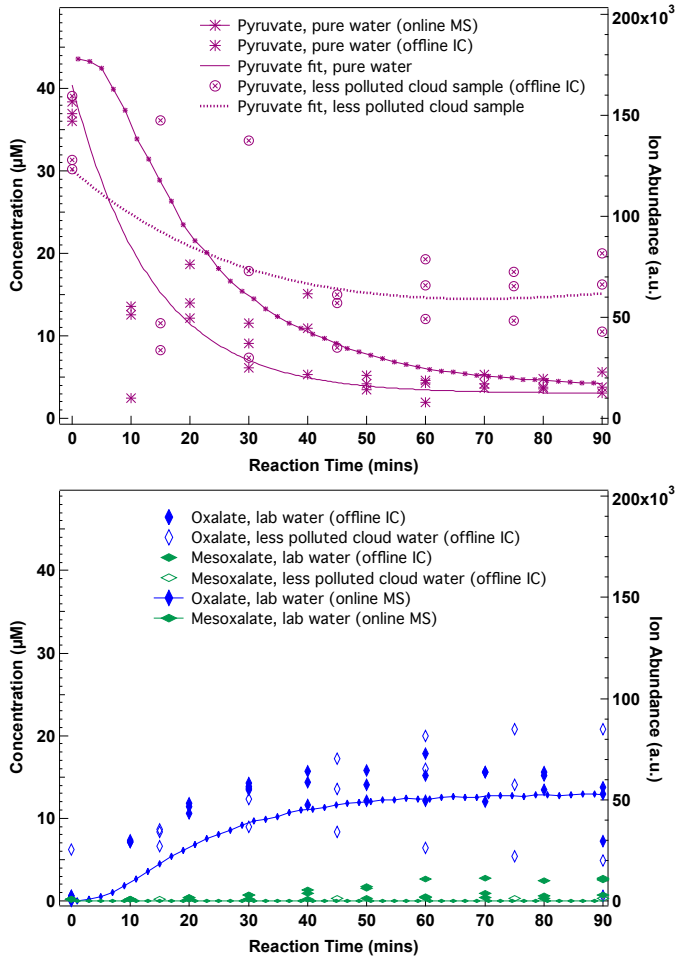

Figure 4-3. Time profiles of (a) the precursor pyruvate; and (b) products oxalate and mesoxalate over the period of the PyrOx and PyrOxA10 experiments (n = 3 for all experiments). Fit lines are intended to show the trends of PyrOx and PyrOxA10; measured initial concentrations of pyruvate and calculated pyruvate rate constants were used as fitting parameters. Online MS time profiles qualitatively follow the pyruvate concentrations measured offline (scaled by relative sensitivity). The unreacted concentration of pyruvate at 90 min was greater in A10 (16±8 μM) than in pure water (3±1 μM), showing that cloud components competed effectively for oxidant or light, and/or that pyruvate was likely generated by cloud component reactions within A10. The oxalate concentration formed after 90 min oxidation was not significantly different between PyrOx (10±8 μM) and PyrOxA10 (9±18 μM), further supporting the hypothesis that substantial pyruvate was formed by cloud component reactions with oxidant or light. Note that mesoxalate is only a small contributor to the TOC after 90 min reaction (11.5%, while oxalic was 26% on average).

4.3.2 Effects of a Cloud Water Matrix on aqSOA Formation Reactions

Three separate experiments were performed to determine whether cloud water matrices alter the oxidation reaction of pyruvate (summarized in Table 4-1 and Figure 4-4): the oxidation of pyruvate within less polluted cloud

water (Mt. Tai sample A10; set of three replicate experiments abbreviated to "PyrOxA10"), the oxidation of pyruvate within more polluted cloud water, diluted and un-diluted (Mt. Tai sample A02; single experiments abbreviated to "PyrOxA02" and "PyrOxA02 dilute"), and the oxidation of pyruvate within a solution of inorganic constituents at similar concentrations to those found in the less polluted cloud sample (single experiment abbreviated to "PyrIn").

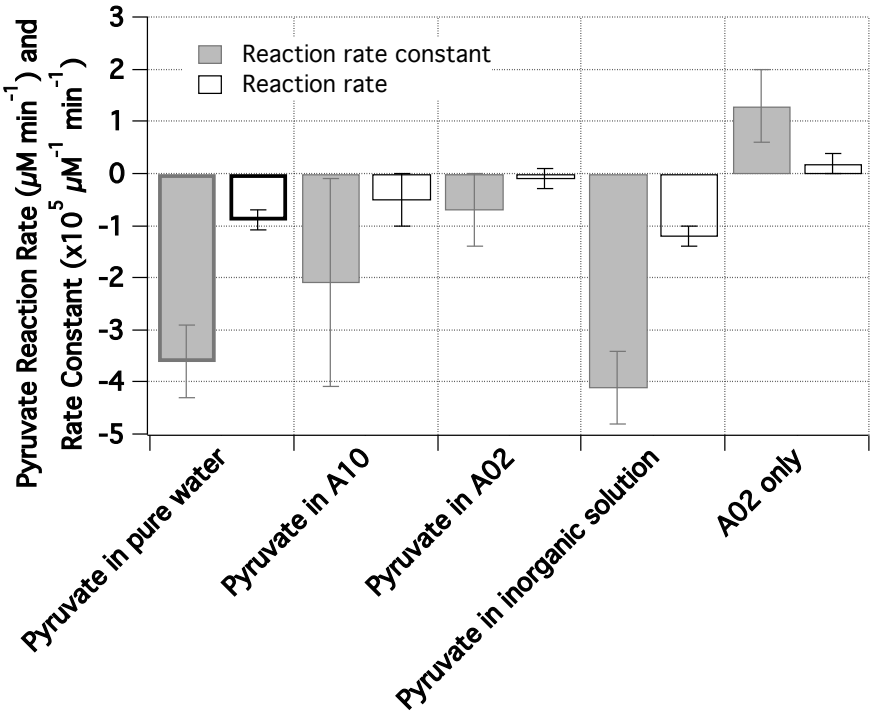

Figure 4-4. Pyruvate reaction rates and rate constants for each matrix examined, including uncertainties (the uncertainty about PyrOx was applied for PyrOxA02, PyrIn, and A02 only). Contrasted with PyrOx, pyruvate oxidation is effectively slower in PyrOxA02, but not in PyrOxA10. Pyruvate was generated in A02 only (sample A02 without added pyruvate but H_2O_2 added; Table A4-1) with a rate constant that could account for the apparent slowing of pyruvate oxidation in PyrOxA02. Inorganic solution components did not significantly change the rate (or rate constant) of pyruvate oxidation.

4.3.3 Oxidation of Pyruvate within Less Polluted Real Cloud Water

Components identified within the less polluted cloud sample (A10) prior to oxidation were LMM acids (including pyruvate), organosulfates, and di-nitrophenol (tentatively identified from the generated formula $C_6H_4N_2O_5$), indicating atmospheric aging and probable influence from regional industrial, urban, transportation, and agricultural biomass burning emissions. Nitrophenols have been associated with aged biomass burning emissions (Harrison et al., 2005), and agricultural fires south of Mt. Tai appear to have contributed to the cloud water composition measured during this period (Desyaterik et al., 2013; Shen et al., 2012). Aromatic carbonyls

have been suggested as photosensitizing components of atmospheric and surface waters (Jammoul et al., 2009); although carbonyls cannot generally be detected using negative mode ESI-MS, carbonaceous components of Mt. Tai cloud water collected during the same time period as those analyzed herein including aromatic carbonyls were detected using UV/visible absorption spectrometry, as discussed by Desyaterik et al., (2013).

The most abundant products in PyrOxA10 identified using the online MS after 90 min of oxidation were similar to those in pure water: LMM carboxylic acids including acetate (the highest abundance signal), formate, $C_2H_4O_3$ (e.g., glycolate), glyoxylate, maleate, malonate, mesoxalate, oxalate, and succinate. Some HMM products of PyrOxA10 were identified; however, no organic S or N species production was detected. The initial pH measured within PyrOxA10 was more basic than that in PyrOx; this is not thought to have affected the radical-radical reaction mechanisms occurring at cloud-relevant concentrations (Lim et al., 2013; Tan et al., 2012). Although the volatile species CO_2, acetate, and formaldehyde are expected to form in the complete oxidation of pyruvate (Lim et al., 2013, 2010), the TOC concentrations measured in discrete cloud water oxidation samples did not change significantly after 90 min, indicating that no substantial losses of volatile organic species occurred.

PyrOxA10 can only be statistically distinguished from PyrOx by the greater final concentrations of pyruvate (Table 4-1 and Figure 4-3), indicating a greater extent of pyruvate oxidation in PyrOx and/or some formation of pyruvate in PyrOxA10 from cloud water component oxidation. Glyoxylate abundance decreased throughout the oxidation, suggesting that only a low concentration of this intermediate was formed (Figure 4-5).

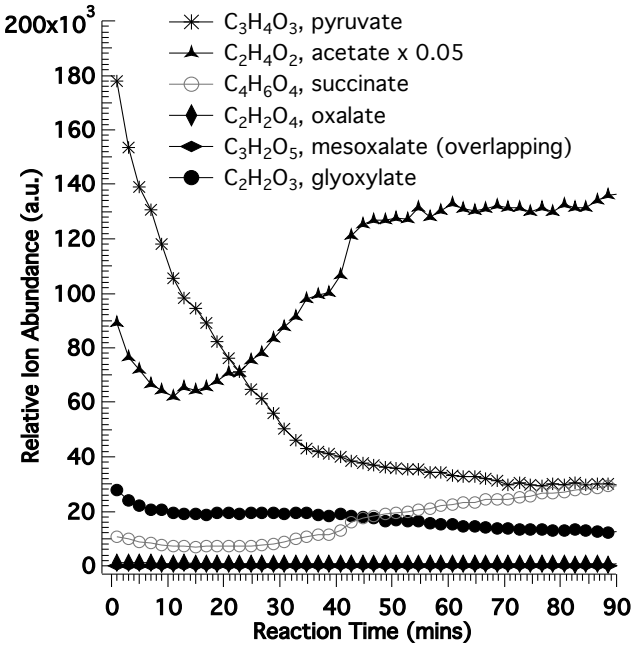

Figure 4-5. Time profiles of the highest abundance oxidation products of PyrOxA10 as measured using online MS (example from third PyrOxA10 replicate oxidation). Plots were smoothed by averaging every 168 data points (140 s), and signals were multiplied by the ratio of initial pyruvate signal in pure lab water to initial pyruvate signal in cloud water sample A10 to eliminate suppression effects by cloud water components. Note that the acetate was scaled (×0.05). Glyoxylate decreased in relative abundance throughout the oxidation, indicating that it was probably produced at low concentrations (although it should be noted that ion suppression due to cloud components could have been changing during the oxidation). Pyruvate signal also decreased throughout the oxidation, with similar relative ion abundance at 90 min as in pure water (Figure 4-2; approximately 20,000 a.u.).

The mesoxalate and oxalate concentrations produced in both reactions were statistically similar, but a high degree of variation was observed in these concentrations in PyrOxA10 after 30 min. Using online MS monitoring, both species remained at low abundance throughout the oxidation. Ionization suppression may have been substantial within online results (despite adjustment for ionization suppression according to the observed suppression in inorganic salt solutions; Fig A4-1). Nitrophenols can be oxidized to give oxalate (Kavitha and Palanivelu, 2005), so it is likely that oxalate was indeed formed and that ionization suppression occurred. No conclusion regarding the oxalate concentration trend can therefore be drawn; however, based on the observed pyruvate and acetate trends, the mechanism in Figure 4-1 may have been effectively slowed in the cloud water matrix compared to that in pure water.

4.3.4 Oxidation of Pyruvate within More Polluted Real Cloud Water

A more polluted cloud water sample (A02) containing a larger number of detectable (using online MS) organic components than in A10 was chosen to further evaluate the effect of cloud water matrices on aqSOA formation

reactions. Observed organic components of A02 (online MS) decreased in abundance throughout the 90 min oxidation, including LMM carboxylic acids, and organic N species such as nitrophenol ($C_6H_5NO_3$) and hydroxy-nitrophenol ($C_6H_5NO_4$; see Table A4-3). Pyruvate was oxidized within A02 ("PyrOxA02") and within diluted A02 (1:4 with pure water by volume; referred to as "PyrOxA02 dilute"). PyrOxA02 yielded little apparent reaction of pyruvate over 90 min (final concentration 30±1 μM) and a significantly slower apparent oxidation than in PyrOx or PyrOxA02 dilute (k=0.7±0.7×10^5 μM^{-1} min^{-1} PyrOxA02; 3.6±0.7×10^5 μM^{-1} min^{-1} PyrOx; 4.8±0.7×10^5 μM^{-1} min^{-1} PyrOxA02 dilute; comparison of the rates of reaction gives the same result). Photolysis of real cloud water components (including H_2O_2) generated oxidant such as $^{\bullet}OH$, indicating that the cloud water had some oxidizing capacity. The average concentration of $^{\bullet}OH$ within more polluted cloud water was ~10% of that introduced via added H_2O_2 photolysis in pure water (see Table 4-1). Oxidation by added $^{\bullet}OH$ of Mt. Tai sample A02 (without added pyruvate, abbreviated as "A02 only") revealed that organic A02 cloud water components could be oxidized by $^{\bullet}OH$, leading to the formation of LMM products, including pyruvate (Table 4-1). Pyruvate production by photo-oxidation of cloud components offset pyruvate oxidation in the experiments and accounted for some or all of the apparent slowing of pyruvate degradation in cloud sample A02: the rate of pyruvate production in A02 only (+0.2±0.2 μM min^{-1}) was not significantly different from that potentially formed in PyrOxA02 (+0.4±0.2 μM min^{-1}; estimated as the difference between the pyruvate reaction rates between PyrOxA02 and PyrOx). Pyruvate was also formed after 15 min oxidation in PyrOxA02 dilute (measured offline using IC-conductivity; Figure A4-2). The formation of LMM acids in PyrOxA02 indicates that abundant organic cloud water constituents were competing for oxidant molecules. Competition for available oxidant by components of A02 is additionally supported by the lower average $^{\bullet}OH$ concentration measured within the polluted cloud water versus pure water (H_2O_2 added in both solutions; see Section 2.3). Oxalate and mesoxalate concentrations at 90 min were not significantly different between PyrOx and PyrOxA02, and only a small number of HMM products were observed in the cloud water oxidation. Future studies should include separation techniques designed to identify possible HMM products and more reproducibly quantify LMM carboxylic acids forming within cloud water samples. These results, overall, suggest that the cloud water components present in cloud samples likely contributed both to in situ pyruvate formation and to a slowing of aqueous pyruvate oxidation by competition for oxidant or incident photons.

4.3.5 Can Inorganic Cloud Constituents Account for Impeded Pyruvate Oxidation in Cloud Water?

An aqueous inorganic salt solution ("PyrIn") with similar concentrations of NH_4NO_3 and $(NH_4)_2SO_4$ to those measured in cloud water sample A10 (20 μM NH_4NO_3 and 50 μM $(NH_4)_2SO_4$) was used to test whether observed pyruvate oxidation slowing could be attributed in part to the presence of inorganic constituents of cloud water. After only 10 min oxidation, the measured pyruvate concentration was below the LOD, and the oxalate concentration after 90 min was not significantly different from that in PyrOx (20 versus 10±8 μM, respectively; see Table 4-1). Pyruvate reaction rates and rate constants were not significantly different from those measured in PyrOx. These results suggest that the observed effects of the cloud matrix in slowing pyruvate oxidation were most likely not associated with major cloud-relevant inorganic ions, including nitrate, sulfate, and ammonium, and indicate that organic constituents within the cloud samples were likely responsible for slowing the net rate of pyruvate loss.

4.4 Conclusions

The aqueous oxidation of pyruvate by $^{\bullet}OH$ has been suggested as an aqSOA formation reaction (Altieri et al., 2006; Carlton et al., 2006; Lim et al., 2005) at wet aerosol relevant concentrations (1–10 mM), and is shown here to form LMM and HMM products that could contribute to SOA mass at cloud relevant concentrations (30 μM). An apparent slowing of pyruvate degradation was observed within real cloud water matrices in less and more polluted regimes. Interactions of nitrate and sulfate ions with $^{\bullet}OH$ and UV light have been observed previously (Zhang et al., 2003), and could theoretically contribute to the observed oxidation slowing. In this work, however, a slowing effect was not observed within inorganic salt solutions at concentrations similar to those found in the less polluted cloud sample used. This is in agreement with the findings of Kirkland et al. (2013) and Tan et al. (2010, 2009), who saw that the aqueous oxidation reactions of glyoxal and methylglyoxal were not impacted substantially by the presence of sulfate, sulfuric acid or nitric acid in solution at cloud relevant concentrations. It is likely that organic constituents of real cloud water caused the apparent slowing effect observed here. No change in chemical mechanism was observed when pyruvate oxidation was carried out within cloud water matrices, based on the observation of similar reaction products. This finding demonstrates that bulk reactions of simple atmospheric water surrogate solutions are relevant for studying chemical mechanisms of aqSOA product formation from pyruvate and similar precursors. Oxidant molecules were formed by photolysis of real cloud sample components (at 254 nm), in agreement with previous studies (Anastasio et al., 1997; Arakaki and Faust, 1998; Faust et al., 1993). A lower

steady state concentration of •OH was generated from the photolysis of H_2O_2 within the cloud water matrix versus pure water; this shows that cloud water components competed for oxidant and/or photons. Further work is needed to show more specifically the mechanisms for the apparent slowing of pyruvate oxidation and any similar occurrence of this effect when different aqSOA precursors are oxidized. For example, high abundance components of cloud samples should be added to oxidation solutions, and the oxygen availability during reaction should be varied to help elucidate reaction mechanisms according to the scheme proposed by Lim et al., (2013). Additionally, replicate oxidation experiments should be carried out using a variety of atmospheric water samples collected from locations with different prevailing atmospheric chemistry schemes and other possible aqSOA precursor molecules. At present, it appears that the net slowing of pyruvate oxidation within real cloud waters is due to cloud constituent competition for •OH and/or absorption of incident photons and is at least partially caused by the offsetting production of pyruvate from photo-oxidation of other cloud water organic compounds.

REFERENCES

Altieri, K.E., Carlton, A.G., Lim, H.-J., Turpin, B.J., Seitzinger, S.P., 2006. Evidence for oligomer formation in clouds: Reactions of isoprene oxidation products. Environ. Sci. Technol. 40, 4956–60.

Altieri, K.E., Seitzinger, S.P., Carlton, A.G., Turpin, B.J., Klein, G.C., Marshall, A.G., 2008. Oligomers formed through in-cloud methylglyoxal reactions: Chemical composition, properties, and mechanisms investigated by ultra-high resolution FT-ICR mass spectrometry. Atmos. Environ. 42, 1476–1490.

Anastasio, C., Faust, B.C., Rao, C.J., 1997. Aromatic carbonyl compounds as aqueous-phase photochemical sources of hydrogen peroxide in acidic sulfate aerosols, fogs, and clouds 1. Non-phenolic methoxybenzaldehydes and methoxyacetophenones with reductants (phenols). Environ. Sci. Technol. 31, 218–232.

Anastasio, C., McGregor, K.G., 2001. Chemistry of fog waters in California's Central Valley: 1. In situ photoformation of hydroxyl radical and singlet molecular oxygen. Atmos. Environ. 35, 1079–1089.

Arakaki, T., Faust, B.C., 1998. Sources, sinks, and mechanisms of hydroxyl radical (•OH) photoproduction and consumption in authentic acidic continental cloud waters from Whiteface Mountain, New York: The role of the Fe(r) (r = II, III) photochemical cycle. J. Geophys. Res. 103, 3487.

Barsanti, K.C., Pankow, J.F., 2006. Thermodynamics of the formation of atmospheric organic particulate matter by accretion reactions—Part 3: Carboxylic and dicarboxylic acids. Atmos. Environ. 40, 6676–6686.

Brantner, B., Fierlinger, H., Puxbaum, H., Berner, A., 1994. Cloudwater chemistry in the subcooled droplet regime at Mount Sonnblick (3106 m asl, Salzburg, Austria). Water. Air. Soil Pollut. 74, 363–384.

Buxton, G. V., Greenstock, C.L., Helman, W.P., Ross, A.B., Tsang, W., 1988. Critical Review of rate constants for reactions of hydrated electrons, hydrogen atoms and hydroxyl radicals (OH/O-) in aqueous solution. J. Phys. Chem. Ref. Data 17, 513.

Canonica, S., Laubscher, H.-U., 2008. Inhibitory effect of dissolved organic matter on triplet-induced oxidation of aquatic contaminants. Photochem. Photobiol. Sci. 7, 547–551.

Carlton, A.G., Turpin, B., Altieri, K.E., Seitzinger, S.P., Reff, A., Lim, H., Ervens, B., 2007. Atmospheric oxalic acid and SOA production from glyoxal: Results of aqueous photooxidation experiments. Atmos. Environ. 41, 7588–7602.

Carlton, A.G., Turpin, B.J., Lim, H., Altieri, K.E., Seitzinger, S.P., 2006. Link between isoprene and secondary organic aerosol (SOA): Pyruvic acid oxidation yields low volatility organic acids in clouds. Geophys. Res. Lett. 33, 1–4.

Chan, K.M., Huang, D.D., Li, Y.J., Chan, M.N., Seinfeld, J.H., Chan, C.K., 2013. Oligomeric products and formation mechanisms from acid-catalyzed reactions of methyl vinyl ketone on acidic sulfate particles. J. Atmos. Chem. 70, 1–18.

Collett, J.L., Daube, B., Munger, J.W., Hoffmann, M.R., 1989. Cloudwater Chemistry in Sequoia National Park. Atmos. Environ. 23, 999–1007.

Crahan, K.K., Hegg, D., Covert, D.S., Jonsson, H., 2004. An exploration of aqueous oxalic acid production in the coastal marine atmosphere. Atmos. Environ. 38, 3757–3764.

De Haan, D.O., Hawkins, L.N., Kononenko, J.A., Turley, J.J., Corrigan, A.L., Tolbert, M.A., Jimenez, J.L., 2011. Formation of nitrogen-containing oligomers by methylglyoxal and amines in simulated evaporating cloud droplets. Environ. Sci. Technol. 45, 984–91.

Demoz, B.B., Collett, J.L., Daube, B.C., 1996. On the Caltech Active Strand Cloudwater Collectors. Atmos. Res. 41, 47–62.

Desyaterik, Y., Sun, Y., Shen, X., Lee, T., Wang, X., Wang, T., Collett, J.L., 2013. Speciation of "brown" carbon in cloud water impacted by agricultural biomass burning in eastern China. J. Geophys. Res. Atmos. 118, 7389–7399.

Donaldson, D.J., Valsaraj, K.T., 2010. Adsorption and reaction of trace gas-phase organic compounds on atmospheric water film surfaces: A critical review. Environ. Sci. Technol. 44, 865–73.

Ervens, B., Herrmann, H., Gligorovski, S., 2003. Temperature-dependent rate constants for hydroxyl radical reactions with organic compounds in aqueous solutions. Phys. Chem. Chem. Phys. 5, 1811–1824.

Ervens, B., Turpin, B., Weber, R., 2011. Secondary organic aerosol formation in cloud droplets and aqueous particles (aqSOA): A review of laboratory, field and model studies. Atmos. Chem. Phys. 11, 11069–11102.

Ervens, B., Volkamer, R., 2010. Glyoxal processing by aerosol multiphase chemistry: towards a kinetic modeling framework of secondary organic aerosol formation in aqueous particles. Atmos. Chem. Phys. 10, 8219–8244.

Ervens, B., Wang, Y., Eagar, J., Leaitch, W.R., Macdonald, A.M., Valsaraj, K.T., Herckes, P., 2013. Dissolved organic carbon (DOC) and select aldehydes in cloud and fog water: the role of the aqueous phase in impacting trace gas budgets. Atmos. Chem. Phys. 13, 5117–5135.

Faust, B.C., Anastasio, C., Allen, J.M., Arakaki, T., 1993. Aqueous-phase photochemical formation of peroxides in authentic cloud and fog waters. Science 260, 73–75.

Feingold, G., Kreidenweis, S., 2000. Does cloud processing of aerosol enhance droplet concentrations? J. Geophys. Res. Atmos. 105, 24351–24361.

Galloway, M.M., Chhabra, P.S., Chan, A.W.H., Surratt, J.D., Flagan, R.C., Seinfeld, J.H., Keutsch, F.N., 2009. Glyoxal uptake on ammonium sulphate seed aerosol: reaction products and reversibility of uptake under dark and irradiated conditions. Atmos. Chem. Phys. 9, 3331–3345.

Griffith, E.C., Carpenter, B.K., Shoemaker, R.K., Vaida, V., 2013. Photochemistry of aqueous pyruvic acid. Proc. Natl. Acad. Sci. U. S. A. 110, 11714–11719.

Guo, J., Wang, Y., Shen, X., Wang, Z., Lee, T., Wang, X., Li, P., Sun, M., Collett, J.L., Wang, W., Wang, T., 2012. Characterization of cloud water chemistry at Mount Tai, China: Seasonal variation, anthropogenic impact, and cloud processing. Atmos. Environ. 60, 467–476.

Guzman, M.I., Colussi, A.J., Hoffmann, M.R., 2006. Photoinduced oligomerization of aqueous pyruvic acid. J. Phys. Chem. A 110, 3619–26.

Harrison, M., Barra, S., Borghesi, D., Vione, D., Arsene, C., Iulianolariu, R., 2005. Nitrated phenols in the atmosphere: a review. Atmos. Environ. 39, 231–248.

Haynes, W.M., Bruno, T.J., Lide, D.R. (Eds.), 2013. Handbook of Chemistry and Physics, 94th ed. CRC Press, Cleveland, OH.

Hegg, D., Covert, D., Jonsson, H., Khelif, D., Friehe, C., 2004. Observations of the impact of cloud processing on aerosol light-scattering efficiency. Tellus 56B, 285–293.

Herckes, P., Valsaraj, K.T., Collett, J.L., 2013. A review of observations of organic matter in fogs and clouds: Origin, processing and fate. Atmos. Res. 132-133, 434–449.

Herrmann, H., Exner, M., Jacobi, H.-W., Raabe, G., Reese, A., Zellner, R., 1995. Laboratory studies of atmospheric aqueous-phase free-radical chemistry: kinetic and spectroscopic studies of reactions of NO3 and SO4- radicals with aromatic compounds. Faraday Discuss. 100, 129–153.

Jammoul, A., Dumas, S., D'Anna, B., George, C., 2009. Photoinduced oxidation of sea salt halides by aromatic ketones: A source of halogenated radicals. Atmos. Chem. Phys. 9, 4229–4237.

John, W., Wall, S., Ondo, J., Winklmayr, W., 1990. Modes in the size distributions of atmospheric inorganic aerosol. Atmos. Environ. 24, 2349–2359.

Kampf, C.J., Jakob, R., Hoffmann, T., 2012. Identification and characterization of aging products in the glyoxal/ammonium sulfate system – implications for light-absorbing material in atmospheric aerosols. Atmos. Chem. Phys. 12, 6323–6333.

Kavitha, V., Palanivelu, K., 2005. Degradation of nitrophenols by Fenton and photo-Fenton processes. J. Photochem. Photobiol. A Chem. 170, 83–95.

Khwaja, H., Brudnoy, S., Husain, L., 1995. Chemical characterization of three summer cloud episodes at Whiteface Mountain. Chemosphere 31, 3357–3381.

Kirkland, J., Lim, Y., Tan, Y., Altieri, K., Turpin, B., 2013. Glyoxal secondary organic aerosol chemistry: effects of dilute nitrate and ammonium and support for organic radical-radical oligomer formation. Environ. Chem. 10, 158–166.

Lee, A.K.Y., Hayden, K.L., Herckes, P., Leaitch, W.R., Liggio, J., Macdonald, A.M., Abbatt, J.P.D., 2012. Characterization of aerosol and cloud water at a mountain site during WACS 2010: secondary organic aerosol formation through oxidative cloud processing. Atmos. Chem. Phys. 12, 6019–6047.

Lee, A.K.Y., Herckes, P., Leaitch, R.W., Macdonald, A.M., Abbatt, J.P.D., 2011a. Aqueous OH oxidation of ambient organic aerosol and cloud water organics: Formation of highly oxidized products. Geophys. Res. Lett. 38, 1–5.

Lee, A.K.Y., Zhao, R., Gao, S.S., Abbatt, J.P.D., 2011b. Aqueous-phase OH oxidation of glyoxal: application of a novel analytical approach employing aerosol mass spectrometry and complementary off-line techniques. J. Phys. Chem. A 115, 10517–10526.

Lee, J., Donahue, N.M., 2011. Secondary organic aerosol coating of synthetic metal-oxide nanoparticles. Environ. Sci. Technol. 45, 4689–95.

Lim, H., Carlton, A.G., Turpin, B.J., 2005. Isoprene Forms Secondary Organic Aerosol through Cloud Processing: Model Simulations. Environ. Sci. Technol. 39, 4441–4446.

Lim, Y.B., Tan, Y., Perri, M.J., Seitzinger, S.P., Turpin, B.J., 2010. Aqueous chemistry and its role in secondary organic aerosol (SOA) formation. Atmos. Chem. Phys. 10, 10521–10539.

Lim, Y.B., Tan, Y., Turpin, B.J., 2013. Chemical insights, explicit chemistry, and yields of secondary organic aerosol from OH radical oxidation of methylglyoxal and glyoxal in the aqueous phase. Atmos. Chem. Phys. 13, 8651–8667.

Lin, P., Yu, J.Z., 2011. Generation of Reactive Oxygen Species Mediated by Humic-like Substances in Atmospheric Aerosols. Environ. Sci. Technol. 45, 10362–10368.

Loeffler, K.W., Koehler, C.A., Paul, N.M., De Haan, D.O., 2006. Oligomer formation in evaporating aqueous glyoxal and methylglyoxal solutions. Environ. Sci. Technol. 40, 6318–6323.

Mazzoleni, L.R., Ehrmann, B.M., Shen, X., Marshall, A.G., Collett, J.L., 2010. Water-soluble atmospheric organic matter in fog: Exact masses and chemical formula identification by ultrahigh-resolution fourier transform ion cyclotron resonance mass spectrometry. Environ. Sci. Technol. 44, 3690–3697.

Page, S.E., Arnold, W.A., McNeill, K., 2011. Assessing the contribution of free hydroxyl radical in organic matter-sensitized photohydroxylation reactions. Environ. Sci. Technol. 45, 2818–2825.

Pocker, Y., Meany, J.E., Nist, B.J., Zadorojny, C., 1969. The Reversible Hydration of Pyruvic Acid I. Equilibrium Studies. J. Phys. Chem. 73, 2879–2882.

Rahn, R., Stefan, M., Bolton, J., 2003. Quantum Yield of the Iodide–Iodate Chemical Actinometer: Dependence on Wavelength and Concentration. Photochem. Photobiol. 78, 146–152.

Sakugawa, H., Kaplan, I.R., Tsai, W., Cohen, Y., 1990. Atmospheric hydrogen peroxide. Environ. Sci. Technol. 10, 29–32.

Sareen, N., Schwier, A.N., Shapiro, E.L., Mitroo, D., McNeill, V.F., 2010. Secondary organic material formed by methylglyoxal in aqueous aerosol mimics. Atmos. Chem. Phys. 10, 997–1016.

Shapiro, E.L., Szprengiel, J., Sareen, N., Jen, C.N., Giordano, M.R., McNeill, V.F., 2009. Light-absorbing secondary organic material formed by glyoxal in aqueous aerosol mimics. Atmos. Chem. Phys. 9, 2289–2300.

Shen, X., Lee, T., Guo, J., Wang, X., Li, P., Xu, P., Wang, Y., Ren, Y., Wang, W., Wang, T., Li, Y., Carn, S.A., Collett, J.L., 2012. Aqueous phase sulfate production in clouds in eastern China. Atmos. Environ. 62, 502–511.

Stefan, M.I., Bolton, J.R., 1999. Reinvestigation of the Acetone Degradation Mechanism in Dilute Aqueous Solution by the UV/H2O2 Process. Environ. Sci. Technol. 33, 870–873.

Stefan, M.I., Hoy, A.R., Bolton, J.R., 1996. Kinetics and Mechanism of the Degradation and Mineralization of Acetone in Dilute Aqueous Solution Sensitized by the UV Photolysis of Hydrogen Peroxide. Environ. Sci. Technol. 30, 2382–2390.

Sun, Y.L., Zhang, Q., Anastasio, C., Sun, J., 2010. Insights into secondary organic aerosol formed via aqueous-phase reactions of phenolic compounds based on high resolution mass spectrometry. Atmos. Chem. Phys. 10, 4809–4822.

Tan, Y., Carlton, A.G., Seitzinger, S.P., Turpin, B.J., 2010. SOA from methylglyoxal in clouds and wet aerosols: Measurement and prediction of key products. Atmos. Environ. 44, 5218–5226.

Tan, Y., Lim, Y.B., Altieri, K.E., Seitzinger, S.P., Turpin, B.J., 2012. Mechanisms leading to oligomers and SOA through aqueous photooxidation: insights from OH radical oxidation of acetic acid and methylglyoxal. Atmos. Chem. Phys. 12, 801–813.

Tan, Y., Perri, M.J., Seitzinger, S.P., Turpin, B.J., 2009. Effects of Precursor Concentration and Acidic Sulfate in Aqueous Glyoxal-OH Radical Oxidation and Implications for Secondary Organic Aerosol. Environ. Sci. Technol. 43, 8105–8112.

Zhang, H., Surratt, J.D., Lin, Y.H., Bapat, J., Kamens, R.M.M., 2011. Effect of relative humidity on SOA formation from isoprene/NO photooxidation: enhancement of 2-methylglyceric acid and its corresponding oligoesters under dry conditions. Atmos. Chem. Phys. 11, 6411–6424.

Zhang, W., Xiao, X., An, T., Song, Z., 2003. Kinetics, degradation pathway and reaction mechanism of advanced oxidation of 4-nitrophenol in water by a UV/H2O2 process. J. Chem. Technol. Biotechnol. 794, 788–794.

Zuo, Y., Hoigné, J., 1994. Photochemical decomposition of oxalic, glyoxalic and pyruvic acid catalysed by iron in atmospheric waters. Atmos. Environ. 2, 1231–1239.

5. AQUEOUS ATMOSPHERIC OXIDATION PROCESSES IN REAL FOG AND CLOUD WATER

Oxidation reactions of organic constituents within droplets of fog, cloud, and wet aerosol can form products with sufficiently low volatility to add secondary organic aerosol mass. While specific molecules such as glyoxal have been characterized as precursors of this aqueous secondary organic aerosol (aqSOA), real atmospheric samples contain a complex system of inorganic and organic chemicals. In addition, the toxicity of organic material that participate in aqueous atmospheric organic processing (AAOP) reactions can change (e.g., addition/removal of NO_2 groups), altering the impact of fog water deposition to ecosystems. AAOP must therefore be studied to understand these reactions and their atmospheric implications fully. This study examined the prominent chemical mechanisms and differences between oxidation reactions within several real atmospheric fog/cloud water samples. Samples included atmospheric water from: Baengnyeong Island (BYI), Republic of Korea, downwind of a polluted region; Mount Tai, China, containing fresh emissions from a highly polluted region of Eastern China; and Casitas Pass (CP), a remote site along the Southern California Coast with regional contributions of chemicals from agricultural, urban, and oil and natural gas emissions. Chemical precursors and products were analyzed in real time during each reaction using high-resolution mass spectrometry, and at discrete time intervals via liquid chromatography/mass spectrometry and ion chromatography. The fog/cloud sample reactions represented different regimes of oxidation, characterized by SO_4^{2-} and organic aromatic species concentrations, as well as apparent age of the sample. Constituents of the Mount Tai cloud water, which were mainly anthropogenic and biomass burning emissions such as nitrophenol, dinitrophenol, and nitrocatechol, were oxidized to longer-chain, often unsaturated species. In contrast, the CP fog water contained abundant biogenic species such as pinonic and pinic acids, and were oxidized to form mostly lower molecular mass carboxylic acids. The more aged BYI fog initially contained carboxylic acids and nitrophenols at lesser concentrations than in the Mount Tai clou dwater and formed mainly organic sulfate esters of carboxylic acids as oxidation products (tentatively identified by molecular formulae). These S-containing species were also observed after all but the least concentrated CP fog water sample oxidation. Carboxylic acids were also abundant products in all oxidation reactions except for BYI fog, in which pyruvate and oxalate were instead degraded, possibly due to metal-carboxylate complex photolysis. The oxidation of aromatic species including 4-nitrophenol and 2,4-dinitrophenol produced distinct species including acrylic and methacrylic acids, which were observed in the oxidation of anthropogenic emissions within real fog/cloud water samples as well. The production of

a variety of polar, oxygenated species through oxidation confirms that AAOP reactions could be responsible for aqSOA formation, particularly in the presence of fresh, concentrated emissions as in cloud water from Mount Tai. Changes in oxidation reactions due to chemical composition of atmospheric water should be further characterized to demonstrate the influence of aqueous chemistry on resulting aqSOA production.

5.1 Introduction

Compounds age chemically in the atmosphere through oxidation processes. These oxidation processes can occur in the gas phase, at surfaces, or in the aqueous phase; differing reactions can occur in these venues (Goldstein and Galbally, 2007; Seinfeld and Pandis, 2006). Those oxidation reactions occurring in the aqueous phase and involving organic species, called aqueous atmospheric organic processing (AAOP) reactions, may account for the formation of a large fraction of unexplained atmospheric organic matter (Chen et al., 2015). Aging reaction within droplets of fog, cloud, and wet aerosol facilitates the transfer of organic carbon between the gas and particle phases in the atmosphere by forming lower volatility products such as low molecular mass (LMM) carboxylic acids. Chemical transformations resulting in lowered volatility of organic matter also occur in the gas phase, but laboratory results have demonstrated that the degree of oxygenation resulting from aqueous oxidation reactions exceeds that from gas phase oxidation reactions, consistent with characteristics of ambient samples (Aiken et al., 2008; Altieri et al., 2008; Chen et al., 2015). Aqueous reactions could additionally explain the formation of organic species that are not currently captured in most empirical speciation studies: only a fraction of the organic species in the atmosphere is typically identified. For example, Hallar et al. (2013) identified 20% on average of particle-phase organics in aerosol samples from a mountaintop site in Colorado using a suite of analytical techniques. It should be noted that there are some examples in which humidity/water content do not have an effect on the overall organic aerosol mass produced from oxidation reactions (Boyd et al., 2015).

Chemicals that act as AAOP precursors are effectively removed from the atmosphere via chemical degradation. Precursors could be pesticides, toxic nitro-aromatic species, and other trace organic atmospheric contaminants (Chang and Thompson, 2010; Chiron et al., 2009; Harrison et al., 2005; Sun et al., 2010). The degradation of organic compounds can change the toxicity of species within fog; for example, the formation in the atmospheric aqueous phase has been suggested for nitrophenols and oxy-PAHs (Raja et al., 2009; Vione et al., 2005), as well as oxidation of these species to form less toxic LMM organics (Trapido and Kallas, 2000; Zhang et al., 2003).

The photo-induced oxidation of organic species within aqueous solutions has been well-studied as a technique for trace organic contaminant removal in municipal and surface waters (Legrini et al., 1993). It is known that aqueous degradation of organics can be accomplished easily by the action of hydroxyl radicals (Keen et al., 2014), or by direct UV photolysis of organics (Sanches et al., 2010) or organometallic complexes (Safarzadeh-Amiri et al., 1997). Degradation can affect a range of species from high molecular mass (HMM) species with complex structures (e.g., Opsahl and Benner, 1998) to LMM carboxylic acids such as acetic acid (Lim et al., 2013; Tan et al., 2012). These reactions are analogous to those occurring in the atmosphere, and simulations of in-cloud, in-fog, and in-wet aerosol oxidation reactions of dissolved organic components have been carried out (Kirkland et al., 2013; Monod et al., 2000; Tan et al., 2009). However, reactions carried out in photoreactors filled with an aqueous solution of an organic chemical standard differ from reactions of real cloud/fog water, at least with respect to the speed of degradation (Bautitz and Nogueira, 2007; Boris et al., 2014; Mavronikola et al., 2009; Trovó et al., 2008). Thus, it is important to study aqueous organic oxidation reactions within real atmospheric water matrices to demonstrate results reflective of true atmospheric processing.

Several studies have shown that oxidation occurs within authentic fog and/or cloud water samples, mainly focusing on the production of oxidant such as hydroxyl radical ($^{\bullet}$OH) within atmospheric water droplets (Anastasio and McGregor, 2001; Anastasio et al., 1994; Arakaki and Faust, 1998; Boris et al., 2014; Faust and Allen, 1992, 1993; Faust et al., 1993; Gelencsér and Varga, 2005; Lee et al., 2011; Stemmler and Gunten, 2000; Zuo and Hoigné, 1993; Zuo and Jones, 1996; Zuo, 2003). Important differences exist between simple solutions of chemical standards and the complex mixtures of inorganic and organic constituents that are real fog and cloud water samples. These include differences in concentration of precursors often not considered in lab simulations, interactions between inorganic and organic species or inorganic species and oxidants/photons, and complex formation between metals and carboxylic acids. Radical reactions are thought to explain most oxidation processes in cloud and fog water since the concentrations of most species are dilute (10 nM – 100 μM), while the organic species concentrations in wet aerosol particles, found in high humidity environments, are greater (1-10 M) and non-radical reactions such as esterifications may occur (Lim et al., 2010). The combination of organic radicals to form "oligomers" is also suggested to be concentration-dependent (Tan et al., 2009), although this may be an instrumental detection limitation (Boris et al., 2014).

Real atmospheric water droplets also contain a large number of organic and inorganic species that can interact with oxidants (and photons), effectively slowing the rate of oxidation of individual organic species (Boris et al., 2014; Glover et al., 2014). Bromide and chloride react with •OH to form radical species, as do carbonate and sulfate. Although it was thought that species such as chlorine radical (•Cl) might react with organic species found in fog/cloud water to form chlorinated products via addition across C-C double bonds, no such products were identified in either standard solutions with added chloride salts or in real polluted cloud water samples (Boris et al., 2014). Carbonate and halide radicals may also react with organics by hydrogen atom (H) abstraction, particularly from an –OH or electron-rich site, actually facilitating the degradation of organic species in a given sample (Glover and Rosario-Ortiz, 2013). Sulfate radicals have been suggested to add across double bonds of LMM organic carbonyls in a similar manner to form CHOS species (Schindelka et al., 2013), although various other photo-oxidation and dark reaction experiments have demonstrated different CHOS species formation mechanisms such as the reaction of sulfuric acid (H_2SO_4) with monoterpene/ozone (O_3) epoxide products (Iinuma et al., 2007), and acid-catalyzed esterification with H_2SO_4 of alcohols/hydrated aldehydes (Liggio et al., 2005). In addition to the oxidant molecule, reaction speed in real atmospheric water samples may be in part dependent on TOC of the water ((Schurman, 2014)), and acidity (Bator and Collett, 1997; Sorooshian et al., 2007).

Aqueous atmospheric organic processing (AAOP) was simulated in the present study by reacting constituents of real cloud and fog water samples with hydroxyl radical (•OH). Precursors and products of AAOP reactions were monitored to explore: (a) prominent chemical mechanisms of AAOP in real aqueous atmospheric samples; (b) differences and similarities between the AAOP reactions within the different samples; and (c) possible impacts of the AAOP reactions in each case on air quality and climate. The simulations in this study employ a high-power UV light for generation of •OH, which causes some photolysis and is likely to cause more rapid reactions than would naturally occur under atmospheric conditions. Control experiments discussing direct photolysis of fog/cloud water constituents should therefore be considered. Qualitative and quantitative analytical approaches were combined to achieve this. Four samples from three global locations where fog/cloud presence is frequent were oxidized, representing differing initial chemical compositions and atmospheric inputs.

5.2 Material and Methods

Four atmospheric water samples (three locations) and four standard chemical species were oxidized in the present work (Table 5-1). Fog and cloud water samples were collected as described elsewhere: Mount Tai, Eastern

China (Tai): Shen et al., 2012; Baengnyeong Island, Korea (BYI): Boris et al., 2016; and Casitas Pass, Southern California Coast (CP): Chapter 3. All samples were collected using a version of a Caltech Active Strand Cloudwater Collector (CASCC), described individually in the study publications listed above, and in detail by Demoz et al. (1996). Droplet diameters (50% cut size) were >3.5 μm in the Tai and CP samples, and >16 μm in the BYI sample. The collected water from a single fog/cloud event at each sampling site (Tai, BYI, CP) was composited into a larger volume such that sufficient liquid was available for at least one oxidation experiment (three replicate oxidation were carried out using the BYI composite). A second CP fog sample composite was made to contrast fog water collected during a fog event with high concentrations (CP3) and low concentrations (CP4) of inorganic and organic constituents. Chemical standards representative of the organic species in the real fog/cloud samples were also oxidized to elucidate mechanisms and products: pinonic acid (PAOx), maleic acid (MalOx), 4-nitrophenol (4NPOx), and 2,4-dinitrophenol (2,4DNPOx).

Table 5-1. Oxidation experiments carried out in the present study.

Abbrev.	Sample	Initial Conc.	Oxidant/Light Source
BYOx (3 reps.)	BYI fog sample composite	--	H_2O_2/UV
CP3Ox	CP fog sample composite	--	H_2O_2/UV
CP4Ox	CP fog sample composite	--	H_2O_2/UV
TaiOx	Mount Tai fog sample composite	--	H_2O_2/UV
BYOx UV photolysis	BYI fog sample composite	--	UV only
BYOx H_2O_2 only	BYI fog sample composite	--	H_2O_2 only
PAOx	Pinonic Acid	3 μM	H_2O_2/UV
MalOx	Maleic Acid	30 μM	H_2O_2/UV
4NPOx	4-Nitrophenol	30 μM	H_2O_2/UV
2,4DNPOx	2,4-Dinitrophenol	3 μM	H_2O_2/UV

5.2.1 Material and Methods: Photoreaction

Photoreaction experiments were carried out using methods similar to those described previously (Boris et al., 2014). Briefly, 40 mL fog/cloud water was reacted in a glass photoreactor (150 mL inner volume) equipped with a recirculating water jacket and magnetic stir bar. The oxidation reactions were initiated with $^{\bullet}OH$, which was generated using a 254 nm UV light (9 Watt) for photolysis of hydrogen peroxide (H_2O_2). The steady state concentration of $^{\bullet}OH$ in the photoreactor system was within the atmospherically relevant range: $5.4\pm0.5\times10^{-14}$ M in deionized water, 3.8×10^{-15} M in authentic cloud water from Mount Tai, China (chemical actinometry; Boris et al., 2014). Discrete 1 mL samples were removed from the reaction solution at 15 min intervals, added to 5 μL bovine catalase (15.9 units/mL), and stored at ~7°C until off-line analysis.

Control experiments were carried out to characterize the reactions of fog/cloud water constituents with H_2O_2 only and by direct UV photolysis because the UV light source used is not tropospherically relevant, and H_2O_2 reaction was considered as a separate oxidation mechanism. The direct UV photolysis experiment resulted in slower and differing reaction mechanisms. Since the H_2O_2 was not chemically preserved in the BYI fog sample used for the control photolysis experiments, it was assumed that there was not sufficient H_2O_2 to generate $^{\bullet}OH$ within the sample. A slow reaction rate was also observed when fog/cloud water constituents were reacted with H_2O_2 only. The TOC degraded by direct photolysis of the BYI fog water composite constituents was only 7.6%, and via H_2O_2 reaction was only 16.8% after 120 min, while $^{\bullet}OH$ achieved 89% TOC reduction after 120 min.

The observed rates of reaction due to $^{\bullet}OH$ attack in the present study are estimated to be atmospherically relevant (fog/cloud $^{\bullet}OH$ concentrations are ~10^{-16} to 10^{-12} M, Anastasio and McGregor, 2001; Ervens et al., 2011; Tan et al., 2010). However, the rates of reaction observed in the presence of other light sources were barely measurable (natural sunlight from 09/25/15 in Fort Collins/40.59° N, 105.15° W and a Newport Oriel LCS-100 solar simulator equipped with a 100 Watt Xe lamp and an AM1.5G light filter to deliver 1 Sun of irradiance were also tested). Oxidation was simulated using the UV lamp and added H_2O_2 in the present study in order to sufficiently observe oxidation processes. Solar simulators have also been previously used to study AAOP reactions (Brinkmann et al., 2003; Faust et al., 1993; Glover et al., 2014; Kitanovski et al., 2014), which highlights the need for additional work in identifying the best practice for accurately simulating atmospheric oxidation in the lab.

Variation observed between oxidation experiments (Figure 5-1) demonstrates that there are variables that have not been controlled in these oxidation reactions and must be explored further. Although a stir bar was effective in introducing oxygen from the surrounding lab air to the solution, oxygen content is one possible driver for this inter-experiment variation. Compressed air and helium from gas cylinders were more effective (based on changes in the rate of degradation) in controlling oxygen in the solution, but caused the reactants in the fog/cloud water to volatilize from the solution. Thus, the stir bar was used in the reactions discussed herein.

5.2.2 Material and Methods: Chemical Analyses

Oxidation of samples was monitored via three separate techniques: (1) online mass spectrometry (online MS); (2) offline liquid chromatography/mass spectrometry (LC/MS); and (3) offline ion chromatography for LMM carboxylic acids (IC). In addition, online UV/visible absorption spectrometry was performed in line with mass

spectrometry during online MS and LC/MS analyses. LC/MS was used to quantify carbonaceous precursors and products including carboxylic acids and phenols from the discrete 15 minute samples. The initial inorganic and organic composition of each sample was quantified via Dionex IC systems (methods described in Boris et al., 2016) and a Sievers 800 Turbo total organic carbon (TOC) analyzer (Boris et al., 2014). Combined, these techniques allowed the identification of precursors, intermediates, products, and predominant mechanisms of reaction.

Some challenges to chemical characterization of real, complex fog/cloud water samples were noted. The SO_4^{-2} peak in the carboxylic acid IC chromatograms co-eluted with oxalic and maleic acids at high SO_4^{-2} concentrations, and outcompeted most carboxylic acid species for ionization within directly injected (online) MS analysis (also observed previously; Boris et al., 2014). Real sample analysis also resulted in increased detection limits due to interfering sample constituents, and the necessity of filtration prior to analysis in high pressure instrumentation.

5.2.3 Material and Methods: Online Analyses

Qualitative analysis of mass spectral data was carried out to identify precursors, intermediates, and products during oxidation experiments, as described in a previous publication (Boris et al., 2014). Each oxidation was monitored online using direct injection via a peristaltic pump to an Agilent electrospray ionization high-resolution time-of-flight mass spectrometer operated in negative mode ((-)-ESI-HR-ToF-MS). The resulting time-resolved mass spectra (approx. two per second) were organized in two ways: (a) time profiles of specific m/z^- values during oxidation experiments; and (b) mass spectra extracted at specific reaction times (e.g., the mass spectrum of BYOx at 30 min). Time profiles were extracted from each data file using Agilent MassHunter software and smoothed using a boxcar smoothing algorithm (Igor; an example of a m/z^- profile before and after smoothing is plotted in Fig. A5-7). Mass spectra were extracted from each oxidation experiment data file at 0, 15, 30, 60, and 120 min reaction time (where 0 min was defined as the time when H_2O_2 addition and/or UV light were initiated) by averaging over one min time intervals. A "precursor mass spectrum" was compiled for each experiment by subtracting the 15, 30, 60, and 120 min reaction time mass spectra from the 0 min reaction time mass spectra and overlaying the resulting spectra. "Product mass spectra" were generated for each oxidation by subtracting the 0 min reaction time mass spectrum from each of the 15, 30, 60, and 120 min mass spectra individually.

The (-)-ESI-HR-ToF-MS detector settings were as follows (for both offline LC/MS and online MS analyses): acquisition m/z^- 65-100 Da at 1.4 spectra s^{-1}; drying gas 350°C and 5 liters min^{-1}; nebulizer 20 psi; fragmentor

voltage 130 V; skimmer voltage 60 V; octupole voltage 150 V; capillary 3500 V. Agilent EI-TOF tuning mix was used for external mass calibration prior to analyses, giving typically <30 ppm mass accuracies (no internal standard solution was used). Online UV/visible absorption spectrometry was performed using an in-line UV/Vis diode array detector (Agilent G1315D). See Appendix 5 for additional information about UV/Vis analyses.

While online MS is useful for identification of polar (de-protonatable) organic species, and the trends determined using this technique are accurate (Boris et al., 2014), the trends in this study were not always in agreement with those measured using IC, likely due to concentrations of carboxylic acids near the IC detection limits. For example, online MS demonstrated an increase in maleate ($C_4H_4O_4$, m/z^- 115.01) during most oxidation reactions, while this product was not significantly different between 0 and 120 min oxidation in IC measurements. Despite this, it was possible to determine overall which detectable (polar, organic) species were most influential in these studies and to propose mechanisms leading to the results described here.

5.2.4 Material and Methods: Offline Analyses

Organic molecules $\geq C_4$ were quantified via HPLC-(-)-ESI-HR-ToF-MS: a Kinetex 2.6 µm particle size XB-C18 column designed for polar organic species separation with 100 Å pore size and 3.00 mm internal diameter was used to separate organic species (carboxylic acids, phenols and S-containing organic species, CHOS) via a 0.1% formic acid/methanol gradient elution. The HPLC-(-)-ESI-HR-ToF-MS system consisted of an Agilent 1100 Series LC with Agilent MSD/ToF detector. The MSD/ToF detector settings were identical to those used in the online MS analyses. Other analyses were carried out using procedures described elsewhere (Boris et al., 2016, 2014). Inorganic anions and cations, as well as carboxylic acids, were quantified using Dionex IC systems with conductivity detectors. A small number of samples were also analyzed after separation using (-)-ESI-HR-ToF-MS detection to confirm the identifications of eluted carboxylic acids. Total organic carbon (TOC) was measured using a Sievers Model 800 Turbo TOC Analyzer in Turbo mode (Boris et al., 2014; see additional notes about TOC analysis in Appendix 5).

Confidence intervals (at the 95% confidence level) were calculated for each species using replicate measured responses ($CI = ts/\sqrt{n}$, where t = critical t value at the 95% confidence level, one-sided, s = standard deviation of replicate responses, n = number of replicate analyses, n=6). Analysis method blanks were generated by analyzing pure lab water in the same manner as samples. The maximum concentration of each species measured within the method blanks was subtracted from the concentrations measured within the samples (blank responses gave 110, 56,

and 25% relative standard deviation for acetate, formate, and oxalate, respectively). Limits of detection (LODs) were calculated from a series of analysis method blanks (LOD = $ts_{blk} \sqrt{[(n_s + n_{blk}) / (n_s \times n_{blk})]}$, where t=critical t value at the 95% confidence level, s_{blk}=standard deviation of method blanks; two-sided; n_s=150=number of samples; n_{blk}=9=number of blanks).

5.3 Results and Discussion

5.3.1 Initial Chemical Composition of Real Fog and Cloud Samples

Three distinct chemical profiles were observed in the real cloud/fog water from three sampling locations (Table 5-2). The Mount Tai cloud water contained primarily organic nitrogen (CHNO) species, highlighting the impact of nearby anthropogenic and biomass burning emissions (Desyaterik et al., 2013), and also a lesser biogenic organic contribution. The two samples from the Southern California Coast (Casitas Pass, CP, fog events 3 and 4) contained mainly biogenic species including pinic acid, pinonic acid, and diaterpenylic acid acetate, but also CHNO species (a smaller contribution of CHNO species was observed in the CP samples than the Tai or BYI samples). The BYI fog water contained a mixture of oxidized species with clear anthropogenic/industrial influence, including phthalic acid derivatives, which have been associated with incomplete combustion of hydrocarbons in motor vehicle exhaust (Kawamura and Kaplan, 1987), CHNO, CHOS, and CHNOS species identified previously as possible monoterpene oxidation products (e.g., $C_{10}H_{17}NO_7S$; Iinuma et al., 2007; Surratt et al., 2008). The CP fog event 3 sample (CP3) contained greater concentrations of all measured inorganic species as well as total organic carbon (TOC) than the CP event 4 sample (CP4), due in part to the lower liquid water content during event 3. In agreement with the apparent anthropogenic versus biogenic origin of organic constituents in each of the fog/cloud water samples, the greatest concentration of the aged anthropogenic species SO_4^{2-} was measured in the BYI fog water (424 μM), followed by the Mount Tai cloud water (406 μM), indicative of an aged combustion emissions impact on these sampling sites. Concentrations of NO_3^- were greatest in BYI fog water (775 μM), followed by CP3 fog water (613 μM), likely from oxidized auto exhaust emissions, and the NH_4^+ concentrations were greatest in the BYI fog water (2010 μM), with concentrations exceeding 1000 μM in all but the CP4 sample. Agriculture is a key land use in Southeast Asia and Southern California, and is the most likely source for fog/cloud water NH_4^+. The pH of the samples ranged between 4.00 (BYI) and 7.03 (CP3). Unsurprisingly, the fog water collected from the sampling sites located east of saltwater bodies (BYI and CP) contained the greatest concentrations of Na^+ and Cl^- (although lower concentrations of Na^+ were measured during the CP event 3 than the Mount Tai cloud water event, possibly due to dust or soil

contributions to Na^+ at Mount Tai). Finally, K^+, which has been suggested as a proxy for biomass burning emissions (Andreae, 1983; Lee et al., 2010), was greatest in the Mount Tai cloud water; this was expected because ash was observed in the cloud water collected at Mount Tai, most likely from field burning in the North China Plain (Desyaterik et al., 2013). TOC concentrations were greatest in the BYI fog sample composite (9.83 mg C L^{-1}) followed by the CP3 fog sample composite (8.81 mg C L^{-1}; Table 5-2).

Carboxylic acids are known products of aqueous organic processing reactions (Ervens et al., 2011; Lim et al., 2010), although they can also originate from gas-phase oxidation of organic compounds (Kawamura et al., 1996; van Pinxteren et al., 2014) or direct emission (Talbot et al., 1988). Aged atmospheric samples will therefore contain a greater carboxylic acid fraction of total organic mass, which can be quantified as the percentage of the TOC mass contributed by quantified carboxylic acids. The percent TOC mass of carboxylic acids for each composited sample is tabulated in Table 5-2: the Mount Tai sample (21.8% TOC mass of carboxylic acids) and BYI sample (43.1% TOC mass of carboxylic acids) contained a greater aged TOC fraction than the samples from CP according to this metric (3.17 and 4.93% TOC mass of carboxylic acids were measured in CP3 and CP4, respectively). It should be noted that the sample composites used in this study likely contained lower concentrations of carboxylic acids than at the time of collection due to microbial activity (Amato et al., 2007) and volatile losses during storage, transfer, and handling of the samples. The diversity of carboxylic acids is also an indicator of atmospheric aging; the BYI sample composite was found to be the most diverse (and thus possibly more aged) of the samples, with four carboxylic acids quantified contributing >5% each of the TOC mass.

Table 5-2. Concentrations and statistics of inorganic species and TOC within sample solutions before oxidation (at t=0 min). The percent of the TOC contributed by quantified carboxylic acids (percent carboxylic acids) is also tabulated, with the confidence limit calculated from replicate analyses of the BYI fog sample carboxylic acids concentrations.

Sample	Species	Conc. *t*=0 min.	Unit	Conf. Int. (95%)	LOD
BYOx	TOC	9.83	mg C L^{-1}	0.03	0.26
	Percent Carboxylic Acids	43.1	%	10.5	--
	pH	4.00	--	0.04	--
	NH_4^+	2010	µM	0.2	0.2
	NO_3^-	775	µM	5	0.04
	SO_4^{-2}	424	µM	0.03	1.8
	Na^+	548	µM	0.19	3
	Cl^-	117	µM	0.008	2
	Ca^{+2}	13.5	µM	0.2	0.1
	K^+	44.7	µM	0.18	3
	Mg^{+2}	4.4	µM	0.19	0.19
	NO_2^-	9.67	µM	0.04	0.04
CP3Ox	TOC	8.81	mg C L^{-1}	0.03	0.26
	Percent Carboxylic Acids	3.17	%	--	--
	pH	7.03	--	0.05	--
	NH_4^+	1050	µM	0.2	0.2
	NO_3^-	613	µM	5	0.04
	SO_4^{-2}	127	µM	0.03	1.8
	Na^+	398	µM	0.19	3
	Cl^-	155	µM	0.008	2
	Ca^{+2}	42.6	µM	0.2	0.1
	K^+	48.3	µM	0.18	3
	Mg^{+2}	28.2	µM	0.19	0.19
	NO_2^-	10.2	µM	0.04	0.04
CP4Ox	TOC	3.22	mg C L^{-1}	0.03	0.26
	Percent Carboxylic Acids	4.93	%	--	--
	pH	6.22	--	0.04	--
	NH_4^+	344	µM	0.2	0.2
	NO_3^-	140	µM	5	0.04
	SO_4^{-2}	39.5	µM	0.03	1.8
	Na^+	70	µM	0.19	3
	Cl^-	68.0	µM	0.008	2
	Ca^{+2}	3.3	µM	0.2	0.1
	K^+	19.2	µM	0.18	3
	Mg^{+2}	2.3	µM	0.19	0.19
	NO_2^-	7.01	µM	0.04	0.04
TaiOx	TOC	6.19	mg C L^{-1}	0.03	0.26
	Percent Carboxylic Acids	21.8	%	--	--
	pH	5.58	--	0.15	--
	NH_4^+	1270	µM	0.2	0.2
	NO_3^-	390	µM	5	0.04
	SO_4^{-2}	406	µM	0.03	1.8
	Na^+	266	µM	0.19	3
	Cl^-	53.3	µM	0.008	2
	Ca^{+2}	79.4	µM	0.2	0.1
	K^+	57.4	µM	0.18	3
	Mg^{+2}	13.9	µM	0.19	0.19
	NO_2^-	7.54	µM	0.04	0.04

5.3.2 Evolution of Carboxylic Acids

Steadily increasing concentrations of acetate were observed during all sample oxidation reactions. The observed production rates of acetate were fitted via exponentially increasing functions: $y=2.2+1.9e^{-0.023x}$ for TaiOx; $y=-16.5+27.4e^{-0.007x}$ for BYOx mean; $y=-3.0+3.1e^{-0.020x}$ for CP3Ox; and $y=-6.1+5.4e^{-0.011x}$ for CP4Ox, where the initial precursor concentration A, the pseudo first order rate constant for acetate formation k, and an empirical constant y_0 are related by $y = y_0 + Ae^{-kx}$. Observed formation rates of acetate between 0 and 120 min oxidation were between

0.12 and 0.25 μM min^{-1} (k=0.007 to 0.023 μM^{-1} min^{-1}), with the slowest acetate formation rate observed in the least polluted sample, CP4, and most rapid acetate formation rate observed in the most polluted sample, from BYI. Concentrations of formate, likewise, steadily increased over the 120 min reactions in all oxidation reactions (0.12 to 0.32 μM min^{-1}; k=0.004 to 0.022 μM^{-1} min^{-1}; Figure 5-1). The slowest formation was observed in the least polluted sample, CP4, and the most rapid formation in the Mount Tai sample. Assuming a droplet lifetime of 30 minutes (Ervens et al., 2013), the observed experimental reaction rates would produce (net) ~3.6-7.5 μM formate and 3.6-9.6 μM acetate during a single droplet lifetime.

The ratio of [acetate]/[formate] in aerosol particles has been suggested as a marker for the origin of the oxidative parent volatile organic compounds (VOCs), with values <1 associated with combustion activities, and values >1 associated with biogenic emissions (Talbot et al., 1988). The effective Henry's Law coefficients are similar at pH 3: 7.1×10^{3} M atm^{-1} acetate and 1.3×10^{4} M atm^{-1} formate, and at pH 7: 1.2×10^{6} M atm^{-1} acetate and 2.0×10^{7} M atm^{-1} formate (at 273K; Haynes et al., 2013; Johnson et al., 1996). Thus, this metric should be relevant for most fog samples, assuming no additional substantial reactive uptake differences between the two species. It was observed that a greater quantity of acetate than formate was produced during AAOP. These results are in agreement with the trend observed by Talbot *et al* (1988). Initially, the ratio of $[acetate]_{aq}/[formate]_{aq}$ was 2.0 in CP3Ox, which might indicate an impact of biogenic emissions (the value also may have changed during storage of the sample). The aqueous oxidation of the biogenic species pinonic acid (PA) resulted in $[acetate]_{aq}/[formate]_{aq}$=2.4, while all other oxidation reactions of samples and standards resulted in $[acetate]_{aq}/[formate]_{aq}$<1 (Figure 5-1). The oxidation of CP4Ox, which contained greater biogenic influence in organic composition than the other samples, reached the greatest value among sample oxidation reactions of $[acetate]_{aq}/[formate]_{aq}$ = 0.91 after 120 min. The value of $[acetate]_{aq}/[formate]_{aq}$ also increased more generally during all oxidation reactions. No detectable formate was produced in the oxidation of maleate.

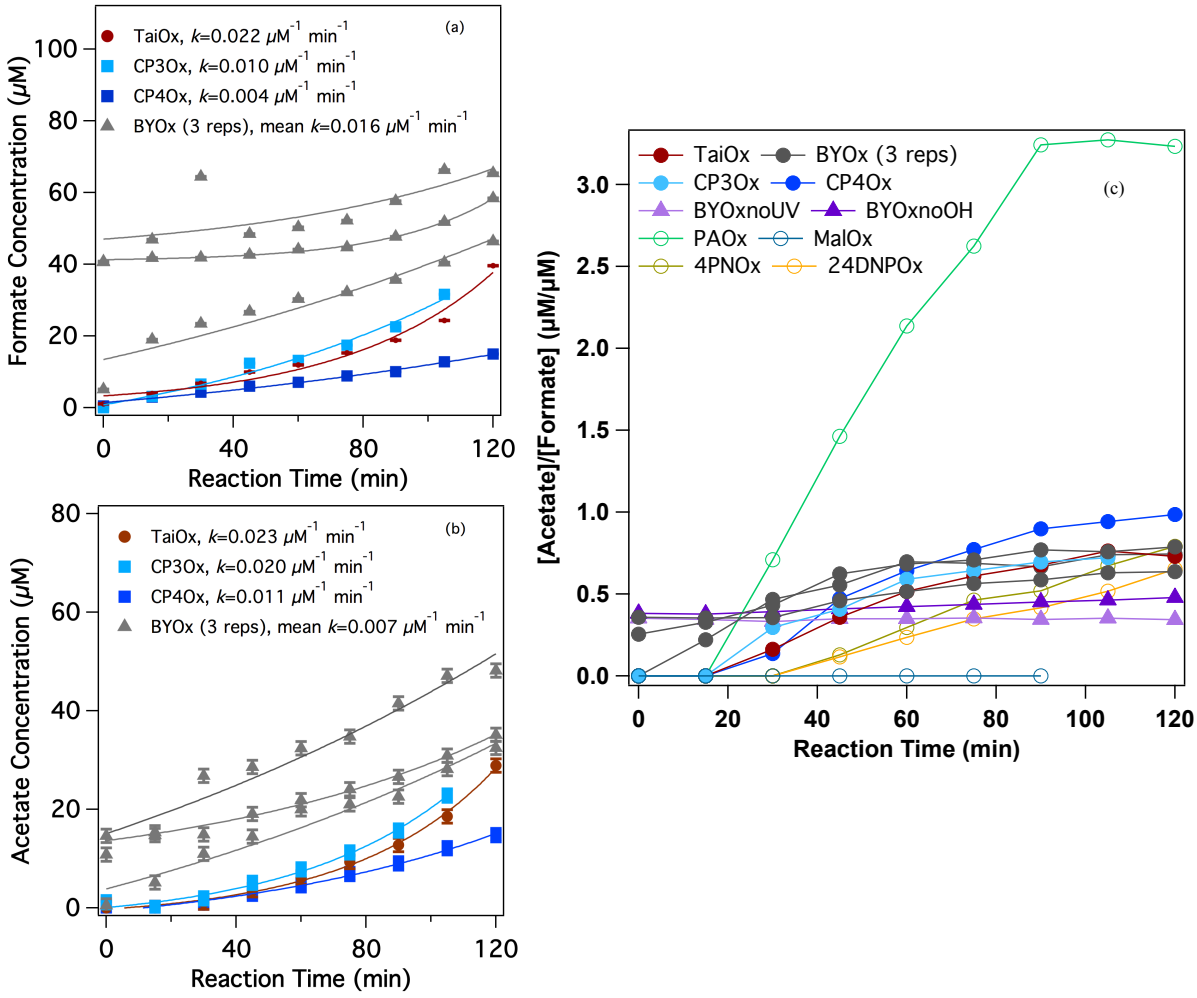

Figure 5-1. Formate concentrations (a) and acetate concentrations (b) measured during oxidation reactions of real fog and cloud water samples. Error bars represent the 95% confidence interval for acetate. Lines are fits to data points of the same color. Reaction rate constants *k* are derived from exponential fits of data points from each oxidation. Acetate/formate concentrations ratios (c) measured during oxidation reactions of standards (open symbols) and real fog/cloud water samples (solid symbols).

Oxalate is frequently the third most abundant carboxylic acid in the ambient atmosphere after acetate and formate, and the most abundant dicarboxylic acid (van Pinxteren et al., 2014 and references therein). It has been suggested that oxalate is a main product of in-cloud oxidation reactions (e.g., Sorooshian and Varutbangkul, 2006), and that it can therefore be used as an atmospheric tracer for such reactions (Warneck, 2003). The trend in oxalate concentration in the present study differed between oxidation experiments: while most reactions demonstrated an increase in oxalate, degradation was observed during the three BYOx replicate oxidation reactions as well as the direct photolysis BYOx control experiment (Figure 5-2 and A5-1). This evidence points to either the degradation of carboxylic acids by $^{\bullet}$OH reaction in BYOx, since the BYI fog sample contained highly oxidized compenents, or the photolysis of metal-oxalate complexes (Si and Ariya, 2008; Sorooshian et al., 2013; Weller et al., 2014a; Zuo and

Hoigné, 1994, 1992) as a dominant process controlling oxalate concentrations in BYOx. Iron-carboxylato complexes are important in terrestrial surface waters, in which 90% of iron (Lipczynska-Kochany, 1992) and 99.97% of Fe(III) (Rue and Bruland, 1995) have been found to be coordinated in such complexes. The anti-correlation between metals and oxalate concentrations in clouds also supports the importance of these complexes in the atmosphere (Safarzadeh-Amiri et al., 1997; Sorooshian et al., 2013; Weller et al., 2014b; Zhang et al., 2016; Zuo and Hoigné, 1994). In the present study, the concentrations of metals were not quantified, but the proximity of the Mount Tai cloud water sampling site to probable sources of atmospheric metal ions makes the Tai sample more likely to have contained metal-carboxylic acid complexes; the greater concentration of oxalate (and also possible presence of metals) in the BYI sample initially versus the other three atmospheric water samples (6.61 μM oxalate in BYI fog water versus <LOD in other samples at t=0 min) could explain the degradation rather than production of oxalate in the BYI sample specifically. Pyruvate, which also forms metal-carboxylato complexes (Weller et al., 2013), also degraded in the $^{\bullet}$OH oxidation (although non-significant) and direct photolysis of the BYI fog water sample. These results highlight two main concerns with the use of oxalate as a molecular marker for aqSOA/AAOP reactions: (1) oxalate is not formed in all aqueous oxidation reactions; and (2) oxalate can be degraded during aqueous oxidation reactions to form lower molecular mass carboxylic acids and CO_2. For example, MalOx produced oxalate at concentrations indistinguishable from zero, as did 2,4DNPOx. Note that while the light source used in the present study is not relevant for the troposphere, Fe-oxalate complexes also degrade in sunlight (Zuo and Hoigné, 1994).

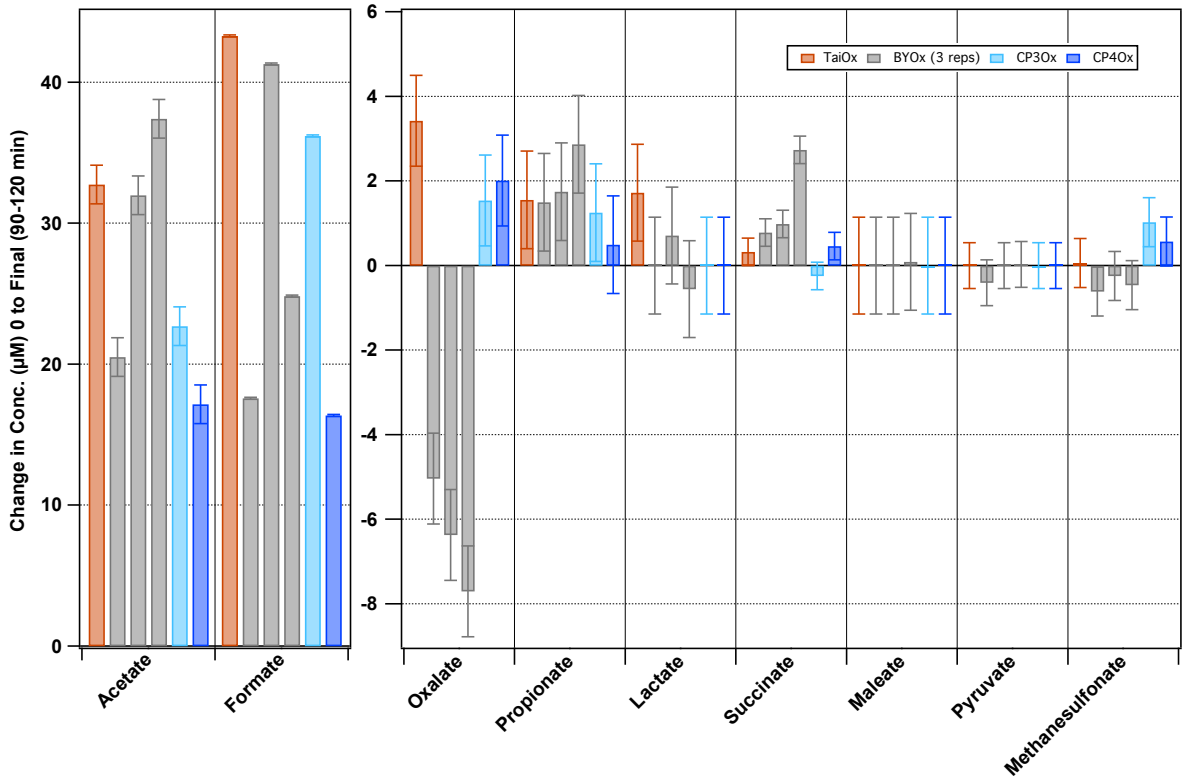

Figure 5-2. Change in concentration of carboxylic acids measured by IC between 0 and 120 min oxidation (or final time). Error bars represent the 95% confidence interval for each carboxylic acid species.

Succinate (saturated C_4 dicarboxylic acid) was thought to be a possible indicator for AAOP reactions, based on online MS results. Succinate production was indeed observed in all samples except CP3Ox. The production during the more aged BYOx was greatest, increasing at t=15 min and remaining at a steady concentration of 5.5-6 µM throughout the remainder of the oxidation.

Methanesulfonate, which originates from marine sources (Zhang et al., 2014) was apparently produced in CP3Ox (significant at the 95% confidence level) and in CP4Ox (significant at the 50% confidence level), which confirms that this species can be formed in the atmospheric aqueous phase (Bardouki et al., 2002). Degradation of methanesulfonate was, in contrast, observed in BYOx (significant at the 80% confidence level), which, again, could result from the lower initial concentrations of higher molecular mass precursors in the aged BYI sample.

Despite the finding that tartrate is a major product of glyoxal oxidation (Tan et al., 2009), tartrate was not identified as a product in any of the sample oxidation reactions in this study (no products with mass m/z^- 149 were found; tartrate was, however, identified as a product of maleate oxidation). Since glyoxal is ubiquitous in the atmosphere (Fu et al., 2008) and reacts at wet aerosol-relevant concentrations (3 mM) to produce tartrate from

aqueous oxidation, this suggests that the particular pathway resulting in its formation, likely a pathway occurring only at greater concentrations than those within the atmospheric samples used here, was not prominent during the reactions in the present study. The (-)-ESI-HR-ToF-MS should be sensitive to the polar, oxygenated structure of tartrate (note that no glyoxal concentrations were measured in the present study).

5.3.3 Mechanisms of Oxidation: Standards

Solutions of chemical standards were subjected to the same oxidation experimental procedures as the fog/cloud samples to qualitatively demonstrate the oxidation mechanisms of particular precursors. Maleic acid, pinonic acid (PA), 4-nitrophenol (4NP), and 2,4-dinitrophenol (2,4DNP) were oxidized (Table 5-1). The initial steps in the mechanisms of oxidation are summarized for maleic acid, PA, and 2,4DNP in Figure 5-3, Figure 5-4 and Figure 5-5, respectively, and demonstrate similar pathways occurring that are characteristic of $^{\bullet}OH$ oxidation in the aqueous phase. The mechanisms of 4NP oxidation were similar to those observed in the 2,4DNP oxidation, and were not summarized in a figure. The pathways for aromatic/unsaturated organic species differ somewhat from the pathways for saturated organic species in that electrophilic $^{\bullet}OH$ addition at a C=C bond typically dominates as the initiating step, while H atom abstraction dominates for saturated species (Atkinson, 1990). Both initiations ($^{\bullet}OH$ addition and H atom abstraction) result in the formation of an alkoxy radical, which then either attacks an O_2 molecule to form a peroxy radical when sufficient O_2 is present (in most atmospheric waters), or takes part in radical-radical reactions to form oligomers in O_2 depleted conditions (Renard et al., 2014). Various steps can occur after this. In the aqueous phase, in contrast to the gas phase where NO_x is available, the peroxy radical is only sometimes reduced to an alkoxy radical. The aqueous peroxy radical may: (1) decompose to form $HO_2^{\bullet}$ and a carbonyl (if a geminal –OH group is present or an aromatic bond can be re-formed); (2) form a tetroxide by joining with a second peroxy radical (even at low organic concentrations such as 10 μM; Cooper et al., 2009); or (3) cyclize to form a bicyclic peroxy intermediate (Von Sonntag et al., 1997). Tetroxides can then decompose via one of several known pathways; the resulting products can be alkoxy radicals or neutral alcohol and carbonyl molecules (Cooper et al., 2009; Lim et al., 2013). The $^{\bullet}OH$ attack can also occur on a side chain; this can result in the removal of the nitro group from a nitrophenol, as demonstrated in the bottom mechanism of Figure 5-3 (Oturan et al., 2000). Particular pathways are suggested in the present work based on the products identified in oxidation experiments and predicted mechanisms.

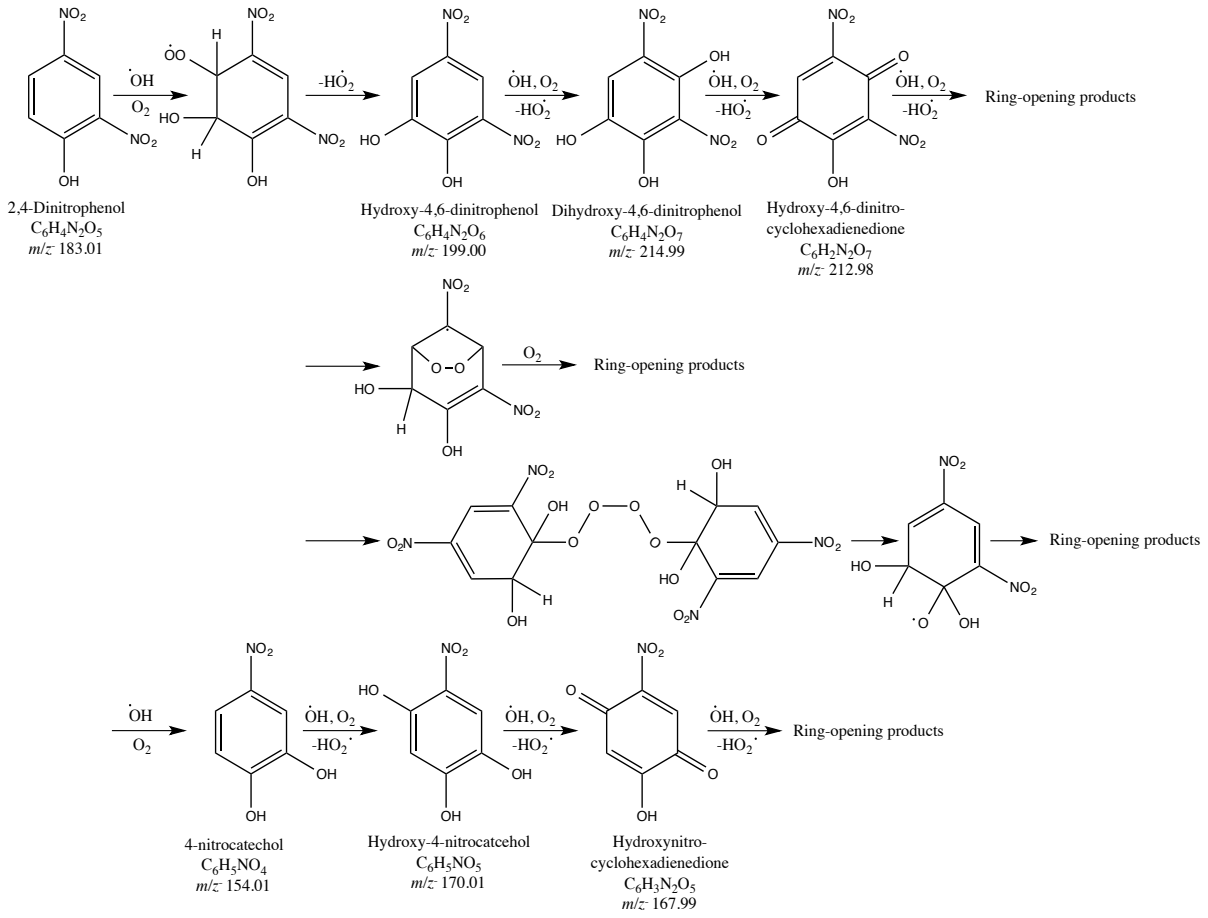

Figure 5-3. First steps in suggested observed mechanism of 2,4DNP oxidation (3 μM). Many ring-opening products were formed, including pyruvate, maleate, succinate, and malonate. The mechanism was initiated by •OH addition to aromatic bonds, followed by peroxy radical formation and a variety of continuing pathways.

The oxidation of 2,4DNP at 3 μM proceeded via multiple pathways (Figure 5-3), each resulting in products with increased oxygen content. Functionalized *para*-hydroquinones were formed, which were easily and reversibly oxidized to the corresponding benzoquinones , the most abundant products detected. Ring-opening species including maleic/fumaric, succinic, malonic, and pyruvic acids were final products of the oxidation after 120 min; all ring-retaining products were degraded after approximately 30 min. The oxidation of 4NP at 30 μM proceeded similarly to 2,4DNP oxidation, by the same pathways, including benzoquinone and substituted benzoquinone formation. Several ring-retaining products with only five carbon atoms were produced as well, likely to be furans/furanones (based on chemical formulae such as $C_5H_4O_2$, $C_5H_4O_3$, $C_5H_4O_4$, $C_5H_4O_5$, and $C_5H_3NO_4$). The cyclization of unsaturated diones has been suggested as a mechanism for furanone and cyclic anhydride formation in atmospheric gas-phase oxidation/photolysis (Bierbach et al., 1994); similar reactions might occur in the atmospheric aqueous phase. Detected ring-opening products of 4NP oxidation included multifunctional C_2-C_6 carboxylic acids with nitro,

aldehyde, alcohol, ketone, and second carboxylic acid groups: products with the possible structures of oxopentanedioic acid ($C_5H_6O_5$), carboxynitropentaldehyde ($C_5H_7NO_5$), dioxohexanedioic acid ($C_6H_6O_6$), and hydroxypentanedioic acid ($C_5H_8O_5$) were detected in 4NPOx.

The oxidation of maleic acid at 30 μM proceeded by •OH addition to the central double bond (Figure 5-4), followed by tetroxide formation and decomposition, to form products including glyoxylic acid and tartaric acid ($C_4H_6O_6$).

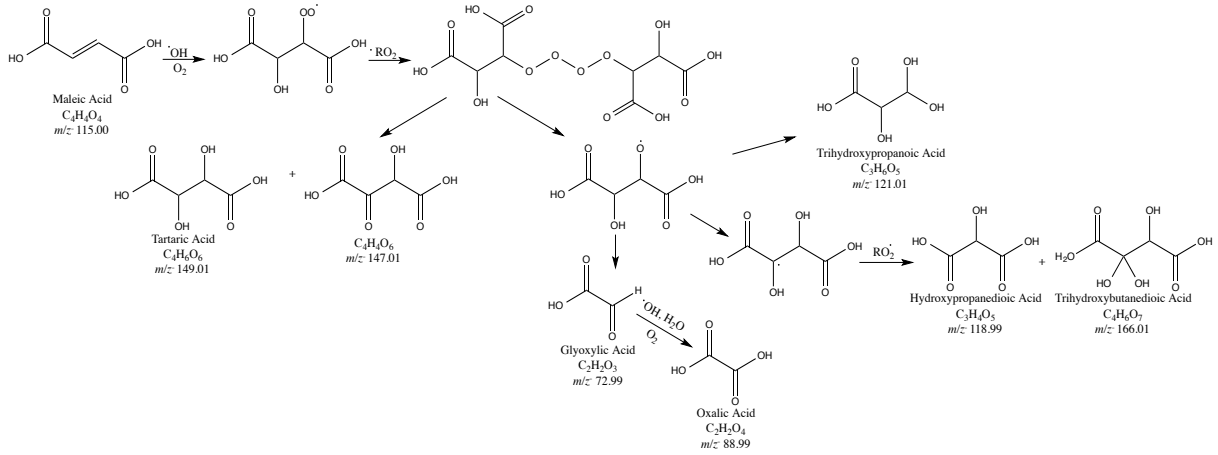

Figure 5-4. First steps in suggested observed mechanism of maleic acid oxidation (30 μM). Additional products including pyruvate and propanoic acid were formed. The mechanism was initiated by •OH addition, followed by tetroxide formation and decomposition.

Other products formed from maleic acid oxidation included malonic acid ($C_3H_4O_4$), trihydroxypropanoic acid ($C_3H_6O_5$), oxobutanoic acid ($C_4H_6O_3$), hydroxymalonic acid ($C_3H_4O_5$), dihydroxymalonoc acid ($C_3H_4O_6$), tetrahydroxypropanic acid ($C_3H_6O_6$), dihydroxyethanic acid ($C_2H_4O_4$), oxalic acid ($C_2H_2O_4$), pyruvic acid ($C_3H_4O_3$), glycolic acid ($C_2H_4O_3$), and dihydroxyacetic acid ($C_2H_4O_4$).

Only the H abstraction mechanism for •OH oxidation was possible for PA (Figure 5-5) since there are no aromatic or double bonds in its structure.

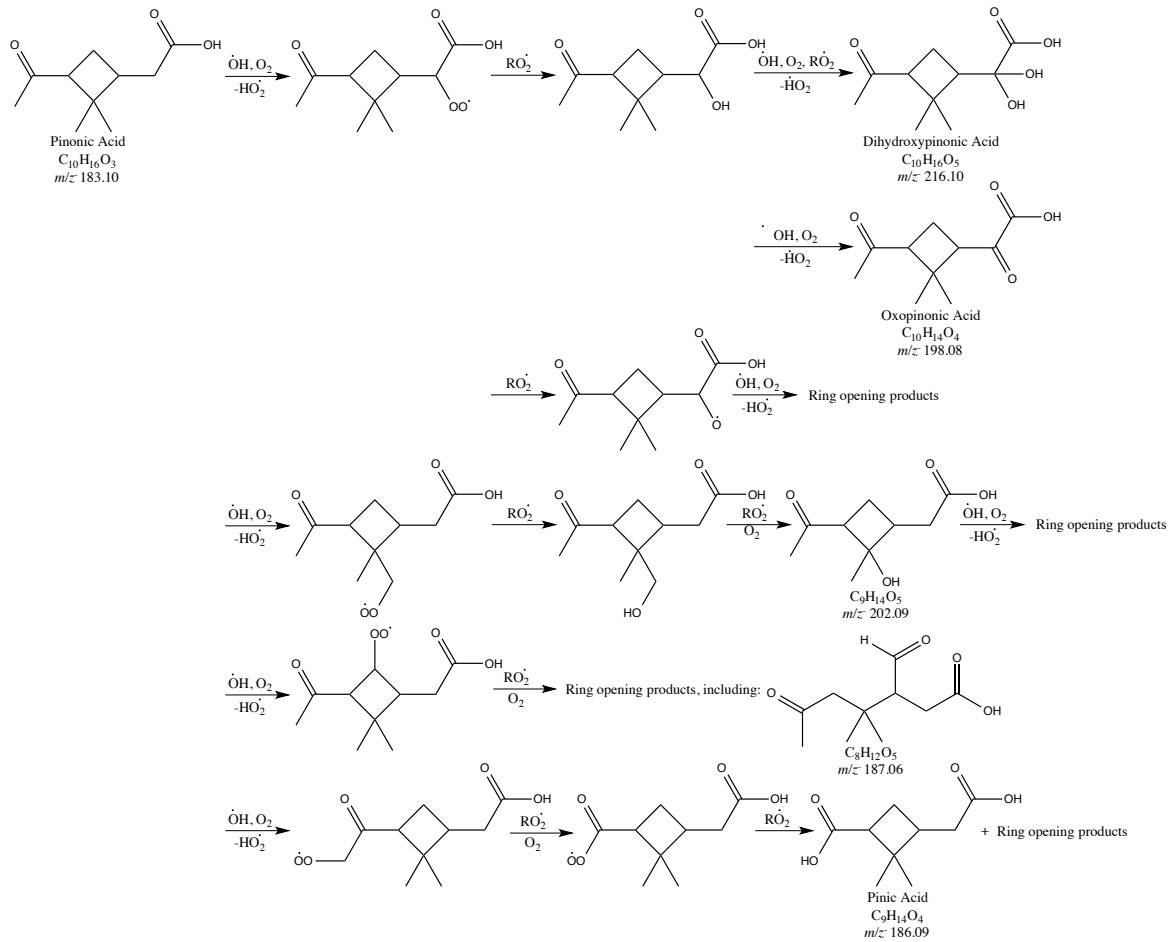

Figure 5-5. Observed mechanism of pinonic acid oxidation (3 μM), including only abundant products detected. All ring-retaining products shown are probably ring-opened to common LMM carboxylic acids. Many species that are prominent products in similar AAOP reactions (Lim et al., 2010) are not detected in the (-)-ESI-HR-ToF-MS, and so are not included in this mechanism.

Gas phase PA •OH oxidation proceeds mainly via H atom abstraction from the methylene C of the $–CH_2COOH$ side chain and the C atoms attaching the butane ring and side chains, followed by addition of O_2 and reduction steps to form an alkoxy radical (Müller et al., 2012). The aqueous oxidation likely occurs via a similar mechanism, although some steps such as 1,2-hydride shifts of alkoxy radicals and tetroxide formation are more likely in the aqueous phase (Lim et al., 2013). The location of •OH attack alters the resulting products, but mechanisms following the H atom abstraction are essentially similar to those observed in the 2,4DNP and maleic acid oxidation reactions. Although the top mechanism in Figure 5-5 demonstrates the individual addition of –OH groups to pinonic acid during oxidation, only products with two –OH additions were observed in the mass spectra. Additional structural

information about the products of aqueous PA oxidation should be explored to demonstrate whether mechanisms suggested in the present study are accurate; an alternative explanation is the formation of peroxides (Bateman et al., 2011).

5.3.4 Precursors of Oxidation: Samples

Mass spectra of each sample oxidation and reaction time profiles of species influenced during oxidation are compiled in Figure 5-6; species identified as precursors and products of sample oxidation are listed in Table A5-2. Oxidation reactions proceeded with some common apparent mechanisms, including formation of a group of products only observed during aqueous oxidation of aromatic precursors. Aromatic species were expected to be most reactive to oxidation, since many reaction mechanisms were possible with the aromatic bonds, followed by unsaturated long-chain species. The differences between quantitative abundance of a compound at 15, 30, 60, and 120 min and its abundance at 0 min oxidation were calculated as a proxy for the most reactive species (Table A5-2; the sensitivity of the (-)-ESI-HR-ToF-MS to analytes likely introduced some bias into the metric.

CHNO species were abundant within the cloud water samples collected at Mount Tai, which were heavily impacted by biomass burning emissions (ash particles were visible in the composite oxidized in this study). Biomass burning was also the most likely source of CHNO species identified within the BYI fog water (Boris et al., 2016). Nitrophenols in the CP3 fog sample were likely from aging of biogenic emission oxidation products and aromatic species in a high NO_x environment (Chapter 3) Additionally, CHNOS species served as precursors in the oxidation reactions, including methylnitrophenol sulfate ester ($C_7H_7NO_6S$) and hydroxynitrophenol sulfate ester ($C_6H_5NO_7S$; both tentatively identified). Since the products of nitrophenol aqueous oxidation were mainly CHO containing, the attack by $^{\bullet}OH$ at nitro groups is therefore a likely mechanism for the oxidation of these species. Even under the high nitrate concentrations observed in the more polluted samples reacted, the nitrophenols served exclusively as reactants rather than products. This included mono- and di-nitrophenols, as well as CHNOS. A CHNOS species ($C_{10}H_{17}NO_7S$; m/z^- 294.06) that was previously identified in ambient aerosol as a nighttime monoterpene/$^{\bullet}NO_3$ oxidation product was also identified as a precursor in BYOx (as well as the direct photolysis of BYI fog water, but not H_2O_2 reaction of BYI fog water).

Oxidation precursors of aromatic species most likely of anthropogenic origin (Kawamura et al., 2013) were identified as precursors in BYOx, CP3Ox and TaiOx. In BYOx, maleic acid ($C_4H_4O_4$, m/z^- 115.01), phthalic acid

($C_8H_6O_4$, *m/z*$^-$ 165.03), and pentenedioic acid ($C_5H_6O_4$, *m/z*$^-$ 129.02) had decreased most in abundance after 15 min oxidation. For CP3Ox, hydroxyphthalic acid ($C_8H_6O_5$, *m/z*$^-$ 181.02) and dinitrophenol ($C_6H_4N_2O_5$, *m/z*$^-$ 183.01) were the most degraded, again indicative of human activities. For TaiOx, dinitrophenol ($C_6H_4N_2O_5$, *m/z*$^-$ 183.01), hydroxynitrophenol, sulfate ester ($C_6H_5NO_7S$, *m/z*$^-$ 233.98), hydroxynitrophenol/nitrocatechol ($C_6H_5NO_4$, *m/z*$^-$ 154.02), and methyldinitrophenol ($C_7H_6N_2O_5$, *m/z*$^-$ 197.03) were the most rapidly degraded species. In contrast, for CP4Ox, the most rapidly degraded species, demonstrated that biogenic species even without unsaturated sites can be rapidly degraded within real fog/cloud samples: a CHNO species of unknown origin ($C_{12}H_{23}NO_3$, *m/z*$^-$ 288.16), pinonic acid ($C_{10}H_{16}O_3$, *m/z*$^-$ 183.10), and pinic acid ($C_9H_{14}O_4$, *m/z*$^-$ 185.08) were the most rapidly degraded.

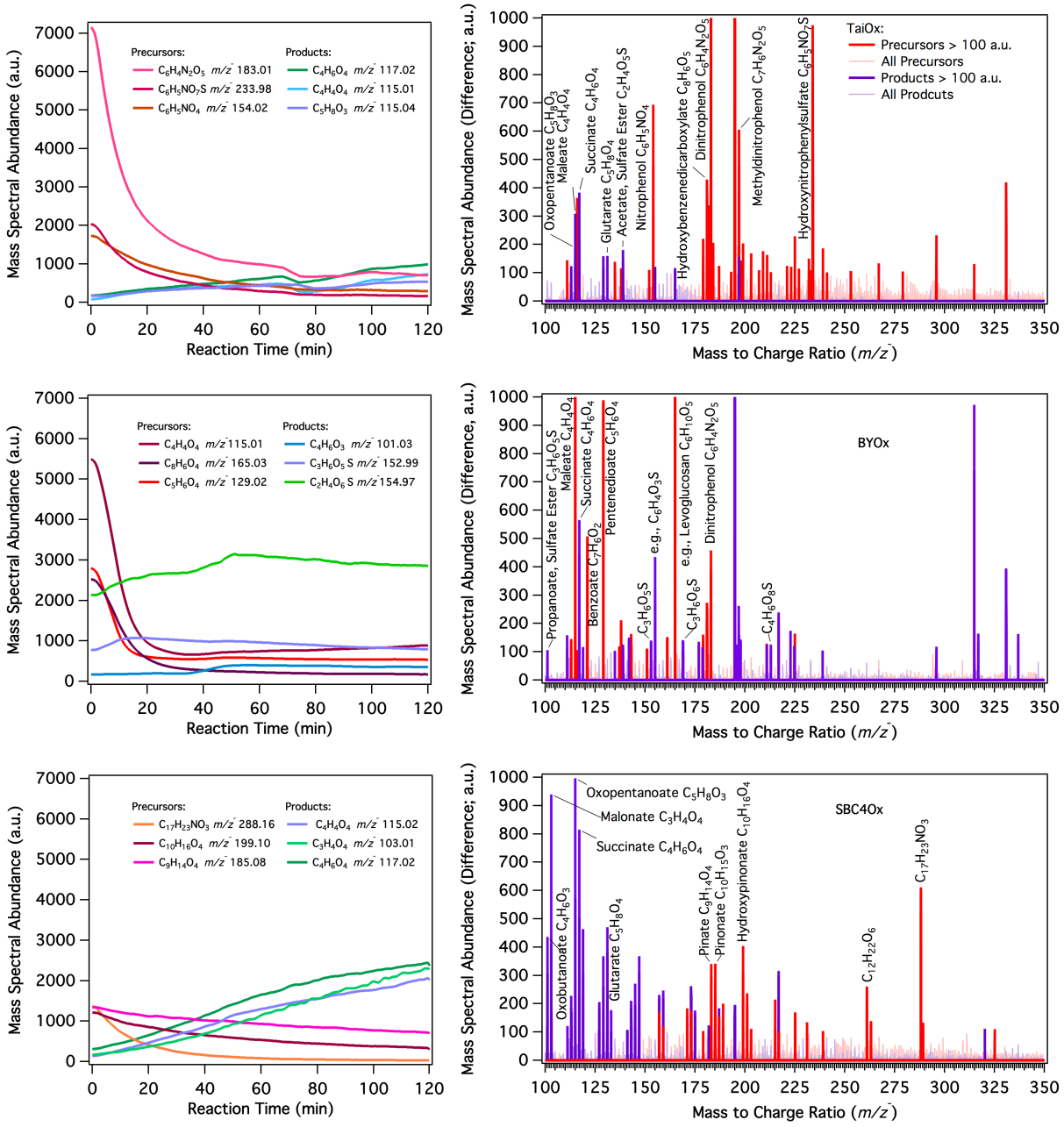

Figure 5-6. Reaction time profiles of mass spectral signals for organic species most influenced by oxidation (left), and mass spectra of precursors and products observed during sample oxidation reactions. Time profiles were smoothed to demonstrate overall trends (500 points, boxcar averaging), and only the three precursors and three products with the greatest change during oxidation were plotted. Mass spectra were calculated as follows: precursors > 100 abundance units (red) and all other precursors (pink) were identified by subtracting spectra at 15, 30, 60, and 120 min oxidation reaction time from the spectrum at 0 min reaction time; products > 100 abundance units (purple) and all other products (lavender) were identified by subtracting the spectrum at 0 min reaction time from the spectra at 15, 30, 60, and 120 min reaction time. Names of species are tentative identifications; "e.g." indicates that multiple formulae were possible at a particular *m/z*.

Quantitative results were mostly in agreement with those from the qualitative online MS analysis. The degradation of 2,4DNP was confirmed in TaiOx and BYOx by quantitative results, but not significantly (95% confidence) in CP3Ox (this could be indicative of a detection limit issue in LC/MS or of a different isomer of dinitrophenol as precursor in CP3Ox). Maleic acid was also not confirmed as having acted as a precursor in BYOx (via IC), suggestive again of a detection limit issue in IC, as compared to the sensitive online MS technique. Also confirmed as precursors via LC/MS were 4-nitrocatechol in TaiOx, and two biogenic species in CP4Ox, pinic and pinonic acids (these two were also degraded quickly, according to LC/MS, in CP3Ox; Figure 5-7).

5.3.5 Products of Oxidation: Samples

Chemical regimes of the fog and cloud water samples initially caused differing oxidation reactions to proceed. Organic S-containing species were prominent products of BYOx and TaiOx, which both began with high organic and sulfate concentrations relative to CP3Ox and CP4Ox. Under the lower S-content chemical conditions of the CP fog water samples, only one CHOS product was formed (tentatively identified as glycolic acid, sulfate ester, $C_2H_4O_6S$ in CP4Ox at 120 min). Despite the supposition that nitrophenols are likely formed in the aqueous phase (Harrison et al., 2005) and experimental evidence demonstrating this process (via $^{\bullet}NO_2$ and $^{\bullet}NO_3$ or HNO_2 reaction with phenol; Barzaghi and Herrmann, 2002; Vione et al., 2003), no CHNO species were formed as a result of oxidation in this study. The formation of $^{\bullet}NO_3$ in clouds has been suggested to occur mainly by scavenging of the radical from the gas phase (after NO_2/O_3 reaction, Chameides, 1986); the lack of fresh $^{\bullet}NO_3$ or precursors from the gas phase in the bulk lab photoreaction may have inhibited reactions that might have occurred in a night-time atmosphere.

During the oxidation of the BYI fog water, CHOS species were formed rapidly (15 min) from LMM compounds (the most abundant was $C_5H_8O_7S$, tentatively identified as hydroxymethyloxobutanoic acid, sulfate ester). At 60 min, pyruvate and methacrylate were observed; these were the only non-S-containing organic products observed using online MS. The CHOS species were likely outcompeting other products within the electrospray ionization source of the online MS, including the LMM carboxylic acid products measured using IC. However, LC/MS separation of the oxidized samples did not allow detection of additional products. Overall, the formation of CHOS species in the BYI fog sample demonstrated that aged fog water constituents could result in a different reaction from the typical progression toward LMM oxygenated products.

The singular oxidation product detected at 15 min reaction time in TaiOx was phthalic acid ($C_8H_6O_4$), indicating that this species can be produced in the atmospheric aqueous phase. Only after further oxidation were unsaturated and oxo-containing carboxylic acids produced. A small number of CHOS species were also identified as products. Phthalic acid was the only product detected with $\geq C_6$ throughout TaiOx, suggesting that the oxidation pathways of the nitrophenols, including 2,4DNP within the Mount Tai cloud water, proceeded via ring-opening mechanisms. No N-containing products were identified, which also suggests that removal of $-NO_2$ groups from the N-containing organic species occurred.

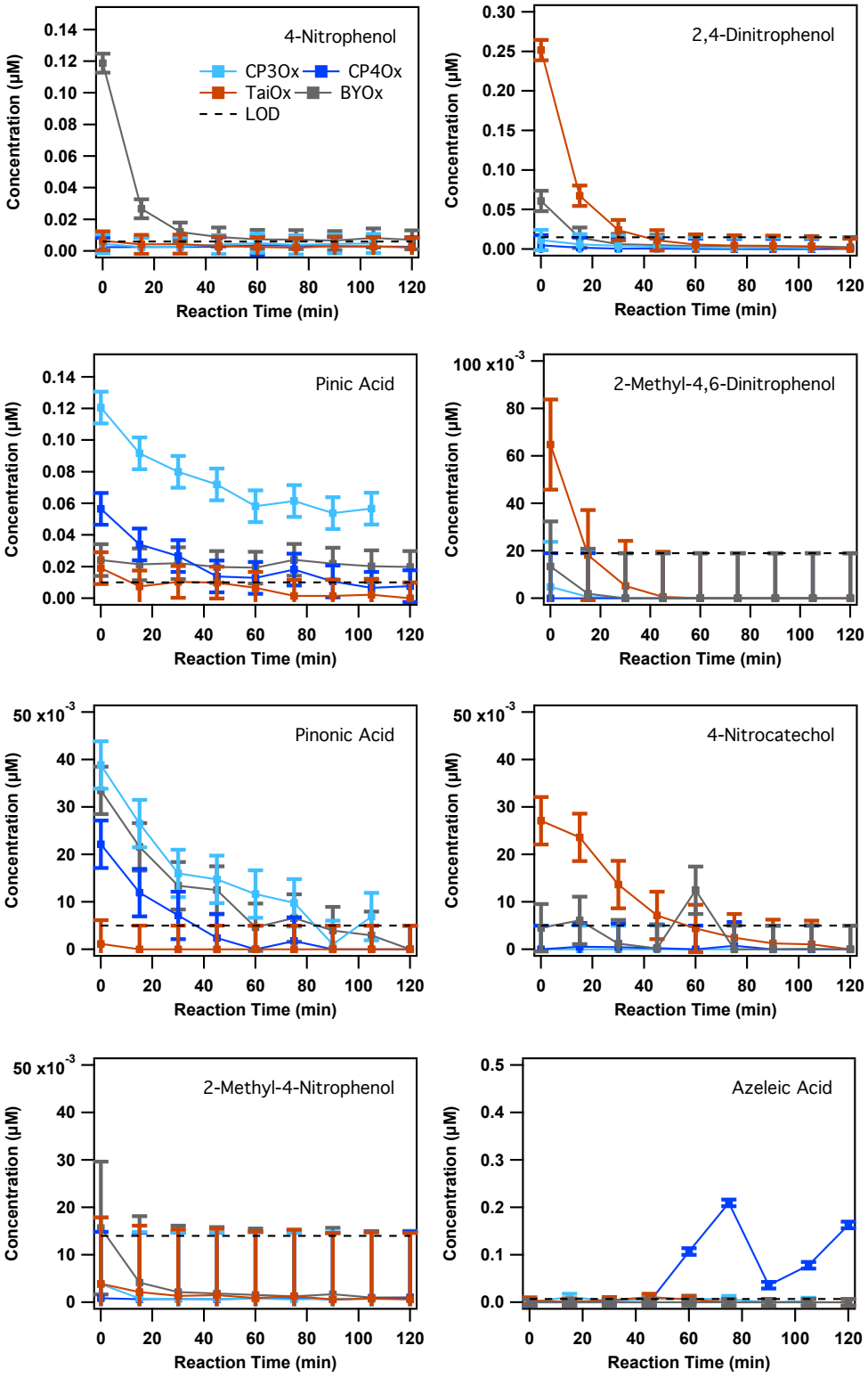

Figure 5-7. Time profiles of nitrophenols and and organic acid cloud water constituents quantified via LC-MS. Error bars represent the 95% confidence interval calculated over replicate standard analyses for each chemical. Limits of detection (LODs) were quantified at 95% confidence over replicate oxidation experiment method blanks, and are represented by dashed black lines.

The oxidation of CP3, which initially contained a mix of aged anthropogenic and biogenic species, produced a CHOS species (tentatively identified as glycolic acid sulfate ester, $C_2H_4O_6S$) and LMM carboxylic acids. There was a clear discrepancy between the products of CP3Ox detected using IC and online MS, highlighting the need to combine online MS with offline quantitative techniques. This discrepancy between instrument signals is due to the competition for ionization in the electrospray source (Tang et al., 2004). Oxidation products of CP3, however, did include some detectable $\geq C_4$ unsaturated and oxo-acids, as well as pyruvate and oxalate. Concentrations of all quantified nitrophenol species (LC/MS) were below the LOD throughout CP3Ox, but were observed to decrease.

The least polluted fog water sample oxidized in the present study, CP4, reacted to form several products also observed in PAOx (e.g., formyldimethylpentanedioic acid and dihydroxydimethylpentanedioic acid), demonstrating the oxidation of biogenic species in real fog water. These species were observed after 30 min CP4Ox reaction time, while LMM organics were observed immediately (after only 15 min). The delayed oxidation (Figure 5-6) appears to be due to slower oxidation of the biogenic species relative to nitrophenol and dinitrophenol as observed in BYOx and TaiOx (this is supported by quantitative LC/MS results; Fig. A5-6). Several of the LMM organic products observed in CP4Ox were not produced in PAOx (or MalOx), including those with double bonds and ketones: acrylic acid ($C_3H_4O_2$), methacrylic acid ($C_4H_6O_2$), hydroxymethacrylic acid ($C_4H_6O_3$), as well as C_5 and C_6 oxo- and unsaturated acids, such as oxopentanoic acid ($C_5H_8O_3$). Methacrylic and hydroxyacrylic acids, however, were observed during 4NPOx, and hydroxyacrylic acid was observed during 2,4DNPOx, suggesting that unsaturated and oxo-acids originate from aqueous oxidation of aromatic species, but not biogenic or straight-chain (including unsaturated) precursors.

Unlike nitrophenols, which are formed in the lab in aqueous solution when dilute nitric acid is added to phenolic species at room temperature, the addition of concentrated sulfuric acid to a phenol is required to form an aromatic organosulfate (Solomons and Fryhle, 2004). Thus, organosulfate formation under aqueous atmospheric conditions is unexpected. Nonetheless, organosulfates have been observed in atmospheric samples and lab experiments: the reaction of H_2SO_4 with isoprene-derived epoxydiols forms products such as 2-methyltetrol sulfate ester (McNeill et al., 2012) and limonene ozonolysis product esters (Iinuma et al., 2007). However, neither the 2-methyltetrol sulfate ester, which is the most common epoxydiol-derived sulfate ester (McNeill et al., 2012), nor products which could be accounted for reasonably by this pathway were detected in the present study. Schindelka et al. (2013) proposed a radical mechanism for sulfation: $SO_4^{\bullet-}$ (formed from photolysis (248 nm) of sulfuric acid and/or potassium

peroxodisulfate) addition across a double bond, followed by peroxy radical formation, reduction to form an alkoxy radical, and loss of an adjacent functional group to form a carbonyl (analogous to the more familiar $^{\bullet}OH$ addition mechanism). Although similar CHOS species were tentatively identified in the present study matching those observed in Schindelka et al. (2013), including glycolaldehyde sulfate ester ($C_2H_4O_5S$), glycolic acid sulfate ester ($C_2H_4O_6S$), and malic acid sulfate ester ($C_4H_6O_8S$), the mechanism proposed by Schindelka requires precursors different from the apparent sulfated species (for example, malic acid), instead beginning with a precursor having a double bond at the site of the ester. For many CHOS species formed in the present study, such as nitrophenol sulfate ester ($C_6H_5NO_7S$), this double bond precursor seems unlikely. Based on the structures of the CHOS compounds tentatively identified in the present study, the most likely mechanism for formation of the CHOS products identified in BYOx and TaiOx is instead S addition by H_2SO_4, similar to the esterification mechanism of carboxylic acids (Deno and Newman, 1950). This mechanism was also suggested by Surratt et al. (2008) for sulfation of a variety of monoterpene products based on structures of the sulfated products confirmed using ion trap MS.

Organic alcohol-sulfate adducts have also been observed in electrospray MS (Cai and Cole, 2002; Perri et al., 2010). The suggested structures for such adducts, however, are not in agreement with the observed chemical formulae in the present study, and adducts therefore cannot explain the observed CHOS species (Figure 5-8). For example, the adduct of hydroxynitrophenol (nitrocatechol) would give a chemical formula of $C_6H_6NO_8S$, while the observed formula is $C_6H_5NO_7S$ (the adduct of nitrophenol would have a formula of $C_6H_6NO_7S$). This logic can be extended to other CHOS species identified in the present study as well. In addition, if the observed CHOS species were simply adducts, they should be formed from the simple analysis of deprotonatable organic species in the presence of H_2SO_4 at similar concentrations to the BYI and Mount Tai fog samples; however, this has not been observed previously under the stated conditions. The CHOS species were instead most likely formed as a result of $^{\bullet}OH$-driven alcohol formation followed by H_2SO_4 esterification, as outlined in Surratt et al. (2008). Only one of the identified CHOS species was detected in the direct photolysis of the BYI sample (tentatively identified as glycolic acid, sulfate ester), confirming that photolysis of neither the H_2SO_4 nor the organic precursors caused most of the CHOS formation.

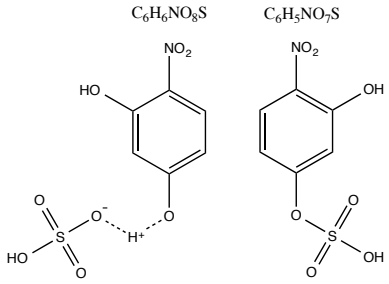

Figure 5-8. CHOS species formed from interaction of H_2SO_4 with nitrocatechol (hydroxynitrophenol), as an example. Adduct due to electrospray ionization process (online and offline MS) as proposed by Cai and Cole (2002; left) does not the match molecular formula identified in the present study, while the covalently bound ester of nitrocatechol (right; formed as suggested by Surratt et al., 2008 and others) does match ($C_6H_5NO_7S$; identified within the Mount Tai sample as a precursor of oxidation).

5.3.6 Atmospheric Implications

Nitrophenols and their derivatives are known to be toxic to aquatic invertebrates as well as to small mammals and plants (Agency for Toxic Substances and Disease Registry, 2011, 1992; Natangelo et al., 1999). 2,4DNP and other nitrophenol species were abundant within the Tai and BYI cloud/fog samples, and also present in the CP fog. Analogous to the advanced oxidation of such species in wastewater and in natural terrestrial waters (Kavitha and Palanivelu, 2005; Zhang et al., 2003), nitrophenols and derivatives were efficiently reacted in real atmospheric water samples to form carboxylic acids and other products. An improvement in air toxicity due to oxidation can therefore be be demonstrated by noting that the rate of removal of 2,4DNP from the authentic cloud/fog samples was -0.012 μM min^{-1} and -0.003 μM min^{-1} after 15 min (k=-0.089 and -1.1 μM^{-1} min^{-1} throughout the oxidation) in TaiOx and BYOx, respectively (see Section 5.3.2, Evolution of Carboxylic Acids, for methodology). Similarly, the following degradation rates for other nitrophenols were observed: 4NP: -0.006 μM min^{-1} (k=-0.12 μM^{-1} min^{-1}) in BYOx, 2-methyl-4,6-dinitrophenol (2m4,6DNP): -0.003 μM min^{-1} (k=-0.084 μM^{-1} min^{-1}) in TaiOx, 4NC: -0.0002 μM min^{-1} (k=-0.022 μM^{-1} min^{-1}) in TaiOx, and 2-methyl-4-nitrophenol (2m4NP): -0.0001 and -0.0008 μM min^{-1} (k=-0.047 and -0.11 μM^{-1} min^{-1}) in TaiOx and BYOx, respectively. Note that these are all second order rate constants. For comparison, the degradation rates of pinonic acid were as follows: -0.0008, -0.0007, and -0.0008 μM min^{-1} (k=-0.028, -0.041, and -0.027 μM^{-1} min^{-1}) in CP3Ox, CP4Ox, and BYOx, respectively; the degradation rates of pinic acid were both -0.002 μM min^{-1} (k=-0.032 and -0.037 μM^{-1} min^{-1}) in CP3Ox and CP4Ox. Rates of degradation were thus overall slower for biogenic, saturated organic species, as anticipated based on mechanisms of oxidation.

The production of aqSOA mass is an expected outcome of AAOP reactions (Ervens et al., 2011). Carboxylic acids produced during the oxidation reactions of real fog/cloud water samples in the present work would contribute to the aqSOA mass production: for example, ~90% and 63% of oxalic and glutaric acids, respectively, have been

observed to be distributed to the particle phase in the real atmosphere (Limbeck et al., 2005). In addition, Ortiz-Montalvo et al. found that addition of NH_4^+ to a solution of carboxylic acids similar to those identified in the present study caused the resulting vapor pressure of the solution to decrease by two orders of magnitude (Ortiz-Montalvo et al., 2014). The net aqueous production of the quantified carboxylic acids (formic and acetic acids, C_2-C_5 dicarboxylic acids, pyruvic acid, propionic acid, lactic acid, and maleic acid) from oxidation reactions of real fog/cloud water samples was as follows: 2.1 mg L^{-1} from CP4Ox, 2.3 mg L^{-1} from CP3Ox, 2.9 mg L^{-1} from the mean of the three BYOx replicates, and 4.5 mg L^{-1} from TaiOx (within 120 min oxidation). This trend in observed carboxylic acid production with greatest values in the fresh, high TOC Mount Tai cloud sample, suggests that aqueous production rates of carboxylic acids are greatest in the presence of fresh, abundant organic emissions. Relative to the TOC concentration, the percent mass carboxylic acids produced in each oxidation was: ~20% in CP4Ox, ~10% in CP3Ox, ~10% in BYOx (mean), and ~20% in TaiOx, demonstrating some commonality between the oxidation reactions. Based on these results, AAOP reactions within fog/cloud therefore would theoretically impact measured organic particulate matter at each sampling site, with greater production of semi-volatile carboxylic acid species within fresh, abundant organic emissions.

5.4 Conclusions

Fog/cloud water collected from the three locations globally and subjected to AAOP reactions in the present study represented differing chemical regimes: the CP4 sample contained lower concentrations of nearly all species measured, and organic species were predominantly biogenic. The CP3 sample, during collection of which LWC was lower than during CP4, contained biogenic species as well as nitrophenols. The BYI fog water sample was the most "polluted" of the samples, containing the greatest concentrations of all measured inorganic species and TOC. Organic species identified within the BYI sample were aged and anthropogenic in origin, including phthalic acid and derivatives, CHNO, and N- and S-containing monoterpene derivatives. Cloud water from Mount Tai used in the present study also contained high concentrations of inorganic species, nearly matching the SO_4^{-2} concentration of the BYI sample. The Mount Tai sample demonstrated a clear anthropogenic and biomass burning influence, but also a contribution from biogenic species.

Initial composition of the fog/cloud water impacted the oxidation experiments most evidently by providing SO_4^{-2} for the formation of CHOS species in some samples (BYOx primarily, but also some in TaiOx and one detectable product in CP4Ox). Although CHNO species were not formed in the oxidation reactions, $^{\bullet}NO_3$ formation was not

likely without NO_2, O_3, or radical reservoir species (Chameides, 1986; Vione et al., 2003). Structure-reactivity relationships of $^{\bullet}OH$ toward organic species in AAOP interactions have been studied previously (Doussin and Monod, 2013). Nitrophenols were degraded more rapidly than biogenic species, as demonstrated using online MS and offline LC/MS, and as anticipated based on previously measured reaction rate constants of aromatic and aliphatic organic species with $^{\bullet}OH$ (Doussin and Monod, 2013). The value of the ratio of $[acetate]_{aq}/[formate]_{aq}$, was confirmed in this study as a metric for oxidation of biogenic versus anthropogenic precursors: values near or exceeding one were from the CP4Ox and PAOx experiments, while other oxidation reactions were clustered below one after 120 min reaction. On the other hand, while oxalate has been discussed as a molecular marker for AAOP reactions, it was instead degraded in the BYOx replicates, 2,4DNPOx, PAOx, and maleate oxidation, suggesting that oxalate should be applied as a molecular marker for such reactions with caution. Metals were not measured in all samples, but the photolysis of metal-carboxylato complexes is suggested to have caused, at least in part, the degradation in some carboxylic acid concentrations over BYOx.

Multiple products not frequently accounted for in models of secondary organic aerosol formation (Tsigaridis et al., 2014) were detected in the oxidation of real fog/cloud water samples. CHOS species, which have recently been more prevalent in organic aerosol discussions (McNeill, 2015; Zhang et al., 2012), were the main observed product category of BYOx. These species were also found to react in the oxidation reactions; in particular, nitrocatechol sulfate ester ($C_6H_5NO_7S$) was detected using online MS as one of the most rapidly reacting precursors in BYOx. These species are proposed to have formed via the mechanism suggested by Surratt et al., (2008), involving esterification of a hydroxy groups by H_2SO_4, driven by the formation of hydroxylated products in the oxidation process. Carboxylic acids are known products of aqueous and gas-phase oxidation reactions, but only a relatively small number of these species are regularly quantified in lab or ambient samples. Additional products frequently detected in the present study included C_5–C_7 acids with oxo- and unsaturated groups, as well as acrylic, methacrylic, and hydroxyacrylic acids. These species were only present in the samples with a substantial contribution from aromatic or unsaturated organic species (mostly of anthropogenic origin); it is suggested that these species may therefore be molecular markers for oxidation of anthropogenic organic emissions.

Oxidation reactions of standard precursors, including 4NP, 2,4DNP, PA, and maleate, differed from the oxidation reactions of real fog/cloud samples in some key ways. The most noticeable of these differences is the complexity of the oxidation reactions of real samples, in which a large number of products were formed. Some

pathways of reaction were the result of interactions between inorganic and organic fog/cloud water components, such as CHOS formation and possibly degradation of carboxylic acids via metal-carboxylato complexation and photolysis. The previous oxidation reactions of chemical standards in the lab to simulate AAOP reactions have included concentrations of individual standards (such as glyoxal) that are more representative of wet aerosol particles; some products of reaction observed in such studies (for example, tartaric acid and organic esterification products, Lim et al., 2010; Tan et al. 2009) were not observed within the oxidation reactions of real fog/cloud samples here.

Implications of this research include the preferential degradation of toxic nitrophenol and aromatic species in fog/cloud water samples via AAOP reactions, occurring at 0.6-1 nM min^{-1} under the experimental conditions here. Additionally, the net formation of carboxylic acids during reactions in fog/cloud water under the experimental conditions was between ~10-20% of TOC, suggesting that AAOP reactions in real fog/cloud water samples could generate aqSOA mass through production and partitioning of semi-volatile carboxylic acid species.

Future research in the area of atmospheric oxidation reactions should include additional studies of oxidation reactions within real fog and cloud water samples to demonstrate the probable regional, seasonal, and diurnal patterns in AAOP. Bulk photoreaction and chemical analysis techniques should also be improved. Polar organic species other than carboxylic acids and phenols should be quantified since it is likely that aldehydes, ketones, and other alcohols are also important intermediates in AAOP reactions (Lim et al., 2013, 2010). Further work is needed to understand and mitigate ESI-MS ionization suppression effects (Annesley, 2003; Kebarle and Verkerk, 2009). Furthermore, transfer at the air-water interface in a real cloud/fog droplet could theoretically provide a source of $^{\bullet}OH$ and aqueous precursors during photo-activity (it has been estimated that $^{\bullet}OH$ is limited in a real droplet environment by mass transfer and kinetic limitations of aqueous $^{\bullet}OH$-producing reactions; Ervens et al., 2014; McNeill, 2015). Continued work toward a more accurate photoreactor setup with quantitative tools for estimation of aqSOA production, such as an environmental chamber setup is needed (Daumit et al., 2014; Nguyen et al., 2011).

REFERENCES

Agency for Toxic Substances and Disease Registry, 1992. Toxicological profile for nitrophenols: 2-nitrophenol, 4-nitrophenol. Atlanta, Georgia.

Agency for Toxic Substances and Disease Registry, 2011. Addendum To the Toxicological Profile for Dinitrophenols. Atlanta, Georgia.

Aiken, A.C., Decarlo, P.F., Kroll, J.H., Worsnop, D.R., Huffman, J.A., Docherty, K.S., Ulbrich, I.M., Mohr, C., Kimmel, J.R., Super, D., Sun, Y., Zhang, Q., Trimborn, A., Northway, M., Zieman, P.J., Canagaratna, M.R., Onasch, T.B., Alfarra, M.R., Prevot, A.S.H., Dommen, J., Duplissy, J., Metzger, A., Baltensperger, U., Jimenez, J.L., 2008. O/C and OM/OC Ratios of Primary, Secondary, and Ambient Organic Aerosols with High-Resolution Time-of-Flight Aerosol Mass Spectrometry. Environ. Sci. Technol. 42, 4478–4485.

Altieri, K.E., Seitzinger, S.P., Carlton, A.G., Turpin, B.J., Klein, G.C., Marshall, A.G., 2008. Oligomers formed through in-cloud methylglyoxal reactions: Chemical composition, properties, and mechanisms investigated by ultra-high resolution FT-ICR mass spectrometry. Atmos. Environ. 42, 1476–1490.

Amato, P., Demeer, F., Melaouhi, A., Fontanella, S., Martin-Biesse, A.-S., Sancelme, M., Laj, P., Delort, A.-M., 2007. A fate for organic acids, formaldehyde and methanol in cloud water: their biotransformation by micro-organisms. Atmos. Chem. Phys. 7, 4159–4169.

Anastasio, C., Faust, B.C., Allen, J.M., 1994. Aqueous phase photochemical formation of hydrogen peroxide in authentic cloud waters. J. Geophys. Res. 99, 8231.

Anastasio, C., McGregor, K.G., 2001. Chemistry of fog waters in California's Central Valley: 1. In situ photoformation of hydroxyl radical and singlet molecular oxygen. Atmos. Environ. 35, 1079–1089.

Andreae, M.O., 1983. Soot carbon and excess fine potassium: Long-range transport of combustion-derived aerosols. Science 220, 1148–1151.

Annesley, T.M., 2003. Ion suppression in mass spectrometry. Clin. Chem. 49, 1041–1044.

Arakaki, T., Faust, B.C., 1998. Sources, sinks, and mechanisms of hydroxyl radical (•OH) photoproduction and consumption in authentic acidic continental cloud waters from Whiteface Mountain, New York: The role of the Fe(r) (r = II, III) photochemical cycle. J. Geophys. Res. 103, 3487.

Atkinson, R., 1990. Gas-phase tropospheric chemistry of organic compounds: A review. Atmos. Environ. Part A. Gen. Top. 24, 1–4.

Bardouki, H., Da Rosa, M.B., Mihalopoulos, N., Palm, W.U., Zetzsch, C., 2002. Kinetics and mechanism of the oxidation of dimethylsulfoxide (DMSO) and methanesulfinate (MSI-) by OH radicals in aqueous medium. Atmos. Environ. 36, 4627–4634.

Barzaghi, P., Herrmann, H., 2002. A mechanistic study of the oxidation of phenol by OH/NO2/NO3 in aqueous solution. Phys. Chem. Chem. Phys. 4, 3669–3675.

Bateman, A.P., Nizkorodov, S. a, Laskin, J., Laskin, A., 2011. Photolytic processing of secondary organic aerosols dissolved in cloud droplets. Phys. Chem. Chem. Phys. 13, 12199–212.

Bator, A., Collett, J.L., 1997. Cloud chemistry varies with drop size. J. Geophys. Res. 102, 28071–28078.

Bautitz, I.R., Nogueira, R.F.P., 2007. Degradation of tetracycline by photo-Fenton process—Solar irradiation and matrix effects. J. Photochem. Photobiol. A Chem. 187, 33–39.

Bierbach, A., Barnes, I., Becker, K.H., Wiesen, E., 1994. Atmospheric Chemistry of Unsaturated Carbonyls: Butenedial, 4-Oxo-2-pentenal, 3-Hexene-2,5-dione, Maleic Anhydride, 3H-Furan-2-one, and 5-Methyl-3H-furan-2-one. Environ. Sci. Technol. 28, 715–729.

Boris, A.J., Desyaterik, Y., Collett, J.L., 2014. How do components of real cloud water affect aqueous pyruvate oxidation? Atmos. Res. 143, 95–106.

Boris, A.J., Lee, T., Park, T., Choi, J., Seo, S.J., Collett, J.L., 2016. Fog composition at Baengnyeong Island in the eastern Yellow Sea: detecting markers of aqueous atmospheric oxidations. Atmos. Chem. Phys. 16, 437–453.

Boyd, C.M., Sanchez, J., Xu, L., Eugene, A.J., Nah, T., Tuet, W.Y., Guzman, M.I., Ng, N.L., 2015. Secondary organic aerosol formation from the β-pinene+NO3 system: effect of humidity and peroxy radical fate. Atmos. Chem. Phys. 15, 7497–7522.

Brinkmann, T., Hörsch, P., Sartorius, D., Frimmel, F.H., 2003. Photoformation of low-molecular-weight organic acids from brown water dissolved organic matter. Environ. Sci. Technol. 37, 4190–8.

Cai, Y., Cole, R.B., 2002. Stabilization of anionic adducts in negative ion electrospray mass spectrometry. Anal. Chem. 74, 985–991.

Chameides, W.L., 1986. Possible role of NO3 in the nighttime chemistry of a cloud. J. Geophys. Res. 91, 5331–5337.

Chang, J.L., Thompson, J.E., 2010. Characterization of colored products formed during irradiation of aqueous solutions containing H2O2 and phenolic compounds. Atmos. Environ. 44, 541–551.

Chen, Q., Heald, C.L., Jimenez, J.L., Canagaratna, M.R., He, L.-Y., Huang, X.-F., Campuzano-Jost, P., Palm, B.B., Poulain, L., Kuwata, M., Martin, S.T., Abbatt, J.P.D., Lee, A.K.Y., Liggio, J., 2015. Elemental Composition of Organic Aerosol: The Gap Between Ambient and Laboratory Measurements. Geophys. Res. Lett. 42, 1–8.

Chiron, S., Comoretto, L., Rinaldi, E., Maurino, V., Minero, C., Vione, D., 2009. Pesticide by-products in the Rhône delta (Southern France). The case of 4-chloro-2-methylphenol and of its nitroderivative. Chemosphere 74, 599–604.

Cooper, W.J., Cramer, C.J., Martin, N.H., Mezyk, S.P., Shea, K.E.O., 2009. Free Radical Mechanisms for the Treatment of Methyl tert -Butyl Ether (MTBE) via Advanced Oxidation/Reductive Processes in Aqueous Solutions. Chem. Rev. 1302–1345.

Daumit, K.E., Carrasquillo, A.J., Hunter, J.F., Kroll, J.H., 2014. Laboratory studies of the aqueous-phase oxidation of polyols: submicron particles vs. bulk aqueous solution. Atmos. Chem. Phys. 14, 10773–10784.

Demoz, B.B., Collett, J.L., Daube, B.C., 1996. On the Caltech Active Strand Cloudwater Collectors. Atmos. Res. 41, 47–62.

Deno, N.S., Newman, S., 1950. Mechanism of Sulfation of Alcohols. J. Am. Chem. Soc. 72, 3852–3856.

Desyaterik, Y., Sun, Y., Shen, X., Lee, T., Wang, X., Wang, T., Collett, J.L., 2013. Speciation of "brown" carbon in cloud water impacted by agricultural biomass burning in eastern China. J. Geophys. Res. Atmos. 118, 7389–7399.

Doussin, J.-F., Monod, a., 2013. Structure–activity relationship for the estimation of OH-oxidation rate constants of carbonyl compounds in the aqueous phase. Atmos. Chem. Phys. 13, 11625–11641.

Ervens, B., Sorooshian, A., Lim, Y.B., Turpin, B.J., 2014. Key parameters controlling OH-initiated formation of secondary organic aerosol in the aqueous phase (asSOA). J. Geophys. Res. Atmos. 119, 3997–4016.

Ervens, B., Turpin, B., Weber, R., 2011. Secondary organic aerosol formation in cloud droplets and aqueous particles (aqSOA): A review of laboratory, field and model studies. Atmos. Chem. Phys. 11, 11069–11102.

Ervens, B., Wang, Y., Eagar, J., Leaitch, W.R., Macdonald, A.M., Valsaraj, K.T., Herckes, P., 2013. Dissolved organic carbon (DOC) and select aldehydes in cloud and fog water: the role of the aqueous phase in impacting trace gas budgets. Atmos. Chem. Phys. 13, 5117–5135.

Faust, B., Allen, J., 1992. Aqueous-phase photochemical sources of peroxyl radicals and singlet molecular oxygen in clouds and fog. J. Geophys. Res. 97, 12913–12926.

Faust, B.C., Allen, J.M., 1993. Aqueous-phase photochemical formation of hydroxyl radical in authentic cloudwaters and fogwaters. Environ. Sci. Technol. 27, 1221–1224.

Faust, B.C., Anastasio, C., Allen, J.M., Arakaki, T., 1993. Aqueous-phase photochemical formation of peroxides in authentic cloud and fog waters. Science 260, 73–75.

Fu, T.-M., Jacob, D.J., Wittrock, F., Burrows, J.P., Vrekoussis, M., Henze, D.K., 2008. Global budgets of atmospheric glyoxal and methylglyoxal, and implications for formation of secondary organic aerosols. J. Geophys. Res. 113, D15303.

Gelencsér, A., Varga, Z., 2005. Evaluation of the atmospheric significance of multiphase reactions in atmospheric secondary organic aerosol formation. Atmos. Chem. Phys. 5, 2823–2831.

Glover, C.M., Mezyk, S.P., Linden, K.G., Rosario-Ortiz, F.L., 2014. Photochemical degradation of Corexit components in ocean water. Chemosphere 111, 596–602.

Glover, C.M., Rosario-Ortiz, F.L., 2013. Impact of halides on the photoproduction of reactive intermediates from organic matter. Environ. Sci. Technol. 47, 13949–13956.

Goldstein, A., Galbally, I., 2007. Known and unexplored Organic constituents in the Earth's atmosphere. Environ. Sci. Technol. 41, 1514–1521.

Hallar, A.G., Lowenthal, D.H., Clegg, S.L., Samburova, V., Taylor, N., Mazzoleni, L.R., Zielinska, B.K., Kristensen, T.B., Chirokova, G., McCubbin, I.B., Dodson, C., Collins, D., 2013. Chemical and hygroscopic properties of aerosol organics at Storm Peak Laboratory. J. Geophys. Res. Atmos. 118, 4767–4779.

Harrison, M., Barra, S., Borghesi, D., Vione, D., Arsene, C., Iulianolariu, R., 2005. Nitrated phenols in the atmosphere: a review. Atmos. Environ. 39, 231–248.

Haynes, W.M., Bruno, T.J., Lide, D.R. (Eds.), 2013. Handbook of Chemistry and Physics, 94th ed. CRC Press, Cleveland, OH.

Iinuma, Y., Müller, C., Böge, O., Gnauk, T., Herrmann, H., 2007. The formation of organic sulfate esters in the limonene ozonolysis secondary organic aerosol (SOA) under acidic conditions. Atmos. Environ. 41, 5571–5583.

Johnson, B.J., Betterton, E.A., Craig, D., 1996. Henry's law coefficient of formic and acetic acids. J. Atmos. Chem. 24, 113–119.

Kavitha, V., Palanivelu, K., 2005. Degradation of nitrophenols by Fenton and photo-Fenton processes. J. Photochem. Photobiol. A Chem. 170, 83–95.

Kawamura, K., Kaplan, I., 1987. Motor exhaust emissions as a primary source for dicarboxylic acids in Los Angeles ambient air. Environ. Sci. Technol. 21, 105–110.

Kawamura, K., Kasukabe, H., Barrie, L.A., 1996. Source and reaction pathways of dicarboxylic acids, ketoacids and dicarbonyls in arctic aerosols: One year of observations. Atmos. Environ. 30, 1709–1722.

Kawamura, K., Okuzawa, K., Aggarwal, S.G., Irie, H., Kanaya, Y., Wang, Z., 2013. Determination of gaseous and particulate carbonyls (glycolaldehyde, hydroxyacetone, glyoxal, methylglyoxal, nonanal and decanal) in the atmosphere at Mt. Tai. Atmos. Chem. Phys. 13, 5369–5380.

Kebarle, P., Verkerk, U.H., 2009. Electrospray: From ions in solution to ions in the gas phase, what we know now. Mass Spectrom. Rev. 28, 898–917.

Keen, O.S., McKay, G., Mezyk, S.P., Linden, K.G., Rosario-Ortiz, F.L., 2014. Identifying the factors that influence the reactivity of effluent organic matter with hydroxyl radicals. Water Res. 50, 408–19.

Kirkland, J., Lim, Y., Tan, Y., Altieri, K., Turpin, B., 2013. Glyoxal secondary organic aerosol chemistry: effects of dilute nitrate and ammonium and support for organic radical-radical oligomer formation. Environ. Chem. 10, 158–166.

Kitanovski, Z., Čusak, A., Grgić, I., Claeys, M., 2014. Chemical characterization of the main secondary organic aerosol (SOA) products formed through aqueous-phase photonitration of guaiacol. Atmos. Meas. Tech. 7, 2457–2470.

Lee, A.K.Y., Herckes, P., Leaitch, R.W., Macdonald, A.M., Abbatt, J.P.D., 2011. Aqueous OH oxidation of ambient organic aerosol and cloud water organics: Formation of highly oxidized products. Geophys. Res. Lett. 38, 1–5.

Lee, T., Sullivan, A.P., Mack, L., Jimenez, J.L., Kreidenweis, S.M., Onasch, T.B., Worsnop, D.R., Malm, W., Wold, C.E., Hao, W.M., Collett, J.L., 2010. Chemical Smoke Marker Emissions During Flaming and Smoldering Phases of Laboratory Open Burning of Wildland Fuels. Aerosol Sci. Technol. 44.

Legrini, O., Oliveros, E., Braun, A.M., 1993. Photochemical Processes for Water Treatment. Chem. Rev. 93, 671–698.

Liggio, J., Li, S., McLaren, R., 2005. Heterogeneous Reactions of Glyoxal on Particulate Matter: Identification of Acetals and Sulfate Esters. Environ. Sci. Technol. 39, 1532–1541.

Lim, Y.B., Tan, Y., Perri, M.J., Seitzinger, S.P., Turpin, B.J., 2010. Aqueous chemistry and its role in secondary organic aerosol (SOA) formation. Atmos. Chem. Phys. 10, 10521–10539.

Lim, Y.B., Tan, Y., Turpin, B.J., 2013. Chemical insights, explicit chemistry, and yields of secondary organic aerosol from OH radical oxidation of methylglyoxal and glyoxal in the aqueous phase. Atmos. Chem. Phys. 13, 8651–8667.

Limbeck, A., Kraxner, Y., Puxbaum, H., 2005. Gas to particle distribution of low molecular weight dicarboxylic acids at two different sites in central Europe (Austria). J. Aerosol Sci. 36, 991–1005.

Lipczynska-Kochany, E., 1992. Degradation of Nitrobenzene and Nitrophenols by Means of Advanced Oxidation Processes in a Homogeneous Phase: Photolysis in the Presence of Hydrogen Peroxide versus the Fenton Reaction. Chemosphere 24, 1369–1380.

Lüttke, J., Scheer, V., Levsen, K., Wünsch, G., Cape, J.N., Hargreaves, K.J., Storeton-West, R.L., Acker, K., Wieprecht, W., Jones, B., 1997. Occurrence and formation of nitrated phenols in and out of cloud. Atmos. Environ. 31, 2637–2648.

Mavronikola, C., Demetriou, M., Hapeshi, E., Partassides, D., Michael, C., Mantzavinos, D., Kassinos, D., 2009. Mineralisation of the antibiotic amoxicillin in pure and surface waters by artificial UVA- and sunlight-induced Fenton oxidation. J. Chem. Technol. Biotechnol. 84, 1211–1217.

McNeill, V.F., 2015. Aqueous organic chemistry in the atmosphere: Sources and chemical processing of organic aerosols. Environ. Sci. Technol. 49, 1237–1244.

McNeill, V.F., Woo, J.L., Kim, D.D., Schwier, A.N., Wannell, N.J., Sumner, A.J., Barakat, J.M., 2012. Aqueous-phase secondary organic aerosol and organosulfate formation in atmospheric aerosols: A modeling study. Environ. Sci. Technol. 46, 8075–8081.

Monod, A., Chebbi, A., Durand-Jolibois, R., Carlier, P., 2000. Oxidation of methanol by hydroxyl radicals in aqueous solution under simulated cloud droplet conditions. Atmos. Environ. 34, 5283–5294.

Müller, L., Reinnig, M.-C., Naumann, K.H., Saathoff, H., Mentel, T.F., Donahue, N.M., Hoffmann, T., 2012. Formation of 3-methyl-1,2,3-butanetricarboxylic acid via gas phase oxidation of pinonic acid – a mass spectrometric study of SOA aging. Atmos. Chem. Phys. 12, 1483–1496.

Natangelo, M., Mangiapan, S., Bagnati, R., Benfenati, E., Fanelli, R., 1999. Increased concentrations of nitrophenols in leaves from a damaged forestal site. Chemosphere 38, 1495–1503.

Nguyen, T.B., Roach, P.J., Laskin, J., Laskin, a., Nizkorodov, S. a., 2011. Effect of humidity on the composition of isoprene photooxidation secondary organic aerosol. Atmos. Chem. Phys. 11, 6931–6944.

Opsahl, S., Benner, R., 1998. Photochemical reactivity of dissolved lignin in river and ocean waters. Limnol. Oceanogr. 43, 1297–1304.

Ortiz-Montalvo, D.L., Häkkinen, S. a K., Schwier, A.N., Lim, Y.B., McNeill, V.F., Turpin, B.J., 2014. Ammonium addition (and aerosol pH) has a dramatic impact on the volatility and yield of glyoxal secondary organic aerosol. Environ. Sci. Technol. 48, 255–62.

Oturan, M.A., Peiroten, J., Chartrin, P., Acher, A.J., 2000. Complete Destruction of p-Nitrophenol in Aqueous Medium by Electro-Fenton Method. Environ. Sci. Technol. 34, 3474–3479.

Perri, M.J., Lim, Y.B., Seitzinger, S.P., Turpin, B.J., 2010. Organosulfates from glycolaldehyde in aqueous aerosols and clouds: Laboratory studies. Atmos. Environ. 44, 2658–2664.

Raja, S., Raghunathan, R., Kommalapati, R.R., Shen, X., Collett, J.L., Valsaraj, K.T., 2009. Organic composition of fogwater in the Texas–Louisiana gulf coast corridor. Atmos. Environ. 43, 4214–4222.

Renard, P., Siekmann, F., Gandolfo, A., Socorro, J., Salque, G., Ravier, S., Quivet, E., Clément, J.-L., Traikia, M., Delort, A.M., Voisin, D., Vuitton, V., Thissen, R., Monod, A., 2013. Radical mechanisms of methyl vinyl ketone oligomerization through aqueous phase OH-oxidation: on the paradoxical role of dissolved molecular oxygen. Atmos. Chem. Phys. 13, 6473–6491.

Renard, P., Siekmann, F., Salque, G., Smaani, A., Demelas, C., Coulomb, B., Vassalo, L., Ravier, S., Temime-Roussel, B., Voisin, D., Monod, A., 2014. Aqueous phase oligomerization of methyl vinyl ketone through photooxidation – Part 1: Aging processes of oligomers. Atmos. Chem. Phys. Discuss. 14, 15283–15322.

Rudich, Y., Talukdar, R.K., Ravishankara, A.R., Fox, R.W., 1996. Reactive uptake of NO3 on pure water and ionic solutions. J. Geophys. Res. Atmos. 101, 21023–21031.

Rue, E.L., Bruland, K.W., 1995. Complexation of iron(III) by natural organic ligands in the Central North Pacific as determined by a new competitive ligand equilibration/adsorptive cathodic stripping voltammetric method. Mar. Chem. 50, 117–138.

Safarzadeh-Amiri, A., Bolton, J.R., Cater, S.R., 1997. Ferrioxalate-mediated photodegradation of organic pollutants in contaminated water. Water Res. 31, 787–798.

Sanches, S., Barreto Crespo, M.T., Pereira, V.J., 2010. Drinking water treatment of priority pesticides using low pressure UV photolysis and advanced oxidation processes. Water Res. 44, 1809–1818.

Schindelka, J., Iinuma, Y., Hoffmann, D., Herrmann, H., 2013. Sulfate radical-initiated formation of isoprene-derived organosulfates in atmospheric aerosols. Faraday Discuss. 165, 237–259.

Schurman, M.I., 2014. Characteristics, Sources, and Formation of Organic Aerosols in the Central Rocky Mountains.

Seinfeld, J.H., Pandis, S.N., 2006. Atmospheric Chemistry and Physics: From Air Pollution to Climate Change. John Wiley & Sons, Inc., Hoboken, New Jersey.

Shen, X., Lee, T., Guo, J., Wang, X., Li, P., Xu, P., Wang, Y., Ren, Y., Wang, W., Wang, T., Li, Y., Carn, S.A., Collett, J.L., 2012. Aqueous phase sulfate production in clouds in eastern China. Atmos. Environ. 62, 502–511.

Si, L., Ariya, P.A., 2008. Reduction of oxidized mercury species by dicarboxylic acids (C2-C4): kinetic and product studies. Environ. Sci. Technol. 42, 5150–5.

Solomons, T.W.G., Fryhle, C.B., 2004. Organic Chemistry, 8th ed. John Wiley & Soons, Hoboken, New Jersey.

Sorooshian, A., Lu, M.-L., Brechtel, F.J., Jonsson, H., Feingold, G., Flagan, R.C., Seinfeld, J.H., 2007. On the source of organic acid aerosol layers above clouds. Environ. Sci. Technol. 41, 4647–54.

Sorooshian, A., Varutbangkul, V., 2006. Oxalic acid in clear and cloudy atmospheres: Analysis of data from International Consortium for Atmospheric Research on Transport and Transformation 2004. J. Geophys. Res. 111, 1–10.

Sorooshian, A., Wang, Z., Coggon, M.M., Jonsson, H.H., Ervens, B., 2013. Observations of Sharp Oxalate Reductions in Stratocumulus Clouds at Variable Altitudes: Organic Acid and Metal Measurements During the 2011 E-PEACE Campaign. Environ. Sci. Technol. 47, 7747–7756.

Stemmler, K., Gunten, U. Von, 2000. OH radical-initiated oxidation of organic compounds in atmospheric water phases: part 1. Reactions of peroxyl radicals derived from 2-butoxyethanol in water. Atmos. Environ. 34, 4241–4252.

Sun, Y.L., Zhang, Q., Anastasio, C., Sun, J., 2010. Insights into secondary organic aerosol formed via aqueous-phase reactions of phenolic compounds based on high resolution mass spectrometry. Atmos. Chem. Phys. 10, 4809–4822.

Surratt, J.D., Gómez-González, Y., Chan, A.W.H., Vermeylen, R., Shahgholi, M., Kleindienst, T.E., Edney, E.O., Offenberg, J.H., Lewandowski, M., Jaoui, M., Maenhaut, W., Claeys, M., Flagan, R.C., Seinfeld, J.H., 2008. Organosulfate formation in biogenic secondary organic aerosol. J. Phys. Chem. A 112, 8345–78.

Talbot, R.W., Beecher, K.M., Harriss, R.C., Cofer, W.R.I., 1988. Atmospheric geochemistry of formic and acetic acids at a mid-latitude temperate site. J. Geophys. Res. 93, 1638–1652.

Tan, Y., Carlton, A.G., Seitzinger, S.P., Turpin, B.J., 2010. SOA from methylglyoxal in clouds and wet aerosols: Measurement and prediction of key products. Atmos. Environ. 44, 5218–5226.

Tan, Y., Lim, Y.B., Altieri, K.E., Seitzinger, S.P., Turpin, B.J., 2012. Mechanisms leading to oligomers and SOA through aqueous photooxidation: insights from OH radical oxidation of acetic acid and methylglyoxal. Atmos. Chem. Phys. 12, 801–813.

Tan, Y., Perri, M.J., Seitzinger, S.P., Turpin, B.J., 2009. Effects of Precursor Concentration and Acidic Sulfate in Aqueous Glyoxal-OH Radical Oxidation and Implications for Secondary Organic Aerosol. Environ. Sci. Technol. 43, 8105–8112.

Tang, K., Page, J.S., Smith, R.D., 2004. Charge competition and the linear dynamic range of detection in electrospray ionization mass spectrometry. J. Am. Soc. Mass Spectrom. 15, 1416–23.

Trapido, M., Kallas, J., 2000. Advanced Oxidation Processes for the Degradation and Detoxification of 4-Nitrophenol. Environ. Technol. 21, 799–808.

Trovó, A.G., Melo, S.A.S., Nogueira, R.F.P., 2008. Photodegradation of the pharmaceuticals amoxicillin, bezafibrate and paracetamol by the photo-Fenton process—Application to sewage treatment plant effluent. J. Photochem. Photobiol. A Chem. 198, 215–220.

Tsigaridis, K., Daskalakis, N., Kanakidou, M., Adams, P.J., Artaxo, P., Bahadur, R., BalkanskII, Y., Bauer, S.E., Bellouin, N., Benedetti, A., Bergman, T., Berntsen, T.K., Beukes, J.P., Bian, H., Carslaw, K.S., Chin, M., Curci, G., Diehl, T., Easter, R.C., Ghan, S.J., Gong, S.L., Hodzic, A., Hoyle, C.R., Iversen, T., Jathar, S., Jimenez, J.L., Kaiser, J.W., Kirkevåg, A., Koch, D., Kokkola, H., Lee, Y.H., Lin, G., Liu, X., Luo, G., Ma, X., Mann, G.W., Mihalopoulos, N., Morcrette, J.-J., Müller, J.-F., Myhre, G., Myriokefalitakis, S., Ng, N.L., O'Donnell, D., Penner, J.E., Pozzoli, L., Pringle, K.J., Russell, L.M., Schulz, M., Sciare, J., Se, Ø., Zhang, X., 2014. The AeroCom evaluation and intercomparison of organic aerosol in global models. Atmos. Chem. Phys. 14, 10845–10895.

van Pinxteren, D., Neusüß, C., Herrmann, H., 2014. On the abundance and source contributions of dicarboxylic acids in size-resolved aerosol particles at continental sites in central Europe. Atmos. Chem. Phys. 14, 3913–3928.

Vione, D., Maurino, V., Minero, C., Borghesi, D., Lucchiari, M., Pelizzetti, E., 2003. New Process in the Environmental Chemistry of Nitrite. 2. The Role of Hydrogen Peroxide. Environ. Sci. Technol. 37, 4635–4641.

Vione, D., Maurino, V., Minero, C., Pelizzetti, E., 2005. Aqueous atmospheric chemistry: Formation of 2,4-dinitrophenol upon nitration of 2-nitrophenol and 4-nitrophenol in solution. Environ. Sci. Technol. 39, 7921–7931.

Von Sonntag, C., Dowideit, P., Fang, X., Mertens, R., Pan, X., Schuchmann, M.N., Schuchmann, H.P., 1997. The fate of peroxyl radicals in aqueous solution. Water Sci. Technol. 35, 9–15.

Warneck, P., 2003. In-cloud chemistry opens pathway to the formation of oxalic acid in the marine atmosphere. Atmos. Environ. 37, 2423–2427.

Weller, C., Horn, S., Herrmann, H., 2013. Photolysis of Fe (III) carboxylato complexes: Fe (II) quantum yields and reaction mechanisms. J. Photochem. Photobiol. A Chem. 268, 24–36.

Weller, C., Tilgner, A., Bräuer, P., Herrmann, H., 2014a. Modeling the impact of iron-carboxylate photochemistry on radical budget and carboxylate degradation in cloud droplets and particles. Environ. Sci. Technol. 48, 5652–9.

Weller, C., Tilgner, A., Bräuer, P., Herrmann, H., 2014b. Modelling the impact of iron-carboxylate photochemistry on radical budget and carboxylate degradation in cloud droplets and particles. Environ. Sci. Technol. 140328152101005.

Zhang, H., Worton, D.R., Lewandowski, M., Ortega, J., Rubitschun, C.L., Park, J., Kristensen, K., Campuzano-Jost, P., Day, D.A., Jimenez, J.L., Jaoui, M., Offenberg, J.H., Kleindienst, T.E., Gilman, J., Kuster, W.C., Gouw, J. De, Park, C., Schade, G.W., Frossard, A.A., Russell, L., Kaser, L., Jud, W., Hansel, A., Cappellin, L., Karl, T., Glasius, M., Guenther, A., Goldstein, A.H., Seinfeld, J.H., Gold, A., Kamens, R.M., Surratt, J.D., 2012.

Organosulfates as Tracers for Secondary Organic Aerosol (SOA) Formation from 2-Methyl-3-Buten-2-ol (MBO) in the Atmosphere. Environ. Sci. Technol. 46, 9437–9446.

Zhang, W., Xiao, X., An, T., Song, Z., 2003. Kinetics, degradation pathway and reaction mechanism of advanced oxidation of 4-nitrophenol in water by a UV/H2O2 process. J. Chem. Technol. Biotechnol. 794, 788–794.

Zhang, Y., Wang, Y., Gray, B.A., Gu, D., Mauldin, L., Cantrell, C., Bandy, A., 2014. Surface and free tropospheric sources of methanesulfonic acid (MSA) over the tropical Pacific Ocean. Geophys. Res. Lett. n/a–n/a.

Zhang, Y.-L., Kawamura, K., Cao, F., Lee, M., 2016. Stable carbon isotopic compositions of low-molecular-weight dicarboxylic acids, oxocarboxylic acids, α-dicarbonyls, and fatty acids: Implications for atmospheric processing of organic aerosols. J. Geophys. Res. Atmos. 121, 3707–3717.

Zuo, Y., 2003. Light-induced formation of hydroxyl radicals in fog waters determined by an authentic fog constituent, hydroxymethanesulfonate. Chemosphere 51, 175–179.

Zuo, Y., Hoigné, J., 1992. Formation of hydrogen peroxide and depletion of oxalic acid in atmospheric water by photolysis of iron (III)-oxalato complexes. Environ. Sci. Technol. 26, 1014–1022.

Zuo, Y., Hoigné, J., 1993. Evidence for Photochemical Formation of H2O2 and Oxidation of SO2 in Authentic Fog Water. Science 260, 71–73.

Zuo, Y., Hoigné, J., 1994. Photochemical decomposition of oxalic, glyoxalic and pyruvic acid catalysed by iron in atmospheric waters. Atmos. Environ. 2, 1231–1239.

Zuo, Y., Jones, R.D., 1996. Photochemical production of carbon monoxide in authentic rainwater. Geophys. Res. Lett. 23, 2769.

6. LABORATORY SIMULATED CLOUD PROCESSING OF BIOMASS BURNING EMISSIONS

Biomass burning (BB) activities are ubiquitous: in agricultural regions where fields are burned, in residential areas where wood is burned for heat and cooking, and in the vicinity of forest fires. Little work has been done, however, to show the effect of liquid water in the atmosphere on BB emissions. Oxidation reactions within droplets of fog, cloud, and wet aerosol are influential in atmospheric composition: low volatility organic products can form, leaving behind aqueous secondary organic aerosol (aqSOA) mass. Trace atmospheric constituents can also be removed by chemical oxidation. This study examines the aqueous oxidation reactions of real BB emissions samples, and, in particular, the precursors and products of those reactions. Gas and particle phase emissions were collected from a small biomass burn (400 g dried Ponderosa Pine) into aqueous solution at approximately 10-fold the equivalent atmospheric liquid water content in clouds using a mist chamber. The BB emissions in the mist chamber extract were oxidized with hydroxyl radical ($^{\bullet}OH$) in triplicate. Chemical analyses of the reaction solution were performed using real-time negative mode electrospray ionization high-resolution time-of-flight mass spectrometry ((-)-ESI-HR-ToF-MS), liquid chromatography (LC) with (-)-ESI-HR-ToF-MS detection for $>C_3$ (more than three C atoms) polar organic species, and ion chromatography (IC) with conductivity detection for $<C_6$ carboxylic acids. The most reactive precursors observed within the samples were hydroquinone and a series of C_4-C_9 multifunctional carboxylic acids. Organic nitrogen species, including 4-methyl-5-nitrocatechol (4M5NC) and 4-nitrocatechol (4NC), were also important precursors, and were quantified during the three replicate oxidations (initially, 4NC: 0.018 ± 0.013 μM, 4M5NC: 0.19 ± 0.07 μM). Degradation of 4NC and 4M5NC in the BB emissions occurred at -0.5% min^{-1} (-0.08 nM min^{-1}) and -0.6% min^{-1} (-1.2 nM min^{-1}), respectively. Products of oxidation included primarily $\geq C_4$ carboxylic acids with similar characteristics to precursors, as well as low molecular mass carboxylic acids (as much as 400 nM min^{-1} of each acid was produced). In particular, the formation of oxalate, which is frequently cited as an abundant product of real aqueous atmospheric organic processing (AAOP), was formed at a mean rate of 40 nM min^{-1}. The net production of semi-volatile carboxylic acids during the oxidations was ~6% of the initial total organic carbon concentration, suggesting that aqSOA is produced as a result of in-cloud oxidations of BB emissions. Additional formation of low-volatility organic material would likely be observed under conditions representative of BB emissions diluted during transport and considering species in addition to small carboxylic acids.

6.1 Introduction

Biomass burning activities, including agricultural burning, biofuel combustion, and forest fires, produce a substantial portion of atmospheric organic aerosol mass globally (15-90%; Bond, 2004; Crutzen and Andreae, 1990; Heald et al., 2006) and in highly populated urban areas (30-70%; Schauer and Cass, 2000). Smoke from forest fires can cause exceedance of the fine aerosol National Ambient Air Quality Standards (NAAQS) even far downwind of a fire: the 2011 Wallow Fire in Arizona, for example, caused exceedance of the NAAQS along the Front Range of Colorado, approximately 500 miles from the fire (Val Martin et al., 2013). An increase is predicted of 54% in annual mean burned area and associated increase of ~0.5 μg m^{-3} in summertime organic carbon mass by 2055 in the western U.S., causing the study of biomass burning (BB) as an organic emissions sources to be especially important (Spracklen et al., 2009).

Transported smoke may interact with light, clouds, and other chemicals during transit, causing transformations within the plume and altering the health, visibility, and climate effects of the smoke. Dry chemical photo-oxidation of BB emissions in the lab decreases the volatility of the organic components, increasing the mass of organic aerosol by factors of 1.5-2.8 (Grieshop et al., 2009b; Hennigan et al., 2011). However, current models under-predict the organic aerosol mass formed in real aged BB emissions (Grieshop et al., 2009a). Some of this additional low volatility material may be produced by the aging of organic species within water droplets in the atmosphere (the aerosol produced is called aqueous secondary organic aerosol, abbreviated as aqSOA). A large fraction of the global atmospheric aerosol mass could be aqSOA: oxalic acid (a suggested chemical tracer of aqSOA, Warneck, 2003) alone is estimated to account for ~5-9% of all water soluble organic carbon (Myriokefalitakis et al., 2011), and the total aqSOA formed via in-cloud reactions may account for a similar mass as anthropogenic secondary organic aerosol globally (13-47 Tg yr^{-1} in-cloud: Lin et al., 2014; 3-25 Tg yr^{-1} anthropogenic: Volkamer et al., 2006). Of the 270-970 Tg yr^{-1} estimated global organic aerosol emissions, up to 17% may thus be contributed by aqueous reactions (assuming an organic mass/organic carbon mass of 1.8 and the annual organic carbon emission estimate from Goldstein and Galbally, 2007). The species that are suggested to contribute most substantially to aqSOA mass include carboxylic acids and oligomers formed by condensation and radical reactions (Ervens et al., 2014; Loeffler et al., 2006; Ortiz-Montalvo et al., 2012). The formation of aqSOA could occur within pyrocumulus or downwind clouds interacting with BB emissions (Slade et al., 2015; Zhao et al., 2014). Field studies have in fact demonstrated that aqSOA formation may be a dominant organic aerosol formation process in forest fire plumes. For example,

measured oxalic acid was above background concentrations in air impacted by both aqueous oxidation and BB emissions (Yu et al., 2005). Similarly, aerosol collected at Yosemite National Park while fires were burning in Oregon contained ~2% by mass of oxalate and an estimated 78% by mass of secondary organic aerosol, while local fire emissions contained only 21% by mass (Engling et al., 2006).

The aqueous processing of BB emissions has been studied in the lab via simplified reactions of chemical species found in smoke (Anastasio et al., 1997; Chang and Thompson, 2010; Santos et al., 2006; Smith et al., 2014; Sun et al., 2010; Zhao et al., 2014), mainly demonstrating a change in the absorptive properties of the species due to oxidation. Most precursors oxidized in these simulations were phenols, which are abundant in organic smoke material (Andreae and Merlet, 2001; Hays et al., 2002). Yu et al. (2014) used a combination of powerful analytical techniques to demonstrate that phenol, guiacol (2-methoxyphenol), and syringol (2,6-dimethoxyphenol) resulted in the formation of multifunctional oxygenated organic species including carboxylic acids and oligomers. While carboxylic acids and their oligomers originate from $^{\bullet}$OH attack, phenolic oligomers have been suggested as products of reaction with triplet excited state aromatic carbonyls (Yu et al., 2014). Low molecular mass (LMM) carboxylic acids and aldehydes are also aqueous oxidation products of other smoke constituents, including abietic acid, levoglucosan, and nitroguaiacol (Slade and Knopf, 2013). Lab-generated aqSOA from phenols is, in addition, chemically similar to ambient wood combustion aerosol transported through foggy conditions (Sun et al., 2010). Organic aerosol produced by in-cloud reactions of BB emissions is thus likely to be prominent in global aerosol mass, and must be further studied to improve current models of climate and air quality.

In the present study, we will directly explore the aqueous chemistry of BB emissions by collecting gaseous organic compounds from small biomass fires into water via mist chambers, initiating oxidation within the aqueous phase emissions, and characterizing the oxidation products. The aims of the current study include: (1) characterizing the chemical changes of water soluble organic compounds in real BB samples due to simulated in-cloud oxidation; and (2) using the quantified oxidation products to estimate the mass of aqSOA formed via in-cloud oxidation of forest fire emissions. The precursors and products of aqSOA determined in this study will be contrasted with those identified in previous work on the dry aging of BB emissions (Grieshop et al., 2009a, 2009b; Hennigan et al., 2012).

6.2 Material and Methods

6.2.1 Methods: Simulated Wildfire Burns at the Powerhouse Building

A series of small biomass burns were conducted using Ponderosa Pine as fuel, which is common to the Western US (Sullivan et al., 2008). A burn enclosure ("Thing One") at the Engineering Department Powerhouse Building of Colorado State University (CSU) in Fort Collins, CO was used. Gaseous emissions from the fires were collected into water using mist chambers (Hennigan et al., 2008). Gas and particle real-time measurements, as well as particle phase emissions collection was also accomplished using various instruments, as described below. Images of the collection setup are presented in Appendix 6. Ponderosa Pine (*Pinus ponderosa*) limbs, needles, cones, pollen packets, and litter were collected as fuel for the simulated fires with the cooperation of the US Forest Service from the Poudre Canyon in northern Colorado and dried at 96°C for 5 hrs in a kiln two days prior to the burn experiments. The dried fuel was massed and placed inside an aluminum pan, atop a single layer of cinderblocks. A small propane torch was used to light the fire. Several burns were carried out; the emissions used in the present work were collected during a burn that consisted of multiple additions of fuel and re-ignition steps throughout the sample collection. The relighting process allowed the collection of both flaming and smoldering phases, and allowed 400 g fuel to be used (final mass of fuel remaining was 77 g, so that 323 g fuel was combusted). The burn persisted for 35 minutes. Relative humidity (RH) and temperature were monitored within the hood during the burns.

6.2.2 Methods: Emissions Sample Collection

Two isokinetic aerosol sampling ports installed in the ducting of the "Thing One" hood were used for sampling of emissions to: (1) the mist chamber; and (2) a series of gas and particle emissions measurements. Emissions were transported to sampling devices from the hood duct using 3/8" Teflon tubing and SwageLok, stainless steel, and Teflon fittings. The real-time gas and particle phase measurements were diluted by ~5% using a 30 L stainless steel dilution chamber ("Hank the Tank") supplied with 13 L min^{-1} clean air from a Teledyne API 751H High Performance Zero Air Generator (controlled via an MKS Type M100B Mass-Flo Controller and a Labjack U12 Series digital input/output device). An Ionicon Analytik GmbH PTR-MS was used to monitor emissions of gas-phase nitrophenols and other species during the burns, but the results will be discussed only in brief to support the current work. Gaseous carbon monoxide (CO, Teledyne 300EU), carbon dioxide (CO_2, LI-COR LI-840A), and water vapor (H_2O_{vapor}, LI-COR LI-840A) were measured in real-time from the contents of the dilution chamber through two 37 mm quartz fiber filters. A TSI butanol condensation particle counter (CPC) also collected particles

from the contents of the mixing chamber. Particle phase emissions were also collected separately onto prebaked quartz fiber filters (37 mm), using a Savillex PFA DOC 47 two-stage filter holder assembly (front and back filters were collected), and then extracted into water (see Appendix 6 for additional information). Flow rates to the CPC, mist chamber, and filter pack were provided by diaphragm pumps and controlled using critical orifices and Mass-Flo Controllers with Labjacks: 8.83 L min^{-1} to the filter pack, 1.3 L min^{-1} to the CO monitor, 0.37 L min^{-1} to the CO_2/H_2O_{vapor} monitor, 1.0 L min^{-1} to the CPC, and 0.5 L min^{-1} to the PTR-MS. The Zero Air generated provided a clean air flow of 0.46 L min^{-1} to the dilution chamber, the flow into the chamber was 9.87 L min^{-1}, and finally, an exhaust line was connected without flow control from the dilution chamber to the room exhaust. Diaphragm pumps were outfitted with HEPA filters so that emissions from the pumps would not interfere with measurements. All flow rates were measured from the experimental setup using pump-action Gillibrators.

The mist chamber was pre-cleaned using 0.5 M HCl solution and deionized water. Just before the emissions were collected, the mist chamber was filled with 25 mL deionized water, which was transferred to and from the mist chamber using a peristaltic pump outfitted with PEEK and Tygon tubing. An aerosol particle filter pack containing a Pall Zeflour filter was placed in line (downstream) with the mist chamber, before the diaphragm pump to ensure that no water reached the pump. Filters were replaced frequently, indicating that some sample may have been lost due to the high flow rate of the air sampled through the mist chamber. The diaphragm air pump (with no critical orifice) provided 29.5 L min^{-1} air flow through the mist chamber, and was started when fuels caught fire. When a burn was complete, the air flow was stopped through the mist chamber. Volatile organic compounds (VOCs) were collected by the mist chamber; only tiny particles (<40 nm) were collected efficiently (50%; see Appendix 6). After collection, mist chamber samples were stored on ice in a cooler for the remainder of the one-day burn study, then frozen in Thermo Scientific 30 mL HDPE amber bottles until analysis (~2 months) and oxidation (~6 months).

6.2.3 Methods: Aqueous Photoreactions

Oxidation reactions of the aqueous mist chamber samples were carried out in a custom-made glass 150 mL photoreactor (4.5 cm inner diameter) with a circulating water jacket (Boris et al., 2014) by introducing $^{\bullet}OH$ from photolysis of H_2O_2 (UV-C light supplied by a 9 Watt submerged AA Aquatics lamp, 254 nm peak wavelength). Liquid was drawn in real time from the reactor to monitor organic chemical trends, and discrete samples were withdrawn every 10-15 min during the reactions for quantitative analyses. A loosely fitting 3D-printed plastic lid covered the photoreactor, but holes for tubing and the UV lamp allowed some exchange with the air in the lab. The

solution was stirred during oxidation to provide a continuous source of O_2 to the solution. The photolysis of solution constituents was not considered: although species such as nitrophenols found in BB emissions can photolyze when exposed to the light source used in this study, the rates of reaction are substantially slower than those observed for reaction with $^{\bullet}$OH (Boris et al., 2014, Chapter 5). Measured concentrations of $^{\bullet}$OH produced in deionized water using the present light source and concentration of H_2O_2 were $5.4\pm0.5\times10^{-14}$ M (Boris et al., 2014); it is expected that steady-state concentrations of $^{\bullet}$OH within the BB emissions in this study were lower due to the presence of species that reacted with $^{\bullet}$OH. The steady state concentration of $^{\bullet}$OH was within the atmospherically relevant range: previous studies have estimated that atmospheric aqueous phase $^{\bullet}$OH concentrations are $\sim10^{-16}$ to 10^{-12} M (Anastasio and McGregor, 2001; Ervens et al., 2011; Tan et al., 2010).

6.2.4 Methods: Online Analyses

Oxidations and chemical analyses were carried out after filtration of the collected BB emissions extracts. Qualitative analysis of mass spectral data was carried out to identify and show trends in abundance of precursors, intermediates, and products during oxidation experiments. Each oxidation was monitored online using (-)-ESI-HR-ToF-MS (see Appendix 6 for settings of the mass spectrometer), resulting in time-resolved mass spectra (approx. two per second). These data were organized in two ways: (a) time profiles of specific m/z^- values during oxidation experiments; and (b) mass spectra extracted at specific reaction times (e.g., the mass spectrum of B4Ox at 30 min). Time profiles were extracted from each data file using Agilent MassHunter software and smoothed using a boxcar smoothing algorithm (Igor). Mass spectra were extracted from each oxidation experiment data file at 0, 15, 30, 60, and 120 min reaction time (where 0 min was defined as the time when H_2O_2 addition and/or UV light were initiated) by averaging over one min time intervals. A "precursor mass spectrum" was also compiled for each experiment by subtracting the 15, 30, 60, and 120 min reaction time mass spectra from the 0 min reaction time mass spectrum and overlaying the resulting subtracted spectra. "Product mass spectra" were likewise generated for each oxidation by subtracting the 0 min reaction time mass spectrum from each of the 15, 30, 60, and 120 min mass spectra individually. Results were averaged over the three replicate reactions. An abundance threshold of 500 a.u. was applied because formula generation is not accurate at low mass spectral abundances.

6.2.5 Methods: Offline Analyses

The chemical composition of the collected mist chamber emissions was quantified prior to the oxidation experiments, including total organic carbon (TOC) concentration (Sievers Model 800 Turbo TOC Analyzer),

specific carboxylic acid concentrations (ion chromatography, IC), specific organic component concentrations (HPLC-(-)-ESI-HR-ToF-MS), and inorganic ion concentrations (IC). Chemical analyses were also carried out at 15 min time intervals during the reaction as well characterizing changes in TOC, carboxylic acid concentrations, and $>C_4$ organic component concentrations. These variables have been used previously to characterize aqSOA product formation (Boris et al., 2014; Desyaterik et al., 2013; Liu et al., 2012; Perri et al., 2009). Discrete 1 mL samples were removed from the oxidation solution at 15 min intervals, added to 5 µL bovine catalase (15.9 units/mL), and stored at ~7°C until off-line analysis. Additional information about chemical analyses can be found in Appendix 6.

6.2.6 Methods: Calculations

Concentrations of gaseous species in mist chamber extracts (before and after oxidation) as measured using the various analytical techniques described above were extrapolated to express the quantities of the gaseous analytes in the air sampled (e.g., µg m^{-3} in air). All calculations reflect a total burn time of 35 min and oxidation time of 120 min. The calculations to convert the extract concentrations to these units were as follows:

$$\frac{\text{A (µmol)}}{\text{vol. extract,diluted (L)}} \times \frac{\text{A (µg)}}{\text{A (µmol)}} \times \frac{\text{vol. extract,diluted(L)}}{\text{vol. extract (L)}} \times \text{vol. extract (L)} = \text{A (µg) collected} \qquad \text{Equation 6-1}$$

$$\text{A (µg) collected} \times \frac{\text{sampling duration (min)}}{\text{vol. air sampled } (m^3)} \times \frac{1}{\text{sampling duration (min)}} = \text{Concentration A } (\mu g\, m^3) \qquad \text{Equation 6-2}$$

The molecular mass of each quantified species was used to convert between the moles and mass of the species. A dilution of the extracts was made prior to each analysis, which was accounted for (filters: 10-fold; mist chamber: 10-fold in oxidation/oxidized discrete samples, 100-fold in analyses before oxidation). The volume of the extract (0.020 L for filter extracts, 0.025 L for mist chamber extracts) was then used to isolate the total mass of the species. Concentrations in the emissions per volume of air were then found by dividing the mass by the total volume of air sampled (the product of the flow rate of the mist chamber, 0.0295 m^3 min^{-1}, and the duration of the mist chamber sample, 35 min). Details about blanks, precision of the analyses, and limits of detection (LOD) can be found in Appendix 6.

6.3 Results and Discussion

6.3.1 Initial Composition of Biomass Burning Emissions

A small Ponderosa Pine fire was carried out, lasting 35 minutes, with multiple flaming and smoldering phases as additional fuel was added and the fire was relit. This approach allowed both phases of burning to be captured within a single sample, which would be observed during a typical wildfire, and also for a substantial mass of emissions to

be collected. The organic concentrations in the present study were representative of what might be found in the cloud droplets just downwind of a forest fire: the total organic carbon (TOC) concentration measured in the mist chamber sample initially was 45.7 mg C L^{-1} (11.1 mg C m^{-3} within the air collected after 10-fold dilution prior to oxidation), intermediate between values observed in cloud water impacted by fresh BB emissions (Mount Tai cloud water, containing up to 100-200 mg C L^{-1}, Shen, 2011) and fog water impacted by transported BB emissions (Baengnyeong Island, Korea fog water, containing 17.0 mg C L^{-1} on average, Boris et al., 2016).

The collected mist chamber sample was acidic (pH 3.29), indicating that carboxylic acids present in the sample would be only partially deprotonated. The most abundant ions measured in the mist chamber extracts were NH_4^+, 0.196 ± 0.005 mg m^{-3}, Cl^-, 0.062 ± 0.004 mg m^{-3}, NO_3^-, 0.0406 ± 0.0019 mg m^{-3}, and SO_4^{2-}, 0.021 ± 0.006 mg m^{-3} (Table 6-1). These constituents likely originated from condensation of gases and some small particle (<40 nm d_p) collection. All ionic species quantifiable in the IC analysis were detected above LOD, with the exception of Mg^{2+}. Mist chamber concentrations of inorganic species were lower than those observed in filter samples because only a minimal number of particles, if any, were collected into the mist chamber (Table A6-2). Even the most abundant inorganic anions did not balance the cation charge (mist chamber extract +/- balance 1.28), suggesting that organic ions influenced in the charge balance of the BB emissions.

Table 6-1. Concentrations and statistics of inorganic species and TOC from mist chamber extract solution before oxidation (at *t*=0 min). The percent of the TOC contributed by quantified carboxylic acids is also tabulated, with the confidence limit calculated from replicate analyses of the carboxylic acid concentrations. Reported values, including pH, are from a diluted extract (10-fold from the mist chamber extract).

Species	Concentration (Mist Chamber)	Confidence Interval (95%)	LOD	Unit
pH	3.29	--	--	--
NH_4^+	196	5	4	μg m^{-3}
NO_3^-	40.6	1.9	1.3	μg m^{-3}
SO_4^{2-}	21	6	4	μg m^{-3}
Na^+	<*LOD*	2	1.7	μg m^{-3}
Cl^-	62	4	3	μg m^{-3}
Ca^{2+}	<*LOD*	8	6	μg m^{-3}
K^+	<*LOD*	6	4	μg m^{-3}
Mg^{2+}	<*LOD*	3	2	μg m^{-3}
NO_2^-	0.009	2	1.7	μg m^{-3}
TOC	11.1	0.07	0.6	mg C m^{-3}
Percent carboxylic acids	18	2	--	%
Lactate	17.5	1.5	0.5	μg m^{-3}
Acetate	182	1	1.1	μg m^{-3}
Propionate	23.5	0.6	1.3	μg m^{-3}
Formate	62.1	0.3	0.04	μg m^{-3}
Pyruvate	4.7	0.5	0.5	μg m^{-3}
Glutarate	5.4	1.7	0.9	μg m^{-3}
Succinate	9.3	1.8	0.5	μg m^{-3}
Malonate	1.2	2	1.2	μg m^{-3}
Maleate	2.0	2	2	μg m^{-3}
Oxalate	2.7	1.1	1.9	μg m^{-3}
4-Nitrophenol	<*LOD*	0.0015	0.3	μg m^{-3}
2-Methyl-4-nitrophenol	<*LOD*	0.003	0.11	μg m^{-3}
4-Nitrocatechol	0.005	0.0012	0.0004	μg m^{-3}
4-Methyl-5-nitrocatechol	<*LOD*	0.003	2	μg m^{-3}
2,4-Dinitrophenol	<*LOD*	0.00007	0.05	μg m^{-3}
Pinonate	<*LOD*	0.0012	0.19	μg m^{-3}
Pinate	<*LOD*	0.002	0.08	μg m^{-3}
2-Methyl-4,6-dinitrophenol	<*LOD*	0.00002	0.05	μg m^{-3}

Detectable concentrations of most quantified carboxylic acids were observed. Greatest concentrations were observed for acetate (182 ± 0.7 μg m^{-3}), formate (62.1 ± 0.3 μg m^{-3}), propionate (23.5 ± 0.6 μg m^{-3}), and lactate (17.5 ± 1.5 μg m^{-3}), with ≤10 μg m^{-3} contributed by other quantified acids. A portion of carboxylic acids not identified using authentic standards was also integrated from IC chromatograms and quantified using the IC-conductivity response to glutarate (likely similar to other carboxylic acids in the sample, based on qualitative online MS results); this category was referred to as "other acids". The percent carboxylic acid mass contributed to the TOC concentration (as mg C m^{-3}) was estimated from the sum of carboxylic acids quantified. The percent TOC of carboxylic acids in the mist chamber was 18 ± 2%, or 17 ± 3% without the inclusion of the "other acids" category. In contrast to the percent carboxylic acids measured in BB impacted cloud/fog samples from the real atmosphere, this was low (52% in fog water from the Yellow Sea during summer, 44% in cloud water from Mount Tai in the Shandong Province of the North China Plain), likely due to aging processes in the real atmosphere.

A series of nitrophenols were quantified via HPLC-(-)-ESI-HR-ToF-MS: 4-nitrophenol (4NP), 2-methyl-4-nitrophenol (2m4NP), 2,4-dinitrophenol (2,4DNP), 2-methyl-4,6-dinitrophenol (2m4,6DNP), 4-nitrocatechol (4NC), and 4-methyl-5-nitrocatechol (4m5NC). These species originate from lignin pyrolysis, and 4m5NC has been suggested as a BB emissions molecular tracer (Iinuma et al., 2010; Mohr et al., 2013). Secondary oxidation processes in the gas and aqueous phases as well as fossil fuel combustion including motor vehicle use can also produce nitrophenols (Harrison et al., 2005; Vione et al., 2005; Zhang et al., 2003). Nitrophenols were anticipated to be detected within the BB emissions from the burning of Ponderosa Pine, but since dinitrophenols most likely form after reaction in the atmosphere, it was not anticipated that 2,4-dinitrophenol or 2-methyl-4,6-dinitrophenol would be detected initially. Indeed, the concentrations of only 4-nitrocatechol and 4-methyl-5-nitrocatechol were above the respective instrumental LODs (LODs: 0.000010-0.03 μM/0.0004-1.3 μg m^{-3} for nitrophenols and nitrocatechols; 0.0007-0.0013 μM/0.04-0.06 μg m^{-3} for dinitrophenols; Fig. A6-4). The concentrations were initially 0.49 ± 0.13 μg m^{-3} 4-nitrocatechol and 8 ± 3 μg m^{-3} 4-methyl-5-nitrocatechol, approximately two to three orders of magnitude greater than those observed in the naturally diluted winter-time real atmosphere downwind of London (~20 ng m^{-3}; Mohr et al., 2013) and in rural Saxony, Germany (10 ng m^{-3}; Iinuma et al., 2010).

6.3.2 Aqueous Oxidation Results: Organic Carbon

The organic carbon (OC) concentration measured before (11.1 mg C L^{-1}) and after oxidation in the three replicate reactions revealed only a small percent degradation of the OC: the mist chamber extract lost on average 14% of OC after 120 min $^{\bullet}OH$ oxidation, leaving 9.6 ± 1.0 mg C L^{-1} after 120 min $^{\bullet}OH$ oxidation (95% confidence interval). The rate of OC loss was less than that anticipated based on previous studies of oxidation: at concentrations of H_2O_2 and 4-nitrophenol within the same order of magnitude as those employed here, $^{\bullet}OH$ oxidation caused the degradation of 4-nitrophenol to more than 90% OC loss after 100 min reaction (Zhang et al., 2003). The difference between this and previous studies is likely the result of the chemical complexity of the BB emissions sample. Aqueous $^{\bullet}OH$ oxidation of organic species within complex samples is slowed due to the competition for oxidant molecules in solution (also observed in polluted cloud samples; Boris et al., 2014). Similar slowing of degradation rates would likely be observed for organic species in the BB emissions based on previous work (Boris et al., 2014).

6.3.3 Aqueous Oxidation Results: Carboxylic Acids

Carboxylic acids were quantified at 15 min intervals during the reaction, using IC analysis of discrete samples (acetate, formate, propionate, lactate, pyruvate, glutarate, succinate, malonate, maleate, and oxalate; Figure 6-1).

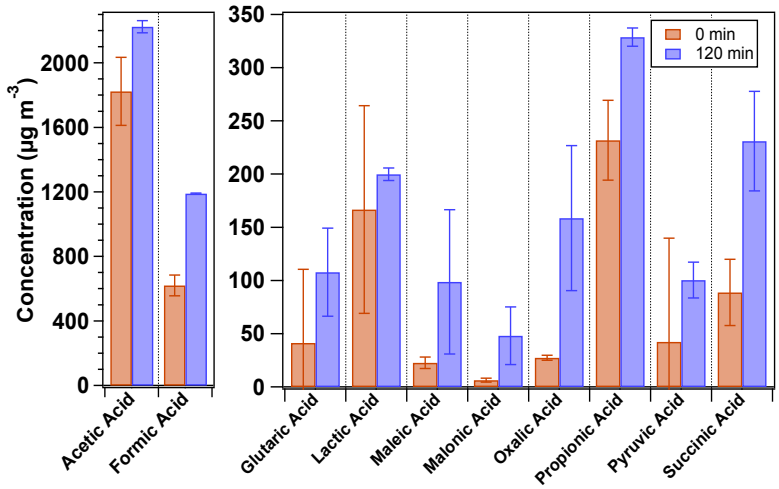

Figure 6-1. Mean concentrations during B4Ox of carboxylic acids at 0 and 120 min oxidation (µg m^{-3} in air). Error bars represent the range of concentrations measured from three replicate oxidations at each time point for each carboxylic acid species.

The concentration of acetate was low relative to that of formate throughout the reactions, which is not typical of aqueous oxidation reactions of standards or fog/cloud water samples (Chapter 5). Oxalate, which is frequently discussed as an aqSOA tracer (Sorooshian and Varutbangkul, 2006; Yu et al., 2005), was formed at an overall rate of 40 nM min^{-1}, less than that for acetate (200 nM min^{-1}) or formate (400 nM min^{-1}), but greater than that for most other acids: propionate (40 nM min^{-1}), succinate (30 nM min^{-1}), pyruvate (20 nM min^{-1}), maleate (20 nM min^{-1}), glutarate (10 nM min^{-1}), malonate (9 nM min^{-1}), and lactate (8 nM min^{-1}). Unidentified carboxylic acid peaks in the IC chromatograms were quantified using the surrogate response of glutarate as "other" acids. The percent carboxylic acids after 120 minutes oxidation was 30 ± 4% (28 ± 5% without "other" carboxylic acids), an increase of 12% (11% without "other") from t=0 min.

6.3.4 Aqueous Oxidation Results: Mechanisms of Oxidation and Qualitative Chemical Analysis

The dominant oxidant was assumed to be •OH during these experiments. Although triplet excited states of organics can also be formed via photo-excitation, and the subsequent reaction of organics with triplet excited states of organic species can be more rapid than •OH attack (Smith et al., 2014), the photosensitization observed previously has been primarily due to the excitation of electrons within non-phenolic aromatic carbonyls. Such species are not readily detectable using (-)-ESI-HR-ToF-MS. Reactions of triplet state organic molecules produce a

majority of covalently bound oligomeric products (Yu et al., 2014), which were also not observed. Structure-reactivity relationships of $^{\bullet}$OH oxidation of organics in the atmospheric aqueous phase have been explored (Doussin and Monod, 2013; Monod and Doussin, 2008; Monod et al., 2005). For organic species with *n*-alkyl chains, the number of CH_2 groups in the precursor molecule has been found to positively correlate with $^{\bullet}$OH reaction rate. The general mechanism of $^{\bullet}$OH attack on organic species proceeds either via H abstraction at the weakest C-H bond to form an alkyl radical (typical for saturated organic species) or electrophilic addition of –OH to a double bond (typical for aromatic or unsaturated organic species). For unsaturated organic molecules, the reaction is known to proceed more rapidly, and is in fact nearly diffusion-limited, with little variation due to substituent groups (Haag and Yao, 1992).

Precursors and products of burn emissions oxidation are summarized in Table 6-2, and changes in abundance with time of the most abundant species are demonstrated in Figure 6-2. Although the initial appearance of a product ion signal as well as the abundance of that signal are probably strongly affected by the sensitivity of the ESI process, the trend of an ionic signal through the duration of the oxidation reaction can still be used to deduce the role of the product in the oxidation. In general, the product ions with greater than 500 abundance units in the mass spectra can be categorized as initial products, intermediates, or final products based on the approximate reaction time at which the signal maximum is reached (Table 6-2). The initial $\geq C_3$ polar organic components of the BB emissions included a variety of multi-functional and dicarboxylic acids, as well as a smaller number of nitrophenolic species. The most reactive species identified via online (-)-ESI-HR-ToF-MS (Figure 6-3) included hydroquinone (m/z^- 109.03, $C_6H_6O_2$), pentenedioate (m/z^- 129.02, $C_5H_6O_4$), and dihydroxypentanoate (m/z^- 133.05 $C_5H_{10}O_4$).

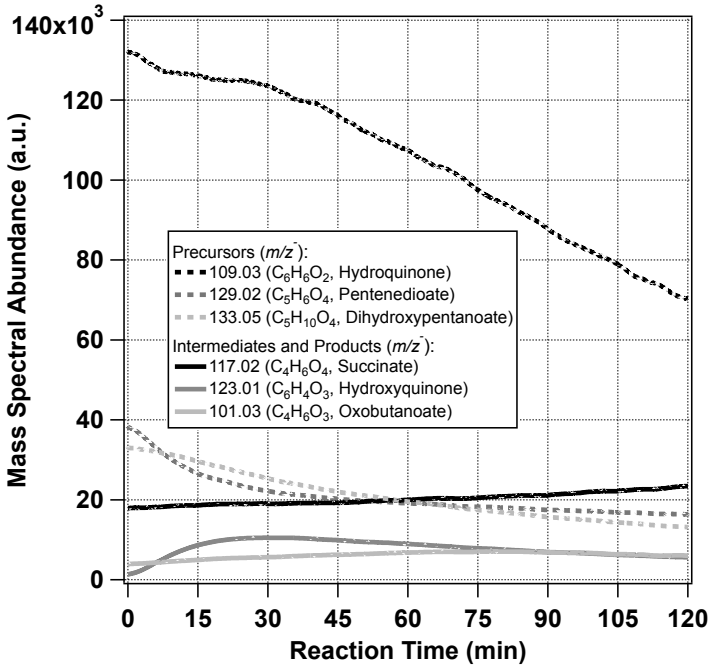

Figure 6-2. Profiles of mass spectral abundances observed via online MS during oxidation of BB emissions (example from replicate 1). The three precursors (dashed lines) and products (solid lines) with greatest changes in magnitude of abundance are plotted. Hydroquinone is more abundant than the other precursors and would continue to decrease in abundance after 120 min oxidation. Note that hydroxyquinone is an intermediate species because it is produced initially, and begins to decrease after approximately 20 min oxidation. Identifications are tentatively made based on formulae.

Although the measured abundance of hydroquinone was much greater than that of the other reactive precursors initially, the (-)-ESI-HR-ToF-MS sensitivity was likely in part responsible for this result. The degradation of even the most reactive precursors was exemplified by a steady decrease in abundance, rather than an exponential decrease, and only a ~50% decrease in hydroquinone abundance (similar to other reactive precursors) was observed after 120 min. This apparent slowing of the degradation was likely due to a competition for oxidant. All constituents were reacted (lost >500 a.u. after 120 min) in at least two replicate oxidation reactions (Table A6-3). Despite the aliphatic nature of dihydroxpentanoate (and other isomers of $C_5H_{10}O_4$), the observed degradation after 30 minutes oxidation was greater than that for other, aromatic and unsaturated precursors. All aliphatic, unsaturated, and phenolic species in the BB emissions in the present study were therefore susceptible to $^{\bullet}$OH attack, despite noted structure-reactivity relationships (Doussin and Monod, 2013). Recent work (Chapter 5) found that nitrophenols were more reactive toward $^{\bullet}$OH attack in real cloud water samples than saturated, biogenic species such as pinonic acid, in contrast with this trend. Electrospray ionization efficiency differences may be the source of some discrepancies between expected and observed trends in contrasted reaction rates of organic species.

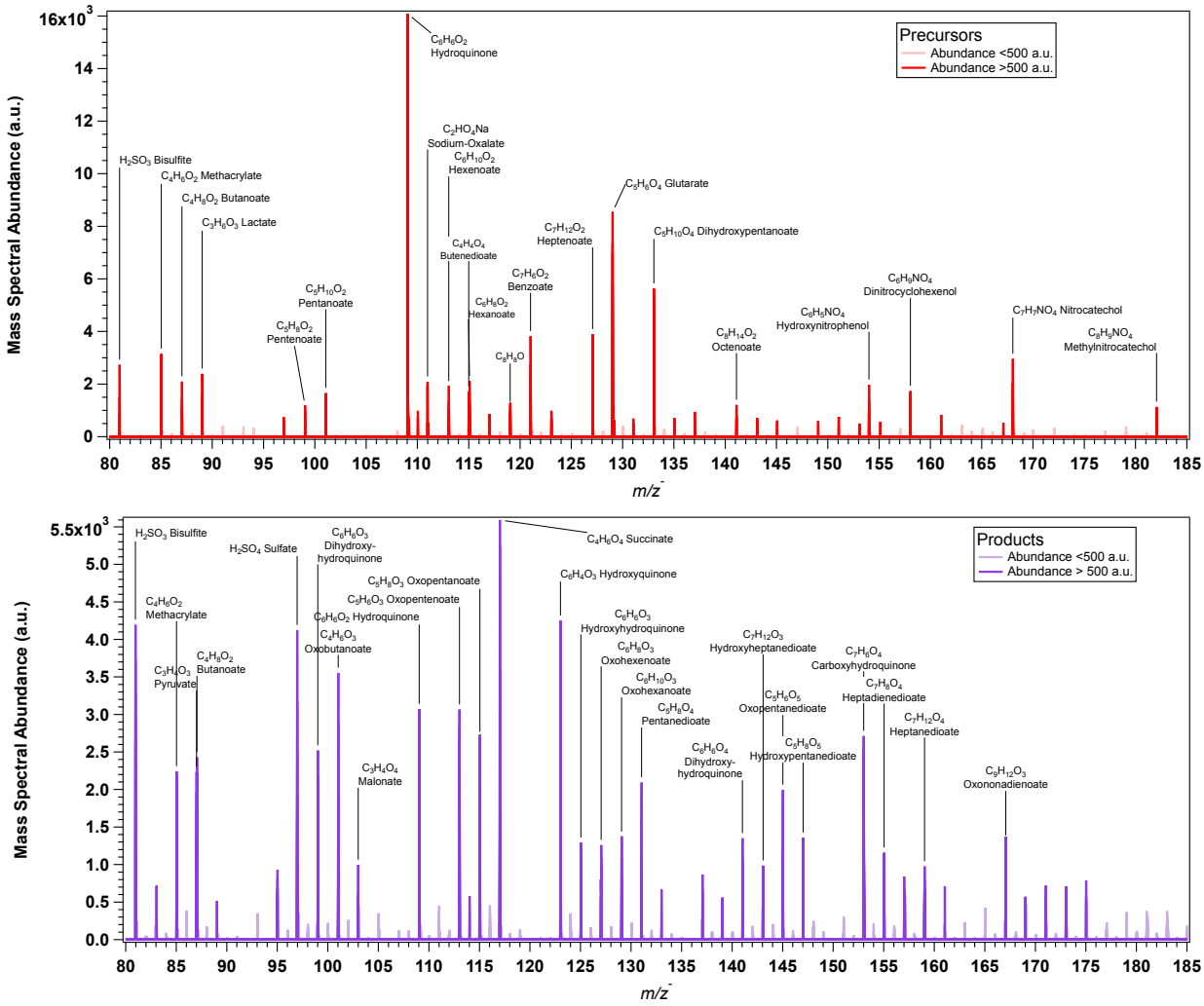

Figure 6-3. Mass spectra of organic species most identified as precursors (top) and products (bottom) of BB emissions oxidation. Mass spectra were calculated as follows: precursors > 500 abundance units (red) and all other precursors (pink) were identified by subtracting spectra at 15 and 30 min oxidation reaction time from the spectrum at 0 min reaction time; products > 500 abundance units (purple) and all other precursors (lavender) were identified by subtracting the spectrum at 0 min reaction time from the spectra at 15, 30, 60, and 120 min reaction time. Names of species are tentative identifications. Products listed include some intermediate species as well. The threshold of 500 a.u. was chosen for determination of formula based on a balance between the need for substantial signal abundance to accurately capture the center of the peak, and a lower signal provided in real time measurements than with LC separation, for which the threshold is typically 5000 a.u. All precursors and products are tabulated in Table A6-3.

Ring-opening as well as ring-retaining products were observed in the oxidation of the BB emissions. However, only a small number of the typically C_2-C_4 carboxylic acids as products of simulated AAOPs of species including glyoxal, methylglyoxal, and methylvinylketone (Altieri et al., 2008; Renard et al., 2014; Tan et al., 2009) were observed during the BB emissions oxidation reactions. Although dimers have been previously observed in the aqueous oxidation of BB emissions components (Chang and Thompson, 2010), no dimers were apparent from the oxidation of the current, gas-phase BB emissions. Products of oxidation became more varied as the oxidation progressed, mainly consisting of oxo-and unsaturated carboxylic acids. The smallest of these products included

malonate and pyruvate, which are C_3. No determination of structure could be made using (-)-ESI-HR-ToF-MS, so oxo-acids could be ketone- or aldehyde-containing. Despite the presence of C_3 and C_4 products, there were also functionalized quinones, present at even 120 min oxidation, indicating that the oxidation process was slowed due to competition. This slowing would theoretically cause the products to be higher in volatility than anticipated if standard solutions of single BB emissions components were oxidized, such as the simple photo-oxidation of a nitrophenol. Thus, although it is clear that a change in volatility would be caused by the AAOP of BB emissions, material with sufficiently low volatility for aqSOA mass formation might not be produced until the emissions (TOC) were diluted somewhat in the atmosphere (recall that TOC concentrations in the oxidation solution were intermediate between values observed within fresh and transported atmospheric water droplets; present study: 45.7 mg C L^{-1} TOC).

Table 6-2. Polar organic species identified within fog and cloud samples via online MS as precursors and products of BB emissions oxidation. Precursors were identified by subtracting t=15 and 30 min reaction time mass spectra from the t=0 mass spectrum (if the mass spectral signal was decreasing between 0 and 30 min); products were identified by subtracting t=0 min reaction time mass spectrum from the t=15, 30, and 120 min reaction time mass spectrum. No plausible identifications could be made for some species. Mean, confidence interval at 95% confidence (CI95) and percent relative standard deviation (RSD) were calculated from the abundances measured in the three replicate oxidation reactions. Only species that were present at >500 a.u. in at least two oxidation replicates are listed; precursor abundances listed are the greater value from 15 and 30 min precursors.

	m/z^-	Formula	Mean Abund. Diff (a.u.)	CI95 Abund. Diff (a.u.)	RSD (%)	Possible Identification
Precursors:	109.03	$C_6H_6O_2$	8873	14587	84	Hydroquinone
	129.02	$C_5H_6O_4$	7633	1596	11	Pentenedioate
	133.05	$C_5H_{10}O_4$	4600	2568	28	Dihydroxypentanoate
	127.08	$C_7H_{12}O_2$	2753	2089	39	Heptenenoate
	121.03	$C_7H_6O_2$	2617	2885	56	Benzoate
	85.03	$C_4H_6O_2$	2310	3932	87	Methacrylate
	168.03	$C_7H_7NO_4$	2270	2639	59	Hydroxynitrocatechol
	115.01	$C_4H_4O_4$	1580	34	1	Maleate
	113.06	$C_6H_{10}O_2$	1483	1081	37	Hexenoate
	115.08	$C_6H_{12}O_2$	1450	1213	43	Hexanoate
	89.03	$C_3H_6O_3$	1380	2453	90	Lactate
	158.05	$C_6H_9NO_4$	1353	935	35	Dinitrocyclohexenol
	119.05	C_8H_8O	1230	309	13	
	154.01	$C_6H_5NO_4$	1137	2025	91	Hydroxynitrophenol
	87.04	$C_4H_8O_2$	1090	2077	97	Butanoate
	110.98	C_2HO_4Na	1013	2243	113	Oxalate, sodium adduct
	101.06	$C_5H_{10}O_2$	1000	1185	60	Pentanoate
	129.09	$C_7H_{14}O_2$	963	674	36	Heptanoate
	141.10	$C_8H_{14}O_2$	937	561	30	Octenoate
	182.05	$C_8H_9NO_4$	723	1236	87	Dimethylnitrocatechol
	215.16	$C_{12}H_{24}O_3$	643	281	22	
	123.06	$C_6H_8N_2O$	590	1068	92	Dimethylpyrimidinol
	99.05	$C_5H_8O_2$	580	1215	107	Pentenenoate
	221.07	e.g, $C_8H_{14}O_7$	500	878	89	
	161.06	$C_6H_{10}O_5$	470	871	94	Levoglucosan
	135.04	$C_8H_8O_2$	440	765	88	Methylbenzoate
	207.05	e.g., $C_7H_{12}O_7$	370	636	87	
Products (0-15 min):	123.01	$C_6H_4O_3$	3213	1657	26	Hydroxyquinone
	153.02	$C_7H_6O_4$	1337	681	26	Carboxyhydroxyhydroquinone
	113.03	$C_5H_6O_3$	1183	499	21	Oxopentanoate
	115.04	$C_5H_8O_3$	673	296	22	Hydroxypentanoate
	87.01	$C_3H_4O_3$	570	1017	91	Pyruvate
	125.03	$C_6H_6O_3$	500	851	87	Hydroxyhydroquinone
	99.01	$C_4H_4O_3$	470	801	87	Oxobutenoate
	167.07	$C_9H_{12}O_3$	457	780	87	
	127.04	$C_6H_8O_3$	407	692	87	Oxohexenoate
Products (0-30 min):	123.01	$C_6H_4O_3$	3693	1811	25	Hydroxyquinone
	153.02	$C_7H_6O_4$	1930	871	23	Carboxyhydroquinone
	113.03	$C_5H_6O_3$	1707	658	20	Oxopentanoate
	99.01	$C_4H_4O_3$	1073	414	20	Oxobutenoate
	87.01	$C_3H_4O_3$	1040	793	39	Pyruvate
	115.04	$C_5H_8O_3$	1003	60	3	Hydroxypentanoate
	101.03	$C_4H_6O_3$	963	386	20	Oxobutanoate
	167.07	$C_9H_{12}O_3$	920	336	19	
	125.03	$C_6H_6O_3$	827	386	24	Hydroxyhydroquinone
	87.04	$C_4H_8O_2$	810	2757	173	Butanoate
	155.04	$C_7H_8O_4$	773	542	36	Pentadienedioate
Products (0-60 min):	127.04	$C_6H_8O_3$	747	199	14	Oxohexenoate

	m/z⁻	Formula	Mean Abund. Diff (a.u.)	CI95 Abund. Diff (a.u.)	RSD (%)	Possible Identification
	173.05	$C_7H_{10}O_5$	553	134	12	Oxoheptanedioate
	85.03	$C_4H_6O_2$	473	1611	173	Methacrylate
	95.01	$C_5H_4O_2$	457	815	91	
	129.06	$C_6H_{10}O_3$	350	596	87	Oxohexanoate
	159.03	$C_6H_8O_5$	337	573	87	Hydroxyhexenedioate
	109.03	$C_6H_6O_2$	310	1055	173	Hydroquionone
	117.02	$C_4H_6O_4$	300	1021	173	Butanedioate
	137.06	$C_8H_{10}O_2$	237	806	173	Octadienoate/Methylguaiacol
	131.04	$C_5H_8O_4$	233	794	173	Pentanedioate
	145.02	$C_5H_6O_5$	220	749	173	Oxopentanedioate
	141.03	$C_6H_6O_4$	217	738	173	Hexadienedioate
	97.03	$C_5H_6O_2$	180	613	173	Pentadienoate
Products (0-120 min):	117.02	$C_4H_6O_4$	4890	2418	25	Butanedioate
	113.03	$C_5H_6O_3$	2957	415	7	Oxopentenoate
	101.03	$C_4H_6O_3$	2820	1695	31	Oxobutanoate
	115.05	$C_5H_8O_3$	2573	483	10	Oxopentanoate
	153.03	$C_7H_6O_4$	2507	665	13	Carboxyhydroquinone
	123.01	$C_6H_4O_3$	2200	343	8	Heptadienoate
	99.01	$C_4H_4O_3$	1987	1281	33	Oxobutenoate
	131.03	$C_5H_8O_4$	1570	1498	49	Hydroxyoxopentenoate
	145.02	$C_5H_6O_5$	1417	1129	41	Oxopentanedioate
	147.03	$C_5H_8O_5$	1350	1464	55	Hydroxypentanedioate
	129.06	$C_6H_{10}O_3$	1343	298	11	Oxohexanoate
	141.03	$C_6H_6O_4$	1180	327	14	Dihydroxyhydroquinone
	127.04	$C_6H_8O_3$	1083	354	17	Oxohexenoate
	87.01	$C_3H_4O_3$	1030	2415	119	Pyruvate
	167.08	$C_9H_{12}O_3$	1013	777	39	
	143.07	$C_7H_{12}O_3$	1003	49	3	Oxoheptanoate
	125.03	$C_6H_6O_3$	967	573	30	Hydroxyhydroquinone
	155.04	$C_7H_8O_4$	953	398	21	Heptadienedioate
	159.04	$C_6H_8O_5$	763	486	32	Hydroxyhexenedioate
	103.01	$C_3H_4O_4$	740	460	32	Malonate
	115.00	C_8H_4O	720	1313	93	
	157.02	$C_6H_6O_5$	690	285	21	Oxohexenedioate
	141.06	$C_7H_{10}O_3$	670	104	8	
	157.09	$C_8H_{14}O_3$	623	23	2	Hydroxyoctanedioate
	173.04	$C_7H_{10}O_5$	463	789	87	Oxoheptanedioate
	97.03	$C_5H_6O_2$	460	792	88	Butadienoate
	175.02	$C_6H_8O_6$	440	791	92	Hydroxyoxohexenedioate
	171.03	$C_7H_8O_5$	430	747	88	Oxoheptenedioate
	139.04	$C_7H_8O_3$	407	697	87	Oxoheptadienoate
	159.06	$C_7H_{12}O_4$	403	688	87	Heptanedioate
	95.01	$C_5H_4O_2$	387	688	88	

6.3.5 Atmospheric Implications

Nitrophenols and their derivatives are known to be toxic to aquatic invertebrates as well as to small mammals and plants (Agency for Toxic Substances and Disease Registry, 2011, 1992; Natangelo et al., 1999). Aqueous oxidation of nitrophenols typically results in the formation of LMM carboxylic acids (Kavitha and Palanivelu, 2005; Trapido and Kallas, 2000; Zhang et al., 2003), which are less harmful (Patnaik, 2006). The degradation of such species through aqueous oxidation therefore results in an overall improvement of health effects on ecosystems.

The two nitrocatechols detected above the instrumental LOD during the aqueous oxidation of the BB emissions, 4NC and 4M5NC, decreased in concentration throughout the oxidation reactions, resulting in mean degradation rates of -0.5% min^{-1} (-0.08 nM min^{-1}; not significant at the 95% confidence level) and -0.6% min^{-1} (-1.2 nM min^{-1}; significant at the 95% confidence level), respectively (Figure 6-4). The oxidation rate of 4NC was similar to that observed during an oxidation of cloud water: removal of 4NC from a cloud sample from Mount Tai, China occurred at a rate of -0.8% min^{-1} (-0.2 nM min^{-1}).

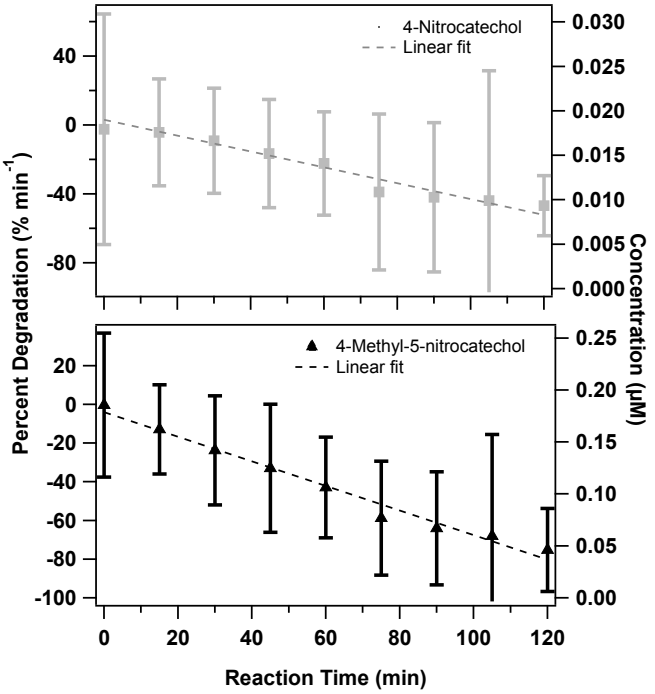

Figure 6-4. Percent of initial concentration of nitrocatechols (left axis) and concentration (μM) quantified via LC/MS with oxidation time. Values are means of three replicate oxidation reactions. Other nitrophenols were quantified, but concentrations were not significantly different from zero. Dashed lines represent linear fits of the concentration trends with time (percent of initial concentration, % min^{-1}): for 4-nitrocatechol, y=-0.461x+3.12; for 4-methyl-5-nitrocatechol, y=-0637x+3.74. Error bars and 95% confidence intervals of concentrations.

In addition to an improvement in the air toxicity, the degradation of organics causes in general the oxygenation of the organic matter, which in turn impacts such atmospheric properties of the collective organic aerosol as hygroscopicity, light absorption (as a result of the oxygenated functional groups present), and volatility. Some relationship between the hygroscopicity of particles and the specific oxygenated functional groups present is observed in lab and field studies, although system-dependent (Massoli et al., 2010; Suda et al., 2014; Wu et al., 2013). A process leading to an increased degree of oxygenation in ambient organic aerosol is not captured by most lab-generated and modeled organic aerosol (Aiken et al., 2008; Heald et al., 2005); this process may inlcude aqueous

oxidation (Chen et al., 2015). Because BB processes account for a substantial fraction of global and regional organic aerosol sources (Heald et al., 2006; Schauer and Cass, 2000), identification of the classes of species produced during aqueous oxidation of BB emissions is important for the estimation of the BB processes contribution to such properties in global aerosol budgets. LMM carboxylic acids can be semi-volatile, and have been found mainly in the particle phase (over 90% for malonic and oxalic acids; Limbeck et al., 2005), especially when cations such as NH_4^+ are present (Ortiz-Montalvo et al., 2014). While the partitioning of organic species between the gas and particle phase is highly dependent on environmental variables such as the concentration of organic particulate matter and ambient organic species vapor pressures (Odum et al., 1996), the net production of carboxylic acids during AAOP reaction can be used as a lower-bound estimate (since no other organic products are included) of whether production of aqSOA might occur. Measured net production of summed carboxylic acids in the oxidation of BB emissions was on average 6.1 mg L^{-1} (3.0 mg C L^{-1}), or ~6% net production of carboxylic acids as a function of the initial TOC in the sample over the two hour oxidation (including unidentified carboxylic acids quantified as "other"). Assuming that partitioning behavior of the produced carboxylic acids would be similar to those observed by Limbeck et al. (2005), this aqueous oxidation of BB emissions could be a substantial contributor to BB organic aerosol. In contrast, dry oxidation of gas and particle phase burn emissions produced 50-280% mass increases, likey including many species in addition to carboxylic acids (Grieshop et al., 2009a; Hennigan et al., 2011). Additional oligomer formation (Tan et al., 2009) or formation of products with $>C_4$ should be considered in future studies of aqueous reactions. It is likely that carboxylic acid production would be greater after some atmospheric dilution of emissions, since slowing of oxidation due to high TOC conditions was observed in the reactions in the present study. Although these bulk aqueous phase photo-oxidation reactions demonstrate a probable contribution to aerosol mass from in-cloud processes, further studies are needed to constrain the impact of these effects on estimated aqSOA mass production. In future work, the quantification of low-volatility C_3-C_9 carboxylic acids, aldehydes, ketones, multifunctional oxygenated species, and oligomers (Tan et al., 2009) should be prioritized to accurately estimate the degree of oxygenation from aqueous oxidation of BB emissions. In particular, the measurement of actual produced aerosol mass (as via aerosol mass spectrometry, Lee et al., 2011, or atomization followed by particle counting, Ortiz-Montalvo et al., 2012) would be useful.

6.4 Conclusions

The aqueous atmospheric oxidation of BB emissions was studied through bulk phase •OH reaction of volatile Ponderosa Pine combustion emissions collected using a mist chamber. The objectives of the study were to characterize the chemical changes of the organic material, estimate whether aqSOA would form, and draw contrast to dry SOA formation from BB emissions. TOC concentrations decreased slightly during the reactions (11.1±0.6 mg C m^{-3} to 9.6±1.0 mg C m^{-3} on average for the three replicate oxidation reactions), indicative of the competition between organic species for oxidant molecules in the complex solution. Carboxylic acids were observed to form during oxidation, as observed in previous simulations (Lim et al., 2010); formation rates were between 8 nM min^{-1} (lactate) and 400 nM min^{-1} (formate). The change in the percentage of TOC accounted for by quantified carboxylic acids increased during the oxidation from 18% to 30%. Emissions constituents included hydroquinone, nitrocatechols, and C_3-C_9 carboxylic acids and ketones/aldehydes including multifunctional species. All organic species within the emissions were observed to degrade appreciably throughout the reaction, in agreement with previous findings that most •OH reaction rates with unsaturated organic species are rapid. Measured degradation rates were also rapid for aliphatic organics, however, in contrast to previously measured rates (Haag and Yao, 1992). Based on the intermediates and products identified by formula, the mechanism of oxidation of the emissions components was thus primarily H abstraction; some aromatic species as well as aliphatic species also apparently underwent •OH addition (for example, hydroxyhydroquinone and hydroxypentenanedioate/hydroxyglutarate). No oligomer formation was apparent, as has been suggested for aqueous interactions of triplet excited state aromatic carbonyls, which are relevant for BB emissions (Yu et al., 2014). The oxidative removal rates of the nitrophenolic species 4NC and 4M5NC were ~10 nM hr^{-1} and 140 nM hr^{-1}, respectively, suggesting that despite some slowing due to the high concentrations of organic substances competing for oxidant, oxidation is an important process for removal of potentially toxic trace organic constituents from the atmosphere. The net production of semi-volatile carboxylic acids through aqueous oxidation reactions was calculated to estimate whether aqSOA production was likely as a result of in-cloud BB emissions oxidation. The result was 6.1 mg L^{-1} production of carboxylic acids on average over the course of the two hour reactions. This was equivalent to approximately 6% addition to the TOC in the BB emissions collected into the mist chamber. Future studies should aim to more accurately quantify the aqSOA mass produced within BB emissions by allowing reactions within suspended droplets rather than in the bulk phase, and quantifying a greater number of organic species contributing to the aqSOA mass formed.

REFERENCES

Agency for Toxic Substances and Disease Registry, 1992. Toxicological profile for nitrophenols: 2-nitrophenol, 4-nitrophenol. Atlanta, Georgia.

Agency for Toxic Substances and Disease Registry, 2011. Addendum To the Toxicological Profile for Dinitrophenols. Atlanta, Georgia.

Aiken, A.C., Decarlo, P.F., Kroll, J.H., Worsnop, D.R., Huffman, J.A., Docherty, K.S., Ulbrich, I.M., Mohr, C., Kimmel, J.R., Super, D., Sun, Y., Zhang, Q., Trimborn, A., Northway, M., Zieman, P.J., Canagaratna, M.R., Onasch, T.B., Alfarra, M.R., Prevot, A.S.H., Dommen, J., Duplissy, J., Metzger, A., Baltensperger, U., Jimenez, J.L., 2008. O/C and OM/OC Ratios of Primary, Secondary, and Ambient Organic Aerosols with High-Resolution Time-of-Flight Aerosol Mass Spectrometry. Environ. Sci. Technol. 42, 4478–4485.

Altieri, K.E., Seitzinger, S.P., Carlton, A.G., Turpin, B.J., Klein, G.C., Marshall, A.G., 2008. Oligomers formed through in-cloud methylglyoxal reactions: Chemical composition, properties, and mechanisms investigated by ultra-high resolution FT-ICR mass spectrometry. Atmos. Environ. 42, 1476–1490.

Anastasio, C., Faust, B.C., Rao, C.J., 1997. Aromatic carbonyl compounds as aqueous-phase photochemical sources of hydrogen peroxide in acidic sulfate aerosols, fogs, and clouds 1. Non-phenolic methoxybenzaldehydes and methoxyacetophenones with reductants (phenols). Environ. Sci. Technol. 31, 218–232.

Anastasio, C., McGregor, K.G., 2001. Chemistry of fog waters in California's Central Valley: 1. In situ photoformation of hydroxyl radical and singlet molecular oxygen. Atmos. Environ. 35, 1079–1089.

Andreae, M.O., Merlet, P., 2001. Emission of trace gases and aerosols from biomass burning. Global Biogeochem. Cycles 15, 955–966.

Bond, T.C., 2004. A technology-based global inventory of black and organic carbon emissions from combustion. J. Geophys. Res. 109, D14203.

Boris, A.J., Desyaterik, Y., Collett, J.L., 2014. How do components of real cloud water affect aqueous pyruvate oxidation? Atmos. Res. 143, 95–106.

Boris, A.J., Lee, T., Park, T., Choi, J., Seo, S.J., Collett, J.L., 2016. Fog composition at Baengnyeong Island in the eastern Yellow Sea: detecting markers of aqueous atmospheric oxidations. Atmos. Chem. Phys. 16, 437–453.

Chang, J.L., Thompson, J.E., 2010. Characterization of colored products formed during irradiation of aqueous solutions containing H2O2 and phenolic compounds. Atmos. Environ. 44, 541–551.

Chen, Q., Heald, C.L., Jimenez, J.L., Canagaratna, M.R., He, L.-Y., Huang, X.-F., Campuzano-Jost, P., Palm, B.B., Poulain, L., Kuwata, M., Martin, S.T., Abbatt, J.P.D., Lee, A.K.Y., Liggio, J., 2015. Elemental Composition of Organic Aerosol: The Gap Between Ambient and Laboratory Measurements. Geophys. Res. Lett. 42, 1–8.

Crutzen, P., Andreae, M.O., 1990. Biomass burning in the tropics: Impact on atmospheric chemistry and biogeochemical cycles. Science (80-.). 250, 1669–1678.

Doussin, J.-F., Monod, a., 2013. Structure–activity relationship for the estimation of OH-oxidation rate constants of carbonyl compounds in the aqueous phase. Atmos. Chem. Phys. 13, 11625–11641.

Engling, G., Herckes, P., Kreidenweis, S.M., Malm, W.C., Collett Jr., J.L., 2006. Composition of the fine organic aerosol in Yosemite National Park during the 2002 Yosemite Aerosol Characterization Study. Atmos. Environ. 40, 2959–2972.

Ervens, B., Renard, P., Ravier, S., Clément, J.-L., Monod, A., 2014. Aqueous phase oligomerization of methyl vinyl ketone through photooxidation – Part 2: Development of the chemical mechanism and atmospheric implications. Atmos. Chem. Phys. Discuss. 14, 21565–21609.

Ervens, B., Turpin, B., Weber, R., 2011. Secondary organic aerosol formation in cloud droplets and aqueous particles (aqSOA): A review of laboratory, field and model studies. Atmos. Chem. Phys. 11, 11069–11102.

Goldstein, A.H., Galbally, I.E., 2007. Known and unexpected organic constituents in the Earth's atmosphere. Environ. Sci. Technol. 41, 1514–1521.

Grieshop, A.P., Donahue, N.M., Robinson, A.L., 2009a. Laboratory investigation of photochemical oxidation of organic aerosol from wood fires 2: analysis of aerosol mass spectrometer data. Atmos. Chem. Phys. 9, 2227–2240.

Grieshop, A.P., Logue, J.M., Donahue, N.M., Robinson, A.L., 2009b. Laboratory investigation of photochemical oxidation of organic aerosol from wood fires 1: measurement and simulation of organic aerosol evolution. Atmos. Chem. Phys. 9, 1263–1277.

Haag, W.R., Yao, C.C.D., 1992. Rate Constants for Reaction of Hydroxyl Radicals With Several Drinking-Water Contaminants. Environ. Sci. Technol. 26, 1005–1013.

Harrison, M., Barra, S., Borghesi, D., Vione, D., Arsene, C., Iulianolariu, R., 2005. Nitrated phenols in the atmosphere: a review. Atmos. Environ. 39, 231–248.

Hays, M.D., Geron, C.D., Linna, K.J., Smith, N.D., Schauer, J.J., 2002. Speciation of gas-phase and fine particle emissions from burning of foliar fuels. Environ. Sci. Technol. 36, 2281–95.

Heald, C.L., Jacob, D.J., Park, R.J., Russell, L.M., Huebert, B.J., Seinfeld, J.H., Liao, H., Weber, R.J., 2005. A large organic aerosol source in the free troposphere missing from current models. Geophys. Res. Lett. 32, 2–5.

Heald, C.L., Jacob, D.J., Turquety, S., Hudman, R.C., Weber, R.J., Sullivan, A.P., Peltier, R.E., Atlas, E.L., De Gouw, J. a, Warneke, C., Holloway, J.S., Neuman, J.A., Flocke, F.M., Seinfeld, J.H., 2006. Concentrations and sources of organic carbon aerosols in the free troposphere over North America. J. Geophys. Res. 111, 1–12.

Hennigan, C.J., Bergin, M.H., Dibb, J.E., Weber, R.J., 2008. Enhanced secondary organic aerosol formation due to water uptake by fine particles. Geophys. Res. Lett. 35, 1–5.

Hennigan, C.J., Miracolo, M. a., Engelhart, G.J., May, a. a., Presto, a. a., Lee, T., Sullivan, a. P., McMeeking, G.R., Coe, H., Wold, C.E., Hao, W.-M., Gilman, J.B., Kuster, W.C., de Gouw, J., Schichtel, B. a., Kreidenweis, S.M., Robinson, a. L., 2011. Chemical and physical transformations of organic aerosol from the photo-oxidation of open biomass burning emissions in an environmental chamber. Atmos. Chem. Phys. 11, 7669–7686.

Hennigan, C.J., Westervelt, D.M., Riipinen, I., Engelhart, G.J., Lee, T., Collett, J.L., Pandis, S.N., Adams, P.J., Robinson, A.L., 2012. New particle formation and growth in biomass burning plumes: An important source of cloud condensation nuclei. Geophys. Res. Lett. 39.

Iinuma, Y., Böge, O., Gräfe, R., Herrmann, H., 2010. Methyl-nitrocatechols: atmospheric tracer compounds for biomass burning secondary organic aerosols. Environ. Sci. Technol. 44, 8453–9.

Kavitha, V., Palanivelu, K., 2005. Degradation of nitrophenols by Fenton and photo-Fenton processes. J. Photochem. Photobiol. A Chem. 170, 83–95.

Lee, A.K.Y., Zhao, R., Gao, S.S., Abbatt, J.P.D., 2011. Aqueous-phase OH oxidation of glyoxal: application of a novel analytical approach employing aerosol mass spectrometry and complementary off-line techniques. J. Phys. Chem. A 115, 10517–10526.

Lim, Y.B., Tan, Y., Perri, M.J., Seitzinger, S.P., Turpin, B.J., 2010. Aqueous chemistry and its role in secondary organic aerosol (SOA) formation. Atmos. Chem. Phys. 10, 10521–10539.

Limbeck, A., Kraxner, Y., Puxbaum, H., 2005. Gas to particle distribution of low molecular weight dicarboxylic acids at two different sites in central Europe (Austria). J. Aerosol Sci. 36, 991–1005.

Lin, G., Sillman, S., Penner, J.E., Ito, A., 2014. Global modeling of SOA: the use of different mechanisms for aqueous-phase formation. Atmos. Chem. Phys. 14, 5451–5475.

Liu, Y., Monod, A., Tritscher, T., Praplan, A.P., DeCarlo, P.F., Temime-Roussel, B., Quivet, E., Marchand, N., Dommen, J., Baltensperger, U., 2012. Aqueous phase processing of secondary organic aerosol from isoprene photooxidation. Atmos. Chem. Phys. 12, 5879–5895.

Loeffler, K.W., Koehler, C.A., Paul, N.M., De Haan, D.O., 2006. Oligomer formation in evaporating aqueous glyoxal and methylglyoxal solutions. Environ. Sci. Technol. 40, 6318–6323.

Massoli, P., Lambe, A.T., Ahern, A.T., Williams, L.R., Ehn, M., Mikkilä, J., Canagaratna, M.R., Brune, W.H., Onasch, T.B., Jayne, J.T., Petäjä, T., Kulmala, M., Laaksonen, A., Kolb, C.E., Davidovits, P., Worsnop, D.R., 2010. Relationship between aerosol oxidation level and hygroscopic properties of laboratory generated secondary organic aerosol (SOA) particles. Geophys. Res. Lett. 37, 1–5.

Mohr, C., Lopez-Hilfiker, F.D., Zotter, P., Prévôt, A.S.H., Xu, L., Ng, N.L., Herndon, S.C., Williams, L.R., Franklin, J.P., Zahniser, M.S., Worsnop, D.R., Knighton, W.B., Aiken, A.C., Gorkowski, K.J., Dubey, M.K., Allan, J.D., Thornton, J. a, 2013. Contribution of nitrated phenols to wood burning brown carbon light absorption in Detling, United Kingdom during winter time. Environ. Sci. Technol. 47, 6316–24.

Monod, A., Doussin, J.F., 2008. Structure-activity relationship for the estimation of OH-oxidation rate constants of aliphatic organic compounds in the aqueous phase: alkanes, alcohols, organic acids and bases. Atmos. Environ. 42, 7611–7622.

Monod, A., Poulain, L., Grubert, S., Voisin, D., Wortham, H., 2005. Kinetics of OH-initiated oxidation of oxygenated organic compounds in the aqueous phase: new rate constants, structure–activity relationships and atmospheric implications. Atmos. Environ. 39, 7667–7688.

Myriokefalitakis, S., Tsigaridis, K., Mihalopoulos, N., Sciare, J., Nenes, A., Kawamura, K., Segers, A., Kanakidou, M., 2011. In-cloud oxalate formation in the global troposphere: a 3-D modeling study. Atmos. Chem. Phys. 11, 5761–5782.

Natangelo, M., Mangiapan, S., Bagnati, R., Benfenati, E., Fanelli, R., 1999. Increased concentrations of nitrophenols in leaves from a damaged forestal site. Chemosphere 38, 1495–1503.

Odum, J.R., Hoffmann, T., Bowman, F., Collins, D., Flagan, R.C., Seinfeld, J.H., 1996. Gas particle partitioning and secondary organic aerosol yields. Environ. Sci. Technol. 30, 2580–2585.

Ortiz-Montalvo, D.L., Häkkinen, S. a K., Schwier, A.N., Lim, Y.B., McNeill, V.F., Turpin, B.J., 2014. Ammonium addition (and aerosol pH) has a dramatic impact on the volatility and yield of glyoxal secondary organic aerosol. Environ. Sci. Technol. 48, 255–62.

Ortiz-Montalvo, D.L., Lim, Y.B., Perri, M.J., Seitzinger, S.P., Turpin, B.J., 2012. Volatility and Yield of Glycolaldehyde SOA Formed through Aqueous Photochemistry and Droplet Evaporation. Aerosol Sci. Technol. 46, 1002–1014.

Patnaik, P., 2006. A Comprehensive Guide to the Hazardous Properties of Chemical Substances: Third Edition, A Comprehensive Guide to the Hazardous Properties of Chemical Substances: Third Edition.

Perri, M.J., Seitzinger, S., Turpin, B.J., 2009. Secondary organic aerosol production from aqueous photooxidation of glycolaldehyde: Laboratory experiments. Atmos. Environ. 43, 1487–1497.

Renard, P., Siekmann, F., Salque, G., Smaani, A., Demelas, C., Coulomb, B., Vassalo, L., Ravier, S., Temime-Roussel, B., Voisin, D., Monod, A., 2014. Aqueous phase oligomerization of methyl vinyl ketone through photooxidation – Part 1: Aging processes of oligomers. Atmos. Chem. Phys. Discuss. 14, 15283–15322.

Santos, A., Yustos, P., Rodriguez, S., Garcia-Ochoa, F., 2006. Wet oxidation of phenol, cresols and nitrophenols catalyzed by activated carbon in acid and basic media. Appl. Catal. B Environ. 65, 269–281.

Schauer, J.J., Cass, G.R., 2000. Source Apportionment of Wintertime Gas-Phase and Particle-Phase Air Pollutants Using Organic Compounds as Tracers Source Apportionment of Wintertime Gas-Phase and Particle-Phase Air Pollutants Using Organic Compounds as Tracers. Environ. Sci. Technol. 34, 1821–1832.

Shen, X., 2011. Aqueous Phase Sulfate Production in Clouds at Mt. Tai in Eastern China. Colorado State University.

Slade, J.H., Knopf, D.A., 2013. Heterogeneous OH oxidation of biomass burning organic aerosol surrogate compounds: assessment of volatilisation products and the role of OH concentration on the reactive uptake kinetics. Phys. Chem. Chem. Phys. 15, 5898–915.

Slade, J.H., Thalman, R., Wang, J., Knopf, D. a., 2015. Chemical aging of single and multicomponent biomass burning aerosol surrogate particles by OH: implications for cloud condensation nucleus activity. Atmos. Chem. Phys. 15, 10183–10201.

Smith, J.D., Sio, V., Yu, L., Zhang, Q., Anastasio, C., 2014. Secondary organic aerosol production from aqueous reactions of atmospheric phenols with an organic triplet excited state. Environ. Sci. Technol. 48, 1049–57.

Sorooshian, A., Varutbangkul, V., 2006. Oxalic acid in clear and cloudy atmospheres: Analysis of data from International Consortium for Atmospheric Research on Transport and Transformation 2004. J. Geophys. Res. 111, 1–10.

Spracklen, D. V., Mickley, L.J., Logan, J. a., Hudman, R.C., Yevich, R., Flannigan, M.D., Westerling, a. L., 2009. Impacts of climate change from 2000 to 2050 on wildfire activity and carbonaceous aerosol concentrations in the western United States. J. Geophys. Res. 114, D20301.

Suda, S.R., Petters, M.D., Yeh, K., Strollo, C., Matsunaga, A., Faulhaber, A., Ziemann, P.J., Prenni, A.J., Carrico, C.M., Sullivan, R.C., Kreidenweis, S.M., Yeh, G.K., Strollo, C., Matsunaga, A., Faulhaber, A., Ziemann, P.J., Prenni, A.J., Carrico, C.M., Sullivan, R.C., Kreidenweis, S.M., 2014. Influence of functional groups on organic aerosol cloud condensation nucleus activity. Environ. Sci. Technol. 48, 10182–90.

Sullivan, A.P., Holden, A.S., Patterson, L.A., McMeeking, G.R., Kreidenweis, S.M., Malm, W.C., Hao, W.M., Wold, C.E., Collett, J.L., 2008. A method for smoke marker measurements and its potential application for determining the contribution of biomass burning from wildfires and prescribed fires to ambient PM 2.5 organic carbon. J. Geophys. Res. 113, D22302.

Sun, Y.L., Zhang, Q., Anastasio, C., Sun, J., 2010. Insights into secondary organic aerosol formed via aqueous-phase reactions of phenolic compounds based on high resolution mass spectrometry. Atmos. Chem. Phys. 10, 4809–4822.

Tan, Y., Carlton, A.G., Seitzinger, S.P., Turpin, B.J., 2010. SOA from methylglyoxal in clouds and wet aerosols: Measurement and prediction of key products. Atmos. Environ. 44, 5218–5226.

Tan, Y., Perri, M.J., Seitzinger, S.P., Turpin, B.J., 2009. Effects of Precursor Concentration and Acidic Sulfate in Aqueous Glyoxal-OH Radical Oxidation and Implications for Secondary Organic Aerosol. Environ. Sci. Technol. 43, 8105–8112.

Trapido, M., Kallas, J., 2000. Advanced Oxidation Processes for the Degradation and Detoxification of 4-Nitrophenol. Environ. Technol. 21, 799–808.

Val Martin, M., Heald, C.L., Ford, B., Prenni, A.J., Wiedinmyer, C., 2013. A decadal satellite analysis of the origins and impacts of smoke in Colorado. Atmos. Chem. Phys. 13, 7429–7439.

Vione, D., Maurino, V., Minero, C., Pelizzetti, E., 2005. Aqueous atmospheric chemistry: Formation of 2,4-dinitrophenol upon nitration of 2-nitrophenol and 4-nitrophenol in solution. Environ. Sci. Technol. 39, 7921–7931.

Volkamer, R., Jimenez, J.L., San Martini, F., Dzepina, K., Zhang, Q., Salcedo, D., Molina, L.T., Worsnop, D.R., Molina, M.J., 2006. Secondary organic aerosol formation from anthropogenic air pollution: Rapid and higher than expected. Geophys. Res. Lett. 33, 1–4.

Warneck, P., 2003. In-cloud chemistry opens pathway to the formation of oxalic acid in the marine atmosphere. Atmos. Environ. 37, 2423–2427.

Wu, Z.J., Poulain, L., Henning, S., Dieckmann, K., Birmili, W., Merkel, M., Van Pinxteren, D., Spindler, G., Müller, K., Stratmann, F., Herrmann, H., Wiedensohler, A., 2013. Relating particle hygroscopicity and CCN activity to chemical composition during the HCCT-2010 field campaign. Atmos. Chem. Phys. 13, 7983–7996.

Yu, J.Z., Huang, X.-F., Xu, J., Hu, M., 2005. When aerosol sulfate goes up, so does oxalate: implication for the formation mechanisms of oxalate. Environ. Sci. Technol. 39, 128–133.

Yu, L., Smith, J., Laskin, a., Anastasio, C., Laskin, J., Zhang, Q., 2014. Chemical characterization of SOA formed from aqueous-phase reactions of phenols with the triplet excited state of carbonyl and hydroxyl radical. Atmos. Chem. Phys. 14, 13801–13816.

Zhang, W., Xiao, X., An, T., Song, Z., 2003. Kinetics, degradation pathway and reaction mechanism of advanced oxidation of 4-nitrophenol in water by a UV/H2O2 process. J. Chem. Technol. Biotechnol. 794, 788–794.

Zhao, R., Mungall, E.L., Lee, A.K.Y., Aljawhary, D., Abbatt, J.P.D., 2014. Aqueous-phase photooxidation of levoglucosan -- A mechanistic study using aerosol time-of-flight chemical ionization mass spectrometry (Aerosol ToF-CIMS). Atmos. Chem. Phys. 14, 9695–9705.

7. CONCLUSIONS AND FURTHER RESEARCH

The current thesis work demonstrated the utility of two approaches to characterizing aqSOA: collection and analysis of real fog water, and lab simulation of aqueous atmospheric oxidation processing (AAOP) reactions in the bulk phase of fog/cloud droplets. These approaches allowed the observation of evidence of aqSOA formation and a qualitative look at predominant mechanisms occurring within the droplets.

7.1 Can We Observe Aqueous Aging of Organics in the Real Atmosphere?

Chemical evidence we have observed in field-based studies for aqSOA formation has included the following. The diversity of carboxylic acids, and their contribution to organic mass in fog samples are enhanced in more aged fog/cloud water samples. Typically, fog/cloud organic matter is composed of 20-50% carboxylic acids (by mass of C) at the time of droplet collection. This percent contribution of carboxylic acids to TOC was on average 52% at Baengnyeong Island in Korea within fog samples that displayed clear evidence of aging (Chapter 2), while only 20% at Casitas Pass in Southern California near biogenic and anthropogenic organic emissions sources (Chapter 3). Lab simulations confirmed that the percent TOC contributed by carboxylic acids increases during further photo-oxidation (with $^{\bullet}OH$ radical). Organic sulfur (OS) species were observed in aged fog water, and appear to be formed during foggy events. Species containing the elements C, H, O, and S were present in Korean fog water, which was aged at the time of collection, and were also observed only during the mature stage of fog in Southern California (suggesting in-fog chemical formation). Aqueous mechanisms for OS species formation have been suggested, and observations of organosulfates in atmospheric aerosol have typically been in humid regions (Iinuma et al., 2007; Schindelka et al., 2013; Surratt et al., 2008). In addition, oxygenated CHO and CHNOS species were apparently formed during fog events in Southern California. Correlations were high between SO_4^{2-} and carboxylic acids in fog water in Korea and Southern California ($r^2 \geq 0.80$). SO_4^{2-} forms primarily in the aqueous phase (Finlayson-Pitts and Pitts, 2000), and carboxylic acids, including oxalate and methanesulfonate, form at least in part in the aqueous phase (Chebbi and Carlier, 1996; Sorooshian et al., 2007; Zhang et al., 2016).

Unfortunately, these points of evidence for aqSOA formation/AAOP occurrence are not without uncertainty. Time-resolved changes in fog chemistry could be due to chemical reactions, but could also be a result of physical changes in the fog (such as deposition of larger, more dilute droplets or evaporation of water to increase fog

constituent concentrations). Additionally, even in the presence of liquid water droplets, it is not possible to rule out gas-phase or surface-driven oxidation reactions rather than aqueous phase reactions as the pathway for observed chemistry. While tracer molecules for aqSOA/AAOP reactions would be an elegant way to observe aqueous oxidation reactions, and even quantify their influence on observed chemistry, current molecular candidates such as oxalate and OS species may not be exclusive to aqueous processes, or representative of all aqueous organic reactions. The main challenge with field studies of aqueous chemistry is therefore that the real atmosphere is complex and most variables cannot be controlled. In contrast, nearly all variables are controlled in bulk-phase lab reactions, meaning that some important factors, including those we currently do not understand, may not be accounted for.

7.2 Can We Accurately Simulate Aqueous Aging using Bulk Phase Reactions in the Lab?

Reactions carried out in bulk aqueous solutions in the lab are useful as a qualitative approach to studying AAOP reactions. Bulk reactions were successfully applied in the present thesis to identify some products and precursors of oxidation reactions, including reactions of chemical standards and of precursors in real fog/cloud water samples. Most previous bulk reaction studies have oxidized chemical standards in water. In the current thesis work, we have demonstrated that the presence of other organic cloud water constituents can overall slow oxidation, and, in the presence of high chemical concentrations, can cause the formation of additional products. Specifically, the reaction rate of pyruvate photo-oxidation was lesser when the reaction was carried out in a real cloud water matrix than in pure deionized water, caused by the competition of other organic cloud water constituents for photons and/or oxidant (Chapter 4). Thus, although organic oxidation in the aqueous phase is suggested to be more rapid than in the gas phase (Monod et al., 2005), real fog water matrices and other true environmental conditions must be considered. When the constituents within several real aqueous atmospheric samples were photo-oxidized (Chapters 5 and 6), the reactions differed based on the structures of the organic precursor molecules, the degree of oxidation ("age"), and SO_4^{2-} concentration in the samples. These differing "regimes" of AAOP resulted in the formation of differing products, including OS species when high SO_4^{2-} concentrations were present. Chemical observations such as these can be made using bulk-phase lab experiments due to the precise control of variables such as light, concentration of precursors and oxidant, and time of oxidation afforded. Some uncertain factors still exist, however, in bulk-phase lab experiments (for example, oxygen availability). The gas/aqueous exchange that occurs at the surface of a droplet cannot be captured by bulk reactions. The result could be an overestimation of aqSOA production (observed by

Daumit et al., 2014 in environmental chamber-based experiments), as organic species are not removed to the gas phase, or underestimation of aqSOA production as oxidant is not continually supplied from the gas phase. Evaporation/condensation cycles of fogs and clouds are also not captured in bulk-phase experiments. Some reactions important in the aqueous phase are in fact driven by evaporation (for example, condensation reaction; Loeffler et al., 2006; Nguyen et al., 2012), and radical-radical reactions could also be enhanced as effective concentrations of organics increase during evaporation (Tan et al., 2009). Even when a drying process is included in modeling or lab simulations, it is unlikely that the drying will be similar to that occurring in the real atmosphere: atomization cannot approximate the effect of fog/cloud cycling and the resulting gas/aqueous equilibria (or lack thereof; Pandis and Seinfeld, 1991). Finally, instrumental limitations currently do not allow all organic matter to be quantified or even identified. Low molecular mass carboxylic acids (11 species) and $\geq C_4$, protonatable species including nitrophenols and biogenic carboxylic acids (12 species) were successfully quantified in the present thesis work. Formulae for a variety (~50-100 per cloud/fog water sample) of additional $\geq C_4$, protonatable species were identified (not quantified due to a lack of chemical standards). Although some polar, oxygenated species can therefore be quantified, oligomeric/high molecular mass products and even some oxygenated compounds such as ketones are infrequently measured in bulk-phase experiments. These compounds may account for a substantial fraction of the organic mass in real fog/cloud water samples as well as AAOP reaction products (Decesari et al., 2005; Lim et al., 2013). This problem is relevant for both field and lab work.

7.3 Priorities for Further Research

In conclusion, priorities in current aqSOA and AAOP research should be to (1) identify unambiguous and easily monitored chemical and/or physical tracers for AAOP; (2) continue to develop advanced lab simulation techniques; and (3) expand fog field studies to include concurrent microphysical and chemical analyses of high and low molecular mass organics. The droplet mode of aerosol size distributions, and species found within it including SO_4^{2-} and oxalate, is a promising candidate for a tracer of AAOP reactions (Crahan et al., 2004; Meng and Seinfeld, 1994), and should be explored more. Current instrumental techniques are capable of making the measurements needed for this work. However, lab simulations that will allow the characterization of AAOP and aqSOA formation details must be advanced. Current techniques are not fully quantitative, and only speciate a portion of the intermediates and products. The aqSOA mass, for example, from glyoxal oxidation in the presence of SO_4^{2-} must be quantified and products speciated, considering evaporation-driven reactions. Environmental chamber techniques, rather than bulk

phase reactions, may be a solution, such as the work of Brégonzio-Rozer et al. (2015) using a stainless steel cloud chamber capable of hosting evaporative cloud cycles by changing pressure (Wang et al., 2011). In-cloud oxidation of isoprene/$^{\bullet}$OH in the aqueous phase was demonstrated to occur more rapidly than in the gas phase (Brégonzio-Rozier et al., 2016). Despite the substantial cost and work to characterize such a chamber, other researchers are using similar rigid cloud chambers (Chang et al., *In Press*; Hoppel et al., 1994), which should expand current understanding of aqSOA formation substantially. Non-rigid Teflon chambers have also been used to study reactions at relative humidity as high as 90% (Daumit et al., 2014; Kalberer et al., 2006; Kroll et al., 2005; Nguyen et al., 2011; Zhang et al., 2011), although wall losses of chemicals and liquid water were often noted. The key advantage of *in-situ* observations is the realistic combination of variables that are afforded by studying the real atmosphere. However, one cost of such studies is the need to monitor a larger number of variables: the microphysical processes in fog must be captured alongside chemistry to identify the effects of aqueous reactions. The separation of droplets into size modes can demonstrate, to some extent, the deposition of larger droplets and evaporation of smaller droplets, although fogs/clouds with constant advection of new air masses remain a challenge to study (van Pinxteren et al., 2016). Finally, a more complete chemical analysis of organics as they are oxidized in AAOP reactions is needed. Currently, molecules that are typically not identified include higher molecular mass species such as HULIS or oligomers, and non-acidic carbonyls. In addition, even for the organic species with acidic groups that can be detected via the common technique of electrospray ionization mass spectrometry (ESI-MS), many cannot be quantified because chemical standards are required. Ultra-high sensitivity analysis of organics can be accomplished by Fourier Transform Ion Cyclotron Resonance Mass Spectrometry (FT-ICR-MS), for example (Altieri et al., 2009), but the method is not quantitative and the data analysis is intense such that only a few samples are typically analyzed in a given study. Radical-radical reaction oligomers of chemical standards have also been identified using coupled traveling wave ion mobility spectrometry/time-of-flight mass spectrometry (IMS-MS), but this technique, again, is not quantitative (Renard et al., 2015). New techniques that allow the identification and quantitation of more organic species must be elucidated to fully characterize AAOP reactions and aqSOA formation.

REFERENCES

Altieri, K. E., Turpin, B. J. and Seitzinger, S. P.: Oligomers, organosulfates, and nitrooxy organosulfates in rainwater identified by ultra-high resolution electrospray ionization FT-ICR mass spectrometry, Atmos. Chem. Phys., 9(7), 2533–2542, doi:10.5194/acp-9-2533-2009, 2009.

Brégonzio-Rozier, L., Giorio, C., Siekmann, F., Pangui, E., Morales, S. B., Temime-Roussel, B., Gratien, A., Michoud, V., Cazaunau, M., DeWitt, H. L., Tapparo, A., Monod, A. and Doussin, J.-F.: Secondary Organic Aerosol formation from isoprene photooxidation during cloud condensation–evaporation cycles, Atmos. Chem. Phys., 16, 1747–1760, doi:10.5194/acpd-15-20561-2015, 2016.

Chang, K., Bench, J., Brege, M., Cantrell, W., Chandrakar, K., Ciochetto, D., Mazzoleni, C., Mazzoleni, L. R., Niedermeier, D. and Shaw, R. A.: A new laboratory facility to study gas-aerosol-cloud interactions in a turbulent environment : The Π Chamber, Bull. Am. Meteorol. Soc., (In Press), 44, doi:10.1175/BAMS-D-15-00203.1, n.d.

Chebbi, A. and Carlier, P.: Carboxylic acids in the troposphere, occurrence, sources, and sinks: A review, Atmos. Environ., 30(24), 4233–4249, 1996.

Crahan, K. K., Hegg, D., Covert, D. S. and Jonsson, H.: An exploration of aqueous oxalic acid production in the coastal marine atmosphere, Atmos. Environ., 38(23), 3757–3764, doi:10.1016/j.atmosenv.2004.04.009, 2004.

Daumit, K. E., Carrasquillo, A. J., Hunter, J. F. and Kroll, J. H.: Laboratory studies of the aqueous-phase oxidation of polyols: submicron particles vs. bulk aqueous solution, Atmos. Chem. Phys., 14(19), 10773–10784, doi:10.5194/acp-14-10773-2014, 2014.

Decesari, S., Facchini, M., Fuzzi, S., Mcfiggans, G., Coe, H. and Bower, K.: The water-soluble organic component of size-segregated aerosol, cloud water and wet depositions from Jeju Island during ACE-Asia, Atmos. Environ., 39(2), 211–222, doi:10.1016/j.atmosenv.2004.09.049, 2005.

Finlayson-Pitts, B. J. and Pitts, J. N.: Acid Deposition: Formation and Fates of Inorganic and Organic Acids in the Troposphere, in Chemistry of the Upper and Lower Atmosphere: Theory, Experiments, and Applications, p. 969, Academic Press, San Diego, CA., 2000.

Hoppel, W. A., Frick, G. M., Fitzgerald, J. W. and Watter, B. J.: A Cloud Chamber Study of the Effect That Nonprecipitating Water Clouds Have on the Aerosol Size Distribution, Aerosol Sci. Technol., 20(1), 1–30, 1994.

Iinuma, Y., Muller, C., Berndt, T., Boge, O., Claeys, M. and Herrmann, H.: Evidence for the Existence of Organosulfates from β-Pinene Ozonolysis in Ambient Secondary Organic Aerosol, Environ. Sci. Technol., 41(19), 6678–6683, doi:10.1021/es070938t, 2007.

Kalberer, M., Sax, M. and Samburova, V.: Molecular Size Evolution of Oligomers in Organic Aerosols Collected in Urban Atmospheres and Generated in a Smog Chamber, Environ. Sci. Technol., 40(19), 5917–5922, 2006.

Kroll, J. H., Ng, N. L., Murphy, S. M., Varutbangkul, V., Flagan, R. C. and Seinfeld, J. H.: Chamber studies of secondary organic aerosol growth by reactive uptake of simple carbonyl compounds, J. Geophys. Res. Atmos., 110(23), 1–10, doi:10.1029/2005JD006004, 2005.

Lim, Y. B., Tan, Y. and Turpin, B. J.: Chemical insights, explicit chemistry, and yields of secondary organic aerosol from OH radical oxidation of methylglyoxal and glyoxal in the aqueous phase, Atmos. Chem. Phys., 13(17), 8651–8667, doi:10.5194/acp-13-8651-2013, 2013.

Loeffler, K. W., Koehler, C. A., Paul, N. M. and De Haan, D. O.: Oligomer formation in evaporating aqueous glyoxal and methylglyoxal solutions, Environ. Sci. Technol., 40(20), 6318–6323, doi:10.1021/es060810w, 2006.

Meng, Z. and Seinfeld, J. H.: On the Source of the Submicrometer Droplet Mode of Urban and Regional Aerosols, Aerosol Sci. Technol., 20(3), 253–265, doi:10.1080/02786829408959681, 1994.

Monod, A., Poulain, L., Grubert, S., Voisin, D. and Wortham, H.: Kinetics of OH-initiated oxidation of oxygenated organic compounds in the aqueous phase: new rate constants, structure–activity relationships and atmospheric implications, Atmos. Environ., 39(40), 7667–7688, doi:10.1016/j.atmosenv.2005.03.019, 2005.

Nguyen, T. B., Lee, P. B., Updyke, K. M., Bones, D. L., Laskin, J., Laskin, A. and Nizkorodov, S. A.: Formation of nitrogen- and sulfur-containing light-absorbing compounds accelerated by evaporation of water from secondary organic aerosols, J. Geophys. Res. Atmos., 117(1), D01207, doi:10.1029/2011JD016944, 2012.

Nguyen, T. B., Roach, P. J., Laskin, J., Laskin, a. and Nizkorodov, S. a.: Effect of humidity on the composition of isoprene photooxidation secondary organic aerosol, Atmos. Chem. Phys., 11(14), 6931–6944, doi:10.5194/acp-11-6931-2011, 2011.

Pandis, S. N. and Seinfeld, J. H.: Should bulk cloudwater or fogwater samples obey henrys law, J. Geophys. Res.-Atmos., 96(91), 10791–10798, doi:10.1029/91JD01031, 1991.

van Pinxteren, D., Fomba, K. W., Mertes, S., Müller, K., Spindler, G., Schneider, J., Lee, T., Collett, J. and Herrmann, H.: Cloud water composition during HCCT-2010: Scavenging efficiencies, solute concentrations, and droplet size dependence of inorganic ions and dissolved organic carbon, Atmos. Chem. Phys., 16, 3185–3205, doi:10.5194/acpd-15-24311-2015, 2016.

Renard, P., Tlili, S., Ravier, S., Quivet, E. and Monod, A.: Aqueous phase oligomerization of α,β-unsaturated carbonyls and acids investigated using ion mobility spectrometry coupled to mass spectrometry (IMS-MS), Atmos. Environ., 130, 153–162, doi:10.1016/j.atmosenv.2015.10.060, 2015.

Schindelka, J., Iinuma, Y., Hoffmann, D. and Herrmann, H.: Sulfate radical-initiated formation of isoprene-derived organosulfates in atmospheric aerosols, Faraday Discuss., 165, 237–259, doi:10.1039/c3fd00042g, 2013.

Sorooshian, A., Lu, M.-L., Brechtel, F. J., Jonsson, H., Feingold, G., Flagan, R. C. and Seinfeld, J. H.: On the source of organic acid aerosol layers above clouds, Environ. Sci. Technol., 41(13), 4647–54, 2007.

Surratt, J. D., Gómez-González, Y., Chan, A. W. H., Vermeylen, R., Shahgholi, M., Kleindienst, T. E., Edney, E. O., Offenberg, J. H., Lewandowski, M., Jaoui, M., Maenhaut, W., Claeys, M., Flagan, R. C. and Seinfeld, J. H.: Organosulfate formation in biogenic secondary organic aerosol, J. Phys. Chem. A, 112(36), 8345–78, doi:10.1021/jp802310p, 2008.

Tan, Y., Perri, M. J., Seitzinger, S. P. and Turpin, B. J.: Effects of Precursor Concentration and Acidic Sulfate in Aqueous Glyoxal-OH Radical Oxidation and Implications for Secondary Organic Aerosol, Environ. Sci. Technol., 43(21), 8105–8112, 2009.

Wang, J., Doussin, J. F., Perrier, S., Perraudin, E., Katrib, Y., Pangui, E. and Picquet-Varrault, B.: Design of a new multi-phase experimental simulation chamber for atmospheric photosmog, aerosol and cloud chemistry research, Atmos. Meas. Tech., 4(11), 2465–2494, doi:10.5194/amt-4-2465-2011, 2011.

Zhang, H., Surratt, J. D., Lin, Y. H., Bapat, J. and Kamens, R. M. M.: Effect of relative humidity on SOA formation from isoprene/NO photooxidation: enhancement of 2-methylglyceric acid and its corresponding oligoesters under dry conditions, Atmos. Chem. Phys., 11(13), 6411–6424, doi:10.5194/acp-11-6411-2011, 2011.

Zhang, Y.-L., Kawamura, K., Cao, F. and Lee, M.: Stable carbon isotopic compositions of low-molecular-weight dicarboxylic acids, oxocarboxylic acids, α-dicarbonyls, and fatty acids: Implications for atmospheric processing of organic aerosols, J. Geophys. Res. Atmos., 121, 3707–3717, doi:10.1002/2014JD022994.Received, 2016.

APPENDICES

APPENDIX 1: STANDARD OPERATING PROCEDURES FOR FOG AND CLOUD WATER ANALYSES

Equipment and Supplies (Shipping Checklist used for 2014 BYI Study)

Instrumentation

- Particulate Volume Monitor (PVM):
- PVM unit (grey plastic box, 14”x39”x26”, approx. 30 kg)
- PVM data logger box containing data logger, RS-232 interface, and power supply unit (grey metal, 24”x21.5”x11.5”, approx. 30 kg)
- Serial cable (RS-232 interface to laptop)
- Amphenol signal cable (PVM to data logger)
- Amphenol power cable (power supply to power converter)
- Foreign step-down power converter if necessary
- Power cord (power converter to wall, if necessary)
- Power cord (PVM to power supply)
- Calibration disk (in plastic storage container)
- Laptop with LoggerNet software and Teamviewer software
- Power cable for laptop
- USB-to-serial adapter cable
- Serial cable (data logger to laptop)
- Signal and/or power extension cords if necessary for site
- Sealable plastic bags and duct tape for each non-Amphenol connection
- U-bolts for mounting PVM (or other mounting supplies)
- Large philips, Small and large flathead screwdrivers
- PVM mounting bracket (metal L-shaped piece)
- Extra air pump (retrofitted pumps available from Dr. Hermann Gerber)

Chemicals (note that some are hazardous):

- Triton X-100 for cleaning CASCC(s)
- pH analyses:
    - pH 4.00 and 7.00 buffer solutions
    - Extra pH electrode storage solution
- Formaldehyde preservation solution:
    - *t*-1,2-Cyclohexylenedinitrilo-tetraacetic acid (CDTA)
    - Sodium hydroxide (10 N solution preferable)
    - Sodium bisulfite
- Peroxides preservation:
    - Conditioning reagent:
    - Fluorescent reagent:
        - Horseradish peroxidase for H_2O_2 preservation (keep at 0°C-5°C/chilled)
        - Potassium hydrogen phthalate
        - *p*-Hydroxyphenylacetic acid (POPHA)
        - Sodium hydroxide (10 N solution preferable)
        - Ethylenediaminetetraacetic Acid (EDTA)
- S(IV) preservation:
    - S(IV) preservative solution:
        - Bovine catalase enzyme for S(IV) preservation (keep at 0°C-5°C/chilled)
        - Formaldehyde solution (37%)
        - *t*-1,2-Cyclohexylenedinitrilo-tetraacetic acid (CDTA)
    - Catalase solution:
- Organic acids preservation:
    - Chloroform (~200 mL)
- Isopropanol for cleaning PVM collimator lens

Supplies for Chemical Analyses (for approximately 100 samples and blanks):

- pH electrode soaking in well-sealed storage solution container

- pH meter with power adapter (battery pack removed)
- Foreign power supply adapter if necessary
- Autopipettes: 100-1000 µL (3), 30-300 µL (3)
- Pipet tips: 200 µL (10 boxes), 1000 µL (8 boxes)
- Gloves (5 boxes)
- Vial racks (2)
- Vial files (5)
- 2 mL cryovials for pH analyses (~60)
- 700 µL plastic autosampler vials for IC analyses (100)
- 1.5-2 mL glass vials with Teflon-lined caps for formaldehyde analyses (100)
- 1.5-2 mL glass vials with Teflon-lined caps for S(IV) analyses (100)
- 1.5-2 mL glass vials with Teflon-lined caps for peroxides analyses (100)
- Extra 1.5-2 mL glass vials with Teflon-lined caps (50)
- 2 mL amber glass vials with Teflon-lined caps for organic acids analyses (100)
- Stirring/heat plate
- Power adapter and/or transformer for stirring/heat plate (if necessary)
- Stir bar
- Squeeze bottle for water
- Water purifying unit with extra filter packs and UV bulb
- Glassware: 250 mL beakers (3), 250 mL Erlenmeyer flasks (2), 10 mL volumetric flasks (2), 100 mL volumetric flasks (6), 250 mL volumetric flasks (2)
- Pasteur pipets with bulbs (10)
- Kimwipes (5 boxes)
- Chemical balance with power cord
- Power adapter and/or transformer for chemical balance (if necessary)
- Large and small weigh boats (20 each), weigh paper
- Microspatula
- Freezer and refrigerator

- Cooler(s) for all chemicals, collected samples and preserved aliquots
- Ice packs for transporting chemicals, samples, and aliquots

Miscellaneous Supplies:

- Folder with 20 log sheets and instrument notes
- Caddy or box for chemical transport between lab and fridge
- Electric label-maker with 4-5 rolls of tape (batteries removed)
- Yellow labeling tape (1 roll)
- Clear packaging tape (5 rolls)
- Duct tape (5 rolls)
- Extra pens, thick and thin permanent markers
- Extra zip-top plastic bags (small and gallon-sized, 2-3 boxes each)
- Zip ties (20-30, medium or large)
- Parafilm (1 box)
- Parts kit with all screws and connectors for CASCC(s) and PVM, plastic bolts and extra tubing for cloudwater collection adapters, wires for collector fan unit(s), electrical tape, duct tape
- Metric and standard Allan wrench sets
- Foil for providing clean surfaces for chemical analyses (2 boxes)
- Medium size crescent wrench
- Extra foreign power adapters (if necessary)
- Boxcutter or other device for cutting tubing
- AA batteries for label maker, 9V battery for pH meter (if removed for transport)
- Q-tips for cleaning PVM collimator lens
- Extra boxes for transport to the U.S.

Size Fractioning Caltech Active Strand Cloudwater Collector (sf-CASCC):

- Stages 1 and 3 (grey plastic box, 12”x39”x26”, approx. 30 kg)
- Stage 2 (similar plastic box needed)
- Fan unit with flow straightener (grey plastic box, 12”x39”x26”, approx. 20 kg)
- Triangular polycarbonate rain cover

- Bottles: 60 @ 60 mL, 48 @ 125 mL, 24 @ 250 mL, 6 @ 500 mL
- Power cable for fan with plastic contact connectors (wired for power converter)
- AC/DC variable power converter (set to 13.3 V, wired for fan unit)
- Rain cover for power converter (plastic box with ventilation works well)
- Trash bags and bungee cords for covering collector during non-use periods
- Toothbrush for cleaning cloud water collector strands and rods
- Spray bottle for cleaning cloud water collector
- Large fertilizer sprayer for cleaning cloud water collector
- Plastic bin large enough to fit CASCC units for washing
- 4 drilled lids with adapter tubing and fittings (for all ports and stages)
- Mounting bracket for correct number of CASCC stages (needs cardboard box)
- Guywires, stands, cement blocks for supporting sf-CASCC

Caltech Active Strand Cloudwater Collector 2 (CASCC2):

- Strand unit (needs plastic shipping box)
- Fan unit (needs shipping box)
- Triangular polycarbonate rain cover
- Stand (this can be a small ladder or bench if sturdy and sufficiently elevated)
- Bottles: 24 @ 60 mL, 24 @ 125 mL, 12 @ 250 mL
- Power cable for fan with plastic contact connectors (wired for power converter)
- AC/DC variable power converter (set to 13.3 V, wired for fan unit)
- Rain cover for power converter (plastic box with ventilation works well)
- Trash bags and bungee cords for covering collector during non-use periods
- Toothbrush for cleaning cloud water collector strands and rods
- Spray bottle for cleaning cloud water collector
- Plastic bin large enough to fit CASCC units for washing
- 4 drilled lids with adapter tubing and fittings (for all ports)
- Guywires, stands, cement blocks for supporting CASCC2

Notes on shipping:

- Batteries should be removed from items shipped via a carrier (UPS/FedEx) and placed in luggage or purchased at the field site location.
- Plastic containers are preferred over cardboard boxes for any heavy items.
- Hazardous materials cannot be shipped via CSU shipping and receiving; chemicals can instead be purchased and shipped by chemical vendors such as Sigma-Aldrich or purchased at the field site location.
- Names of items listed on shipping forms must be non-scientific; for example, a particulate volume monitor can be called a "water detector". Note that these names should not be inaccurate, but should be easily translatable and understandable so that opening the package is not necessary for customs to ensure that no hazardous or non-allowable items are shipped into the field site country.
- Shipping forms accompanying boxes should list serial numbers of any large, expensive, or otherwise important items contained in each box. This allows customs (in particular, in South Korea) to verify that the items are non-hazardous and secure for entry into the country.
- Customs fees: It may be possible to simply export the items to the destination country rather than shipping them for short-term entry. Depending on the size and nature of the shipment, this may decrease the cost of customs fees.

Size-Fractionating CalTech Active Strand Cloudwater Collector (sf-CASCC)

(Source: Operating Procedures Manual, Cloudwater Collection and Analysis, Colorado State University Department of Atmospheric Science)

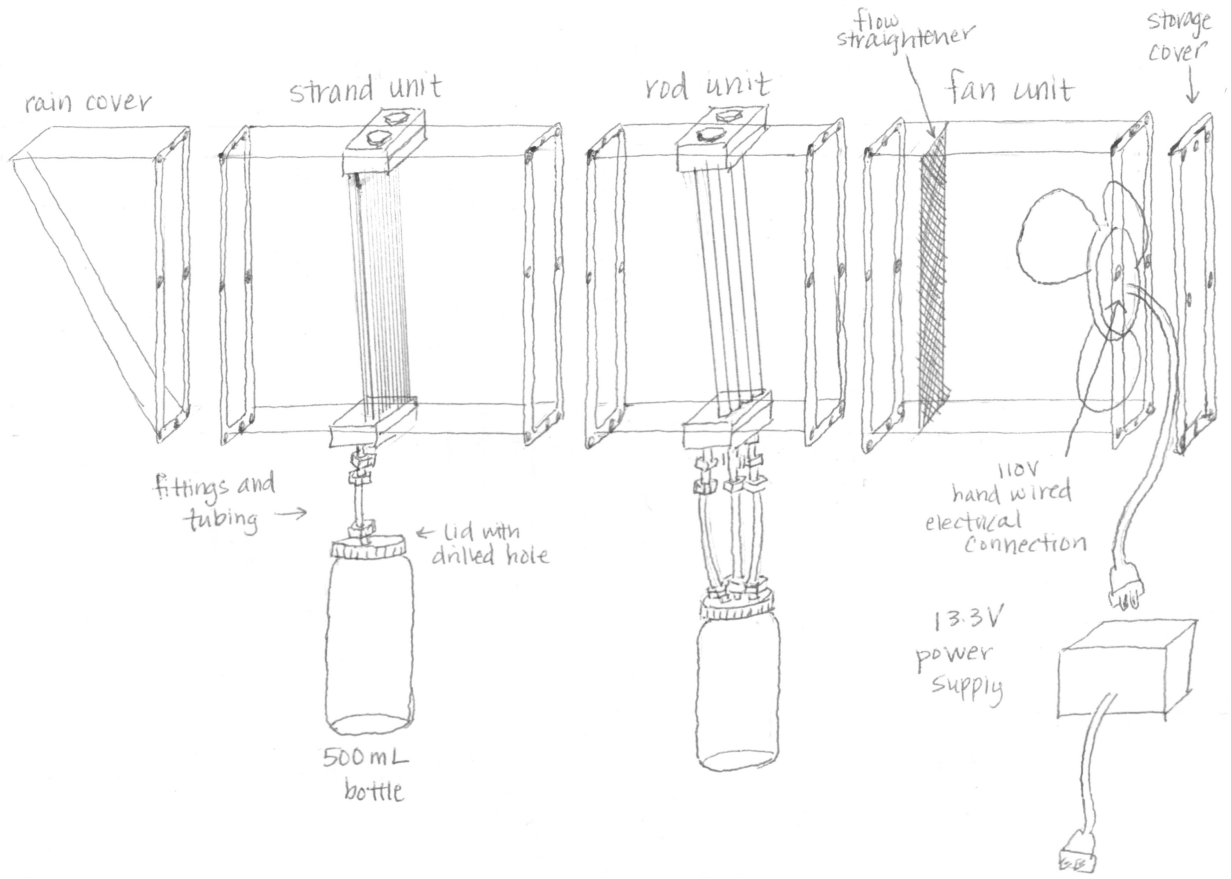

Figure A1-1. Size-fractionating Caltech Active Strand Cloudwater Collector (sf-CASCC) setup schematic

Overview

The CASCC collector (Caltech Active Strand Cloudwater Collector) is an active Cloudwater collector with Teflon strand and rod collection surfaces and a fan to pull the air past the strands/rods. The collector is housed in a rectangular PlexiGlas box. There are small hose connections for Teflon tubes at the bottom of the collector where the sample is collected. The sf-CASCC is a relatively large CASCC model equipped with two or three stages of strand or rod cassettes. The largest size fraction of cloud drops is collected on cylindrical Teflon rods in the front of the collector, which are aimed toward the fan and downward into several collection bottles. A mid-size fraction of

cloud drops can be collected on smaller rods. The smallest size fraction of cloud drops is collected on Teflon strands strung on cassettes (these strands are also what is used in the CASCC2).

Cleaning

Contaminants can accumulate in the CASCC during fog events, and should be removed prior to collection of fog from the next event. The Teflon strands in particular should be kept as clean as possible. Regular cleaning between fog events can be done using a spray bottle containing deionized water for small CASCCs; for larger CASCCs, a higher power sprayer such as that used for dispensing fertilizer can be used to spray through the collector body. Side doors in some of the collector units can be opened for easier access to the strands and rods.

Blanks

After thorough cleaning of the collector, blanks can be taken. Use a spray bottle to spray deionized water onto the collection strands. Spray approximately 500 mL into the collector. The water should run down the strands, into the Teflon trough, into the tube and then into the collection bottle. Use the first 300 mL or so to rinse the bottle and then discard the rinse water. Collect the final 100 mL of rinse water in the collection bottle, transfer 30 mL into a clean, labeled 30 mL polyethylene bottle, and discard the rest. A separate deionized water blank should be collected for each cloud/fog event.

Strand and rod cassettes

The three cassettes that hold the strands can be easily removed from the collector. On the top of the collector there are two flathead screws. Remove these screws and pull out the PlexiGlas section on top of the collection strands. Each of the three cassettes of Teflon strands can now be removed. These should be soaked and then rinsed with copious quantities of deionized water. A film may build up on the strands after sampling. This can be removed with a 1:100 aqueous solution of Triton X-100 surfactant and a clean KimWipe.

Housing

The PlexiGlas housing of the CASCC2 does not contact the cloud drops, but should be cleaned anyway. Spray the inside of the collector with deionized water and then carefully wipe the surfaces with a clean KimWipe. Alternatively, for more thorough cleaning, the housing can be submerged in a tub of deionized water.

Base of the collector

Pay special attention to cleaning the Teflon trough at the bottom of the collector. A film may form on this surface as well. This can also be cleaned with a 1:100 aqueous solution of Triton X-100 surfactant. Make sure this trough is well-rinsed after cleaning. Reinsert the clean cassettes of Teflon strands. Replace the PlexiGlas section on top of the strands and tighten the two screws.

Collection bottle and tube

Rinse the Teflon tube and collection bottle. The collection bottle is a 125 or 250 mL polyethylene narrow-necked bottle. Replace the bottle if it appears damaged or soiled. Attach the Teflon tube and collection bottle to the collector. The collector may need to be balanced between two small tables to allow the tube to hang down.

Storage

Dry the collector with KimWipes, cover the inlet with Parafilm, remove the collection bottle and tube and place the entire collector into a bag. Tape the bag securely to make sure it does not blow away or allow insects or birds to enter the collector. Place Parafilm over the end of the sample tube, making sure you keep the connector pieces secure (ferrule and nut) and place it and the collection bottle in a clean plastic bag.

Setup for Collection

The CASCC collector is mounted on a three-meter pole. The pole mounts to an H-shaped base with four bolts; the H-shaped base should be used regardless of the stand type to hold together the units of the CASCC. Use cinder blocks or water containers to stabilize the base.

There is an extra arm that provides stability for the front stage of the collector. It is attached with two u-bolts and four nuts. Lay the pole and base down flat on the ground. Insert the u-bolts over the pole near the tape marks on the pole. Place the flat plate of the arm over the bolts and lightly snug down the nuts.

Select a position that faces the collector into the prevailing wind, if no precipitation is expected, and refasten the four bolts. If precipitation is expected, it is best to position the collector inlet at right a angle to prevailing wind.

The sf-CASCC is held in place by a tie-down strap. The small fraction collection tube should protrude through the flange and the large drop sampling tube should sit behind the stabilizing arm. Place the collector on the top of the pole. Press the stabilizing arm up under the lip of the collector inlet and snug down the u-bolts tightly. Fasten the

tie-down strap across the top of the small drop collection portion of the collector to ensure it does not come loose from the stand.

Generally, two people are required to erect the sf-CASCC. One person can help lift from the front while another pulls on a guy wire from the back. Insert the hook from the guy wire into the eye on the pole and grasp it firmly in both hands. The other person can start lifting the collector from the front, gradually shifting down to push on the pole once the collector is raised out of reach. The person with the guy wire will then use one foot to pull down on the base of the collector.

Since the sf-CASCC is heavy and top-heavy, make sure the base is well stabilized. Place the hooks on the guy wires through the eye-bolts on the pole, fully loosen the turnbuckles, pull the wires out from the pole and pound in the stakes. Tighten the turnbuckles to make sure the wires are taut. These should also be tightened daily.

Power is supplied to the collector through a waterproof box that houses the power switch. The box is mounted to the pole. The cord on the back of the connector has an Amphenol connector which screws into the bottom of the box. A 120V A/C plug exits the box. Plug this cord in and ensure that the fan will turn on when the switch inside the box is thrown.

To prevent the bottles from coming loose in high winds, tape or cable tie the line to the pole. Ensure that the collection bottles will not be too heavy to remain connected to the collector by placing a support underneath the bottles, especially during heavy fog events; the sampling bottles can sit on top of the power box.

Cover the entire collector with a clean plastic bag until you are ready to begin sampling. Before each event, ensure that enzyme solutions (peroxidase and catalase) are active (see specific sections on H_2O_2 and S(IV) analyses for these instructions).

Collection

Log sheets (see Appendix A) should be used to record sample collection. Since the goal will be to collect sufficient volumes of fog water for several analyses including photo-oxidation experiments, sample collection times should depend on the flow of water into the sample bottle as well as any observed changes in meteorology or chemical composition during a fog event. Typical collection periods will be 3-5 hours.

The Particulate Volume Monitor (PVM) will be used to measure liquid water content (LWC); fog samples will be collected when LWCs greater than the specified threshold (0.05 g m^{-3}) are observed. The threshold may be reset for the sampling region, depending on the density of the fog/cloud.

When to begin sampling

Visibility should be less than ¼ mile (400 meters) to begin sampling, as a general rule. In practice, it is difficult to judge distance accurately at night when it is foggy. If possible, locate a landmark that should normally be visible at night which is approximately 400 meters away. Streetlights work very well for this since they are regularly spaced.

If no landmark is available, you can leave a light or flashlight on near the collectors and walk away from the collectors until you can no longer see the light. Try this form several directions, in case the fog appears thick from one direction but not from another.

Since starting the collectors too early would contaminate the collection surfaces with aerosol particles, and this would mean having to re-clean all the collectors, it is better to wait several minutes to see if the fog persists than to start the collectors when the fog is not thick enough.

In order to have consistent data, sampling periods should begin and end on the hour. Less than one hour is required to collect a sufficient volume of fog water with CASCC samplers. CASCC collectors collect water quickly and should be started when the fog forms. Run the samplers continuously until the fog dissipates, changing sample at the start of each hour. Collection bottles can be emptied into polyethylene containers of the appropriate volume (eliminate headspace as much as possible to avoid interaction with any gaseous contaminants).

The collector should be turned off prior to the end of the event to prevent evaporation (and thus concentration of the samples) within the collector.

Sampling periods for the collectors may be shortened to determine how rapidly changes in fog composition occur. Special directions will be provided for this situation if needed.

How to start collector

Once you've decided it's time to sample, remove the plastic bags from the collector. Turn the power on to the collector fan. Make sure the fan is rotating in the correct direction: as viewd from the back of the collector, the fan

should be rotating counter-clockwise so that air is flowing into the collector. The fan also has an arrow indicating the proper rotation direction.

Check that the sampling lines on the collector are connected and, once some water begins to accumulate, check that the water is flowing into the sample collection bottle. Record times and observations in the log sheet.

Caltech Active Strand Cloudwater Collector Version 2 (CASCC2)

(Source: Operating Procedures Manual, Cloudwater Collection and Analysis, Colorado State University Department of Atmospheric Science)

Overview

The CASCC2 collector is an active cloudwater collector with Teflon strand collection surfaces and a fan to pull the air past the strands. The collector is house in a rectangular PlexiGlas box. There is a small hose connection for a Teflon tube at the bottom of the collector where the sample is collected.

Cleaning

Contaminants can accumulate in the CASCC2 during fog events, and should be removed prior to collection of fog from the next event. The Teflon strands in particular should be kept as clean as possible. Regular cleaning between fog events can be done using a spray bottle containing deionized water. Side doors in some of the collector units can be opened for easier access to the strands and rods.

Blanks

After thorough cleaning of the collector, blanks can be taken. Use a spray bottle to spray deionized water onto the collection strands. Spray approximately 500 mL into the collector. The water should run down the strands, into the Teflon trough, into the tube and then into the collection bottle. Use the first 300 mL or so to rinse the bottle and then discard the rinse water. Collect the final 100 mL of rinse water in the collection bottle, transfer 30 mL into a clean, labeled 30 mL polyethylene bottle, and discard the rest.

Strand and rod cassettes

The three cassettes that hold the strands can be easily removed from the collector. On the top of the collector there are two flathead screws. Remove these screws and pull out the PlexiGlas section on top of the collection strands. Each of the three cassettes of Teflon strands can now be removed. These should be soaked and then rinsed with copious quantities of deionized water. A film may build up on the strands after sampling. This can be removed with a 1:100 aqueous solution of Triton X-100 surfactant and a clean KimWipe.

Housing

The PlexiGlas housing of the CASCC2 does not contact the cloud drops, but should be cleaned anyway. Spray the inside of the collector with deionized water and then carefully wipe the surfaces with a clean KimWipe. Alternatively, for more thorough cleaning, the housing can be submerged in a tub of deionized water.

Base of the collector

Pay special attention to cleaning the Teflon trough at the bottom of the collector. A film may form on this surface as well. This can also be cleaned with a 1:100 aqueous solution of Triton X-100 surfactant. Make sure this trough is well-rinsed after cleaning. Reinsert the clean cassettes of Teflon strands. Replace the PlexiGlas section on top of the strands and tighten the two screws.

Collection bottle and tube

Rinse the Teflon tube and collection bottle. The collection bottle is a 125 or 250 mL polyethylene narrow-necked bottle. Replace the bottle if it appears damaged or soiled. Attach the Teflon tube and collection bottle to the collector. The collector may need to be balanced between two small tables to allow the tube to hang down.

Storage

Dry the collector with KimWipes, cover the inlet with Parafilm, remove the collection bottle and tube and place the entire collector into a bag. Tape the bag securely to make sure it does not blow away or allow insects or birds to enter the collector. Place Parafilm over the end of the sample tube, making sure you keep the connector pieces secure (ferrule and nut) and place it and the collection bottle in a clean plastic bag.

Setting Up for Collection

The CASCC2 collector is mounted on a three meter pole. The pole mounts to an H-shaped base with four bolts. Use cinder blocks or water containers to stabilize the base. The collector attaches to a flange on top of the pole with four hex-head bolts. Remove the collector from the bag, place it on the shelf of the ladder and then climb the ladder. Attach the collector using the four bolts and an Allen wrench. Removing the four Allen bolts that are threaded up into the bottom of the mounting bracket will allow the collector to rotate. Select a position that faces the collector into the prevailing wind, if no precipitation is expected, and refasten the four bolts. If precipitation is expected, it is best to position the collector inlet at a right angle to the prevailing wind.

Power is supplied to the collector through a waterproof box that houses the power switch. The box is mounted to the pole. The cord on the back of the connector has an Amphenol connector which screws into the bottom of the box. A 120V A/C plug exits the box. Plug this cord in and ensure that the fan will turn on when the switch inside the box is thrown.

To prevent the bottles from coming loose in high winds, tape or cable tie the line to the pole. Ensure that the collection bottles will not be too heavy to remain connected to the collector by placing a support underneath the bottles, especially during heavy fog events; the sampling bottles can sit on top of the power box.

If you anticipate high winds or a long set-up time, the three guy wires should be attached. Loosen the three turnbuckles all the way and then insert the hooks into the three eye bolts on the pole. Loop the other end of the wires around the stakes. Pull the lines out from the collector and then pound in the stakes with a 2-pound hammer. Try to ensure the guy wires are not set up so that you have to walk by them to access another instrument. The wires become almost invisible at night during fog events and can cause injury if you trip over them. Tighten the turnbuckles until the lines are taut. Check the tightness of the guy wires daily.

Collection

It is very important to keep everything which might come in contact with the samples very clean. Latex examination gloves should be worn when handling samples, and these should be rinsed thoroughly with deionized water.

It is also important to keep the deionized water from becoming contaminated. If there is any question whether a squeeze bottle has become contaminated (by falling on the ground, handling of the tube, etc.), it should be emptied and thoroughly rinsed with deionized water.

Labeling and recording

Bottles should be labeled with a permanent marker and with a paper label to make sure every sample is correctly identifiable by other scientists, and after coming into contact with water.

The volume of sample collected should dictate the size of the bottle used. Polyethylene bottles with 30, 60, and 125 mL volumes should be used for the sf-CASCC and the CASCC2.

Each sample should be labeled with a code of the form SCCMMDDYY#, where S represents the sampling site, CC represents the fog collector type, MM represents the month, DD represents the date, YY represents the year, and ## represents the sample number collected with that collector at that site on that date. Codes for sampling site and collector types are listed at the bottom of the project log sheets. The date used for nighttime fog should be the date corresponding to the morning at the end of the fog event. For example, if a fog sample is collected from the CASCC2 collector at Bakersfield from 10:00-11:00 pm on the night of 12/24/14, and is the second CASCC2 sample collected during that event, the sample should be labeled BCC12259502. Note the use of 12/25 as the sample date since the event is expected to bridge the dates of 12/24 and 12/25.

Log sheets (see the example at the end of this Appendix) should be used to record sample collection. Since the goal will be to collect sufficient fog water for several analyses including photo-oxidation experiments, sample collection times should depend on the flow of water into the sample bottle as well as any observed changes in meteorology or chemical composition during a fog event. Typical collection periods will be 3-5 hours.

The Particulate Volume Monitor (PVM) will be used to measure liquid water content (LWC); fog samples will be collected when LWCs greater than the specified threshold (0.05 g m^{-3}) are observed. The threshold may be reset for the sampling region, depending on the density of the fog/cloud.

When to begin sampling

Visibility should be less than ¼ mile (400 meters) to begin sampling, as a general rule. In practice, it is difficult to judge distance accurately at night when it is foggy. If possible, locate a landmark that should normally be visible at night which is approximately 400 meters away. Streetlights work very well for this since they are regularly spaced.

If no landmark is available, you can leave a light or flashlight on near the collectors and walk away from the collectors until you can no longer see the light. Try this form several directions, in case the fog appears thick from one direction but not from another.

Since starting the collectors too early would contaminate the collection surfaces with aerosol particles, and this would mean having to re-clean all the collectors, it is better to wait several minutes to see if the fog persists than to start the collectors when the fog is not thick enough.

In order to have consistent data, sampling periods should begin and end on the hour. Less than one hour is required to collect a sufficient volume of fog water with CASCC samplers. CASCC collectors collect water quickly and should be started when the fog forms. Run the samplers continuously until the fog dissipates, changing sample at the start of each hour. Collection bottles can be emptied into polyethylene containers of the appropriate volume (eliminate headspace as much as possible to avoid interaction with any gaseous contaminants).

The collector should be turned off prior to the end of the event to prevent evaporation (and thus concentration of the samples) within the collector.

Sampling periods for the collectors may be shortened to determine how rapidly changes in fog composition occur. Special directions will be provided for this situation if needed.

Massing sample bottles

Every sample should be massed and the value recorded in the field logbook. In order to determine how much water was present in the sample bottle, we need measurements of how much the bottles weigh when labeled and capped, but without any sample.

After leveling and taring the balance, mass a sample bottle and record the reading and type of bottle on the project sheet. After fog water has been collected in the bottle, re-mass the bottle and record the final mass. Keep in mind that the density of water is approximately 1 g /ml and check that the approximate mass of the volume collected makes sense relative to the mass measured.

How to start collector

Once you've decided it's time to sample, remove the plastic bags from the collector. Turn the power on to the collector fan. Make sure the fan is rotating in the correct direction: as viewd from the back of the collector, the fan should be rotating counter-clockwise so that air is flowing into the collector. The fan also has an arrow indicating the proper rotation direction.

Check that the sampling lines on the collector are connected and, once some water begins to accumulate, check that the water is flowing into the sample collection bottle. Record times and observations in the log sheet.

Sample removal

Before beginning sampling, label and weigh two collection bottles (with caps on) for each CASCC collector stage. Write the tare weight on the bottle label for later use. Taking samples from the sf-CASCC and CASCC2 collectors is then relatively simple and quick. First, gently shake the collector by tugging on one of the guy wires. This ensures that all of the sample collected will flow down the sampling tube and into the collection bottle. Next, remove the collection bottle from the end of the sampling line by unscrewing the polyethylene top. Replace the collection bottle with the second bottle previously prepared for that collector stage, using the second cap to cap the collection bottle just removed.

Operating Procedure: Gerber Scientific, Inc. Particulate Volume Monitor (PVM-100)

Source: Operator's Manual for Model PVM-100 (GSI, 1993)

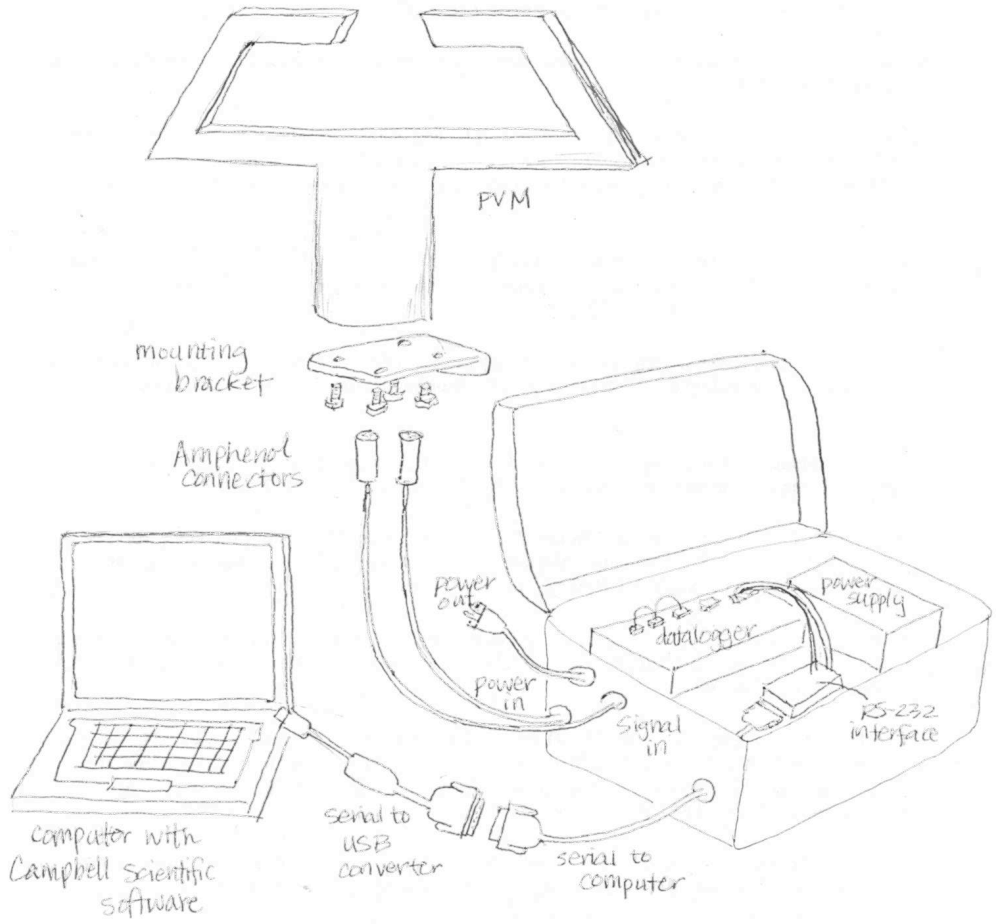

Figure A1-2. Particulate Volume Monitor (PVM) setup schematic.

Cleaning and Maintenance

Prior to use and regularly during use, empty volume within the arms should be cleaned so that no insects, dust build-up, or spider webs interact with the laser beam of the PVM. Additionally, the collimator lens should be regularly cleared of any condensation when high liquid water contents and/or wind directions parallel to the arms are observed. The following cleaning procedure should be used:

- Remove the weather cover to the transmitter and pull the air tube off of the elbow on the manifold.
- Remove the collimator lens assembly from the arm by removing the two screws that hold the assembly in place, and by removing heater B.

- Clean the collimator lens which is permanently attached to the lens holder. A suggested method for cleaning: Use luke warm water and mild saop (with no lotion content) and cotton swab to wash the front and the rear surface of the lens. Rinse with clean luke warm water, and blow off any drops that remain on the lens (residue from evaporated droplets will cause a large optical offset). Cleaning the lens with organic type cleaners is also possible. Avoid excessive use of the organic cleaners because they tend to soften the epoxy that holds the lens in place.
- Reassemble the collimator lens assembly, install in the arm, and attach heater B and air tube. Note that the lens holder must be installed with the "TOP" up.

If insects are common, insecticide tape can be used on the inside of the arms (not to the end of the receiver arm).

The filtered air flow to the transmitter arm should also be regularly checked: the flow may be blocked without a change in the sound of the instrument running.

The PVM is not designed to operate in a condensing atmosphere (in cloud) with the power to the instrument turned off. Six heaters in the instrument are used to keep condensation from forming inside. When power must be turned off (e.g., lightning activity), turn off the instrument's power for the minimum amount of time. For longer periods of time without power, bring the instrument indoors.

The air pump has a rated lifetime of about 1 year. In an atmosphere with significant ozone content, the pump lifetime is less. Replacement air pumps are available from GSI. Replace the air pump in the following manner: remove the cylindrical cover of the electronic enclosure; remove 4 screws that hold down each temperature control board. Gently move these boars aside without unsoldering any wires. Unsolder pump leads from terminal strip directly below the lower temperature control board, and unscrew the clamp that holds the pump in place. Pull off the plastic tubing from the bottom and side of the pump. To install the new pump, reverse this procedure. If used under ambient conditions, the air filter has an indefinite lifetime.

Removal of the cylindrical cover to the electronic enclosure:

- Turn the power switch to OFF and unplug the instrument from the wall.
- Remove the 6 screws that hold the cover in place, while the instrument is held standing upside down.

- Carefully and slowly raise the enclosure until it clears the instrument so that internal components are not damaged.

Setup for Collection

- Attach the mountain bracket to the 4 bolts on the base plate of the electronics enclosure.
- Use the pipe clamps to clamp the instrument to a vertical or horizontal pipe not larger than 5 cm (2 in.) outside diameter. The PVM can be mounted in a fixed position. The effect of wind direction on the instrument's outputs is small because of the large separation between transmitter and receiver arms, and the narrowness of the arms. However, the ideal position of the PVM is with the arms perpendicular to the wind. In this position the effect of extreme weather on the instrument's optics is minimal.
- Attach the power cord to the power connector on the base plate, and plug the power cord into a proper main power receptacle. For safety reasons, and the accurate operation of the PVM-100, it is necessary that the instrument is properly grounded through the ground conductor of the power cord. The main receptacle should have a ground terminal with continuity to a good local ground.
- Attach the signal cable to the output connector on the base plate. Connect the tinned leads of the other end of the cable to recording means with an input impedance of at least 10 KOhm per channel.
- Turn the power switch on the base plate ON, and remove the tape covering the openings in the arms.

Calibration

The following calibration procedure adjusts the sensitivity of the PVM-100, nulls out voltage offsets, and checks the health of the electronics, laser diode, and detectors:

a. Permit the instrument to warm up for 10 minutes before starting the calibration procedure.

b. Block the laser beam between the arms of the instrument with an opaque object, and adjust the ZERO potentiometers located on the base plate to produce voltage outputs of 0.000 V for channels 1 and 2. This procedure removes the electronic offset in the voltage output of each channel.

c. Hold the open end of the calibration disk against the opening on the receiver arm. Adjust the fine SPAN controls on the base plate to produce output voltages in channels 1 and 2 equal to the calibration voltages listed in CALIBRATION DATA. (If the fine SPAN controls do not have sufficient range to obtain the desired voltages, use the coarse SPAN control.) The fine SPAN adjustment on the base plate is preset to

about its center position to give equal room for adjustment in both directions. In case the required calibration voltages cannot be obtained by adjusting the fine SPAN controls, the coarse SPAN control located on the main board must be used:

1. Adjust the fine SPAN control to about its central position.
2. Remove the cylindrical cover from the electronic enclosure (power OFF).
3. Adjust the coarse SPAN controls R4 in channels 1 and 2 to obtain the required calibration voltages (power ON), while holding the calibration disk against the receiver arm opening.
4. Find adjust the SPAN with the fine SPAN adjust on the base plate. Re-attach the cover with power OFF.
5. Repeat steps (2) and (3) twice.
6. Remove the calibration disk from the receiver arm, and use the ZERO potentiometers on the base plate to produce outputs of 0.000 V in channels 1 and 2. This procedure removes the optical offset in the voltage output of each channel. (Note: if the laser beam is now blocked, negative voltages equivalent to the optical offset will appear in channels 1 and 2.)
7. The optical offset voltages are typically 10-20 mV. These voltages will become larger as the collimator lens becomes dirty through use. The ZERO potentiometers on the base plate have a large adjustment range so that large optical offsets can be nulled out. It is good practice to clean the collimator lens when the optical offsets exceed about 50 mV.

Table A1-1. PVM calibration data.

Parameter	Ch. 1 PSA (cm^2 m^{-3})	Ch. 2 LWC (g m^{-3})	Ch. 1 3.75 μm (km^{-1})	Ch. 2 10.6 μm (km^{-1})	Ch. 3 R_e (μm)
Calibration Voltage (V)	0.705	0.117			
Scaling Factor	3000	1.00			10

V1 (divider scaling) = 2.000V, V2 (denominator limit) = 2.000V

The output voltages in the channels 1, 2, and 3 must be multiplied by the scaling factors given in the preceding table to produce values of the parameters listed in the table.

The calibration voltages for 3.75 μm and 10.6 μm aerosol optical extinction are referenced to oceanic aerosol at a relative humidity of 80%. When values of the extinctions are desired for other aerosol types and relative humidities, correction factors must be applied to the calibration voltages. See Gerber (1991) for details.

Collection

The instrument should be operated when liquid water forms at the surface level, to detect whether fog particles are present. If fog is present (if the atmospheric liquid water content is 0.05 g m^{-3}), the cloud water collectors should be started.

Teardown and Shipping

The PVM-100 is shipped in a large plastic case with foam that fits to the instrument. Accessories including the calibration unit can be put in the case with the instrument.

Overview of Analyses

The following analyses can be carried out for each fog sample collected; analyses are listed in order of priority:

pH

Pipet 0.5 mL sample to a clean plastic centrifuge vial. Label the sample. Analyze immediately (seem Operating Procedure: pH Analysis: Measurement).

Inorganic Anions and Cations

Pipet 0.5 mL sample to a clean 0.8 mL plastic autosampler vial. Label the vial with the sample name and "IC". Freeze as soon as possible.

Total S(IV)

Pipet 1 mL sample into a 1.5 mL plastic autosampler vial. Add 100 µL "S(IV) preservative solution". Add 100 µL bovine catalase solution. Cap and mix completely. Label the vial with the sample name and "S(IV)". Freeze as soon as possible.

Total Formaldehyde

Pipet 1 mL sample to a clean 1.5 mL glass autosampler vial. Add 100 µL "formaldehyde preservative solution". Cap and mix completely. Label the vial with the sample name and "HCHO".

Peroxides

Pipet 1 mL sample to a 2 mL plastic autosampler vial. Add 200 µL "conditioning reagent". Add 200 µL "fluorescent reagent". Cap and mix completely. Label the vial with the sample name and "H_2O_2". Freeze as soon as possible.

Organic Acids

Pipet 50 µL CH_2Cl_2 to a clean 2 mL plastic autosampler vial. Add 0.5 mL sample. Cap and mix completely. Label the vial with the sample name and "OA". Freeze as soon as possible.

Carbonaceous Precursors

Aliquots for this analysis (0.5 mL sample to a clean 2 mL glass autosampler vial) will be taken at CSU after shipping to the US.

Water Soluble Organic Carbon

Aliquots for this analysis (1 mL sample, diluted to 5 mL in a brown plastic bottle) will be taken at CSU after shipping to the US. The sample should be filtered using a rinsed filter with <1μm pore size should be carried out before dilution.

The total sample volume per sample for these analyses will be 6 mL. All remaining sample can be used for photo-oxidations; if there is insufficient sample volume from some samples, the samples can be combined to make a composite over a reasonable time period (this is particularly relevant if the samples are from the same fog event and the chemical parameters measured for the samples are similar).

Operating Procedure: pH Analysis

Analysis Location

Analysis will be carried out at the sampling location (within approximately one hour of collection).

Calibration

- Calibration should be carried out immediately after cloudwater collectors have been started and are successfully collecting. At least two points (pH 4 and 7) should be used to calibrate the pH meter and electrode.
- The pH meters are Orion models 250A or 290A. These meters are nearly identical. To attach the electrode (Cole-Parmer EW-05990-45 electrode) to the meter, twist the silver-colored BNC connector onto the top of the meter. Ensure that a battery is installed or that the power adapter is plugged into the meter and into the wall socket (the adapter is useful for 110-220V wall supplies, although this should be verified).
- Turn on the pH meter by pressing the "ON" button. To deactivate the automatic power shutoff feature, press "2nd-setup", press "yes" until you reach page "1-4", then turn it "off" by pressing the up arrow. Press measure to return to measurement mode. Setup menus are also listed on the back of the meter. If the meter should shut off for any reason, the calibration data is saved, and you simply have to press the "ON" button.
- Adjust the temperature shown at the bottom of the screen to the temperature of the room you're working in by pressing the "up" or "down" arrows on the front of the meter. Look at the pH buffer solution bottles for the exact pH of the buffer solutions at the current temperature in your lab area.
- Rinse the electrode into a beaker with deionized water. Place four clean 1 mL cryovials into a vial holder. Pipette 1 mL of pH 4 buffer into two vials and pipette 1 mL of pH 7 buffer into the two other vials. Two of these vials (one pH 4 and one pH 7) will be for washing, and the others for calibration.
- Rinse the pH electrode with deionized water and place in the wash pH 7 buffer. Remove it, and then place it in the calibration pH 7 vial. Press "2nd" then "Cal" on the pH meter. The display should show some numbers and then the word "calibrate" should appear on the top of the screen. Wait for the meter to beep and display "ready" (this could be a minute or so). If the correct value is shown (this should be the value you read on the buffer solution bottle), press "yes" and remove the electrode from the pH 7 buffer. If not, press the up and down buttons to select the correct value, then select "yes". The meter will then ask for a second calibration point.
- Rinse the electrode with deionized water and shake it gently, until no more water drips off. Place it into the wash pH 4 buffer, remove it and then place it into the 2nd pH 4 buffer. Wait for the meter to beep and display

"ready", and then see what pH the meter is reading. If the correct value is shown, press "yes". If not, press the up and down buttons to select the correct value, then select "yes". Remove the electrode from the pH 4 buffer, rinse it with deionized water, and place it into a vial containing storage solution.

- The "slope" value that appears on the pH meter after the calibration should be 100 +/- 2 (between 98 and 102). If this is not true, the calibration should be repeated until the "slope" is within this range. If a higher pH range is desired, a pH 10.00 buffer can be used. The 250A meter will not prompt for a third point, and a second calibration should be done. The 290A meter will prompt for the third point, which can be carried out using the pH 10.00 buffer solution, or avoided by pressing "measure" after the second calibration point is accepted.
- Check buffers between every 3-5 samples, or every half hour. The pH should be within 0.03 pH units.

Measurement

- Place two 1 mL polyethylene cryovials into a vial holder. Pipette 500 µL sample into one vial for washing the electrode, and 1 mL sample into the other vial for measurement. Rinse the electrode with water and shake to remove excess water. Place the pH probe into the wash vial. Remove the probe from the first vial and shake off excess solution. Place the probe into the second vial, making sure it is in contact with the sample. Write down the pH on the project log sheet when the reading first stabilizes (typically approximately 1-3 min). If the equilibration process takes longer than ~5 sec, parafilm or foil should be placed over the top of the sample so that atmospheric CO_2 is not allowed to equilibrate with the solution and change the pH.
- Repeat the measurement three times, and report the mean value of these three pH values. Record all three measurements in your lab notebook for future reference.
- Rinse the electrode with deionized water and place it into the storage solution. If the electrode will not be used again for at least ~30 min, wrap the top of the storage solution vial with Parafilm.

Storage of Samples

No sample storage is necessary because pH should be measured at the cloud water/fog water collection site. Buffer solutions should not be emptied down the drain; they can be thrown out or emptied into a non-halogenated waste jar. Water from rinsing the pH electrode can be dumped down the drain.

Operating Procedure: Cation and Anion Ion Chromatography

Principle of Analysis

Dionex ion chromatograph (IC) systems are attached to a Dionex autosamplers that allow random access to the sampling vials. This allows you to run the same standards at the beginning and end of each run of samples. In addition, the autosampler can be programmed to automatically run duplicate samples.

To make sure that the IC is running properly while unattended during a long run, periodic duplicates are run as well as standards. At the beginning of each run of samples, regardless of whether they are run for anions, cations, or organic acids, a deionized water blank is loaded. Then ten standards are run, followed by another blank sample. Ten samples are then run, the last of which is injected twice. After this duplicate, one of the standards is run. Samples continue to be run in groups of ten, ending with a duplicate injection followed by a standard injection, until the sample set to be analyzed is complete. At the end of the samples, all ten standards are run again before turning off the instrument.

This procedure provides a check on whether the response of the instrument changes during the course of a run as well as information on the reproducibility of the injections.

Calibration

- Stock solutions of anions, cations, and organic acids should be prepared for the analyses. The anion and cation stock solutions can be prepared in advance and stored in polyethylene bottles in the refrigerator for up to a week. The organic acids tock solution should be prepared immediately before analysis.
- The anion stock solution is prepared as follows: 0.005 M chloride (0.292 g/L sodium chloride), 0.01 M nitrate (0.850 g/L sodium nitrate), 0.01 M nitrite (0.690 g/L sodium nitrite), and 0.005 M sulfate (0.710 g/L sodium sulfate). Mass the above chemicals and place them in a clean 1 L volumetric flask. Fill the flask half way with deionized water and gently shake the flask to dissolve the crystals. Sonicate if the crystals do not dissolve, and if a sonication bath is available. Fill the flask to 1 L with deionized water and invert three times to mix.
- The cation stock solution is prepared as follows: 0.0025 M calcium (0.368 g/L calcium chloride di-hydrate)), 0.0025 M magnesium (0.508 g/L magnesium chloride hexa-hydrate), 0.01 M ammonium (0.535 g/L ammonium chloride), 0.005 M sodium (0.292 g/L sodium chloride), and 0.005 M potassium (0.373 g/L potassium chloride). Mass the above chemicals and place them in a clean 1 L volumetric flask. Fill the flask half way with deionized

water and gently shake the flask to dissolve the crystals. Sonicate if the crystals do not dissolve, and if a sonication bath is available. Fill the flask to the 1 L mark with deionized water and invert three times to mix.

- The organic acids stock solution is prepared as follows: 0.01 M acetate (0.820 g/100 mL sodium acetate), 0.01 M formate (0.680 g/100 mL sodium formate), 0.005 M oxalate (1.261 g/100 mL oxalic acid), 0.01 M propionate (0.961 g/100 mL sodium propionate), 0.01 M pyruvate (1.100 g/100 mL sodium pyruvate). Mass the above chemicals and place them in a clean 1 L volumetric flask. Fill the flask half way with deionized water and gently shake the flask to dissolve the crystals. Sonicate if the crystals do not dissolve, and if a sonication bath is available. Fill the falsk to the 1 L mark with deionized water and invert three times to mix.
- Preparation of standards from stock solutions: All these dilutions are prepared in the same way. Wear cleaned (rinsed) latex examination gloves when preparing the standards to prevent contamination. Pipette the appropriate amount of stock solution into a clean 100 mL volumetric flask. Fill the flask with deionized water to the fill line. Mix thoroughly by inverting 3-5 times. Transfer the solution to the appropriately labeled standard polyethylene bottle. The bottle volume is only 30 mL and there will be 100 mL solution; rinse the bottle thoroughly with the stock solution twice and fill the bottle.

Table A1-2. Calibration solutions for anion ion chromatography.

Standard Number	Concentration (µM)	Volume Stock Sltn. to 100 mL (µL)
1	2 µM NO_3^-, NO_2^-/ 1.67 µM PO_4^{-3}/1 µM Cl^-, SO_4^{-2}	20
2	4/2.67/2	40
3	10/6.67/5	100
4	20/13.3/10	200
5	50/33.3/25	500
6	100/66.7/50	1000
7	200/133/100	2000
8	400/267/200	4000
9	800/533/400	8000
10	1600/1070/800	16000

Table A1-3. Calibration solutions for cation ion chromatography.

Standard Number	Concentration (μM)	Volume Stock Sltn. to 100 mL (μL)
1	1 μM Na^{+},K^{+}/0.5 μM Ca^{+2},Mg^{+2}	20
2	4/2/1	40
3	10/5/2.5	100
4	20/10/5	200
5	50/25/12.5	500
6	100/50/25	1000
7	200/100/50	2000
8	400/200/100	4000
9	800/400/200	8000
10	1600/800/400	16000

Table A1-4. Calibration solutions for organic acids ion chromatography.

Standard Number	Concentration (μM)	Volume Stock Sltn. to 100 mL (μL)
1	2 μM acetate, formate, pyruvate, propionate, 1 μM oxalate	20
2	4/2	40
3	10/5	100
4	20/10	200
5	50/25	500
6	100/50	1000
7	200/100	2000
8	400/200	4000
9	800/400	8000
10	1600/800	16000

Inorganic Anion Analysis (SAX IC)

Analysis Location

Analysis will be carried out at Hankuk University of Foreign Studies in Seoul, Korea

Analysis

- Anions are analyzed with a Dionex AS41-SC analytical column preceded by a AG4A-SC guard column. Suppression is with a Dionex Anion Self Regenerating Suppressor (ASRS-1), and detection is by a Dionex conductivity detector. An AS3500 autosampler is used to introduce the samples into the column. The sample loop volume is 50 μL.
- The anion eluent is 1.8 mM sodium carbonate/1.7 mM sodium bicarbonate. The eluent is prepared from a stock solution of 180 mM sodium carbonate/170 mM sodium bicarbonate. 20 mL stock solution is added to a clean plastic 2 L eluent reservoir which is then filled with deionized water (with a conductivity of at least 18 mega ohm-cm) to the 2 L mark. The eluent is then degassed with helium for five minutes.
- The eluent stock solution is prepared by adding 19.08g sodium carbonate and 14.28 g sodium bicarbonate to a clean 1 L glass volumetric flask and adding deionized water to the 1 L mark. This solution should be stored in a tightly capped polyethylene bottle in the refrigerator.
- The pump is primed for one minute at 9 mL per minute with the waste bypass valve open. The valve is then closed, and the system is started with a flow rate of 2 mL per minute and left to equilibrate for one hour before starting analyses. Note the time, pressure and total conductivity in the IC logbook now and hourly with the instrument is running. Expected background conductivity for the cation analysis is approximately 2.8 μS.
- Previously prepared IC vials are then loaded into the racks of the autosampler. A set of ten cation standards at varying solutions is also loaded into vials and placed into the autosampler (see “Calibration”).

Inorganic Cation Analysis (SCX IC)

Analysis Location

Analysis will be carried out at Hankuk University of Foreign Studies in Seoul, Korea

Analysis

- Cations are analyzed with a Dionex CS-12 analytical column preceded by a CG-12 guard column, with a Dionex cation self regerating suppressor (CSRS-1) operating in auto suppression recycle mode. Detection is with a Dionex conductivity detector. Injections are made by an AS3500 autosampler with a 50 µL sample loop.
- The eluent is 20 mM methanesulfonic acid (MSA), prepared from concentrated MSA and deionized water. 2.6 mL concentrated MSA is added to a 2 L plastic eluent reservoir. Deionized water is added to the 2 L mark, and the eluent is then degassed with helium for five minutes.
- The pump is primed for one minute at 9 mL per minute with the waste bypass valve open. The valve is then closed, and the system is started with a flow rate of 1 mL per minute and left to equilibrate for one hour before starting analyses. Note the time, pressure and total conductivity in the IC logbook now and hourly with the instrument is running. Expected background conductivity for the cation analysis is between 1 and 2 µS.
- Previously prepared IC vials are then loaded into the racks of the autosampler. A set of ten cation standards at varying solutions is also loaded into vials and placed into the autosampler (see "Calibration").

Organic Acid Analysis (WAX IC)

Analysis Location

Analysis will be carried out at the Atmospheric Science Department at Colorado State University.

Collection of Samples

A 1 mL aliquot of each collected fog sample will be filtered through a washed 0.2 µm syringe filter and stored, frozen, in a 2 mL glass autosampler vial until analysis. To each vial should be added 20 µL chloroform prior to storage.

Analysis

- Organic acids are analyzed with a Dionex AS11-HC analytical column preceded by a AG11 guard column. Suppression is with a Dionex Anion Self Regenerating Suppressor (ASRS-1), and detection is by a conductivity detector. An AS3500 autosampler introduces the samples to the column. The sample loop volume is 100 µL.

- The organic acids eluents are 5 mM sodium hydroxide and 100 mM sodium hydroxide. The eluents are usually prepared from sodium hydroxide pellets: 200 mg and 4.00g sodium hydroxide, respectively, are added to a clean 1 L volumetric flask, which is filled with water. The eluent is degassed with helium for five minutes.
- The pump is primed for one minute at 9 mL per minute with the waste bypass valve open. The valve is then closed, and the system is started with a flow rate of 1 mL per minute and left to equilibrate for one hour before starting analyses. Note the time, pressure and total conductivity in the IC logbook now and hourly with the instrument is running. Expected background conductivity for the cation analysis is approximately 1-2 µS.
- Previously prepared IC vials are then loaded into the racks of the autosampler. A set of ten cation standards at varying solutions is also loaded into vials and placed into the autosampler (see "Calibration").
- The separation method for the organic acid IC analysis is as follows:

Flow rate: 1.2 mL min^{-1}
Injection volume: 80 µL
Detector collection rate: 5.00 Hz
Gradient:
Solvent A = deionized water;
Solvent B = 5 mM NaOH;
Solvent C = 100 mM NaOH

Time (min)	Solvent Ratio
Initial	80% A/20% B
0	80% A/20% B (Inject)
6.50	80% A/20% B
25.00	82% A/18% C
30.00	82% A/18% C
40.00	70% A/30% C
45.00	70% A/30% C
46.00	80% A/20% B
50.00	80% A/20% B

Total analysis time: ~53 min including injection time

Operating Procedure: S(IV) Analysis

Principle of Analysis

Since S(IV) in cloudwater can be readily oxidized by H_2O_2, O_3, and O_2 in the presence of transition metals, samples should be preserved as soon as possible after collection. Preservation is accomplished by adding a preserving solution containing formaldehyde, CDTA (*t*-1,2-cyclohexylenedinitrilo-tetraacetic acid) and sodium hydroxide. The method for preparing the S(IV) preserving solution is described below. The ratio of preservation solution to cloudwater is 1:15.

The principle of preservation is that S(IV) reacts rapidly with formaldehyde to form hydroxymethanesulfonate (HMS). HMS is stable in the preserved cloudwater samples since it is not easily oxidized. HMS formed in the preserved cloudwater can then be easily decomposed to free S(IV) before analysis. CDTA in the preservative solution prevents interference of trace metals in the S(IV) analysis. A catalase solution is also added to the samples to destroy any H_2O_2 in cloudwater, since aqueous oxidation of S(IV) by H_2O_2 is a very fast reaction and could interfere with the measurements. Preserved samples should be kept at 4°C until analysis.

S(IV) in cloud sample is preserved as HMS. During analysis HMS is first decomposed to HCHO and free S(IV) by adding strong base, and then free S(IV) and HCHO can react with acidic pararosaniline to form a purple compound, which can be measured spectrophotometrically. A mechanism for the color compound formation is recommended by Dasgupta (1980):

$(NH_2Ph)_3C^+ + HCHO \rightarrow (NH_2Ph)_2C^+PhNHCH_2OH \rightarrow (NH_2Ph)_2C^+PhNHCH_2SO_3H$

$(NH_2Ph)_2C^+PhNHCH_2OH \rightarrow (NH_2Ph)_2C^+PhNHCH_2SO_3H$

$(NH_2Ph)_2C^+PhNHCH_2SO_3H + HCHO \rightarrow$ etc.

Optimum color development is reached at approximately 14 min.

Calibration

Authentic standards of S(IV) containing species at various concentrations in the range anticipated should be analyzed using the described method to generate a calibration curve.

Storage of Samples

Pipet 1 mL cloudwater into a 1.5 mL plastic autosampler vial. Add 100 µL "S(IV) preservative solution". Add 100 µL bovine catalase solution. Cap and mix completely. Label the vial with the sample name and "S(IV)". Keep frozen, if possible, until analysis.

Catalase Enzyme Activity Test

Pipette 1 mL deionized water into a 1.5 mL glass vial. Add 100 µL 1.0 mM H2O2 solution and 100 µL catalase solution. Cap and mix completely. Add 200 µL "conditioning reagent and 200 µL "fluorescent reagent". Cap and mix completely. Label with the date and "catalase check."

Measurement

- Connect the Shimadzu UV-1800 UV/visible absorption spectrophotometer to a computer via a USB cable. Turn on the spectrophotometer (power button is on the bottom of the right side of the instrument). Wait for the instrument self-checks, then press "Enter" at the login screen (no password should be set). From the main menu, select "Other", followed by "PC Control".
- From the computer, install the spectrophotometer. Follow the New Hardware setup wizard and insert the UV Probe software CD when prompted.
- Open the UV Probe application and select "Instrument Bar" from the "View" menu. Add an instrument by selecting "Add" from the "Instrument" menu. Follow the wizard, entering the model name (UV-1800) and the serial number listed on the side of the instrument. It may be necessary to check the computer's system configurations to verify the number of the USB port to which the instrument is connected. Select the "Photometric" module from the "Window" menu, then select the button showing the name of the instrument just added, and click "Connect".
- Create a new collection method by selecting "New" from the "File" menu, then "Method" from the "Edit" menu. Configure the method as follows:

  Wavelength Type: Point
  Column Name: "WL580.0"
  Wavelength (nm): 580
  Click "Add", then "Next>".
  Type: Multi-Point

Formula: Fixed Wavelength
Units: “uM”
WL1: WL580.0
Abs = f(Conc) (selected)
Order of Curve: 1st
Zero Interception: not selected
Click “Next>”.
Data Acquired by: Instrument
Sample Repetitions: 3
“Prompt before repeat” selected
“None” selected
Click “Next>”.
Select a filename and click “Finish”.

- Use clean 4.5 × 4.5 × 45 mm plastic cuvettes with tapered bases (the square 1 cm cuvettes are too large for this analysis). Place the longer pathlength side of the cuvette into the line of the instrument beam (short side facing toward the front/back of the instrument) so that the pathlength is 1 cm.
- Autozero: Put a deionized water-filled cuvette in the front and the back positions in the spectrophotometer, then click “Auto Zero”.
- Set up the standard table: In the Photometric Standard Table, enter the names and concentrations of the S(IV) standards with three replicate rows each (use different names for each; e.g., “Std 1-1”).
- Measure the standards: When measuring absorbance, put the blank reference cuvette into the back holder and the sample cuvette into the front holder. Pipette 0.75 mL of standards 1, 2, 3, 4 and 5 each into 1.0 cm cuvettes (three replicates of each), add 62 µL 2.5 M NaOH solution to each and mix completely, add 280 µL PRA working solution to each and mix completely, and start timer. After approximately 14.0 min, place each cuvette into the front holder of the spectrophotometer, close the lid, select the standard in the Standard Table and click “Measure Std.” Three replicates and a mean value of absorbance are recorded. Record all values in a separate notebook and immediately clean the cuvettes.
- Clean cuvettes: Rinse each cuvette with deionized water five times, then allow to soak for 30 min – 1 hour. Rinse again with deionized water three times, then allow to dry. If a stain is visible on the cuvette, dilute nitric acid and/or hydrogen peroxide can be used to remove the discoloration. Consult the UV-1800 Instruction Manual for further information.

- Measure blanks: Pipette 0.75 mL deionized water into a 1.0 mL cuvette (make three replicates), add 62 μL M NaOH solution and mix completely, then add 280 μL PRA working solution and mix completely. Start a timer, and measure the absorbance after approximately 14.0 min.
- Measure the catalase enzyme activity: Pipette 0.75 mL preserved catalase enzyme solution into a 1.0 mL cuvette, add 62 μL M NaOH solution and mix completely, then add 280 μL PRA working solution and mix completely. Start a timer, and measure the absorbance after approximately 14.0 min.
- Measure samples: Pipette 0.75 mL sample into a 1.0 cm cuvette, add 62 μL 2.5 M NaOH solution and mix completely, add 280 μL PRA working solution and mixing completely. Start the timer and measure the absorbance after approximately 14.0 min. For each set of 10 samples, repeat the analysis of one sample three times to find the reproducibility of the sample analysis.

Solutions:

0.125 M NaOH solution:

Dissolve 0.5 g NaOH in a 100 mL flask, diluted to 100 mL with deionized water.

S(IV) preservative solution:

Pipette 1.0 mL 0.125 M NaOH solution into a 250 mL flask. Add 0.0275 g CDTA and shake the solution until all solid is completely dissolved. Add 2.125 mL commercial formaldehyde solution (37%) and dilute to 250 mL with deionized water.

Catalase solution:

Dissolve 200 μL commercial catalase solution (105 mg/mL and activity of 58000/mg) to 50 mL deionized water.

PRA (pararosaniline, $C_{19}H_{19}N_3O$) stock solution:

Dissolve 0.25 g PRA in a 250 mL flask, add 20.625 mL concentrated HCl and dilute to 250 mL with deionized water. Because the PRA solid is hard to dissolve completely, the solution should be filtered through a 1.0 μm pore size Nylon membrane filter after the PRA solid is dissolved as much as possible.

PRA working solution:

Add 16 mL concentrated HCl to 13.2 mL PRA stock solution, then dilute to 100 mL with deionized water.

M NaOH solution:

Dissolve 10 g NaOH in a 100 mL flask and dilute to 100 mL with deionized water.

S(IV) stock solution (5.0 mM):

Dissolve 0.0630 g Na_2SO_3 in deionized water, add 6.5 mL S(IV) preserving solution and then dilute to 100 mL with deionized water

S(IV) working solutions:

Add 20 μL S(IV) stock solution to a 100 mL volumetric flask, add 6.5 mL S(IV) preservative solution and dilute to 100 mL with deionized water. Repeat with 40, 100, 200, and 400 μL of S(IV) stock solution to prepare the remaining standards. The S(IV) standard concentrations are 1.0, 2.0, 5.0, 10.0, and 20.0 μM, respectively.

Quality Control

Relative standard deviations of standard measurements should be <10% and the LOD should be close to 0.25 μM for S(IV).

Notes on S(IV) Analysis

- Sample dilution by adding preservative and catalase solutions:
  - S(IV) in cloud samples has been diluted 1.2 times by adding 100 μL S(IV) preservative solution and 100 μL catalase solution to 1.0 mL of sample, whereas HMS in cloud samples has been diluted 1.3 times by adding the reagents. There are two ways to get actual concentrations in cloud samples. One way is to add the same reagents to the standard and do a calibration curve with these standards. Alternatively, multiply the anaytcail concentrations by a dilution factor of 1.2 and 1.3 for total S(IV) and HMS respectively.
- Effect of formaldehyde concentration on the S(IV) analysis:
  - Formaldehyde plays important roles not only on color development but also on the method sensitivity. Formaldehyde is one of the reactants in the mechanism which produces the purple compound which is

measured by the spectrophotometer. Therefore the amount of formaldehyde in samples can influence the speed of color development. The more formaldehyde added, the faster the color develops.

- On the other hand, formaldehyde can also decrease method sensitivity by the way that it competes with pararosaniline to react with free S(IV). During this process HMS is first decomposed to free S(IV) and formaldehyde, then acidic pararosaniline is added to the sample for color development. As long as the sample is acidified, formaldehyde would have a chance to react with free S(IV) to form HMS. Consequently, less S(IV) would react with pararosaniline and the method sensitivity would be decreased.
- Because of these two opposite effects of formaldehyde on the color development, there should be an optimum amount of formaldehyde added which enhances color development but does not speed up the reaction so much that it decreases sensitivity. This optimum amount of formaldehyde was determined by experiment. Results showed that the maximum sensitivity can be reached between 10 and 20 mM HCHO. At this concentration, it takes 12-14 min for color development. Therefore the concentration of 20 mM formaldehyde is a good compromise between color development and sensitivity.

- Interference of organic materials with the S(IV) analysis:
  - Because the S(IV) analysis is based on color measurement, background color in cloud samples could interfere with the analysis by masking the S(IV) absorption. In most cloudwater samples, background color is due to organic materials, therefore for samples with high organic content, the colorimetric method can cause errors in S(IV) analysis. If organic amines are also present, they could compete with pararosaniline for S(IV). This would reduce the color development and give a lower measurement of S(IV) than was actually present.

Operating Procedure: Formaldehyde Analysis

Analysis Location

Analysis will be carried out at university lab.

Principle of Analysis

In the presence of small amounts of formaldehyde, 2,4-pentanedione and ammonia can react with formaldehyde quantitatively to form a yellow product, diacetyldihydrolutidine (DDL). DEL can be measured with a fluorescence spectrophotometer. Since the amount of DDL produced equals the amount of formaldehyde present in solution (provided 2,4-pentanedione and ammonia are in excess), the formaldehyde concentration can be determined from the amount of DDL (Dong and Dasgupta, 1987).

Sample preservation

Formaldehyde can form a stable compound, HMS, in the presence of bisulfite. HMS can later be decomposed to formaldehyde to be analyzed. A formaldehyde preservation solution containing bisulfite is added on site. The volume ratio of preservative to sample is 1:10. Preparation of the HCHO preservation solution is as follows (20 mM NaOH, 10 mM CDTA, 3 mM $NaHSO_3$):

Heat and stir together in a glass container:

0.08 g sodium hydroxide

0.3644 g *t*-1,2-Cyclohexylenedinitrilo-tetraacetic acid

0.0294 g sodium bisulfite

Deionized water to 100 mL total volume

After the solution cools, measure the pH to ensure that it is approximately 4.8.

Calibration

An authentic formaldehyde standard at several concentrations should be used to generate a calibration curve in the concentration range anticipated to be in the samples.

Storage of Samples

Pipet 1 mL cloudwater to a clean 1.5 mL glass autosampler vial. Add 100 μL "formaldehyde preservative solution". Cap and mix completely. Label the vial with the sample name and "HCHO".

Analysis procedure

- Prepare the solutions below, then set up the Shimadzu RF-1501 spectrometer (see below for instructions to use a fluorescence plate reader and heating unit instead). Turn on the instrument. Allow about 30 seconds for warm-up, then turn on the xenon lamp switch. After the instrument self-checking is completed, select "quantitative" mode at the main menu and input the following parameters:

    Number of standards = 5
    Excitation wavelength = 412 nm
    Emission wavelength = 510 nm
    Unit of concentration = μM
    Number of repetitions = 1
    Instrument parameters:
        Excitation bandwidth = 10 nm
        Emission bandwidth = 10 nm
        Response = 0.25 sec
        Sensitivity = High
        Auto shutter = On

- Save your parameters to one of the file banks, then press the "Return" key to return to the "Quantitative" screen and press the "F2" key to do a calibration curve. Input standard concentrations one by one as requested and select "Meas." mode. Make sure the fluorescent intensity showing up at the upper right corner of the screen is highlighted, which means that the shutter is closed. If it is not highlighted, press the "Shutter key before opening the door of the sample compartment. Now the instrument is ready to start the calibration.
- To re-zero the instrument with deionized water and reagent blank, measure a deionized blank first. Pipet 70 μL deionized water into a 0.5 mL microcentrifuge vial, add 20 μL 5 mM H2O2 solution, 20 μL sodium ethylenediamine-tetraacetic acid (EDTA) solution and 70 μL HCHO "reaction reagent". Heat the solution at 80°C for exactly 2 min with the Temp-Blok heater, then cool it at room temperature for exactly 8 min. Pipet 150 μL solution into the black fluorescence micro-cuvette and put the cuvette into the cuvette holder. Make sure that the unpolished side of the cuvette is facing the front of the instrument. Press the "Shutter" key (i.e. open the

shutter door) and press the “Auto Zero key to re-zero the instrument. Press the “Shutter” key again to close the shutter door.

- Alternatively, if a fluorescence plate reader such as an Ultra-Fast skirted 96-well polypropylene polymerase chain reaction plate (Life Science Products, Inc., LS-9855-25Black) will be used, samples and standards can be pipetted (70 μL) into the plate reader along with reaction reagent, H_2O_2 solution, and EDTA buffer solution. The plate containing reagents and samples/standards can be heated (e.g., in a Peqlab PeqStar 96 Universal Gradient Heating Unit) to 80°C for 2 min, and allowed to react inside the heating unit at 23°C for 30 min (the lid temperature may be set to 110°C). The product, DDL, can then be quantified using the fluorescence plate reader at an excitation wavelength of 412 nm and an emission wavelength of 510 nm. The mean of three replicate formaldehyde measurements (three wells) can be used for each sample. A method should be set in the plate reader and the heating unit prior to analysis.

Calibration

- Construct the calibration curve with the standard solutions. Measure the fluorescence intensity by pressing the “Start” key. After the calibration curve is finished, press the “F3” key to start the sample measurements.
- Solutions:

HCHO stock solution (0.0206 M):

0.2765 g sodium hydroxymethylsulfonate (NaHMS)

10 mL “HCHO preservation solution”

Dilute to 100 mL with water

HCHO standard solutions:

Pipette 10, 20, 50, 100 and 200 μL HCHO stock solution into five 100 mL flasks. Add 10 mL “HCHO preservative solution” and dilute to 100 mL with deionized water. The standard concentrations are 2.06, 4.12, 10.30, 20.60, and 41.20 μM.

HCHO reaction reagent (2.0 M ammonium acetate, 0.05 M acetic acid, 0.02 M 2,4-pentanedione):

15.418 g ammonium acetate

300 μL acetic acid

200 μL 2,4-pentanedione

Dilute to 100 mL with deionized water

Na_4 EDTA/NaOH solution (0.05 M Na_4EDTA, 0.1 M NaOH):

1.2612 g $Na_4EDTA\text{-}4H_2O$

0.4 g NaOH

Dilute to 100 mL with deionized water

5.0 mM H_2O_2 solution:

30 μL commercial H_2O_2 solution (~30%)

Dilute to 100 mL with deionized water

Quality Control

The relative standard deviation of standard measurements within ~30 nm should be <10%, and the limit of detection (LOD) should be ~0.4 μM.

Operating Procedure: Peroxides Analysis

Analysis Location

Analysis will be carried out at the university lab.

Principle of Analysis

The measurement of hydroperoxides using a fluorescence spectrophotometer measures both hydrogen peroxide and organic peroxide. For simplicity hydrogen peroxide will be used here to denote hydroperoxides.

Hydrogen peroxide can be reduced by a hydrogen donor molecule, such as *p*-hydrooxyphenylacetic acid (POPHA), in the presence of peroxidase. A dimeric product can be formed and measured quantitatively by a fluorescence spectrophotometer (Lazrus et al., 1986). One molecular dimer is produced from one molecule of hydrogen peroxide. The hydrogen peroxide concentration in cloduwater can therefore be determined by measuring the dimer concentration. Hydrogen peroxide is very active chemically, however, requiring immediate analysis or preservation on site as soon as possible after cloudwater is taken from the collectors.

H_2O_2 solution concentrations can be calibrated using potassium iodide. Hydrogen peroxide reacts with iodide to form iodine. The iodine produced reacts with iodide in solution to for I3-., which can be measured with the spectrophotometer. The reaction stoichiometry is as follows:

$H_2O_2 + 2I^- + 2H^+ \rightarrow I_2 + 2H_2O$

$I_2 + I^- \rightarrow I_3^-$

Sample Preservation

Hydrogen peroxide in cloudwater samples is preserved on site by addition of POPHA to form a stable dimer. The sample preservation is accomplished by adding 200 μL "conditioning agent" and 200 μL fluorescent reagent to 1.0 mL cloudwater. The conditioning reagent contains potassium hydrogen phthalate (KHP), which acts as a buffer (pH 5.5), and EDTA, which can also act as a buffer (pH 5.5) and prevents interference by metal ions. Preparation of the conditioning and fluorescent reagents is as follows:

H_2O_2 conditioning reagent:

Heat and stir to dissolve:

7.147 g KHP (to pH ~4.00)

80 mL deionized water

Add 10 M NaOH solution to pH ~5.5 (~2.88 mL)

Add, then dilute to 100 mL with deionized water:

0.028 g EDTA

H_2O_2 fluorescent reagent:

Heat and stir to dissolve:

7.147 g KHP (to pH ~4.00)

80 mL deionized water

Add 10 M NaOH solution to pH ~5.5 (~2.88 mL)

Add, then dilute to 100 mL with deionized water:

0.1218 g POPHA

0.0027 g peroxidase

Calibration of H_2O_2 Solution

- The H_2O_2 concentration in solution can be determined by the amount of I_3^-. Pipette 2.0 mL I_3^- standard solution into a cuvette and measure absorbance at 352 nm with 1% KI solution as the blank reference. Repeat for each standard. Pipette 2.0 mL H_2O_2 calibration solution and measure its absorbance and I_3^- concentration. Repeat the measurement three times and record the average.
- According to the reaction stoichiometry, one mole of H_2O_2 can produce one mole of I_3^-. Therefore the concentration of commercial H_2O_2 solution can be calculated as follows:

Micromolar H_2O_2 commercial concentration

= (commercial H_2O_2 percentage/100*density commercial H_2O_2 solution*1000/34 = 0.2325*commercial H_2O_2 percentage

Micromolar H_2O_2 calibration solution concentration

= Molar H_2O_2 commercial concentration*(3.35/100)*(0.5/100)*(2/100)

= 0.3235*commercial H_2O_2 percentage*(3.35/100)*(0.5/100)*(2/100)

= 1.084*commercial H_2O_2 percentage

= 1.084*I_3^- concentration in H_2O_2 calibration solution

- Solution preparation:

1% KI in 0.1 M phosphate buffer:

Dilute to 1000 mL with deionized water:

13.6 g KH_2PO_4

58 µL concentrated H_3PO_4 (85%)

10.0 g KI

I_3^- stock solution (5.0 mM):

Dilute to 100 mL with deionized water:

1.2 g KI

0.1269 g iodine

Keep at room temperature for one day before use.

I_3^- standard solutions:

Pipette 50, 100, 200, 500, 1000 and 2000 µL of I_3^- stock solution into six 100 mL volumetric flasks and add 1% KI solution to the 100 mL line. The concentrations of the standard I_3^- are 2.5, 5.0, 10.0, 25, 50, and 100 µM.

H_2O_2 stock solution 1:

Dilute to 100 mL with deionized water:

1.35 mL commercial H_2O_2 solution (~30%)

H_2O_2 stock solution 2:

Dilute to 100 mL with deionized water:

100 µL H_2O_2 stock solution 1

H_2O_2 calibration solution:

Dilute to 100 mL with 1% KI solution:

2.0 mL H_2O_2 stock solution 2

Storage of Samples

Pipet 1 mL cloudwater to a 2 mL plastic autosampler vial. Add 200 µL "conditioning reagent" and 200 µL "fluorescent reagent". Cap and mix completely. Label the vial. Freeze as soon as possible.

Calibration

- Prepare the solutions below, then set up the Shimadzu RF-1501 spectrometer (see below to use a plate reader instead). Turn on the instrument. Allow 30 seconds for warm-up, then turn on the lamp. After the instrument self-check is complete, select "quantitative" at the main menu and input the parameters:

  Number of standards = 6
  Excitation wavelength = 320 nm
  Emission wavelength = 400 nm
  Unit of concentration = µM
  Number of repetitions = 1
  Instrument parameters:
  Excitation bandwidth = 10 nm
  Emission bandwidth = 10 nm
  Response = 0.25 sec
  Sensitivity = High
  Auto shutter = On

- Save your parameters to one of the file banks, then press the "Return" key to return to the "Quantitative" screen and press the "F2" key to do a calibration curve. Input standard concentrations one by one as requested and select "Meas." mode. Make sure the fluorescent intensity showing up at the upper right corner of the screen is highlighted, which means that the shutter is closed. If it is not highlighted, press the "Shutter key before opening the door of the sample compartment. The instrument is ready to calibrate.
- To re-zero the instrument with reagent blank, load a clean cuvette as follows: Pipette 80 µL deionized water into a 0.5 mL microcentrifuge vial, add 20 µL conditioning reagent, 20 µL fluorescent reagent and 20 µL 0.4 M NaOH solution, mix completely and transfer the solution to the fluorescence cuvette. *The solution ratios are*

different for blanks/standards and samples. Put the cuvette into the cuvette holder. Make sure that the unpolished side of the cuvette is facing the front of the instrument. Press the "Shutter" key (open the shutter door) and press the "Auto Zero" key to re-zero the instrument. Press the "Shutter" key again.

- Construct the calibration curve with the standard solutions. For each one follow the same procedure you followed for the reagent blank: 80 µL sample into a 500 µL microcentrifuge vial, add 20 µL conditioning reagent, 20 µL fluorescent reagent and 20 µL 0.4 M NaOH solution, mix completely and transfer it to the fluorescence cuvette. Measure the fluorescence intensity by pressing the "Start" key. Solutions:

  H_2O_2 stock solutions:

  Pipette 3.35 mL commercial 30% H_2O_2 solution into a clean 100 mL flask and dilute to 100 mL with deionized water.

  Pipette 500 µL of H_2O_2 stock solution 1 into a clean 100 mL flask and dilute to 100 mL with deionized water.

  H_2O_2 standard solutions:

  Pipette 20, 50, 100, 200, 500, 1000, 2000 µL H2O2 stock solution 2 into separate clean 100 mL flasks and dilute to 100 mL with deionized water. Concentrations of the standard solution are 0.34, 0.85, 1.70, 3.40, 8.50, 17.0 µM, respectively.

Measurement

- After the calibration curve is complete, press the "F3" key to start sample measurements. Since the conditioning and fluorescent reagents have already been added to the cloud sample on-site, you only need to add the NaOH solution before measuring: pipette 120 µL preserved sample into cuvette, add 20 µL NaOH, mix and measure fluorescent intensities. Record measurements in the lab notebook.
- Alternatively, if a fluorescence plate reader such as an Ultra-Fast skirted 96-well polypropylene polymerase chain reaction plate (Life Science Products, Inc., LS-9855-25Black) will be used, blanks and standards can be pipetted (80 µL) into the plate with conditioning reagent (20 µL), fluorescent reagent (20 µL), and 0.4 M NaOH (20 µL). Samples can be pipetted (120 µL) into the plate along with 0.4 M NaOH solution (20 µL); because samples were presereved, no conditioning or fluorescent reagents are necessary. The dimeric product can then be quantified using the fluorescence plate reader at an excitation wavelength of 320 nm and an emission

wavelength of 400 nm. The mean of three replicate peroxides measurements (three wells) can be used for each sample. A method should be set in the plate reader prior to analysis.

Peroxidase Enzyme Activity Test

Pipette 1 mL deionized water into a 1.5 mL glass vial. Add 100 µL 1.0 mM H_2O_2 solution, 200 µL "conditioning reagent, and 200 µL "fluorescent reagent". Cap and mix completely. Label with the date and "peroxidase check."

Quality Control

The relative standard deviation of standard measurements within ~30 nm should be <5%, and the limit of detection (LOD) for standard 3 should be ~0.06 µM.

Operating Procedure: Water Soluble Organic Carbon (WSOC, Sievers Turbo)

Analysis Location

Analysis will be carried out at the university lab.

Principle

Total organic carbon (TOC) can measured via several instruments; TOC measurement by a Sievers 900 Turbo analyzer requires only a small volume of sample (0.5-5 mL), so is useful for fog and cloud samples that typically have low volume. This instrument is a two-channel system measuring the conductivity of carbonate before (channel one) and after (channel two) UV/chemical oxidation of carbonaceous species in the sample. The two channels allow measurement, therefore, of inorganic carbon and total carbon, respectively; the difference of these two channels is the TOC.

Calibration

Calibration is not necessary for the Sievers Turbo Organic Carbon Analyzer because calibration is carried out during instrument maintenance. Calibration can be carried out, however, by measuring the concentration of organic carbon in a commercial standard of oxalic acid.

Storage of Samples

Samples should be kept frozen, if possible, until TOC analysis. Because no special storage is necessary to maintain the organic carbon concentration in the samples, the aliquot for TOC analysis can be taken from a cloudwater sample just before analysis. Prior to dilution, the samples can be thawed on a lab bench, and refrigerated between thawing and analysis. Wide-mouth amber polyethylene bottles are generally used for storage. Methylene chloride or chloroform should not be used.

Analysis

- The Sievers Turbo TOC unit can be kept powered on, but not collecting data; alternatively, the Sievers unit can be collecting background data from the large glass deionized water reservoir on the lab bench. During data collection, the instrument measures total carbon and total inorganic carbon, then the difference is calculated to give TOC concentration. The output is read by a custom designed program within LabView that allows the data to be viewed during analysis and also exports the data to a comma separated value (.csv) file. The name of this file and location can be specified within the LabView program.

- To start an analysis, power on the instrument, then select the "Start Analysis" option from the main menu. Several self tests are run after "Start Analysis" is selected, which could take up to 24 hours for a steady background signal. Make sure that deionized water is kept in the reservoir during this time, and that the valve on the right side of the instrument is aligned to draw from the reservoir. If water is being drawn from the reservoir for long periods of time, the water should be replaced approximately every 24 hours.
- After the instrument is started and a steady background signal is read (this should be 50-100 ppb), a background sample should be analyzed. Fill a sample container with 5-10 mL deionized water, place the orange intake tubing into the sample, and cover with Parafilm or foil. On the Labview program, select the desired file folder and name for the background sample, then start a new sample collection. Turn the valve on the Sievers instrument so that the deionized water is drawn from the sample container into the instrument. Allow the instrument to analyze the deionized water for 5-10 minutes, until at least one minute of steady TOC data is collected. Stop the analysis using the Labview program and place a deionized water sample in place of the background sample to allow the instrument to continue running until the first sample is analyzed.
- Repeat the steps for the background sample for each actual sample, including dilution such that the TOC will be approximately within the 50 ppb – 50 ppm linear range of the detector in turbo mode, and also such that the sample is at least 5 mL in volume.
- After the final sample data has been collected and the sample analysis is stopped using the Labview program, the instrument can be put into standby. The data can be opened in a spreadsheet application and the organic carbon and time columns plotted to show the period during which the TOC signal was steady. Calculate the average of the TOC signal over this period, which will be in ppm = $\mu g\ C\ m^{-3}$.

REFERENCES

Bertman, S. B., Roberts, J. M., Parrish, D. D., Buhr, M. P., Goldan, P. D., Kuster, W. C., Fehsenfeld, F. C., Montzka, S. a. and Westberg, H.: Evolution of alkyl nitrates with air mass age, J. Geophys. Res., 100(D11), 22805, doi:10.1029/95JD02030, 1995.

Boris, A. J., Lee, T., Park, T., Choi, J., Seo, S. J. and Collett, J. L.: Fog composition at Baengnyeong Island in the eastern Yellow Sea: detecting markers of aqueous atmospheric oxidations, Atmos. Chem. Phys., 16, 437–453, doi:10.5194/acp-16-437-2016, 2016.

Buxton, G. V., Greenstock, C. L., Helman, W. P., Ross, A. B. and Tsang, W.: Critical Review of rate constants for reactions of hydrated electrons, hydrogen atoms and hydroxyl radicals (OH/O-) in aqueous solution, J. Phys. Chem. Ref. Data, 17(2), 513, doi:10.1063/1.555805, 1988.

Chang, H.: The Processing of Aerosol Particles and Soluble Trace Gases by Chemically Heterogeneous Radiation Fogs, Colorado State University., 2004.

Dasgupta, P. K., Decesare, K. and Ullrey, J. C.: Determination of Atmospheric Sulfur Dioxide without Tetrachloromercurate (II) and the Mechanism of the Schiff Reaction, Anal. Chem., 52, 1912–1922, doi:10.1021/ac50062a031, 1980.

Deguillaume, L., Charbouillot, T., Joly, M., Vaïtilingom, M., Parazols, M., Marinoni, a., Amato, P., Delort, a.-M., Vinatier, V., Flossmann, a., Chaumerliac, N., Pichon, J. M., Houdier, S., Laj, P., Sellegri, K., Colomb, a., Brigante, M. and Mailhot, G.: Classification of clouds sampled at the puy de Dôme (France) based on 10 yr of monitoring of their physicochemical properties, Atmos. Chem. Phys., 14(3), 1485–1506, doi:10.5194/acp-14-1485-2014, 2014.

Desyaterik, Y., Sun, Y., Shen, X., Lee, T., Wang, X., Wang, T. and Collett, J. L.: Speciation of "brown" carbon in cloud water impacted by agricultural biomass burning in eastern China, J. Geophys. Res. Atmos., 118(13), 7389–7399, doi:10.1002/jgrd.50561, 2013.

Dong, S. and Dasgupta, P.: Fast fluorometric flow injection analysis of formaldehyde in atmospheric water, Environ. Sci. Technol., 2(6), 581–588, doi:10.1021/es00160a009, 1987.

Elbert, W., Hoffmann, M. R., Krämer, M., Schmitt, G. and Andreae, M. O.: Control of solute concentrations in cloud and fog water by liquid water content, Atmos. Environ., 34(7), 1109–1122, doi:10.1016/S1352-2310(99)00351-9, 2000.

Ellrod, G. P. and Gultepe, I.: Inferring low cloud base heights at night for aviation using satellite infrared and surface temperature data, Pure Appl. Geophys., 164, 1193–1205, doi:10.1007/s00024-007-0214-7, 2007.

Ervens, B., Sorooshian, A., Lim, Y. B. and Turpin, B. J.: Key parameters controlling OH-initiated formation of secondary organic aerosol in the aqueous phase (asSOA), J. Geophys. Res. Atmos., 119(119), 3997–4016, doi:10.1002/2013JD021021, 2014.

Feng, Y., Ramanathan, V. and Kotamarthi, V. R.: Brown carbon: A significant atmospheric absorber of solar radiation, Atmos. Chem. Phys., 13, 8607–8621, doi:10.5194/acp-13-8607-2013, 2013.

Gong, S. L., Barrie, L. A., Prospero, J. M., Savoie, D. L., Ayers, G. P., Blanchet, J.-P. and Spacek, L.: Modeling sea-salt aerosol in the atmosphere 2. Atmospheric concentrations and fluxes, J. Geophys. Res., 102(D3), 3819–3830, 1997.

Guo, J., Wang, Y., Shen, X., Wang, Z., Lee, T., Wang, X., Li, P., Sun, M., Collett, J. L., Wang, W. and Wang, T.: Characterization of cloud water chemistry at Mount Tai, China: Seasonal variation, anthropogenic impact, and cloud processing, Atmos. Environ., 60, 467–476, doi:10.1016/j.atmosenv.2012.07.016, 2012.

De Haan, H. and De Boer, T.: Applicability of light absorbance and fluorescence as measures of concentration and molecular size of dissolved organic carbon in humic Lake Tjeukemeer, Water Res., 21(6), 731–734, doi:10.1016/0043-1354(87)90086-8, 1987.

Hegg, D. A., Gao, S. and Jonsson, H.: Measurements of selected dicarboxylic acids in marine cloud water, Atmos. Res., 62(1-2), 1–10, doi:10.1016/S0169-8095(02)00023-6, 2002.

Helms, J. R., Stubbins, A., Ritchie, J. D., Minor, E. C., Kieber, D. J. and Mopper, K.: Absorption spectral slopes and slope ratios As indicators of molecular weight, source, and photoleaching of chromophoric dissolved organic matter, Limnol. Oceanogr., 53(3), 955–969, 2008.

Herckes, P., Valsaraj, K. T. and Collett, J. L.: A review of observations of organic matter in fogs and clouds: Origin, processing and fate, Atmos. Res., 132-133, 434–449, doi:10.1016/j.atmosres.2013.06.005, 2013.

Hoffer, A., Kiss, G., Blazsó, M. and Gelencsér, A.: Chemical characterization of humic-like substances (HULIS) formed from a lignin-type precursor in model cloud water, Geophys. Res. Lett., 31, L06115, doi:10.1029/2003GL018962, 2004.

Huang, J.: Carbonate Radical in Natural Waters, University of Toronto., 2000.

Kahnt, A., Iinuma, Y., Mutzel, A., Böge, O., Claeys, M. and Herrmann, H.: Campholenic aldehyde ozonolysis: a mechanism leading to specific biogenic secondary organic aerosol constituents, Atmos. Chem. Phys., 14(2), 719–736, doi:10.5194/acp-14-719-2014, 2014.

Lazrus, A. L., Kok, G. L., Lind, J. a, Gitlin, S. N., Heikes, B. G. and Shetter, R. E.: Automated Fluorometric Method for Hydrogen Peroxide in Air, Anal. Chem., 58, 594–597, doi:10.1021/ac00294a024, 1986.

Lee, B. H., Mohr, C., Lopez-Hilfiker, F. D., Lutz, A., Hallquist, M., Lee, L., Romer, P., Cohen, R. C., Iyer, S., Kurtén, T., Hu, W., Day, D. A., Campuzano-Jost, P., Jimenez, J. L., Xu, L., Ng, N. L., Guo, H., Weber, R. J., Wild, R. J., Brown, S. S., Koss, A., de Gouw, J., Olson, K., Goldstein, A. H., Seco, R., Kim, S., McAvey, K., Shepson, P. B., Starn, T., Baumann, K., Edgerton, E. S., Liu, J., Shilling, J. E., Miller, D. O., Brune, W., Schobesberger, S., D'Ambro, E. L. and Thornton, J. A.: Highly functionalized organic nitrates in the southeast United States: Contribution to secondary organic aerosol and reactive nitrogen budgets, Proc. Natl. Acad. Sci., 113(6), 201508108, doi:10.1073/pnas.1508108113, 2016.

Malm, W. C., Sisler, J. F., Huffman, D., Eldred, R. A. and Cahill, T. A.: Spatial and Seasonal Trends in Particle Concentration and Optical Extinction in the United-States, J. Geophys. Res., 99(D1), 1347–1370, 1994.

Medinas, D. B., Cerchiaro, G., Trindade, D. F. and Augusto, O.: The carbonate radical and related oxidants derived from bicarbonate buffer., IUBMB Life, 59(May), 255–262, doi:10.1080/15216540701230511, 2007.

Munger, J. W.: The chemical composition of fogs and clouds in Southern California, California Institute of Technology., 1989.

Odum, J. R., Hoffmann, T., Bowman, F., Collins, D., Flagan, R. C. and Seinfeld, J. H.: Gas particle partitioning and secondary organic aerosol yields, Environ. Sci. Technol., 30(8), 2580–2585, doi:10.1021/es950943+, 1996.

Pankow, J. F.: An absorption model of gas/particle partitioning of organic compounds in the atmosphere, Atmos. Environ., 28(2), 185–188, doi:10.1016/1352-2310(94)90093-0, 1994.

Pankow, J. F. and Asher, W. E.: SIMPOL.1: A simple group contribution method for predicting vapor pressures and enthalpies of vaporization of multifunctional organic compounds, Atmos. Chem. Phys., 8, 2773–2796, doi:10.5194/acpd-7-11839-2007, 2008.

Pathak, R. K. and Chan, C. K.: Inter-particle and gas-particle interactions in sampling artifacts of PM2.5 in filter-based samplers, Atmos. Environ., 39(9), 1597–1607, doi:10.1016/j.atmosenv.2004.10.018, 2005.

Seinfeld, J. H. and Pankow, J. F.: Organic atmospheric particulate material., Annu. Rev. Phys. Chem., 54(1), 121–140, doi:10.1146/annurev.physchem.54.011002.103756, 2003.

Shen, X.: Aqueous Phase Sulfate Production in Clouds at Mt. Tai in Eastern China, Colorado State University., 2011.

Shen, X., Lee, T., Guo, J., Wang, X., Li, P., Xu, P., Wang, Y., Ren, Y., Wang, W., Wang, T., Li, Y., Carn, S. A. and Collett, J. L.: Aqueous phase sulfate production in clouds in eastern China, Atmos. Environ., 62, 502–511, doi:10.1016/j.atmosenv.2012.07.079, 2012.

Shilling, J. E., Chen, Q., King, S. M., Rosenoern, T., Kroll, J. H., Worsnop, D. R., Decarlo, P. F., Aiken, A. C., Sueper, D., Jimenez, J. L. and Martin, S. T.: Loading-dependent elemental composition of α-pinene SOA particles, Atmos. Chem. Phys., 9(3), 771–782, doi:10.5194/acp-9-771-2009, 2009.

Tan, Y., Perri, M. J., Seitzinger, S. P. and Turpin, B. J.: Effects of Precursor Concentration and Acidic Sulfate in Aqueous Glyoxal-OH Radical Oxidation and Implications for Secondary Organic Aerosol, Environ. Sci. Technol., 43(21), 8105–8112, 2009.

Zhang, Q., Worsnop, D. R., Canagaratna, M. R. and Jimenez, J.-L.: Hydrocarbon-like and oxygenated organic aerosols in Pittsburgh: insights into sources and processes of organic aerosols, Atmos. Chem. Phys., 5, 3289–3311, doi:10.5194/acp-5-3289-2005, 2005.

FOG COLLECTION LOG SHEET

Date(s): _____ Operator(s): _____ Collector: _____

Notes: _____

_____

Sample	Start Date	Start Time	End Time	Empty Bottle	Bottle + Sample	pH/time	IC Vials (2)	Peroxides	TOC Vial	LC Vial	Notes, Time Aliquots Completed	Organic Acids Vial
SSCCMMDD#	DD/MM	HH:MM	HH:MM	WW.W g	WW.W g	P.PP HH:MM					Winds calm, HH:MM	

Site Code: BY Fog Collector Codes (CC): CASCC2-CC, sf-CASCC Large – CL, sf-CASCC Small – CS, ETCH Large – EL, ETH Small – ES, IESL Large – ISL, IESL Medium – IM, IESL Small - IS

APPENDIX 2: FOG COMPOSITION AT BAENGNYEONG ISLAND IN THE EASTERN YELLOW SEA: DETECTING MARKERS OF AQUEOUS ATMOSPHERIC OXIDATIONS

Methods: Chemicals

Chemical standards and solvents were purchased as follows: malonic acid (99%), 4-nitrophenol (98%), and 2,4-dinitrophenol (98%) were purchased from Acros organics. Glutaric acid (99%), oxalic acid (99.999%), benzoic acid (99%), succinic acid (99+%), pyruvic acid (98%), propionic acid (99+%), 2-methyl-4-nitrophenol (97%), maleic acid (99%), *cis*-pinonic acid (98%), and 2,4- pentanedione (99+%) were purchased from Aldrich. Inorganic salt standards (Six Cation-II and Seven Anion Standards) were purchased from Dionex and diluted. Formaldehyde (37% aqueous/methanol), sodium hydroxide pellets, potassium iodide (KI; 99.6%), iodine (100.0%), potassium hydrogen phthalate (99.95%), sodium carbonate (HPLC grade), and sodium bicarbonate (certified ACS) were purchased from Fischer. Ammonium acetate (≥99.0%), *para*-hydroxy-phenylacetic acid (POPHA; ≥98.0%), $Na_4EDTA \bullet 4H_2O$ (≥99%), CDTA (≥98%), parafuchsin (containing pararosaniline), methanesulfonic acid (MSA; ≥99.0%), acetic acid (99%), formic acid (~98%), adipic acid (≥99%), *n*-valeric acid (≥99%), azelaic acid (98%), and 4,6-dinitro-*o*-cresol (2-methyl-4,6-dinitrophenol; ≥98%) were purchased from Fluka. Salicylic acid (≥99.0%), monobasic potassium phosphate (99.99%), and catalase enzyme from bovine liver were purchased from Sigma. Buffers for pH measurement (pH 4, 7), hydrogen peroxide (30% *w/w* aqueous solution), and Triton X-100 non-ionic detergent were obtained from Sigma-Aldrich. Pinic acid was obtained from the Sigma-Aldrich Library of Rare Chemicals (no purity characterization was carried out). Horseradish peroxidase (Type VI, 250-330 units/mg solid using pyrogallol) was purchased from both Fisher Scientific and Sigma. Anhydrous sodium sulfite was purchased from Chempure Lab Chemicals (99.9%). Methanol and acetonitrile (LCMS grade) were purchased from Honeywell.

Stock standards of organic acids (100 mM) were prepared in water, with the exception of valeric and succinic acids, which were prepared using ~2% methanol in water. Stock standards of nitrophenols (4 and 10 mM) were prepared using up to 40% methanol and/or 4% acetonitrile in water.

Methods: Chemical Analysis

All chemical analyses were carried out without prior filtration of the collected fog water. Most analyses were carried out using procedures previously employed for fog and cloud samples (e.g., Collett et al., 1999; Benedict et

al., 2012). Information about purchased chemicals can be found in the Supporting Information. S(IV), which includes dissolved sulfur dioxide, bisulfite, sulfite, and hydroxymethanesulfonate (HMS), was measured after reaction with 4,4'-[(4-Imino-2,5-cyclohexadien-1-ylidene)methylene]dianiline (pararosaniline) via UV/visible absorption spectrometry (Shimadzu UV-1800 spectrophotometer) at 580 nm according to a modified procedure introduced by Dasgupta et al. (1980; 1981). Formaldehyde was reacted with 2,4-pentanedione and ammonia to form diacetyldihydrolutidine (DDL), which can be measured via fluorescence spectrometry at an excitation wavelength of 412 nm and an emission wavelength of 510 nm (BioTek Synergy H1 fluorescence plate reader, Peqlab PeqStar 96 Universal Gradient Heating Unit, and Ultra-Fast skirted 96-well polypropylene polymerase chain reaction plates) following a procedure published by Dong and Dasgupta (1987). Formaldehyde naturally complexed in the form of HMS is included in the quantified formaldehyde using this method. The mean of three replicate formaldehyde measurements was used for each sample. Total peroxides (organic peroxides and hydrogen peroxide) were reacted with para-hydroxy-phenyl- acetic acid (POPHA) to form a fluorescent dimer in the presence of horseradish peroxidase (412 nm excitation, 510 nm emission; Biotek fluorescence plate reader; Lazrus et al., 1986). A solution of triiodide (I_3^- from KI/I_2) was used to calibrate the stock solution of hydrogen peroxide. The mean of three replicate peroxides measurements was used for each sample. TOC was measured using a Sievers Model 800 Turbo TOC Analyzer in Turbo mode (via digestion of carbonaceous material to CO_2 followed by conductivity detection). Major inorganic ions were quantified using a Dionex DX-500 ion chromatography (IC) system with conductivity detection; cations were separated along a Dionex CS12A analytical column with an installed CG12 guard column and CSRS ULTRA II suppressor using MSA as eluent; anions were separated along a Dionex AS14A analytical column with an installed AG14A guard column and ASRS ULTRA II suppressor using CO_3^{2-}/HCO_3^- eluent. Organic acids were analyzed using a gradient Dionex IC system with a Dionex AS11-HC analytical column, AG11 guard column, and ASRS ULTRA II suppressor using NaOH eluent and a conductivity detector. A small number of samples were also analyzed after separation using (-)-ESI-HR-ToF-MS to confirm the identifications of eluted organic acids. Additional organic molecules were identified via HPLC-(-)-ESI-HR-ToF-MS: a Kinetex 2.6 μm 60 particle size XB-C18 column designed for polar organic species separation with 100 Å pore size and 3.00 mm internal diameter was used to separate organic species (higher molecular mass organic acids, phenols and organosulfates) via a 0.1% formic acid/methanol gradient elution. The HPLC-(-)-ESI-HR-ToF-MS system consisted of an Agilent 1100 Series LC with Agilent MSD/ToF detector. Agilent EI-TOF tuning mix was used to perform

external mass calibration prior to analyses, initially giving ±1 ppm mass accuracy. Mass accuracies during analysis are tabulated in Table 2, and are typically <15 ppm. External calibrations performed on the HPLC-(-)-ESI-HR-ToF-MS were linear (r^2>0.90). Mass spectral results were filtered so that only species with abundances ≥ 500 abundance units (a.u.) were included. A mass range of 100 to 300 Da was chosen for inclusion in the analyses of these species to exclude organic species identified via IC (organic acids) and compounds with uncertain formula assignments at higher masses.

Methods: Statistical Calculations

Limits of detection (LODs) were estimated from blanks collected after each event during the sampling campaign, and calculated as $ts\sqrt{((N_s+N_{blk})/(N_s*N_{blk}))}$ where N_{blk} is the number of replicate blanks, N_s is the number of replicate samples, t is the Student's t-statistic value for the given N_{blk} at the one-tailed 95% confidence level, and s is the standard deviation of the replicate blanks. Uncertainties were calculated as $ts/\sqrt{N_s}$ for replicate standard solutions at a median concentration from each calibration curve, where N is the number of standard replicates (≥3), t is the Student's t-statistic value for the given N at the two-tailed 95% confidence level, and s is the standard deviation of the standard replicates.

Results: Changes in Composition during Fog Events

Constraining the processes leading to composition changes during a fog event is difficult. Trends in concentrations of major ions are shown in Figure A2-4 for two fog events through which multiple fog water samples were collected (2 and18 July). Although clearly demonstrating that AAOP reactions occurred during these events is not possible, there are changes during the fog events that are apparent within the measured chemical and physical parameters. During the dissipation stage of fogs observed on 2 and 18 July, the LWC decreased and concentrations of all species measured increased. While LWC and constituent concentrations have a generally inverse relationship during the events, the LWC explains 25% or less of concentration variation (r2≤0.25) in samples overall for small and large samples. On 18 July (Figure A2-4, right), the decrease in the magnitude of concentrations at 7:30 am agrees with previously observed depositional velocities for individual inorganic species (Herckes et al., 2007). Throughout the two fog events, changes in total low molecular mass organic acid concentrations, which might reflect oxidation of organic species within the fog water, are either low or follow trends of other inorganic species, consistent with a dominance of physical processes. The lack of clear evidence for supporting or negating aqueous

organic reactions within these specific fog events emphasizes the utility of laboratory studies in which many chemical and physical variables can be controlled.

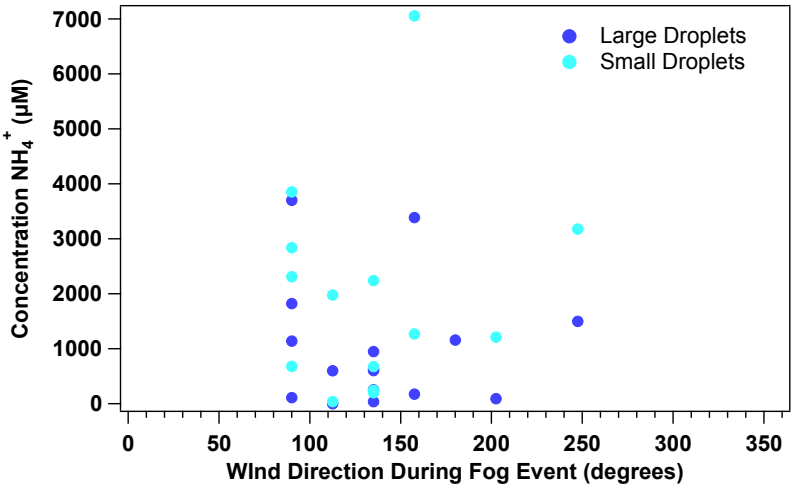

Figure A2-1. Ammonium concentrations during fog events as a function of wind directions measured at co-located meteorological station. No correlation can be observed between NH_4^+ and wind, showing that the source of this species was likely long-rang transport as NH_4NO_3.

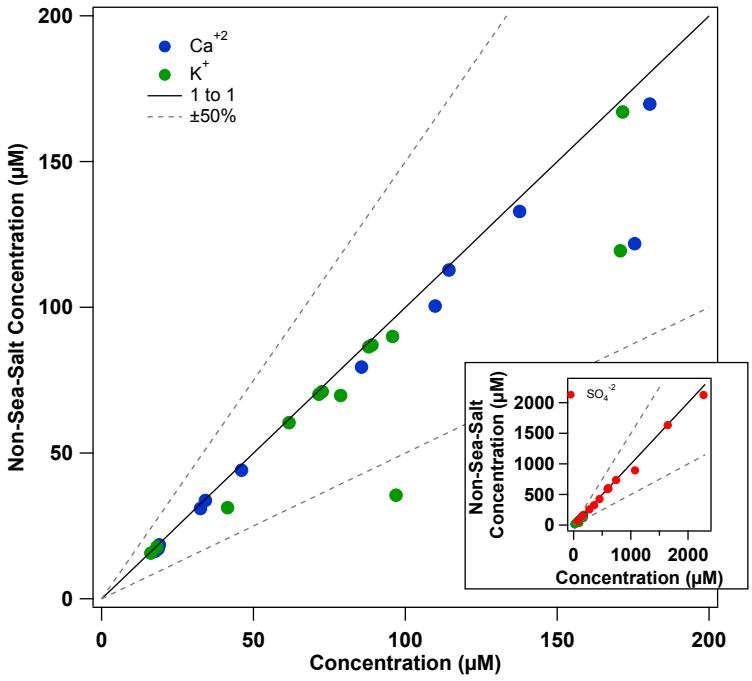

Figure A2-2. Non-sea salt (nss) components of several ionic species, calculated using molar ratios of species and Na^+ in sea salt. Area between solid line denoting 100% nss contribution and dashed line denoting 50% below includes most data points. Inset shows nss-SO_4^{2-} contribution. nss-Cl^- concentrations are sometimes well below zero (due to Cl^- depletion) and are therefore not shown.

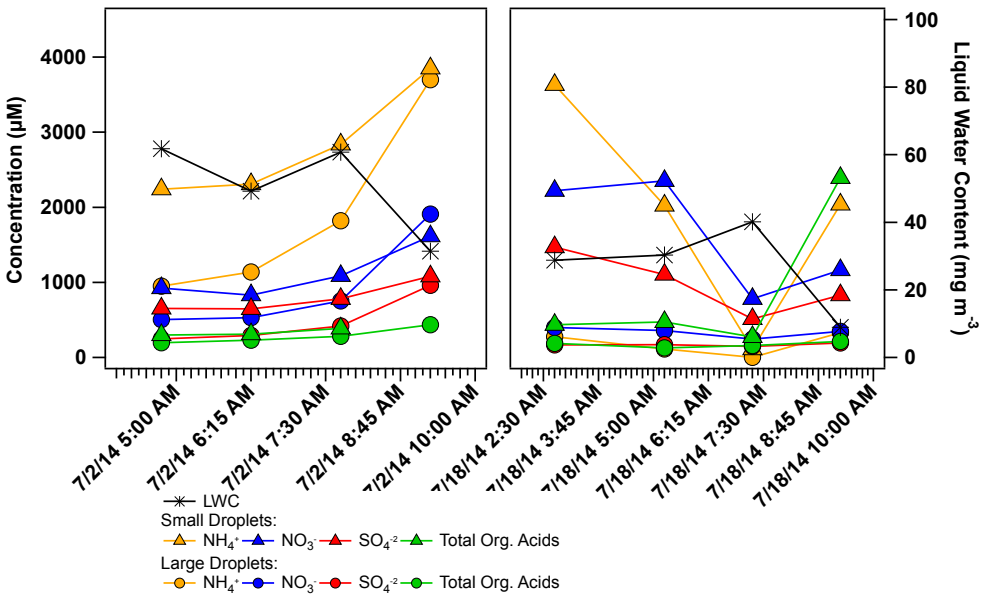

Figure A2-3. Chemical trends with time for two fog events during which multiple fog water samples were collected (on the mornings of 2 and 18 July 2014). LWC was calculated as the mean value measured by the PVM through the duration of each fog sample (times along the bottom of the plot are at the start of each sampling period).

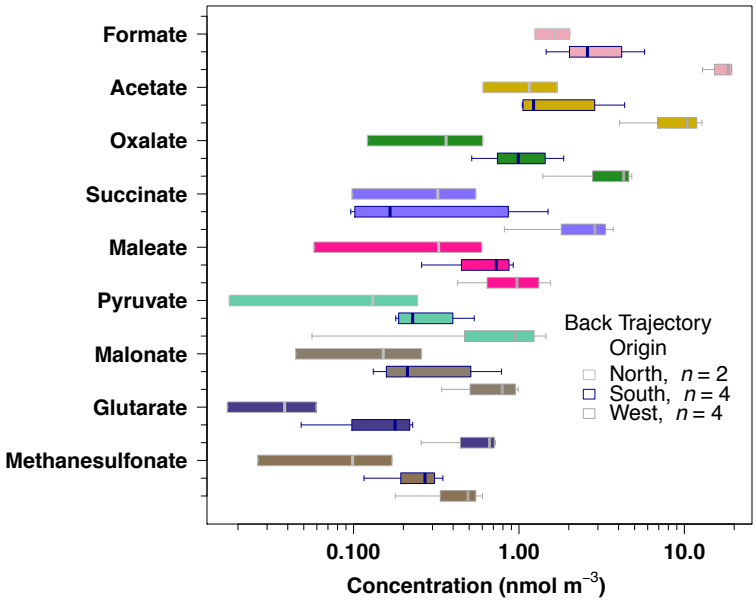

Figure A2-4. Sector analysis of most abundant organic acids, demonstrating that highest concentrations of organic acids originated from the west. Note that samples from the east were low in volume so that organic acids analyses were not performed (samples collected on 5 and 6 June 2014).

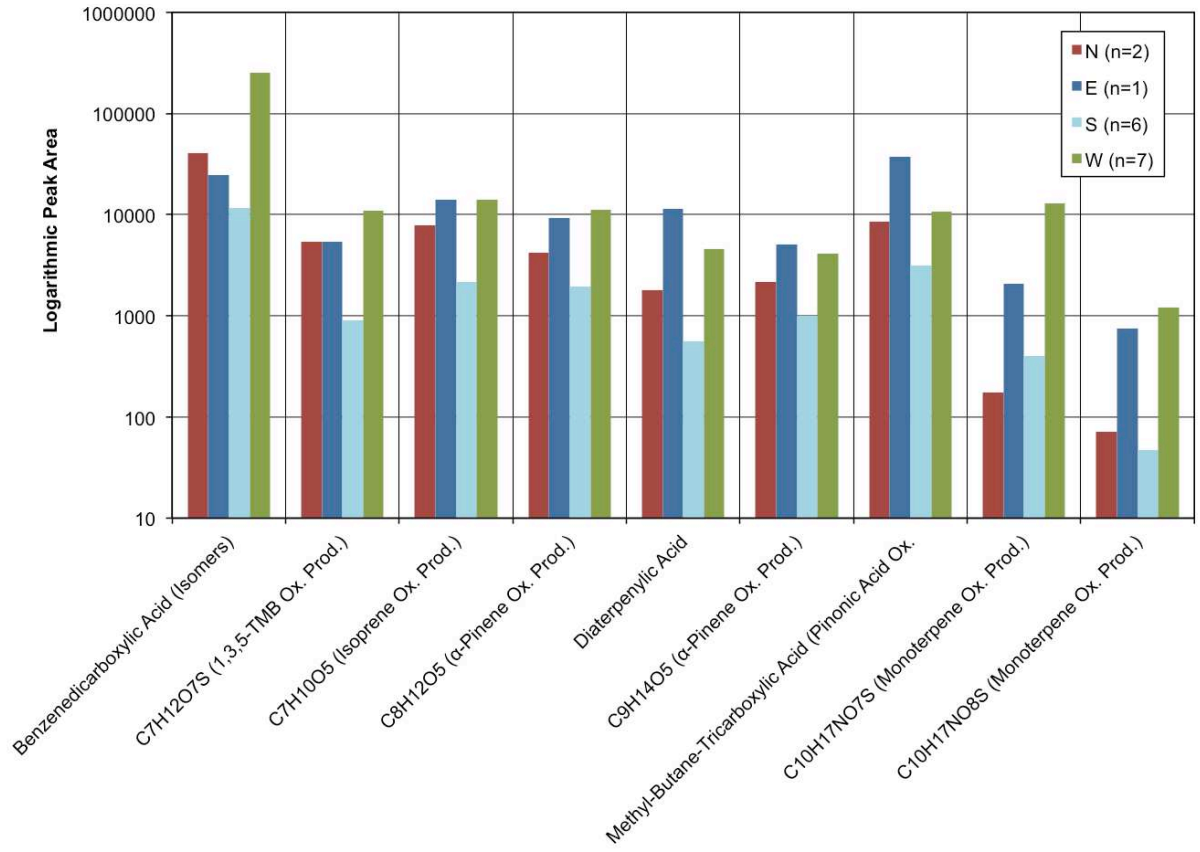

Figure A2-5. Peak areas of tentatively identified anthropogenic (two categories on left) and biogenic (two categories on right) species in BYI fog water (see Table 2). Samples with westerly back trajectories contained the greatest quantities of the anthropogenic species, while the samples collected with westerly trajectories and an easterly trajectory (*n*=1) contained the greatest quantities of the biogenic species. Samples with southerly back trajectories (from over the sea) contained the smallest quantities of most species. Note that sensitivities of the mass spectrometer to these species are highly variable, and no calibration has been made for these compounds.

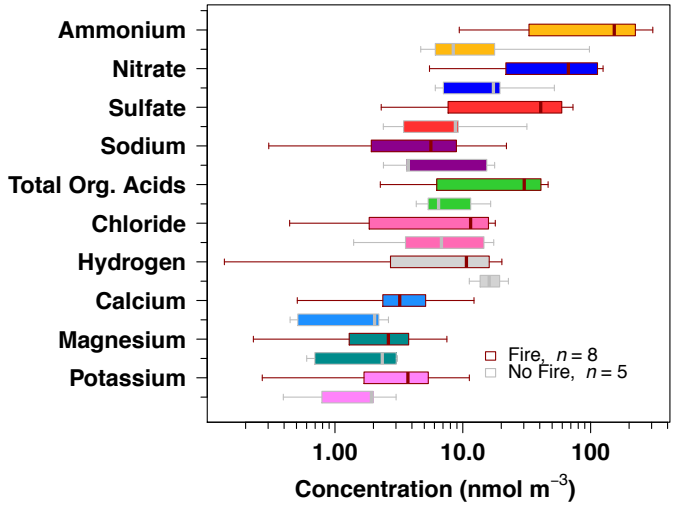

Figure A2-6. Contrast of most abundant species in fog samples between days with fire impact (based on qualitative observation of fires in MODIS fire product outputs, co-located with back trajectories). Note that fire periods included the samples from 07/02/14, which typically contained the greatest concentrations of most abundant species; this is likely due to sources other than fires. A larger sample set might allow a more conclusive determination of the regional fire impact on fog chemistry at BYI.

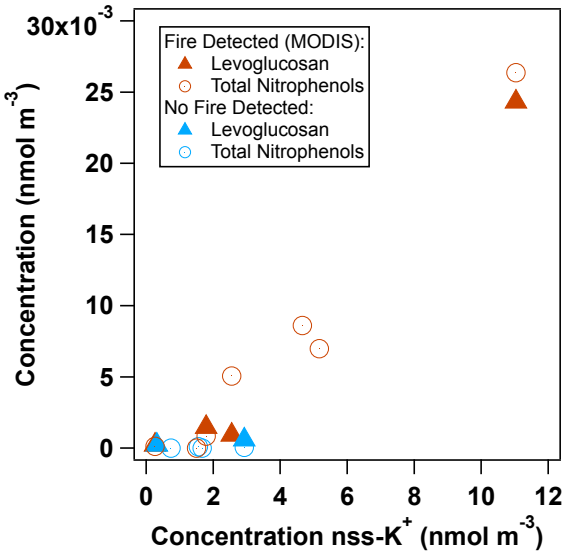

Figure A2-7. Correlation of levoglucosan (triangles) and total nitrophenol (circles) concentrations with those of nss-K^+. Air equivalent concentrations were used to remove the impact of liquid water content between fog samples. Levoglucosan concentrations were only analyzed in six fog samples, representative of most fog events (the fog samples from the event on 18 June were not analyzed due to contamination by CASCC cleaning solution; four samples were analyzed from days when fire was detected; two from days when no fire was detected). The overall correlation of nitrophenols with nss-K^+ was r^2=0.93 (n=11, p<0.001).

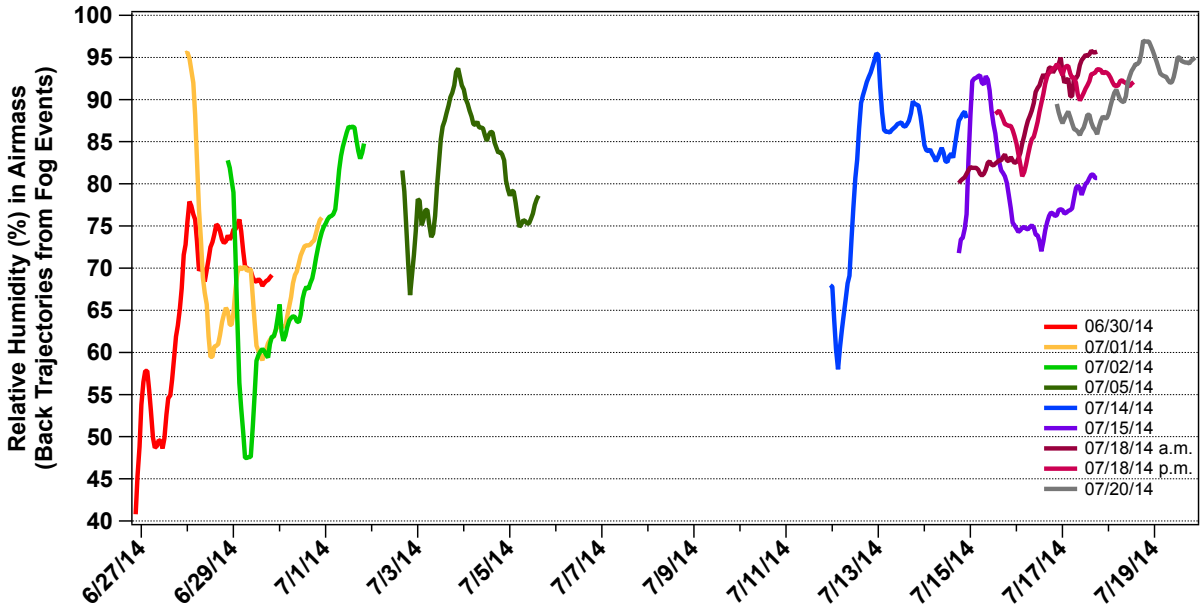

Figure A2-8. Relative humidity outputted from HySPLIT back trajectories initialized at the beginning of each fog event sampled in this study. All samples with the exception of that collected on 30 June were impacted by air masses that had been at high RH (>80%) for a portion of the previous 72 hours.

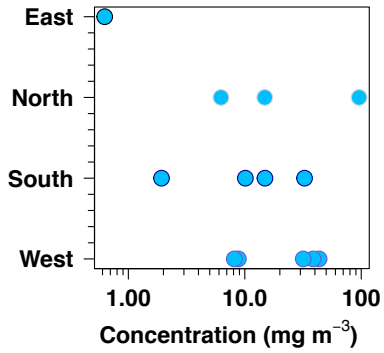

Figure A2-9. Liquid water contents (mg m^{-3}) measured during fog water events at BYI, categorized by direction of back trajectory. The category "East" contains only one sample, but this sample was collected during the lowest LWC of the field campaign. No other apparent dependence of LWC on air mass origin direction can be observed.

Table A2-1. Meteorological and sample variables recorded during fog events. Sample masses are volume-weighted means.

Date and Time	End Time	Duration (min)	Temperature (°C)	Wind Dir. (Deg)	Sample Mass (g)
6/30/14 5:02	8:00	175	20.4	247.5	20.76
7/1/14 7:21	9:16	116	21.4	135	211.23
7/1/14 9:16	12:05	169	19.9	135	47.67
7/2/14 4:45	6:15	90	20.4	135	74.34
7/2/14 6:15	7:45	90	19.1	90	66.05
7/2/14 7:45	9:15	90	19.1	90	54.31
7/2/14 9:14	11:30	135	20.1	90	22.59
7/6/14 3:16	6:40	205	21.1	0	2.44
7/14/14 20:45	22:45	120	24.3	157.5	18.52
7/18/14 2:46	4:45	120	23.2	202.5	33.96
7/18/14 5:15	7:15	120	21.5	135	23.06
7/18/14 9:14	10:15	60	21.9	90	2.20
7/20/14 6:15	8:15	120	22.3	112.5	74.32

Table A2-2. Concentrations of measured inorganic species during fog events. Unless specified, units of chemical species are μM, with the exception of that for pH (unitless).

Date and Time	pH	NH_4^+	SO_4^{-2}	NO_3^-	NO_2^-	Cl^-	Ca^{+2}	Na^+	Mg^{+2}	K^+	S(IV)	Charge Balance (+/-)
6/30/14 5:02	3.54	2914	606.2	1674	1.6	111	114	70	56	88	2.17	1.14
7/1/14 7:21	4.14	253	72.0	185	*0.3*	22	19	24	13	16	0.250	1.02
7/1/14 9:16	4.37	632	155.0	370	2.2	30	34	20	15	18	0.684	1.08
7/2/14 4:45	3.77	2076	601.8	873	1.9	90	33	71	48	73	1.40	1.10
7/2/14 6:15	3.93	2153	601.3	792	1.7	118	19	63	44	72	1.39	1.14
7/2/14 7:45	3.98	2723	742.2	1050	1.9	140	46	88	50	89	1.87	1.16
7/2/14 9:14	3.67	3840	1072	1638	3.1	219	34	2921	53	97	1.89	1.76
7/6/14 3:16	n.m.	4044	2272	4897	4.1	900	175	2445	276	171	n.m.	0.73
7/14/14 20:45	5.00	6088	1645	2247	5.6	381	138	213	120	172	6.27	1.18
7/18/14 2:46	3.69	1113	451.6	687	*0.3*	418	110	425	91	79	4.92	1.00
7/18/14 5:15	3.74	650	355.7	758	1.4	489	180	487	88	41	1.67	0.87
7/18/14 9:14	n.m.	668	273.2	383	2.1	279	86	275	40	96	n.m.	1.07
7/20/14 6:15	3.48	1750	592.3	772	1.2	95	18	59	52	62	3.49	0.98

Table A2-3. Concentrations of measured TOC and low molecular mass organic acids during fog events. Units of organic acids are μM.

Date and Time	TOC (ppmC)	Acetate	Propionate	Formate	MSA	Pyruvate	Valerate	Succinate	Malonate	Maleate	Oxalate	Glutarate	Total Organic Acids
6/30/14 5:02	24.7	121	0.929	115	18.6	15.2	0.943	47.6	24.8	58.8	69.4	3.30	476
7/1/14 7:21	n.m.	160	1.07	101	1.79	0.79	0.245	3.31	1.48	3.04	5.86	0.92	280
7/1/14 9:16	4.66	40.8	0.998	84.1	1.77	1.19	0.676	6.58	3.00	3.87	8.16	1.16	152
7/2/14 4:45	14.2	66.9	1.06	81.0	9.15	6.86	1.27	29.7	11.0	15.3	54.8	8.42	286
7/2/14 6:15	20.2	67.6	1.16	110	7.50	6.61	0.838	26.6	9.19	12.5	49.5	8.58	301
7/2/14 7:45	24.8	91.2	1.20	129	7.50	10.7	1.63	36.8	11.2	16.2	58.2	12.4	376
7/2/14 9:14	21.3	n.m.	n.m.	n.m.	n.m.	n.m.	n.m.	n.m.	n.m.	n.m.	n.m.	n.m.	n.m.
7/6/14 3:16	n.m.	n.m.	n.m.	n.m.	n.m.	n.m.	n.m.	n.m.	n.m.	n.m.	n.m.	n.m.	n.m.
7/14/14 20:45	n.m.	202	1.36	532	12.9	5.02	3.78	52.6	22.5	42.2	110	18.3	1002
7/18/14 2:46	n.m.	19.3	0.418	35.8	7.18	3.58	0.213	9.15	7.45	19.6	29.7	5.59	138
7/18/14 5:15	n.m.	59.0	0.353	26.6	6.05	5.35	0.337	6.21	6.21	21.3	18.6	2.78	153
7/18/14 9:14	n.m.	640	0.528	42.7	6.71	38.8	0.436	6.19	6.05	20.6	16.2	4.61	783
7/20/14 6:15	8.97	49.7	0.600	57.6	6.12	7.03	1.01	26.8	14.7	18.4	35.7	5.51	223

Table A2-4. Concentrations of measured organic species during fog events. Unless specified, units of chemical species are μM. Pinonate was also quantified, but no measurable values were found within fog samples. Grey, italicized values: Not significantly different from 0 because value was less than LOD or less than uncertainty (95% CI).

Date and Time	Peroxides	Formaldehyde	2-Methyl-4,6-Dinitrophenol	4-Nitrophenol	2,4-Dinitrophenol	2-Methyl-4-Nitrophenol	Benzoate	Salicylate	Adipate	Pinate	Azelate
6/30/14 5:02	1.1	21	*0*	0.04	0.02	*0.00007*	0.03	0.11	0.15	0.01	0.04
7/1/14 7:21	3.7	6	*0*	*0*	*0*	*0*	*0*	*0*	*0*	*0*	*0*
7/1/14 9:16	15.2	3	*0*	*0*	*0.008*	*0*	0.02	*0.07*	0.04	*0.009*	*0.002*
7/2/14 4:45	0.6	4	*0.00002*	*0*	0.024	*0*	0.06	*0.06*	0.10	*0.006*	0.03
7/2/14 6:15	0.4	4	*0.0004*	*0*	0.04	*0*	0.08	*0.06*	0.11	*0.007*	0.04
7/2/14 7:45	0.6	6	*0.0012*	0.05	0.06	*0.00004*	0.11	0.10	0.14	0.01	0.04
7/2/14 9:14	0.4	7	n.m.	n.m.	n.m.	n.m.	n.m.	n.m.	n.m.	n.m.	n.m.
7/6/14 3:16	n.m.	n.m.	n.m.	n.m.	n.m.	n.m.	n.m.	n.m.	n.m.	n.m.	n.m.
7/14/14 20:45	58.9	9	*0.004*	0.14	0.07	0.04	0.14	0.15	0.14	*0.009*	0.04
7/18/14 2:46	1.0	3	*0*	*0*	*0.0001*	*0*	*0.001*	*0.03*	0.15	0.02	0.03
7/18/14 5:15	0.6	n.m.	*0*	*0*	*0*	*0*	*0.000003*	*0.03*	0.16	*0.005*	0.09
7/18/14 9:14	n.m.	n.m.	*0*	*0*	*0*	*0*	*0.00008*	*0.02*	0.02	*0.00003*	*0*
7/20/14 6:15	3.7	3	*0*	*0*	*0.0001*	*0*	0.02	*0.06*	0.05	0.03	*0*

APPENDIX 3: EVOLVING ANTHROPOGENIC EMISSIONS AND AQUEOUS AGING WITHIN FOG ON THE SOUTHERN CALIFORNIA COAST

Methods: Fog Water Collection

The ss-CASCC was mounted approximately 1 m from the ground. Its flow rate was calculated using the measured average air velocities from a previous study (Chang, 2004): battery power varied during sampling periods, with an approximate average voltage of 11.5 V, giving a flow rate of 25.7 m^3 min^{-1}. Pre-baked amber glass bottles (40-500 mL) were used for ss-CASCC sample collection and storage. The CASCC2 was mounted on a stand approximately 2.5 m from the ground and was powered by a 120 VAC supply from the gasoline-powered campaign vehicle motor. The flow rate measured by Chang (2004) was 8.2 m^3 min^{-1} (the vehicle motor was allowed to run during sampling, but care was taken to place the tailpipe away and downwind of the collectors). Polypropylene bottles (70-500 mL) were used for collection and storage of CASCC2 samples. The CASCCs were cleaned prior to each fog event with deionized water. Fog water collection method blanks were collected after every cleaning. Limits of detection (LODs) were calculated using these blanks and are tabulated in Table 1. Collected fog water was kept in a cooler on ice for a short period of time (less than eight hours) prior to separation into aliquots for specific chemical analyses. The fog water was divided into aliquots for analyses, and remaining fog water was refrigerated before transport on ice to the laboratory, and finally stored frozen prior to further analyses.

Methods: Chemical Analyses of Fog Water Constituents

Formaldehyde was measured following a procedure published by Dong and Dasgupta (1987) by reaction with 2,4-pentanedione and ammonia to form diacetyldihydrolutidine (DDL), which was quantified via fluorescence spectrometry. Three aqueous solutions were prepared: (1) a reaction reagent containing 2 M $NH_4C_2H_3O$, 0.05 M $C_2H_4O_2$, and 0.02 M 2,4-pentanedione; (2) a buffer/metal chelating solution containing 0.05 M sodium ethylenediaminetetraacetic acid ($Na_4EDTA \bullet 4H_2O$) and 0.1 M NaOH; and (3) 5 mM H_2O_2 to oxidize excess S(IV) generated after reforming formaldehyde from its preserved derivative, HMSA. Standards for calibration were prepared from formaldehyde-sodium bisulfite adduct (NaHMS) and 20 mM NaOH/10 mM [1,2-cyclohexanediyldinitrilo]tetraacetic acid(CDTA)/3 mM $NaHSO_3$}. Samples and standards were pipetted (70 μL) into an Ultra-Fast skirted 96-well polypropylene polymerase chain reaction plate (Life Science Products, Inc., LS-9855-25 Black) along with reaction reagent, H_2O_2 solution, and EDTA buffer solution. The plate containing

reagents and samples/standards were heated (Peqlab PeqStar 96 Universal Gradient Heating Unit) to 80°C for 2 min, and solutions were allowed to react inside the heating unit at 23°C for 30 min (the lid temperature was set to 110°C). The product, DDL, was quantified using a BioTek Synergy H1 fluorescence plate reader at an excitation wavelength of 412 nm and an emission wavelength of 510 nm. Complexed formaldehyde in the form of hydroxymethanesulfonate is included in the quantified formaldehyde using this method. The mean of three replicate formaldehyde measurements was used for each sample.

Total organic carbon (TOC) concentration was measured using a Sievers Model 800 Turbo TOC Analyzer in Turbo mode ($UV/H_3PO_4/(NH_4)_2S_2O_8$ digestion of carbonaceous material to CO_2 followed by conductivity detection). The mean of 3-5 mins TOC measurements at 10 sec sampling frequency was used. A custom LabView program was used for TOC data collection.

Major inorganic ions were quantified using a Dionex DX-500 ion chromatography (IC) system with conductivity detection; cations were separated along a Dionex CS12A analytical column, CG12 guard column, and CSRS ULTRA II suppressor using methanesulfonic acid (MSA) as eluent; anions were separated along a Dionex AS14A analytical column, AG14A guard column, and ASRS ULTRA II suppressor using carbonate/bicarbonate eluent. All inorganic ion external calibrations were linear (r^2>0.9) with the exception of that for NH_4^+, which typically exhibits a non-linear (third order polynomial) response using this system. An Igor program was used to solve for $[NH_4^+]_{aq}$

Organic acids were measured using a gradient Dionex IC system with a Dionex AS11-HC analytical column, AG11 guard column, and ASRS ULTRA II suppressor using sodium hydroxide eluent and a conductivity detector. A 100 µL injection of each sample/standard was made using a Dionex AS50 autosampler and the eluent gradient was as follows: 1 mM NaOH for 6.5 min, NaOH concentration was increased for 18.5 min to 18 mM NaOH and held for 5 min, NaOH concentration was increased for another 20 min to 30 mM NaOH and held for 5 min, NaOH concentration was decreased to the initial 1 mM concentration over 1 min and held for 4 min. Data analyses were performed using Dionex PeakNet and Chromeleon software. A small number of samples were also analyzed after separation using ESI-(-)-HR-ToF-MS to confirm the identifications of eluted organic acids. All organic acid external calibrations were linear (r^2>0.9).

Additional organic molecules were identified and/or quantified via high performance liquid chromatography followed by negative electrospray ionization high-resolution time-of-flight mass spectrometry (HPLC-ESI-(-)-HR-

ToF-MS) from each chloroform-preserved aliquot (no substantial differences were observed in organic composition between chloroform-preserved and un-preserved samples). This method was previously used to identify fog water constituents (Boris et al., 2016).A Kinetex 2.6 μm particle size XB-C18 column designed for polar organic species separation with 100 Å pore size and 3.00 mm internal diameter was used to separate organic species ($\geq$\ce{C4}organic acids, phenols and organosulfates) via a 0.1\% aqueous formic acid/methanol gradient elution. The HPLC-ESI-(-)-HR-ToF-MS system consisted of an Agilent 1100 Series LC with Agilent MSD/ToF detector. Agilent EI-TOF tuning mix was used to perform external mass calibration prior to analyses. Mass accuracies during analysis are tabulated in Table 2, and are typically <15 ppm. External calibrations performed on the HPLC-HR-ToF-MS were linear (r^2>0.90). Agilent MassHunter Qualitative Analysis software was used for data analyses.

Figure A3-1. Example sampling setup demonstrating deployment of CASCC2 (left) and ss-CASCC (right) as well as location with respect to road and campaign vehicle.

Methods: Chemicals

Stock standards of organic acids (100 mM) were prepared in water, with the exception of valerate and succinate, which were prepared using ~2% methanol in water. Stock standards of nitrophenols (4 and 10 mM) were prepared using up to 20% acetonitrile in water. Chemical standards and solvents were purchased as follows: malonic acid (99%, 4-nitrophenol (98%), and 2,4-dinitrophenol (98%) were purchased from Acros organics. Glutaric acid (99%), oxalic acid (99.999%), succinic acid (99+%), pyruvic acid (98%), propionic acid (99+%), 4-nitro-catechol (97%), 2-methyl-4-nitrophenol (97%), maleic acid (99%), *cis*-pinonic acid (98%), and 2,4-pentanedione (99+%) were

purchased from Aldrich. Inorganic salt standards (Six Cation-II and Seven Anion Standards) were purchased from Dionex and diluted. Formaldehyde (37%aqueous/methanol), sodium hydroxide pellets, sodium carbonate (HPLC grade), and sodium bicarbonate (certified ACS) were purchased from Fischer. Ammonium acetate (≥99.0%), $Na_4EDTA•4H_2O$ (99%), methanesulfonic acid (MSA; ≥99.0%), acetic acid (99%), formic acid (~98%), adipic acid (≥99%), *n*-valeric acid (≥99%), azelaic acid (98%), and 4,6-dinitro-o-cresol (2-methyl-4,6-dinitrophenol; ≥98%) were purchased from Fluka. Monobasic potassium phosphate (99.99%) was purchased from Sigma. 4-methyl-5-nitrocatechol (98%) was additionally purchased from Santa Cruz Biotechnology. Buffers for pH measurement (pH 4, 7), hydrogen peroxide (30% w/w aqueous solution), and Triton X-100 non-ionic detergent were obtained from Sigma-Aldrich. Pinic acid was obtained from the Sigma-Aldrich Library of Rare Chemicals (no purity characterization was carried out). Methanol and acetonitrile (LCMS grade) were purchased from Honeywell.

Methods: Volatile Organic Compounds in Grab Samples

A total of 48 individual VOCs were quantified from the canister samples using a five detection channel, three GC analytical system which employed three flame ionization detectors (FIDs), one electron capture detector (ECD) and one mass spectrometer (MS). For each sample, trace VOCs within a 1363 cm^3 (STP) aliquot of air were trapped on a glass bead filled loop immersed in liquid nitrogen. After the sample was trapped, the loop was isolated, warmed to 80°C, and the VOCs were injected to the GC inlet. The carrier gas (ultra-high purity He) flushed the contents of the loop and the stream was split into five parts, with each sub-stream feeding a separate GC column/detector pair as follows: (1) a CP-Al_2O_3/Na_2SO_4 PLOT column (Varian-Chrompack; 50 m×0.53 mm i.d., 10 μm film thickness) connected to an FID was used to measure C_2-C_7 NMHCs; (2) a VF-1ms column (Varian-Chrompack; 60 m×0.32 mm i.d., 1 μm film thickness) connected to an FID measuring C_4-C_{10} NMHCs; (3) A Restek XTI-5 column (Restek; 30 m×0.25 mm i.d., 0.25 μm film thickness) coupled to an FID was used to measure selected OVOCs (not quantified in this study); (4) an OV-1701 column (Ohio Valley Specialty Chemical; 60 m×0.25 mm i.d. 1 μm thickness) connected to an ECD was used to measure C_1-C_5 alkyl nitrates; (5) an OV-624 column (Ohio Valley Specialty Chemical; 60 m×0.25 mm i.d., 1.4 μm thickness) connected to an MS measured C_6-C_{10} NMHCs. Multiple standard concentrations were used during sample analysis (analyzed every 10 samples). Data from GC/ECD and GC/FID analyses were analyzed using Shimadzu Class-VP software, and data from GC/MS analyses of VOCs were analyzed using Shimadzu LabSolutions software. The gases analyzed included C_2-C_{10} hydrocarbons and C_1-C_5 alkyl

nitrates. The relative standard deviation (RSD) of the peak areas for each compound in the standards, was 1-30\% for the aliphatic and alicyclic hydrocarbons, 8-25% for the alkyl nitrates, and 2-21% for aromatic hydrocarbons.

Methods: Fog Water Composites

Fog water was composited into larger volume samples for GC/MS analysis. The objective of the analysis was to determine the non- or slightly polar VOCs and semi-VOCs within the fog water; thus, it was sufficient to determine the concentrations observed within each event, rather than within the time-resolved samples of each event. This allowed sufficient liquid fog water volume for analysis of each event composite, as well as the analysis of a fog collection method blank composite. The composites were made as described in Table 1.

Volumes of fog water samples used in composites for GC/MS analysis. The aliquots used in each composite were determined based on the total volume collected in each sample (more sample was used in a composite for samples with large volumes)

Table A3-1. Masses aliquotted to composites of fog water samples for GC/MS analysis.

	Mass of Sample Aliquotted to Composite (g)					Total Composite Mass (g)
Event 1	10th 22:05	11th 00:05	11th 02:05	11th 04:05	11th 06:05	
	40.04	30.12	45.13	49.92	29.93	195.14
Event 2	11th 21:55	12th 02:00	12th 03:00	12th 04:00	12th 06:00	
	12.78	45.08	37.84	55.12	40.05	190.87
Event 3	12th 21:30	12th 23:30	13th 01:30	13th 03:30	13th 05:30	
	14.93	34.91	55.31	7.57	15.17	127.89
Event 4	14th 00:50	14th 01:50	14th 02:50	14th 03:50	14th 04:50	
	34.99	49.98	50.01	34.97	34.94	204.89
Blank	10th 21:45	11th 21:40	12th 21:00	13th 22:30		
	38.32	38.56	76.55	38.6		192.03

Methods: Trace VOCs in Fog Water

Fog samples remaining after the analyses discussed in the previous paragraph were aliquotted for analysis of volatile trace organic compounds via gas chromatography/mass spectrometry (GC/MS; HP Model 6890 with 5973 mass selective detector housed at Arizona State University). An HP-5 capillary column (95% dimethylpolysiloxane/5% phenyl-methylpolysiloxane; 30 m×250 μm×0.25 μm i.d.) was used in splitless injection mode (temperature profile: initial hold time at 65°C of 10 min, gradient at 10°C min^{-1} to 300°C, and isothermal hold for 20 min). Composites of each fog event were made in order to provide sufficient liquid water for detection via GC/MS (~200 mL); the specific quantities used in the composites are listed in Table SI-X. Composites were vacuum filtered through pre-baked 47 mm quartz fiber filters; the resulting filtrate and filter-adhering materials were

extracted and analyzed separately as the "dissolved" and "insoluble" fractions of the fog water, respectively. The insoluble fraction was extracted from the filters using the following procedure: filters were sonicated in 10 mL dichloromethane (DCM; Fisher, Optima Grade) for 20 min, three times, and the DCM was allowed to evaporate in a chemical hood to a total volume of 10-15 mL under nitrogen at ~10 psi. The dissolved fraction was extracted into DCM solvent as follows: to each composited filtrate was added ~10 g NaCl (Fluka, ≥99.5%) and 0.5 M HCl (EMD Chemicals, 36.5-38.0%) to pH 2-3 (~7-15 drops; pH was measured using MicropHast 0-14 pH strips); the resulting solution was liquid/liquid extracted into three 25 mL aliquots of DCM in a 1000 mL separatory funnel, and blown down to 10-15 mL under nitrogen. Remaining NaCl was removed by filtering each extract through a 10 mL Millipor Multifit glass syringe with a luer-lock metal filter holder containing pre-baked quartz fiber filter material, a metal frit and o-rings. Sample was lost from events 2 and 3 composites during the liquid/liquid extraction: ~119 mL and ~5 mL were saved, respectively. Internal standard responses were used to determine the concentrations in all samples despite these losses, resulting in an order of magnitude lower peak area of decanoic-d_{19} acid in composite 3, but no substantial difference in the peak area in composite 2 versus the two other composites. Methyl esters of organic acids were produced by derivatization with lab-generated diazomethane (50 μL reagent to 50 μL extract). Trimethylsilyl esters and ethers of organic acids and alcohols, respectively, were produced via derivatization with *N*,*O*-*bis*(trimethylsilyl) trifluoroacetamide/1% trimethylchlorosilane (Sigma Aldrich; 50 μL reagent to 50 μL extract, followed by heating at 65°C for 3 hrs). Extracts of dissolved and insoluble fractions in DCM were each blown down under nitrogen to a final volume of 50 μL, measured using a glass syringe, and injected (1 μL) as methyl esters, trimethylsilyl esters, and directly without derivatization into the GC/MS. All glassware, syringes, and metal tools used in analysis were washed with 18.0 MΩ water and isopropanol (Fisher, Optima Grade), then baked overnight at 110-120°C.

Internal standards used in GC/MS analyses of fog water included (Cambridge Isotope): *n*-tetracosane-d_{50}, *n*-triacontane-d_{62}, *n*-hexatriacontane-d_{74}, *n*-eicosane-d_{42}, *n*-hexadecane-d_{34}, naphthalene-d_8, benzophenone-d_5, coronene-d_{12}, chrysene-d_{12}, toluene-d_8, benzo[e]pyrene-$_{d12}$, vanillin-$^{13}C_6$, benzaldehyde-2,3,4,5,6-d_5, 1,6-anyhydro-beta-D-gluose-$^{13}C_6$ (isotopically labeled levoglucosan), D-glucose-d_7, palmitic acid-d_{31}, staeric acid-d_{35}, decanoic acid-d_{19}, and cholesterol-2,2-3,4,4,6-d_6 (CDN Isotopes). Calibrations used for analyses were linear (r^2>0.9; force through zero); *N*,*N*-diethyltoluamide (Sigma Aldrich) and C_{10}-C_{20} *n*-alkanoic acids were calibrated. Azelaic and adipic acids were quantified using the response factor of the C_{20} *n*-alkanoic acid as a surrogate standard.

Calibration curves were constructed using the summed areas of three characteristic ions for each compound, normalized to the response (three summed characteristic ions) of decanoic-d_{19} acid. The internal standard was chosen to be decanoic-d_{19} acid because of its molecular mass similarity to the quantified compounds. A fog collection method blank (water sprayed into the collector for cleaning prior to sample collection during the campaign, composited from four separate fog collection method blanks) as well as an extraction method blank (water from Arizona State University water purification system) were treated as samples and filtered, extracted, and analyzed in the same manner. However, no blank values were subtracted from measured sample concentrations. Data analysis was performed using MSD ChemStation Enhanced Data Analysis Software.

Concentrations measured within event composites were extrapolated to values estimated to be within each fog sample added to the composites. This was done by multiplying the concentration of an analyte measured in a composite by the fraction of the total composite mass that was contributed by a given sample. The resulting estimated concentrations of adipate in fog samples were lower than concentrations measured using LC-(-)-ESI-HR-ToF-MS (slope = 0.3, r^2 = 0.5); tabulated total *n*-alkanoic acid concentrations should therefore be seen only as estimates.

It is possible that some vaporization of volatile species from fog water accounts for the lack of volatile organic components detected in fog water: glass bottles containing fog samples were refrigerated rather than frozen during storage to avoid losing sample from broken glass bottles.

Methods: Air Equivalent Concentrations Calculation

Fog water air equivalent concentrations were calculated for species to demonstrate their atmospheric quantities, normalized to the LWC of the fog during a particular fog event. The result of this calculation is sometimes also called cloud water loading, and has been used in many other studies of fog and cloud water composition (Deguillaume et al., 2014; Elbert et al., 2000; Herckes et al., 2013). The calculation is shown in Eqn. A3-1.

$$\frac{nmol\ i}{m^3\ air} = \frac{\mu mol\ i}{L\ sample} \times \frac{L}{1000\ mL} \times \frac{mL}{1.00\ g} \times g\ sampled \times \frac{hr}{m^3\ air} \times hr\ sampling\ time \times \frac{1000\ nmol\ i}{\mu mol\ i} \qquad \text{Equation A3-1}$$

Methods: Meteorological and Satellite Data

Infrared satellite images of the Southern California coastal area were retrieved from GOES-West archives and processed using a product to highlight night-time low clouds and fogs (in shades of blue, based on certainty of

presence; Figure A3-11). Specifically, the product displays the difference between 10.7 window IR and 3.9 shortwave IR (Ellrod and Gultepe, 2007). Time resolution of retrievals was between 15 min and 1 hr.

Archived observations from atmospheric soundings were downloaded from the University of Wyoming Upper Air Soundings site (http://weather.uwyo.edu/upperair/sounding.html), initialized from the Oakland International Airport (station ID 72493/OAK) at 00:00 and 12:00 GMT between 10 and 14 June.

Archived Model Output Statistics (MOS) results were downloaded from the Iowa Environmental Mesonet (IEM) National Weather Service MOS Download Interface (http://mesonet.agron.iastate.edu/mos/fe.phtml) with Eta/NAM input. Data from the most recent model output were used for each time point (three-hourly) between 3 and 15 June, initialized from the Oxnard Airport weather station (KOXR).

Volatile Organic Compounds Empirical Orthogonal Function Analysis

Patterns within concentrations of volatile organic compounds (VOCs) quantified within grab samples collected during fog events and at VOC source sites were identified using empirical orthogonal function (EOF) analysis (Figure A1-1, Figure A3-7, and Figure A3-8). This technique uses mathematical transformations of data organized into a matrix (typically with dimensions of the sample measurements such as chemical concentrations $\times$ sampling time) to find relationships between the sample measurements that mathematically describe the data. For example, EOF analysis has been used to describe the sources of organic acids in cloud water (Hegg et al., 2002). There was some uncertainty in the EOF analysis in the present study because of the possible dependence between [VOC]s and small sample size (n=30); histograms were, however, Gaussian according to the chi-square test for goodness of fit at α=0.1. EOF1, explaining 45% of variance in [VOC]s, was characterized by elevated concentrations of ethane, propane, and most aromatic species (Figure A3-8), and was associated with the sample collected at the oil spill site along the freeway. EOF1 was therefore likely to be indicative of O&NG extraction emissions, but no samples collected during fog events were correlated with this EOF. High concentrations of acetylene, benzene, and toluene were characteristic of EOF2, explaining 12% of variance in [VOC]s. The emissions source described by EOF2 most influenced the composition of samples collected along the freeway, at the O&NG processing site, and at Serra Cross Park platform, suggesting that EOF2 represented motor vehicle traffic. The contribution of EOF2 to the fog sample collected at 7:25 am on 13 June (during event three) was also observed, likely due to morning traffic along the road at the collection site. In addition, EOF3 apparently described an aged

VOC factor, characterized by high concentrations of alkyl nitrates, and EOF4 described a biogenic VOC factor characterized by high concentrations of the pinenes. EOF3 and EOF4 had limited apparent impact on fog sampling periods (9 and 6% of variation, respectively). Impact on fog samples by these EOFs is described by the individual PC values for the fog samples; no apparent similarities between fog sampling periods were demonstrated, and most influences as demonstrated by EOFs were minimal in magnitude. This was surprising particularly for EOF4 with biogenic influence.

Alkyl Nitrates Analysis

The age of the air masses during fog events were estimated using the ratios of alkyl nitrate to parent alkane concentrations. These ratios can be used to determine the age of air masses by assuming that alkyl nitrates: (a) are formed entirely as secondary products of nitration reactions (reaction with NO) in the atmosphere; (b) that the branching ratio for alkyl nitrate formation versus reduction of the alkyl peroxy radical is constant despite changes in the atmospheric temperature, pressure, and [NO_x] between collected air samples; and (c) that the degradation of alkyl nitrates is accounted for by reaction with $^{\bullet}OH$ at mean diurnal [$^{\bullet}OH$] and photolysis (Bertman et al., 1995). Based on proximity to a major city and the substantial concentrations of NO_3^-} measured within the fog water, it can be assumed that the alkyl nitrate formation process was not limited at CP due to [NO_x] and that variation in [alkyl nitrates] measured can be attributed to secondary formation reactions. Since the observed alkyl nitrate to alkane ratios should, under these assumptions, be dependent only on the reaction rate constants, branching ratios for formation and degradation of alkyl nitrates, and time such that previously modeled and observed relationships between the age of air masses and concentration ratios (Bertman et al., 1995). The resulting ratios of alkyl nitrates to parent alkanes are summarized in Figure A3-9. The greatest values of the ratios were observed during late evening samples, at the beginning of the fog events. It is unlikely that subsequent decreases in the observed ratios are a result of degradation of the alkyl nitrates because the major known loss mechanisms for alkyl nitrates are reaction with $^{\bullet}OH$ and photolysis, which should not occur at night. It is therefore more likely that the ratios changed due to the influx of in air masses overnight or the lowering of the nocturnal mixing layer and resultant increase in alkane concentrations. However, there was no apparent dependence of either alkane concentrations or alkyl nitrate/parent alkane ratios on wind direction, parent alkane concentrations, time of day, or summed organic acids concentrations. Ratios measured were lowest at potential VOC source sites including the Refugio State Beach oil spill cleanup site and the oil spill site along Interstate 5; the greatest ratios were observed within the air sampled at the upwind site at

Gaviota State Beach. This is in agreement with the suggestion that the advection of air masses through the fog sampling site were most likely the dominant factor in the variation of these ratios; higher values were associated with more background, remote air, while lower values were associated with air impacted by regional VOC emissions. Based on the discrepancy between previously reported modeled/estimated and measured alkyl nitrate/alkane ratios (Bertman et al., 1995), it is not useful to extrapolate the ages estimated from ratios measured in previous studies to the ratios measured at CP in 2015.

Aerosol Measurements at Ventura

Aerosol samples (<2.5 μm diameter particles) were collected using a Thermo Anderson Hi-Volume Air Sampler at an air flow rate of approximately 1.1 m^3 min^{-1}. All aerosol samples were collected at Serra Cross Park (34.285, -119.296, 230 m A.S.L. near Grant Park) in Ventura. Filters were re-wrapped after collection in baked heavy duty aluminum foil and sturdy paper folders, sealed in plastic bags, and kept refrigerated or frozen. Punches of filters were extracted into 18.0 MΩ water via sonication with heat: five 25 mm punches were placed into a Falcon 16 mL polystyrene test tube, capped and extracted into 10 mL over 45 min, and into an additional 5 mL over 45 min. Extracts were combined and filtered using a 0.2 μm PTFE syringe filter to remove quartz filter fibers. Extracts were then frozen in Thermo Scientific 30 mL high density polyethylene amber bottles until analysis (~1 month). Filter field blanks were collected by placing a clean filter into the aerosol sampler for six to eight hr. without power to the air pump. Extraction method blanks were also generated by carrying out the filter extraction process with clean filter punches from the same quartz fiber filter batch as the sampled filters. LODs specific to each analysis (e.g., IC) were calculated from a combination of filter extraction method, filter field method, cloud water collector method, and deionized water blank (18.0 MΩ water analyzed using each method, including IC) responses.

Aerosol samples were also collected in 1985/6 at a similar site within Grant Park. The site has been well visited on most summer days since the 1960s because it overlooks the city and ocean, and also is the location of the historical Serra Cross. There is an adjacent parking lot at the site that may have introduced some vehicle emissions to the collected aerosol. The aerosol concentrations $[NO_3^-]_{aerosol}$ and $[SO_4^{-2}]_{aerosol}$ at this site were lower in 1985/86 than in 2015, while $[\text{organic acid}]_{aerosol}$ and $[NH_4^+]_{aerosol}$ were greater in 1985/86 (Figure A3-10). Measured $[Ca^{+2}]_{aerosol}$ was approximately equivalent in the 1985/86 and 2015 measurements. It is likely that the differences in 1985/6 and 2015 aerosol constituent concentrations are due to several major influences: (1) enhanced vehicle traffic at the Serra Cross parking lot in 2015; (2) sampling artifacts such as re-partitioning of semi-volatile organics acids,

HNO_3, and HCl in the 2015 samples due to longer sampling times than 1985/6 and interactions of collected chemicals (Pathak and Chan, 2005; Nylon and Teflon filter media and backup filters were used in 1985/6); and (3) decreased concentrations of some species due to regulation of industrial and mobile source emissions; (4) seasonal differences in temperature and/or emissions, including variations in sea spray aerosol formation (Gong et al., 1997); or (5) enhanced Cl^- depletion in 2015 as a result of decreased $[NH_4^+]_{aerosol}$. Note that for the aerosol measurements made in 1986, *n*=35, while for the 2015 study, *n*=5. Aerosol samples were also collected during fog events at CP in 1986 (*n*=38); the aerosol constituent concentrations were similar to those measured at Ventura in 1986.

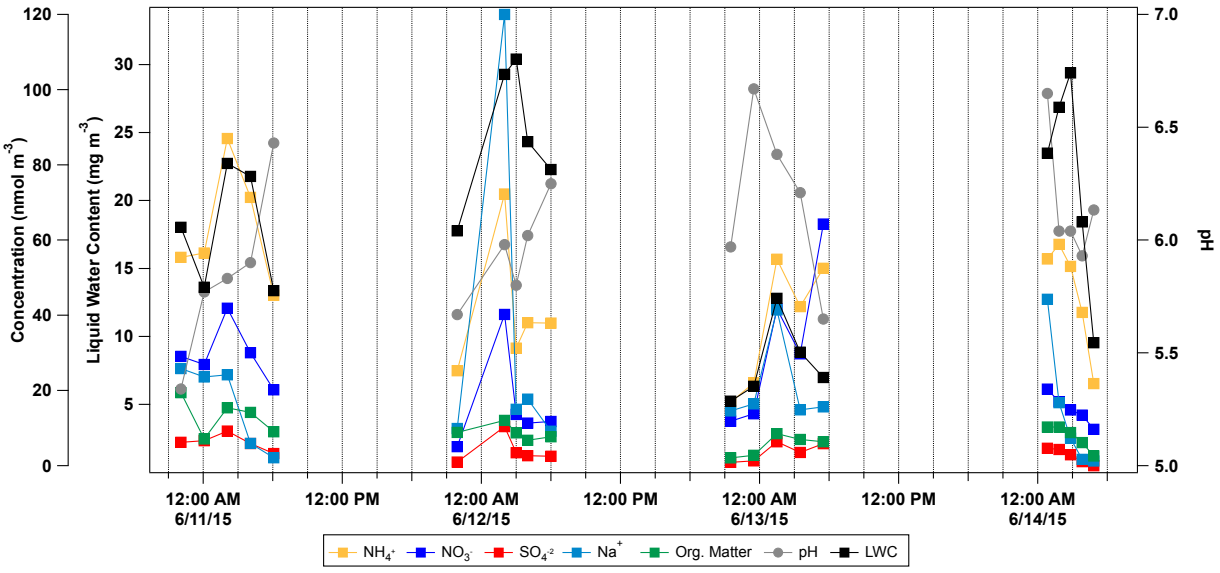

Figure A3-2. Major trends of fog water chemical components in Southern California fog. LWC is estimated from CASCC2 sample mass collected and sampling duration.

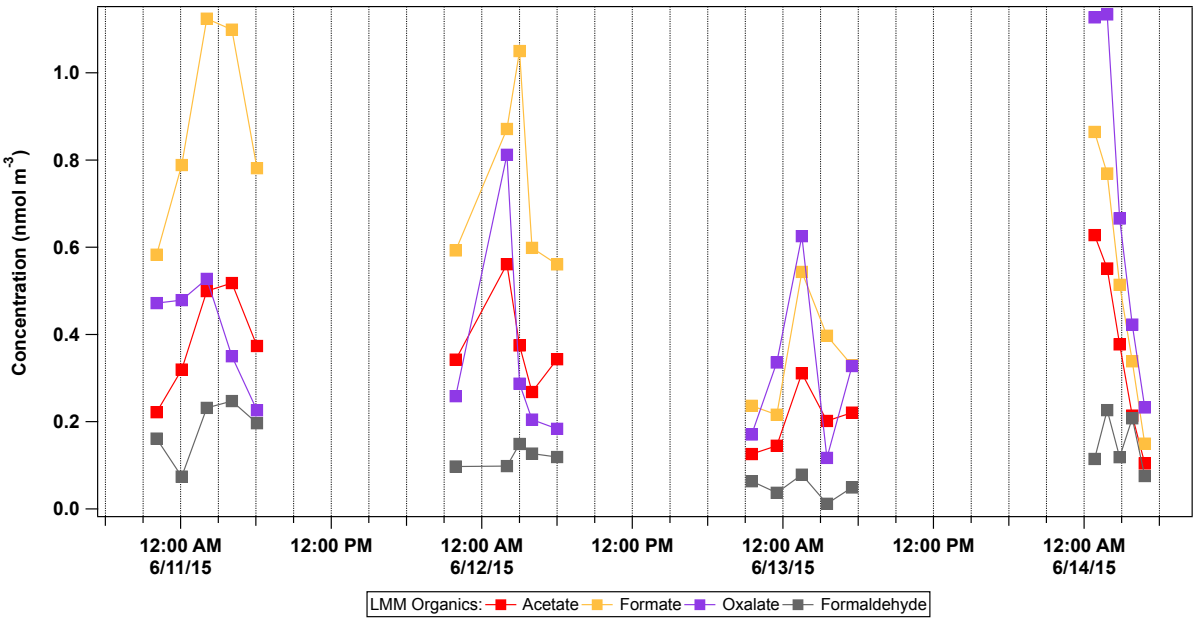

Figure A3-3. Major trends of low molecular mass organic fog water chemical components in Southern California fog. Concentrations scale well with NH_4^+ concentrations.

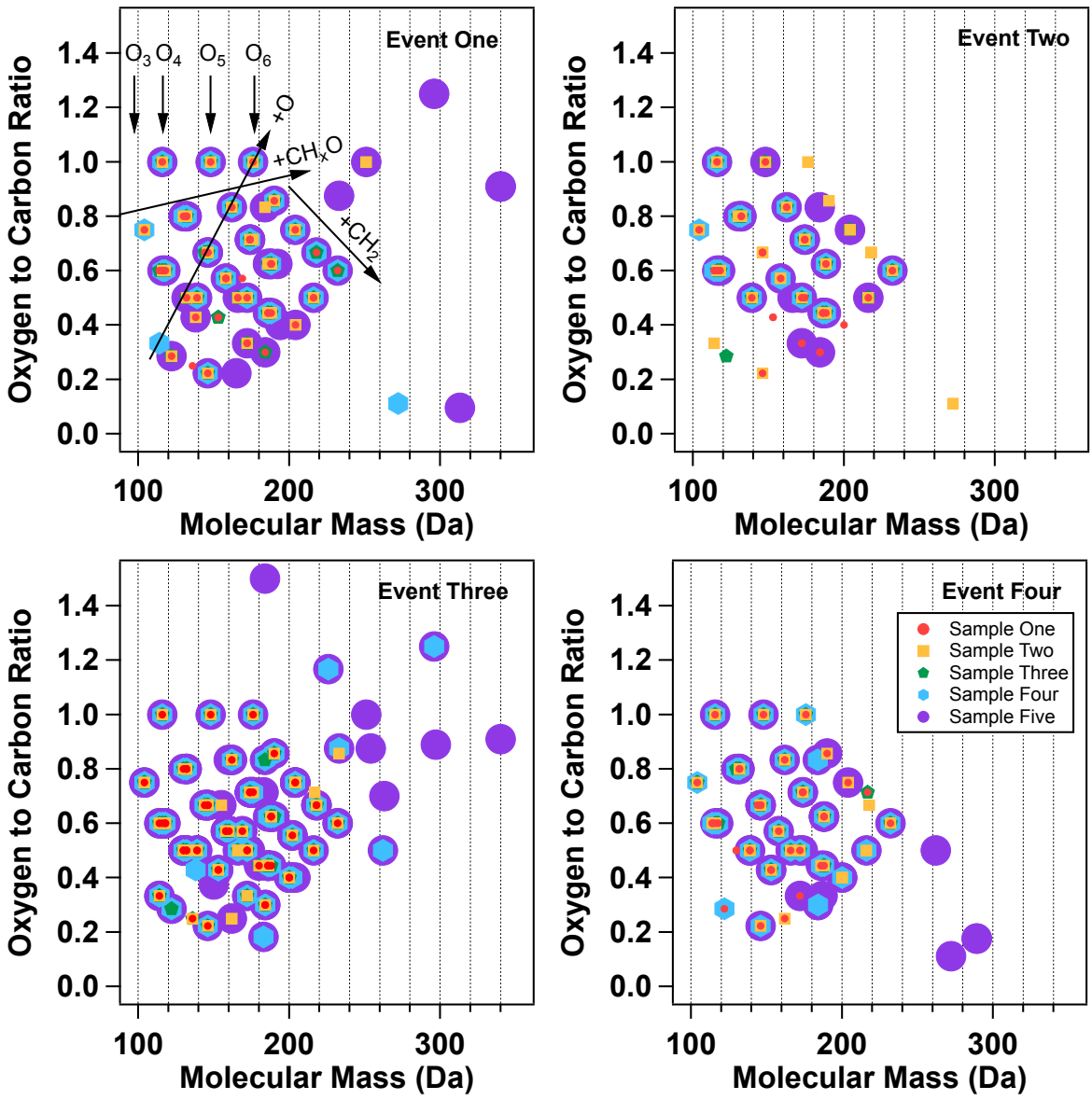

Figure A3-4. Polar, organic compounds identified via LC-ESI-(-)-HR-ToF-MS. Molecular composition within the fog is illustrated via a plot of the ratio of the number of oxygen/carbon atoms (O/C ratios) versus accurate mass measured (Da), in all fog events. The first through fifth samples in time are represented by different colors and sizes of points: small, red points are first sample in each event, large, purple circles are last sample in each event. Series of compounds appearing diagonally with decreasing O/C ratios at increasing molecular mass differ mostly by CH_2, with the same number of O atoms through each series.

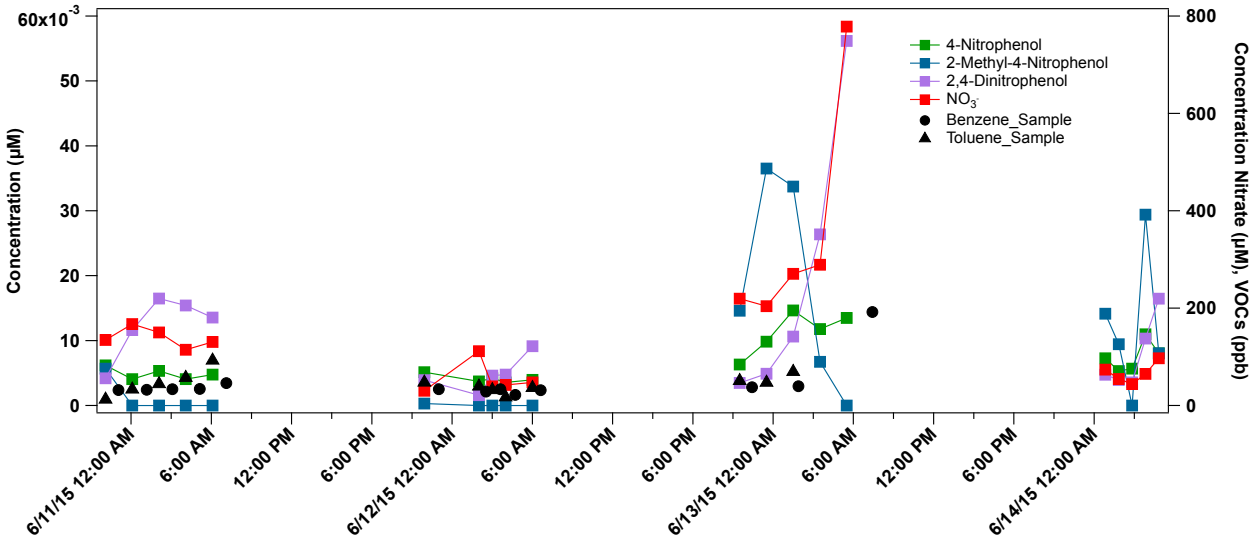

Figure A3-5. Trends in nitrophenol species quantified in CP fog samples using LC-(-)-ESI-HR-ToF-MS. Possible precursors for secondary atmospheric formation of nitrophenols are also shown, including \ce{NO3-}, toluene, and benzene.

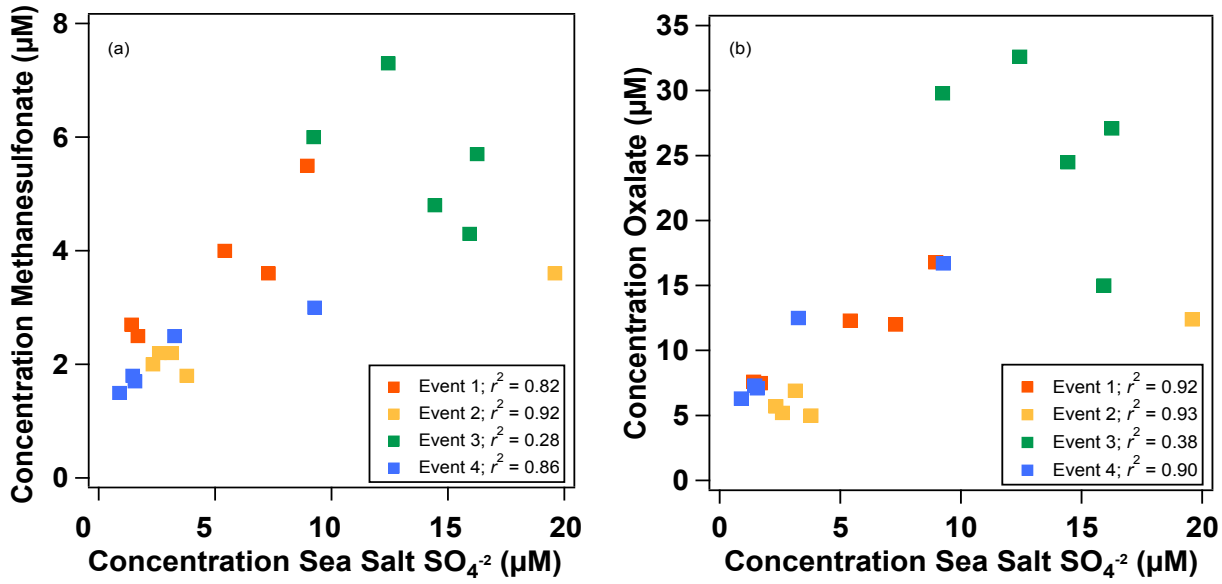

Figure A3-6. Correlations of (a) methanesulfonate and (b) oxalate with non-sea salt SO_4^{-2} concentrations within Southern California fog samples. For all analyses, n=20.

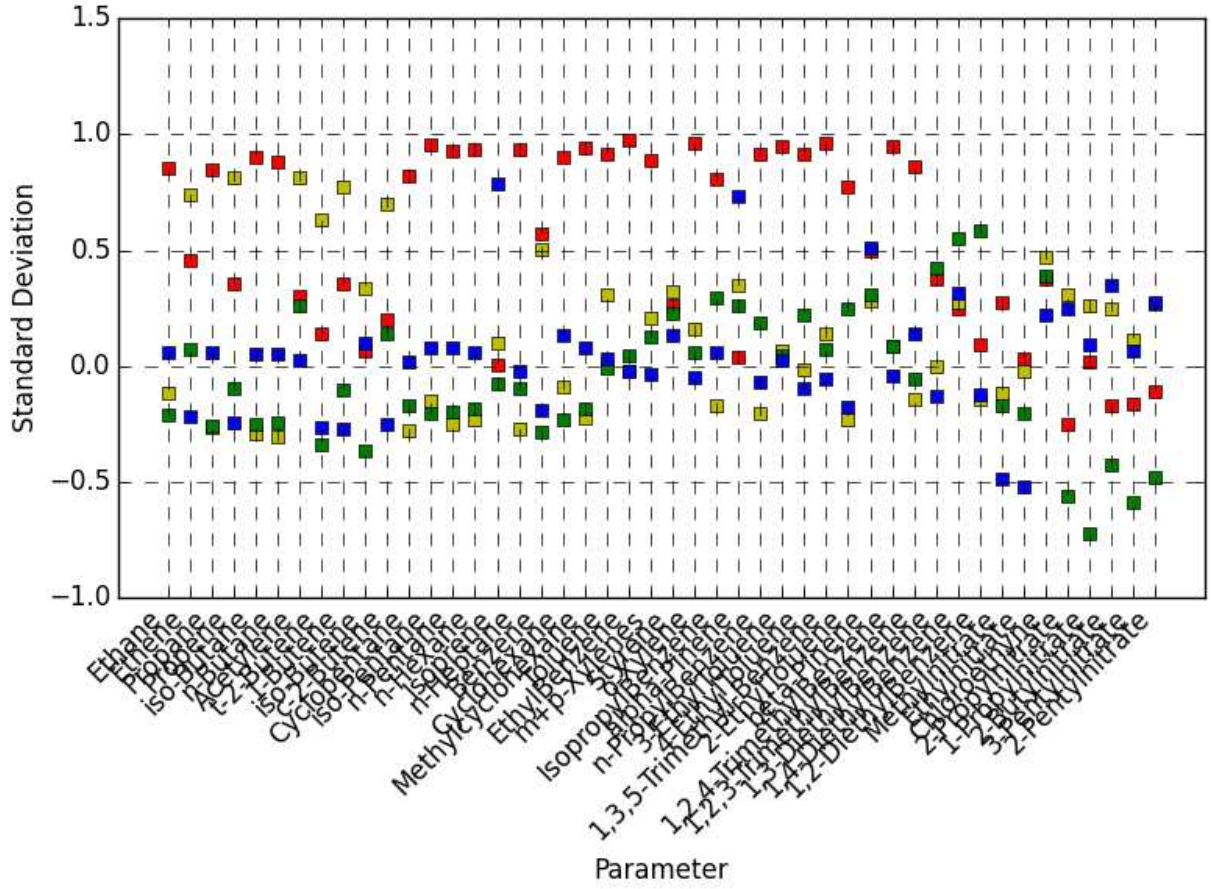

Figure A3-7. EOFs describing patterns in the VOCs measured during fog events and at probable VOC source sites. Larger values of standard deviation indicate greater involvement of a particular chemical species in an EOF. Red squares represent EOF1, with elevated concentrations of alkanes and aromatic species corresponding to a crude oil signature; yellow squares represent EOF2, with elevated concentrations of alkenes indicating a vehicular/processed oil signature; green squares represent EOF3 (negative values demonstrate greater impact), distinguished by elevated concentrations of alkylnitrates likely demonstrating an aged air signature; and blue squares represent EOF4, with elevated biogenic hydrocarbons concentrations.

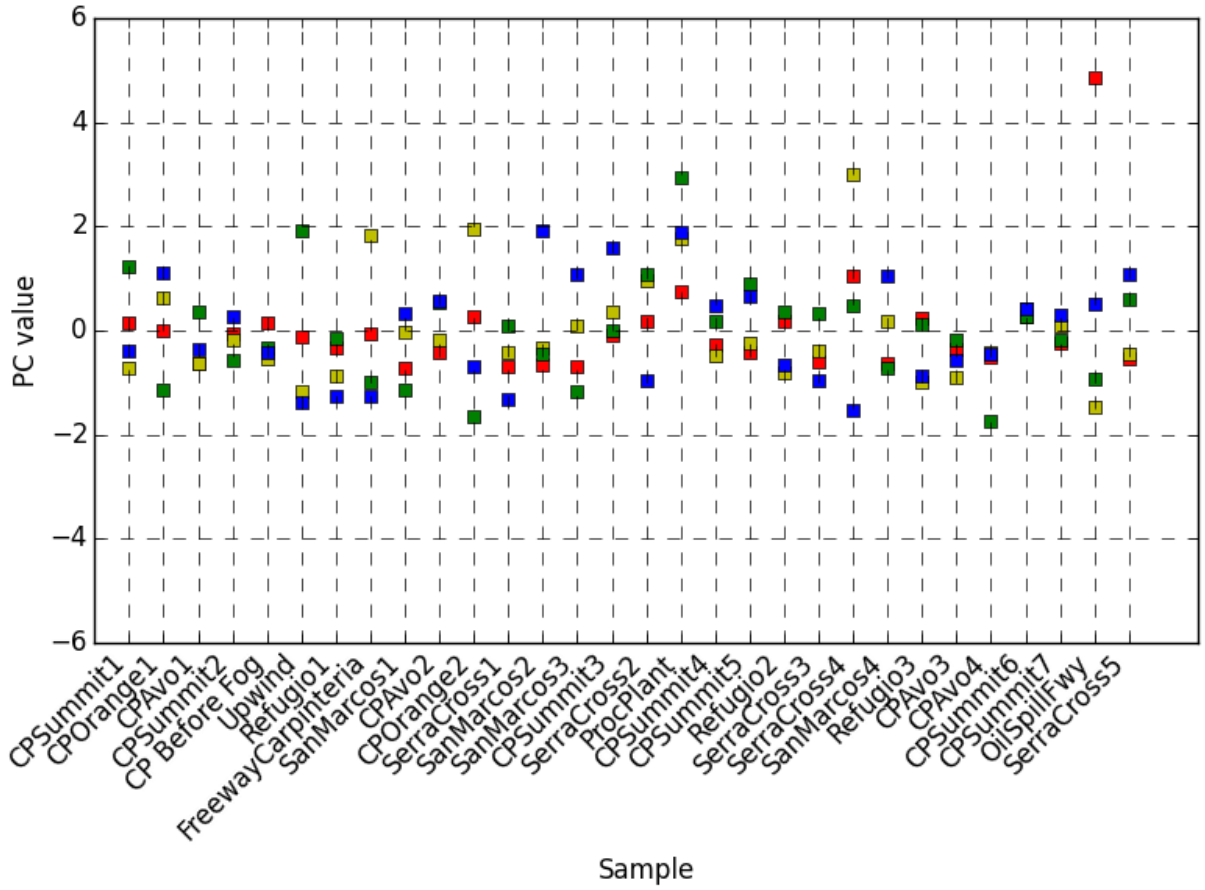

Figure A3-8. Principle components (PCs) of EOFs describing patterns in the VOCs measured during fog events and at probable VOC source sites. Larger values indicate more impact of a source (as described by an EOF) on air collected at a particular location and time. Red squares represent EOF1, corresponding to a crude oil signature that is influential at the oil spill site along the freeway; yellow squares represent EOF2, indicating a vehicular/processed oil signature as typified by the freeway and oil processing plant in Carpinteria; green squares represent EOF3, distinguished by elevated concentrations of alkyl nitrates likely demonstrating an aged air signature that was found in some fog-laden air, and during the sunny afternoon at the oil spill site and the San Marcos Road; and blue squares represent EOF4, which is representative of a biogenic impact, and had an influence during afternoon grab sampling periods at San Marcos Road as well as at the oil processing plant in Carpinteria and during some fog events.

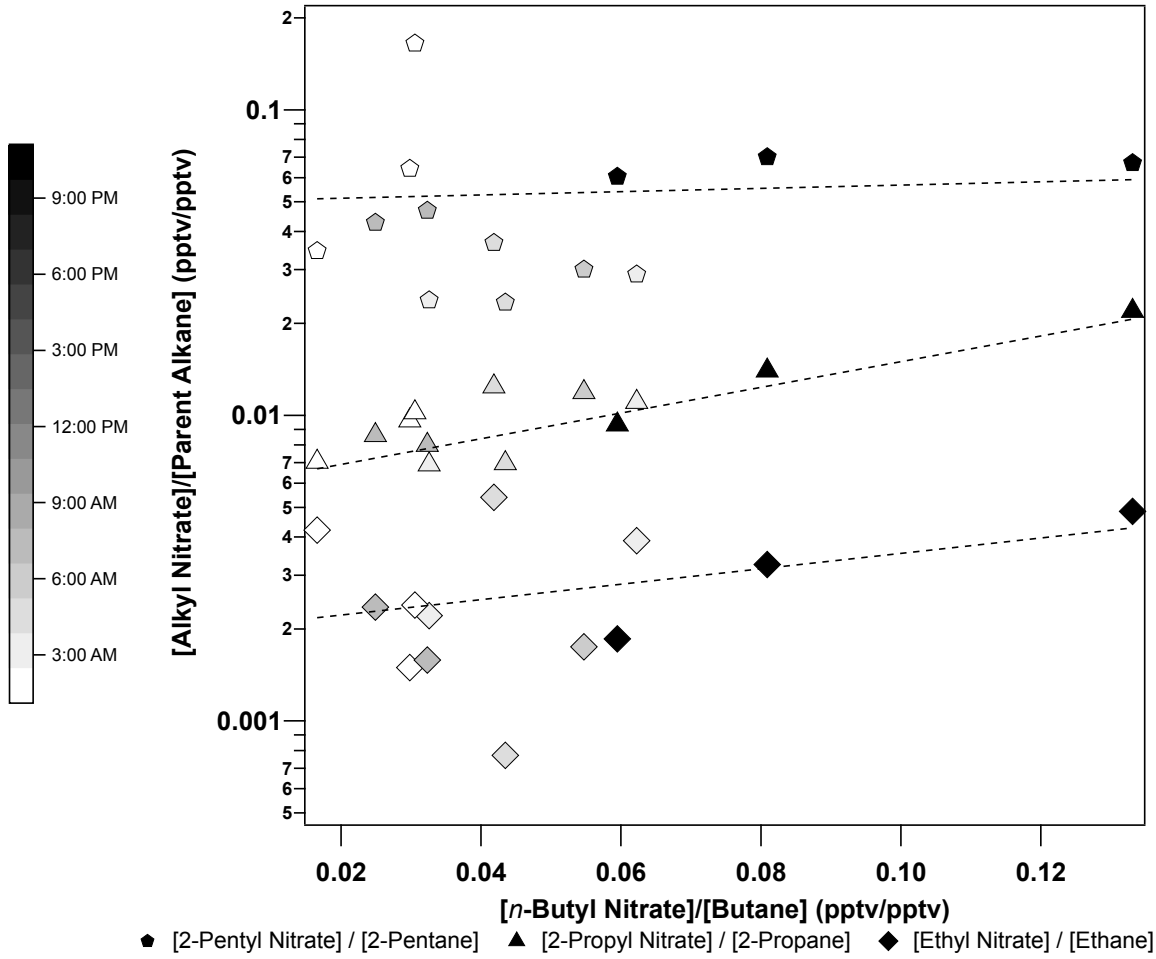

Figure A3-9. Ratios of alkyl nitrate to parent alkane concentrations measured in gaseous grab samples during the fog sampling periods. The greatest enhancements in [*n*-butyl nitrate]/[butane] and [2-propyl nitrate]/[2-propane] were observed before midnight, which is suggested here to indicate advection of emissions containing fresh alkanes overnight as winds shifted from westerly to onshore (also see Figure A3-12 for wind measurements).

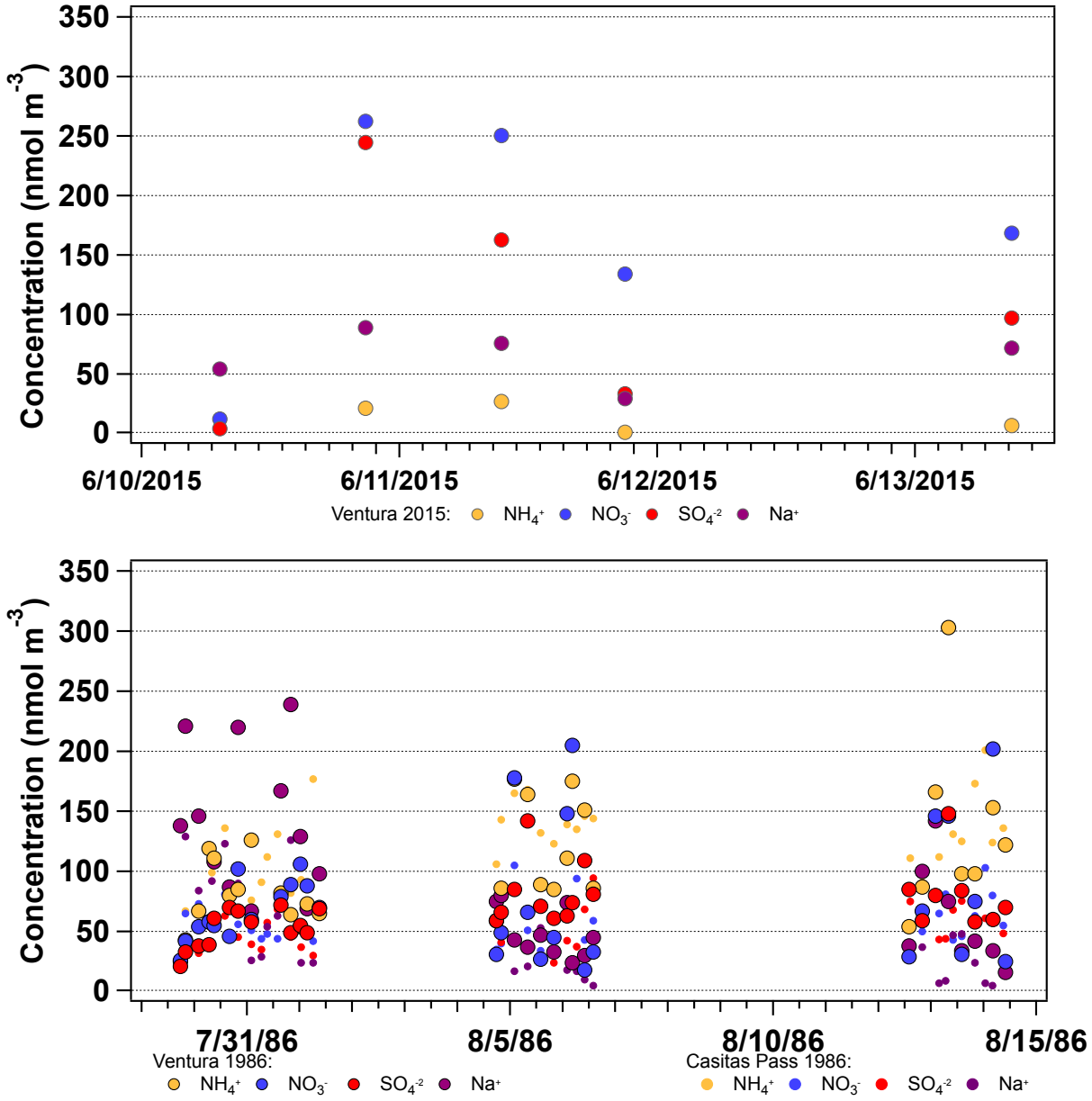

Figure A3-10. Aerosol phase concentrations of inorganic species observed in the 2015/current study (top), and in the 1985/86 study. Measurements were made during both studies at a hill site above Ventura, California, and are plotted in the larger markers. Smaller circular markers in the bottom graph represent concentrations of aerosol species measured at the fog sampling site along CP road in 1986. Concentrations of NO_3^-, SO_4^{-2}, and Na^+ were similar in the studies, but NH_4^+ concentration were greater in the 1985/86 study. Note that the aerosol sampling period in the 1985/86 study was later in the summer than in the 2015 study, so that higher temperatures might have caused increased volatile emissions of NH_4^+.

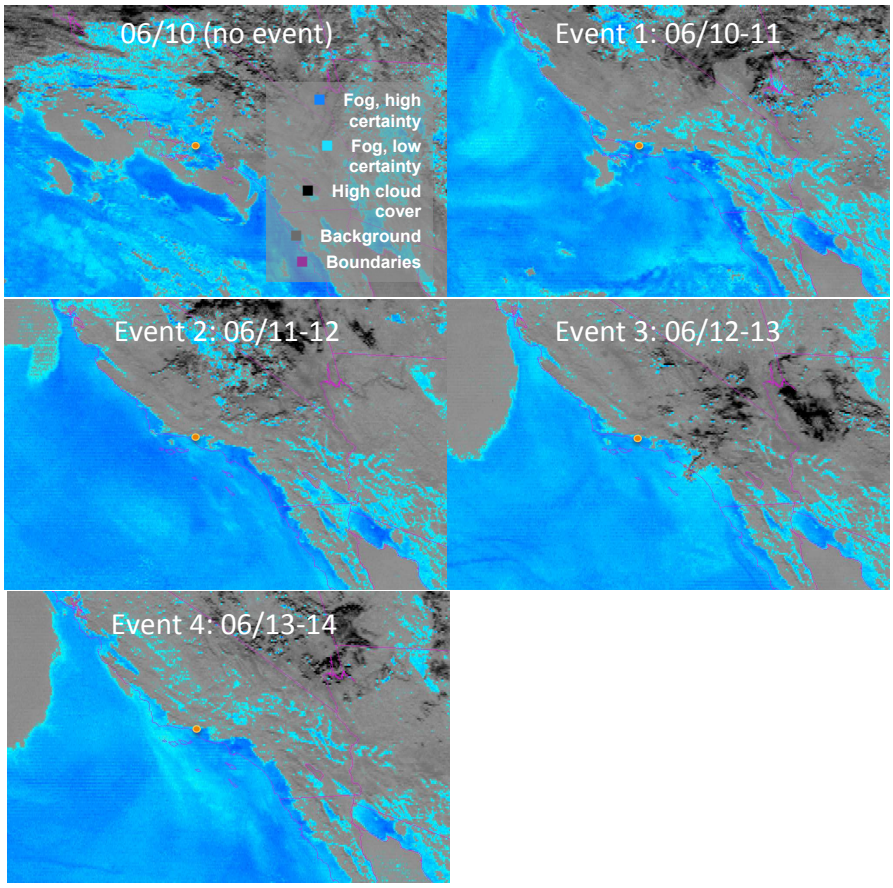

Figure A3-11. Satellite images retrieved from the Geostationary Operational Environmental Satellite (GOES)-West satellite imager, displaying a night-time "fog product" (the difference between 10.7 window IR and 3.9 shortwave IR, Ellrod and Gultepe, 2007). All panes were retrieved for approximately 0:00 local time. Shades of blue correspond to cloud, with darker hues designating areas with higher confidence of cloud presence (note that some blue regions over land do not correspond to cloud). The sampling area is designated in each pane as an orange circle. The extent of the fog/stratus cloud cover is obviously greater on nights when fog was collected than on the night of 9/10 June, and was obviously present inland by midnight during each fog event. Based on additional time-resolved satellite images, the fog typically moved inland at approximately 10 pm. Greatest liquid water content values were observed during event 4 (13/14 June). Data retrieved and processed by Dr. Dan Lindsey of the National Oceanographic and Atmospheric Administration Center for Satellite Applications and Research.

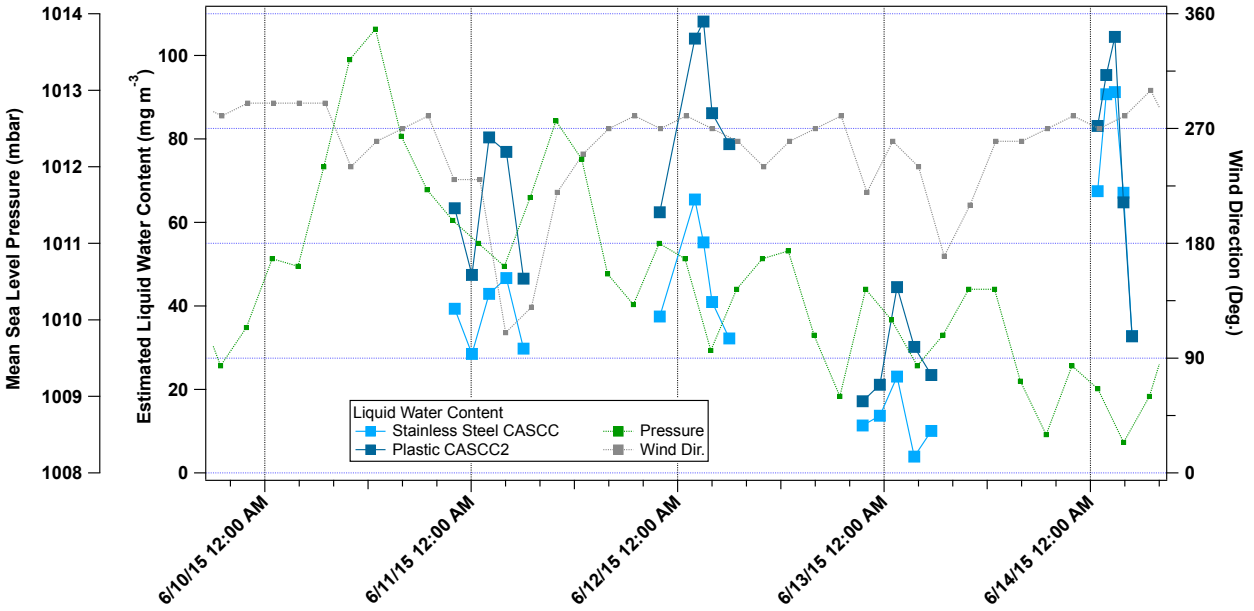

Figure A3-12. Weather parameters and LWCs observed before and during the 2015 fog sampling campaign. Model output statistics (MOS) were retrieved from the University of Wyoming Department of Atmospheric Science website for the nearest possible location to the sampling site, Oakland, California. The passage of a front is visible in the pressure and wind direction traces. Regional winds were from the west through the majority of the sampling period, although locally, a sea breeze was present in the late afternoon through evening, bringing moist air onshore. Fog was sufficiently dense for collection after 9 June, when atmospheric pressure began to decrease and the dewpoint rose. Estimated LWCs from the two cloudwater collectors differed at times, likely due to battery power to the ss-CASSC. For this reason, CASCC2 LWC values were used when discussing trends in this study.

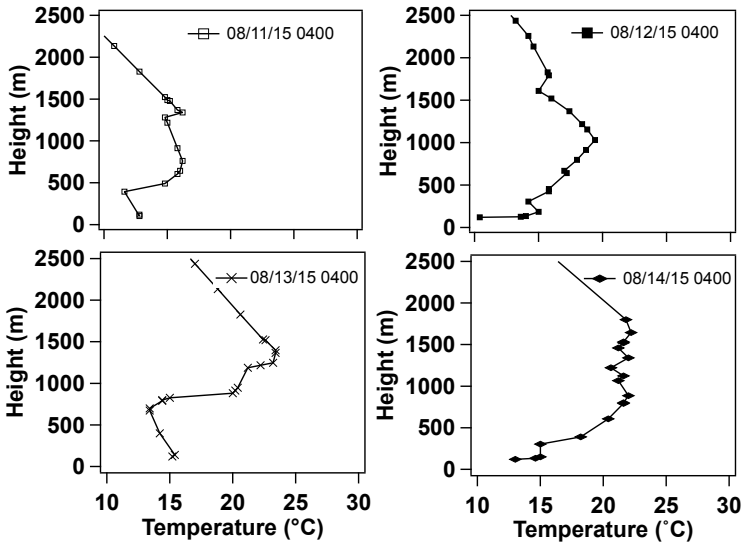

Figure A3-13. Soundings from archived observations from Vandenburg Air Force Base, on the California Coast north of Santa Barbara. Obvious temperature inversions are present in the temperature profiles, although the lapse rates measured during the fog collection campaign in 1985/86 were steeper within the inversion layers (rawinsonde data from Point Mugu; Munger, 1989). Inversion tops in both fog studies were at a height of approximately 1000 m. Data retrieved from University of Wyoming Atmospheric Science Department website.

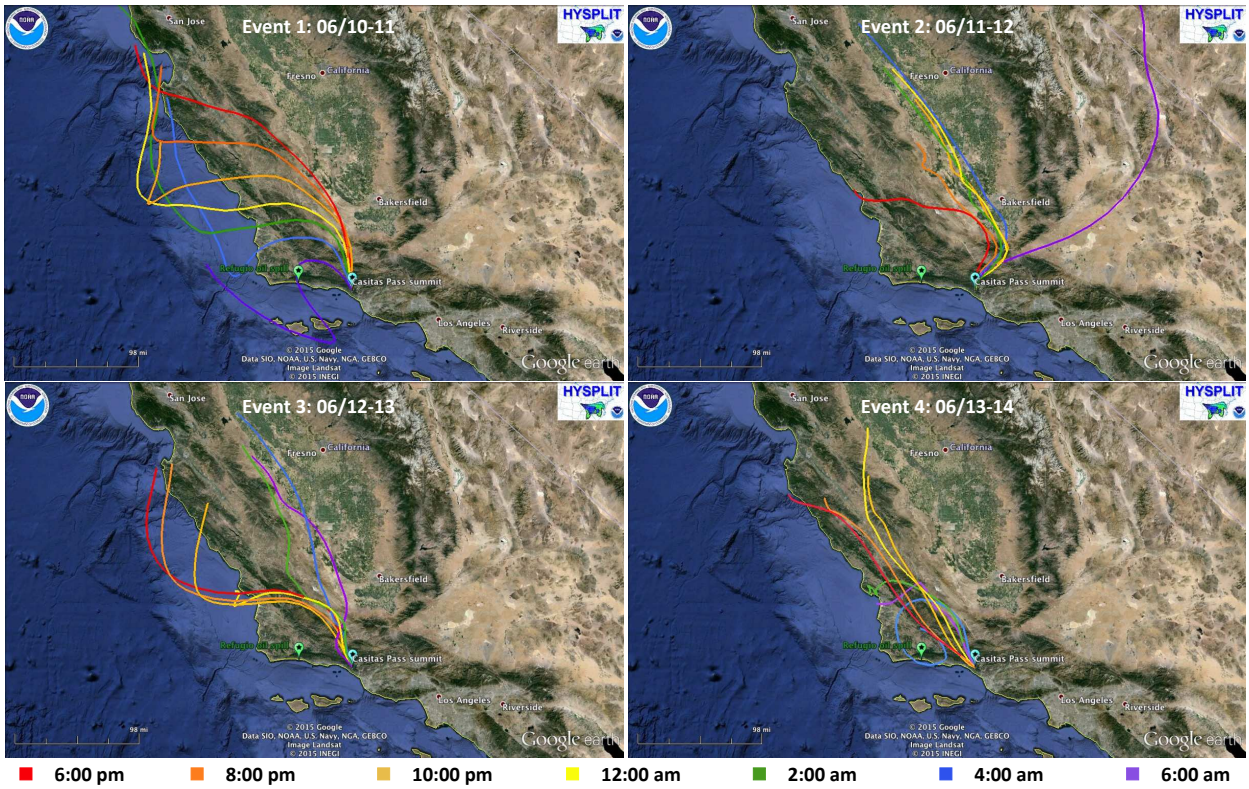

Figure A3-14. Back trajectories generated using NOAA HySPLIT every two hours on evenings with fog events sampled in June 2015. Back trajectories were 12 hr in duration. Markers designate the site of the Refugio oil spill (further west; green) and CP summit (blue). Back trajectory traces were overlaid on a map using Google Earth.

Table A3-2. Fog sample collection dates and times, pH (measured at the sampling site), and mass of collected fog from both samplers. Charge balance calculated from organic and inorganic species concentrations.

	Start Date	Start Time	End Time	pH	Collected, ss-CASCC (g)	Collected, CASCC2 (g)	(ss-CASCC)	Balance (+/-)	(ppmC)
Event 1	10-Jun	22:05	0:05	5.34	121.3	62.4	39.3	1.13	16.1
	11-Jun	0:05	2:05	5.77	87.9	46.7	28.5	1.12	9.05
	11-Jun	2:05	4:05	5.83	132.3	79.1	42.9	1.1	10.3
	11-Jun	4:05	6:05	5.9	144	75.7	46.7	1.08	10
	11-Jun	6:05	8:05	6.43	91.9	45.8	29.8	1.09	11.2
Event 2	11-Jun	21:55	0:36	5.67	39.5	21	37.5	1.14	8.2
	12-Jun	2:00	3:00	5.98	101	51.2	65.5	1.3	6.4
	12-Jun	3:00	4:00	5.8	85.2	53.2	55.3	0.88	4.7
	12-Jun	4:00	6:00	6.02	126.3	84.8	41	1.41	4.78
	12-Jun	6:00	8:00	6.25	99.4	77.5	32.2	1.63	5.8
Event 3	12-Jun	21:30	23:30	5.97	35.1	16.9	11.4	1.24	10.8
	12-Jun	23:30	1:30	6.67	42.3	20.8	13.7	1.28	10.4
	13-Jun	1:30	3:30	6.38	71.2	43.8	23.1	1.17	11.2
	13-Jun	3:30	5:30	6.21	12.1	29.7	3.92	0.72	14
	13-Jun	5:30	7:30	5.65	31	23.1	10.1	0.84	16.8
Event 4	14-Jun	0:50	1:50	6.65	104.1	40.9	67.5	1.15	7
	14-Jun	1:50	1:50	6.04	139.9	46.9	90.7	1.19	6.1
	14-Jun	2:50	2:50	6.04	140.7	51.4	91.2	1.18	4.89
	14-Jun	3:50	3:50	5.93	103.5	31.9	67.1	1.21	5.9
	14-Jun	4:50	4:50	6.13	101.1	32.2	32.8	1.21	6.45

Table A3-3. Aerosol sample constituent concentrations from past (summer 1985 and 1986, Munger, 1989) and current (June 2015) studies at a hill site in Ventura, California. Concentrations of aerosol constituents measured during the 1985/1986 campaign at CP were similar to those measured at Ventura. All concentrations are in units of nmol m^{-3}. Values below the LOD are shown in italics.

	Aerosol Loading, 1986 (nmol m^{-3})			Aerosol Loading, 2015 (nmol m^{-3})		
Chemical	Mean	Min	Max	Mean	Min	Max
NH_4^+	90	16	239	11.3	*<LOD*	27
NO_3^-	76	18	205	166	12.3	262
Na^+	90	16	239	64.1	29.4	89.1
Cl^-	58	*<LOD*	200	7.6	*<LOD*	17
SO_4^{-2}	67	21	148	108	4.3	244
Ca^{+2}	13	5	31	14.2	6.8	19.4
Mg^{+2}	9.8	1.5	26.5	3.9	0.7	6.8
K^+	--	--	--	1.1	0.4	1.8
Formate	81	38	260	*<LOD*	*<LOD*	1.3
Acetate	74	36	123	*<LOD*	*<LOD*	1.3

Table A3-4. Mean, minimum, and maximum concentrations of organic and inorganic species quantified in fog samples collected at CP (via extraction into a non-polar solvent, methylation, and GC/MS analysis). All concentrations are given in μg L^{-1} from 50 μL final extract volumes; acids were quantified as methyl esters.

Soluble						
	Event 1	Event 2	Event 3	Event 4	Blank	LOD
n-Alkanoic Acids						
C_7	1.54	2.97	8.78	1.78	1.11	0.3
C_8	<*LOD*	<*LOD*	<*LOD*	<*LOD*	<*LOD*	0.5
C_9	7.4	<*LOD*	<*LOD*	<*LOD*	<*LOD*	2
C_{10}	<*LOD*	<*LOD*	<*LOD*	<*LOD*	<*LOD*	2
C_{11}	<*LOD*	<*LOD*	<*LOD*	<*LOD*	<*LOD*	2
C_{12}	<*LOD*	<*LOD*	<*LOD*	<*LOD*	<*LOD*	3
C_{13}	<*LOD*	<*LOD*	<*LOD*	<*LOD*	<*LOD*	3
C_{14}	<*LOD*	3.04	5.32	<*LOD*	<*LOD*	3
C_{15}	<*LOD*	<*LOD*	<*LOD*	<*LOD*	<*LOD*	3
C_{16}	10.5	12.49	82.8	8.83	9.82	2
C_{17}	<*LOD*	<*LOD*	<*LOD*	<*LOD*	<*LOD*	2
C_{18}	12.1	12.5	67.9	9.87	10.9	0.3
C_{19}	<*LOD*	<*LOD*	<*LOD*	<*LOD*	<*LOD*	0.3
C_{20}	<*LOD*	<*LOD*	<*LOD*	<*LOD*	<*LOD*	0.3
C_{21}	<*LOD*	<*LOD*	<*LOD*	<*LOD*	<*LOD*	0.3
C_{22}	<*LOD*	<*LOD*	<*LOD*	<*LOD*	<*LOD*	0.3
C_{23}	<*LOD*	<*LOD*	<*LOD*	1.49	<*LOD*	0.3
Adipate	2.69	5.28	49.2	3.68	1.01	0.09
Azelate	4.4	10.2	73.1	8.67	1.43	0.2
N,N-diethyl-toluamide	12.1	10.9	5.21	20.2	<*LOD*	1.3
CPI	1.59	1.06	1.44	3.2	<*LOD*	--
Insoluble						
	Event 1	Event 2	Event 3	Event 4	Blank	LOD
n-Alkanoic Acids						
C_7	0.365	0.83	1.18	0.559	<*LOD*	0.08
C_8	<*LOD*	<*LOD*	<*LOD*	<*LOD*	<*LOD*	0.2
C_9	<*LOD*	<*LOD*	<*LOD*	<*LOD*	<*LOD*	0.5
C_{10}	<*LOD*	<*LOD*	<*LOD*	<*LOD*	<*LOD*	0.6
C_{11}	<*LOD*	<*LOD*	<*LOD*	<*LOD*	<*LOD*	0.5
C_{12}	<*LOD*	<*LOD*	<*LOD*	<*LOD*	<*LOD*	0.5
C_{13}	1.68	2.14	<*LOD*	<*LOD*	<*LOD*	0.5
C_{14}	<*LOD*	<*LOD*	<*LOD*	<*LOD*	<*LOD*	0.4
C_{15}	<*LOD*	<*LOD*	<*LOD*	<*LOD*	<*LOD*	0.4
C_{16}	2.16	1.22	0.665	5.83	<*LOD*	0.4
C_{17}	<*LOD*	<*LOD*	<*LOD*	<*LOD*	<*LOD*	0.4
C_{18}	1.38	1.19	1.55	3.26	<*LOD*	0.2
C_{19}	<*LOD*	<*LOD*	<*LOD*	<*LOD*	<*LOD*	0.2
C_{20}	<*LOD*	<*LOD*	<*LOD*	<*LOD*	<*LOD*	0.2
C_{21}	<*LOD*	<*LOD*	<*LOD*	<*LOD*	<*LOD*	0.13
C_{22}	<*LOD*	<*LOD*	<*LOD*	<*LOD*	<*LOD*	0.12
C_{23}	<*LOD*	1.34	<*LOD*	1.7	<*LOD*	0.11
Adipate	0.83	1.33	1.48	0.82	<*LOD*	0.05
Azelate	1.23	3.2	1.47	0.64	<*LOD*	0.03
N,N-diethyl-toluamide	3.51	5.1	14.1	4.05	<*LOD*	0.1
CPI	2.53	4.59	13.17	4.12	9.43	--

Table A3-5. Fog sample concentrations of inorganic species.

	Start Date	Start Time	Ca^{2+} (μM)	Cl^- (μM)	K^+ (μM)	Mg^{2+} (μM)	Na^+ (μM)	NH_4^+ (μM)	NO_2^- (μM)	NO_3^- (μM)	SO_4^{2-} (μM)
	10-Jun	22:05	12.7	103	12.7	16.9	120	249	3.4	135	34.9
	11-Jun	0:05	14.6	96	15.1	15.1	148	340	7.5	167	49.1
Event 1	11-Jun	2:05	8.4	67	12.6	9.4	89.4	306	8.8	150	37.8
	11-Jun	4:05	5	36	8	3.3	27.8	263	6.7	114	27.6
	11-Jun	6:05	19.7	37	7.4	5.1	23.2	280	5.6	131	29.8
	11-Jun	21:55	7.3	47	5.3	*<LOD*	51.7	120	2.7	30.4	12.1
	12-Jun	2:00	38.7	283	21.8	43.9	324	197	5.5	112	32.4
Event 2	12-Jun	3:00	5	52	2.7	5.7	43	84.6	3.1	39.4	13.4
	12-Jun	4:00	11.8	52	5	8.4	62.5	128	3.8	42.2	14.3
	12-Jun	6:00	33.9	30	4.5	8.8	38.4	140	4.5	47.6	15
	12-Jun	21:30	67.2	199	14.1	34.8	263	300	7	220	43.1
	12-Jun	23:30	63.7	165	18.6	36.1	239	312	7.7	204	40.4
Event 3	13-Jun	1:30	63.9	188	22.3	40.5	269	352	9.1	270	50.7
	13-Jun	3:30	35.2	112	19.2	22.8	153	404	10.3	289	48.6
	13-Jun	5:30	72.8	139	20.3	40.1	205	640	15.8	778	90
	14-Jun	0:50	18	128	7.9	18.4	153	189	3.9	73.7	21.4
	14-Jun	1:50	12.4	51	6	8.8	53.8	176	3.3	54.6	17.7
Event 4	14-Jun	2:50	5.7	34	4.1	2.8	24	145	3.6	44	12.5
	14-Jun	3:50	8.1	44	5.2	3.4	14.7	182	3.2	65	12.2
	14-Jun	4:50	17	46	9.6	5.6	25.6	200	4	97	15

Table A3-6. Fog sample concentrations of Polar Organic Species.

Start Date	Start Time	4-Nitrophenol (nM)	2-Methyl-4-Nitrophenol (nM)	2,4-Di-Nitrophenol (nM)	Adipate (nM)	Pinonate (nM)	Pinate (nM)	Azelate (nM)	Total Nitrophenols (nM)
10-Jun	22:05	0.006	0.006	*<LOD*	0.075	0.055	0.007	0.08	0.016
11-Jun	0:05	0.004	*<LOD*	0.012	0.055	0.056	0.003	0.12	0.016
11-Jun	2:05	0.005	*<LOD*	0.016	0.083	0.039	0.012	0.08	0.022
11-Jun	4:05	0.004	*<LOD*	0.015	0.06	0.036	0.007	0.09	0.019
11-Jun	6:05	0.005	*<LOD*	0.014	0.061	0.047	0.013	0.14	0.018
11-Jun	21:55	0.005	*<LOD*	0.004	0.078	0.039	0.019	0.14	0.009
12-Jun	2:00	0.004	*<LOD*	*<LOD*	0.051	0.025	*<LOD*	0.09	0.005
12-Jun	3:00	0.004	*<LOD*	0.005	0.031	0.02	*<LOD*	0.04	0.009
12-Jun	4:00	0.004	*<LOD*	0.005	0.035	0.024	*<LOD*	*<LOD*	0.008
12-Jun	6:00	0.004	*<LOD*	0.009	0.046	0.043	0.005	0.07	0.013
12-Jun	21:30	0.006	0.015	*<LOD*	0.199	0.06	0.009	0.1	0.024
12-Jun	23:30	0.01	0.037	0.005	0.206	0.07	0.016	0.13	0.055
13-Jun	1:30	0.015	0.034	0.011	0.179	0.059	0.015	0.1	0.059
13-Jun	3:30	0.012	0.007	0.026	0.14	0.059	0.02	0.18	0.045
13-Jun	5:30	0.014	*<LOD*	0.056	0.158	0.09	0.036	0.22	0.07
14-Jun	0:50	0.007	0.014	0.005	0.113	0.022	0.006	0.07	0.026
14-Jun	1:50	0.005	0.009	0.004	0.09	0.029	*<LOD*	0.05	0.019
14-Jun	2:50	0.006	*<LOD*	0.004	0.058	0.04	*<LOD*	0.03	0.009
14-Jun	3:50	0.011	0.029	0.01	0.063	0.044	0.007	0.06	0.051
14-Jun	4:50	0.008	0.008	0.016	0.088	0.076	0.009	0.22	0.033

Table A3-7. Fog sample concentrations of low molecular mass organic species.

Start Date	Start Time	HCHO (μM)	Lactate (μM)	Acetate (μM)	Propionate (μM)	Formate (μM)	MSA (μM)	Pyruvate (μM)	Valerate (μM)	Glutarate (μM)	Succinate (μM)	Malonate (μM)	Maleate (μM)	Oxalate (μM)
10-Jun	22:05	4.1	2.3	8	1.1	21	3.6	1.7	0.3	1.8	4.41	5.6	0.6	12
11-Jun	0:05	2.6	3.4	16	2.1	39	5.5	2.9	0.2	2.2	5.82	7.1	0.6	16.8
11-Jun	2:05	5.4	2.6	14	1.8	32	4	2	0.2	1.6	3.98	5.4	0.2	12.3
11-Jun	4:05	5.3	0.7	16	1.3	33	2.5	1	0.3	1	2.88	0.2	0.3	7.5
11-Jun	6:05	6.6	2.6	19	2	39	2.7	1.1	0.3	2.6	3.35	0.2	0.3	7.6
11-Jun	21:55	2.6	2.4	13	1.2	22	2.2	1.4	0.2	0.8	0.56	1.6	0.3	6.9
12-Jun	2:00	1.5	2.3	13	1.3	19	3.6	1.7	0.2	1.3	2.36	4.2	0.4	12.4
12-Jun	3:00	2.7	1.5	8	0.8	23	2.2	0.9	0.2	0.8	1.59	2.1	0.5	5.2
12-Jun	4:00	3.1	1.5	7	0.5	16	1.8	0.7	0.2	0.5	1.13	1.5	0.4	5
12-Jun	6:00	3.7	2.7	10	11	17	2	1.3	0.2	0.7	1.37	1.8	1.1	5.7
12-Jun	21:30	5.6	5.1	17	2.5	32	4.3	4.1	0.2	3.2	1.72	7.4	0.3	15
12-Jun	23:30	2.7	5	16	2.2	24	4.8	2.9	0.2	4	3.57	10.6	0.5	24.5
13-Jun	1:30	3.4	5.2	16	2.2	28	5.7	4.7	0.2	3.8	5.28	10.3	0.4	27.1
13-Jun	3:30	3	6.2	16	2.1	31	6	4.2	0.3	4.9	6.27	12.5	1.1	29.8
13-Jun	5:30	4.9	7.7	22	2.5	33	7.3	4.6	0.2	5.5	4.94	10.2	1.5	32.6
14-Jun	0:50	1.7	3.3	18	1.8	24	3	2.2	0.2	2.9	4.78	7.2	0.2	16.7
14-Jun	1:50	2.5	2.7	13	1.5	19	2.5	2.1	0.2	2.1	3.54	5.5	0.5	12.5
14-Jun	2:50	1.3	2	8	1	11	1.8	1.7	0.2	1.6	2.52	3.7	0.7	7.3
14-Jun	3:50	3.1	3.4	8	1.1	12	1.5	1.6	0.3	1.5	1.98	2.6	0.7	6.3
14-Jun	4:50	2.3	11.5	7	1	11	1.7	2.2	0.7	1.5	1.38	2	0.6	7.1

Table A3-8. Fog water constituents tentatively identified via (-)-ESI-ToF-MS. "x" markers indicate whether the species were identified in each sample during the four fog events observed.

			Event 1					Event 2						Event 3					Event 4				
m/z⁻	Formula	t_R (min)	6/10/15 22:05	6/11/15 0:05	6/11/15 2:05	6/11/15 4:05	6/11/15 6:05	6/11/15 21:55	6/12/15 2:00	6/12/15 3:00	6/12/15 4:00	6/12/15 6:00	6/12/15 21:30	6/12/15 23:30	6/13/15 1:30	6/13/15 3:30	6/13/15 5:30	6/14/15 0:50	6/14/15 1:50	6/14/15 2:50	6/14/15 3:50	6/14/15 4:50
103.04	C4H8O3	3.2	x	x		x		x	x		x			x	x	x	x			x		
103.04	C4H8O3	2.3											x	x	x	x	x	x	x	x	x	
108.10	C9H16O3	19.4																				
113.02	C5H6O3	3.9												x	x	x	x	x				
113.02	C5H6O3	2.5	x	x	x			x			x		x	x		x	x	x	x		x	
113.06	C6H10O2	13.5														x						
113.06	C6H10O2	5.5												x	x	x	x					
113.06	C6H10O2	11.3							x				x		x	x	x					
115.00	C4H4O4	2.1	x	x	x	x	x	x	x	x	x	x	x	x	x	x	x	x	x	x	x	x
115.04	C5H8O3	3.2	x	x	x	x																
115.04	C5H8O3	4.1												x	x	x			x			
115.04	C5H8O3	8.6															x					
115.04	C5H8O3	2.9	x	x	x	x	x	x	x	x	x	x	x	x	x	x	x	x	x	x	x	x
117.06	C5 H10 O3	3.5	x	x	x	x	x	x	x	x	x	x	x	x	x	x	x	x		x	x	x
117.06	C5H10O3	4.7											x	x		x	x					
121.03	C7H6O2	9.9	x	x	x	x	x			x					x	x	x	x			x	
122.08	C9H14O4	9.9																		x		
129.02	C5H6O4	3.3	x	x		x	x		x	x	x	x	x	x	x	x	x			x	x	x
129.06	C6H10O3	7.1											x	x	x	x	x	x				
129.06	C6H10O3	8.3															x					
129.06	C6H10O3	6.2											x	x	x		x	x				
131.03	C5H8O4	3.3	x	x		x	x	x	x	x	x	x	x	x	x	x	x	x	x	x	x	x
131.03	C5H8O4	4.5	x	x	x	x	x	x	x	x	x	x	x	x	x	x	x	x	x	x	x	x
131.04	C5H8O4	6											x	x	x	x	x					
131.07	C6H12O3	7.4		x	x	x	x						x	x	x	x	x					
131.11	C6H12O3	8.1											x				x					
135.04	C8H8O2	12.4	x	x									x	x	x							
137.02	C7H6O3	8.9														x						
137.02	C7H6O3	16.6		x		x	x															
138.02	C6H5NO3	13.3	x	x	x	x	x	x	x	x	x	x	x	x	x	x	x	x	x	x	x	x
138.02	C6H5NO3	13.5	x		x								x	x	x	x	x	x	x		x	x
143.03	C6H8O4	2.6	x	x	x								x	x	x	x	x	x				
143.04	C6H8O4	3.3														x	x					
143.04	C6H8O4	7.1															x					
145.05	C6H10O4	2.5						x	x				x	x		x	x	x	x	x	x	
145.05	C6H10O4	7.6	x	x	x	x	x	x	x				x	x	x	x	x	x	x	x	x	x
145.05	C9H6O2	9.6	x	x	x	x	x	x	x				x	x	x	x	x	x	x		x	x
145.05	C6H10O4	2.8	x						x					x		x	x	x			x	x
145.05	C6H10O4	7.8	x	x	x	x	x	x					x	x	x	x	x		x		x	x
145.05	C6H10O4	9.2											x	x	x	x	x					
147.03	C5H8O5	2.0	x	x	x	x	x	x	x	x		x	x	x	x	x	x	x	x	x	x	x
149.02	C8H5O3	9.5															x					
152.03	C7H7NO3	19.7	x	x	x			x					x	x	x	x		x	x	x	x	x
152.03	C7H7NO3	18.2	x	x	x			x					x	x	x	x	x	x	x	x	x	x
154.01	C6H5NO4	10.4												x			x					
157.05	C7H10O4	6.5	x	x	x	x	x	x			x		x	x	x	x	x	x			x	x
157.05	C7H10O4	5.4	x	x					x			x	x	x	x	x	x		x	x	x	
159.03	C6H8O5	2.02															x					
159.06	C7H12O4	4.4													x	x	x					
159.07	C7H12O4	6.9														x	x					
159.07	C7H12O4	11.6															x					
159.07	C7H12O4	10.8															x					
159.07	C7H12O4	10.4											x	x	x	x	x					
159.07	C7H12O4	13.4															x					
161.03	C8H6N2O2	19.8												x			x	x	x			
161.04	C6H10O5	2.6															x					
161.05	C6H10O5	2.3	x	x	x	x	x	x	x	x	x	x	x	x	x	x	x	x	x	x	x	x
164.07	C9H11NO2	3.4					x															
165.02	C8H5O4	11.2												x								

165.02	C8H6O4	10.1	x	x	x	x	x					x		x	x	x	x	x	x	x	x	x
168.03	C7H7NO4	10.5	x	x									x	x	x	x	x					
171.06	C8H12O4	8.5	x	x	x	x	x	x	x	x	x	x	x	x	x	x	x	x	x	x	x	x
171.07	C8H12O4	9.0															x					
171.07	C8H12O4	7.2											x	x	x	x	x					
171.10	C9H16O3	15.8		x				x														
171.10	C9H16O3	20.1	x	x	x	x	x	x				x		x	x	x	x	x				x
173.04	C7H9O5	3.5		x	x		x	x	x				x	x	x	x	x	x				
173.04	C7H10O5	2.6														x	x					
173.05	C7H10O5	4.4	x	x	x	x	x		x	x	x	x	x	x	x	x	x	x	x	x	x	x
173.05	C7H10O5	2.3											x	x	x	x	x					
173.05	C7 H10 O5	3.1	x	x	x	x	x	x	x	x	x	x	x	x	x	x	x	x	x	x	x	x
173.08	C8H14O4	15.9						x									x					x
175.03	C6H8O6	2.1	x	x	x	x	x		x				x	x	x	x	x	x	x	x	x	
175.06	C7H12O5	9.5				x										x	x					
175.06	C7H12O5	7.6															x					
175.06	C7H12O5	9.5															x					
175.06	C7H12O5	4.1											x	x		x	x					
175.06	C7H12O5	3.5	x											x		x	x					
179.03	C9H8O4	15.5											x	x	x		x					
182.01	C7H5NO5	19.1															x					
182.02	C11H5NO2	17.2														x	x					
183.00	C4H8O6S	2.0															x					
183.01	C6H4N2O5	15.3				x	x					x			x	x	x				x	x
183.10	C10H16O3	19.3											x	x								
183.10	C10H16O3	16.4	x	x	x		x	x				x	x	x	x	x	x				x	x
183.10	C10H16O3	17.8						x								x	x					x
185.04	C8H10O5	9.3			x	x	x															
185.05	C8H10O5	9.2					x									x	x					
185.08	C9H14O4	8.5	x	x	x	x	x	x	x	x	x	x	x	x	x	x	x		x		x	x
185.08	C9H14O4	10.7															x					
185.08	C9H14O4	11.1											x	x	x	x	x					
185.08	C9H14O4	18.1	x	x	x	x	x					x		x	x	x	x					
185.08	C9H14O4	10.0											x	x	x	x	x	x				
185.08	C9H14O4	13.8						x									x					
186.11	C9H17NO3	14.6																				x
187.06	C8H12O5	8.1	x	x	x	x	x						x	x	x	x	x	x	x	x	x	x
187.06	C8H12O5	5.2	x	x	x	x	x	x	x	x	x	x	x	x	x	x	x	x	x			x
187.06	C8H12O5	4.1													x	x						
187.06	C8H12O5	6.2		x		x	x			x			x	x	x	x	x					x
187.06	C8H12O5	3.8													x	x	x					
187.10	C9H16O4	19.9	x	x	x	x	x	x	x	x	x	x	x		x	x	x	x	x	x	x	x
189.04	C710O6	2.1	x	x	x	x	x		x				x	x	x	x	x	x	x			x
189.04	C7H10O6	3.8													x	x	x					
189.08	C8H14O5	6.8													x	x	x					
191.09	C8H16O5	2.7					x															
193.05	C10H10O4	12.3					x															
199.10	C10H16O4	10.3															x					
199.10	C10H16O4	13.4											x	x	x	x	x		x			x
199.10	C10H16O4	10.9	x					x					x	x	x	x	x		x		x	x
201.08	C9H14O5	4.9															x					
201.08	C9H14O5	11.3											x	x	x	x	x					
201.08	C9H14O5	7.4															x					
201.11	C10H18O4	10.7														x	x					
203.05	C8H12O6	2.3														x	x					
203.05	C8H12O6	3.1												x		x	x					
203.06	C8H12O6	9.0	x	x	x	x	x		x	x		x	x	x	x	x	x	x	x			x
203.06	C8H12O6	9.2											x	x			x					
203.13	C10H20O4	20.2		x		x	x										x					
204.15	C9H16O7S	10.7															x					
215.09	C10H16O5	12.2	x	x	x	x	x	x	x	x		x	x	x	x	x	x	x		x		x
216.00	C7H7NO5S	10.1												x				x		x		
217.07	C9H14O6	13.5	x	x	x		x		x				x	x	x	x	x		x			
217.07	C9H14O6	10.8												x	x	x	x					
217.07	C9H14O6	11.2							x				x	x	x	x	x					
225.01	C6H10O7S	2.7	x													x	x					
231.09	C10H16O6	8.6															x					
231.09	C10H16O6	14.1	x	x	x		x	x	x	x	x	x	x	x	x	x	x	x	x	x	x	x
231.99	C7H7NO6S	10.4												x								
232.05	C8H10NO7	9.2					x									x	x					

250.06	C8H13NO8	7.7		x	x							x			
253.04	C8H14O7S	12.7										x			
261.13	C12H22O6	19.1									x	x			x
262.09	C10H17NO7	17.5									x				
271.17	C18H24O2	9.3				x									x
288.16	C17H23NO3	9.3												x	
288.16	C17H23NO3	9.3												x	
295.04	C8H12N2O10	9.2		x						x	x				
296.04	C9H15NO8S	18.4									x				
312.10	C21H15NO2	2.6		x											
339.10	C11H20N2O10	20.1			x							x			
339.10	C11H20N2O10	19.3		x											

APPENDIX 4: HOW DO COMPONENTS OF REAL CLOUD WATER AFFECT AQUEOUS PYRUVATE OXIDATION?

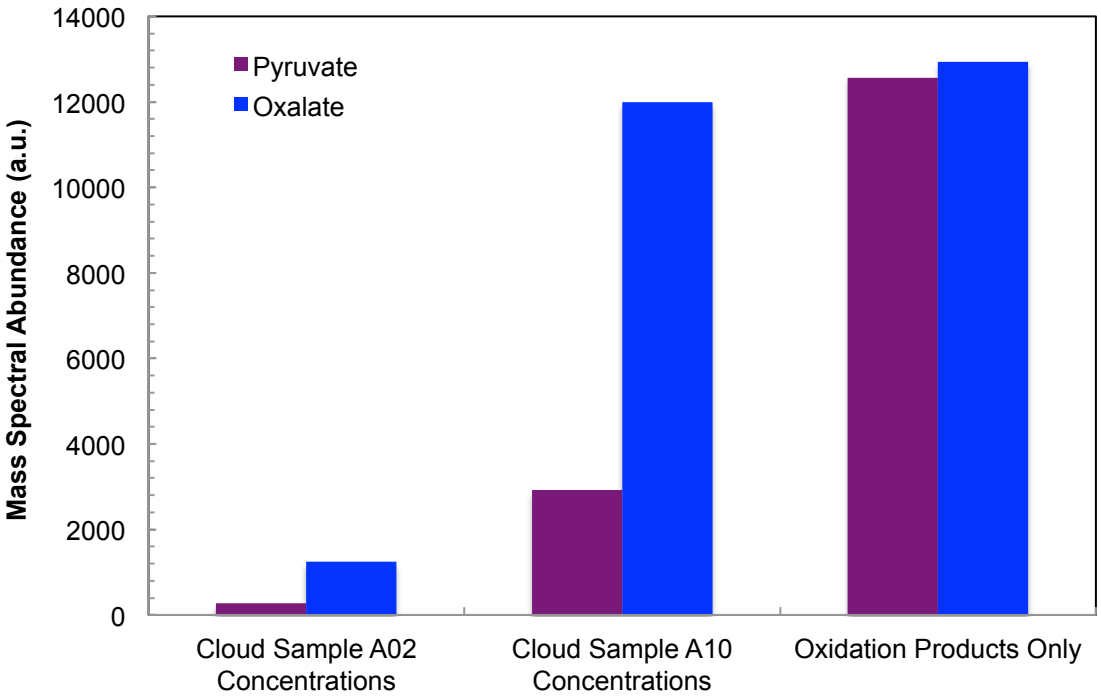

Figure A4-1. Suppression effects encountered when introducing cloud-relevant inorganic salt concentrations to the ESI-HR-ToF-MS. Mass spectral response (shown in mass spectral abundance units) decreases by an order of magnitude when 1400 μM ammonium nitrate and 1200 μM ammonium sulfate (concentrations similar to those in cloud sample A02) are introduced to the 90-min oxidation products of pyruvate.

Table A4-1. Starting parameters in control and •OH measurement experiments (n=1 in all cases). Concentrations of pyruvate were measured using IC-conductivity and salicylate measured using LC-UV/vis (202±4 nm absorbance). Mount Tai cloud water sample A01 was collected directly prior to A02 and was of similar composition. Uncertainties are ±90% CI. Concentrations of •OH were measured using salicylate degradation (values used in calculations for pyruvate oxidations are shown in parentheses). The literature rate constant of 1.6×10^{10} M^{-1} sec^{-1} (Buxton et al., 1988) was used for salicylate oxidations.

	Initial H_2O_2 conc. (μM)	Initial pyruvate conc. (μM)	Initial salicylate conc. (μM)	Initial UV-C light photon flux (Einsteins sec^{-1})	•OH conc. (M)	Measured reaction rate (μM min^{-1})	Reaction rate constant (μM^{-1} min^{-1})
Salicylate in cloud sample A01	150	0	22.3	1×10^{-7}	3.1×10^{-14}	-0.7	1.6×10^{10}
Salicylate in cloud sample A02, no H_2O_2	0	0	51.7	1×10^{-7}	5.0×10^{-15}	-0.2	1.6×10^{10}
Salicylate in pure water	150	0	30.2	1×10^{-7}	6.9×10^{-14}	-2.0	1.6×10^{10}
Salicylate in pure water (rep. 2)	150	0	16.2	1×10^{-7}	6.7×10^{-14}	-1.0	1.6×10^{10}
Salicylate in pure water (rep. 3)	150	0	23.6	1×10^{-7}	6.3×10^{-14}	-1.4	1.6×10^{10}
Salicylate in pure water, no H_2O_2	0	0	23.8	1×10^{-7}	1.2×10^{-14}	-0.3	1.6×10^{10}
Pyruvate in pure water, no H_2O_2	0	34	0	1×10^{-7}	(6.9×10^{-8})	-0.1	4.5×10^{4}
Pyruvate in pure water, no UV	150	36	0	0	(6.9×10^{-8})	-1.0	4.2×10^{5}

Table A4-2. Carbonaceous components of less polluted cloud sample (A10; collected on 07/04/2008). IC-ESI-HR-ToF-MS separation and detection at 0 min reaction was used to obtain accurate ion formulae. Fewer components are present in this sample in comparison to those detected in the polluted cloud sample A02; detected components include some organic acids and inorganic species.

m/z^-	Probable Ion Formula	Accuracy (mDa)
59.015	$C_2H_4O_2$	-0.95
60.994	CH_2O_3	-0.64
69.035	C_4H_6O	-0.63
85.030	$C_4H_6O_2$	-0.5
87.009	$C_3H_4O_3$	-0.38
94.981	CH_4SO_3	5.26
111.009	$C_5H_4O_3$	-0.08
112.017	$C_5H_5O_3$	0.08
113.024	$C_5H_6O_3$	0.23
129.056	$C_6H_{10}O_3$	-0.20
131.034	$C_5H_8O_4$	0.58
139.040	$C_7H_8O_3$	0.37
157.014	$C_6H_6O_5$	0.42
175.024	$C_6H_8O_6$	0.96
183.002	$C_6H_4N_2O_5$	3.13
201.040	$C_8H_{10}O_6$	0.36
219.051	$C_8H_{12}O_7$	-0.09
227.055	$C_{10}H_{12}O_6$	1.64
271.047	$C_{11}H_{12}O_8$	-0.97
272.991	$C_cH_{10}O_{10}S$	0.52

Table A4-3. Components of polluted cloud sample (A02; collected on 06/19/2008). IC-ESI-HR-ToF-MS separation and detection at 0 min was used to generate accurate ion formulae. Influence from biomass burning was suggested by the presence of soot/ash particles, nitrated aromatic species in the sample, and the transport and sample composition of Desyaterik et al. (2013).

m/z^-	Possible Formula	Accuracy (mDa)
110.977	No good match	
138.020	$C_6H_5NO_3$	-0.69
138.972	$C_2H_4O_5S$	-1.42
140.987	No good match	
152.988	$C_3H_6O_5S$	-1.33
154.015	$C_6H_5NO_4$	-0.42
154.967	No good match	
165.019	$C_8H_6O_4$	-0.04
173.045	$C_7H_{10}O_5$	0.57
181.018	$C_5H_{10}O_5S$	-0.34
182.011	$C_7H_4NO_5$	-1.52
183.002	$C_6H_4N_2O_5$	3.09
184.983	No good match	
189.042	$C_7H_{10}O_6$	-1.4
198.993	$C_4H_8O_7S$	-0.22
203.055	$C_8H_{12}O_6$	1.24
209.013	$C_6H_{10}O_6S$	-0.76
211.001	$C_9H_7O_4S$	0.69
213.007	$C_7H_6N_2O_6$	8.03
223.029	No good match	
225.008	$C_6H_9O_7S$	-4.05
226.996	No good match	
229.008	$C_5H_{10}O_8S$	2.55
231.994	$C_6H_5N_2O_8$	3.69
233.973	$C_6H_5NO_7S$	-1.23
239.024	$C_7H_{12}O_7S$	-0.9
241.018	$C_{10}H_{10}O_5S$	-0.22

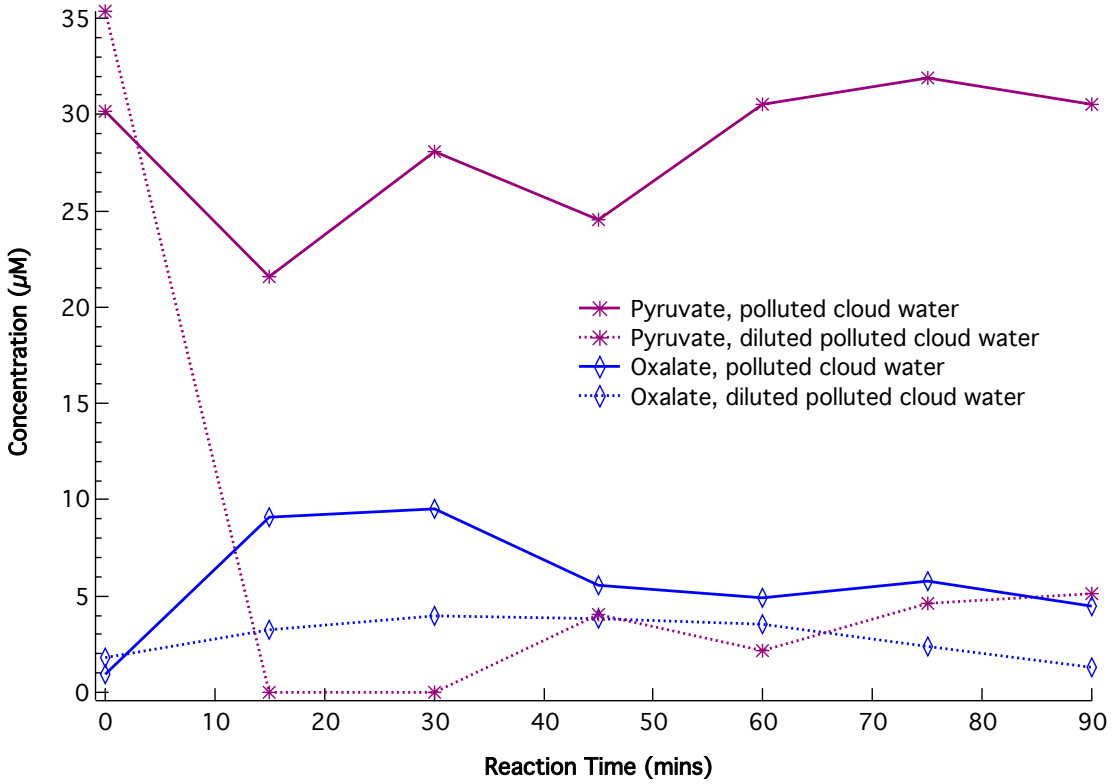

Figure A4-2. Compared oxalate and pyruvate concentration profiles (measured offline using IC-conductivity) in polluted cloud water sample A02 and diluted A02 (1:4 in water). Both oxidations include approximately 30 μM initial pyruvate concentration. A small decrease in oxalate production was observed in PyrOxA02 dilute as compared to PyrOxA02; this suggests that oxalate was produced from organic cloud water components or that additional oxidant molecules were generated by reactions of cloud water components. Pyruvate degradation was more rapid in PyrOxA02 dilute, in agreement with results of the PyrOxA10 and PyrOx experiments. Pyruvate production within the cloud sample components was likely responsible for part of the apparent slowing of pyruvate oxidation in the PyrOxA02 reaction, as shown by the increase in pyruvate concentrations after 15 min in both A02 reactions.

APPENDIX 5: AQUEOUS ATMOSPHERIC OXIDATION PROCESSES IN REAL FOG AND CLOUD WATER

Total Organic Carbon Analysis

The concentrations of total organic carbon were measured before and after each oxidation (using a Sievers 800 Turbo, described in the Method section of this paper). However, the values after oxidation were frequently greater than those measured before oxidation; since no carbon should have been added to the system during oxidation, it is unlikely that these measurements are accurate. It is instead probable that either: (a) the concentration of TOC before oxidation was underestimated in at least some samples due to incomplete UV/chemical oxidation during TOC measurement of carbonaceous species; or (b) some TOC was added by discrete sampling methods (only low concentrations of organic acids were detected in oxidation method blanks, however). The conversion of inorganic to organic carbon via carbonate radical formation via addition of carbonate radicals to organic molecules has not been documented (Huang, 2000; Medinas et al., 2007). Contrast between a 30 μM standard of 4-nitrophenol and the theoretical TOC concentration of this solution were within the estimated 5% error of this instrumental method (2.16 ppmC theoretical versus 2.15 ppmC measured), demonstrating that the instrument was functioning properly at the time of the analyses. In addition, TOC in the sample composites were re-measured several months after the oxidation experiments and analyses, with results similar to the original measurements. Because of this discrepancy, TOC measurements after oxidation (at t=120 min) were only reported to contrast the control experiments (without UV and without H_2O_2) with the UV/H_2O_2 BYOx experiment.

Changes in Absorption of Light by Samples

Light absorption is an important characteristic of chemical components within aerosol and atmospheric water because of the change in visibility degradation and energy distribution within the atmosphere. Feng *et al.* (2013) suggested that 19% of global anthropogenic aerosol light absorption might be due to brown carbon species (those absorbing within the visible light range). Oxidative changes to

brown carbon could increase or decrease absorptive properties within different wavelength ranges: the fragmentation of conjugated double bond structures could cause the absorption band to shift and/or diminish in intensity, while an increasing degree of oxygenation due to functionalization processes would likely enhance the absorption of species, particularly at low (180-250 nm) wavelengths. The change in light absorption in the ultraviolet and visible ranges (190-900 nm) within cloud and fog water samples, as well as in relevant standards, was measured throughout each oxidation experiment. Due to an equilibration period of the UV/visible absorption signal for each sample after the sampling line was introduced, the initial measured absorption spectrum varied (10-50 min).

The metric E2:E3, defined as the ratio between the total solution absorption of light at 254 nm and that at 365 nm, has been used previously to describe the development of higher molecular mass molecules through photodegradation of terrestrial aquatic dissolved organic matter (De Haan and De Boer, 1987; Helms et al., 2008). The value of E2:E3 therefore may provide some insight into the portion of unidentified organic matter in real samples, and whether there is any formation/degradation of large molecules (De Haan & De Boer classified E2:E3 ratios for molecular size ranges <5 nm, 5-10 nm, 10-20 nm, 20-35 nm, and 35-200 nm). The value of E2:E3 reflects a change in the light absorption by organic compounds during oxidation, which is typified by greater absorption at low wavelengths (i.e., 254 nm) after reaction. In the case of terrestrial water systems where concentrations of organics are greater than in atmospheric waters, aqueous oxidation products of a functionalized benzoic acid absorbed at higher wavelengths than those of the original compound, suggestive of oligomerization to form substances similar to humic and fulvic acids (Hoffer et al., 2004). Atmospheric water organic concentrations may more likely generate absorption at lower wavelengths due to the breaking of conjugated molecules and the formation of low molecular mass, carbonyl-containing molecules that can absorb in the 190-250 nm range due to n $\rightarrow$ π^* transition (this is expected for fog and cloud; wet aerosol particles may be more similar to terrestrial waters). Relatively greater absorption of light at 254 nm versus 365 nm would result in E2:E3 > 1, such that values of E2:E3 are expected to increase during oxidation.

The result of most oxidation experiments was a decrease in the absorption of light at 254 nm (UV-C) and 365 nm (UV-A). The change in absorption of light 365-900 nm was minimal. It was found that the metric E2:E3 was not relevant for the UV/vis spectra collected from the atmospherically relevant standards and atmospheric water samples because the wavelengths selected varied similarly to one another within the oxidations, and because the scale of the change in absorption was not reflected by the metric. The change in absorption at specific wavelengths should instead be employed to describe the absorptive changes due to AAOPs (Δ210, Δ254, and Δ450, representing the far UV, near UV, and visible ranges, respectively).

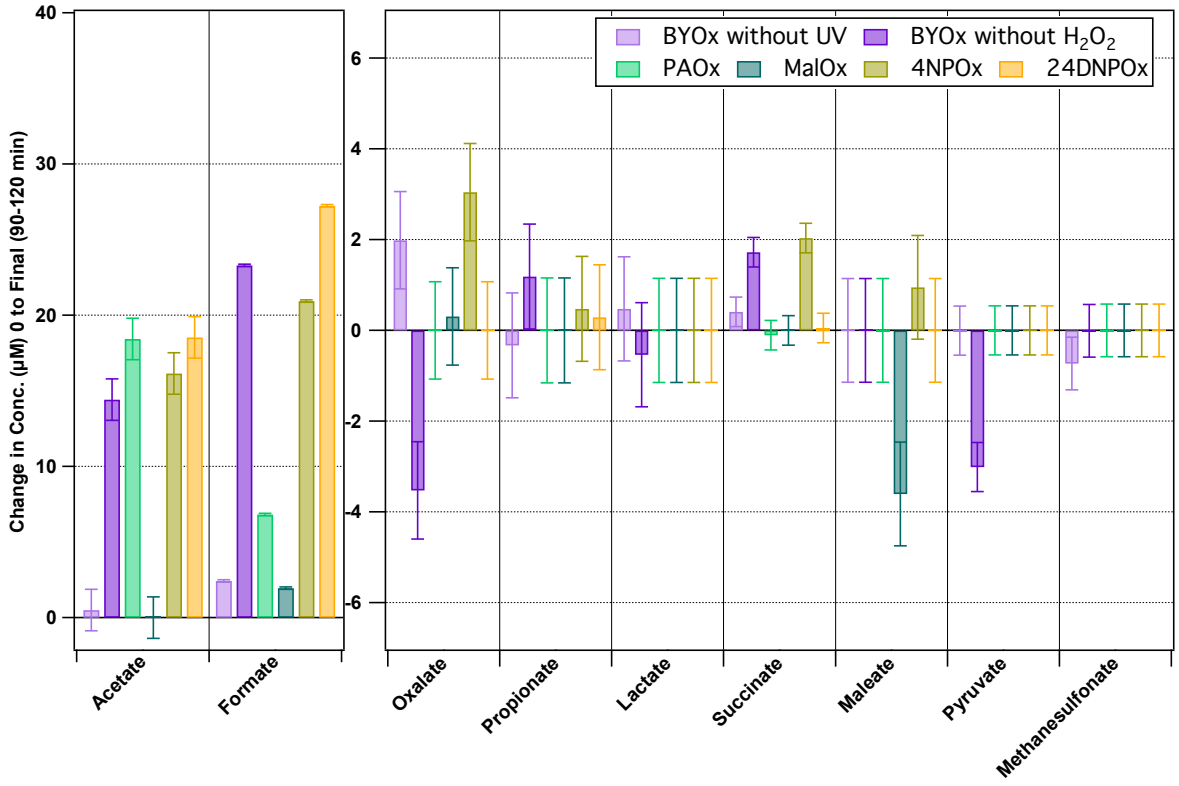

Figure A5-1. Change in concentration of organic acids between 0 and 120 min oxidation (or final time) of control experiments and authentic standards. Error bars represent the 95% confidence interval for each organic acid species.

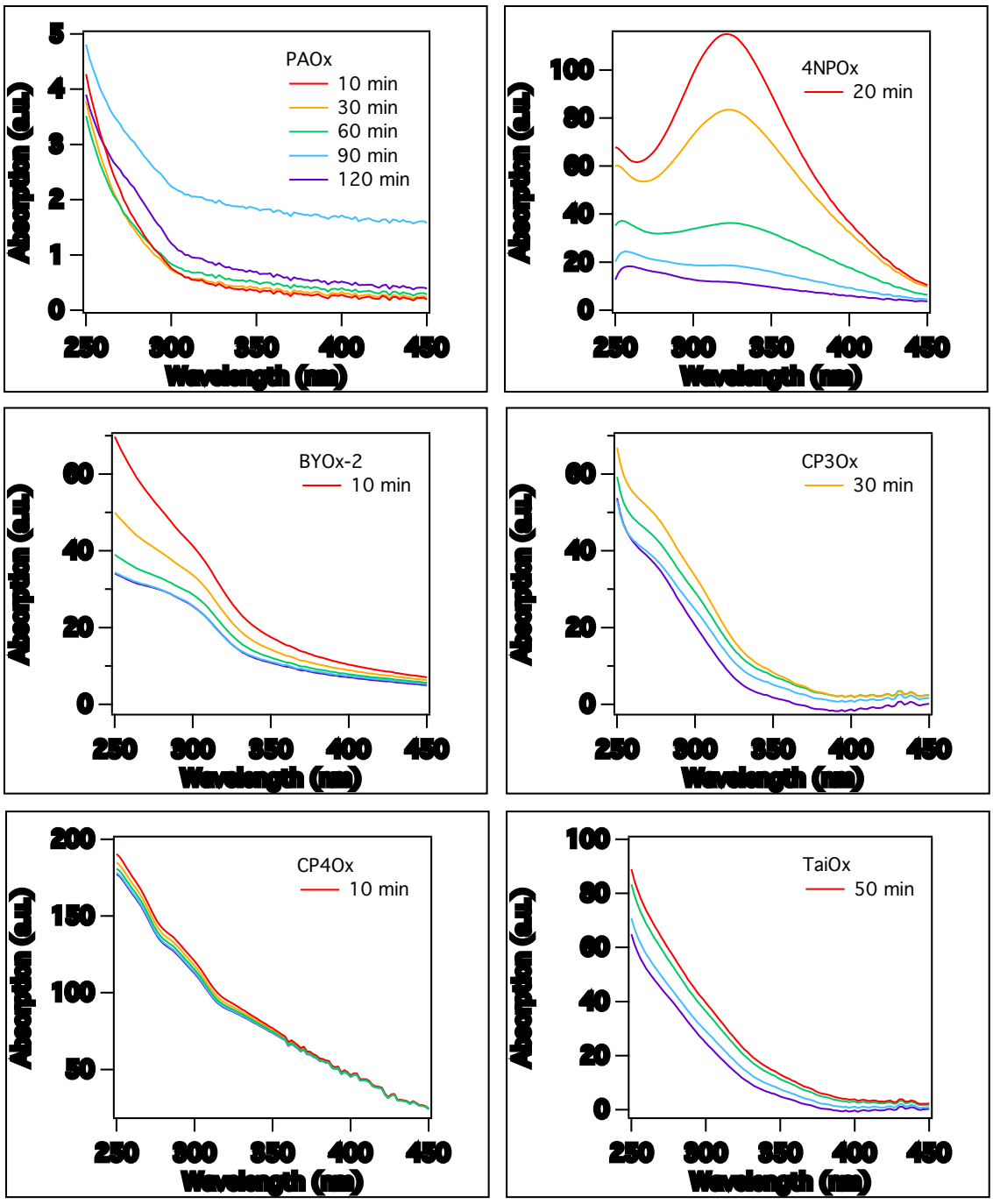

Figure A5-2. Ultraviolet/visible absorption spectra (250-450 nm) during oxidations of samples and standards. Experiment abbreviations are as follows: PAOx = pinonic acid; 4NPOx = 4-nitrophenol; BYOx-2 = Baengnyeong Island, Korea fog sample composite replicate #2; CP3Ox = Casitas Pass, Calif. fog sample event 3 composite; CP4Ox = Casitas Pass, Calif. Fog sample event 4 composite; TaiOx = Mount Tai, China cloud water sample composite. Spectral colors are as follows: Red = Initial spectrum (10-50 min); Yellow = 30 min; Green = 60 min; Blue = 90 min; Purple = 120 min. Notes: the scale of each y-axis is different; absolute values of absorption should be compared between spectra due to auto-zeroing at the beginning of each oxidation; absorption in the 750-850 nm range was subtracted from each spectrum in order to mitigate some of the auto-zeroing effect.

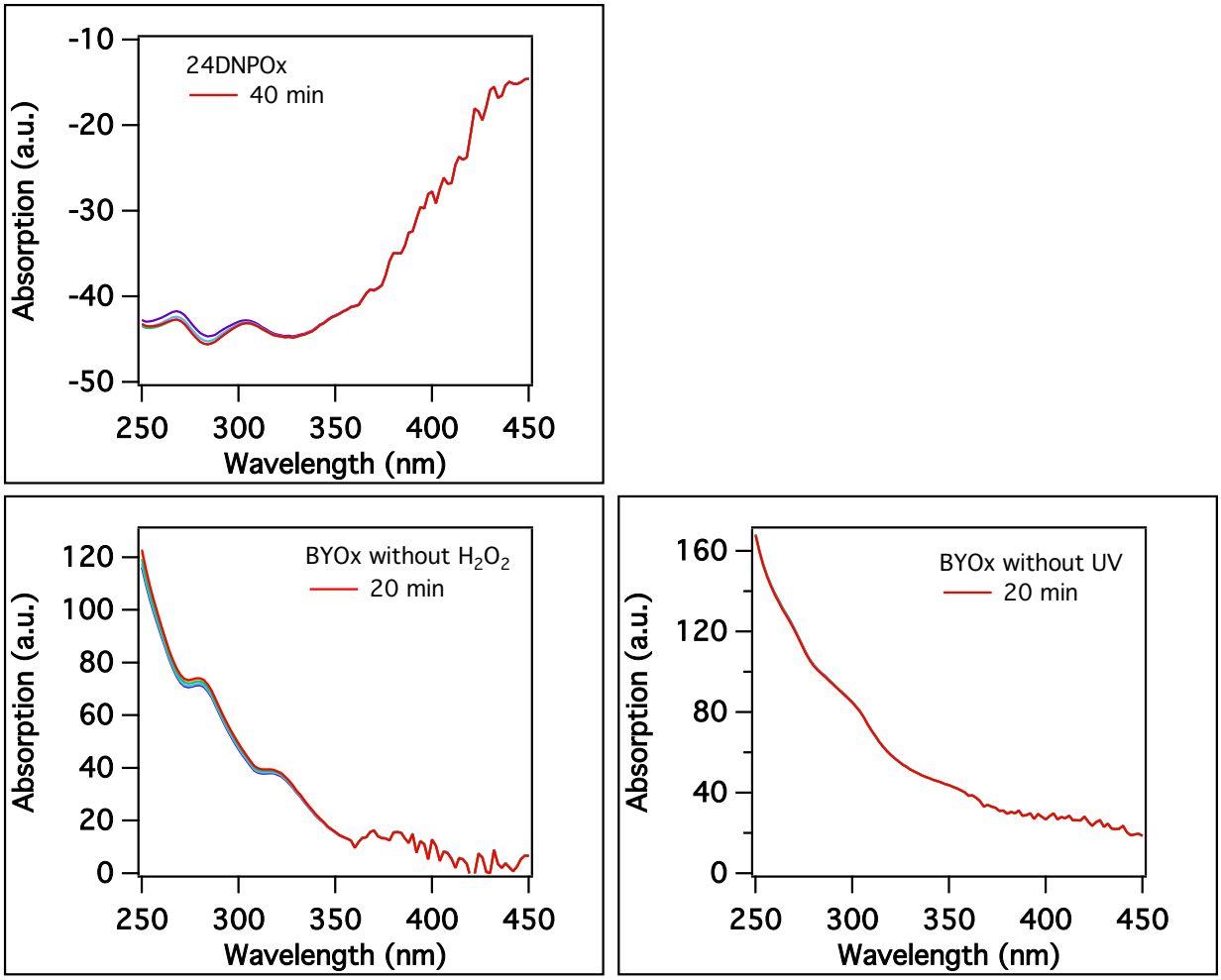

Figure A5-3. Ultraviolet/visible absorption spectra (250-450 nm) during oxidations of samples and standards. See Figure A5-2 for experiment abbreviations and spectral colors.

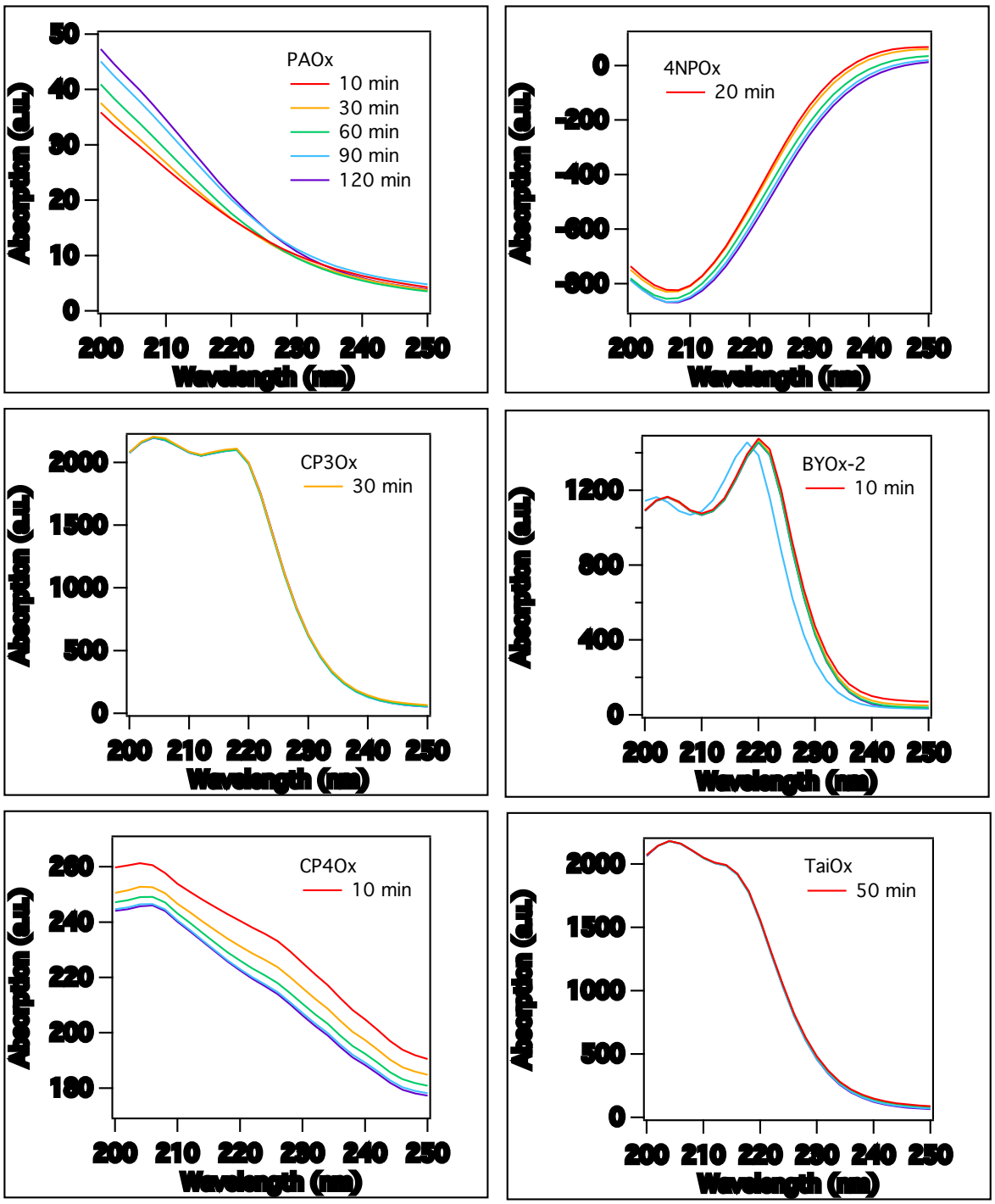

Figure A5-4. Ultraviolet/visible absorption spectra (200-250 nm) during oxidations of samples and standards. See Figure A5-3 for experiment abbreviations and spectral colors.

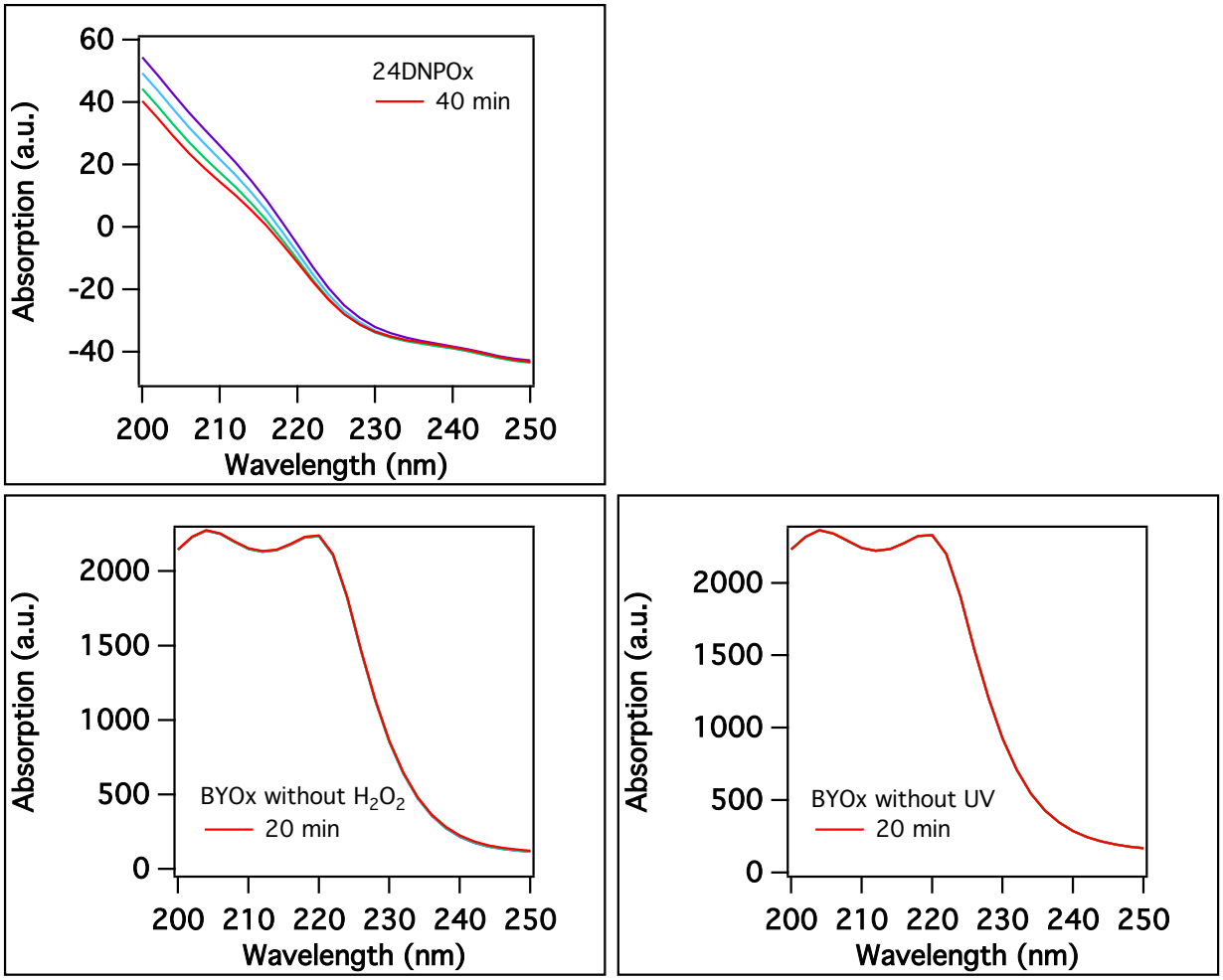

Figure A5-5. Ultraviolet/visible absorption spectra (200-250 nm) during oxidations of samples and standards. See Figure A5-4 for experiment abbreviations and spectral colors.

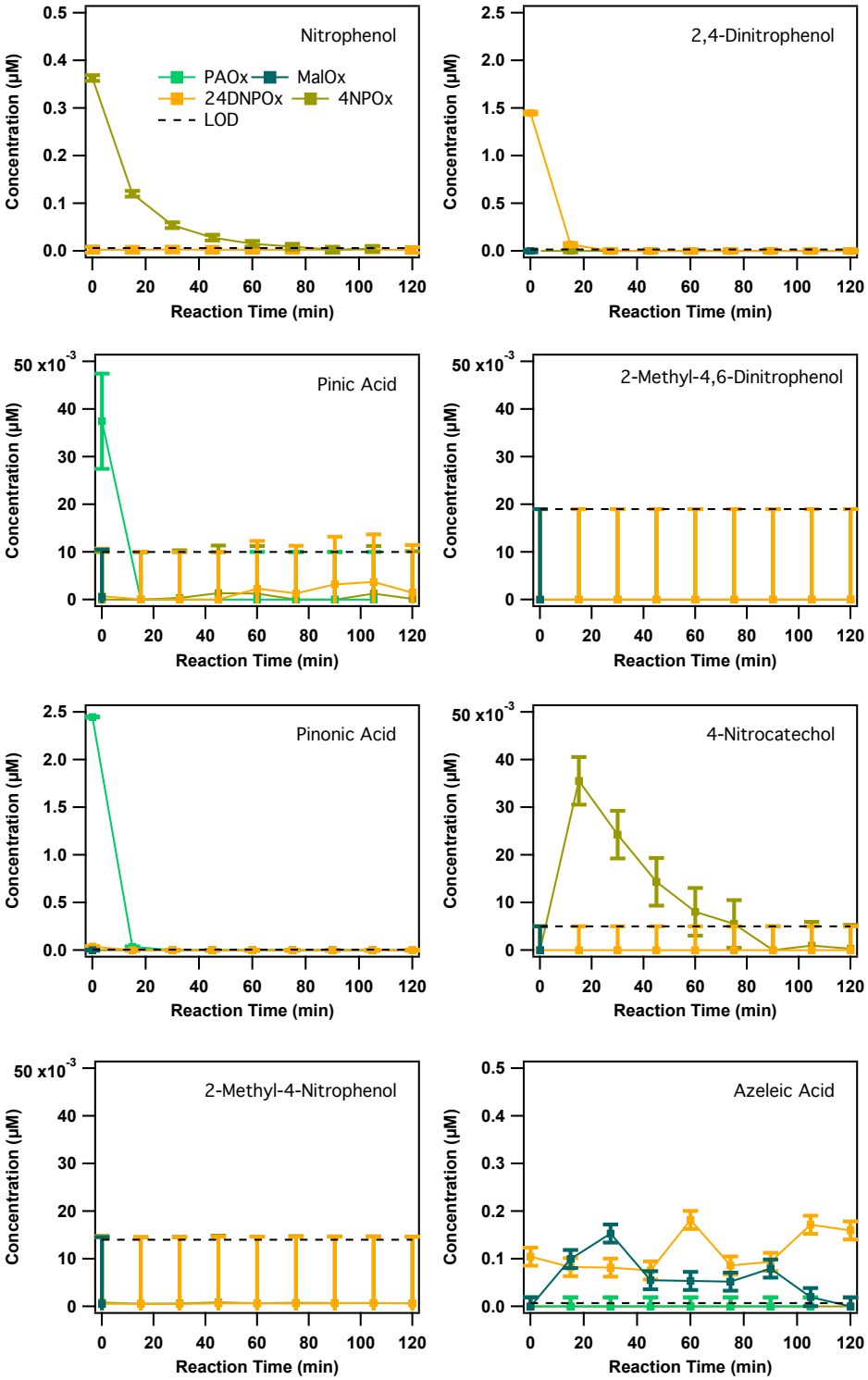

Figure A5-6. Time profiles of nitrated and organic acid standard oxidation precursors, intermediates, and products quantified via LC-MS. Error bars represent the 95% confidence interval calculated over replicate standard analyses for each chemical. Limits of detection (LODs) were quantified at 95% confidence over replicate oxidation experiment method blanks, and are represented by dashed black lines.

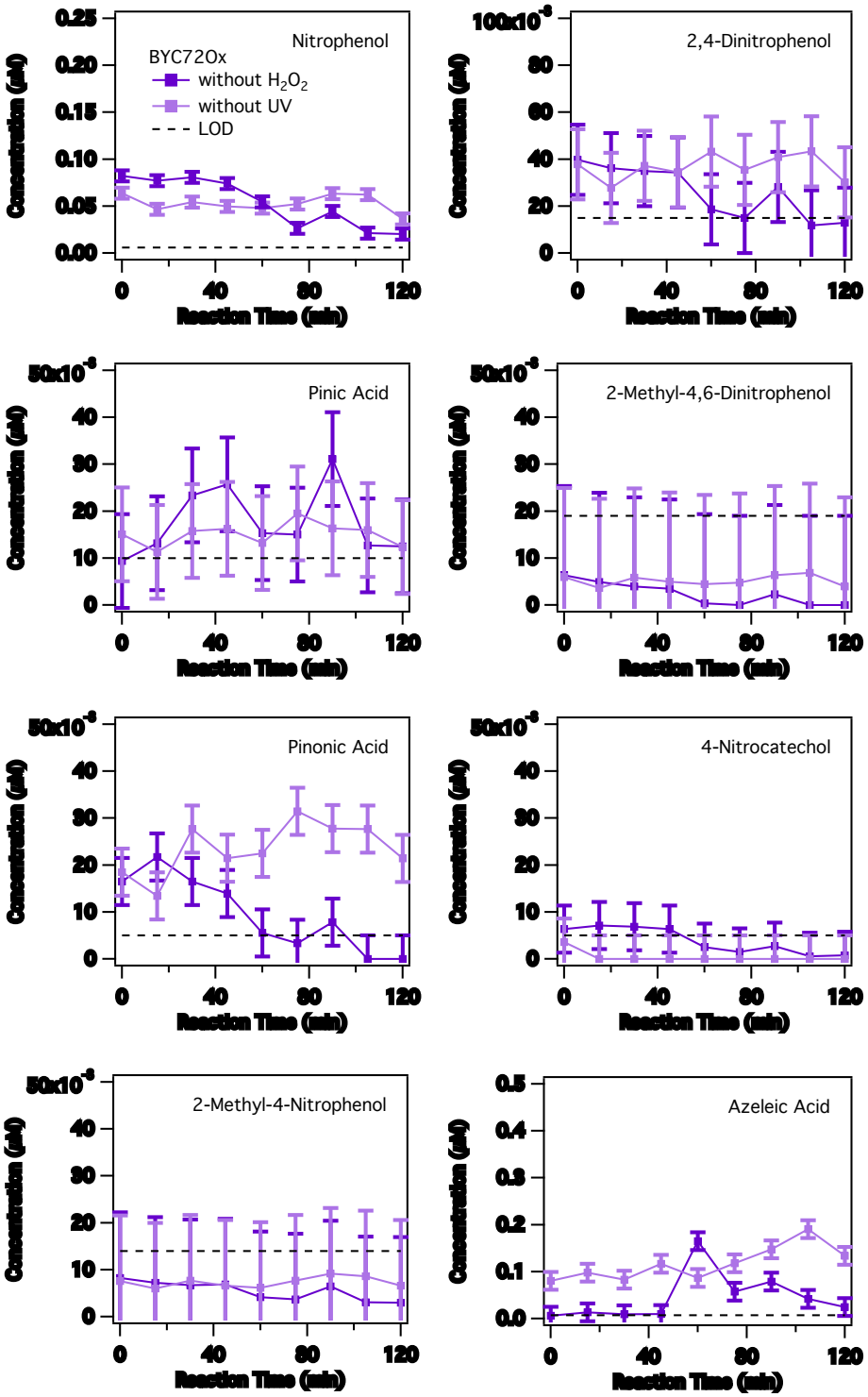

Figure A5-7. Time profiles of nitrated and organic acid control oxidation experiment precursors, intermediates, and products via LC-MS. Error bars represent the 95% confidence interval calculated over replicate standard analyses for each chemical. Limits of detection (LODs) were quantified at 95% confidence over replicate oxidation experiment method blanks, and are represented by dashed black lines.

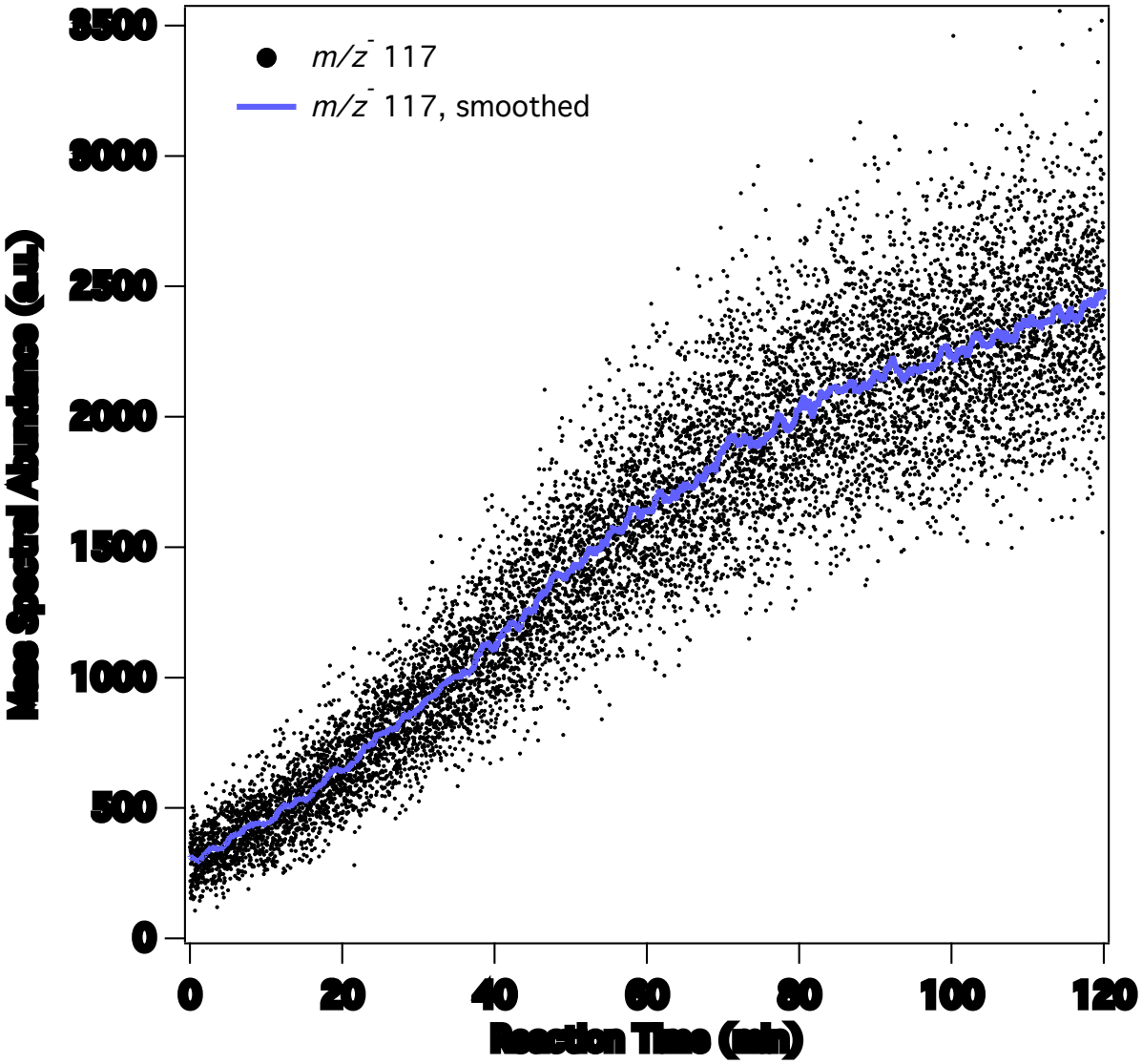

Figure A5-8. Example mass spectral profile (SBC4Ox, m/z^- 117) demonstrating the similarity between the trends in the raw and smoothed data.

Table A5-1. Polar organic compounds identified within fog and cloud samples via online ESI-HR-ToF-MS as precursors and products of oxidation, for sample oxidations as well as the control experiment BYOx without H_2O_2. Precursors were identified by subtracting t=15 and 30 min reaction time mass spectra from the t=0 mass spectrum; products were identified by subtracting t=0 min reaction time mass spectrum from the t=15, 30, 60, and 120 min reaction time mass spectrum. Multiple plausible formulae were identified for species prefixed with "e.g."; no plausible identifications could be made for some species. Formulae were only generated for species with mass spectral abundances >100 a.u. One species, succinic acid, was identified as a product of direct photolysis of the BYI sample (in the BYOx without H_2O_2), and is listed in grey italicized font.

BYOx				
Precursors:	m/z^-	Formula	Abund. (a.u.)	Possible Identification
	113.03	$C_5H_6O_3$	150	Oxopentenoic acid
	115.01	$C_4H_4O_4$	2000	Maleic acid
	121.03	$C_7H_6O_2$	540	Benzoic acid
	129.02	$C_5H_6O_4$	1000	Pentenedioic acid
	137.03	$C_7H_6O_3$	120	Hydroxybenzoic acid
	138.03	$C_6H_5NO_3$	210	Nitrophenol
	143.04	$C_6H_8O_4$	140	Hexenedioic acid
	150.96	$C_3H_4O_5S$	110	Hydroxyacrylaldehyde, sulfate ester
	161.05	$C_6H_{10}O_5$	160	Levoglucosan
	165.03	$C_8H_6O_4$	1100	Phthalic acid
	169.02	$C_4H_{10}O_5S$	90	Oxoheptadienedioic acid
	179.04	$C_9H_8O_4$	168	Methylphthalic acid
	181.02	$C_8H_6O_5$	290	Hydroxyphthalic acid
	183.01	$C_6H_4N_2O_5$	460	Dinitrophenol
	197.02	$C_7H_6N_2O_5$	150	Methyldinitrophenol
	225.02	$C_6H_{10}O_7S$	170	Methylglyoxal oxidation product (Sareen et al., 2010)
	294.07	$C_{10}H_{17}NO_7S$	100	Nighttime monoterpene oxidation product (Iinuma et al., 2007a; Surratt et al., 2008)
Products (0-15 min):	138.98	$C_2H_4O_5S$	105	Glycolaldehyde, sulfate ester
	152.99	$C_3H_6O_5S$	130	Hydroxyacetone, sulfate ester
	154.97	$C_2H_4O_6S$	200	Glycolic acid, sulfate ester
	168.99	$C_3H_6O_6S$	110	Lactic acid, sulfate ester
	211.00	$C_5H_8O_7S$	110	Hydroxymethyloxobutanoic acid, sulfate ester
Products (0-30 min):	*117.03*	*$C_4H_6O_4$*	*190*	*Succinic acid*
	138.98	$C_2H_4O_5S$	120	Glycolaldehyde, sulfate ester
	152.99	$C_3H_6O_5S$	140	Hydroxyacetone, sulfate ester
	154.97	$C_2H_4O_6S$	280	Glycolic acid, sulfate ester
	168.99	$C_3H_6O_6S$	110	Lactic acid, sulfate ester
	211.00	$C_5H_8O_7S$	90	Hydroxymethyloxobutanoic acid, sulfate ester
	212.98	$C_4H_6O_8S$	100	Malic acid, sulfate ester
Products (0-60 min):	87.01	$C_3H_4O_3$	110	Pyruvic acid
	101.03	$C_4H_6O_3$	450	Methacrylic acid
	117.02	*$C_4H_6O_4$*	*140*	*Succinic acid*
	138.98	$C_2H_4O_5S$	120	Glycolaldehyde, sulfate ester
	152.99	$C_3H_6O_5S$	440	Hydroxyacetone, sulfate ester

	154.97	$C_2H_4O_6S$	440	*Glycolic acid, sulfate ester*
	168.99	$C_3H_6O_6S$	280	Lactic acid, sulfate ester
	196.98	$C_4H_6O_7S$	110	Hydroxyoxobutanoic acid, sulfate ester
	211.00	$C_5H_8O_7S$	100	Hydroxymethyloxobutanoic acid, sulfate ester
	212.98	$C_4H_6O_8S$	130	Malic acid, sulfate ester
Products (0-120 min):	*117.019*	*$C_4H_6O_4$*	*570*	*Succinic acid*
	138.97	$C_2H_4O_5S$	120	Glycolaldehyde, sulfate ester
	154.97	$C_2H_4O_6S$	330	*Glycolic acid, sulfate ester*
	168.98	$C_3H_6O_6S$	330	Lactic acid, sulfate ester
CP4Ox				
Precursors:	*m/z*$^-$	Formula	Abund. (a.u.)	Possible Identification
	157.09	$C_8H_{14}O_3$	170	Pinic acid oxidation product
	171.10	$C_9H_{16}O_3$	130	α-pinene ozonolysis product (Shilling et al., 2009)
	183.01	$C_6H_4N_2O_5$	100	Dinitrophenol
	183.10	$C_{10}H_{16}O_3$	340	Pinonic acid
	185.08	$C_9H_{14}O_4$	350	Pinic acid
	199.10	$C_{10}H_{16}O_4$	410	Hydroxypinonic acid
	201.11	$C_{10}H_{18}O_4$	240	Hydrated pinonic acid
	225.16	$C_{13}H_{22}O_3$	170	
	261.14	$C_{12}H_{22}O_6$	280	
	263.13	$C_{15}H_{20}O_4$	140	Sesquiterpene oxidation product
	288.16	$C_{17}H_{23}NO_3$	630	
	487.31	e.g., $C_{22}H_{49}N_3O_{10}$	100	
	514.33	e.g., $C_{22}H_{49}N_3O_{10}$	220	
Products (0-15 min):	71.01	$C_3H_4O_2$	150	Acrylic acid
	72.99	$C_2H_2O_3$	180	Glyoxylic acid
	73.03	$C_3H_6O_2$	150	Propanoic acid
	75.01	$C_2H_4O_3$	150	Glycolic acid
	85.03	$C_4H_6O_2$	170	Methacrylic acid
	115.04	$C_5H_8O_3$	410	Oxopentanoic acid
	117.02	$C_4H_6O_4$	100	Succinic acid
	129.05	$C_6H_{10}O_3$	100	Oxohexanoic acid
	131.04	$C_5H_8O_4$	110	Hexenedioic acid
Products (0-30 min):	71.01	$C_3H_4O_2$	290	Acrylic acid
	72.99	$C_2H_2O_3$	390	Glyoxylic acid
	73.03	$C_3H_6O_2$	220	Propanoic acid
	75.01	$C_2H_4O_3$	310	Glycolic acid
	85.03	$C_4H_6O_2$	290	Methacrylic acid
	87.01	$C_3H_4O_3$	460	Pyruvic acid
	87.05	$C_4H_8O_2$	120	Butanoic acid
	88.99	$C_2H_2O_4$	120	Oxalic aicd
	101.03	$C_4H_6O_3$	150	Hydroxymethacrylic acid
	103	$C_3H_4O_4$	140	Malonic acid
	115.04	$C_5H_8O_3$	290	Oxopentanoic acid
	117.02	$C_4H_6O_4$	240	Succinic acid

	127.04	$C_6H_8O_3$	100	Oxohexenoic acid
	129.04	$C_6H_{10}O_3$	400	Oxohexanoic acid
	131.04	$C_5H_8O_4$	220	Glutaric acid
	143.04	$C_6H_8O_4$	110	Hexenedioic acid
	145.02	$C_5H_6O_5$	120	Hydroxypentenedioic acid
	157.05	$C_7H_{10}O_4$	130	Heptanedioic acid
	159.03	$C_6H_8O_5$	130	Hydroxyhexenedioic acid
	173.05	$C_7H_{10}O_5$	150	Dihydroxydimethylpentanedioic acid (PAOx)
	175.03	$C_6H_7O_6$	110	Tricarballylic acid
	187.06	$C_8H_{12}O_5$	130	Formyldimethylpentanedioic acid (PAOx)
Products (0-60 min):	71.01	$C_3H_4O_2$	100	Acrylic acid
	72.99	$C_2H_2O_3$	330	Glyoxylic acid
	73.03	$C_3H_6O_2$	100	Propanoic acid
	75.01	$C_2H_4O_3$	320	Glycolic acid
	85.03	$C_4H_6O_2$	410	Methacrylic acid
	87.01	$C_3H_4O_3$	980	Pyruvic acid
	87.05	$C_4H_8O_2$	210	Butanoic acid
	88.99	$C_2H_2O_4$	310	Oxalic acid
	89.03	$C_3H_6O_3$	160	Lactic acid
	101.03	$C_4H_6O_3$	310	Hydroxymethacrylic acid
	103.01	$C_3H_4O_4$	410	Malonic acid
	103.04	$C_4H_8O_3$	120	Hydroxybutanoic acid
	115.03	$C_5H_8O_3$	820	Oxopentanoic acid
	117.02	$C_4H_6O_4$	530	Succinic acid
	127.04	$C_6H_8O_3$	190	Oxohexenoic acid
	129.04	$C_6H_{10}O_3$	260	Methyloxopentanoic acid
	131.04	$C_5H_8O_4$	380	Glutaric acid
	133.01	$C_4H_6O_5$	110	Malic acid
	143.04	$C_6H_8O_4$	190	Hexenedioic acid
	147.03	$C_5H_8O_5$	140	Hydroxyglutaric acid
	157.05	$C_7H_{10}O_4$	650	Pinic acid oxidation product
	159.03	$C_6H_8O_5$	220	Hydroxyhexenedioic acid
	173.05	$C_7H_{10}O_5$	270	Dihydroxydimethylpentanedioic acid (PAOx)
	175.03	$C_6H_8O_6$	160	Tricarballylic acid
	185.05	$C_8H_{10}O_5$	110	Isoprene oxidation product (Nguyen et al., 2011)
	189.04	$C_7H_{10}O_6$	110	Monoterpene oxidation product (Kundu et al., 2012)
	201.04	$C_8H_{10}O_6$	140	Pentenedicarboxylic acid
	215.06	$C_9H_{12}O_6$	100	Pinic acid oxidation product
Products (0-120 min):	85.03	$C_4H_6O_2$	120	Methacrylic acid
	87.01	$C_3H_4O_3$	850	Pyruvic acid
	88.99	$C_2H_2O_4$	360	Oxalic acid
	89.03	$C_3H_6O_3$	150	Lactic acid
	101.03	$C_4H_6O_3$	440	Hydroxymethacrylic acid
	103.01	$C_3H_4O_4$	940	Malonic acid

	111.05	$C_6H_8O_2$	130	Hexadienoic acid
	113.04	$C_5H_6O_3$	240	Oxopentenoic acid
	115.02	$C_4H_4O_4$	1010	Maleic acid
	115.03	$C_5H_8O_3$	700	Oxopentanoic acid
	117.02	$C_4H_6O_4$	890	Succinic acid
	125.06	$C_7H_{10}O_2$	300	Heptadienoic acid
	127.04	$C_6H_8O_3$	210	Oxohexenoic acid
	131.04	$C_5H_8O_4$	830	Pentenedioic acid
	133.02	$C_4H_6O_5$	190	Malic acid
	143.04	$C_6H_8O_4$	510	Hexenedioic acid
	145.05	$C_6H_{10}O_4$	190	Hexendioic acid
	147.03	$C_5H_8O_5$	140	Hydroxyglutaric acid
	154.97	$C_2H_4O_6S$	120	Glycolic acid, sulfate ester
	157.05	$C_7H_{10}O_4$	250	Norpinic acid oxidation product
	159.03	$C_6H_8O_5$	250	Hydroxyhexenedioic acid
	161.01	$C_5H_6O_6$	100	Hydroxyoxopentanedioic acid
	171.03	$C_7H_8O_5$	100	Oxoheptenedioic acid
	173.05	$C_7H_{10}O_5$	250	Dihydroxydimethylpentanedioic acid (PAOx)
	175.03	$C_6H_8O_6$	180	Tricarballylic acid
	185.05	$C_8H_{10}O_5$	100	Isoprene oxidation product (Nguyen et al., 2011)
	187.06	$C_8H_{12}O_5$	110	Formyldimethylpentanedioic acid (PAOx)
	201.05	$C_8H_{10}O_6$	170	Pinic acid oxidation product
	215.06	$C_9H_{12}O_6$	100	Pinic acid oxidation product

CP3Ox

Precursors:	*m/z*-	Formula	Abund. (a.u.)	Possible Identification
	171.07	$C_8H_{12}O_4$	360	Octanenedioic acid
	173.06	$C_7H_{10}O_5$	400	Oxoheptanedioic acid
	182.02	$C_7H_5NO_5$	170	Carboxynitrophenol
	183.01	$C_6H_4N_2O_5$	220	Dinitrophenol
	183.1	$C_{10}H_{16}O_3$	310	Pinonic acid
	185.08	$C_9H_{14}O_4$	380	Pinic acid
	187.06	$C_8H_{12}O_5$	940	Hydroxynorpinic acid
	189.07	*e.g.,* $C_8H_{14}O_3S$	320	
	199.1	$C_{10}H_{16}O_4$	440	Hydroxypinonic acid (Kahnt et al., 2014)
	201.08	$C_9H_{14}O_5$	450	Hydroxypinic acid
	203.06	$C_8H_{12}O_6$	720	Methylbutanetricarboxylic acid (MBTCA); pinonic acid oxidation product (Szmigielski *et al.,* 2007)
	215.09	$C_{10}H_{16}O_5$	490	α-Pinene oxidation product (Kahnt et al., 2014)
	217.09	$C_9H_{14}O_6$	590	Dihydroxypinic acid
	229.07	$C_{10}H_{14}O_6$	270	α-Pinene oxidation product (Kahnt et al., 2014)
	231.08	$C_{10}H_{16}O_6$	420	Diaterpenylic acid acetate (Kahnt et al., 2014)
	250.06	e.g., $C_8H_{13}NO_8$	300	Monoterpene oxidation product
	262.09	e.g., $C_{10}H_{17}NO_7$	110	α-Pinene oxidation product (Lee et al., 2016)
	264.08	e.g., $C_9H_{15}NO_8$	120	Monoterpene oxidation product
	276.08	$C_{10}H_{15}NO_8$	100	Nitroxydiaterpenylic acid acetate
	278.09	$C_{10}H_{17}NO_8$	160	Monoterpene oxidation product
	288.16	$C_{13}H_{23}NO_6$	180	

	294.08	*e.g.,* $C_{17}H_{13}NO_4$	130	
	295.05	$C_{10}H_{16}O_8S$	190	Dihydroxypinonic acid, sulfate ester
	309.09	*e.g.,* $C_{15}H_{18}O_5S$	100	
	325.09	$C_{17}H_{14}N_2O_5$	170	
	356.1	$C_{22}H_{15}NO_4$	220	
Products (0-15 min):	115.03	$C_5H_8O_3$	110	Oxopentanoic acid
Products (0-30 min):	115	$C_4H_4O_4$	140	Maleic acid
	115.04	$C_5H_8O_3$	330	Oxopentanoic acid
	117.02	$C_4H_6O_3$	100	Succinic acid
	129.02	$C_5H_6O_4$	120	Pentenedioic acid
Products (0-60 min):	115	$C_4H_4O_4$	120	Maleic acid
	115.04	$C_5H_8O_3$	220	Oxopentanoic acid
	117.02	$C_4H_6O_4$	130	Succinic acid
	125.06	$C_7H_{10}O_2$	430	Heptadienoic acid
	129.02	$C_5H_6O_4$	100	Pentenedioic acid
	129.06	$C_6H_{10}O_3$	110	Methyloxopentanoic acid
Products (0-120 min):	101.03	$C_4H_6O_3$	120	Oxobutanoic acid
	113.03	$C_5H_6O_3$	110	Oxopentenoic acid
	115.01	$C_4H_4O_4$	580	Maleic acid
	117.02	$C_4H_6O_4$	310	Succinic acid
	129.03	$C_5H_6O_4$	270	Pentenedioic acid
	129.06	$C_6H_{10}O_3$	150	Methyloxopentanoic acid
	131.04	$C_5H_8O_4$	220	Glutaric acid
	145.05	$C_6H_{10}O_4$	170	Adipic acid
	209.95	*e.g.,* C_7HNO_5S	340	

TaiOx

Precursors:	m/z^-	Formula	Abund. (a.u.)	Possible Identification
	138.02	$C_6H_5NO_3$	120	Nitrophenol
	152.04	$C_7H_7NO_3$	110	Methylnitrophenol
	154.02	$C_6H_5NO_4$	730	Hydroxynitrophenol
	179.04	$C_9H_8O_4$	170	Methylphthalic acid
	181.02	$C_8H_6O_5$	140	Hydroxyphthalic acid
	182.01	$C_7H_5NO_5$	290	Carboxynitrophenol
	183.01	$C_6H_4N_2O_5$	3170	Dinitrophenol
	184.01	$C_7H_7NO_5$	190	Hydroxymethoxynitrophenol
	187.07	$C_8H_{12}O_5$	210	Hydroxynorpinic acid
	193.05	$C_{10}H_{10}O_4$	100	Dimethylphthalic acid
	197.03	$C_7H_6N_2O_5$	680	Methyldinitrophenol
	199	$C_4H_8O_7S$	210	Methylglyceric acid, sulfate ester (Nguyen et al., 2011; Schindelka et al., 2013)
	203.06	$C_8H_{12}O_6$	170	Methylbutanetricarboxylic acid (MBTCA); gas phase pinonic acid oxidation product (Szmigielski et al., 2007)
	207.04	$C_7H_{12}O_5S$	110	Monoterpene oxidation product, sulfate ester
	209.05	$C_7H_{14}O_5S$	180	Monoterpene oxidation product, sulfate ester
	211.05	$C_8H_8N_2O_5$	100	Dimethyldinitrophenol
	213.02	$C_7H_6N_2O_6$	100	Methoxydinitrophenol
	221.08	$C_7H_{14}N_2O_6$	130	Hydroxydinitroheptanol
	223.07	$C_{11}H_{12}O_5$	120	Sinapic acid (Biogenic; Gao et al., 2006)

	225.02	$C_8H_6N_2O_6$	230	Acetyldinitrophenol
	227	$C_5H_8O_8S$	120	Hydroxypentenedioic acid, sulfate ester
	232	$C_7H_7NO_6S$	150	Methylnitrophenol, sulfate ester
	233.98	$C_6H_5NO_7S$	980	Hydroxynitrophenol, sulfate ester
	239.03	$C_9H_8N_2O_6$	190	Dimethyldinitrobenzoic acid
	241.05	$C_7H_{14}O_7S$	100	Dihydroxypentanoic acid, sulfate ester
	253.05	$C_{10}H_{10}N_2O_6$	110	
	267.06	$C_{12}H_{12}O_7$	130	Syringol oxidation product (Yu et al., 2014)
	279.06	$C_{10}H_{16}O_7S$	110	Hydroxypinonic acid, sulfate ester
Products (15 min):	165.02	$C_8H_6O_4$	110	Phthalic acid
Products (30 min):	113.03	$C_5H_6O_3$	100	Oxopentenoic acid
	115.01	$C_4H_4O_4$	150	Maleic acid
	115.04	$C_5H_8O_3$	100	Oxopentanoic acid
	117.02	$C_4H_6O_4$	120	Succinic acid
	129.02	$C_5H_6O_4$	110	Pentenedioic acid
	165.02	$C_8H_6O_4$	120	Phthalic acid
	196.98	$C_4H_6O_7S$	100	Hydroxyoxobutanoic acid, sulfate ester
Products (60 min):	113.03	$C_5H_6O_3$	130	Oxopentenoic acid
	115.01	$C_4H_4O_4$	200	Maleic acid
	115.04	$C_5H_8O_3$	140	Oxopentanoic acid
	117.02	$C_4H_6O_4$	220	Succinic acid
	129.02	$C_5H_6O_4$	120	Pentenedioic acid
	138.97	$C_2H_4O_5S$	150	Glycolaldehyde, sulfate ester
	196.98	$C_4H_6O_7S$	140	Hydroxyoxobutanoic acid, sulfate ester
	210.99	$C_5H_8O_7S$	100	Hydroxyoxopentanoic acid, sulfate ester
Products (120 min):	113.02	$C_5H_6O_3$	120	Oxopentenoic acid
	115.01	$C_4H_4O_4$	330	Maleic acid
	115.04	$C_5H_8O_3$	190	Oxopentanoic acid
	117.02	$C_4H_6O_4$	390	Succinic acid
	129.02	$C_5H_6O_4$	160	Pentenedioic acid
	131.04	$C_5H_8O_4$	170	Glutaric acid
	138.97	$C_2H_4O_5S$	190	Glycolaldehyde, sulfate ester
	154.97	$C_2H_4O_6S$	120	Glycolic acid, sulfate ester

BYOx without H_2O_2

Precursors:	*m/z*-	Formula	Abund. (a.u.)	Possible Identification
	71.01	$C_3H_4O_2$	3140	Acrylic acid
	72.99	$C_2H_2O_3$	390	Glyoxylic acid
	73.03	$C_3H_6O_2$	580	Propanoic acid
	75.01	$C_2H_4O_3$	140	Glycolic acid
	85.03	$C_4H_6O_2$	930	Methacrylic acid
	88.99	$C_2H_2O_4$	100	Oxalic acid
	103.00	$C_3H_4O_4$	390	Malonic acid
	115.00	$C_4H_4O_4$	2220	Maleic acid
	129.02	$C_5H_6O_4$	1140	Pentenedioic acid
	133.01	$C_4H_6O_5$	290	Malic acid

	294.07	$C_{10}H_{17}NO_7S$	160	Nighttime monoterpene oxidation product (Iinuma et al., 2007a; Surratt et al., 2008)
Products (15 min):	117.02	$C_4H_6O_4$	320	Succinic acid
	131.04	$C_5H_8O_4$	110	Glutaric acid
	154.97	$C_2H_4O_6S$	110	Glycolic acid, sulfate ester
	181.02	$C_8H_6O_5$	140	Hydroxyphthalic acid
	183	$C_6H_4N_2O_5$	120	Dinitrophenol
	195.1	$C_{11}H_{16}O_3$	170	
	197.01	$C_8H_6O_6$	170	
Products (30 min):	117.02	$C_4H_6O_4$	430	Succinic acid
	131.04	$C_5H_8O_4$	130	Glutaric acid
	154.97	$C_2H_4O_6S$	150	Glycolic acid, sulfate ester
	181.02	$C_8H_6O_5$	220	Hydroxyphthalic acid
	183.01	$C_6H_4N_2O_5$	110	Dinitrophenol
	197.01	$C_8H_6O_6$	240	
Products (60 min):	117.02	$C_4H_6O_4$	300	Succinic acid
	181.02	$C_8H_6O_5$	230	Hydroxyphthalic acid
	197.01	$C_8H_6O_6$	280	
	241	$C_9H_6O_8$	100	
Products (120 min):	117.02	$C_4H_6O_4$	140	Succinic acid
	181.02	$C_8H_6O_5$	230	Hydroxyphthalic acid
	197.01	$C_8H_6O_6$	270	

APPENDIX 6: LABORATORY SIMULATED CLOUD PROCESSING OF BIOMASS BURNING EMISSIONS

Filter Collection

Particle phase emissions were also collected separately onto prebaked quartz fiber filters (37 mm), using a Savillex PFA DOC 47 two-stage filter holder assembly (front and back filters were collected), and then extracted into water. Filter samples were handled using tweezers cleaned with isopropanol, and were stored after collection in aluminum foil. Backup quartz filters were used within the aerosol particle filter packs to determine whether artifact (positive, via gas adsorption on the filter or negative, via re-volatilization of semi-volatile species) formation had occurred. On average, 44% of pinonic acid and 4-nitrocatechol, and 33% of adipic acid were on the backup filter (these were the only species with measurable quantities detected from organic acids IC and HPLC-(-)-ESI-HR-ToF-MS analyses on both the back and front filters). Pinonic acid has been observed on backup filters used in field studies in greater abundance than other, less volatile biogenic carboxylic acids (Warnke et al., 2006). Since pinonic and adipic acids were additionally measured at similar concentrations in mist chamber extracts, it is possible that either type of artifact formed. Backup filter concentrations were therefore not added to sample concentrations because no determination could be made about the origin of the contents of the backup filters.

Estimated Particle Collection to Mist Chambers

The loss of particles due to sampling to the filters and mist chamber was explored by estimating: (1) turbulent flow-driven diffusive and inertial losses in the sample tubing; and (2) the deviation from isokinetic sampling at the connection between sample tubing and hood ducting. Due to the high flow rate (5000 L min^{-1}) and the broad diameter (0.16 m) of the ducting from the hood, the transmission of particles was assumed to be unchanged within the ducting. In addition, the temperature in the hood measured during the burn simulations remained at 72-73°F, so no thermophoretic effects on particle behavior (or emissions volatility) were expected. The value of the Reynolds number, Re, is defined by the relationship $Re = \rho_g d_t V/\eta$, where ρ_g is the density of the surrounding gas, d_t is the inner diameter of the tubing, V is the mean velocity of the surrounding gas, and η is the viscosity of the fluid (Hinds, 1999). At standard conditions and assuming SI units, $Re \approx 66000 V d_t$; using a flow rate of 28 liters of air per minute into the 3/8" inner diameter tubing to the mist chamber, V was determined to have a value of 3.7 m s^{-1}. A value of $Re \approx (66000 \times 3.5 \text{ m s}^{-1} \times 0.0095 \text{ m}) = 3200$ was calculated for the mist chamber sampling, indicative of a turbulent

flow inside the tubing. For the filter pack, a lesser value of Re ≈ (66000 × 1.1 m s^{-1} × 0.0095 m) = 956 was calculated, indicating laminar flow. The value of d_p at which 50% of particles were lost to the wall was calculated for each sampler using equations for the penetration efficiency to the wall of the sample tubing (Hinds, 1999; Yin and Dai, 2015). In the case of turbulent flow (the mist chamber), the penetration P = number particles outside the streamlines / number particles within the streamlines = $\exp[(-4V_{dep}L)/(d_tV)]$ where V_{dep}, the deposition velocity of the particles, was calculated by $V_{dep} = (0.04V/Re^{1/4})(\rho_g D/\eta)^{2/3}$, L is the length of the tubing, and D is the diffusion coefficient of the particle, dependent on the particle diameter. For the laminar flow case, this was approximated as $P = 0.819\exp(-11.5\mu) + 0.0.975\exp(-70.1\mu)$, with μ, the dimensionless deposition parameter = $4DL/\pi d_t^2V$. Calculated values of d_p at which $P = 0.5$ were approximately 4 nm for the mist chamber and 2 nm for the filter pack, but particles with d_p>40 nm were removed with at least P=0.95 (above d_p=150 nm, $P \geq 0.99$) in the mist chamber, while all particles d_p>20 nm were collected with an asymptotic efficiency of approximately (1-P) ≈ 0.1 onto the filters, suggesting that only the smallest particles were efficiently collected by the mist chamber, and filter packs collected particles >4 nm with 10-50% efficiency. A substantial fraction of aerosol particles generated from the combustion of Ponderosa Pine are greater than 20 nm, with most particle mass at approximately 200 nm diameter and a second particle mode in the course size range (Hays et al., 2002). Thus, the collected particles (filter) are only representative of a portion of aerosol generated in the burn, and most particles were not collected into the mist chamber. The measured particle phase total organic carbon (OC) mass on the filter was approximately five-fold less than that measured previously per kg fuel for Ponderosa Pine (estimated 5.8 g OC kg^{-1} fuel in the present study, but 27.8 g OC kg^{-1} fuel in Hays et al., 2002), in agreement with these calculations. In addition, collection of the emissions to the mist chamber was found to be subisokinetic (6.9 m s^{-1} actual; 21.9 m s^{-1} required for isokinetic), such that the emissions entering the tubing may have been enriched in larger diameter particles (Hinds, 1999).

Instrumental Methods

The MSD/ToF detector settings were as follows (for both offline LC/MS and online MS analyses): acquisition m/z^- 65-100 Da at 1.4 spectra s^{-1}; drying gas 350°C and 5 liters min^{-1}; nebulizer 20 psi; fragmentor voltage 130 V; skimmer voltage 60 V; octapole voltage 150 V; capillary 3500 V. Agilent EI-TOF tuning mix was used to perform external mass calibration prior to analyses, initially giving ±1 ppm mass accuracy. Mass accuracies during analysis were typically <30 ppm (no internal standard solution was used during analyses because reference ions interfere with ionization of analytes).

Organic molecules $\geq C_3$ were quantified via HPLC-(-)-ESI-HR-ToF-MS, which consisted of an Agilent 1100 Series LC with Agilent MSD/ToF detector. A Kinetex 2.6 μm particle size XB-C18 column designed for polar organic species separation with 100 Å pore size and 3.00 mm internal diameter was used to separate nitrophenols via a 0.1% formic acid/methanol gradient elution. The MSD/ToF detector settings were identical to those used in the online MS analyses. External calibrations performed on the HPLC-(-)-ESI-HR-ToF-MS were linear ($r^2 > 0.90$).

Water used in extracting and dilution emissions was deionized (>18MΩ). All chemical analyses were carried out without prior filtration of the collected fog water. Most analyses were carried out using procedures previously employed for fog and cloud samples collected in our lab (e.g., Collett et al., 1999; Benedict et al., 2012). Major inorganic ions were quantified using a Dionex DX-500 IC system with conductivity detection; cations were separated along a Dionex CS12A analytical column, CG12 guard column, and CSRS ULTRA II suppressor using 20 mM methanesulfonic acid (MSA) as eluent; anions were separated along a Dionex AS14A analytical column, AG14A guard column, and ASRS ULTRA II suppressor using carbonate/bicarbonate eluent. Carboxylic acids were quantified using a gradient Dionex IC system with a Dionex AS11-HC analytical column, AG11 guard column, and ASRS ULTRA II suppressor using a 1-40 mM sodium hydroxide (NaOH) eluent gradient and a conductivity detector. Note that because conductivity is a non-specific detection mechanism, only demonstrating the presence and not identities of acids, some uncertainty in the identity of the acid corresponding to each chromatographic peak exists (Fig. A6-3). Although MS was used in line with IC to confirm the order of separation, differences in reaction time caused by increased separation time between the IC and MS, as well as sensitivity of the MS to particular acids, made this analysis certain as well. All inorganic ion and carboxylic acid external calibrations were linear (r^2>0.99) with the exception of that for ammonium, which typically exhibits a non-linear response using this system. Ammonium concentrations were determined after dilution (to result in <100 μM concentrations) in cases where the concentration in the sample exceeded the linear range of the method. Overloading of the cation exchange chromatography column caused this upper limit. Total organic carbon (TOC) concentration was measured using a Sievers Model 800 Turbo TOC Analyzer in Turbo mode (two-channel conductivity analysis after CO_2-permeable membrane separation: channel one converts carbonaceous material to CO_2 by UV and chemical oxidation, channel two measures inorganic CO_2). Stock standards of carboxylic acids (100 mM) were prepared in water, with the exception of valeric and succinic acids, which were prepared using ~2% methanol in water. Stock standards of nitrophenols (4 and 10 mM) were prepared using up to 20% acetonitrile in water.

Blanks and Figures of Merit

Two types of method blanks were generated: field blanks from the filter pack and mist chambers, and chemical analysis method blanks from each chemical analysis method. Chemical analysis method blanks were generated for carboxylic acids, inorganic ions, and $\geq C_3$ organic components by analyzing deionized water in the same manner as samples. Field blanks collected prior to sampling of BB emissions contained higher concentrations of carboxylic acids and nitrophenols than most samples; the blanks were collected by pumping air from the hood prior to beginning the burn processes onto filters/into mist chamber extract at the same flow rate as was used for sample collection. It is likely that the sampling lines still contained products of previous burns; fortunately, the blank was collected for approximately one hour, such that much of the material from previous burns was likely removed.

Blank subtractions were not performed, but confidence intervals were instead generated to quantify the possible error in each measurement. Confidence intervals (at the 95% confidence level) were calculated for each chemical species quantified using replicate measured responses of chemical standards ($CI = ts/\sqrt{n}$, where t = critical t value at the 95% confidence level, one-sided, s = standard deviation of replicate carboxylic acid standard analysis responses, n = number of replicate carboxylic acids standards analyses (n=3). Limits of detection (LODs) were calculated from a series of chemical analysis method blanks ($LOD = \bar{x}_{blk} + t\, s_{blk}\sqrt{[(n_s+n_{blk})/(n_s \times n_{blk})]}$, where $\bar{x}_{blk}$=mean of chemical analysis method blanks; t=critical t value at the 95% confidence level, s_{blk}=standard deviation of chemical analysis method blanks; two-sided; n_s=number of samples (carboxylic acid IC: n_s=27; LC: n_s=27); n_{blk}=number of blanks (carboxylic acid IC: n_{blk}=9, LC: n_{blk}=16). LODs (instrumental) and confidence intervals (95%) were extrapolated from the units of the mist chamber extract using the flow rate, extract volume, and dilution factor of the collection technique.

Particle Phase Components of Smoke

Smoke components with $\geq C_6$ were in general found at higher concentration in the filter than mist chamber extracts. Abundant species included adipic, azeleic, and pinonic acids, as well as 4NC; all other $\geq C_6$ organics were below the method detection limits of the HPLC-(-)-ESI-HR-ToF-MS. Levoglucosan (or other carbohydrate with formula $C_6H_{10}O_5$) was detected only as a product in the aqueous $^{\bullet}OH$ oxidation of the BB emissions. Results from the PTR-MS confirmed that gas phase 4NC and other nitrophenols were detected (Table A6-1).

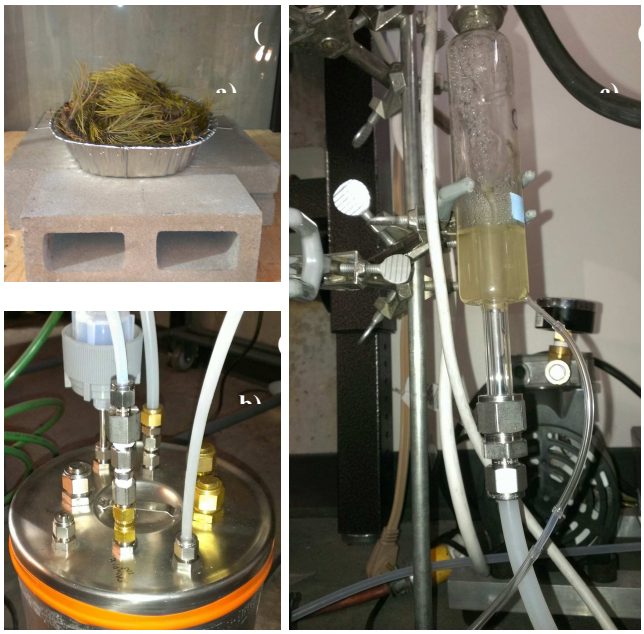

Figure A6-1. Photos of setup for simulated burns and collection of smoke: (a) burn platform with fuel in hood; (b) mixing chamber with connections to filter pack, CO, zero air inlet, and waste air outlet; (c) mist chamber with water containing emissions from burns (air flows upward through apparatus, causing spray of water to form and drip down walls).

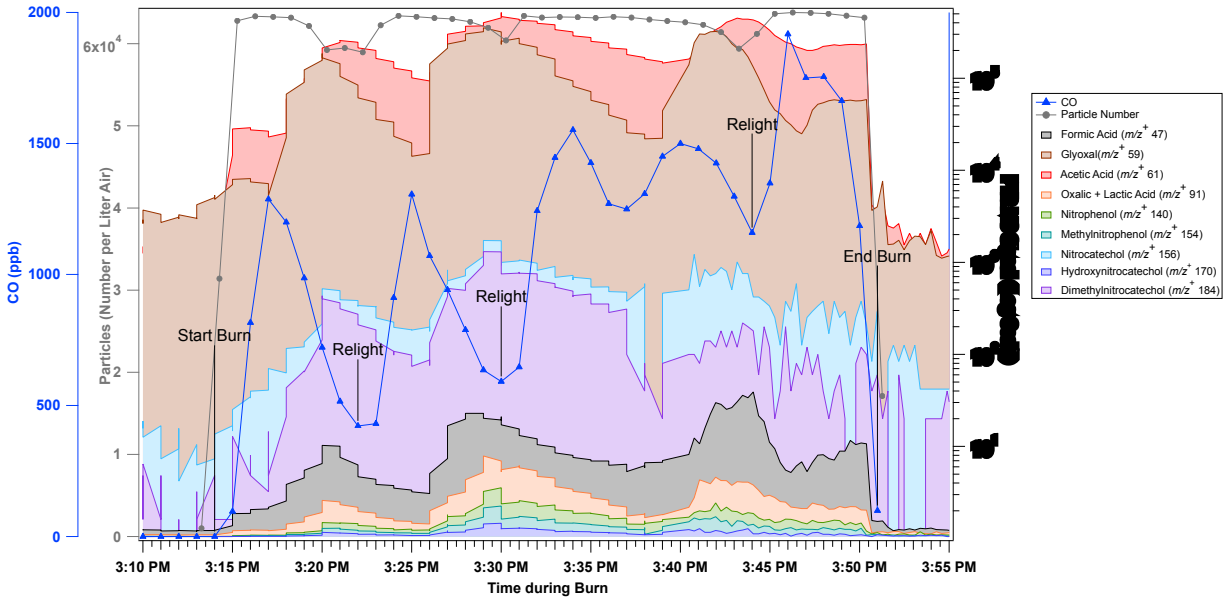

Figure A6-2. Carbon monoxide (CO), particle number, and PTR-MS gas-phase organic species measurements through the duration of the burn demonstrating a fluctuation of the flaming and smoldering phases throughout the burn. The fuel was relit and additional fuel was added throughout the burning process to achieve this fluctuation. Particle number was nearly at the instrument maximum throughout the burn, and uncertain at the measured high number concentration; however, the decrease in number concentration coincident with the decreases in CO confirms the suggested decrease in emissions when combustion subsided. PTR-MS measurements were not calibrated such that only signal was available. Identifications were made purely based on *m/z*; since the MS signal has only unit mass resolution, these identifications are uncertain.

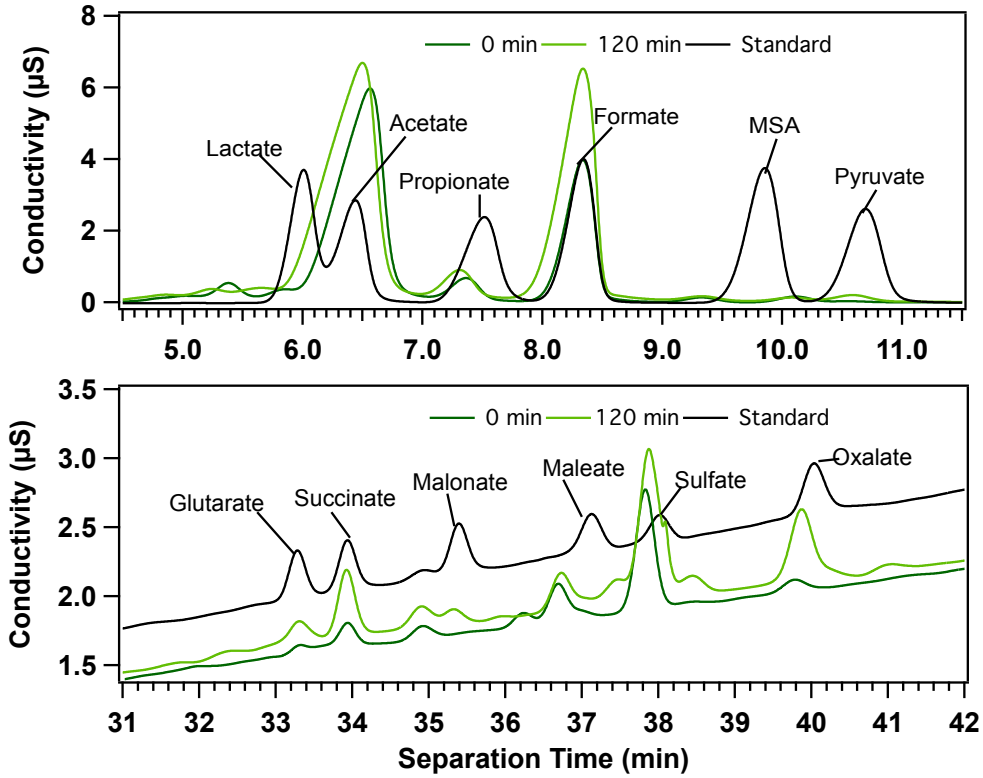

Figure A6-3. Chromatogram window from oxidation at 0 and 120 min from IC-conductivity separations displaying retention times characteristic of quantified acids. Many fewer peaks are present in the chromatograms than in the IC-MS chromatograms due to the greater sensitivity of the MS detector and the selectivities of both detectors. Chromatogram traces were shifted for this figure so that formate and succinate peaks were aligned in the top pane and bottom pane, respectively.

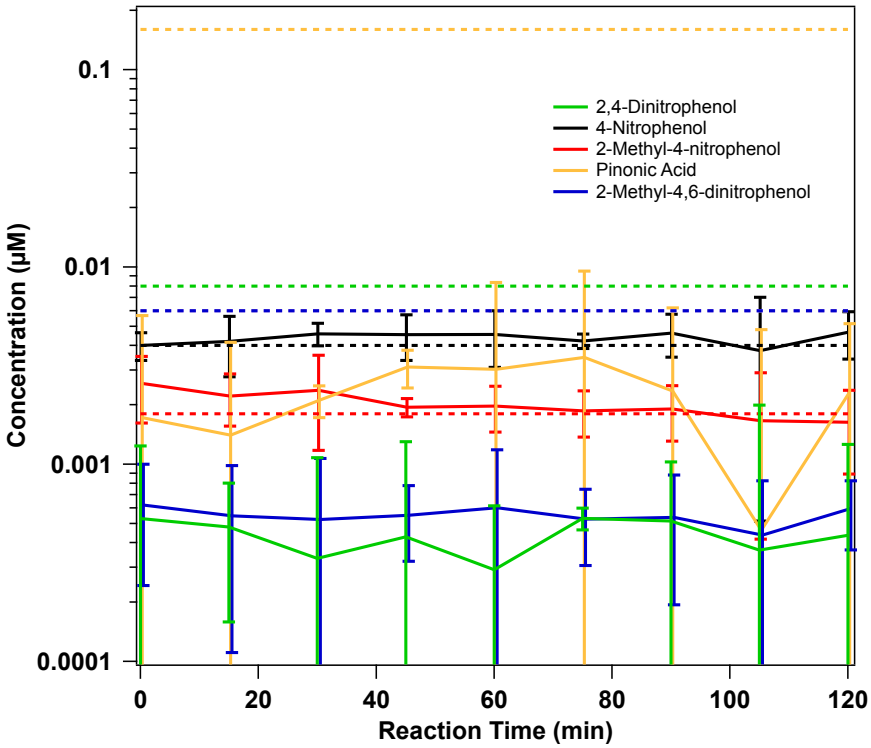

Figure A6-4. Concentrations of organic species with $\geq C_3$ quantified via LC/MS throughout the oxidation. Instrumental LODs calculated from 17 replicate deionized water analyses are displayed as dashed lines for each species. Error bars indicate the 95% confidence intervals for each species at each time point, based on the three replicate oxidation experiments. 4-nitrocatechol and 4-methyl-5-nitrocatechol concentrations were above the respective instrumental LODs and are not plotted. Pinic acid concentrations were less than zero, and are not plotted.

Table A6-1. Concentrations and statistics of inorganic species and TOC collected onto filters (before oxidation). The percent of the TOC contributed by quantified organic acids (percOA) is also tabulated, with the confidence limits (95%) calculated from replicate analyses of the organic acids concentrations. Reported pH is from a 10-foled diluted extract. Concentrations, LODs (instrumental) and confidence limits (95%) were extrapolated from values measured in the extract (μM) using the flow rates, extract volume, and dilution factor of the collection technique.

Species	Concentration (Filter)	Confidence Limit (95%)	LOD	Unit
pH	4.35	--	--	--
NH_4^+	2.96	0.18	0.06	mg m^{-3}
NO_3^-	2.02	0.06	0.04	mg m^{-3}
SO_4^{-2}	0.5	0.2	0.14	mg m^{-3}
Na^+	2.88	0.08	0.06	mg m^{-3}
Cl^-	1.82	0.13	0.10	mg m^{-3}
Ca^{+2}	0.5	0.3	0.19	mg m^{-3}
K^+	2.7	0.2	0.15	mg m^{-3}
Mg^{+2}	*<LOD*	0.09	0.07	mg m^{-3}
NO_2^-	0.47	0.08	0.06	mg m^{-3}
TOC	3.32	0.03	0.26	mg C m^{-3}
PercOA	14	--	--	%
Lactate	187	5	1.4	μg m^{-3}
Acetate	330	3	5	μg m^{-3}
Propionate	103	2	5	μg m^{-3}
Formate	201	1.9	0.3	μg m^{-3}
Pyruvate	16.6	1.4	1.6	μg m^{-3}
Glutarate	11	3	2	μg m^{-3}
Succinate	4	4	1.3	μg m^{-3}
Malonate	12	5	3	μg m^{-3}
Maleate	38	5	5	μg m^{-3}
Oxalate	60	3	6	μg m^{-3}
4-Nitrophenol	*<LOD*	0.04	7	μg m^{-3}
2-Methyl-4-nitrophenol	*<LOD*	0.09	3	μg m^{-3}
4-Nitrocatechol	0.12	0.03	0.010	μg m^{-3}
4-Methyl-5-nitrocatechol	1.18	0.08	50	μg m^{-3}
2,4-Dinitrophenol	*<LOD*	0.0019	1.4	μg m^{-3}
Pinonate	*<LOD*	0.03	5	μg m^{-3}
Pinate	*<LOD*	0.06	2	μg m^{-3}
2-Methyl-4,6-dinitrophenol	*<LOD*	0.0006	1.2	μg m^{-3}

Table A6-2. Polar organic compounds identified within mist chamber extracts via online ESI-HR-ToF-MS as precursors and products of oxidation, for BB emissions oxidations. Precursors were identified by subtracting *t*=15 and 30 min reaction time mass spectra from the *t*=0 mass spectrum (if the mass spectral signal was decreasing between 0 and 30 min); products were identified by subtracting *t*=0 min reaction time mass spectrum from the *t*=15, 30, 60, and 120 min reaction time mass spectrum. Multiple plausible formulae were identified for species prefixed with "e.g."; no plausible identifications could be made for some species. Formulae were only generated for species with mass spectral abundances >500 a.u. because of the uncertainty in determining formulae at low abundance; species only detected >500 a.u. in one replicate oxidation are greyed. If no well-matched or logical formulae could be generated, the ion was omitted from the table. The confidence interval at 95% confidence (CI95) and the relative standard deviation percent (RSD) were calculated from the abundances measured in the replicate oxidations.

	m/z$^-$	Formula	Abund. Diff. (a.u.) Rep. 1	Abund. Diff. (a.u.) Rep. 2	Abund. Diff. (a.u.) Rep. 3	Mean Abund. Diff (a.u.)	CI95 Abund. Diff (a.u.)	RSD (%)	Possible Identification
Precursors:	109.03	$C_6H_6O_2$	1760	16570	8290	8873	14587	84	Hydroquinone
	129.02	$C_5H_6O_4$	7200	8570	7130	7633	1596	11	Pentenedioic acid
	133.05	$C_5H_{10}O_4$	3190	5770	4840	4600	2568	28	Dihydroxypentanoic acid
	127.08	$C_7H_{12}O_2$	2500	3920	1840	2753	2089	39	Heptenenoic acid
	121.03	$C_7H_6O_2$	2840	3960	1050	2617	2885	56	Benzoic acid
	73.03	$C_3H_6O_2$	7760	0	0	2587	8805	173	Propanoic acid
	71.02	$C_3H_4O_2$	7000	0	0	2333	7943	173	Acrylic acid
	85.03	$C_4H_6O_2$	3500	3430	0	2310	3932	87	Methacrylic acid
	168.03	$C_7H_7NO_4$	3070	3020	720	2270	2639	59	Nitrocatechol
	115.01	$C_4H_4O_4$	1570	1600	1570	1580	34	1	Maleic acid
	113.06	$C_6H_{10}O_2$	1260	2110	1080	1483	1081	37	Hexenoic acid
	115.08	$C_6H_{12}O_2$	1150	2160	1040	1450	1213	43	Hexanoic acid
	89.03	$C_3H_6O_3$	1710	2430	0	1380	2453	90	Lactic acid
	158.05	$C_6H_9NO_4$	1470	1760	830	1353	935	35	Dinitrocyclohexenol
	119.05	C_8H_8O	1340	1300	1050	1230	309	13	
	154.01	$C_6H_5NO_4$	1400	2010	0	1137	2025	91	Hydroxynitrophenol
	87.04	$C_4H_8O_2$	1160	2110	0	1090	2077	97	Butanoic acid
	110.98	C_2HO_4Na	790	2250	0	1013	2243	113	Oxalic acid, sodium adduct
	101.06	$C_5H_{10}O_2$	790	1680	530	1000	1185	60	Pentanoic acid
	129.09	$C_7H_{14}O_2$	910	1330	650	963	674	36	Heptanoic acid
	141.1	$C_8H_{14}O_2$	830	1260	720	937	561	30	Octenoic acid
	75.01	$C_2H_4O_3$	2480	0	0	827	2814	173	Glycolic acid
	109.07	C_7H_9O	2270	0	0	757	2576	173	Methylphenol
	182.05	$C_8H_9NO_4$	1030	1140	0	723	1236	87	Methylnitrocatechol
	215.16	$C_{12}H_{24}O_3$	610	800	520	643	281	22	
	123.06	$C_6H_8N_2O$	0	1070	700	590	1068	92	Dimethylpyrimidinol
	99.05	$C_5H_8O_2$	510	1230	0	580	1215	107	Pentenenoic acid
	221.07	e.g, $C_8H_{14}O_7$	640	860	0	500	878	89	
	161.06	$C_6H_{10}O_5$	0	880	530	470	871	94	Levoglucosan
	135.04	$C_8H_8O_2$	580	740	0	440	765	88	Methylbenzoic acid
	207.05	e.g., $C_7H_{12}O_7$	600	510	0	370	636	87	

	137.03	$C_7H_6O_3$	0	950	0	317	1078	173	Salicylic acid
	151.06	$C_8H_8O_3$	0	790	0	263	896	173	Syringol
	143.11	$C_8H_{16}O_2$	0	740	0	247	840	173	Oxanoic acid
	145.06	$C_6H_{10}O_4$	0	630	0	210	715	173	Hexenedioic acid
	149.05	e.g., $C_4H_{10}N_2O_4$	0	630	0	210	715	173	
	155.11	$C_9H_{16}O_2$	0	560	0	187	635	173	Nonenoic acid
	111.05	$C_6H_8O_2$	0	530	0	177	601	173	Cyclohexadienediol
	167.11	$C_{10}H_{16}O_2$	0	530	0	177	601	173	Decadienoic acid
	131.04	$C_5H_8O_4$	0	520	0	173	590	173	Pentenedioic acid
	153.09	$C_9H_{14}O_2$	0	500	0	167	567	173	
Products (0-15 min):	123.01	$C_6H_4O_3$	3350	3980	2310	3213	1657	26	Hydroxyquinone
	153.02	$C_7H_6O_4$	1490	1580	940	1337	681	26	Carboxyhydroxy-hydroquinone
	113.03	$C_5H_6O_3$	1390	1260	900	1183	499	21	Oxopentanoic acid
	87.04	$C_4H_8O_2$	0	0	2230	743	2530	173	Butanoic acid
	85.03	$C_4H_6O_2$	0	0	2220	740	2519	173	Methacrylic acid
	115.04	$C_5H_8O_3$	830	530	660	673	296	22	Hydroxypentanoic acid
	87.01	$C_3H_4O_3$	1010	0	700	570	1017	91	Pyruvic acid
	125.03	$C_6H_6O_3$	740	760	0	500	851	87	Hydroxyhydroquinone
	99.01	$C_4H_4O_3$	730	680	0	470	801	87	Oxobutenoic acid
	167.07	$C_9H_{12}O_3$	720	650	0	457	780	87	
	89.02	$C_3H_6O_3$	0	0	1280	427	1452	173	Lactic acid
	127.04	$C_6H_8O_3$	620	600	0	407	692	87	Oxohexenoic acid
	137.06	$C_8H_{10}O_2$	870	0	0	290	987	173	
	155.04	$C_7H_8O_4$	0	710	0	237	806	173	Heptadienedioic acid
	161.05	$C_6H_{10}O_5$	700	0	0	233	794	173	Levoglucosan
	95.02	$C_5H_4O_2$	0	690	0	230	783	173	
	73.03	$C_3H_6O_2$	0	0	660	220	749	173	Propanoic acid
	173.05	$C_7H_{10}O_5$	580	0	0	193	658	173	Oxoheptanedioic acid
	109.07	$C_7H_{10}O$	0	0	570	190	647	173	
	101.03	$C_4H_6O_3$	570	0	0	190	647	173	Oxobutanoic acid
Products (0-30 min):	123.01	$C_6H_4O_3$	4260	4190	2630	3693	1811	25	Hydroxyquinone
	153.02	$C_7H_6O_4$	2150	2220	1420	1930	871	23	Carboxyhydroquinone
	113.03	$C_5H_6O_3$	1900	1900	1320	1707	658	20	Oxopentanoic acid
	99.01	$C_4H_4O_3$	1200	1190	830	1073	414	20	Oxobutenoic acid
	87.01	$C_3H_4O_3$	1410	610	1100	1040	793	39	Pyruvic acid
	115.04	$C_5H_8O_3$	1030	1010	970	1003	60	3	Hydroxypentanoic acid
	101.03	$C_4H_6O_3$	1040	1110	740	963	386	20	Oxobutanoic acid
	167.07	$C_9H_{12}O_3$	1080	940	740	920	336	19	
	125.03	$C_6H_6O_3$	930	950	600	827	386	24	Hydroxyhydroquinone
	87.04	$C_4H_8O_2$	0	0	2430	810	2757	173	Butanoic acid
	155.04	$C_7H_8O_4$	750	1060	510	773	542	36	Pentadienedioic acid

	127.04	$C_6H_8O_3$	810	800	630	747	199	14	Oxohexenoic acid
	173.05	$C_7H_{10}O_5$	630	500	530	553	134	12	Oxoheptanedioic acid
	85.03	$C_4H_6O_2$	0	0	1420	473	1611	173	Methacrylic acid
	95.02	$C_5H_4O_2$	0	810	560	457	815	91	
	129.06	$C_6H_{10}O_3$	0	530	520	350	596	87	Oxohexanoic acid
	159.03	$C_6H_8O_5$	510	500	0	337	573	87	Hydroxyhexenedioic acid
	109.03	$C_6H_6O_2$	930	0	0	310	1055	173	Hydroquionone
	117.02	$C_4H_6O_4$	900	0	0	300	1021	173	Butanedioic acid
	137.06	$C_8H_{10}O_2$	710	0	0	237	806	173	Octadienoic acid
	131.04	$C_5H_8O_4$	700	0	0	233	794	173	Pentanedioic acid
	145.02	$C_5H_6O_5$	660	0	0	220	749	173	Oxopentanedioic acid
	141.03	$C_6H_6O_4$	650	0	0	217	738	173	Hexadienedioic acid
	97.03	$C_5H_6O_2$	540	0	0	180	613	173	Pentadienoic acid
Products (0-120 min):	117.02	$C_4H_6O_4$	3490	5800	5380	4890	2418	25	Succinic acid
	113.03	$C_5H_6O_3$	2930	3180	2760	2957	415	7	Oxopentenoic acid
	101.03	$C_4H_6O_3$	1900	3610	2950	2820	1695	31	Oxobutanoic acid
	115.05	$C_5H_8O_3$	2290	2700	2730	2573	483	10	Oxopentanoic acid
	153.03	$C_7H_6O_4$	2890	2250	2380	2507	665	13	Carboxyhydroquinone
	123.01	$C_6H_4O_3$	2400	2080	2120	2200	343	8	Heptadienoic acid
	99.01	$C_4H_4O_3$	1260	2520	2180	1987	1281	33	Oxobutenoic acid
	131.03	$C_5H_8O_4$	700	1890	2120	1570	1498	49	Hydroxyoxopentenoic acid
	145.02	$C_5H_6O_5$	930	2050	1270	1417	1129	41	Oxopentanedioic acid
	147.03	$C_5H_8O_5$	600	2090	1360	1350	1464	55	Hydroxypentanedioic acid
	129.06	$C_6H_{10}O_3$	1180	1370	1480	1343	298	11	Oxohexanoic acid
	141.03	$C_6H_6O_4$	1110	1370	1060	1180	327	14	Dihydroxyhydroquinone
	127.04	$C_6H_8O_3$	900	1260	1090	1083	354	17	Oxohexenoic acid
	87.01	$C_3H_4O_3$	0	700	2390	1030	2415	119	Pyruvic acid
	167.08	$C_9H_{12}O_3$	1330	570	1140	1013	777	39	
	143.07	$C_7H_{12}O_3$	980	1000	1030	1003	49	3	Oxoheptanoic acid
	125.03	$C_6H_6O_3$	1300	840	760	967	573	30	Hydroxyhydroquinone
	155.04	$C_7H_8O_4$	790	1180	890	953	398	21	Heptadienedioic acid
	159.04	$C_6H_8O_5$	500	990	800	763	486	32	Hydroxyhexenedioic acid
	103.01	$C_3H_4O_4$	610	1010	600	740	460	32	Malonic acid
	115.00	C_8H_4O	0	1320	840	720	1313	93	
	157.02	$C_6H_6O_5$	550	840	680	690	285	21	Oxohexenedioic acid
	141.06	$C_7H_{10}O_3$	650	730	630	670	104	8	
	157.09	$C_8H_{14}O_3$	610	630	630	623	23	2	Hydroxyoctanedioic acid
	173.04	$C_7H_{10}O_5$	0	710	680	463	789	87	Oxoheptanedioic acid
	97.03	$C_5H_6O_2$	0	630	750	460	792	88	Butadienoic acid
	175.02	$C_6H_8O_6$	0	790	530	440	791	92	Hydroxyoxohexenedioic acid

	171.03	$C_7H_8O_5$	0	720	570	430	747	88	Oxoheptenedioic acid
	139.04	$C_7H_8O_3$	650	570	0	407	697	87	Oxoheptadienoic acid
	159.06	$C_7H_{12}O_4$	580	0	630	403	688	87	Heptanedioic acid
	95.01	$C_5H_4O_2$	0	530	630	387	665	88	
	85.03	$C_4H_6O_2$	0	0	760	253	862	173	Methacrylic acid
	133.01	$C_4H_6O_5$	0	680	0	227	772	173	Hydroxybutenedioic acid
	114.02	$C_4H_5NO_3$	0	580	0	193	658	173	
	139.01	$C_6H_4O_4$	0	570	0	190	647	173	Dihydroxyquinone
	189.04	$C_7H_{10}O_6$	0	570	0	190	647	173	Hydroxyoxopentanedioic acid
	169.01	$C_7H_6O_5$	0	550	0	183	624	173	Trihydroxybenzoic acid
Unreactive:	128.04	$C_5H_7NO_3$			X				Nitrocyclopentenol
	145.05	$C_6H_{10}O_4$			X				Glutarate
	163.07	$C_6H_{12}O_5$	X						Hydroxyhexanedioate
	169.13	$C_{10}H_{18}O_2$	X						Decenoate
	175.04	$C_{10}H_8O_3$			X				
	187.09	$C_9H_{16}O_4$	X						Nonanedioate
	193.07	$C_7H_{14}O_6$			X				
	197.07	$C_6H_{14}O_7$	X						
	201.06	$C_{12}H_{10}O_3$	X						
	203.07	$C_7H_{12}N_2O_5$	X						
	211.09	$C_6H_{16}N_2O_6$	X						
	219.07	$C_{12}H_{12}O_5$			X				
	235.08	$C_6H_{12}O_2$			X				Hexanoate
	237.08	$C_7H_{14}N_2O_7$	X						

APPENDIX 7: STANDARD OPERATING PROCEDURES FOR OXIDATIONS AND OFFLINE IC AND LC/MS ANALYSES

Cloud and Fog Water Analysis Operating Procedure: Performing Online Aqueous Photo-oxidations

- Sample Volume: Samples should be at least 40 mL in volume to allow a full oxidation reaction (approximately 120 minutes at 0.25 mL min^{-1} online mass spectral analysis, with five offline samples; see Table below). The 250 mL photoreactor can be used to react solutions of this volume.

Table A7-1. Sample volumes needed for specific sampling intervals during photo-oxidations.

Sampling interval	Sample Volume	Total Sample Number	Total Volume Needed
10 min	2 ml	13	26
15 min	2 ml	9	18
30 min	2 ml	5	10

- Precursor Concentration: The concentration of the precursor(s) should be environmentally relevant; glyoxal, for example, is found in wet aerosol particles at concentrations up to 3000 μM and in fog or cloud droplets in the range of 30-300 μM. While other precursors such as homovanillic acid (HVA) are not found in concentrations this high, it is acceptable to use a concentration at least initially that might allow the identities of the products to be determined. It should be noted, however, that the products will likely be different when a different concentration of the precursor is oxidized (Tan et al., 2009).

- Oxidant: Hydroxyl radical is currently understood to be the most prevalent oxidant in atmospheric waters (Ervens et al., 2014), and can be generated by introducing H_2O_2 and light (either at 253.9 nm or using a solar simulator to give a full spectrum) to the solution. The concentration should be environmentally relevant, although higher and lower concentrations are acceptable for experimental reasons. Approximately 15 μM is relevant for cloud droplets, although a range of values has been measured (e.g., Shen et al., 2012). Some studies have employed a 5:1 ratio of oxidant (as H_2O_2) to precursor concentrations to allow full oxidation. Other oxidants are known; in particular, nitrate and nitrite radicals as well as high energy light and singlet oxygen are likely relevant in aqueous secondary organic aerosol (SOA) formation.

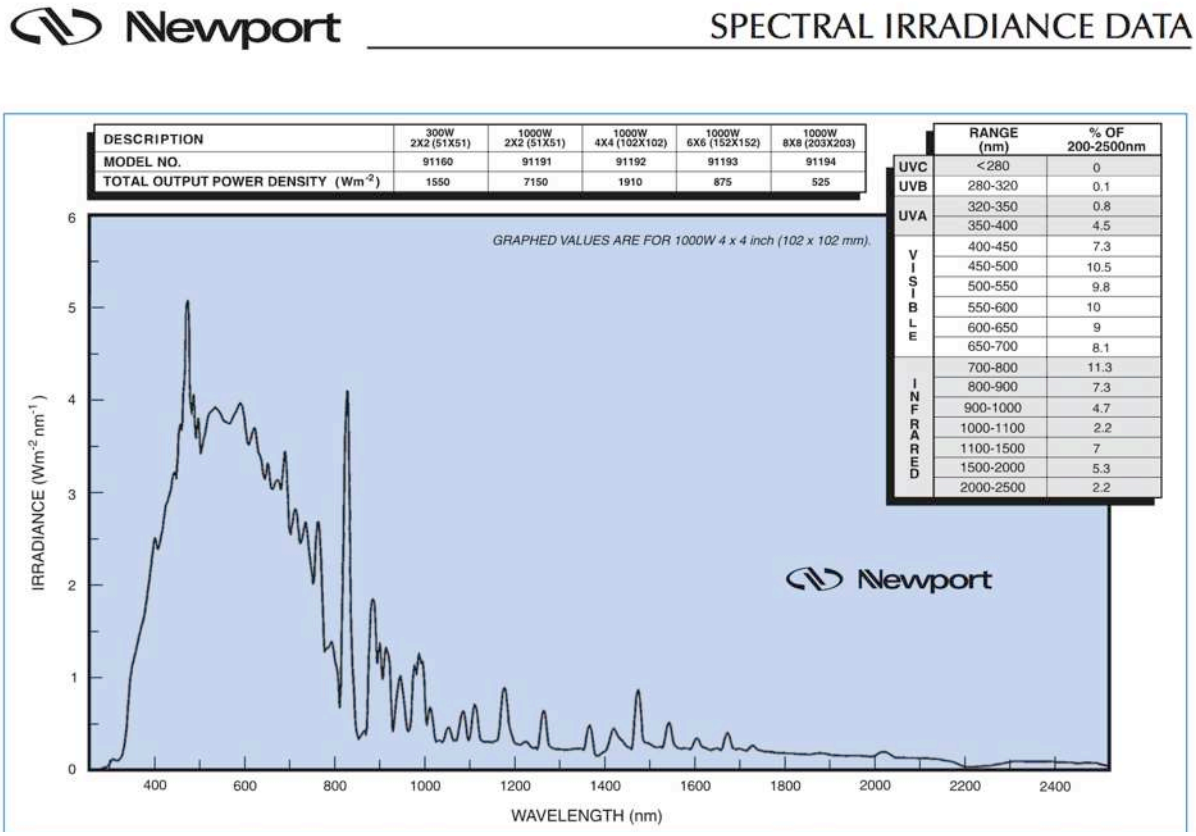

Figure A7-1. Spectra irradiance from a Newport Oriel simulator similar to the LCS-100 simulator in our lab.

- Light Source: Two major options exist for providing light to a photoreaction in our lab (as of 07/23/2015): an ultraviolet lamp with peak wavelength 253 nm, which is submerged directly into the reaction solution, or a solar simulator, which is directed downward onto the solution. The ultraviolet source generates hydroxyl radical easily, but can also cause photolysis of the compounds in the solution that's not representative of real

atmospheric photolysis (because it's only a small bandwidth –not the spectrum of the sun). On the other hand, the simulator does provide an approximation of the solar spectrum (Figure A7-1), but with a lower hydroxyl radical generation capacity. While the spectrum is mostly accurate for the visible range of the spectrum, the generated irradiance in the ultraviolet range is low, and has not been characterized well.

- Whether to use offline/discrete sampling: Although getting discrete samples for analysis via the Sievers TOC analyzer, organic acids ion chromatograph, or pH electrode is useful, it makes the oxidation process more strenuous (depending on the interval between the discrete samples), and timing can be an issue for products of oxidation that continue to be degraded as the sample sits in the sample vial awaiting analysis. *To avoid loss of products/continued reaction after drawing discrete samples from the reaction vessel, have vials prepared with a small amount (~10 microliters) bovine catalase, and put the sample immediately in the refrigerator or a refrigerator autosampler tray. Analyze samples within 24 hours –or as soon as possible. Complete lack of reactant and product molecule detection after less than 24 hours has been observed in some cases.*

Introduction of the sample to the mass spectrometer (online mass spectrometry)

- Choice of pump: The two most important factors in choosing a pump for introducing the sample directly into the mass spectrometer for online analysis are the minimization of time spent by the sample within the tubing between the photoreactor and mass spectrometer, and the minimization of noise resulting from the pumping process. Two types of pumps have been tested with the photoreactor: a simple peristaltic pump and a nanopump made for LC analysis. While the nanopump introduces low flow rates to the mass spectrometer (which provides increased sensitivity if the sample is complex or contains high concentrations of inorganic acids), the noise introduced to the mass spectrometer signal by this pump is irregular and large in magnitude. This may originate from bubbles trapped within the long lengths of tubing required for use of this pump. An additional feature of the nanopump is that additives can be mixed into the sample prior to injection into the mass spectrometer that can potentially help with reproducibility between oxidation experiments (although this was not observed when the nanopump was used with 1-5% methanol and 0.1% formic acid added). The peristaltic pump introduces noise (10-20% of signal) at regular intervals, which can be easily removed by using smoothing algorithms in many data analysis software packages, but the tubing required for a simple peristaltic pump has a large inner diameter, which increases the time spent by the sample between photoreactor and mass spectrometer. Overall,

the peristaltic pump is likely to be the best option in most experiments because it is simpler to use and provides removable noise in the mass spectrometer signal.

- Contamination in tubing: Contamination visible in the mass spectrometer signal is a common issue before and after oxidation reactions. This is likely due to the use of chemicals that adhere (due to solubility) to the tubing and inner surfaces between the photoreactor and mass spectrometer. When this occurs, the first measure taken should be to "wash" the tubing by flowing solvent/water through the system for long periods of time (up to several hours). If this does not eliminate the contamination issue, the plate of the ionization source within the mass spectrometer can be cleaned using a cotton swab and water/isopropanol mixture (or similar). The mass spectrometer should be put into "standby" mode and the sample tubing should be unscrewed from the source before opening the source. *Care should be taken when opening the ionization source: do not try this for the first time without supervision.* A third option is to replace the tubing that might be contaminated.
- Flow rate: Sample should be introduced to the mass spectrometer at flow rates generally less than 1 mL/min; if possible, 100-200 microliters/min is optimal.

Mass spectrometer specifications

- Mass calibration: Before each day of analyses, the mass spectrometer should be calibrated so that the m/z^- values are accurate, and so that formulae can be generated easily.
- Start the mass spectrometer: From standby (green light is visible on the mass spectrometer itself), open the Agilent MassHunter Workstation Data Acquisition software. Select an appropriate method without LC separation, but with some flow (from the bin pump or the photoreactor) to the mass spectrometer, and ensure that the system is prepared for this method (column in place, if any, eluent bottles full, etc.). Click the "On" button on the top right of the window. The instrument, including the LC bin pump, will start, in all methods.
- From the top left of the Agilent MassHunter Workstation Data Acquisition software, select "Tune" from the "Context drop-down menu. The tuning window will open. Change the window range in the first tab on the bottom right to "0.1%T", de-select masses in the bottom center <1700, and in the final tab on the bottom right, select the "low mass range".
- Introduce a tune mix to the mass spectrometer: A diluted (1:20 in acetonitrile) solution of the Agilent EI tuning mix is used for this process. Use a 2 mL plastic syringe, luer-lock adapter with peak tubing, and syringe pump (<200 microliters/min) to introduce the tuning mix to the mass spectrometer. *Do not allow the peaks to reach*

>10,000 abundance units because some of the compounds in the tune mix can persist in the mass spectrometer/tubing after use and are difficult/time consuming to remove.

- From the first tab, click "calibrate" and wait until the result shows. Click this two additional times, and record the final calibration.
- Exit the tuning mode by selecting "Acquisition" from the "Context" drop-down menu at the top left of the window.
- Mass spectrometer parameters (method): See below for specific parameters used in analysis of samples online during photoreactions (saved as method "Ali Online_fullox_12-16-14.m"):
- WPS Tab: This tab (regarding the autosampler) is unimportant for online analyses. Stop Time should be set to "No limit" (under Options sub-tab).
- Bin Pump Tab: Flow should be set to 0 ml/min. Stop Time should be set to "No limit". Post time should be set to "Off".
- Column Tab: This tab (regarding the autosampler) is unimportant for online analyses. Stop Time should be set to "No limit". Post time should be set to "Off".
- DAD Tab: If the UV/visible absorption spectrometer will be used in-line to monitor the absorption of the photoreaction solution components, "Store" should be checked under the Spectrum section on the Setup sub-tab. Set the Range on the same sub-tab to 190-900nm with a 2nm step. Stop Time should be set to "No limit". Ensure that "UV" and "Vis" are selected under Required Lamps on the Options sub-tab. See *s, decrease the VCap voltage)* for other settings on this tab.

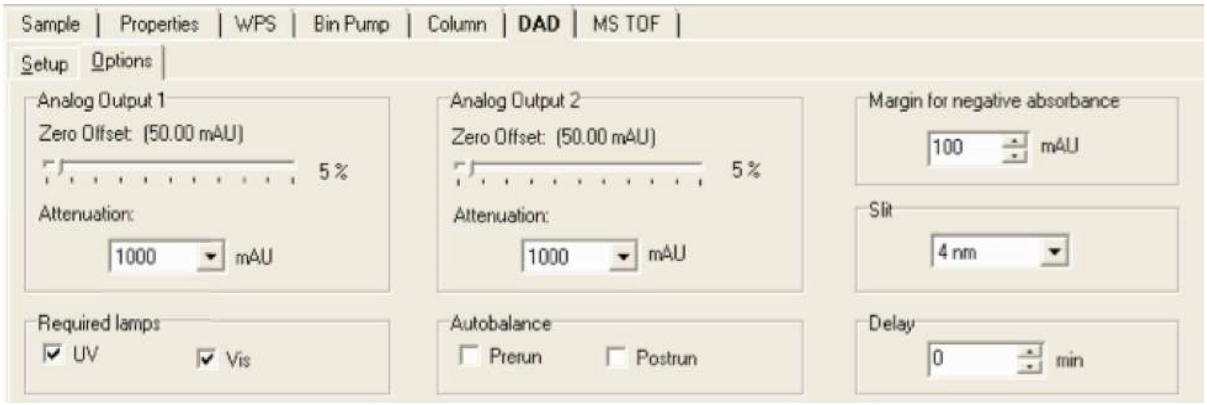

Figure A7-2. Parameters for collection online UV/visible absorption spectrometer data during photoreactions.

- MS TOF Tab: Stop Time should be set to “No Limit/As Pump”. Follow the parameters as set in F, Figure A7-4, Figure A7-5, and Figure A7-6 and as below:

Source sub-tab:

Gas Temp: 350°C,

Drying Gas: 5 l/min

Nebulizer: 20 psig,

Fragmentor: 130 V

Skimmer: 60 V

OCT 1 RF Vpp: 150 V

VCap: 3500 V

Capillary should read 0.00 uA, Chamber should read 0.00 uA (these will increase in the event of arcing; if this occurs, decrease the VCap voltage).

Acquisition sub-tab:

Mass Range 65-100 m/z

Acquisition Rate 1.4 spectra/s

Acquisition Time 713.9 ms/spectrum

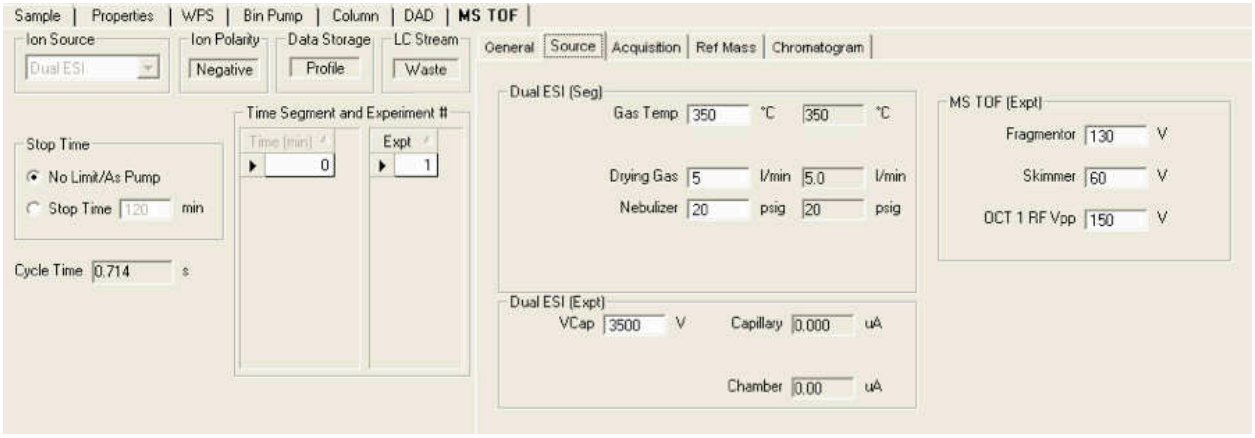

Figure A7-3. Parameters for MS TOF tab > Source sub-tab during online mass spectrometry data collection for photoreactions.

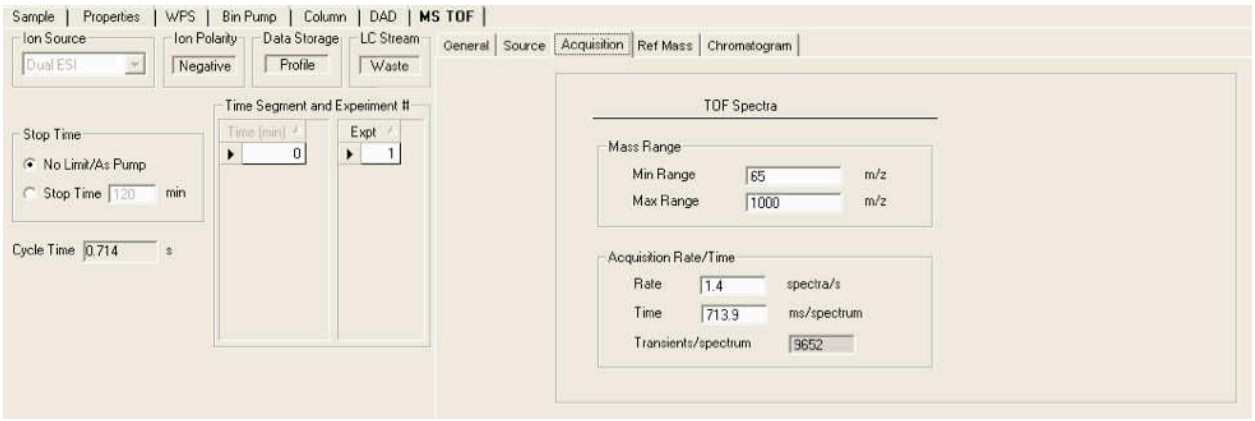

Figure A7-4. Parameters for MS TOF tab > Acquisition sub-tab during online mass spectrometry data collection for photoreactions.

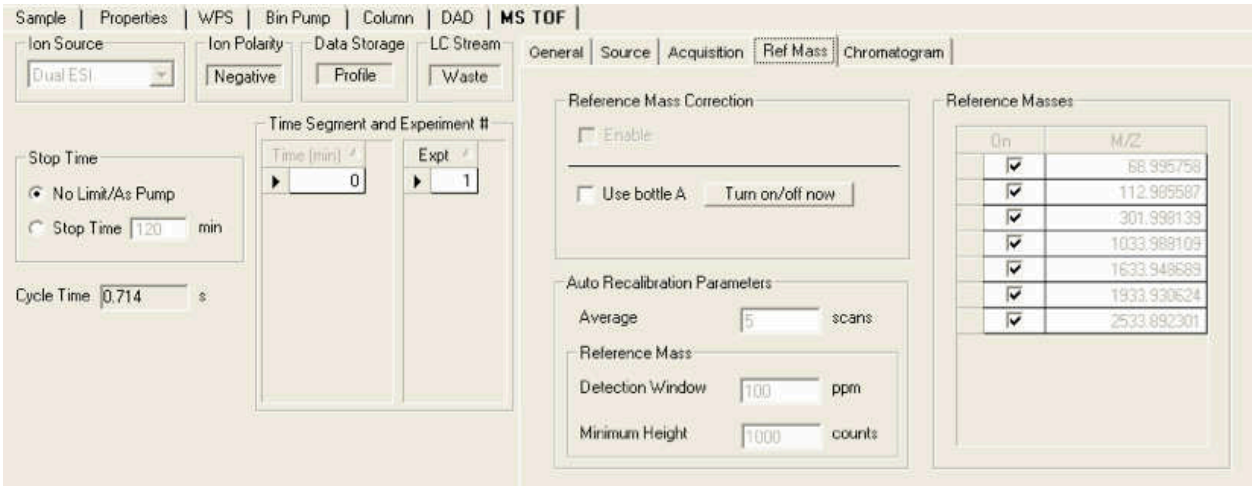

Figure A7-5. Parameters for MS TOF tab > Ref Mass sub-tab during online mass spectrometry data collection for photoreactions.

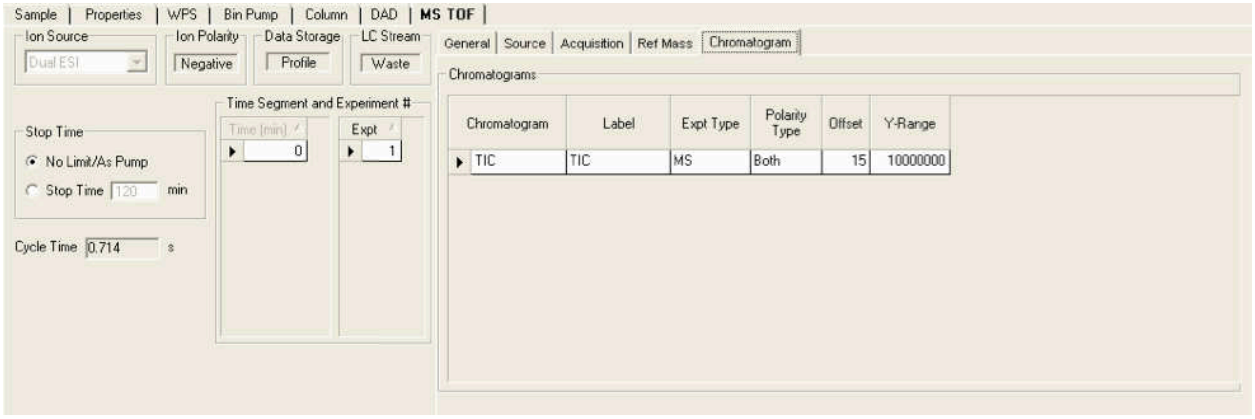

Figure A7-6. Parameters for MS TOF tab > Chromatogram sub-tab during online mass spectrometry data collection for photoreactions.

Discrete sampling (for offline analyses)

- Preparation for discrete sampling: Clean a plastic 3 mL syringe with Luer lock tip by filling one small beaker with deionized water and rinsing the syringe with 10 full syringe volumes into a second, empty beaker. Connect (screw) the syringe Luer lock tip to a Luer lock adapter, and screw a ~2-3 foot piece of brown or yellow PEEK tubing to the adapter using a plastic ferrule and screw. Place the unconnected end of the PEEK tubing through a small hole in the cap of the photoreactor, and down into the photoreactor. Stabilize the rest of the tubing and syringe such that the discrete samples can be withdrawn during the oxidation without having to move the protective covering keeping your eyes and skin from exposure to the UV lamp (or simulator). Keep the two beakers, along with extra deionized water in a closed container, at the benchtop for cleaning of the syringe between discrete samples. To avoid loss of products/continued reaction after drawing discrete samples from the reaction vessel, prepare 1.5 mL autosampler vials with a small amount (~10 microliters) bovine catalase solution (diluted approximately 10 times from the manufacturer standard). Cap all vials. Label all vials with the name of the oxidation, the date, and the time of the discrete sample (e.g., "BYOx 03-18-15 0 min"). Dispense bovine catalase to and label one additional vial beyond those for the discrete samples for a method blank; label but *do not dispense bovine catalase* to a vial for total organic carbon (TOC) analysis at 120 minutes oxidation. If TOC measurement will be made at 0 minutes oxidation, label a vial for this purpose as well. Put the vials in the refrigerator in a vial rack or in a refrigerator autosampler tray. If the organic acids IC will be used, power on the system and allow several deionized water blanks to run using the same method that will be used for the discrete samples.
- Draw a method blank. Fill the photoreactor with deionized water to test the online MS method and to allow for a method blank for the discrete sample analyses. Remove the method blank labeled autosampler vial from the refrigerator. Draw a discrete sample of water through the syringe, ensuring that several tubing volumes of water are pulled through the tubing if there is any possible contamination in the tubing. Re-clean the syringe (rinse with 10 full syringe volumes of water) before drawing the blank if necessary. Draw the blank by filling the syringe to ~1.5 mL, pushing a small amount back into the tubing to keep water from spilling out of the tubing (to ~1.25 mL), and disconnect the syringe from the Luer lock adapter. Dispense the solution into the correctly labeled autosampler vial by angling the vial and touching the syringe tip to the lower side of the vial mouth (if the solution is dispensed too rapidly or straight up-and-down, the solution will form a layer of surface tension

and spill over the mouth of the vial). If this method of dispensing does not work, an additional Luer lock adapter and small length of PEEK tubing can be used to dispense the solution. Care should be taken to clean the entire dispensing apparatus (syringe or syringe with additional Luer lock adapter and PEEK tubing) after each discrete sample is dispensed by rinsing the apparatus with 10 full syringe volumes of deionized water. Reattach the syringe to the discrete sampling tubing line at the photoreactor, first expelling any water from the rinse process, filling with air, and pushing the air into the tubing after making the connection to the Luer lock so that no old solution remains in the tubing..

- Draw a discrete sample at 0 min oxidation. Just before the oxidation is initiated by adding H_2O_2 solution and/or UV light, draw a sample using the method described in the previous step, and dispense it to the correctly labeled vial. Immediately shake the vial to disperse the bovine catalase and put the capped vial in a refrigerated location. Rinse the syringe (and apparatus for dispensing solution) 10 times with deionized water. Reattach the syringe to the discrete sampling tubing line at the photoreactor, first expelling any water from the rinse process, filling with air, and pushing the air into the tubing after making the connection to the Luer lock so that no old solution remains in the tubing.
- Draw discrete samples at the given time interval using the instructions in the steps above. At 120 minutes oxidation (or final time step), dispense additional liquid volume if any remains to both the final IC/LC analysis vial and the vial for final TOC analysis.
- Analyze samples within as soon as possible, taking special attention to minimize time samples remain out of refrigeration (even minutes may make a difference). Organic acids IC measurements are very sensitive to this timing. Complete lack of reactant and product molecule detection after less than 24 hours has been observed in some cases.

Data analysis

- Online mass spectrometry data: The Agilent MassHunter Qualitative Analysis software can be used for this. Note that on computers with more recent versions of Windows than Windows XP, this software has copious problems. A copy of both versions of the software should be on cds in a drawer near the mass spectrometer. Even in the earlier version of this software, the techniques for analyzing data are tedious and different from other software ---this takes some getting used to. *It is important to note in your results (and make clear to your audience) that the sensitivity of electrospray ionization depends on multiple variables and does not necessarily reflect the mass-normalized or molar abundances of the compounds in the sample.*
- Extract mass spectra at each discrete time interval:
    - Average over one minute time period
    - Set >500 or >1000 a.u. threshold in Method Editor
    - Generate formulae for each peak in mass spectra by loosely highlighting each peak, right clicking, and selecting "generate formula". Settings in Method Editor can be un-intuitive and tricky.
    - Subtract "background" spectrum from each mass spectrum
- Generate extracted ion chromatograms (EICs) for interesting *m/z* values:
    - For one EIC: Within the Spectrum Preview or Spectrum Results Window, zoom in on a peak (drag a box around the peak or right click and slide on the bottom axis of the spectrum). Select the area just around that peak and double click.
    - For multiple EICs: Right click on any TIC Scan/chromatogram in the Data Navigator, select "Extract chromatograms". A window will appear. Select one or multiple (ctrl/cmd/shift) data files under List of opened data files at left. Select "EIC" from the Type drop-down menu. In the m/z value(s): box, enter the *m/z* values of interest, separated by a comma (in some versions of the software, a semi-colon is used to separate these –be sure to copy your *m/z* values before selecting OK in case this is one of those versions, since it will delete your selection). Select OK.
- Clean up EICs/time profiles using another data analysis program: Use smoothing algorithms such as "smooth" in Igor to eliminate noise from the EICs (alternatively called time profiles). Delete data points before the beginning of the oxidation process. To export the raw data within chromatograms, Click Actions > Export all

chromatograms to CSV file. This will export the chromatograms that are checked in the Data Navigator to a CSV file within each separate data file (all in one, long column).

- Ion chromatographs from the organic acids system: PeakNet version 5.21 is used to view and integrate conductivity chromatograms. This software is also flawed and can be frustrating to use, but is currently the best tool for this analysis. Integrate each peak in all chromatograms, including in deionized water blanks (these are needed for calculating the limit of detection for the analysis).
- Sievers Total organic carbon: Data collected from the Labview VI are saved as a .txt file and can be opened in Excel. Create a scatter plot of the TOC and time values to find the beginning and end of the time period during which accurate data points were collected. Find the average of the TOC values within this period.
- **Reversed phase liquid chromatography-mass spectrometry for offline analyses**
- The following settings for LC/MS analysis should be used (or a variation on the settings) for analysis of carbonaceous species in the samples/standards being oxidized.
- Specifications: The instrument is an Agilent 1100 series high performance liquid chromatograph with a gradient mixer (no degassing helium cylinder required) and an optional in-line UV/visible absorption spectrometer (Agilent DAD). The chromatography column used is a Kinetex 2.6 μm particle size XB-C18 column designed for polar organic species separation with 100 Å pore size and 3.00 mm internal diameter. A gradient elution with 0.1% formic acid and methanol is used to achieve separation.
- After the online MS analysis of an oxidation, there is frequently contamination of the tubing and/or inlet to the MS by solution components (this is especially true if any nitrophenols were contained in the solution being oxidized). ***The MS should be kept on and deionized water should be pumped through the MS so that any contamination can be minimized before LC/MS analysis is begun.***
- Connect the system: Ensure that the proper connection is made to the specified chromatography column port on the LC stack (verify this by allowing a small amount of eluent to run through the system without a column or any tubing attached to the six-way valve on the bottom unit of the stack). If UV/vis analysis is desired, connect the UV/vis in line after the chromatography column and before the MS. If the MS was not mass accuracy calibrated in the previous 24 hours, see the instructions in this document for doing so.
- Find the method “Ali_aromatic_short_n.d” and ensure that the following settings are selected:

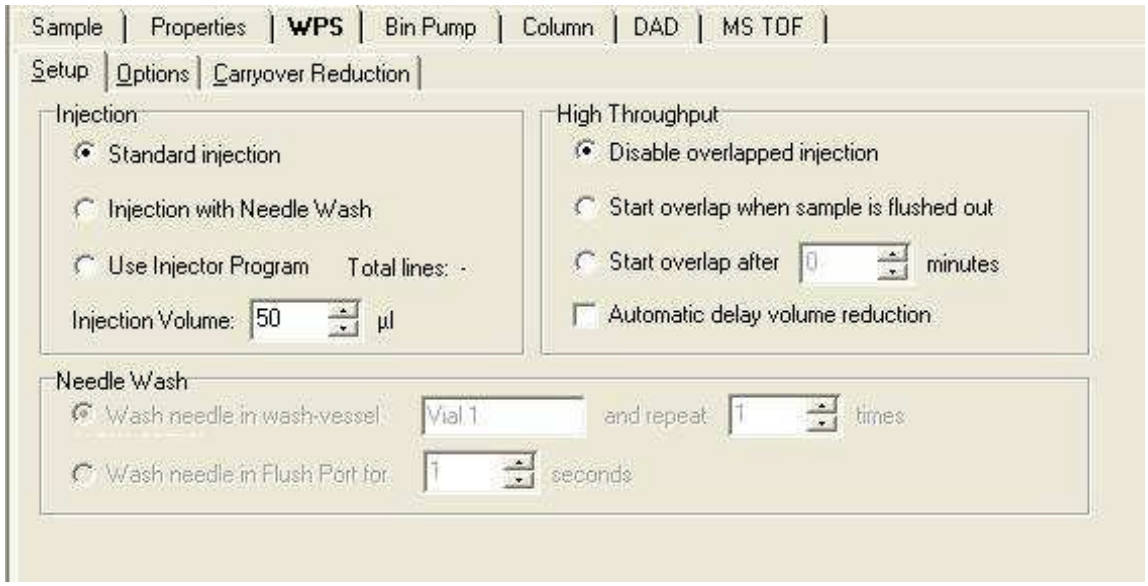

Figure A7-7. Settings in LC/MS method for analysis of carbonaceous species in discrete (offline) samples.

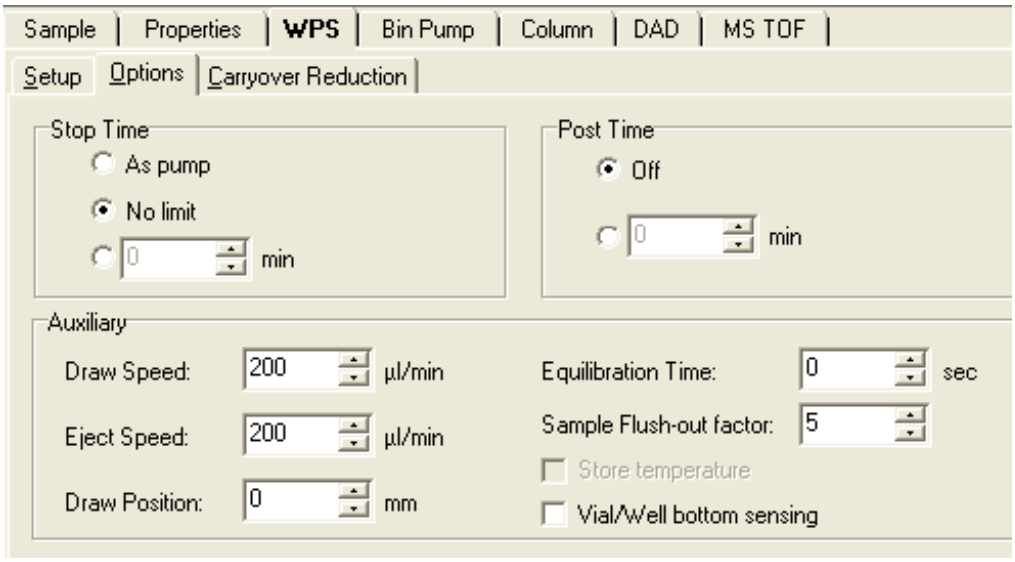

Figure A7-8. Settings in LC/MS method for analysis of carbonaceous species in discrete (offline) samples.

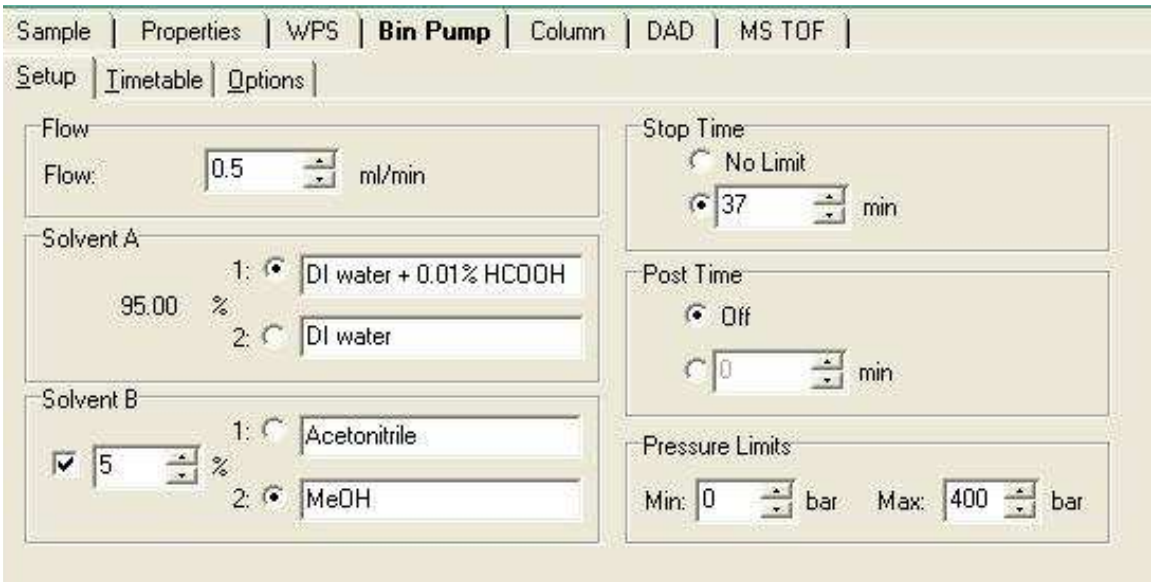

Figure A7-9. Settings in LC/MS method for analysis of carbonaceous species in discrete (offline) samples.

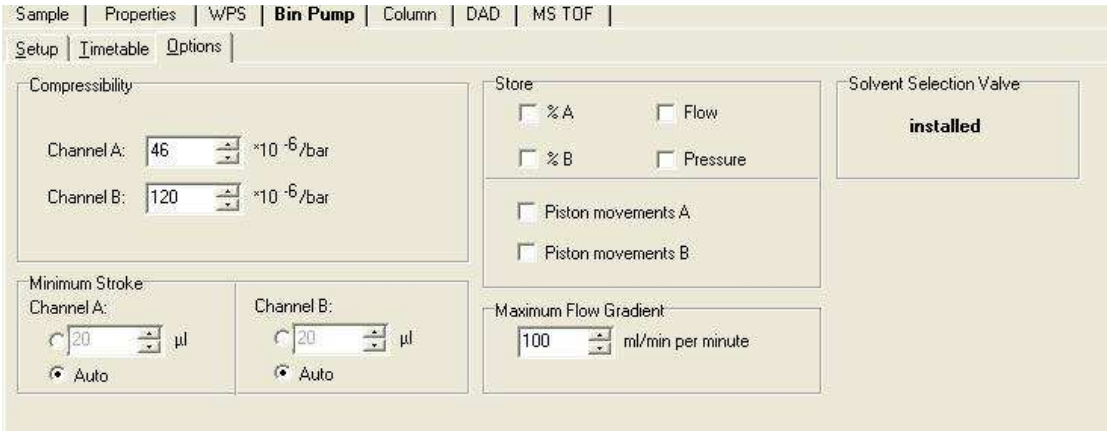

Figure A7-12. Settings in LC/MS method for analysis of carbonaceous species in discrete (offline) samples.

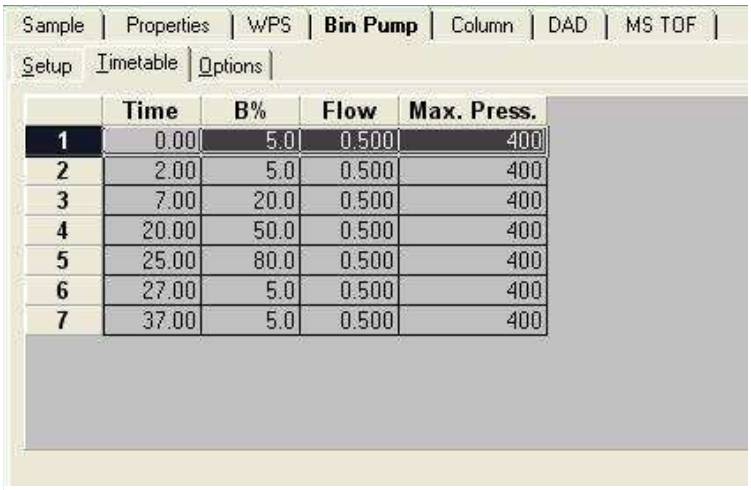

	Time	B%	Flow	Max. Press.
1	0.00	5.0	0.500	400
2	2.00	5.0	0.500	400
3	7.00	20.0	0.500	400
4	20.00	50.0	0.500	400
5	25.00	80.0	0.500	400
6	27.00	5.0	0.500	400
7	37.00	5.0	0.500	400

Figure A7-10. Settings in LC/MS method for analysis of carbonaceous species in discrete (offline) samples.

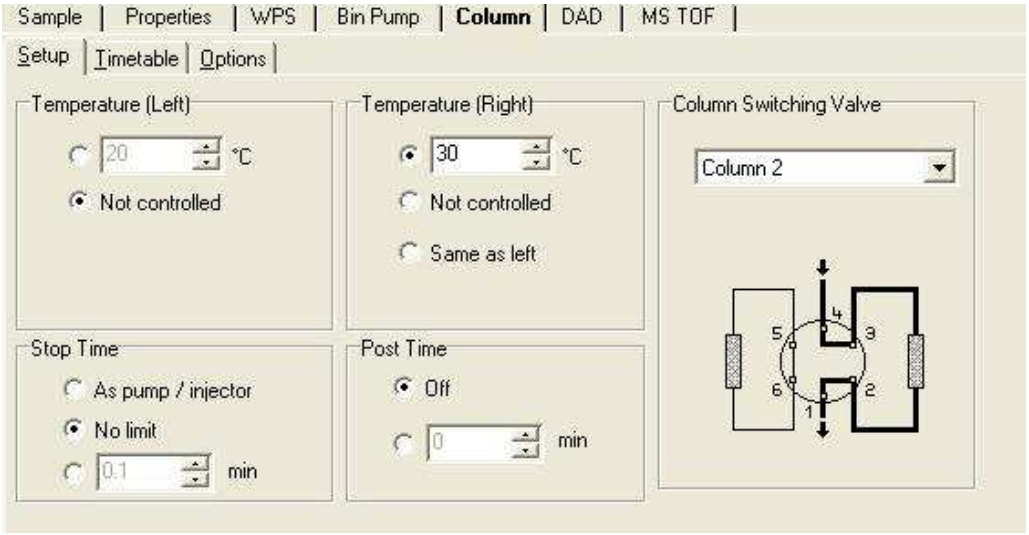

Figure A7-11. Settings in LC/MS method for analysis of carbonaceous species in discrete (offline) samples.

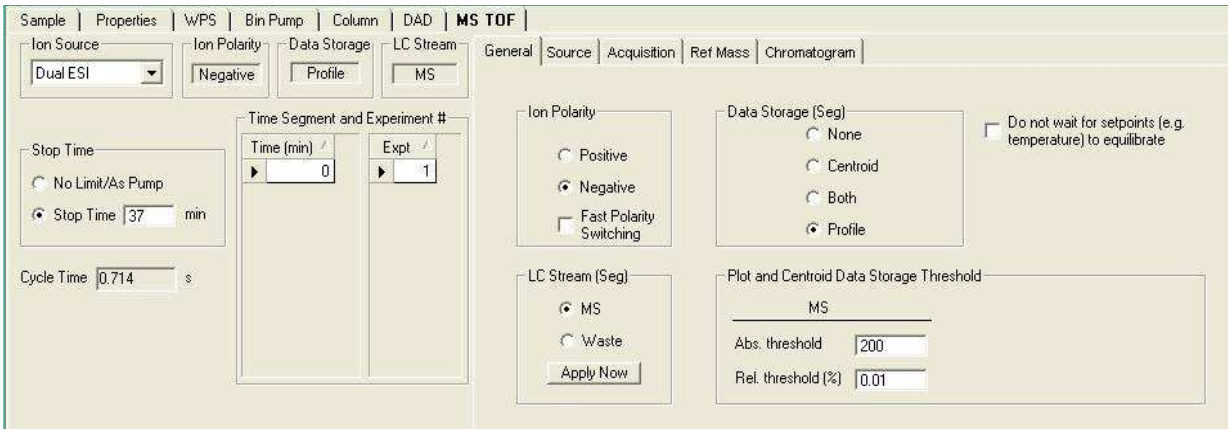

Figure A7-13. Settings in LC/MS method for analysis of carbonaceous species in discrete (offline) samples.

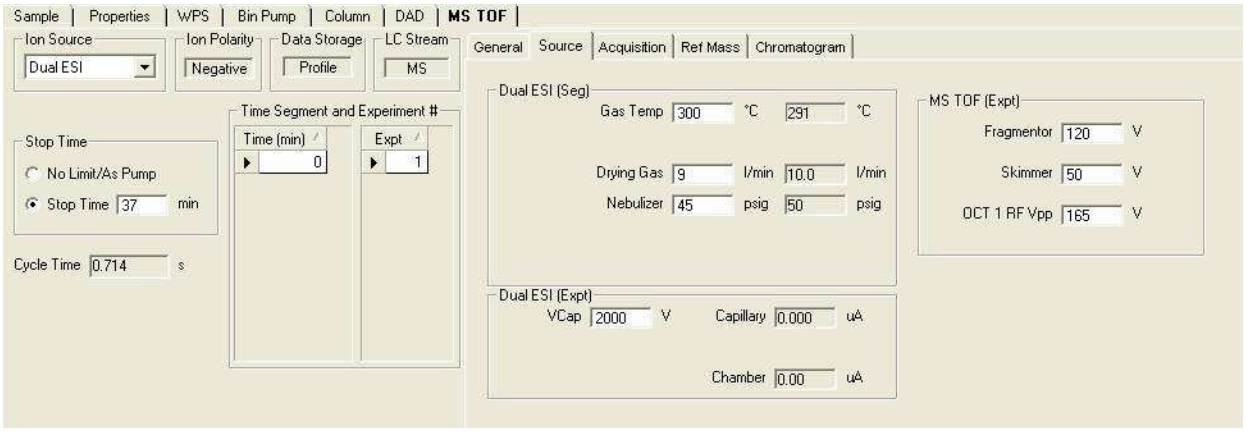

Figure A7-14. Settings in LC/MS method for analysis of carbonaceous species in discrete (offline) samples.

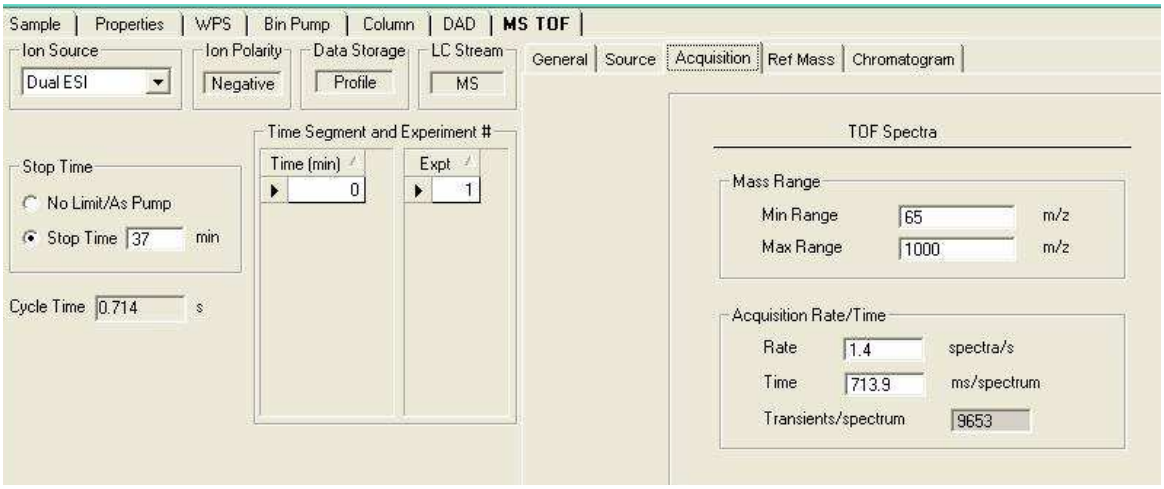

Figure A7-15. Settings in LC/MS method for analysis of carbonaceous species in discrete (offline) samples.

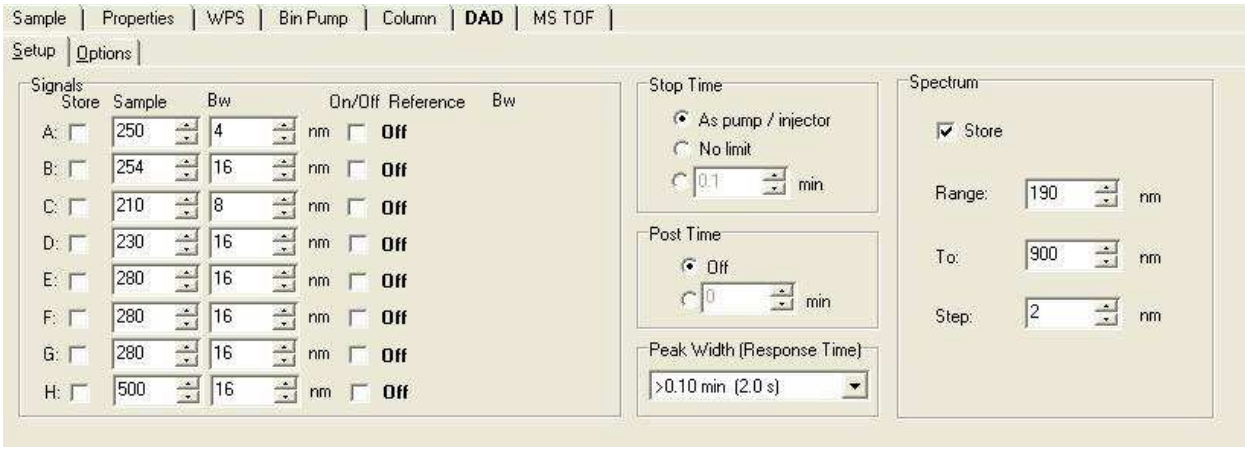

Figure A7-16. Settings in LC/MS method for analysis of carbonaceous species in discrete (offline) samples.

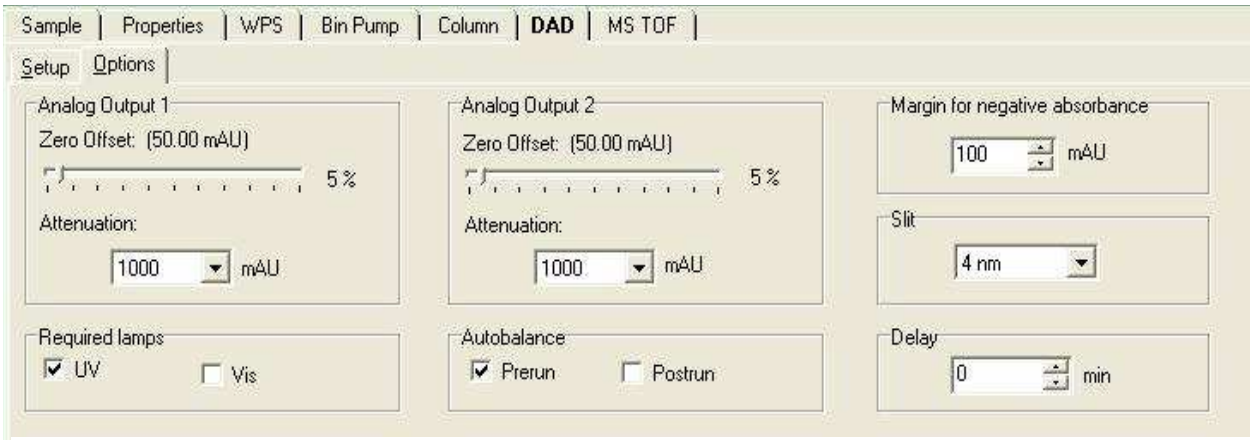

Figure A7-17. Settings in LC/MS method for analysis of carbonaceous species in discrete (offline) samples.

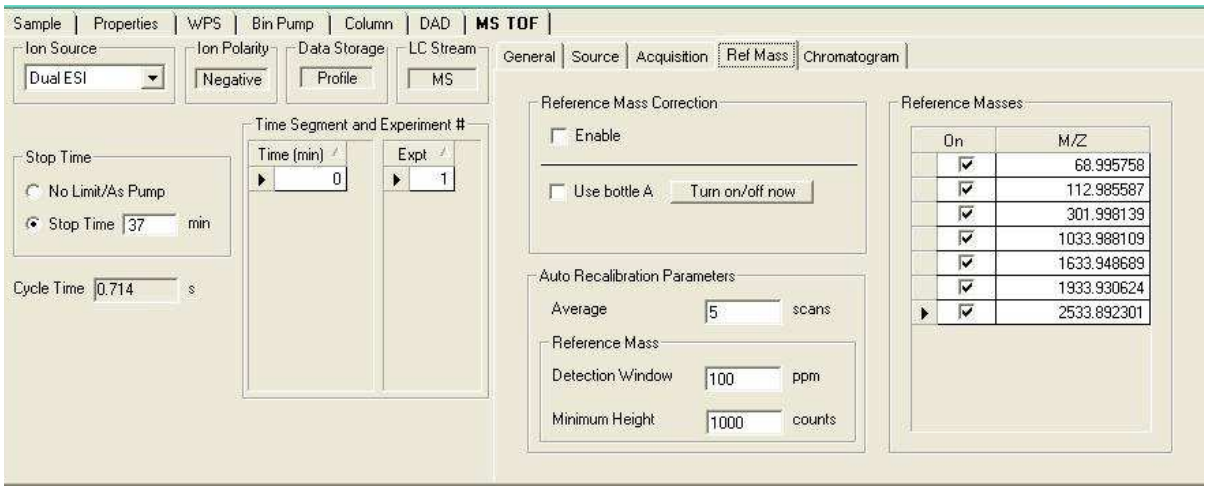

Figure A7-18. Settings in LC/MS method for analysis of carbonaceous species in discrete (offline) samples.

- Place vials in an autosampler sample holder and make a worklist. Remove the vials from the refrigerator and place them in an autosampler vial holder. Be sure to add several standards to be analyzed between samples, as well as deionized water blanks (approximately one blank and standard analysis should be added per every five sample analyses). At least three deionized water blanks should also be analyzed before starting the sample analyses to ensure that the system is running properly and to remove any contaminants in the chromatography column, tubing, etc. Make and save a new worklist in the Agilent MassHunter software to match the order of the autosampler vials in the LC/MS autosampler.
- Start the method when the system is free of contaminants (typically all contaminants will be <500 a.u., with the exceptions between m/z^- 65-1000 Da of sulfuric acid and oligomers, and lactic acid). Do so by pressing the "Start Worklist" button (the picture on the button is of several vials) on the Agilent MassHunter software.
- Calibrate. Before or after analyzing the samples, use the volumes and concentrations in Table A7-2. Volumes and concentrations of standards to be used in calibration of C18 LC/MS analysis of carbonaceous species.to generate standards for calibration of the LC/MS method. Verify that external calibrations performed on the HPLC-(-)-ESI-HR-ToF-MS are linear ($r^2 > 0.90$).

Table A7-2. Volumes and concentrations of standards to be used in calibration of C18 LC/MS analysis of carbonaceous species.

	C18 Analysis					
Final Concentrations (micromolar):	0.01	0.05	0.1	0.25	0.5	1
Adipic more concentrated (uM):	0.25	1.25	2.5	6.25	12.5	25
		1. Dilute to 100 uM solutions: Vol to add to 10 mL totaL (uL):			**2. Dilute to 1 uM solutions:** Vol to add to 10 mL totaL (uL):	
	Start Conc. 4 mM ->		250		Start Conc. 100 uM -->	100
	Start Conc. 10 mM >		100			
	Start Conc. 100 mM --->		10			
3. Into final autosampler vials:	**Std 1**	**Std 2**	**Std 3**	**Std 4**	**Std 5**	**Std 6**
Vol working solution to add (uL) @ 1 uM:	15	75	150	375	750	1500
Vol water to add (uL):	1485	1425	1350	1125	750	0
2,4-dinitrophenol, 4-nitrophenol, 2-methyl-4,6-dinitrophenol, benzoic acid, 4-methyl-5-nitrocatechol, pinic acid, pinonic acid, 2-methyl-4-nitrophenol, azeleic acid, adipic acid, 4-nitrocatechol						

Ion chromatography separation of organic acids

- Specifications: Organic acids can be measured using a gradient Dionex weak anion exchange ion chromatography (IC) system: an AS11-HC analytical column, AG11 guard column, and ASRS ULTRA II suppressor using a 1-40 mM sodium hydroxide (NaOH) eluent gradient and an ED40 conductivity detector. A small number of samples can also be analyzed after IC separation using (-)-ESI-HR-ToF-MS detection to confirm the identifications of eluted organic acids.
- Configure the system. If the system has already been used recently and all components are connected to the computer, skip this step. Connect all modules via network connection box, and connect the box to a computer with PeakNet (which needs Windows 2000 or previous). Power on the computer and all modules. Open PeakNet. From the PeakNet Main Menu, select the "Configure" program. Select "Module Inventory" button in the Configure program. Using the popup menu, select the modules you have connected to the system. Save the configuration and exit the Configure program.
- Make the method. If the method has already been made, skip this step. From the PeakNet Main Menu, select the "Method Editor" program. Select "New" under the "File" menu. Select the appropriate system and add all unassigned modules in use to the method configuration. Exit the popup window. A new method has been created called "Method1". Double click on the gradient pump (e.g., GP40) module and ensure that the pump is on, pressure limits are 0.00-20.00 MPa, piston size is standard, and eluents are A: water, B: 15 mM NaOH, C:

100 mM NaOH. Select “OK” to the move to the next screen. At Time=”Init”, eluents should be %A=80, %B=20, and flow rate should be 1.5 mL/min. Click “Enter” when these settings have been selected to change the settings. Select “0.00” min from the Time dropdown menu. At Time=”0.00”, the settings will be identical to those at Init. Click Enter. Continue setting the following times as follows: 12.00 min: %A=80, %B=20; 23.00 min: %A=0, %B=100; 28.00 min: %A=90, %C=10; 42.00 min: %A=85, %C=15; 46.00 min: %A=85, %C = 15; 47.00 min: %A=80, %B=20; 50.00 min: %A=80, %B=20. If present, select the “Oven” button and set the temperature to 35°C. Select Exit. Double click on the autosampler (e.g., AS50) module and set the mode at Init to LOAD (CSV=A), and at 0.00 to INJECT (CSV=A). Click the “Setup” button and set the tray temperature to 4°C and sample needle height to 2 mm. Select “Exit”. Single click on the detector module (e.g., ED40). Set the Data Collection Time to 50.00 in at 5.00 Hz with units of µS (plotted between -1 and 10 µS). Double click the detector module. Set the Range to 10; add a “0.00” minute time and check the “Offset” option at that time. Add a “0.5” minute time and select the “begin” option at that time. Select “Exit”. Save the method and exit the Method Editor program.

- Create a schedule. Select the “Schedule Editor” from the PeakNet Main Menu. A new schedule will be created, or an old schedule can be opened and saved as a new name to use as a template. The following settings should be set:
- Sample: Choose a vial number in the autosampler
- Sample Type: “Sample”
- Level: *Leave blank*
- Method: Choose the method created in the previous step or “Taehyoung Method”.
- Data File: Browse to a folder where the data should be saved and enter a file name (preferably without spaces or symbols; should be short).
- Volume: 100 (µL).
- Dilution, Weight, Int. Std.: these will be set to “1” automatically.

Once all the blanks (at least three to begin the worksheet, and one every five samples/standards), calibration standards (see calibration section below; a standard should be analyzed between every five samples as well), and samples have been entered into the schedule, add a “Stop” to the schedule using a vial position that contains deionized water and using a method that is identical to the main method, but that has no eluent flow or injection

sequence, and that turns off the suppressor (*the suppressor is the most important part of this: if the suppressor is left on while not in use, particularly without eluent flow, it will substantially shorten the lifetime of the suppressor*). Save the schedule and exit the Schedule Editor program.

- Check the settings manually on the autosampler to ensure that the syringe volume, sample loop volume, syringe draw speed are set to the correct values. Ensure that the needle is properly aligned and do a rinse step if the autosampler has not been used for some time.
- Start the system. The organic acids IC should be started and run for at least one hour, and at least two deionized water blanks should be analyzed, prior to analysis of samples or standards. Turn on the valve at the helium gas cylinder and ensure that <5 kPa pressure is flowing to the eluent bottles. From the PeakNet main menu, select "Run". Select "Open Sequence" and browse to the sequence you created in step d. When you select "Ok", the system will begin to run eluent at the Init ratios, and turn on the suppressor. Ensure that the system is working properly (system pressure should be approximately 2700-2900 psi, signal should be between -1 and 2 μS). Start the analysis (the "Play" button on the right; the Play button on the left puts the system into the Init mode that is currently running). Be sure to check back on the system before any samples or standards are analyzed so that the sequence can be stopped in time to allow additional water blank analyses if needed.

Note that the schedule can be created and started before the discrete samples are collected; if a vial is not present, the item in the schedule will be skipped.

- Troubleshooting notes: If the autosampler screen displays an error relating to the syringe, and the schedule has halted, restart the autosampler and restart the schedule from the first schedule item that was not completed. All data should be checked to ensure that no electronic or mechanical noise interfered with the signal; some samples may need to be rerun. If the background is unstable with a regular wave-like pattern along the baseline, turn off the suppressor (Select "Direct Control" from the "Run" menu) and the eluent flow, open the prime valve on the pump, and prime for at least a full minute. If the baseline noise continues, try priming for several minutes. If the noise still persists, consult the manual for the gradient pump: the troubleshooting/maintenance section discusses replacement of the rinse/piston seals and check valves. If these items do need to be replaced, be sure to note the date of replacement on a piece of tape inside the gradient pump door. *While the eluent is not running through the system, the suppressor current should always be turned off.* Eluents may also be

contaminated with carbon dioxide, etc., after months of not being used. These should be replaced. To remake the eluents, deionized water (Millipor system or equivalent) can be used in bottle A, a solution from NaOH pellets of 200 mg/1L deionized water can be used in bottle B (5 mM NaOH), and a solution of 4 g NaOH pellets to 1L deionized water can be used in bottle C (100 mM NaOH). Mix well or leave cap off and sonicate to entirely dissolve pellets. Close eluent bottles tightly. When connecting plastic nuts and screws, make tight connections, but *not too tight*. Particularly when the connection is between plastic and metal, as in the six-way valve of the AS50, the plastic pieces can shred and get stuck inside the nut/valve. Removal of plastic pieces is best done with a sharp object stuck firmly into the plastic as if using a screw driver. NaOH can degrade these plastic pieces over time, and it is a good idea to replace them in the long term. NaOH can additionally build up inside the tubing and cause leaks. Water or even sulfuric acid can be run through *parts* of the system to remove blockages, in either direction. Sulfuric acid can contaminate the column, so care should be taken to avoid this from happening. Consult the column or suppressor manual for additional information about these cleaning processes.

- Calibration: See the chart below for volumes and concentrations to be used in calibrating the organic acids IC. Solutions of the lowest molecular mass species should be remade regularly (in particular, formate and acetate should be remade on a weekly basis; oxalate and lactate should be remade on a monthly basis). All standard responses should be checked over time for linearity between calibrations/analyses. Note that no internal standard is typically used in IC (nor is it typical in LC/MS). All organic acid external calibrations should be linear (r^2>0.99).

Table A7-3. Calibration volumes and concentrations to be used in the calibration of the response of organic acids in the organic acids IC system.

	Organic Acids Analysis							
	1. Dilute to 1 mM Solutions: Vol to add to 10 mL totaL (uL): Start Conc. 100 mM --->		100	2. Dilute to 100 uM Solutions: Vol to add to 10 mL totaL (uL): Start Conc. 1 mM -->		1000		
	Standard Solution Number							
	1	2	3	4	5	6		
Final Conc, uM:	1	3	5	10	30	50	100	200
3. Into final autosampler vials:								
vol at 1mM:				15	45	75	150	300
vol at 100 uM:	15	45	75					
Vol water:	1485	1455	1425	1485	1455	1425	1350	1200
Acetate, propionate, maleate, oxalate, formate, MSA, pyrvuvate, valerate, glutarate, succinate, malonate								

Oxidation Logsheet

Date: Reaction performed by:

Reactant(s), concentration(s): Oxidant, concentration:

Light source: Total desired time of oxidation (e.g., 60 min or 90 min):

Online flow rate: Online MS? Yes No Online UV/vis? Yes No

Offline/discrete sample vol.: Time interval (e.g., 10 or 15 min):

Total vol. for offline, online analyses: Total vol. at *t*=0 (when oxidant and/or light added):

Reaction Time (min)	MS Recorded Time (min)	Discrete Sample (check)	Notes
0			

Oxidation Logsheet

Date: Reaction performed by:

Reactant(s), concentration(s): Oxidant, concentration:

Light source: Total desired time of oxidation (e.g., 60 min or 90 min):

Online flow rate: Online MS? Yes No Online UV/vis? Yes No

Offline/discrete sample vol.: Time interval (e.g., 10 or 15 min):

Total vol. for offline, online analyses: Total vol. at *t*=0 (when oxidant and/or light added):

Reaction Time (min)	MS Recorded Time (min)	Discrete Sample (check)	Notes
0			

APPENDIX 8: CASE STUDY: ORGANIC ACIDS AT MOUNT TAI, CHINA

Empirical orthogonal function (EOF) analysis was performed on a dataset of chemical parameters within orgographically lifted organic acids collected from Mount Tai in the North China Plain. The Mountain is located within Shangdong Province, which has been found to have the highest measured SO_2 and NO_x concentrations within China, resulting primarily from industrial and agricultural processes (Guo et al., 2012). Although organic acids could have been emitted directly to the atmosphere or formed within the atmospheric through secondary gas-phase processing, an exploration was made with the goal of identifying PCs with aqueous processing signatures within the Mount Tai organic acids and other collected chemical parameters, based on known chemical and physical relationships of variables. It can be assumed that there is no autocorrelation between most data points since most samples were taken independently in time, but there are some samples that were taken con- secutively during a single cloud event (these will certainly have some autocorrelation). Since the data sampling rate was irregular, however, removing the effect of autocorrelation would be difficult. In order to avoid underestimating the error (North et al., 1982) in each resulting EOF, only one point per event will be calculated in the effective sample size.

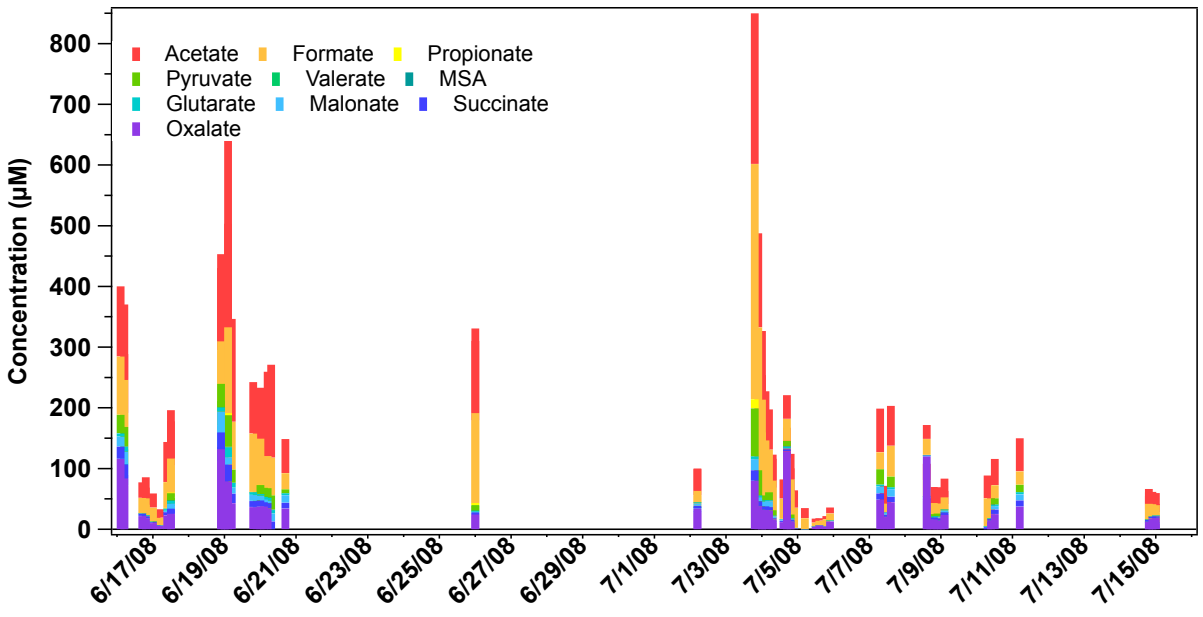

Figure A8-1. Concentrations of organic acids measured in cloud samples from Mount Tai, China.

Again, the eigenanalysis using standardized data was more useful, but for some variables, seeing the magnitude

of the difference between EOFs is useful. For example, EOF_1 (red) repre- sents samples with low ionic concentrations overall, but in particular in the unstandardized plot of the EOFs with respect to each parameter, sodium (Na^+), nitrate (NO_3), and chloride (Cl^-) concentrations have large absolute deviations from the mean of the sample set. Since the units are equivalent for these (and the charge, because the unit is micro normal), it is probable that the species sodium nitrate ($NaNO_3$) and sodium chloride (NaCl) were low in these samples in particular. These might be from marine sources or continental dust sources.

Note that the analysis was run without the inclusion of the d "date time" parameter, and no substantial change was observed from the EOF and PC patterns presented here.

EOF_1 (45% variance, red) describes a characteristic post-monsoonal (later date), high liquid water cloud event with high pH (basic), high hydrogen peroxide (H_2O_2), but low values of generally all other chemical species. This signature might represent samples with low concentrations of oxidant (note that the median PC is slightly negative for this EOF) that have not yet reacted in the atmosphere and have left relatively high concentrations of ionic and organic species in the samples.

EOF_2 (12% variance, yellow) describes a second type of sample collected later in the sampling period with low mass and higher concentrations of species (possibly samples of fog droplets that have been partially evaporated at the end of an event). For the opposite trend (the median PC is again negative), the sample is more dilute and might be from larger, early fog event droplets.

EOF_3 (9% variance, green) describes a sample type with high pH, TOC, and concentrations of species that might be found in the gas phase (formaldehyde –HCHO, acetate, formate, propionate, and pyruvate). The opposite of this EOF gives a possible

Median values for the PCs were all slightly negative, with a possible secondary mode at a slightly positive value in each, although this is difficult to discern due to the small number of samples.

Since the number of samples collected during a second study of the atmospheric aqueous phase was small (only about 6 usable samples after all nans were removed), this subset of samples (fog collected at Baengnyeong Island, South Korea in the Yellow Sea) was added to the Mt. Tai, China orographically lifted cloud sample dataset, and EOF analysis was performed. The results are shown in Figures 5 and 6; Although the PCs are mostly unchanged, EOF_1 is changed by a small amount, and EOF_2 and EOF_3 are quite different. All median values of the PCs were again slightly negative, with a possible secondary mode in each PC that was slightly positive. EOF_1 was likely associated, in most samples, with high concentrations of most species, high acidity, and relatively low peroxide (oxidant) concentration. The bimodality would make sense if we had some oxidized and some unoxidized samples, which is what we are generally looking for in these samples.

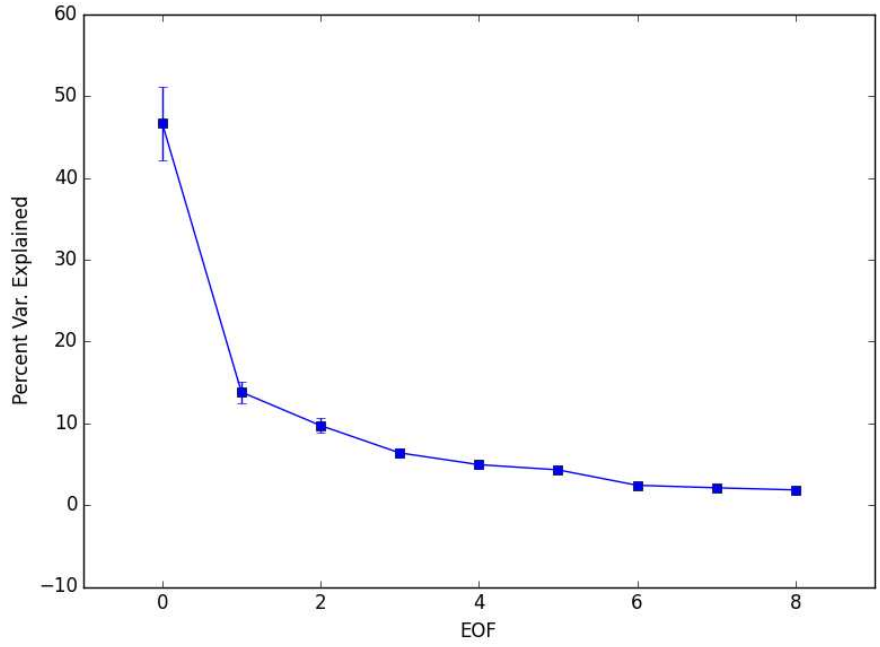

Figure A8-2. Plot of the percent variance explained by each standardized EOF.

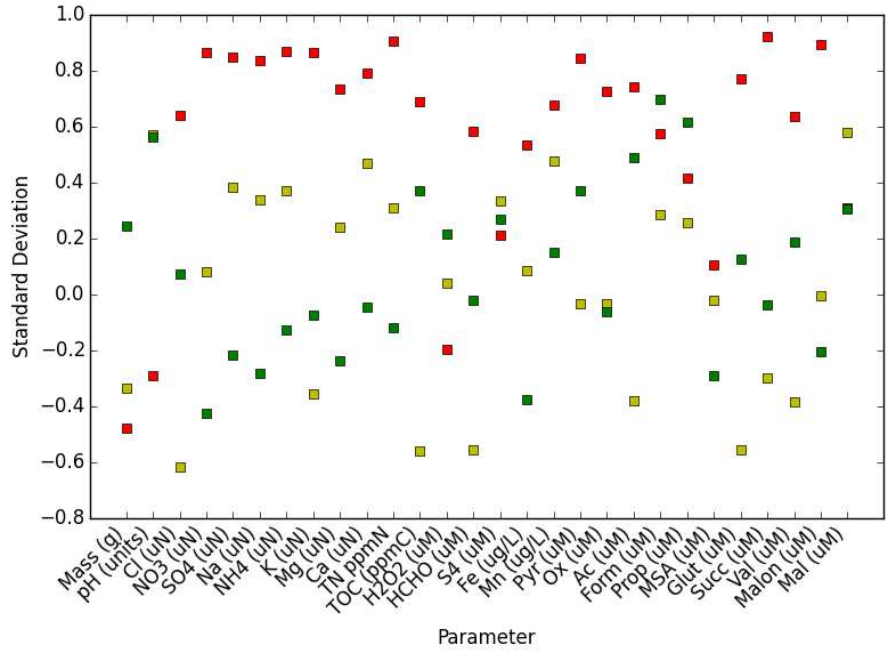

Figure A8-3. Plot of the variance for each variable included in each standardized EOF (the eigenvalues for the first three principal components). EOFs are shown in yellow (E0), green (E1), and red (E2).

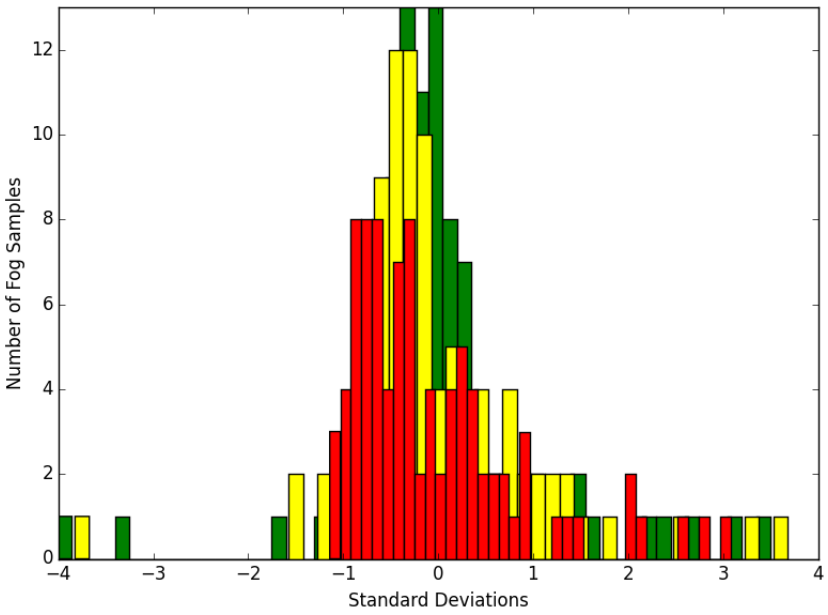

Figure A8-4. Histograms of the convective features in the dataset binned by the values of PC_1 (red), PC_2 (yellow), and PC_3 (green; all PC values are standardized). These can be interpreted as showing which/how many of the convective features resemble EOFs 1, 2, and 3, respectively.

Table A8-1. Organic acids concentrations measured in Mount Tai cloud water samples (from 2008; Shen, 2011).

Date and Time	Pyruvate (μM)	Oxalate (μM)	Acetate (μM)	Formate (μM)	Propionate (μM)	Methanesulfonate (μM)	Glutarate (μM)	Succinate (μM)	Valerate (μM)	Malonate (μM)	Maleate (μM)	Percent Org. Acids (%)
6/16/08 2:24	30.0926	115.89	115.728	96.0454	0	0	5.2604	20.1596	0.590472	16.436	207.162	53.2979
6/16/08 4:48	23.0483	71.9535	97.4633	59.6743	0	0	4.18754	18.0392	0	14.4695	3.88096	27.3739
6/16/08 4:48	32.0297	83.8845	124.252	77.3836	0	0	8.31168	23.2154	0.349876	20.8248	6.70183	29.254
6/16/08 16:48	0.229881	21.9371	25.6567	25.4196	0	0	0.381587	3.65057	0	0	0	20.6384
6/16/08 19:12	0	15.0236	28.3861	21.3585	0	0	1.50207	2.62499	0	0	5.97489	18.2091
6/16/08 19:12	0.283066	18.4379	34.6266	27.7895	0	0	1.38865	3.22397	0	0	6.28259	19.6793
6/17/08 0:00	0	10.3125	23.363	23.1169	0	0	0.810664	1.47685	0	0	30.0105	41.571
6/17/08 2:24	0	5.70121	11.7433	2.62589	0	0	0.500397	0.0088353	0	0	1.05739	16.3652
6/17/08 4:48	0	5.63521	14.2428	12.4003	0	0	0.473613	0.345686	0	0	0	15.9501
6/17/08 9:36	0	23.1203	66.1762	42.6689	1.1513	0.563629	3.03708	5.15878	0	2.01754	8.19537	14.6146
6/17/08 12:00	9.26531	25.6362	73.4726	51.7264	0.996681	1.03207	3.6744	7.05529	0	5.18562	21.2941	24.027
6/17/08 12:00	11.6253	24.8706	79.5469	55.9755	1.13536	1.13423	4.8308	9.19993	0	7.92775	48.5671	27.0158
6/18/08 21:36	40.0834	110.816	136.105	83.0525	0	0	7.61083	25.8603	0.304185	26.7797	190.867	42.2346
6/18/08 21:36	38.5203	131.958	143.673	70.1513	0	0	6.97181	27.5469	0.20038	34.3666	114.107	38.2061
6/19/08 0:00	21.1937	73.4132	99.679	49.771	0	0	5.19838	16.2125	0	18.0784	37.3795	34.4799
6/19/08 0:00	14.6229	2.4982	90.6346	45.5139	0.5689	0	4.10238	11.8145	0	8.79299	22.785	23.636
6/19/08 0:00	0	37.862	172.602	63.9723	0	0	5.94258	10.9722	0	2.72466	6.94329	14.2684
6/19/08 2:24	27.3761	43.5576	305.789	97.0539	0.293393	0	9.24958	15.9373	0	4.00407	0	11.1195
6/19/08 2:24	51.871	78.9553	437.225	141.398	3.29764	0	16.5058	27.5447	0.800239	12.3444	0	9.6003
6/19/08 4:48	22.044	42.9416	169.487	78.671	0	0	7.90101	15.8183	0	9.66212	25.4709	19.9062
6/19/08 19:12	0	36.7075	84.8594	96.3382	0	0.0506303	4.57488	9.85628	0.0844048	10.0249	226.74	84.619

6/19/08 21:36	14.754	24.3111	72.2889	53.4832	0	0	3.59888	8.64123	0.0880845	7.14071	45.8615	37.7753
6/20/08 0:00	14.5751	37.8186	83.8404	76.2063	0.269443	0	2.99752	9.77683	0.067221	7.63482	148.556	65.5709
6/20/08 0:00	0	24.6492	65.1625	52.8977	0	0	1.89385	5.24788	0	2.11211	71.0883	47.7055
6/20/08 2:24	11.2639	29.8035	73.3741	40.3697	0.43849	0	2.55138	4.83115	0	3.49493	0	23.5856
6/20/08 2:24	14.7181	37.4842	109.423	46.6456	0	0	4.24782	7.0502	0.239442	4.52979	0	18.1516
6/20/08 4:48	15.442	34.7858	138.891	52.9269	0	0.250989	5.00322	8.37144	0	4.03692	44.25	18.6481
6/20/08 7:12	23.7434	0	153.132	62.245	0	0.0787173	6.28539	12.9198	0	12.7485	53.4092	22.7926
6/20/08 16:48	6.53059	33.9368	56.4027	26.7033	0	0	2.88045	9.76221	0	12.6608	107.454	39.818
6/26/08 0:00	9.46246	24.3838	139.326	147.967	3.56207	0	1.65932	3.46148	0	0.93731	2576.91	635.222
6/26/08 0:00	9.95904	22.2419	131.636	137.377	2.23303	0	1.84475	3.81267	0.0439844	1.28105	2881.78	707.689
7/2/08 4:48	0	34.3187	37.1188	18.941	0	0	1.95809	4.11115	0.0557307	3.87435	650.943	182.424
7/2/08 4:48	0	26.94	43.1008	19.3376	0	0	2.07392	4.03149	0	3.74928	801.953	213.006
7/3/08 19:12	79.2593	79.7366	257.582	387.391	15.0922	0	4.06802	17.4802	0.129432	18.3948	1065.66	97.4465
7/3/08 21:36	41.7819	38.3204	155.079	235.091	0	0	3.02702	8.07797	0	6.18527	826.512	179.329
7/4/08 0:00	23.72	22.2294	113.099	157.661	0.271925	0	1.72146	4.3639	0	3.71692	507.883	175.922
7/4/08 0:00	17.1379	18.6082	94.2495	117.98	0	0	1.18132	3.4328	0.0965976	1.30045	410.774	200.725
7/4/08 0:00	0	18.468	81.4969	103.526	0	0	1.45764	3.09236	0	2.0374	97.3933	90.026
7/4/08 2:24	6.8828	16.6504	66.3102	87.7185	0	0	0.962535	2.33962	0	1.77289	41.1159	62.6872
7/4/08 2:24	0	32.1923	80.8157	99.0414	0	0	1.98762	5.79235	0	7.54978	82.4664	64.2769
7/4/08 4:48	13.2854	31.1795	66.381	69.9774	0	0	1.64335	5.5982	0	9.41039	10.2184	38.1214
7/4/08 7:12	9.01062	15.7229	42.6014	49.0417	0	0	1.06255	2.60338	0	3.01935	231.05	157.26
7/4/08 7:12	1.25974	11.2901	48.2628	53.0411	0	0	0.920916	1.50872	0	0	210.123	187.762
7/4/08 14:24	0	11.9072	31.7778	33.4198	0	0	0.806949	2.33149	0	1.89312	115.974	116.394
7/4/08 16:48	9.02308	128.61	39.1975	36.1739	0	0	3.64322	3.25592	0	1.06326	105.082	132.636
7/4/08 16:48	17.2962	19.5834	49.3962	70.5679	0	0	4.08298	3.83868	0	2.67397	90.5256	71.4558
7/4/08 19:12	5.97473	13.5038	42.1675	57.7594	0	0	2.67045	2.26917	0	0	203.507	155.608
7/4/08 19:12	0	10.7426	37.8702	49.4352	0	0	1.78264	0.812575	0	0	203.145	174.142

7/4/08 21:36	0	1.33077	29.0883	33.0268	0	0	0.25251	0.666533	0	0	115.597	154.32
7/5/08 4:48	0	0	16.8578	18.2471	0	0	0.0370309	0	0	0	91.9286	180.751
7/5/08 12:00	0	4.27752	6.81186	6.50359	0	0	0.10212	0	0	0	5.91681	34.8848
7/5/08 14:24	0	6.30727	4.40321	7.26275	0	0	0.433971	0	0	0	0	22.5965
7/5/08 19:12	0	4.45051	5.02079	11.9726	0	0	0.341027	0	0	0	0	17.4912
7/5/08 21:36	0	12.8106	10.0538	11.4506	0	0	0.987346	0.681156	0	0	24.0588	42.0583
7/7/08 7:12	25.5386	48.5795	71.8017	27.9002	0	0	2.9749	10.4192	0.211599	11.2613	887.176	166.557
7/7/08 9:36	0	20.1222	29.1599	14.3441	0	0	0	3.69269	0	4.24764	130.026	65.7842
7/7/08 12:00	0	11.4972	20.6946	11.587	0	0	0.653974	1.73276	0	1.1768	41.9934	40.038
7/7/08 14:24	17.6447	44.7973	66.0252	50.6805	0	0	2.90419	8.75193	0	12.5965	770.375	186.191
7/8/08 14:24	0	47.5974	26.8691	26.0324	0	0	1.23519	3.30913	0	2.89098	181.709	132.02
7/8/08 14:24	0	119.645	22.9595	26.5525	0	0	0.912749	1.75677	0	0	0	88.8738
7/8/08 16:48	0	10.674	14.2512	13.3444	0	0	0.838419	1.05754	0	0	1.27919	24.064
7/8/08 16:48	0	12.3744	22.1781	21.802	0	0	1.27917	2.42397	0	0	0	25.0519
7/8/08 19:12	3.91427	16.5008	26.1991	18.5194	0	0	1.40569	3.18169	0	0	30.9166	45.2963
7/8/08 19:12	4.28069	13.3612	25.5584	16.6235	0	0	1.69656	3.06105	0	0	62.6561	62.3019
7/8/08 21:36	4.92365	14.9031	27.3655	16.0976	0	0	1.53721	3.42974	0	1.18063	89.7825	67.1061
7/8/08 21:36	0	10.7556	21.5016	18.7705	0	0	1.03036	2.34853	0	0	41.5269	51.1317
7/8/08 21:36	3.14902	9.27287	21.5797	24.7384	0	0	0.969697	2.12113	0	0	48.5169	67.2109
7/9/08 0:00	0	10.8884	23.3008	28.8742	0	0	0.552832	2.20186	0	0	72.6127	85.3326
7/9/08 0:00	0.860652	10.6071	21.9468	26.418	0	0	1.3628	2.1757	0	0.334492	57.6548	64.0425
7/9/08 2:24	0	23.7215	31.0335	20.1927	0	0	1.92499	4.29029	0	2.40149	123.142	75.5015
7/9/08 2:24	0	22.2329	22.1262	13.0527	0	0	1.34665	3.17733	0	1.32124	79.651	55.1786
7/10/08 7:12	0	0	37.8148	46.1251	0	0	1.31127	3.52611	0	0	32.9356	54.5184
7/10/08 9:36	0	8.77475	21.871	26.5202	0	0	1.07324	2.0759	0	0	6.61154	34.0696
7/10/08 9:36	0	13.8186	23.6716	19.2062	0	0	1.34618	3.26859	0	0	25.5967	42.3278
7/10/08 12:00	10.6349	25.0434	43.0747	21.5133	0	0	2.36274	7.28046	0	5.90004	81.1973	53.7334

7/11/08 4:48	12.266	37.3116	54.4717	22.2565	0	0	3.35056	10.2136	0	10.077	153.458	63.3979
7/14/08 19:12	0	12.5309	24.3843	25.6412	0	0	0.968404	2.9163	0	0	36.7572	56.9186
7/14/08 19:12	0	10.0216	21.2841	19.8761	0	0	1.0017	2.45193	0	0.0381055	31.5337	54.1349
7/14/08 19:12	0	9.56147	21.1695	27.5997	0	0	0.474579	1.80176	0	0	52.0559	90.7822
7/14/08 21:36	0	11.9524	20.4525	26.9403	0	0	0.635883	1.78445	0	0	18.0146	64.9511
7/14/08 21:36	0	17.7078	21.6467	17.0736	0	0	0.575604	2.70171	0	0	3.0887	44.4744
7/15/08 0:00	0	18.644	20.1774	16.7282	0	0	0.555693	2.98632	0	0.79863	1.84829	42.8803
7/15/08 0:00	0	9.70561	13.4439	16.9073	0	0	0.551181	1.01992	0	0	3.06118	28.9837
6/29/10 4:48	7.70944	20.9949	60.6022	76.9256	3.82382	5.73425	2.67161	16.6183	1.56206	8.15388	20.7099	35.5532
6/30/10 7:12	1.57447	7.88358	125.318	87.7741	3.86383	2.22159	1.58975	3.21556	1.41557	2.01543	6.03952	143.734
7/1/10 4:48	4.40667	19.0593	49.1134	79.875	3.95809	3.05332	3.47209	11.2092	2.26859	4.0918	7.71211	60.4416
7/1/10 7:12	4.50376	20.7561	50.9422	98.5079	4.17703	2.97643	3.5417	12.327	1.93359	3.68926	7.45581	52.6647
7/1/10 7:12	7.01896	24.2685	67.0782	102.869	4.35363	3.0888	3.96603	16.8251	2.69916	5.12938	10.5214	45.0844
7/1/10 12:00	21.0712	98.6022	220.187	247.142	3.08272	3.28421	50.4194	137.471	8.08859	40.4334	26.5	80.1598
7/19/10 7:12	3.9923	14.4693	34.8105	50.7163	3.59933	2.9576	2.27312	9.52191	2.04049	5.36818	9.19295	72.3841
8/26/08 17:26	8.89839	29.3149	68.2555	56.2136	0.624099	0.293627	3.08166	7.9359	0.258552	4.88848	177.087	81.9692

APPENDIX 9: MATERIALS FOR OUTREACH PROGRAMS

Chemical Oxidation

Background: Everything around you is composed of chemical elements, and each chemical element is made of tiny, identical bits called atoms. Inside each atom is a number of protons and neutrons, which are located in the center of the atom, and electrons, which move around the outer part of the atom. The protons and neutrons don't change much, but in nature, it is very common for the electrons to be lost, or for extra electrons to be added to an atom. This type of change to atoms is called "oxidation" when electrons are lost, and "reduction" when electrons are gained. An easy way to remember is this "OiL RiG": oxidation is loss; reduction is gain. This experiment will show two parts: (1) a gain of electrons, or reduction, of manganese (Mn) atoms, and (2) a loss of electrons, or oxidation, from carbon (C) atoms. These reactions show two very different, very cool things that happen when we just add or remove electrons from atoms.

Question: What happens when you add electrons to an element? How much does it change?

(1) Experiment: Colorful Oxidation States

MATERIALS NEEDED:

- 250mL flask
- 0.15M sugar solution
- 0.33M NaOH
- A few mL of a dilute $KMnO_4$ solution
- Safety equipment (goggles, gloves)

PROCEDURE:

1. Add equal volumes of sugar and NaOH solutions to the flask.
2. Add 5-10 drops of a $KMnO_4$ solution, too much $KMnO_4$ will make the color changes too dark to see.

(2) Experiment: Ozonolysis of limonene

Question: Can we make particles by mixing two gases (ozone and pinene) together?

MATERIALS NEEDED:

– 1L Erlenmeyer flask

– O_3 (ozone) generating UV light

– Lime peel

– Aquarium pump

– ozone scrubber

PROCEDURE:

1. Make ozone in flask (make sure it's covered!)
2. Add limonene by putting freshly cut lime peel in flask
3. Shine a laser pointer through the flask and see what happens